Cranfield UNIVERSITY
Silsoe

Microarray Ltd

Institute of Bioscience and technology

EngD

2005

Daniel William Mills

Towards a commercial microelectrode array based sensor for improved chlorine detection

Supervisor: Professor S.P.J. Higson

Presented 31st March 2005

This degree is submitted in partial fulfilment of the requirements for the degree of Doctor of Engineering

Abstract

The commercial development of a disposable aqueous chlorine sensor based on a novel microelectrode array fabrication process is described.

Non-conducting poly(*o*-phenylenediamine) films are firstly used to passivate conductive surfaces. Ultrasonic ablation of passivated electrode assemblies then results in the formation of a plurality of wells to expose the underlying conductive substrate, thereby forming a microelectrode array.

Microelectrode arrays produced in this manner can be exploited within many electrochemical sensing applications; however, portable aqueous chlorine detection has been selected by Microarray Limited (the industrial sponsors of this project) as a primary vehicle for launching its generic production technology. The scale of microelectrode array production has been extended from that of individual gold sputter-coated glass slide electrodes - to the simultaneous production of hundreds of low-cost screen printed carbon-ink based sensors.

A focus has been directed at all stages towards permitting the cost-effective large-scale mass production of sensors with a view to challenging existing portable aqueous chlorine measurement technologies both in terms of performance and unit cost. Based on volume batches of 250,000, it has been calculated that Microarray Limited sensors can be manufactured for a unit cost of approximately 2.5 pence, sufficiently low to provide scope for a competitive yet profitable sale price. The Microarray Limited aqueous chlorine detection system has improved the limit of detection from 0.01 ppm to 0.005 ppm total chlorine without sacrificing accuracy. Furthermore, this novel approach to aqueous chlorine detection offers numerous key benefits to the customer including reduced testing time, a more straightforward operation and the elimination of harmful reagents.

Product development has been described from an initial concept through to a pre-production phase. The development of an innovative generic sensor packaging technology is also described.

Acknowledgements

I would like to thank my supervisor Professor Séamus Higson for providing his guidance during the course of my research. Similarly I wish to thank Doctor Stuart Collyer for his valueable assistance with both technical and none technical aspects of my research programme. I would also like to express thanks to my family and friends for providing their continued support and encouragement throughout the duration of my EngD.

Table of contents

CHAPTER 1

Rationale for research

The main focus of this research programme has been to develop an aqueous chlorine measurement device, to have superiority over existing technologies in terms of sensitivity, cost and application. This objective has been realised through combining the development of an innovative microelectrode array manufacturing technique with careful sensor design and materials selection.

Chlorination has provided the main method for microbial disinfection for over a century. As a relatively strong oxidising agent, chlorine is toxic to most micro-organisms by causing rupture of the cell wall, or by disrupting enzyme activity. These fundamental toxic effects have experienced very little resistance from disease causing microbes, and serve to protect the health of millions of people around the world. Chlorination of water must be carefully controlled as too little will provide inadequate disinfection, while too much wastes resources and can result in the water possessing a bad taste and odour. At even higher concentrations, chlorinated water can be toxic and may damage skin or other tissues coming into contact with it.

Despite chlorination being long-established in first-world countries as a means to reduce disease, poor water quality continues to pose a major threat to human health in developing countries. In contrast to the west, poorer third-world countries are less concerned with acceptable water taste and odour, instead being challenged to supply their populations with microbiologically safe water at an affordable cost. One United Nations report suggests that over 5 million people, most of them children, die each year from diseases related to poor-quality drinking water (United Nations, 2001). However, more recent statistics produced by the World Health Organisation indicate a lower incidence of 1.6 million deaths in the developing world during 2003 (World Health Organisation, 2004). Moreover, the number of people who suffer each year from diseases linked to dirty water easily runs into billions (European Environment Agency, 2002). Despite increasing awareness as to the benefits of clean drinking water, in most cases third-world populations are growing faster than their country's water supply and sanitation infra-structures, causing the situation to worsen.

Of further concern are the delicately balanced ecosystems of our rivers and lakes, where aquatic life is particularly sensitive to even trace amounts of chlorine. Environmental regulation reflects this accordingly (78/659/EEC, 1997), (2000/60/EC, 2000); however there is currently no cost effective field measurement method available for the ultra-low concentrations of aqueous chlorine stipulated (≤0.005 mg/l total residual chlorine). Removing samples of water to the laboratory for analysis is impractical, as chlorine can be unstable, reacting readily with organic molecules and being sensitive to both light and temperature.

Existing field chlorine measurement technologies rely on wet-chemical colourimetric methods, whereby a chemical is added to the solution to react with chlorine and produce a colour change. Chlorine concentration is then estimated by measuring the absorbance of a light source through the mixture. This process requires a skilled operator, separate hazardous chemical reagents and lengthy test procedures. Furthermore, the low sensitivity of colourimetric methods has resulted in a failure to enforce the levels of chorine stipulated by environmental regulation.

Microarray limited is an R&D company specialising in developing and exploiting new intellectual property for electrochemical sensor applications (Figure 1.1). Company headquarters are based in Manchester (UK) and research is carried out at Cranfield University at Silsoe, Institute of Bioscience and Technology.

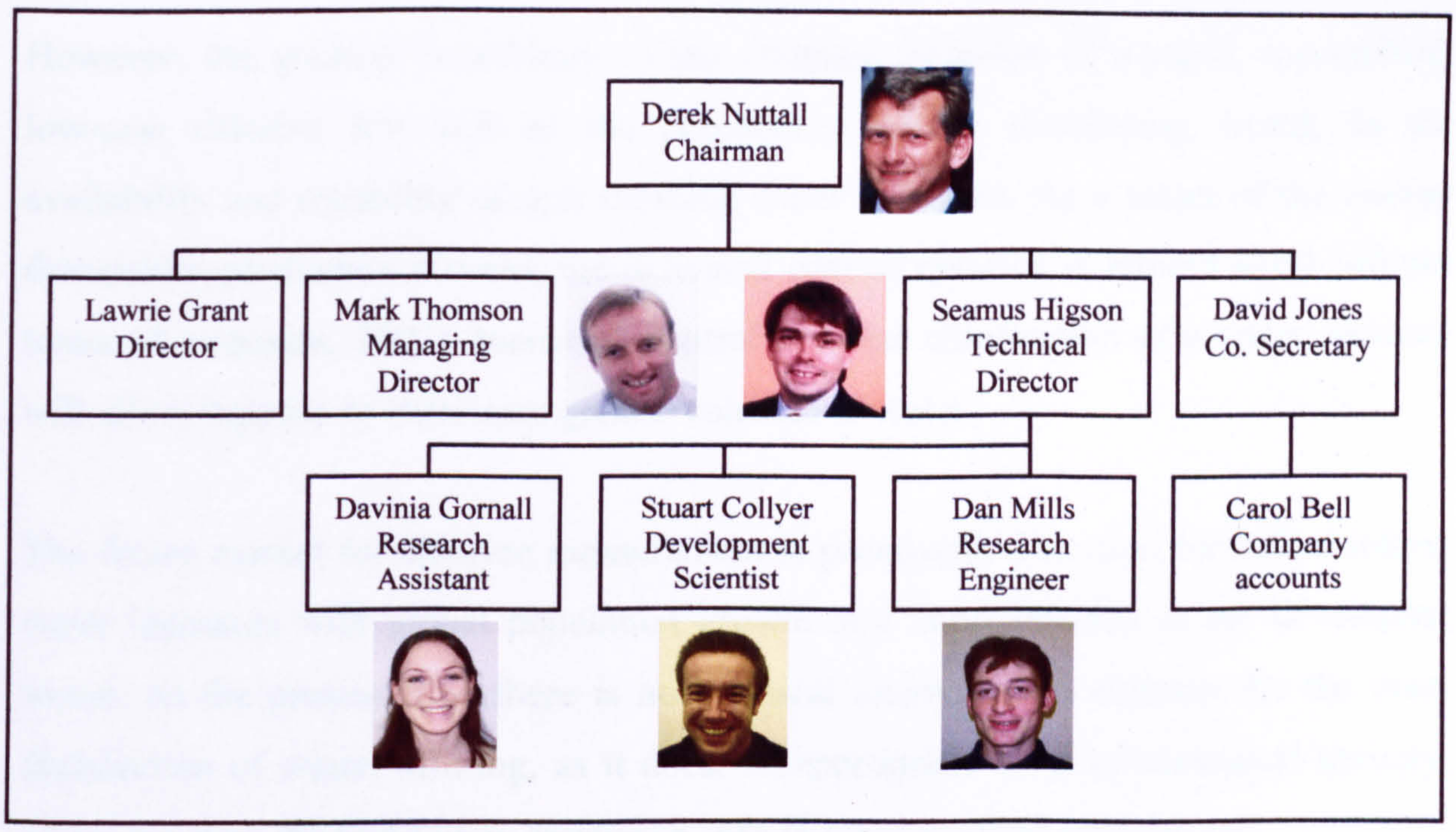

Figure 1.1: The Microarray Limited company structure

Microarray Limited has developed a commercial aqueous chlorine measurement system offering a number of improvements over existing chlorine measurement methods. Key advantages include increased sensitivity, fast, reagentless sampling, reduced operator skill and sensor stir-independence derived from a microelectrode array sensor configuration. Intellectual property ownership exists for the novel microelectrode array manufacturing method, which allows the simultaneous production of thousands of sensors in a short time and at low cost (Higson, Filed 19th November 1996, published October 1996). The generic stir-independent sensor manufacturing technology offers the advantage of providing a signal which is unaffected by flow or movement of the sample liquid, and can in the future be applied to measurement of further analytes of importance. Microarray Limited has received investment towards targeting of the chlorine measurement market from a number of sources, including academic institutions and venture capitalists, as well as the UK Environmental Agency who are keen to be able to enforce environmentally safe levels of chlorine in river water.

However, the greatest beneficiary of the commercialisation of a rapid, low-skilled, low-cost chlorine test will be the populations of the developing world, as the availability and reliability of safe drinking water increases. As a result of the energy demanding production process, the delivered cost of chlorine is around $160-300 per tonne (Rosemount, 2002). Increased control over the chlorination of a water network will allow supplies to chlorinate greater volumes of water.

The future market for chlorine measurement is promising. The need for safe drinking water increases with global population growth and improvements in the developing world. At the present time there is no practical alternative to chlorine for the mass disinfection of water, offering, as it does, an appropriate level of biological toxicity, while avoiding the build-up in resistance seen in other medical applications.

D. W. Mills

Cranfield University, Silsoe

CHAPTER 2

Introduction and literature review

D. W. Mills

Cranfield University, Silsoe

2.1 Chemical sensors

Ever increasing demand for improved healthcare, environmental protection and process control has driven a global surge in chemical measurement technologies. Traditionally such analysis has been restricted to the laboratory, with incurred disadvantages such as a delay in measurement and the low throughput commonly associated with expensive equipment and highly trained personnel. It seems reasonable therefore that industry has pushed towards a lower cost solution based upon the mass production of miniaturised sensors which can be applied by low skilled operators, or even the consumer himself. Whilst reducing cost, this allows the generation of large amounts of data in a shorter space of time, providing comprehensive information on complex and dynamic systems. This is of particular importance to environmental monitoring which involves large scale, field-based measurement, such as the chlorination of water systems.

2.1.1 Chemical sensor definitions, technologies and markets

In order to describe chemical sensors, it is necessary to broadly define the sensor technologies available. It is possible to classify sensors in a number of ways, for example, the type of variable detected, (temperature, pressure, strain, etc.), sensing technology utilised (e.g., photoelectric, magnetic, acoustical), the sensing device itself (thermocouple, bourdon tube, strain gauge, etc.) or by application (process control, aerospace, appliance, motor vehicle, etc.).

Stetter *et al* broadly define sensor technology into two groups: *physical* sensors and *chemical* sensors (Stetter *et al*, 2003). Physical sensors are used to measure physical properties such as temperature (e.g. thermistors, thermocouples), and pressure (e.g. piezoelectric crystal microbalance). These devices have been able to approach the general requirements of an ideal sensor in that they are sensitive, selective for the parameter of interest, robust, reliable, easy to use and inexpensive due to established mass production.

Chemical sensors differ from physical sensors in that they have a chemical or molecular target to be measured, thereby providing information to the user about the chemical nature of the sensor environment. A chemical sensor can be defined as a device which can convert a chemical property (e.g. concentration) into a measurable signal. The chemical sensing process involves the *molecular recognition* of a chemical species (target analyte) and the *transduction* of the chemical information into a measurable signal.

An official definition is provided by IUPAC, stating that 'a chemical sensor is a device which transforms chemical information into analytical signal. Each chemical sensor consists of two parts: a receptor and a transducer. The receptor part transforms chemical information into a form of energy measured by the transducer, which generates the analytical signal' (IUPAC, 1997a).

The chemical sensors market as a whole is dominated by key players such as Roche, Johnson & Johnson, Bayer, NGK Spark Plug, Abbott Laboratories, Captive and Robert Bosch, who accounted for most of the $2.8 billion of U.S. chemical sensor market sales in 2003 (Figure 2.1). This is due primarily to their dominance of large market sectors like glucose monitoring biosensors and automotive oxygen sensors.

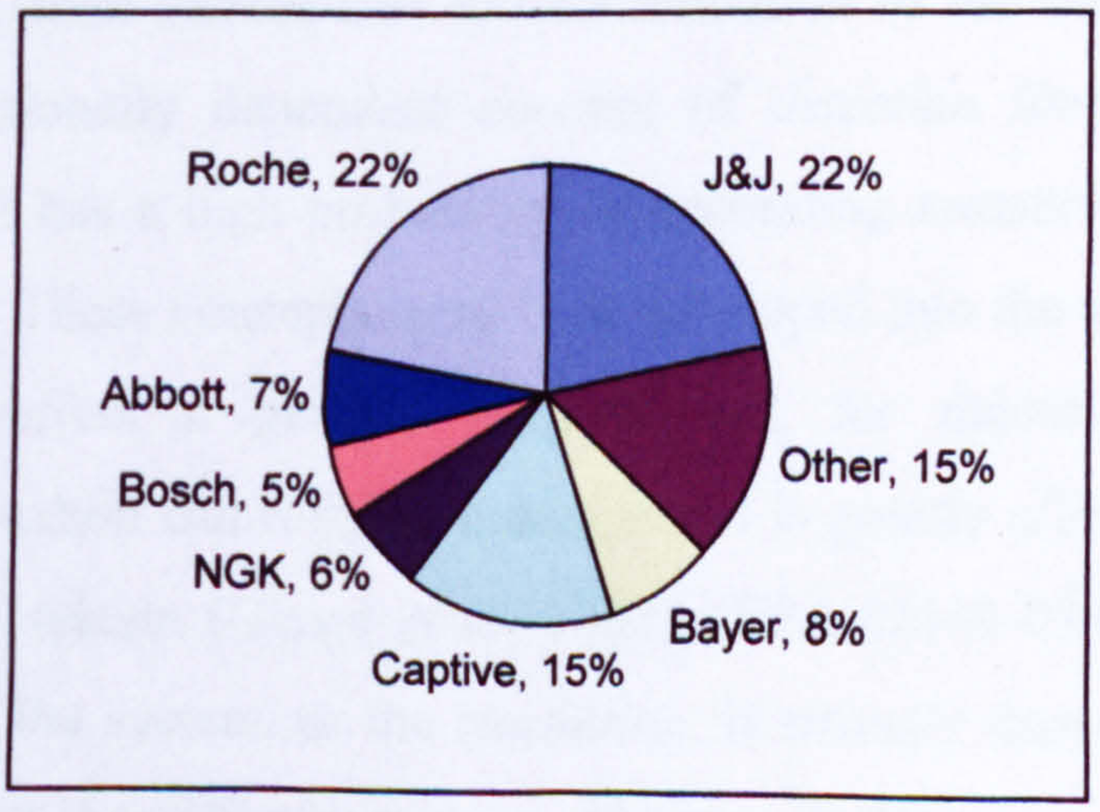

Figure 2.1: U.S. Chemical Sensor Market Share 2003 ($2.8 billion)

There are a number of performance criteria applicable to chemical sensors. *Selectivity* of a sensor, the ability to discriminate between different substances, is one of the most important performance criterions and has received the most chemical sensing research in recent times (Janata & Josowicz, 1998). Selectivity for a particular chemical is usually provided by a membrane, for example Nafion, which screens analytes based on size and charge exclusion or by an ion selective frit such as the ion selective glasses used in pH electrodes. *Accuracy* refers to how close the measured value is to the true value, and requires the certainty of a result to be quantified in terms of determinate, indeterminate and gross errors. Generally speaking, accuracy is expected to be better than ±5% (Eggins, 2002). *Precision*, or reliability, is a measure of how repeatable the results are. For example, if the same solution is measured a number of times, then ideally exactly the same result should be obtained each time. However, in practice this is not the case, as there are limitations to the level of reproducibility of the sensor manufacturing processes, as well as experimental limitations.

The *sensitivity range*, or *working concentration range*, is concerned with detection and quantitation within the concentration range of interest. Since 1968, most of the literature in this area has referred to the work of Dr. Lloyd Currie who, using statistical decision theory, strove to develop an internationally standardised method for comparing the capability of different measurement techniques (Currie, 1968), (Currie, 1995), (Zorn *et al*, 1999). He defined the term *critical value* as the measured value at which there is a small chance that the concentration of the sample is zero, and the related and functionally dependent concept of *detection limit*, which refers to a concentration that has a high probability of generating measured values greater than the critical value. These concepts were later developed into the *method detection limit* (MDL), which offers a general purpose tool for determining the minimum concentration a method can reliably measure and is greatly affected by the signal-to-noise ratio of the system (Glaser *et al*, 1981), (EPA-821-R-03-005, February 2003). The *sensitivity* of the system, or the *resolution*, is strongly dependent on the linearity and the gradient of the calibration curve. Modern electronics can easily decipher the signal response of a sensor, which will have a mathematical relationship to the

concentration of analyte. The more linear and steeper the curve, the more easily individual concentrations can be determined.

The *response time* of a sensor is a key performance criterion as it has a direct impact on the working efficiency of the testing party. For this reason a response time of 60 seconds or less is generally expected, although a great deal depends on the sensor construction, whereby multiple selectivity layers or slow reaction kinetics can limit responsiveness. *Recovery time* is the time which must elapse before the sensor can perform another test. This should ordinarily be less than a few minutes, however in the case of single-use (disposable) sensors, this is not an issue. Finally, the *stability* of a sensor may pose a significant problem for continuous in-line measurement. When sensors are exposed to an impure medium, a build up of material on the electrode surface may occur over time, often resulting in a decrease in sensor response. Single use, disposable sensors suffer much less from this problem due to the short period of time that they are exposed to solution. However, both types of sensors must possess adequate storage stability, so that long term storage under reasonable conditions does not produce any significant variation in results. Chemical sensors may be sub-classified into the following groups (Cattrall, 1997):

Electrochemical – The most common type of chemical sensor, incorporating conductimetric, amperometric and potentiometric transducers (including ion-selective electrodes and ion-selective field effect transistors).

Optical – Sensors which rely on light absorbance, reflectance and luminescence based measurement and are sometimes termed *optodes*.

Mass sensitive – Material adsorbed onto the surface of an oscillating piezoelectric crystal causes a shift in the resonant frequency. This change can be measured and calibrated to indicate target analyte concentration.

Calorimetric – Heat sensitive devices incorporating a transducer such as a thermistor to measure the heat energy released from a chemical reaction.

The field of electrochemical sensors continues to dominate at both the research and the commercial level, comprehensively reviewed by Janata *et al* (Janata and Josowicz, 1998) and more recently by Bakker (Bakker, 2004). The generic term 'electrochemical sensor' refers to a device which functions by transducing the oxidation, or reduction, of an analyte of interest into an electrical signal.

The three types of electrochemical sensor offer different degrees of selectivity, namely *conductimetric, potentiometric, and voltammetric* (Brett & Brett, 1998). In *conductimetric* sensors, solution resistance is measured to assess concentration. Although this method is not analyte specific, it can provide generic information in respect to total ion concentration. Gas sensors often employ this type of analysis, frequently based on semi-conducting metal oxides, for example SnO_2 is used to detect carbon monoxide (Malinovskaya *et al*, 2001).

Potentiometric methods involve the equilibrium potential of an indicator electrode to be measured at almost zero current against a selected reference electrode. Since no current flows, this has the advantage of not consuming any analyte. The use of an ion selective frit over the electrode surface can provide good selectivity for a particular species, with detection limits as low as $1x10^{-5}$ M. A familiar example of such a potentiometric sensor is the pH meter, which has a broad response range, a fast and stable response to the concentration of H^+ ions, and is relatively stir independent (Wang, 2000). Recent potentiometric research has focused on reducing detection limits to trace levels (Bakker & Pretsch, 2002), (Umezawa *et al*, 2002).

Voltammetric sensors interrogate the analyte solution by applying a sweeping oxidative or reductive potential and recording the current that flows. As the potential increases (or decreases), a peak current is observed at potentials in excess of the oxidation or reduction potentials of the electroactive species; the current observed is proportional to its concentration. It is also possible to step directly to the relevant potential and measure the current, this approach is known as an *amperometric* analysis. Historically voltammetry developed from the discovery of polarography in 1922 by the Czech

chemist Jaroslav Heyrovsky using a dropping mercury electrode (Heyrovsky, 1922) (Heyrovsky, 1948). Disadvantages to this method include significant stir dependence due to the role of mass transport, as well as some consumption of analyte. However, amperometric electrochemical sensors have been found to be relatively robust in use, and are highly sensitive with detection limits reported as low as $2x10^{-13}$ M (Kim *et al*, 2001). Amperometric sensors are used most commonly in portable industrial safety monitors, where they account for nearly all of the market. The sensors are well suited to this application as amperometric devices are stable, fast, durable, compact, require very little power and are relatively cheap to mass produce. It is worth noting that the mass transport dependency and sensitivity to solution movement is negated in the case of a microelectrode array sensor configuration.

It is also possible to modify a chemical sensor by the incorporation of a biochemical sensing element coupled in some way to a transducer. Known as a *biosensor*, these devices utilises the specificity found in natural biological processes to detect and measure an inorganic, organic, or biological analyte. A typical definition of a biosensor is 'a self contained analytical device that incorporates a biologically active material in intimate contact with an appropriate transduction element for the purpose of detecting (reversibly and selectively) the concentration or activity of molecular species in a sample' (Guilbault, 1976). Crucially, biosensors are able to benefit from the selectivity found in natural biological systems, and can be grouped by their biological component (e.g. enzyme, antibody, DNA), or by their transduction element (e.g. electrochemical, optical, acoustic, calorimetric). Figures 2.2 illustrates the 'lock-and-key' principle in a biosensor (Wang, 1995).

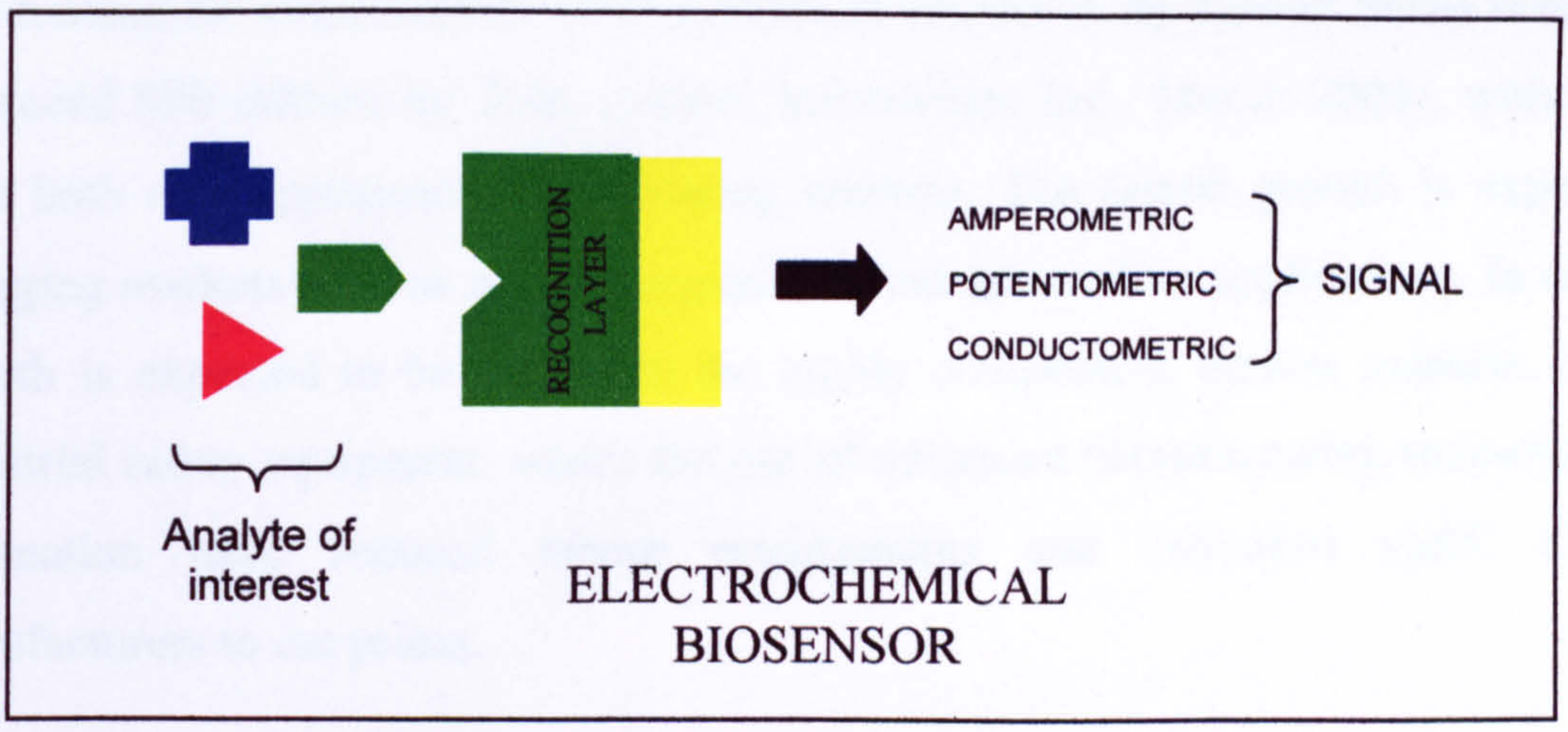

Figure 2.2: Biorecognition and signal transduction

A biosensor can usually be considered to be a sub-set of chemical sensors because the methods of transduction, or sensor platforms, are similar to those for chemical sensors. The first commercial example of a biosensor was the famous Exactech Medisense® blood glucose meter launched in the U.S. in 1986. The diabetes monitoring market worldwide is estimated to exceed $26 billion by 2007 (BCC Research, 2002) and in 2002 commanded 85% of the world commercial biosensors market (Newman *et al*, May 2002). However, as yet, glucose test strips have remained the only truly high volume quantitative biosensor application, since enzymes other than the glucose oxidase used in these biosensors are more susceptible to stability issues and batch-to-batch variation. Home pregnancy test kits, based on antibody entrapment, have proved to be highly successful qualitative diagnostic devices, and in 2002 retail sales in the UK exceeded that for blood glucose kits by £30 million (Mintel, September 2003).

The type of chemical sensor being developed within this research program does not require a biological sensing element, and instead relies on electroanalytical methods and non-biological surface modification to impart sensitivity and selectivity. Once developed, the device will function to measure chlorine via direct amperometric electrochemical reduction.

The demand for amperometric electrochemical sensors in the United States is expected to exceed $90 million by 2006 (Global Information Inc., March 2004), with growth from both new applications and existing markets. The fastest growth is expected in emerging markets such as medical equipment and automotive applications. In contrast, growth is expected to be slower in the highly competitive mature markets, such as industrial safety equipment, where the use of advanced manufacturing technology and automation have reduced labour requirements and increased yield, allowing manufacturers to cut prices.

Year	1992	1996	2001	2006	2011
Electrochemical sensor demand ($ millions)	250	460	620	815	1055
Electrochemical Sensor demand (millions of units)	13.5	27.8	34.8	47.3	62.7
Average cost per unit ($)	18.50	16.55	17.80	17.25	16.85
Demand by technology ($ millions):					
Potentiometric	220	410	545	705	880
Amperometric	29	46	68	92	127
Conductimetric	1	4	7	18	48
Demand by market area ($ millions):					
Industrial	153	325	438	577	735
Environmental monitoring	71	97	129	163	202
Medical / diagnostic	12	20	29	42	64
Other	14	18	24	33	54

Table 2.1: Electrochemical sensors demand in the United States of America

Table 2.1 indicates the trend for electrochemical sensors demand in the United States (Freedonia Group International, April 2002). The market sector is expanding rapidly, even allowing for a reduction in average sensor unit cost. Potentiometric sensors are the most common chemical sensor measurement technology, resulting from the enormous market for industrial process safety and control.

2.1.2 Amperometric electrochemical sensors and the scope for aqueous chlorine measurement

Amperometric (or voltammetric) techniques rely on the measurement of current flow through a cell at an applied potential. This technique can allow the quantitative determination of certain organic and inorganic compounds in solution by initiating their oxidation (or reduction) and measuring the accompanying current flow between the working and counter electrode. One of the most famous examples of an amperometric chemical sensor is the Clark oxygen electrode (Clark, 1956). This device could quantify the concentration of oxygen in blood or tissue fluid by electrochemically reducing the oxygen at a platinum electrode and measuring the current (Equation 2.1).

$$\beta - D - glu\cos e + O_2 \xrightarrow{GOD} gluconolactone + H_2O_2 \qquad (2.1)$$

The device was subsequently modified to enable the determination of glucose concentration by incorporating an enzyme layer as a biological recognition entity (Clark & Lyons, 1962). In this device, glucose oxidase would cause the reduction of glucose near to the electrode surface, thereby consuming oxygen (Equation 2.2). The reduction in oxygen at the electrode surface was inversely proportional to the concentration of glucose.

$$\tfrac{1}{2}O_2 + 2H^+ + 2e^- \xrightarrow{-600mV\,(vs.\ Ag/AgCl)} H_2O \qquad (2.2)$$

The operational stability of the enzyme layer, previously contained by an oxygen permeable membrane, was then enhanced by entrapping the enzyme into a polyacrylamide matrix in contact with the electrode surface (Updike & Hicks, 1967). As the original design relied directly on the reduction of oxygen, it was found to be sensitive to ambient oxygen levels which could cause a signal drift. For this reason,

Clark reversed the polarity of the device so that the sensor became insensitive to oxygen, instead responding to the hydrogen peroxide enzymatically produced in Equation 2.1 (Clark, 1970). Unfortunately there was a drawback: electroactive interferents commonly found in blood, for example ascorbic acid and uric acid, could also be oxidised at this potential and so affect the signal. However, Clark's ideas finally became a commercial reality with the successful re-launch of the Yellow Springs Instrument Company (Ohio, U.S.) in 1975. This was the first whole blood glucose analyser, and incorporated a novel permselective barrier to exclude these interferents (Figure 2.3).

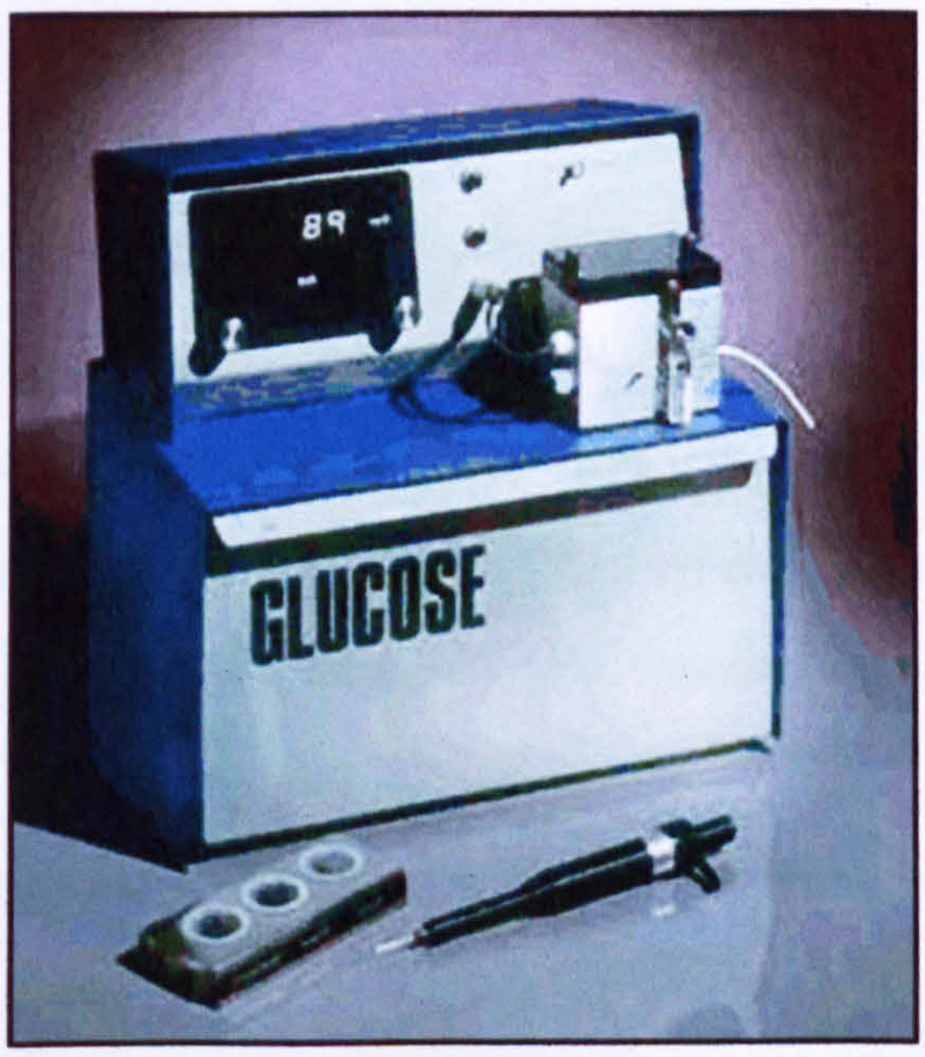

Figure 2.3: The YSI 23A instrument for whole blood glucose analysis

The success of this device paved the way for the development of a blood glucose self-diagnosis device for diabetes sufferers. A ferrocene mediator was developed which could entrap the enzyme and also act as an electron shuttle instead of molecular oxygen (Cass *et al*, 1984). Figure 2.4 illustrates the reversible oxidation and reduction action of ferrocene in the sensor. It can be seen that the mediator is not consumed in the process and is able to continue to shuttle electrons from the enzyme following re-oxidation at the working electrode.

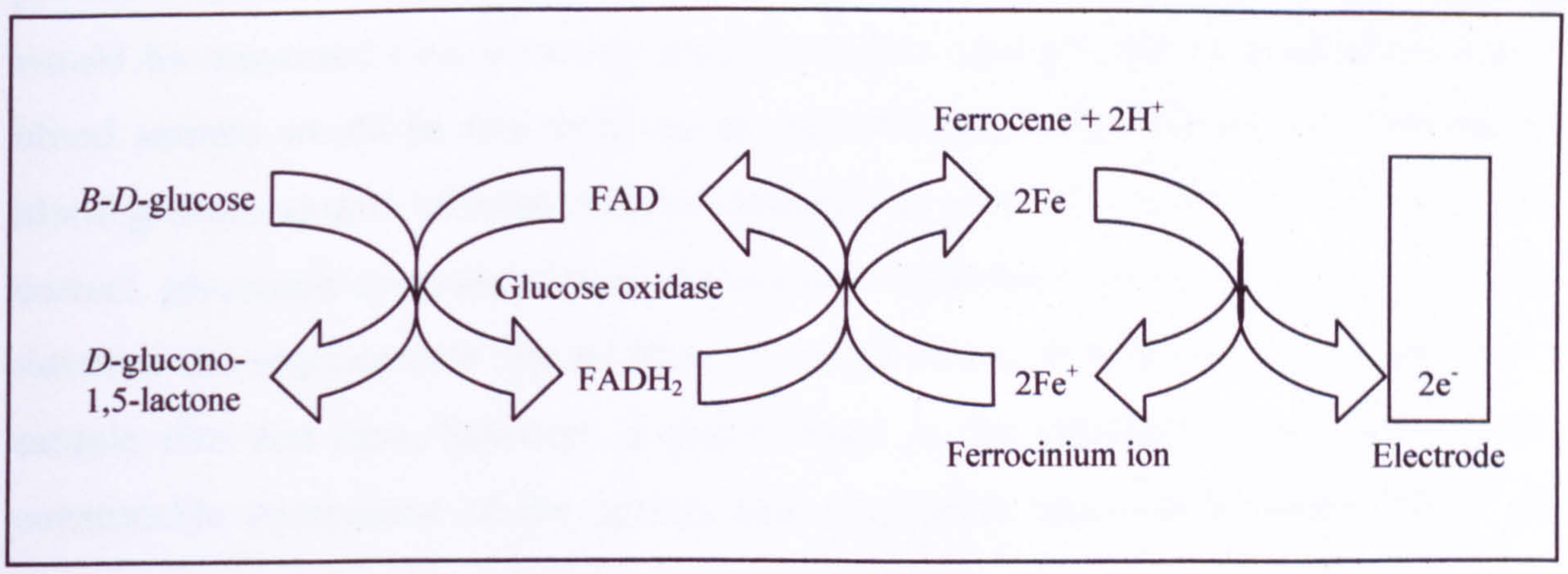

Figure 2.4: Ferrocene mediated glucose oxidase electron transfer

As well as circumventing the reliance of amperometric enzyme sensors on oxygen partial pressure, ferrocene mediated amperometry found success by facilitating the low-cost screen printing manufacture of single use disposable sensors (Cardosi & Turner, 1989). As a result, the Exactech Medisense® blood glucose self diagnosis system was developed and commercialised with resounding success (Figure 2.5).

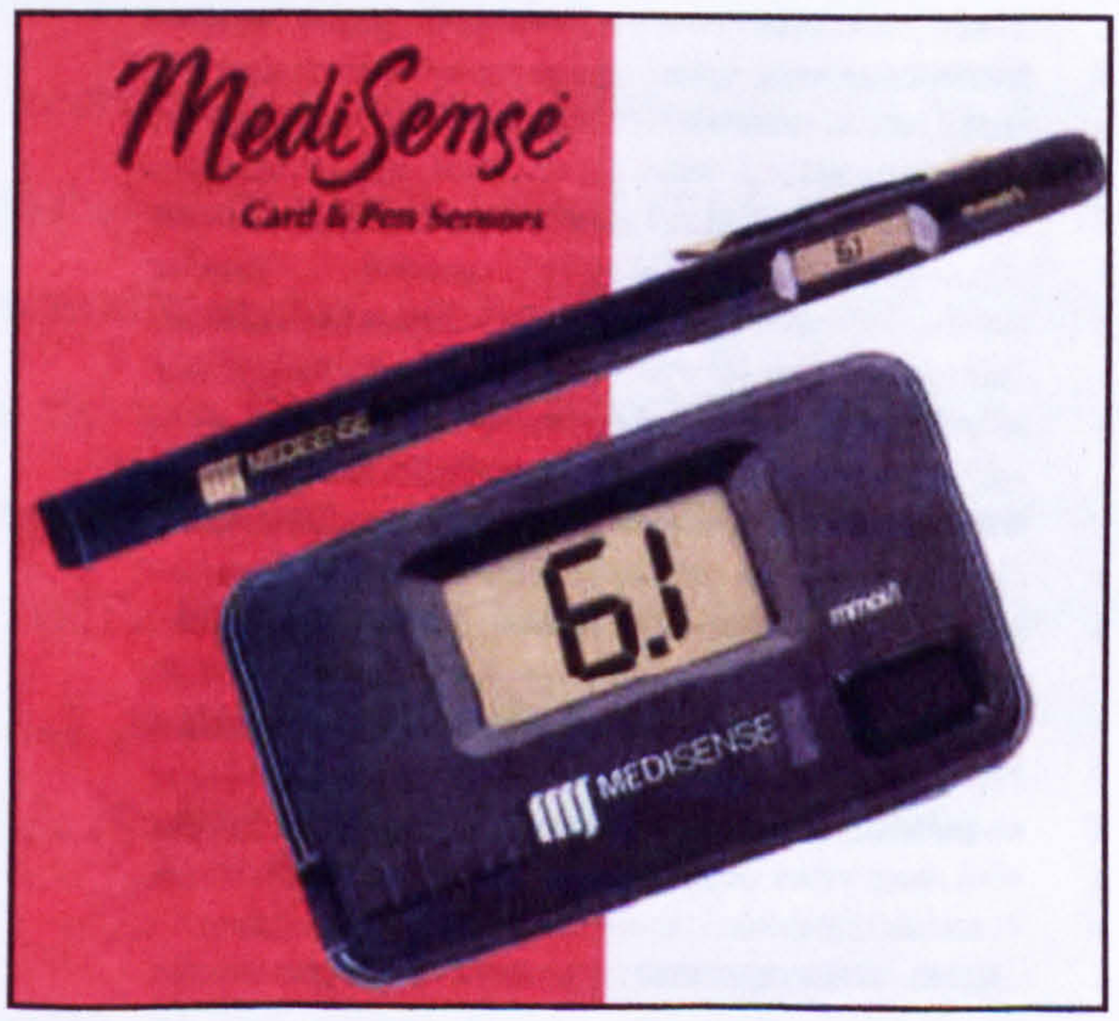

Figure 2.5: The Medisense® blood glucose sensor pen (1987) and 'credit card' design (1989)

The system comprised of a hand-held potentiostat, and miniaturised disposable screen printed strips (electrodes) which receive a small spot of the user's blood. Current flow would be measured over a twenty second window and glucose concentration in the blood sample would be indicated via an incorporated LCD display. The Medisense blood glucose system allowed diabetes sufferers to accurately detect, and if necessary correct, glycaemic episodes without the need for centralised laboratory analysis. It also satisfied the requirements for an ideal chemical sensor in terms of cost, specificity, sample size and time, however, a major factor in the commercial success was the consumable component of the system (the disposable test strips) which created an enormous repeat-purchase market.

The Medisense® blood glucose self diagnosis system serves as a good example for the successful commercialisation of a portable analytical system, which provides an alternative to centralised laboratory-based methods. Chemical sensors have benefited from the increasing power of computers, materials selection, design and processing tools, allowing them to make great inroads into pharmaceutical therapy, process-control optimisation and environmental monitoring to satisfy the ever increasing need for data (Bilitewski & Turner, 2000), (Janata, 2001). Furthermore, with growing world socio-political discordance, and increasing availability of explosives and bio-chemical agents to terrorist organisations, governments are paying a great deal of interest to chemical sensors and biosensors for the purpose of security and defence monitoring (Iqbal *et al*, 2000), (Wang *et al*, 2003). A new class of chemical sensors known as electronic 'noses' or 'tongues' have also emerged, primarily in the food industry. These devices are able to detect the hundreds of compounds which contribute to an aroma or flavour, and then make an assessment as to food quality (Kress-Rogers *et al*, 2001). Freshness of food can be also be assessed by the detection of biogenic amines such as putrescine and cadaverine (Gokoglu *et al*, 2003) or levels of essential amino acids (Sarkar *et al*, 1999) (Kelly *et al*, 2000).

Prior to the introduction of the Medisense® system, diabetes patients were able to self-test via a urine-based dipstick test based on colour change technology. This system could only offer a low level of accuracy as it was very difficult to quantify the results

which relied on the subjective comparison against a colour reference chart. Furthermore, the operative steps required to perform a test were, for obvious reasons, unpopular. The advent of an accurate, quantitative, and easy-to-use system based on the new biosensor technology guaranteed a rapid and comprehensive capture of the market.

It is possible to draw parallels between the successful Medisense technology and that of a new technology for the measurement of aqueous chlorine. Like glucose, it is possible to measure chlorine in the laboratory via electrochemical methods, but in the field only by using colourimetry based methods (discussed in detail in Section 2.5). As was the case with glucose measurement, an enormous market already exists for aqueous chlorine detection, and customers express dissatisfaction with the accuracy of the established measurement technology as well as the required skill and time of operation (Boswell, 2001). If a new field-based aqueous chlorine measurement system can improve upon these performance characteristics, then it will have gained a competitive advantage. However, it is important to recognise that even with these improvements, winning customers over to the new technology is likely to require more persuasion. For example, the current available technology may be inscribed into the various control systems of an organisation, therefore requiring a revision and validation of new procedures, as well as re-training. This inertia could be overcome by offering significant added-value features to the new system. Customers are prepared to receive benefits over an existing system, but will be reluctant to make any sacrifices in terms of performance, or more importantly, cost. A major advantage of an electrochemical sensor based approach would be the ability to measure both free and total chlorine in a single test. This feature could provide real benefits to organisations, since this could offer significant savings in terms of time and money. Improvements in limits of detection and accuracy would also provide a major advantage in some industries. Significantly, a market niche could be developed for the proposed chlorine measurement system, since it would permit enforcement of the low levels of chlorine stipulated by environmental regulation - levels which are below those achievable using existing technology (78/659/EEC, 1997). A pivotal feature of the Microarray Limited chlorine measurement system is the stir-independent characteristic imparted through its

microelectrode array configuration. Ordinarily, electrochemical sensors are prone to signal fluctuation as a consequence of solution movement and diffusion gradients which affect the mass transport of analyte to the electrode surface. The development of an innovative, cost-effective method of microelectrode array manufacture could circumvent these problems and help bring disposable, amperometric sensor-based detection to the forefront of aqueous chlorine measurement.

Commercial success would be likely to follow from a similar marketing strategy employed in the Medisense® case. Based on a one-off instrument purchase followed by the repeat purchase of a disposable sensor component, this strategy is well proven in other markets, for example within the inkjet printer market with disposable print cartridges, and also the mobile phone market in which the cost of handsets to the consumer is subsidised by network providers. In both cases the organisation will sell the 'instrument' component at a discounted rate since this will act as a vehicle for future sales.

2.2 Electrochemistry

The science of electrochemistry is concerned with the interrelation of electrical and chemical effects. Broadly speaking, electrochemistry is fundamental to numerous phenomena, such as metallic corrosion, electroplating technologies, batteries, the production of aluminium and chlorine, and electrochromic displays. Dynamic electrochemistry is the study of electron transfer reactions between electrodes and reactant molecules, which are normally in solution. Typical factors to affect the dynamics of an electrode reaction include:

- the transport of material to and from the electrode and solution
- the electrode potential and temperature of the system
- the physical and chemical properties of the electrode surface (e.g. activity)
- the reactivity of the species in solution
- the nature of the interfacial region over which the electron transfer occurs

In order to understand the principle of dynamic electrochemistry, equilibrium electrochemistry and the process of electrolysis must first be considered. Bard & Faulkner have provided a comprehensive review of electrochemical methods; key elements are detailed below (Bard & Faulkner, 2001).

2.2.1 Electron transfer and energy levels

An electrode reaction may be driven by the application of a potential difference (known as voltage) to the working electrode in an electrochemical cell. One volt, V, describes the potential difference between two points when one joule of energy (J) is used to move one coulomb of charge (Q) through the conducting material (Equation 2.3).

$$V = Joule / Coulomb \qquad (2.3)$$

Potential difference can also be related to current (I) and resistance (R) by Ohms Law, whereby a potential of one volt appears across a resistance of one ohm when a current of one ampere flows (Equation 2.4).

$$V = IR \qquad (2.4)$$

The behaviour of electrons within a metal can be partly understood by considering Fermi-levels (E_F). The crystal structure of metals comprises of closely packed atoms, strongly overlapping due to a sea of delocalised electrons. A piece of metal therefore does not possess individual, well defined electron energy levels as would exist for a single atom of the same material. Instead, a continuum of levels exists with the available electrons filling the energy states from the lowest level upwards. The *Fermi-level* (E_f) corresponds to the energy of the highest occupied orbital (Figure 2.6)

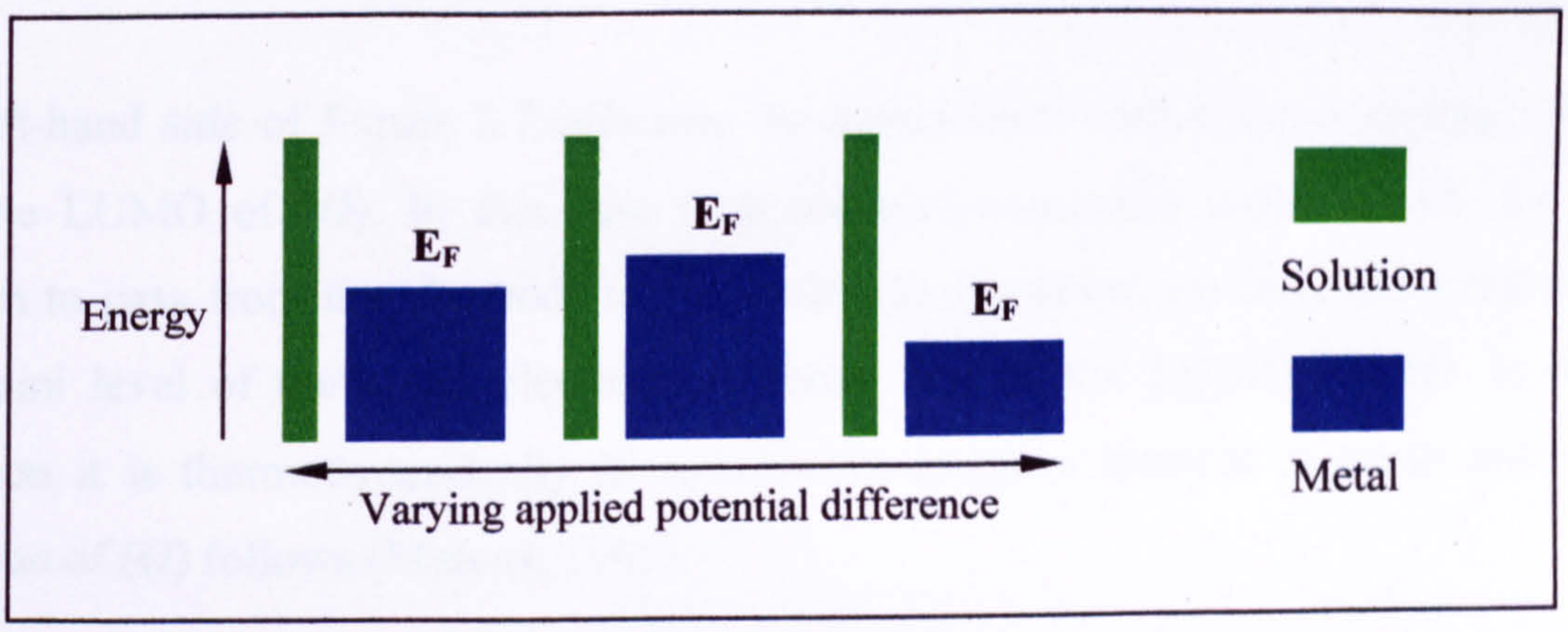

Figure 2.6: Variation of Fermi energy level in a metal with applied voltage

It can be seen that an energy level is not fixed and can be moved by supplying electrical energy, i.e. the Fermi-level can be altered by means of an applied potential difference. It is then possible, depending on the position of the Fermi-level within the metal, that the oxidation or reduction of a species in solution may be thermodynamically feasible. Figure 2.7 illustrates the Fermi-level of an atom of metal as part of an electrode along with the orbital energies (*HOMO* and *LUMO*) of a molecule (***O***) in solution. The term *HOMO* refers to the highest occupied molecular orbit, and is also known as the valence band; the term *LUMO* refers to the lowest unoccupied molecular orbital, sometimes called the conduction band. The energy spacing between them (*the band gap*) attributes a materials' conductive properties, with a large gap existing for a typical insulator, compared to almost zero difference for a good conductor such as metal.

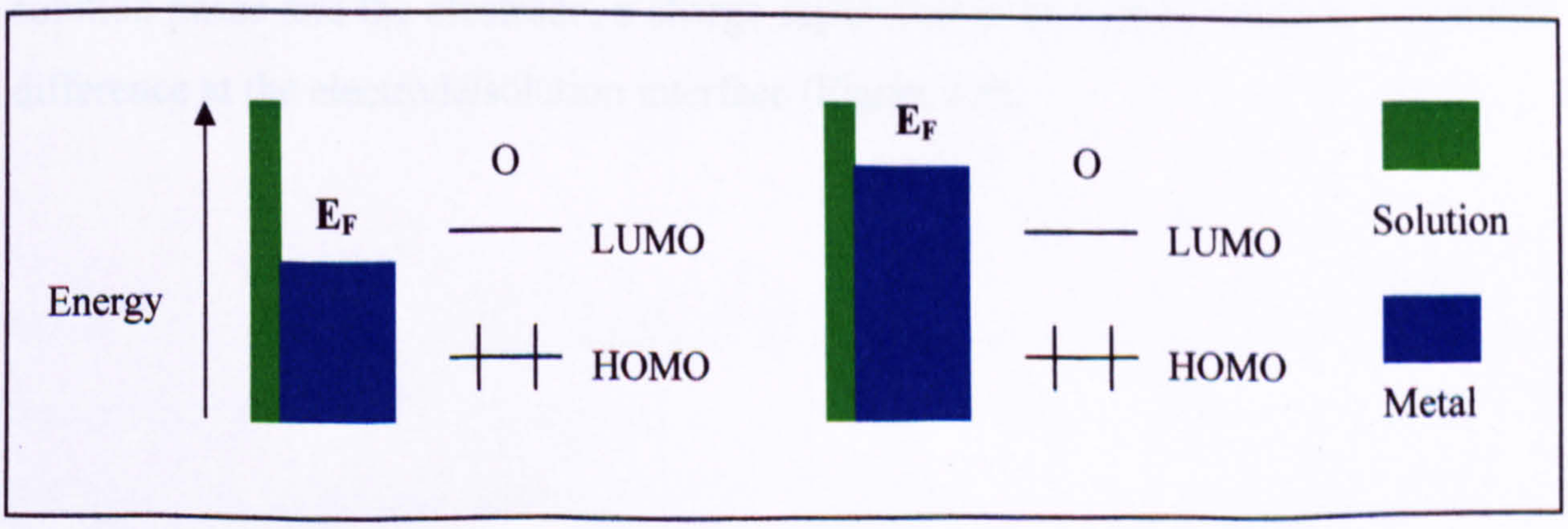

Figure 2.7: Thermodynamic favourabilities for electron transfer

The left-hand side of Figure 2.7 indicates the Fermi-level with a lower energy value than the LUMO of (***O***). In this case it is thermodynamically *unfavourable* for an electron to pass from the electrode to the molecule. However, on the right-hand side the Fermi level of the metal electrode is above that of the LUMO of (***O***). In this condition it is thermodynamically *favourable* for electron transfer to occur and the reduction of (***O***) follows (Marcus, 1965).

2.2.2 Equilibrium electrochemistry and electrolysis

Equilibrium electrochemistry can allow the relatively simple determination of thermodynamic parameters, including entropies and enthalpies, and equilibrium constants including activities and solution pH. An electrode process generally involves the transfer of charge across the interface between an electrode (usually metallic, termed ***m***), and a species in solution (***aq***) (Equation 2.5).

$$Fe^{3+}(aq)+e^{-}(m)\leftrightarrow Fe^{2+}(aq) \qquad (2.5)$$

In order for the components of the system to move towards equilibrium concentration, a source (or sink) of electrons must be present, such as the metallic electrode used in the example above. As the reaction involves the transfer of an electron between the solution phase and the electrode, a charge separation is developed creating a potential difference at the electrode/solution interface (Figure 2.8).

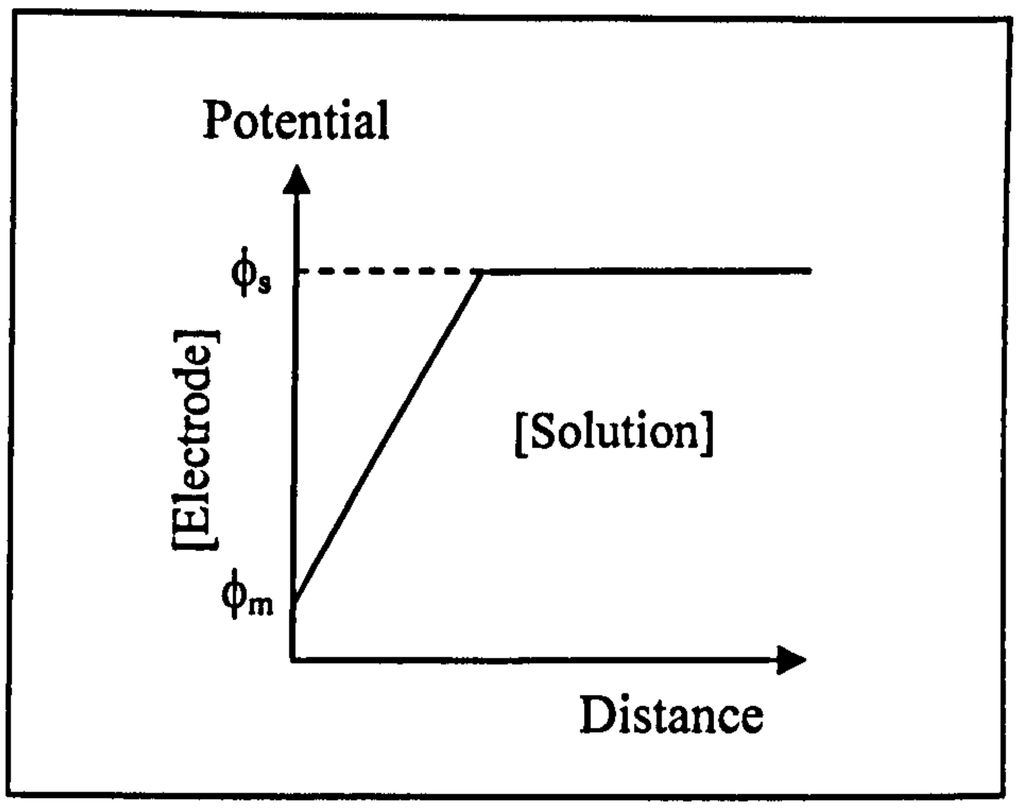

Figure 2.8: The potential drop across the electrode/solution interface

Figure 2.8 illustrates the potential drop ($\Delta\phi_{m/s}$) across an electrode/solution interface, which is the difference between the solution potential, ϕ_s, and the electrode potential, ϕ_m (Equation 2.6).

$$\Delta\phi_{m/s} = \phi_m - \phi_s \qquad (2.6)$$

In order to measure and control the potential difference at the working electrode ($\Delta\phi_{m/s}$), a reference electrode is introduced to the system which has a constant potential drop across its interface with the solution. Potential difference, E, is then calculated relative to the reference potential (Equation 2.7)

$$E = (\phi_m - \phi_s) + ref \qquad (2.7)$$

Experimentally, equilibrium potentials can be determined via an electrochemical cell comprising two half-cells separated by a porous membrane or salt bridge. One cell contains the species of interest (e.g. Fe^{3+}/Fe^{2+}) and the other contains a reference electrode, ideally a standard hydrogen electrode (SHE). Both half-cells are connected by a high impedance voltmeter. Provided that no current is allowed to pass then

E (potential) will rapidly reach a steady state equilibrium potential (E_e) which is dependant on the concentrations of Fe^{2+} and Fe^{3+}.

The standard hydrogen electrode is defined as having an absolute potential of zero and offers a convenient method to report the potentials of half-cells relative to this reference. For a general charge transfer reaction, in which ***n*** electrons are transferred (Equation 2.8).

$$O(aq) + ne^{-}(m) \leftrightarrow R(aq) \qquad 2.8$$

where ***O*** is the oxidised species, and ***R*** is the reduced form.

From this, Nernst shows that the potential difference established under equilibrium conditions is given by the following equation:

$$E_e = E^{\Theta} + \frac{RT}{nF} \ln \frac{O}{R} \qquad 2.9$$

where E_e, the equilibrium potential of the electrode results from E^{Θ}, the standard electrode potential of the reaction, and the concentrations of ***O*** and ***R*** at the electrode surface (under equilibrium conditions this is the same as in the bulk solution).

In the case where current is allowed to flow, the application of a potential with a different value to E_e can induce the exchange of electrons between the electrode and the molecules in solution. This transfer results in a change in the oxidation state of the species; this process is called electrolysis.

$$Fe^{2+}(aq) \rightarrow Fe^{3+}(aq) + e^{-}(m) \qquad 2.10$$

$$Fe^{3+}(aq) + e^{-}(m) \rightarrow Fe^{2+}(aq) \qquad 2.11$$

The species in solution may lose an electron, becoming oxidised (Equation 2.10), or may become reduced by gaining an electron (Equation 2.11).

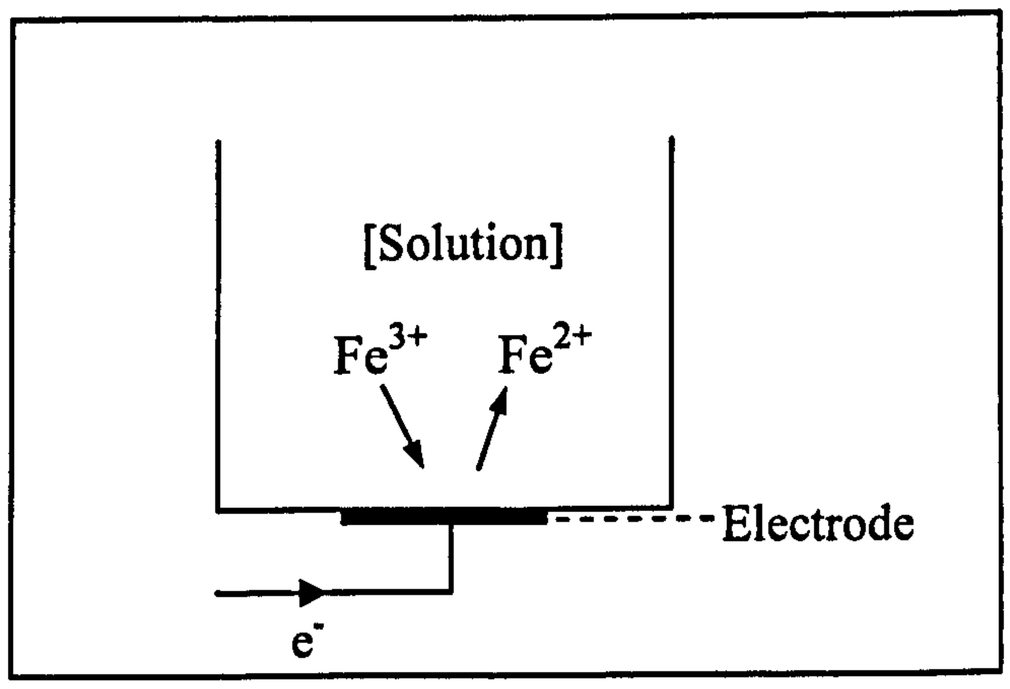

Figure 2.9: The reduction of Fe^{3+} (*aq*) to Fe^{2+} (*aq*)

Equation 2.12 indicates the magnitude of the current (***i***) that will be obtained from the reduction of Fe^{3+} in the cell illustrated in Figure 2.7 above.

$$i = AFj \qquad (2.12)$$

where ***F*** is the Faraday constant (96,485 C/mol), ***A*** is the electrode area (in this case 1 cm^2), and ***j*** is the amount of material reaching the electrode each second, known as the *flux*, given by Equation 2.13.

$$j = k_0\left[Fe^{3+}\right]_0 \qquad (2.13)$$

where k_o is the heterogeneous rate constant for the electron transfer reaction, and $[Fe^{3+}]_0$ refers to the concentration of the reactant at the electrode surface. Since the rate of depletion of reactant at the electrode surface is generally faster than the rate of replenishment from the bulk solution, this latter term specifically refers to the concentration at the interfacial region and not necessarily to that in the bulk solution.

The electrolytic current observed is therefore dependant on both the mass transport of reactants to the electrode surface, and the rate of the heterogeneous electron transfer kinetics, which in turn is dependant on the applied potential (Section 2.2.2).

2.2.3 Dynamic Electrochemistry

Dynamic electrochemistry generally refers to the subset of electrochemical systems in which equilibrium is not established. A comprehensive review of the subject was written by Anderson *et* al and includes key topics such as voltammetry, amperometry, coulometry and electrochemical impedance spectroscopy (Anderson *et al*, 1998).

Consider an electron transfer reaction (Equation 2.14).

$$O(aq) + ne^{-}(m) \xleftrightarrow{k_{red}/k_{ox}} R(aq) \qquad 2.14$$

O represents a molecule in an oxidised state, requiring n electrons to be converted into the reduced species, ***R***. If it assumed that there are arbitrary amounts of (***O***) and (***R***) in the solution, the total current flowing, i, is the sum of the reductive (i_c) and oxidative (i_a) currents (Equation 2.15).

$$i = i_a + i_c = nFAk_{ox}[R]_0 - nFAk_{red}[O]_0 \qquad 2.15$$

where A is the electrode area (cm^2), F is the Faraday constant, n is the number of electrons transferred, $[\ ]_0$ represents the surface concentrations of either (***O***) or (***R***), and k_{red} and k_{ox} are the rate constants for the reductive and oxidative steps respectively.

Equation 2.15 can be simplified for a single electron transfer reaction to:

$$i = FA(k_{ox}[R]_0 - k_{red}[O]_0) \qquad 2.16$$

It is noted that in the case where reaction 2.12 is at equilibrium (therefore satisfying the Nernst Equation 2.9), then current flow has ceased since the rate of reduction of $[O]$ equals the rate of oxidation of $[R]$, i.e.

$$k_{red}[O]_0 = k_{ox}[R]_0 \qquad 2.17$$

Using transition state theory based on chemical kinetics it is possible to relate the free energies of activation to the rate constant k_{ox} and k_{red}. Figure 2.10 indicates the reaction path whereby reactants $O_{(aq)}$ and $e^-_{(m)}$ must overcome the transition state energy barrier to form reaction products, $R_{(aq)}$. When the Gibbs free energy criterion, ΔG, is negative, a reaction can proceed spontaneously.

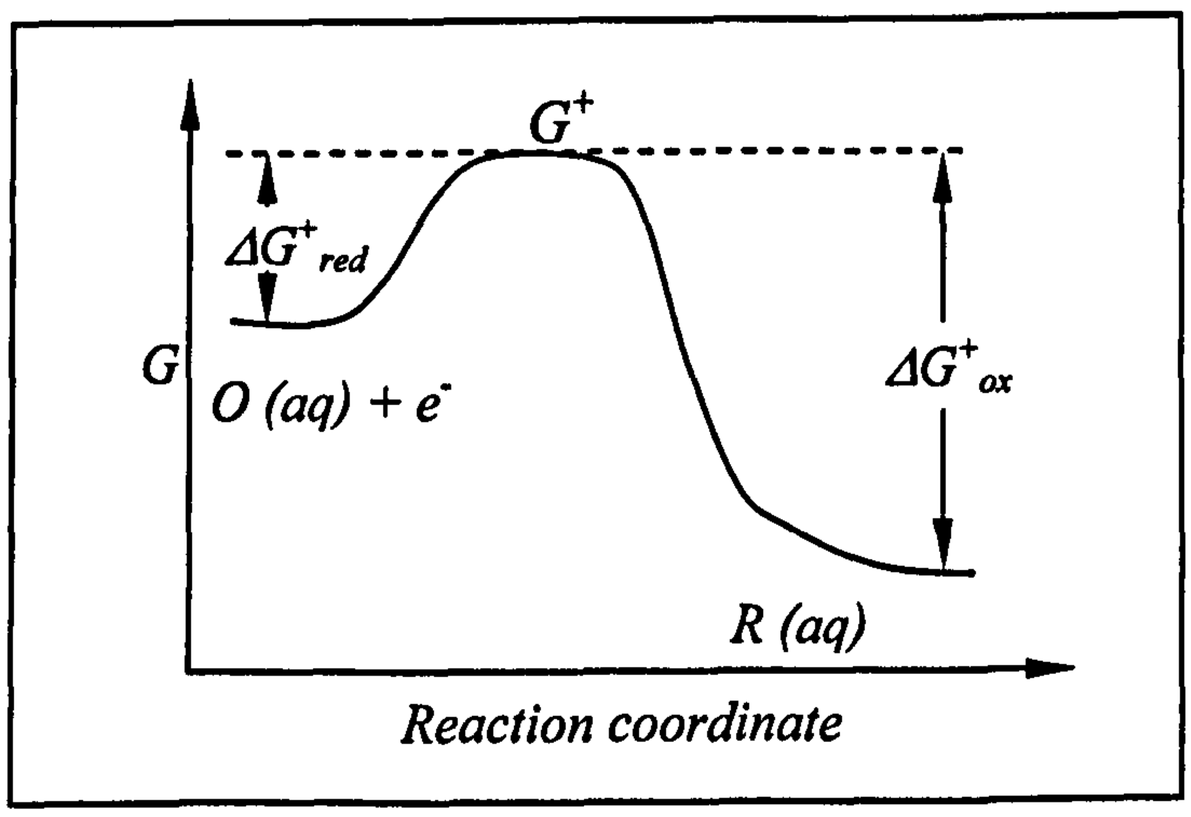

Figure 2.10: Free energy plot for a single electron reduction reaction

The rate of this reductive reaction can be described by Equation 2.18.

$$k_{red} = Ae^{\frac{-\Delta G^{+}_{red}}{RT}} \qquad 2.18$$

where ΔG^{+}_{red} is the free energy of activation, R is the gas constant, T is the temperature (K), and in this case A refers to a 'frequency factor' which accounts for the rate of collision of the electroactive molecule with the surface of the electrode.

The free energies of activation for the electrode reaction are related to both the chemical properties of the reactants and their response to applied potential. The kinetic model described above is analogous to that of homogeneous chemistry. However, as mentioned in section 2.2.2, it can be seen that electrochemical reactions are influenced by the interfacial potential ($\Delta\phi_{m/s}$). It is necessary to establish how this affects transition state theory when applied to electrode kinetics. Consider Equation 2.17 below:

$$Fe^{3+}(aq) + e^{-}(m) \leftrightarrow Fe^{2+}(aq) \qquad 2.19$$

The free energy associated with reactants (Fe^{3+} and e^{-}) is:

$$G_{Fe^{3+}} = \text{constant} + 3F_{\phi_s} - F\phi_m \qquad 2.20$$

$$\text{or,} \quad G_{Fe}{}^{3+} = \text{constant} + 2F_{\phi_s} - F(\phi_m - \phi_s) \qquad 2.21$$

The free energy associated with the product (Fe^{2+}) is:

$$G_{Fe^{2+}} = \text{constant'} + 2F_{\phi_s} \qquad 2.22$$

At this stage the *transfer co-efficient,* or *symmetry* factor (α) is introduced which reflects the sensitivity of the transition state to the drop in electrical potential between the metal and the solution. If α ($0<\alpha<1$) is close to zero, then the transition state is thought to resemble the reactants in its potential dependence, whereas when the value approaches unity, the transition state behaves more like the product. In fact, α is typically found to be close to 0.5 for most reactions, which suggests an intermediate behaviour and allows Equations 2.21 and 2.22 to be reduced to:

$$G_{Fe^{3+}} = \text{constant''} + 2F_{\phi_s} - (1-\alpha)F(\phi_m - \phi_s) \qquad 2.23$$

From the equations above it is evident that changes to the solution potential (ϕ_s) or the metal potential (ϕ_m) will affect the free energy barriers to reduction and oxidation, and alter the kinetics of the electrode reaction. In practice, it is necessary to utilise more than one electrode. For example, a single microelectrode which passes a very low current only requires two electrodes, the working and reference (which has a fixed electrode/solution interface potential). Larger currents require the incorporation of a third electrode, a *counter electrode*, which can act as a sink or source of electrons.

When applied potential (E) equals the equilibrium potential (E_e) then there is no net current flow. Electrolysis becomes thermodynamically viable only when a potential different to the equilibrium potential is applied. This difference, known as the *over-potential* (η), can be calculated as follows:

$$\eta = E - E_e \qquad 2.24$$

In order to describe interfacial rates (k_{red} and k_{ox}) in terms of a two or three electrode cell, Equations 2.18, 2.21 and 2.22 must be modified into the following relationship:

$$k_{red} = A\exp\left(\frac{\Delta G^{+}_{red}}{RT}\right)\exp\left(\frac{-\alpha F\eta}{RT}\right) \qquad 2.25$$

$$k_{ox} = A\exp\left(\frac{\Delta G^{+}_{ox}}{RT}\right)\exp\left(\frac{(1-\alpha)F\eta}{RT}\right) \qquad 2.26$$

where:

$$\Delta G^{+}_{ox} = \Delta G^{+}_{0} - (1-\alpha)F\left(E_e - E^{\Theta}\right) \qquad 2.27$$

$$\Delta G^{+}_{red} = \Delta G^{+}_{0} + \alpha F\left(E_e - E^{\Theta}\right) \qquad 2.28$$

Equations 2.25 and 2.26 can be further simplified by the introduction of the standard heterogeneous rate constant, k^{0}_{red} and k^{0}_{ox}, which are independent of over-potential, η.

$$k^{0}_{red} = k^{0}_{red}\exp\left(\frac{-\alpha F\eta}{RT}\right) \qquad 2.29$$

$$k^{0}_{ox} = k^{0}_{ox}\exp\left(\frac{(1-\alpha)F\eta}{RT}\right) \qquad 2.30$$

The incorporation of Equations 2.29 and 2.30 into Equation 2.16 now allows the generation of the Butler-Volmer equation (Butler, 1924), (Erdey-Grúz & Volmer, 1930), which provides the relationship between the net current, i, flowing at the working electrode, and the over-potential, transfer coefficients, temperature and the concentrations of the reactants and products.

$$i = i_0\left(\frac{[R]_0}{[R]_{bulk}}\exp\left\{\frac{(1-\alpha)F\eta}{RT}\right\} - \frac{[O]_0}{[O]_{bulk}}\exp\left\{\frac{(-\alpha F\eta)}{RT}\right\}\right) \qquad 2.31$$

It can be seen that the Butler-Volmer equation includes a scaling factor i_0, known as the standard exchange current, which in the case of zero current flow provides a further relationship between k^0_{red} and k^0_{ox} (Equation 2.32).

$$i_0 = FAk^0[R]^{\alpha}_{bulk}[O]^{1-\alpha}_{bulk} \qquad 2.32$$

The Butler-Volmer equation can be further simplified if the solution is well stirred, such that the surface concentration of the reactants and products approaches that of the bulk solution, i.e. where $[R]_0 = [R]_{bulk}$ and $[O]_0 = [O]_{bulk}$ (Equation 2.33).

$$i = i_0\left(\exp\left\{\frac{(1-\alpha)F\eta}{RT}\right\} - \exp\left\{\frac{-\alpha F\eta}{RT}\right\}\right) \qquad 2.33$$

Figure 2.11 illustrates the effect of the magnitude i_0 on current as a function of over-potential.

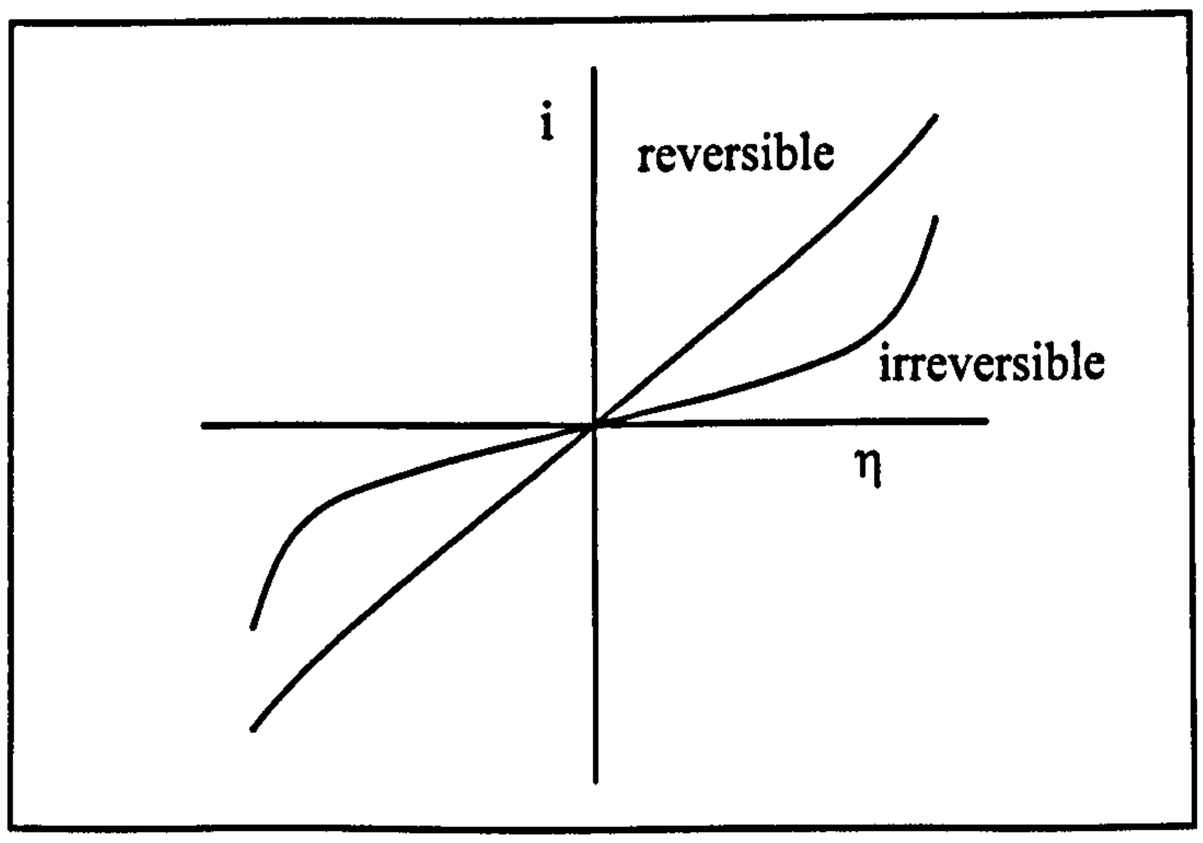

Figure 2.11: The effect of i_0 on process reversibility

In the case of a large value of i_0, only a very small potential needs be applied in order to produce significant current flow. Conversely, for a process with a small value of i_0, irreversible behaviour is exhibited requiring a high over-potential to induce current flow. It is possible to further simplify the Butler-Volmer equation in the case of an irreversible reaction where the applied potential results in a strong oxidative process with negligible reduction (Equation 2.34) and vice versa (Equation 2.35).

$$\ln i = \ln i_0 + \frac{(1-\alpha)F}{RT}\eta \qquad 2.34$$

$$\ln(-i) = \ln i_0 - \frac{\alpha F}{RT}\eta \qquad 2.35$$

From the above equations it is possible to determine the value of α via the process of Tafel analysis, in which ln(i) is plotted against E. By analysing both the reductive and the oxidative processes, it is also possible to determine the standard exchange current (i_0) by extrapolation of the Tafel lines (Figure 2.12) (Tafel, 1905).

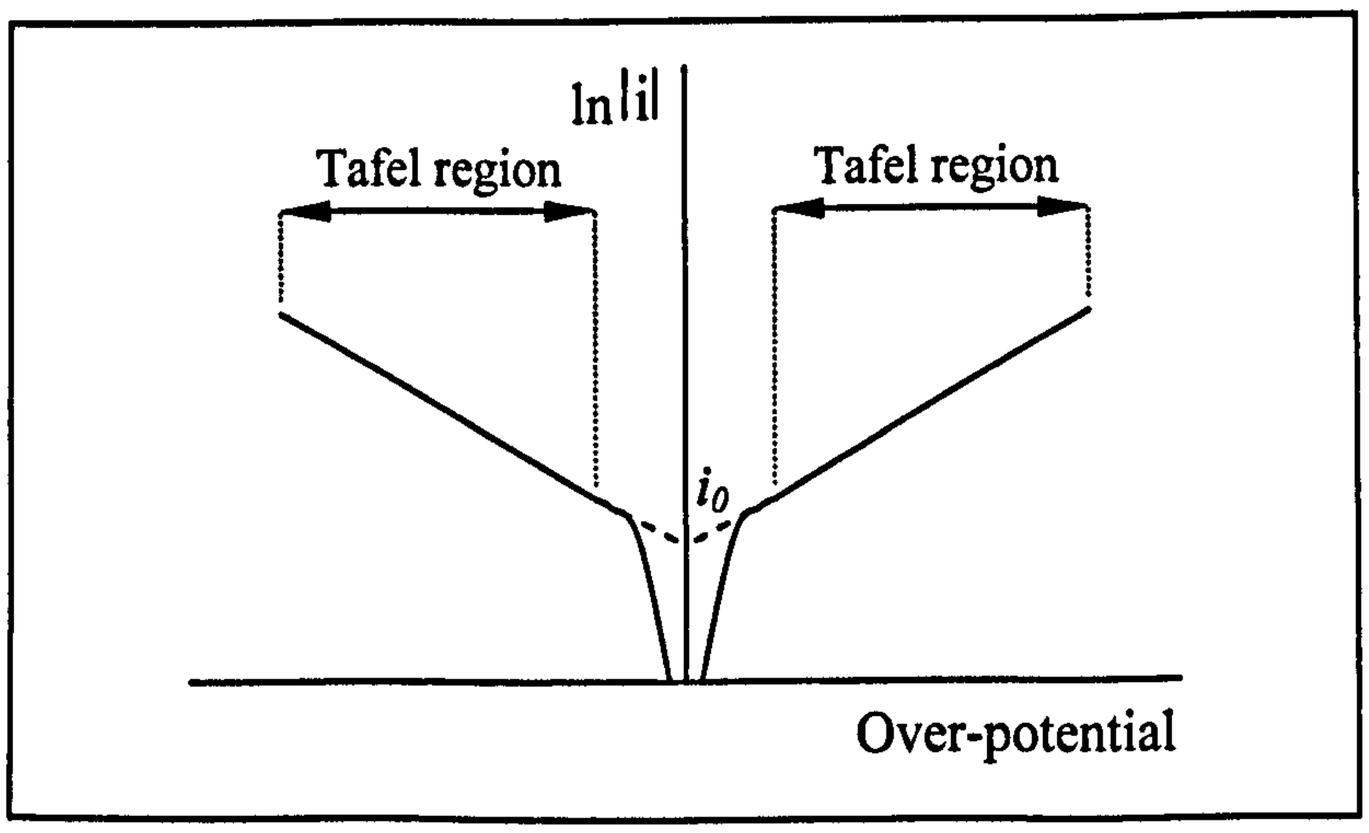

Figure 2.12: Determination of i_0 via Tafel analysis

2.2.4 Mass transport

Previous discussions have been concerned with the rates of electron transfer occurring at electrode surfaces. However, in order for those reactions to occur, material has to be supplied and removed, thereby introducing the concept of mass transfer (Figure 2.13).

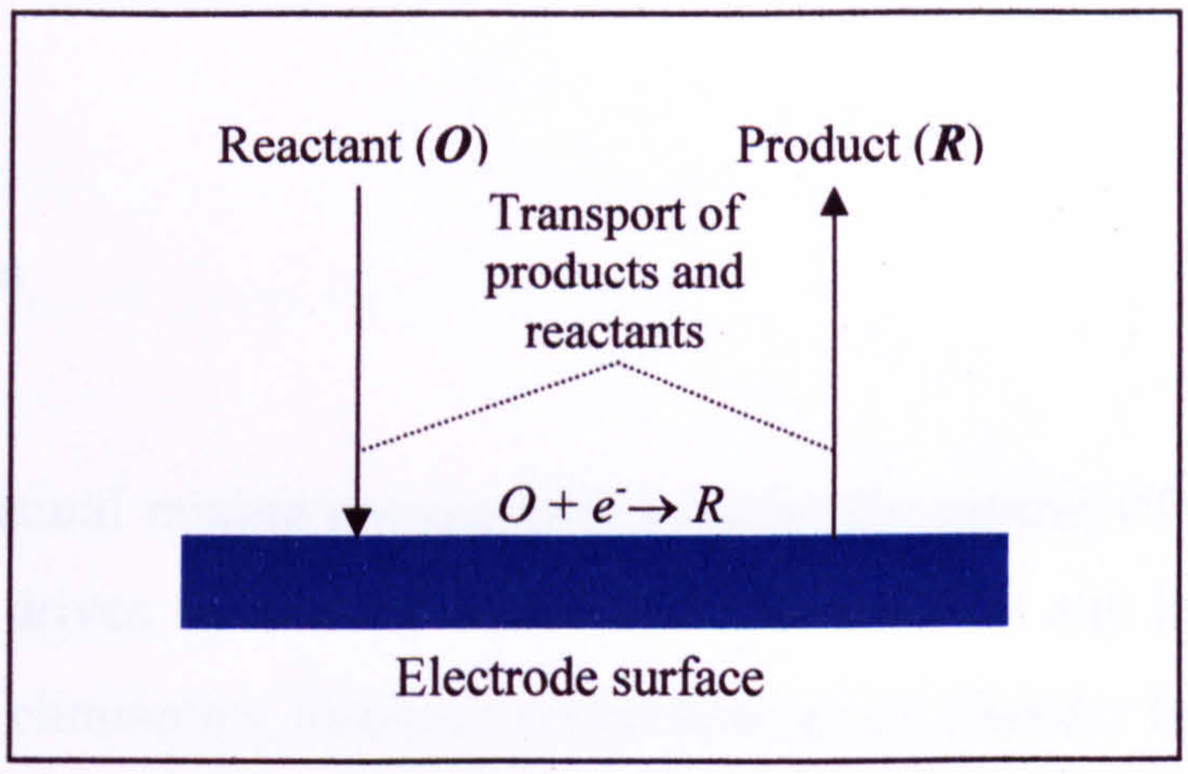

Figure 2.13: Mass transfer to and from the electrode surface

Depending on which process is slower for a given system, the overall reaction rate may be limited by either the kinetics of the electron transfer, or by the rate at which material is able to be transported to the electrode surface. Given the ability for a small change in potential to cause a relatively large increase in the reaction kinetics, it follows that mass transport effects may become critical to the analysis of a system. If Equation 2.36 is considered, it can be seen that for a fixed electrode area, A, current flow is dependent on both the reaction rate, k_{red}, and the surface concentration of the reactant, $[O]_0$.

$$i_c = -FAk_{red}[O]_0 \qquad 2.36$$

Therefore, if the rate constant is large enough such that any reactant close to the electrode surface is immediately converted into the reaction product, then the current will be controlled by the amount of fresh reactant reaching the surface over time from the bulk solution.

There are three forms of mass transport which are known to greatly affect an electrochemical experiment, namely:

- Diffusion
- Convection
- Migration

2.2.4.1 Diffusion

Diffusion is a natural mixing process facilitated by the natural vibration of atoms and molecules. It is driven by entropy which seeks to even out any inhomogeneities in a system, thereby eliminating localised concentrations as disorder is spread through the system. The rate of diffusion, first described mathematically by Fick, is dependent upon the concentration gradient (Fick, 1855). In this model it is assumed that the electrode is perfectly flat and of infinite dimensions. The direction of mass transport to and from the electrode occurs in a direction normal to the electrode surface. Ignoring any electrostatic effects, the rate of diffusion at a given point in the solution is dependent on the concentration gradient at that point. Fick's first law of diffusion terms this flow of material *flux* (Equation 2.37).

$$flux = j = -D_B \frac{\delta[B]}{dx} \qquad 2.37$$

where *[B]* is the concentration of reactant B, D_B is the diffusion coefficient of B (typically around 10^{-5} cm^2s^{-1}), and δx represents the change in distance from the electrode surface. Fick's first law therefore describes the rate of change of concentration of species B at a point as a function of distance. In practice, it is often more useful to describe the change of concentration at a point as a function of time. This can be achieved by calculating the change in concentration within the region (x) to ($x + \delta x$) during the time interval (δt) within area A (Figure 2.14).

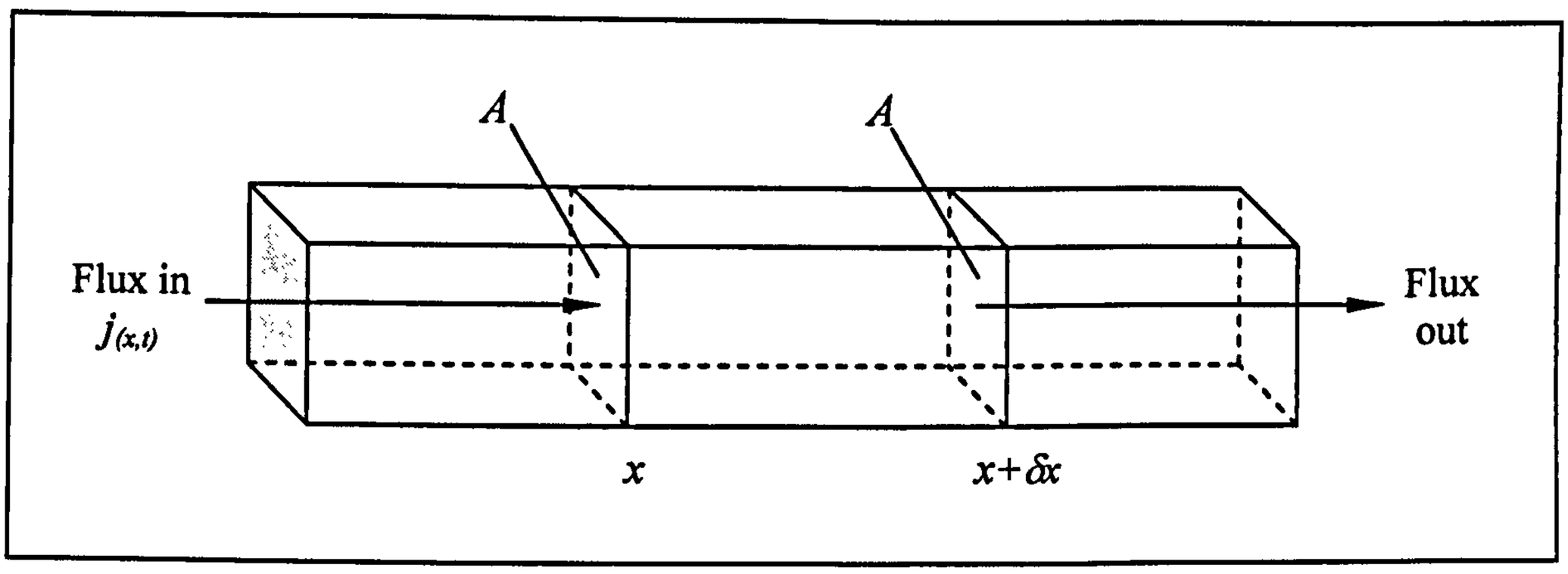

Figure 2.14: Schematic describing Fick's second law of diffusion

The difference in the concentration of B entering plane x and leaving through plane $x+\delta x$ is given by the *mass conservation equation* below:

$$[B]_{(x,t+\delta t)} A\,\delta x - [B]_{(x,t)} A\,\delta x = j_{(x,t)} A\,\delta t - j_{(x+\delta x,t)} A\,\delta t \qquad 2.38$$

Equation 2.38 can be rearranged to give the general conservation equation:

$$\frac{\delta}{\delta t}[B]_{(x,t)} + \frac{\delta}{\delta x} j_{(x,t)} = 0 \qquad 2.39$$

Substitution of Fick's first law (Equation 2.37) into this equation yields Fick's Second law of diffusion (Equation 2.40).

$$\frac{\delta[B]}{\delta t} = D_B\left(\frac{\delta^2[B]}{\delta x^2}\right) \qquad 2.40$$

This equation allows the prediction of concentration changes of reactants or products close to the electrode surface as a function of time. It is also possible to extend the equation to incorporate diffusion in more than one direction, for example the three Cartesian directions x, y and z (Equation 2.41).

$$\frac{\delta[B]}{\delta t} = D_B \frac{\delta^2[B]}{\delta x^2} + D_B \frac{\delta^2[B]}{\delta y^2} + D_B \frac{\delta^2[B]}{\delta z^2} \qquad 2.41$$

In the case of a planar electrode in a solution containing reactant, ***B***, prior to the application of potential, the concentration of reactant at the electrode surface ($[B]_0$) is equal to that of the bulk solution ($[B]_{bulk}$). If an oxidative potential is applied, where ***B*** reacts to form, form B^+, a concentration gradient is formed which extends between the electrode surface, where $[B] = 0$, and the bulk solution, where $[B] = [B]_{bulk}$. The concentration gradient created causes a flux of unreacted ***B*** towards the depleted area, and conversely flux of product, B^+, out into the bulk solution. As electrolysis proceeds, the diffusion layer extends further into solution, and becomes less linear as it reaches into the bulk solution (Figure 2.15)

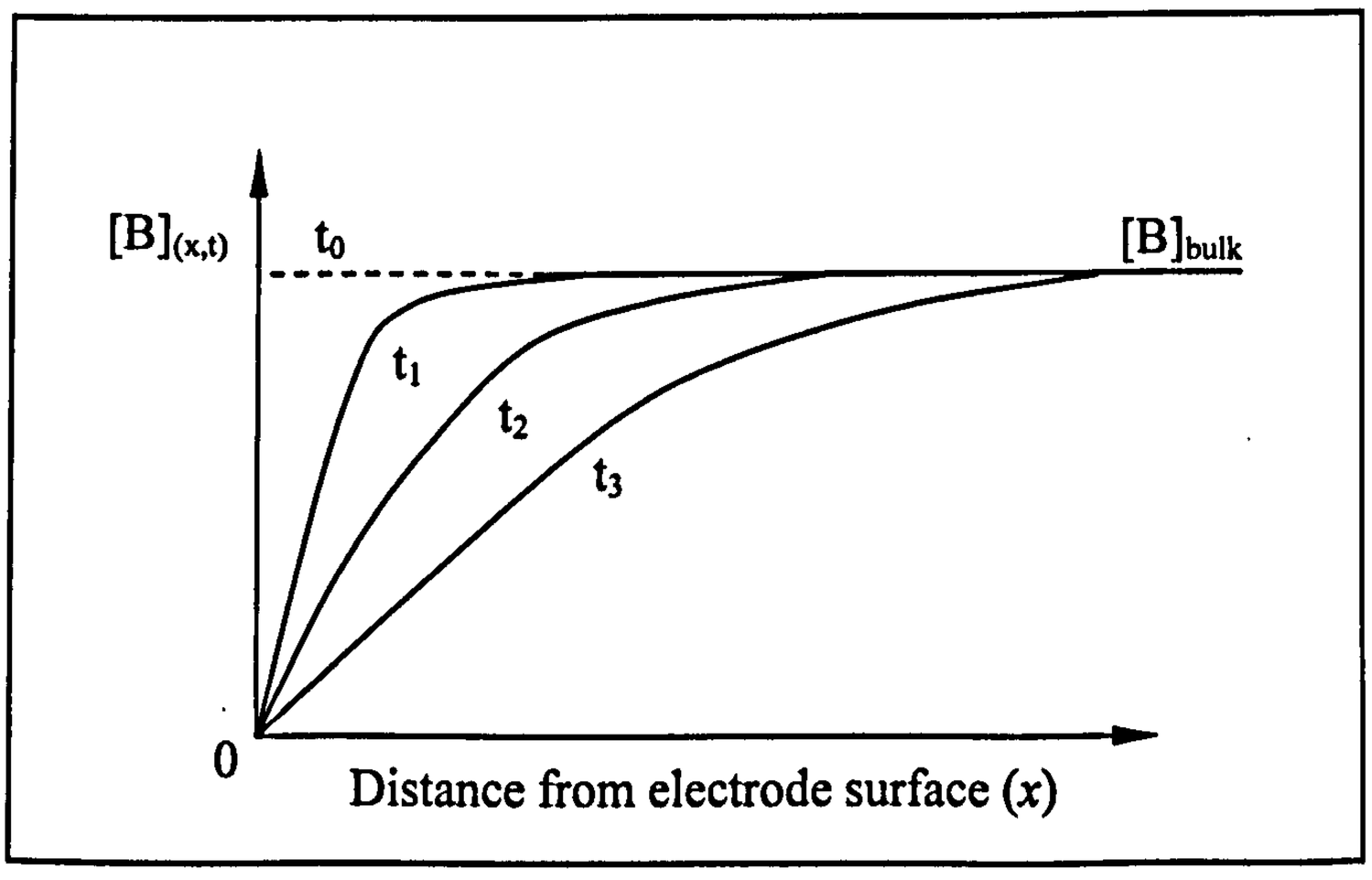

Figure 2.15: The growth of diffusion layer thickness (x) with time (t)

Under steady state conditions, transport within the linear portion of the diffusion layer can be attributed to diffusion alone, whereas further out into solution, natural convection begins to make a significant contribution to mixing. Nernst estimated the size of the diffusion layer thickness (δ) by extrapolation of the linear portion of the

curves in Figure 2.15. For electrodes of millimetre dimensions, under normal experimental conditions, the Nernst diffusion layer thickness is approximately 0.05 mm. Equation 2.42 describes the thickness of the diffusion layer, δ:

$$D\left(\frac{\delta[B]}{\delta x}\right) = D\frac{([B]_{bulk} - [B]_0)}{\delta} \qquad 2.42$$

when $[B]_0 = 0$,

$$D\left(\frac{\delta[B]}{\delta x}\right)_0 = D\frac{[B]_{bulk}}{\delta} = k_d[B]_{bulk} \qquad 2.43$$

In this equation, k_d, represents the mass transfer coefficient ($=D/\delta$). Equations 2.44 and 2.45 indicate the corresponding mass transfer coefficient and diffusion layer thickness respectively:

$$k_d = \left(\frac{D}{\pi t}\right)^{1/2} \qquad 2.44$$

$$\delta = (\pi D t)^{1/2} \qquad 2.45$$

2.2.4.2 Convection

Convection represents the mechanical movement of material within a solution. Two types of convection may be usefully defined: natural convection and forced convection.

Natural convection can arise from thermal gradients/density differences which may be present in any solution. For example, an exothermic electrolysis reaction occurring at

the electrode surface will cause localised temperature increases with the associated changes in solution density. This form of convection, which is generally undesirable as it is difficult to predict, begins to have a significant effect after a time scale of 10 to 20 seconds for electrodes of millimetre dimensions or higher.

Forced convection involves the artificial movement of the solution via, for example, stirring or gas bubbling, and is generally on a much faster scale than other forms of solution movement. By deliberately introducing mechanical mixing of the solution, it is possible to significantly reduce the contribution of natural convection and allow for the quantitative prediction of mass transport to the electrode via Equation 2.46.

$$\frac{\delta[B]}{\delta t} = -v_x \frac{\delta[B]}{\delta x} \qquad 2.46$$

Since reactants must be transported to the electrode surface for a reaction to occur, it follows that the maximum observable current is limited by the rate at which reactant reaches the electrode/solution interface. Assuming the electrode potential is sufficient to convert all reactant at the surface (such that $[B]_0 = 0$), then a limiting current is reached (Equation 2.47).

$$i_L = \frac{D_B F A [B]_{bulk}}{\delta_d} \qquad 2.47$$

2.2.4.3 Migration

When a potential is applied to an electrode, an electric field is generated which extends into the solution ($\delta\phi/\delta x$). In turn, this field can cause the movement of ions to or from the electrode, and is termed *migration* (Equation 2.48).

$$j_m \propto -u[B]\frac{\delta\phi}{\delta x} \qquad 2.48$$

where the migratory flux, j_m, is proportional to the concentration of the ion, ***[B]***, the electric field ($\delta\phi/\delta x$), and the ionic mobility factor (u), which incorporates solution viscosity and ionic size and charge.

Under certain conditions, migration effects can complicate electrochemical experiments. For example, when electrolysis at an electrode surface is considered, charge transfer results in a localised change in ionic concentration and a subsequent change in the electrical potential in the solution at that point. This in turn causes a change in the electric field ($\delta\phi/\delta x$) and so consequently a change in the migratory flux and rate of electrolysis follows.

In order to eliminate the effects of migration, a high concentration of chemically and electrochemically inert supporting electrolyte can be added to the solution (typically around 0.1M, or 100 times the concentration of reactant). The generation and removal of anions and cations at the electrode surface during electrolysis now causes a re-distribution of the anions and cations of the supporting electrolyte allowing the maintenance of near electrical neutrality in the region, apart from that directly adjacent to the electrode surface. The maintenance of electroneutrality therefore prevents the build up of electric fields ($\delta\phi/\delta x$) and so mass transport is no longer significantly affected by Equation 2.48, which can be neglected.

The addition of supporting electrolyte also provides a number of other benefits to an electrochemical system. Firstly, a high concentration of electrolyte increases the conductivity of solution and prevents solution resistance from limiting the current flow rather than the reaction of interest. A second benefit of a large excess of electrolyte is that the distance (δx) over which the electrode/solution interface potential drop ($\phi_{m/s}$) occurs is reduced to around 100-200 nm. As well as preventing potential gradients and

migration effects outside this region, it means that reactants close enough to the electrode surface will experience the full driving force ($\phi_{m/s}$) and can allow 'tunnelling' of electrons to and from the electrode surface. It follows, therefore, that outside this narrow region, mass transport must occur by either diffusion or convection.

The third advantage is that the high concentration of supporting electrolyte ions compared to that of the reactants and products, means that the ionic strength of the solution remains relatively constant throughout the experiment. This in turn allows the activity coefficients of the reactants and products, which are highly sensitive to ionic strength, are kept constant. The result is that the potentials required for electrolysis (predicted by the Nernst equation) and the rate of reactions are also kept constant throughout the experiment.

2.2.5 The electrode/solution interface - the electrical double layer

Within an electrolyte bulk, all ions and solvent molecules are in an isotropic environment. When a metal surface disrupts the electrolyte, an unequal distribution of charges from the ions and polar solvent molecules accumulates near to the electrode surface. Polarisation of an electrode will further enhance the effect on the solution structure, including the arrangement of dipolar molecules, polarised atoms, electrons and ions, such that oppositely charged species are attracted, and vice-versa. This charge separation generates a capacitive charge associated with the formation of the interfacial region *electrical double layer*. Current will be seen to flow as a result of these effects, and may necessitate a pre-conditioning time for electrodes before use (Higson & Vadgama, 1993).

Many models have been put forward to explain the nature of the electrical double layer, all of which assume that there are no faradaic processes occurring at the electrode. The model which gave rise to the term 'electrical double layer' was first put forward by Helmholtz (Von Helmholtz, 1853). Helmholtz considered the ordering of positive and negative charges in a rigid fashion on the two sides of the

electrode/electrolyte interface to give rise to a double layer. The interactions between the ions in solution and the electrode surface were assumed to be electrostatic in nature and resulted from the fact that a metal electrode holds a charge density (q^m), which arises from either an excess or a deficiency of electrons at the electrode surface. In order for the interface to remain neutral, the charge held on the electrode is balanced by the redistribution of ions close to the electrode surface. This ordering is restricted to the interface and does not extend further out into solution; therefore the electrochemical effects observed can be compared to that of a parallel capacitor. Helmholtz's view of this region is shown in Figure 2.16.

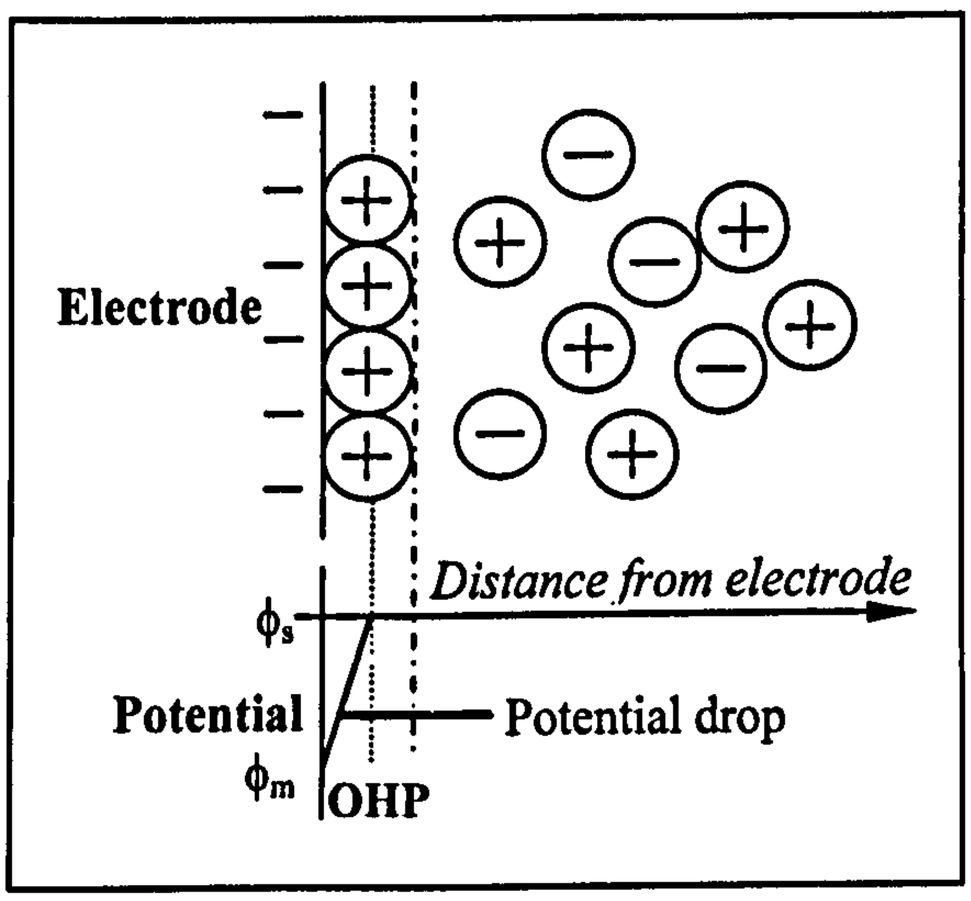

Figure 2.16: The Helmholtz double layer showing the rigid arrangement of ions

The attracted ion is able to approach the electrode to a distance limited by its solvation shell. The plane drawn directly through the centre of these ions is called the Outer Helmholtz Plane (OHP), whereby all the excess charge on the electrode is balanced by the ions forming the OHP. It is this dual charge format which denoted the term 'electrical double layer'. The model of Helmholtz, while providing a basis for rationalising the behaviour of this region does not account for many factors, such as diffusion or mixing in the solution, the possibility of adsorption on to the surface, or the interaction between solvent dipole moments and the electrode surface.

Gouy and Chapman (Gouy, 1910), (Chapman, 1913) independently developed the electrical double layer model to account for a dispersion of the charged layer due to Brownian motion. A dynamic 'diffuse layer' was now conceived, in which point charges allowed some of the potential drop to occur beyond the OHP (Figure 2.17).

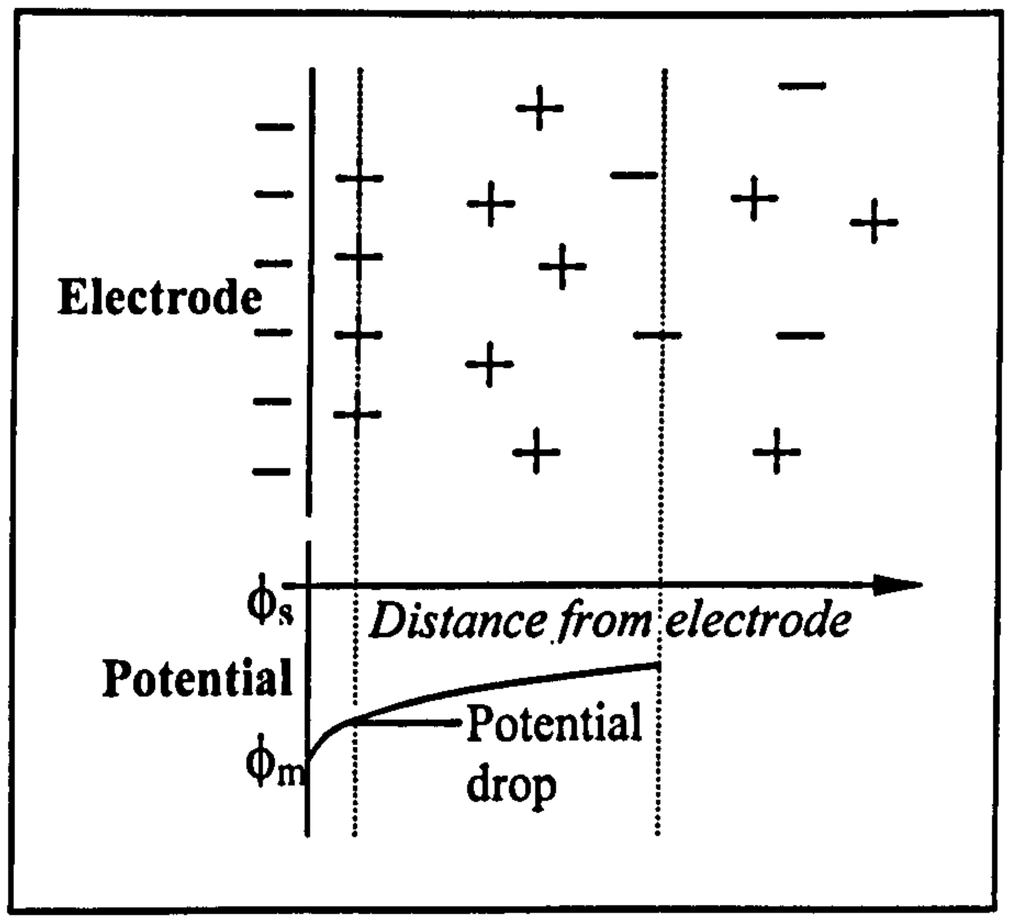

Figure 2.17: The Gouy-Chapman model of the electrical double layer

In 1924 Stern combined the Helmholtz and Gouy-Chapman models to suggest that the double layer was formed by a compact layer of ions adjacent to the electrode surface, followed by a diffuse layer extending into the bulk solution (Stern, 1924). This configuration leads to a sharp drop in potential between the electrode surface and the OHP, then a slower potential drop as you move further into solution (Figure 2.18).

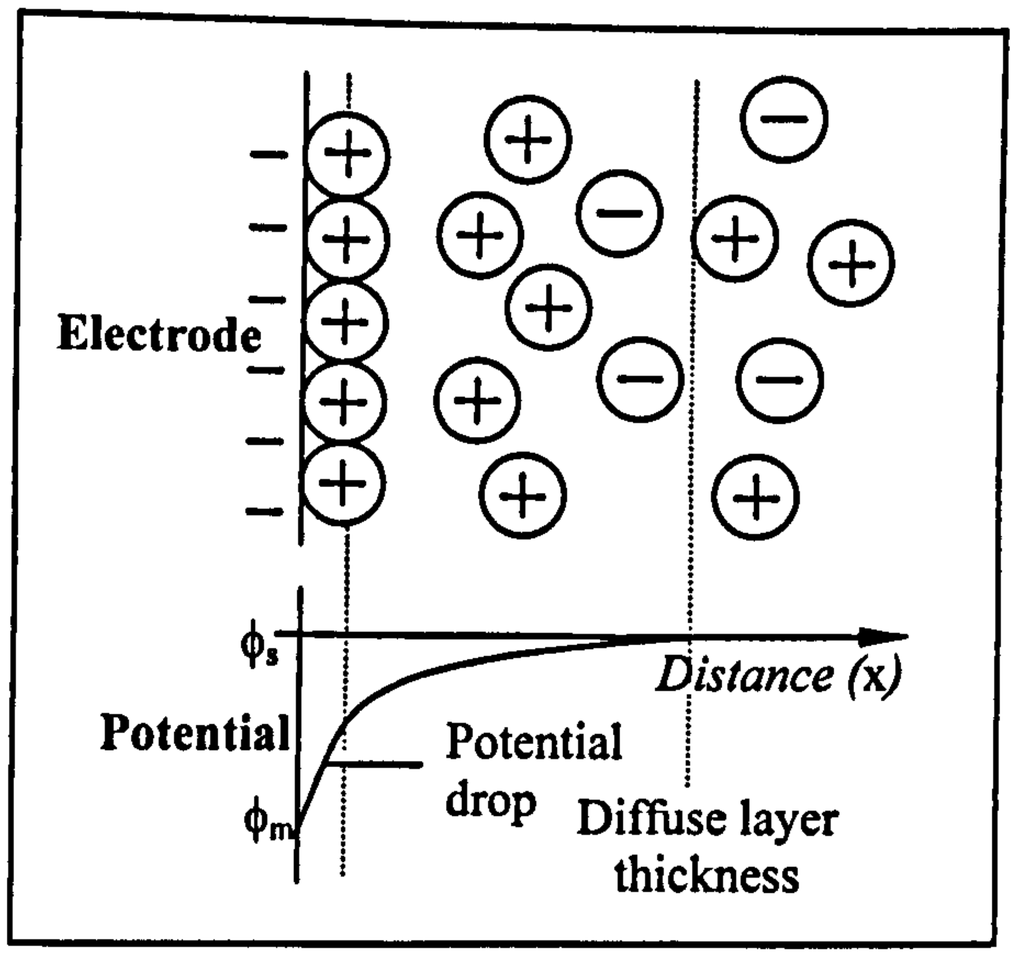

Figure 2.18: The Stern model of the electrical double layer

Grahame (Grahame, 1947) extended the model proposed by Stern to include a third region in which an ion can lose its solvent shell as it approaches the electrode surface, and is therefore able to adsorb onto the electrode surface. The inner Helmholtz plane (IHP) passes through the centres of these ions. The outer Helmholtz plane (OHP) passes through the centre of the solvated and non-specifically adsorbed ions; the diffuse region is found beyond the OHP (Figure 2.19).

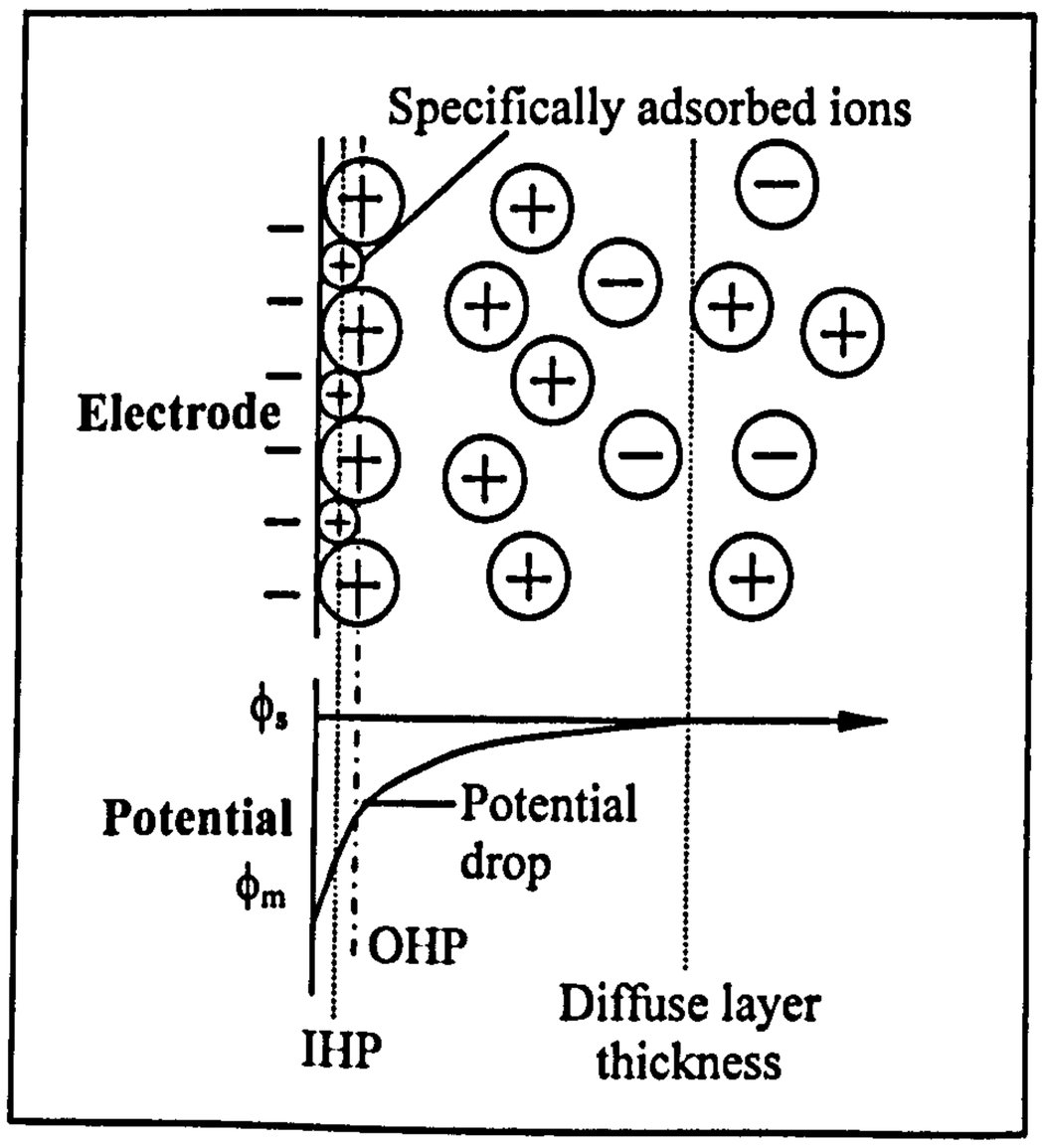

Figure 2.19: The Grahame model of the electrical double layer

The Grahame model was later extended to include dipolar solvents, such as water at the interfacial region (Figure 2.20) (Bockris *et al*, 1963) .

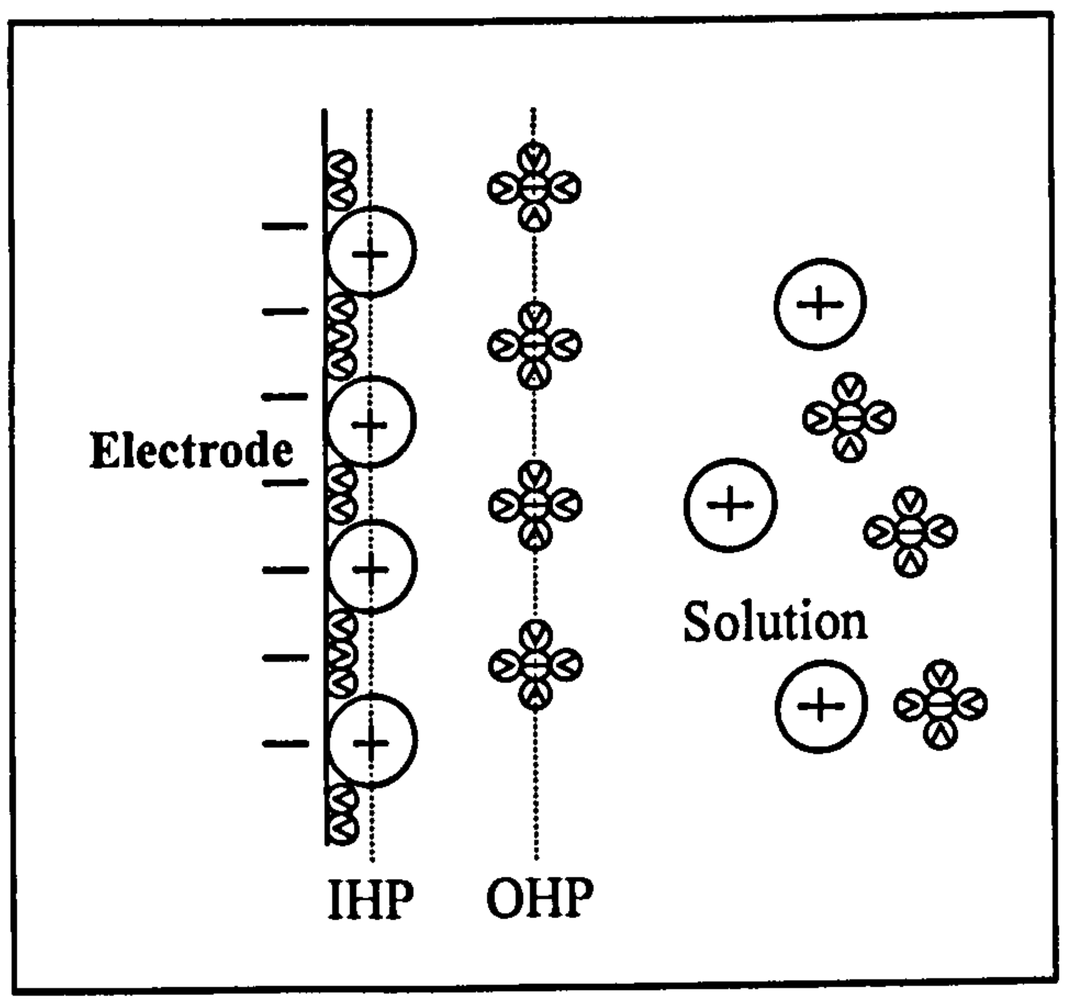

Figure 2.20: The Bockris *et al* electrical double layer model

Although beyond the scope of this thesis, many modifications and improvements have been made to these models with the latest approaches using numerical modelling to follow the redistribution effects as the electrode potential is varied (Vlachy, 1999).

2.2.6 Voltammetry

Voltammetric analysis was first developed by the Czech chemist Jaroslav Heyrovsky (Heyrovsky, 1922) with the development of polarography in 1922. The common characteristic of all voltammetric techniques is that they involve the application of a potential (***E***) to an electrode and the monitoring of the resultant current (***i***) flowing through the cell. Generally, the applied potential is varied or the current is monitored over a period of time (***t***), which means that voltammetric analysis can be described as some function of ***E***, ***i***, and ***t***. They are considered to be active techniques (as opposed to passive methods such as potentiometry) because the applied potential forces a change

in the concentration of an electroactive species by electrochemical oxidation or reduction.

The analytical advantages of the various voltammetric techniques includes excellent sensitivity with a large linear concentration range for both organic and inorganic species (typically 10^{-12} to 10^{-1} M), a large number of useful solvents and electrolytes, a wide range of temperatures, rapid analysis times (in the order of seconds), simultaneous determination of a number of analytes, and the ability to determine kinetic and mechanistic parameters due to a well developed theory.

Analytical chemists routinely use voltammetric techniques for the quantitative determination of a variety of dissolved organic and inorganic materials. Physical, biological and inorganic chemists widely use voltammetric techniques for investigating reductive and oxidative process in various media, adsorption processes on surfaces, and mass transport and reaction mechanisms. Voltammetric methods are also applied to the determination of compounds of pharmaceutical interest, and when coupled with high pressure liquid chromatography (HPLC), they are effective tools for the analysis of complex mixtures.

2.2.6.1 Experimental investigations of current / measurement characteristics

The simplest approach to the measurement of current and voltage characteristics is to use a two electrode system, one of which carries out the reaction of interest (termed the *working* electrode), and the other provides a stable potential (termed the *reference* electrode) so that the potential difference between the working electrode and the solution can be controlled.

The working electrode should be made of an inert material, as well as being a good electrical conductor, typically gold or platinum. More recently glassy carbon, graphite and carbon pastes have been used due to their relatively low materials cost and ease of

production. Although potential values are not absolute, the standard hydrogen electrode (SHE) is used for the calculation of standard electrode potentials. Unfortunately, the standard hydrogen electrode is cumbersome and more commonly silver/silver chloride (Ag/AgCl) and saturated calomel electrodes (SCE) are employed. These devices are able to maintain a stable potential in solution and have a fixed offset to the potential of the SHE. It is important to maintain the position of the reference electrode as closely as possible to the working electrode in order to minimise the effect of ***iR*** (*Ohmic*) drop. It assumed that a finite current flows when a potential, ***E***, is applied between a large working electrode and a reference electrode.

$$E = (\phi_m - \phi_s) + iR + (\phi_s - \phi_{ref}) \qquad 2.49$$

where (ϕ_m-ϕ_s) is the driving force for electrolysis at the working electrode, the term ***iR*** represents the potential drop in solution due to the passage of current (***i***) through a solution with resistance (***R***) between the electrodes, and (ϕ_s-ϕ_{ref}) is the potential drop at the reference electrode/solution interface (primarily controlled by the chemical composition of the reference electrode).

In electrochemical systems where only a small current flows (for example at a microelectrode), the term ***iR*** can be neglected, and since (ϕ-ϕ_{ref}) is fixed according to the electrode chemical composition, Equation 2.49 can be simplified to:

$$E = (\phi_m - \phi_s) + \text{constant} \qquad 2.50$$

Any changes in potential are therefore directly related to the driving force (ϕ_m-ϕ_s). Unfortunately in the case of larger electrodes, the term ***iR*** is no longer negligible and so cannot be neglected. Furthermore, the passage of large currents through the reference electrode can alter its chemical composition and cause a change in the value of (ϕ_s-ϕ_{ref}).

As mentioned in section 2.2.2, this creates the need for a third electrode, called a *counter*, or *auxiliary*, electrode which acts as a source or sink of electrons. The area of the counter electrode should ideally be 2-10 times larger than that of the working electrode in order to prevent electron supply causing a rate limiting step. It may also be required to separate the working and counter electrode via a semi-permeable membrane or frit if the products formed at the counter electrode would cause interference.

The three-electrode system is controlled by a device called a *potentiostat* which can prevent any current from passing through the reference electrode, thereby stabilising its potential.

Different techniques can be employed to polarise the working electrode in either a two- or three-electrode system, and allow voltammetric experiments to be performed in a number of ways. *Linear-sweep voltammetry* involves the polarisation of the working electrode from a value E_1 to E_2 at a constant sweep rate, v (Figure 2.21). If this potential sweep is then reversed, i.e. from E_2 to E_1, then the process is termed *cyclic voltammetry*. These processes will now be described in more detail.

2.2.6.2 Cyclic voltammetry

Cyclic voltammetry is one of the most widely used experimental approaches in dynamic electrochemistry. The process can be characterised by a triangular potential cycle (Figure 2.21).

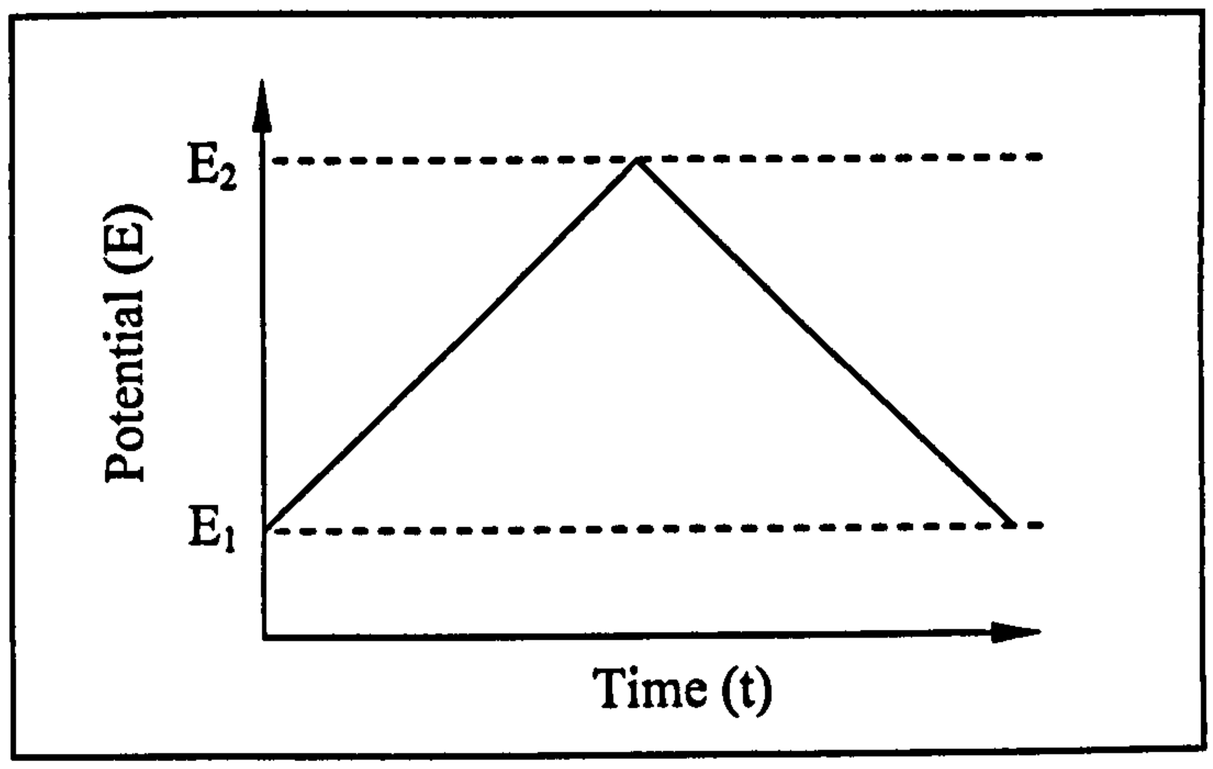

Figure 2.21: The variation of potential with time during cyclic voltammetry

If the voltammetry is performed in stationary solution, Fick's second law of diffusion can be used to predict the mass transport of species *B* to the working electrode (described by Equation 2.40). For the case of *irreversible* electrode kinetics, it is possible to analyse the current / voltage shown in the linear-sweep voltammogram (Figure 2.22).

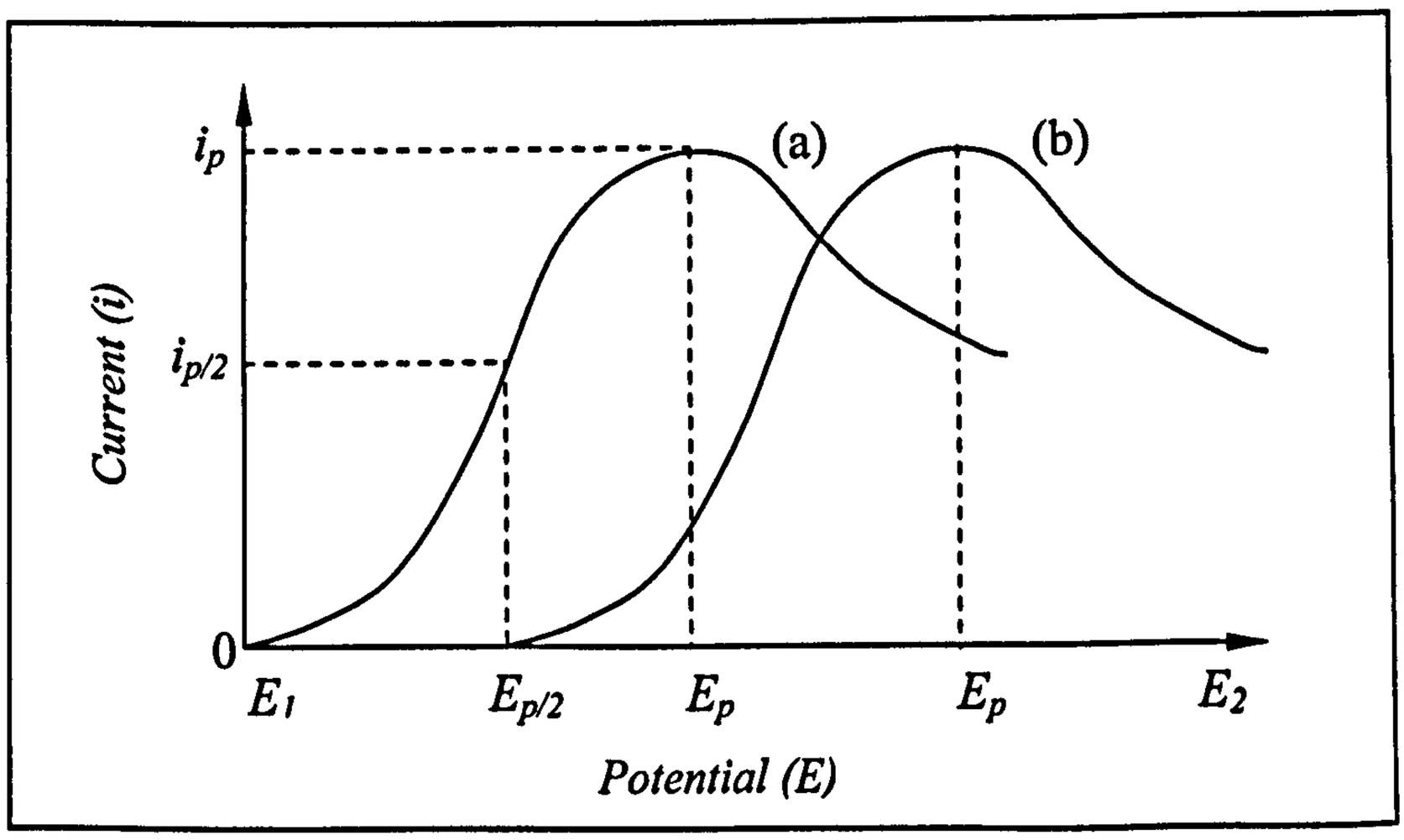

Figure 2.22: Potential vs. current sweep for (a) a reversible electron transfer reaction and (b) an irreversible electron transfer reaction

Initially, the applied potential is insufficient to induce electron transfer and so no current will flow. As the potential is increased, larger electrochemical rate constants (k_{red} and k_{ox}) are experienced such that the current rises with time until the concentration of species B at the electrode surface ($[B_0]$) decreases and mass transport becomes the limiting factor. The peak current, i_p, therefore represents the balance between an increasingly heterogeneous rate constant and the beginning of a decrease in surface concentration of reactants. Beyond i_p, the current begins to drop as the supply of reactants to the electrode surface limits the current.

In the case of a reversible electrode reaction, the rapid electrode reaction kinetics involved produces a significant current, which flows as soon as the reaction becomes thermodynamically viable (Figure 2.22a). The peak potential, E_p, in a perfectly reversible electrode reaction is constant and independent of sweep rate, whereas for irreversible reactions (2.22b), the faster sweep rates will shift E_p to a more negative potential for reduction, or a more positive potential in the case of oxidation. This relationship is represented by Equation 2.51 and 2.52.

For a reversible reaction:

$$\left|E_p - E_{\frac{p}{2}}\right| = 2.20\frac{RT}{F} \qquad 2.51$$

For an irreversible reaction:

$$\left|E_p - E_{\frac{p}{2}}\right| = 1.86\frac{RT}{\alpha F} \qquad 2.52$$

In either case, i_p, is directly proportional to the concentration of B, and increases with sweep rate. This is explained by considering Fick's first law, which indicates that i_p is a reflection of the concentration gradient of B near the electrode, which in turn is controlled by the thickness of diffusion layer. An increase in the sweep rate will mean a reduced time for electrolysis and allow an increase in i_p due to a thinner diffusion

layer. It follows that the shape of the forward sweep is therefore dependent on the reversibility of the redox couple.

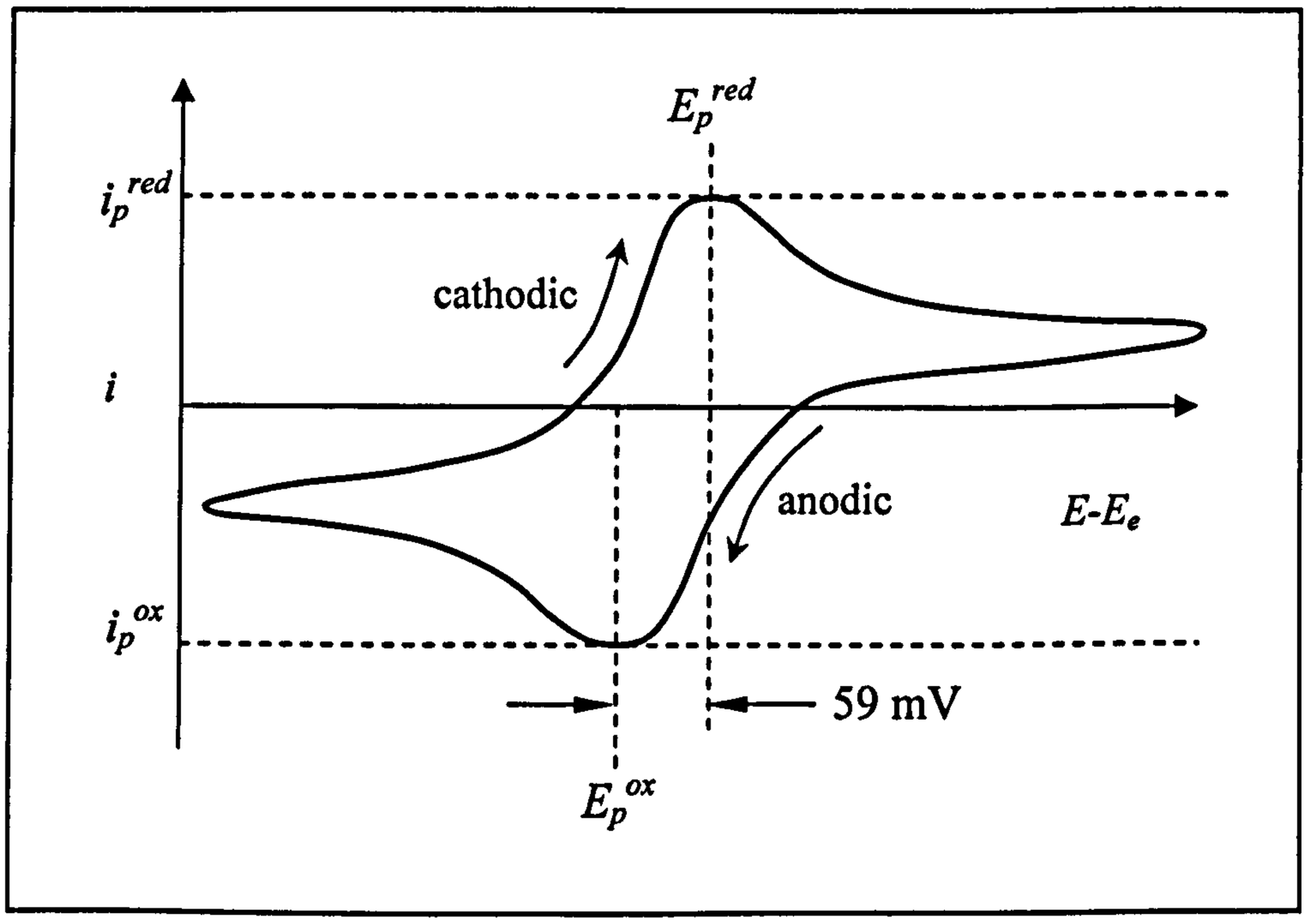

Figure 2.23: Cyclic voltammogram for a reversible electron transfer reaction

Figure 2.23 shows a voltammogram for a typical reversible single electron transfer reaction. As the potential is swept towards the cathodic direction, increasing amounts of reactants are converted, until a reduction peak is reached (E_p^{red}). Following this peak, large quantities of product surround the electrode and form their own diffusion gradient away from the electrode surface. The flux of reactant is no longer sufficient to satisfy the Nernst equation, resulting in a steady decrease in current. Upon reaching E_2, the potential sweep is reversed in the anodic direction and reaction products generated in the forward sweep are converted back to their original form. Current flow will increase until E_p^{ox} is reached, where a depletion of the diffusion layer causes a decrease in current, mirroring that of the forward (cathodic) sweep. In a truly reversible reaction the heights of the forward and reverse peaks are of equal magnitude (Equation 2.54), and are separated by a potential of approximately n/59 mV (at 25°C) (Equation 2.54), as predicted by the Nernst equation, (where n is the number of

electrons per molecular oxidation/reduction). For a given set of conditions, peak separation for a perfectly reversible couple will not change with scan rate. It follows that for a reversible reaction involving the transfer of ***n*** electrons, peak separation can be described as follows:

$$\left|E_p^{ox} - E_p^{red}\right| = 2.218\frac{RT}{nF} = \frac{n}{59} \qquad 2.53$$

$$\frac{i_p^{ox}}{i_p^{red}} = 1 \qquad 2.54$$

In real cyclic voltammograms, the faradaic response is superimposed onto a charging current which is approximately equal for both the forward and reverse scan directions. The correction required to ascertain the true values of i_p^{ox} and i_p^{red}, makes their measurement somewhat imprecise. Consequently, cyclic voltammetry is not thought to be an ideal method for quantitative evaluation of system properties that must be derived from peak heights, such as the rate constant of a coupled heterogeneous reaction, or the concentration of the electroactive species. This technique is often employed as a first step in voltammetric analysis since it offers a rapid semi-quantitative method for identifying electroactive material present in a solution.

So far, reactions have been described in terms of being reversible, where the reverse peak is equal and opposite to that of the forward sweep, and irreversible, where reaction products cannot be converted back to their original oxidation state. However, the majority of redox couples fall between the two extremes, exhibiting what is described as quasi-reversible behaviour, which is generally characterised by a smaller reverse peak current (i_p^{ox}). The return peak will only appear if the scan rate is sufficiently fast so as to reach the required potentials before the material has time to diffuse away into the bulk solution. Furthermore, the peak separation of quasi-reversible reactions is proportional to the scan rate. The measurement of the peak

potentials of the forward and reverse reactions with scan rate can allow the calculation of standard rate constants.

2.2.6.3 Chronoamperometry

Chronoamperometric techniques involve the polarisation of the working electrode at a fixed potential in a quiescent solution. The potential is stepped from E_1, where no reaction takes place, to one at which all species which reach the electrode surface react (E_2), as shown in Figure 2.24 (a). Current flow is recorded against time (t), as shown in Figure 2.24 (b).

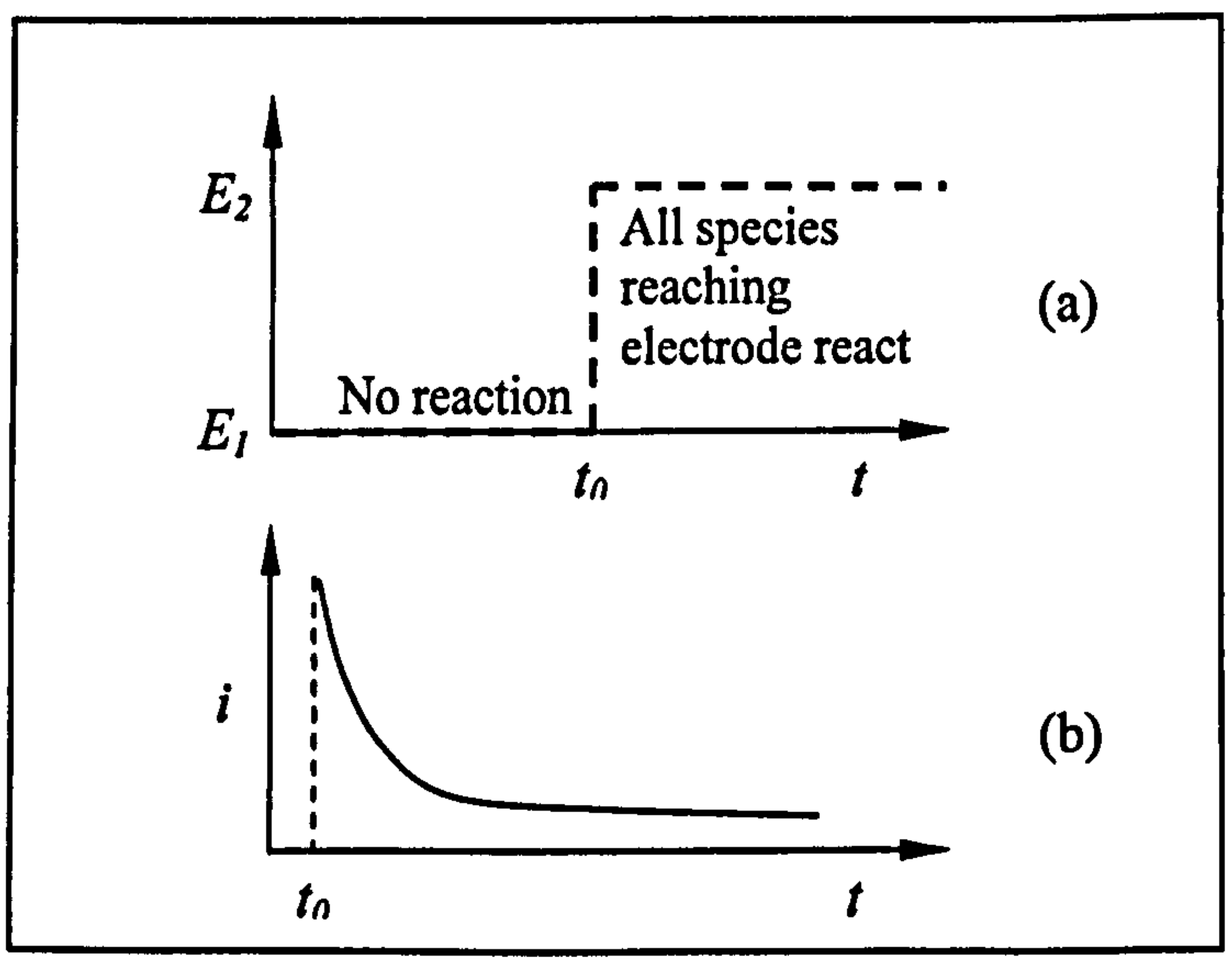

Figure 2.24: Chronoamperometry: (a) the potential step, (b) current response to the applied potential as a function of time

Immediately following the application of potential, E_2, a large current is observed resulting from the relatively high (bulk) concentration of reactant at the electrode surface. As the reactant is consumed, and the concentration gradient extends into solution, the current can be seen to decay to a steady-state value controlled by the rate of diffusion given by the case of a planar electrode in a quiescent solution.

For an electrode of normal dimensions in static conditions, the current flow is described by the Cottrell Equation (Cottrell, 1902), which is derived from Fick's second law of diffusion:

$$i = \frac{nFA[B]_{bulk} D_B^{1/2}}{(\pi t)^{1/2}} \qquad 2.55$$

where i is the current measured at time (t), n is the number of electrons transferred per mole, F is the faraday constant, A is the electrode area, $[B]$ bulk is the bulk concentration of the measured species, D_B is the diffusion coefficient of species B.

2.2.7 Microelectrodes

Until now we have considered electrochemical processes occurring at electrodes of macroscopic dimensions, and for the case where the rate of electron transfer is fast, and relatively slow linear diffusion renders the measured current to be under diffusional control. Diffusion controlled behaviour is frequently problematic for electroanalysis, since any convection in the solution will affect the diffusion gradients in the solution, and so cause a change to the electrode response. Although the use of microelectrodes in electrochemistry dates back to the early 1800s, with the work of William Wollaston, they have only experienced widespread use in relatively recent times. This is largely because a suitable combination of technology, instrumentation, and developed theory enabling the practical use of microelectrodes has only been developed in relatively recent years (Imisides *et al*, 1996). Because of these developments, the use of microelectrodes has become one of the most actively pursued fields in electroanalytical chemistry. The advantages of very small electrodes was recognised for many years by physiologists (Silver, 1987), (Logman *et al*, 2000), (Xu *et al*, 2002) who envisaged minimally invasive, in vivo electrodes immune to movement in the surrounding medium. Advantages of microelectrodes in environmental monitoring applications has

also been well recognised, in particular that of trace metal monitoring (Tercier-Waeber *et al*, 1999), (Koudelka-Hep & van der Wal, 2000), (Cunningham *et al*, 2001), (Gobet *et al*, 2003). However, it was through the work of Wightman and Fleischmann that the wider applications to electrochemistry were realised (Wightman, 1981), (Fleischmann *et al*, 1987), (Pons & Fleischmann, 1987).

The definition of a microelectrode, the smallest of which are sometimes known as ultramicroelectrodes, continues to receive debate (Amatore, 1995), (Shoup & Szabo, 1984). Functionally, one definition suggests that the electrode must be smaller than the thickness of the diffusion layer to prevent the signal being diffusion limited (Dayton *et al*, 1980). A further definition provided by Bard and Faulkner describes a microelectrode as having a characteristic surface dimension smaller than 25 μm (less than the width of a human hair) (Bard & Faulkner, 2001). This critical dimension could refer to the width of the band, or the radius of the disc electrode (common examples are illustrated in Figure 2.25). The development of carbon nanotube technology has allowed the dimensions of microelectrodes to be reduced to the sub-micron level (~100 nm) (Campbell *et al*, 1999), (Dimaki & Boggild, 2004). For electrodes with dimensions of around 10 nm or lower, termed nanodes (Penner *et al*, 1990), experimental behaviour begins to differ from that predicted by theory (Morris *et al*, 1987), (Norton *et al*, 1990).

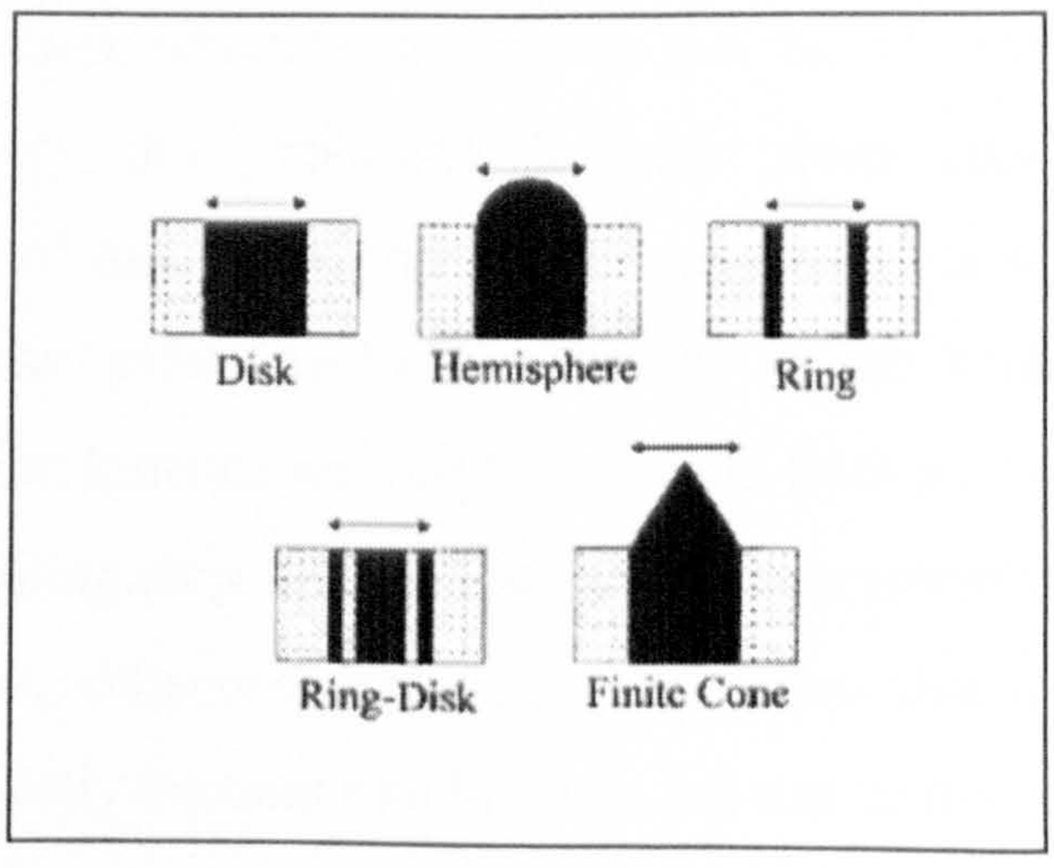

Figure 2.25: The cross-sectional views of various microelectrodes (Zoski, 2002)

As exhibited in Figure 2.25, microelectrodes may take a number of forms including a hemisphere, an disc, a ring, a band or even interdigitated electrodes (IDE) (Paeschke *et al*, 1995), (Wang *et al*, 1998), each possessing its own diffusion characteristics. However, this work and any calculations herein are concerned with the flat, inlaid disc microelectrode type (typically ≤10 μm diameter), which lends itself more easily to high volume production.

Small scale sensors of this type can offer a number of performance advantages over macroelectrodes, including stir-independent properties, and higher signal-to-noise ratios resulting from higher sensitivity, reduced double layer capacitance and Ohmic drop (Section 2.2.6.1). Despite performance advantages, the high volume commercialisation of microelectrodes has been limited thus far by the difficulty and cost associated with their manufacture.

2.2.7.1 Mass transport and reaction kinetics at microelectrodes

The ultra-small dimensions of microelectrodes provide a number of performance advantages over macroelectrodes. Firstly, current measured is a function of area, and as a consequence the currents passed by microelectrodes are extremely small (of the order of 1×10^{-9} amps or below). Advantageously, this means that the amount of electrolysis occurring is also very small, which in turn means that the diffusion layers around such electrodes will be very thin, resulting in very steep concentration gradients. Consequently, the rate of mass transport to microelectrodes is much greater than for macroelectrodes and can offer invaluable benefits in the study of fast reactions. Ordinarily, when reaction kinetics are fast then results from an experiment will reflect the slowest, or rate limiting step, such as the supply of materials via diffusion. In the case of microelectrodes, enhanced mass transport means that other factors such as electrode kinetics frequently become rate limiting and can be investigated.

A further advantage of a smaller current is that the effects of solution resistance (Ohmic drop) become minimised. This means that the need for high levels of electrolyte in solution is negated to certain extent, and so it is possible to allow the use of non-polar solvents such as benzene or toluene to be used as the reaction medium instead of water.

Finally, information on electrode processes can be gained by sweeping the potential whilst measuring the current. Ordinarily, in addition to electrolysis, a change in potential causes a re-structuring of the electrical double layer producing a 'charging current' which can mask the reaction under interrogation. The reduced area of microelectrodes allows a major reduction in the magnitude of the capacitive 'transient' current, permitting equilibrium to be attained in very short time scales as well as allowing useful reaction data to be obtained at very fast sweep-rates.

Figure 2.26 illustrates the diffusion profile to the surface of a hemispherical microelectrode compared to that of a planar electrode.

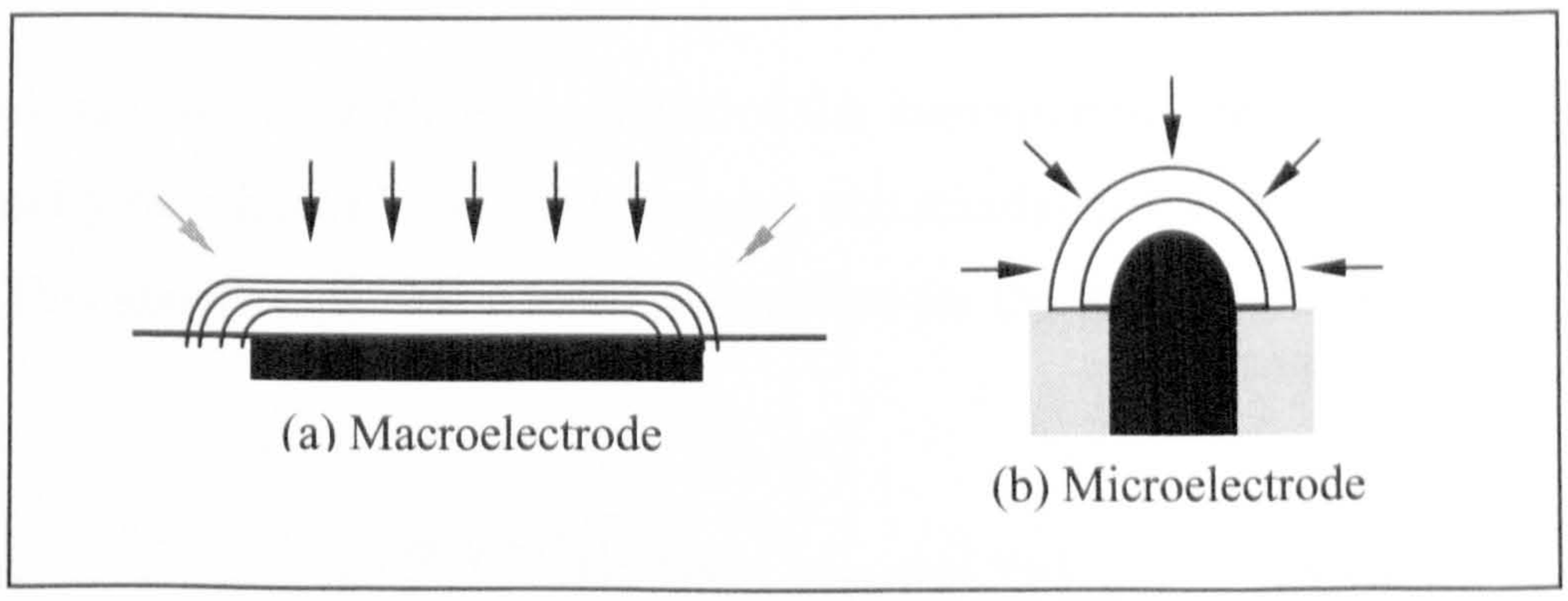

Figure 2.26: Diffusion profile to a macroelectrode (a) and a hemispherical microelectrode (b)

It can be seen that the diffusion gradient to the surface of the macroelectrode follows a linear profile (as was seen in Figure 2.15). In the case of a hemisphere of diameter ≤10 μm (close to the thickness of the diffusion layer), the electrode is fully and uniformly accessible for the supply of material (Figure 2.26b). Using the same

boundary conditions as for linear diffusion, Cottrell described the current flow for a hemispherical electrode (Equation 2.56).

$$I(t) = nFAJ = nFAD[B]_{bulk}\left[\frac{1}{(\pi Dt)^{\frac{1}{2}}} + \frac{1}{r_0}\right] \qquad 2.56$$

This is the Cottrell equation modified to include a spherical term, dependent on the reciprocal of the electrode radius, r_0. In the case of macroelectrodes (where $r_0 \geq 5$ μm), currents measured at a spherical electrode match those predicted by planar diffusion, whereby current decreases with time until equilibrium is reached. The dependency of the current flow at hemispherical microelectrodes with time is greatly reduced (Equation 2.57).

$$r_0 = \frac{(\pi Dt)^{1/2}}{10} \qquad 2.57$$

The result is that the smaller the radius of the hemispherical microelectrode (r_0), the more rapidly the effect of time (t) decreases, and steady-state current is obtained much sooner. This allows Equation 2.56 to be modified for the case of a microelectrode:

$$I = \frac{2\pi r^2 nFD_B[B]_{bulk}}{r} = 2\pi nrFD_B[B]_{bulk} \qquad 2.58$$

In practice, it is normally much easier to produce electrodes with two-dimensional geometry, generally prepared mechanically or lithographically. Fortunately, if the dimensions of the hemisphere are close to that of the diffusion layer thickness, then hemispherical diffusion will be permitted if the electrode is flattened into a disc shape (Figure 2.27).

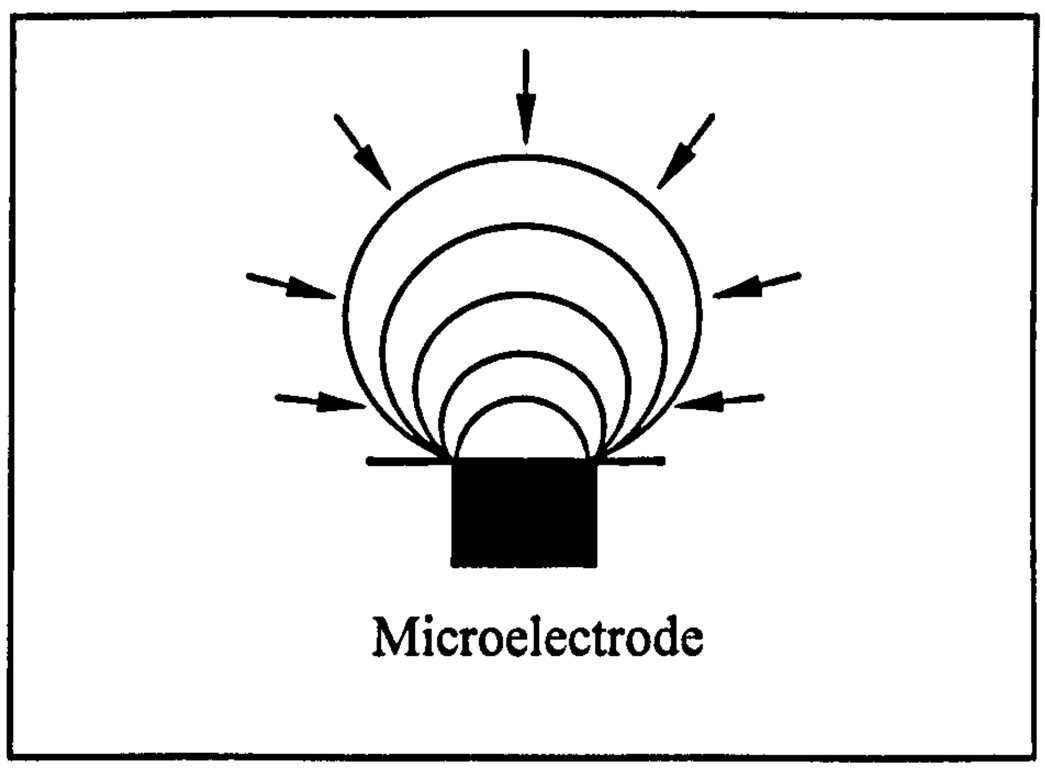

Figure 2.27: Schematic of the diffusion profile to a disc microelectrode

The disc radius, r_0, now becomes a quarter of the sphere perimeter (Equation 2.59).

$$r_0 = \frac{2\pi r_{hemisphere}}{4} \qquad 2.59$$

can be rearranged to:

$$r_{hemisphere} = \frac{2r_0}{\pi} \qquad 2.60$$

By substituting Equation 2.60 into Equation 2.58, it is possible to obtain a relatively simple expression for the steady-state current at a disc microelectrode, obtained after a few seconds and which varies with radius rather than area (Shoup and Szabo, 1984):

$$I = 4nFr_0 D_B [B]_{bulk} \qquad 2.61$$

The rapid attainment of steady-state current is illustrated in Figure 2.28.

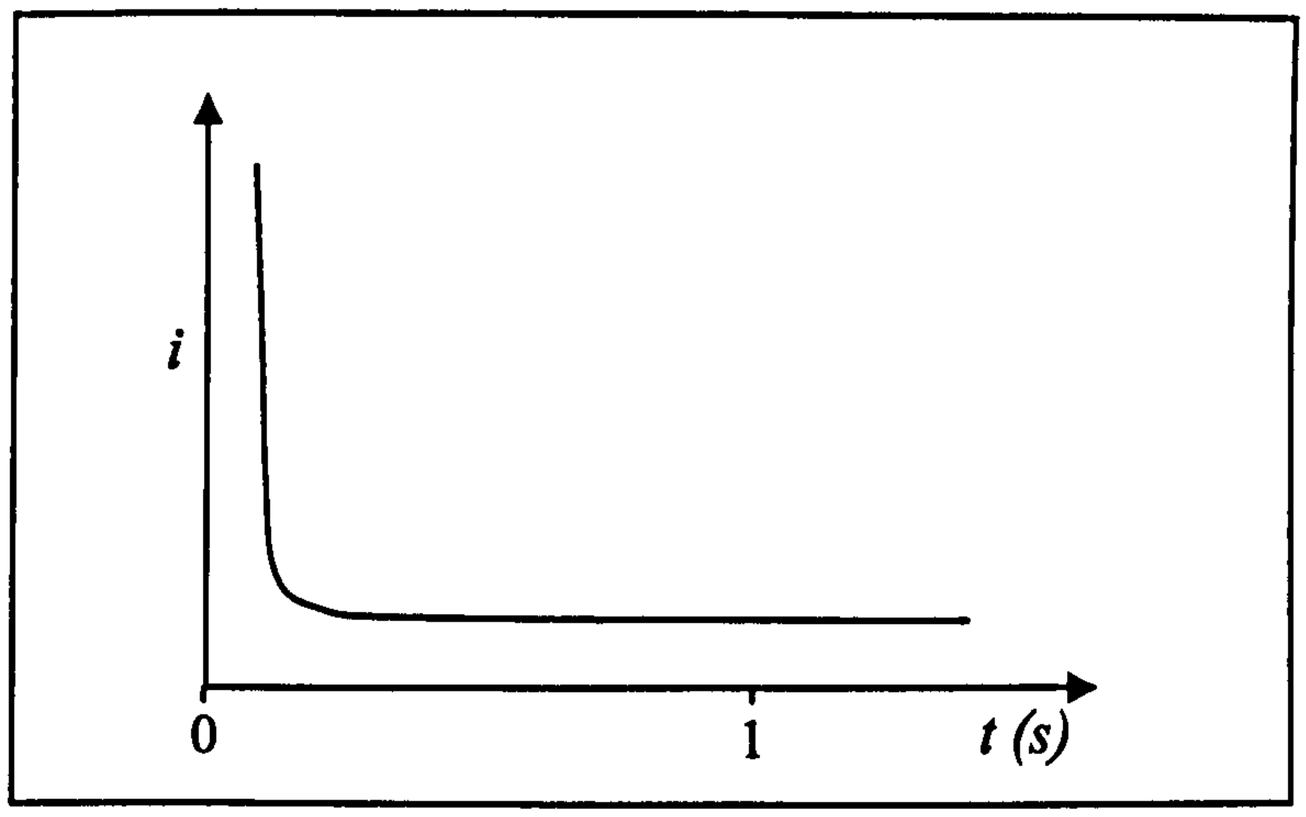

Figure 2.28: Current vs. time on a microelectrode

The Cottrell equation for a macroelectrode (Equation 2.55) predicts that the concentration gradient will continue to extend into solution with time (Figure 2.15). However in the case of microelectrodes, the penetration of the diffusion layer is limited, illustrated in Figure 2.29.

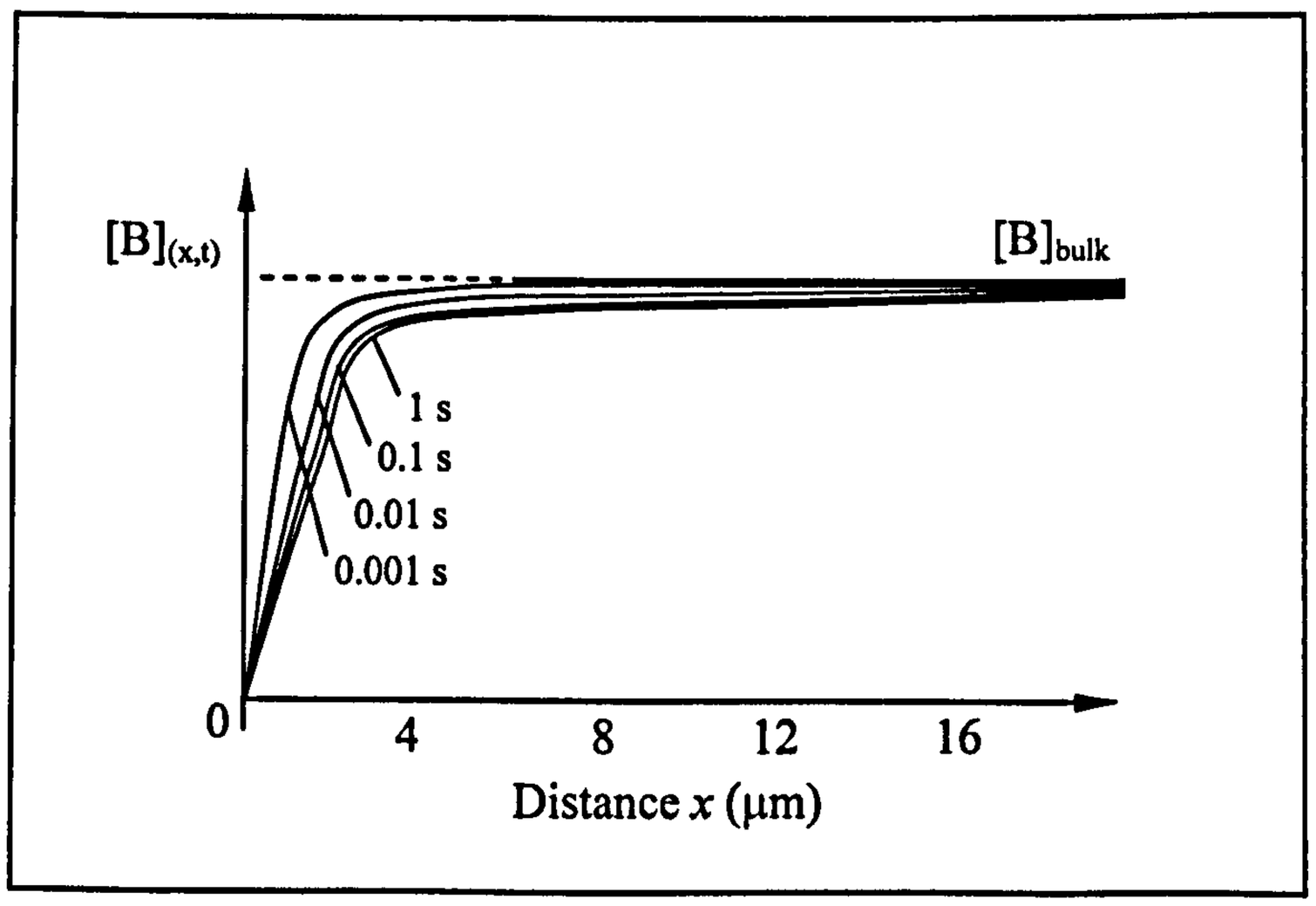

Figure 2.29: Concentration profile versus distance from microelectrode

As a consequence of their small size and enhanced (hemispherical) diffusion, microelectrodes exhibit a modified form of the cyclic voltammogram experienced with macroelectrodes (Figure 2.30).

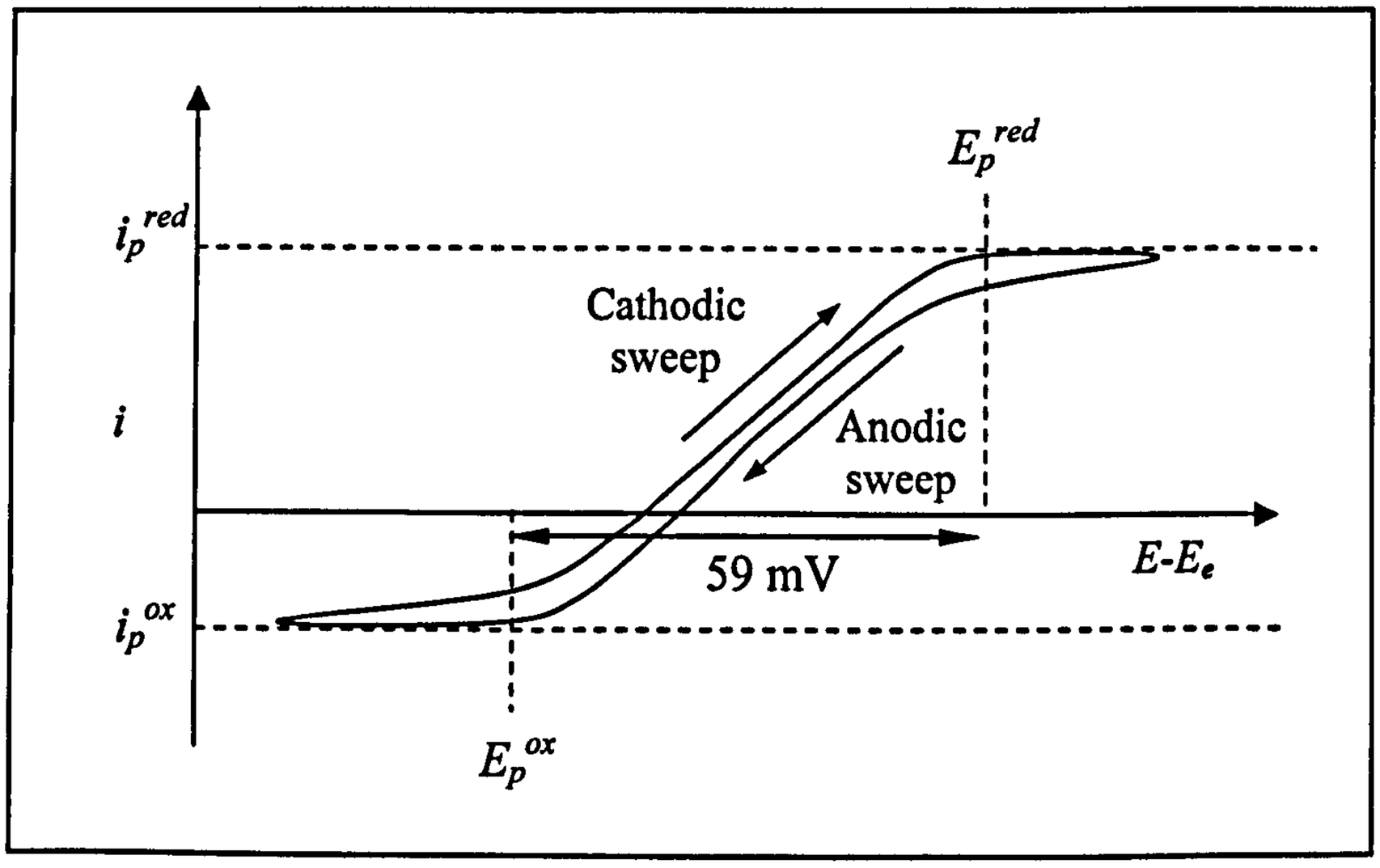

Figure 2.30: Cyclic voltammogram for a reversible electron transfer reaction at a microelectrode

It can be seen that after E_p^{red} is reached, the current does not start to decay as the rate of mass transport is sufficient to prevent the flux of material to the electrode from becoming depleted. The form of this curve is termed *sigmoidal*, and the reaction kinetics are now the rate limiting factor. Consequently, the effect of convection (being many orders of magnitude faster than diffusion) is eliminated, and imparts the greatest benefit of microelectrode behaviour: *stir independence.*

2.2.7.2 Microelectrode arrays

In spite of the inherent advantages of microelectrodes in terms of stir independence, lowered Ohmic drop, fast kinetics, enhanced sensitivity, rapidly attained steady-state and improved Faradaic-to-capacitive currents, their small size do present some drawbacks. Given that signal size is dependent electrode area, it follows that a microelectrode will only generate a very small current (typically of the order of picoamps). This places a serious demand on the instrumentation equipment used to prevent the signal being swamped by electrical noise. However, it is possible to circumvent the problem of a small signal if multiple microelectrodes in the same system are connected in parallel. The result is that a significant current can be obtained, whilst retaining the inherent performance advantages of a single microelectrode. Such assemblies are termed *microelectrode arrays* (Figure 2.31) (Ross *et al*, 1992).

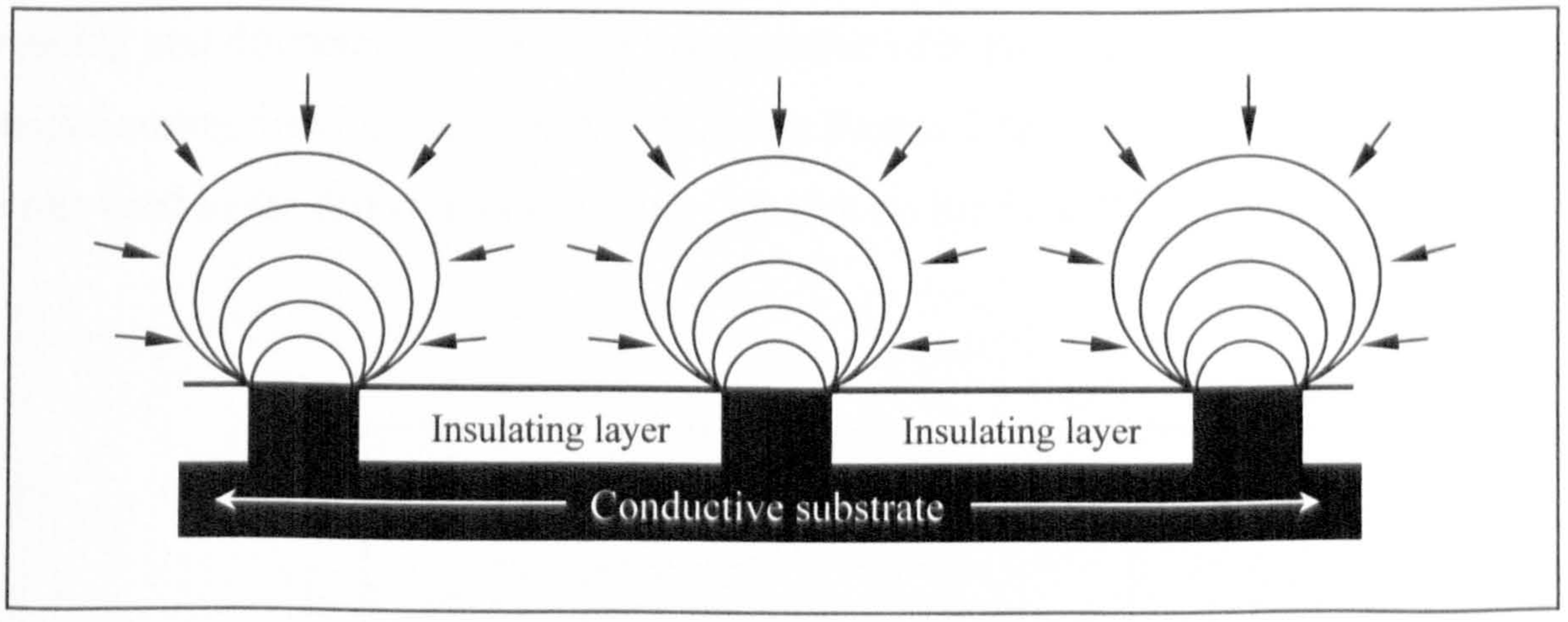

Figure 2.31: Microelectrode array configuration

The combination of a number of microelectrodes does however add some complexity to the situation. In the case of a relatively a low packing density, the signal response will simply be that of individual microelectrodes, multiplied by the number, ***N***, contained in the array (Equation 2.62) (Aoki *et al*, 1989).

$$I = N.(4nFr_0 D_B [B]_{bulk}) \qquad 2.62$$

In practice, however, this is only achieved if the spacing between electrodes is sufficiently large, such that there is no interaction between the individual electrodes as they begin to compete for mass transport. In the case where electrodes are closer together, the system will initially behave in the same way as it would with larger spacing. However, as the diffusion layers begin to move towards equilibrium, the individual diffusion shells begin to overlap and cause a reduction in the hemispherical diffusion of material to the electrode surfaces. This effect, termed *shielding*, is dependent on electrode size, density and distribution and in extreme cases may result in the sensor array behaving like a macroelectrode electrode of the same area (Amatore *et al*, 1983).

Morf proposed a convenient model allowing the optimisation of microelectrode disc spacing and diameter to maximise the response of a given array while minimising the neighbouring disc interactions (Morf, 1996). Figure 2.32 helps to illustrate some of the terms used in the following discussion (Morf & de Rooij, 1997).

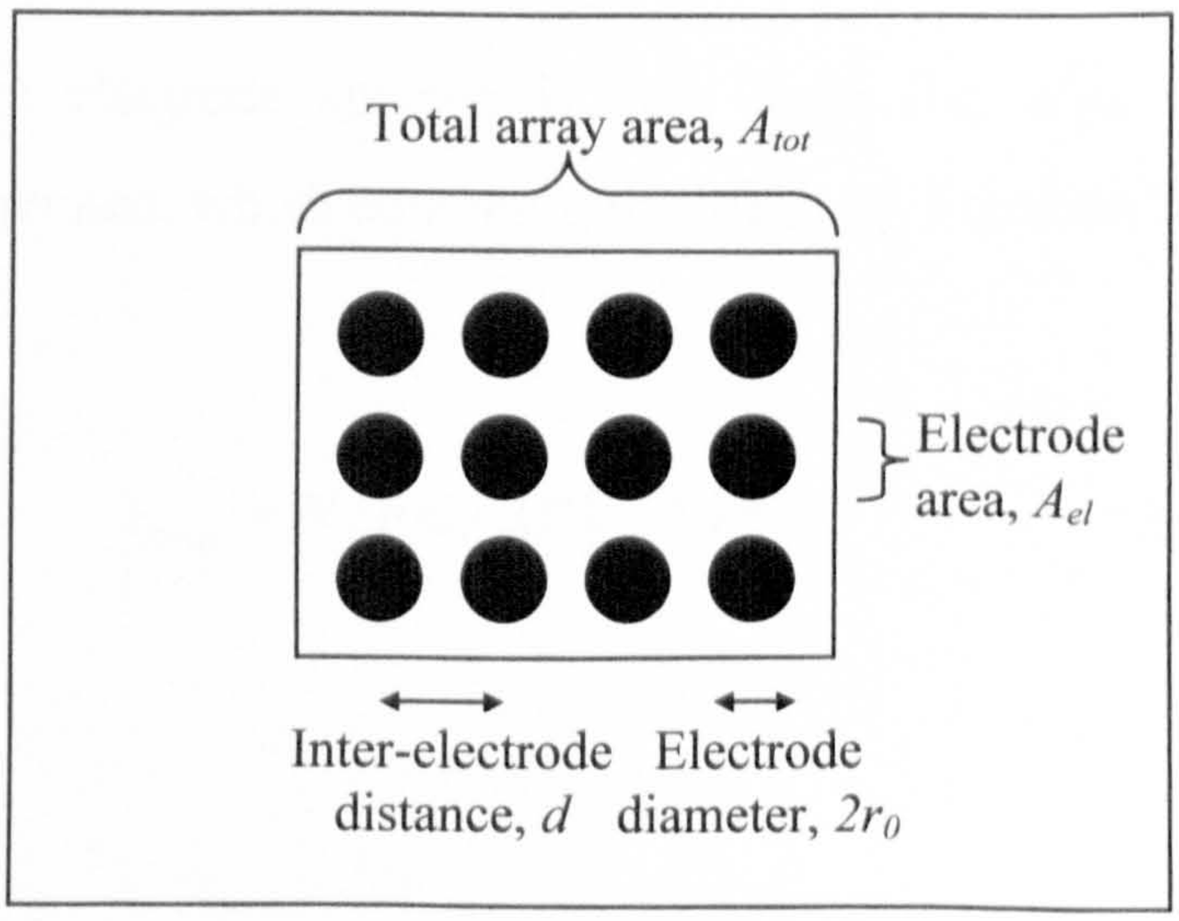

Figure 2.32: Schematic representation of an array of inlaid disc microelectrodes

Accordingly, equation 2.63 describes the limiting current of a microelectrode array:

$$i_{array} = FnD_B[B]_{bulk} \cdot \left[\left(\frac{1 - A_{el}^{1/2}}{d} \right)^2 \cdot \frac{a_0}{NA_{el}} + \frac{\delta}{A_{tot}} \right]^{-1} \qquad 2.63$$

where A_{el} is the active area of the electrode surface, d is the mean distance between the centres of the neighbouring electrodes ($[d=A_{tot}/N)]^{1/2}$), A_{tot} is the total surface area of the array including the inactive zones, a_0 is the apparent radius of the individual electrodes ($a_0 = [\pi/4].r_0$) and δ is the thickness of the diffusion layer (cm).

It is possible to simplify this equation for the case where $A_{el}^{1/2} \approx 2r_0$ (Equation 2.64)

$$i_{array} = \frac{\left(FnD_B[B]_{bulk}.A_{tot}\right)}{\delta + \frac{\left(d - 2r_0\right)^2}{4r_0}} \qquad 2.64$$

For the case where electrode spacing is very large (i.e. $d^2 r_0$ and $d^2 >> 4r_0.\delta$), Equation 2.65 is generated, which equates to the idealised Equation 2.62.

$$i_{array} = N.\left(FnD_B[B]_{bulk}\right).4r_0 \qquad 2.65$$

2.2.7.3 Conventional microelectrode fabrication methods

Although numerous variations exist for conventional microelectrode manufacture, they can all be divided into two main categories: (a) techniques based on glass capillary/epoxy encapsulation of metallic wires or carbon fibres, or (b) those based on microfabrication techniques (Madou, 1997). The former has been widely used in the field of neurophysiology now for over 50 years, allowing the *in-vivo* positioning of sensors very close to neurons, causing only minimal damage to the supporting tissues (Loeb *et al*, 1995). Comprehensively reviewed by Zoski, these methods are only applicable for the production of single microelectrodes (Zoski, 2002).

Microfabrication techniques take advantage of thin-film and thick-film technologies originally developed for the manufacture of integrated circuits, and can be used to produce microelectrode array sensor chips (Feeney & Kounaves, 2000). Production of photo-lithographically formed microelectrode arrays has dramatically increased in recent years. This technology effectively constructs thin-film patterns of conductive materials onto silicon wafers into well-defined micron geometries. In general, a silicone wafer with a thermally grown oxide layer is coated with a seed layer (~10 nm) of chromium or titanium. Thin films of materials such as iridium, platinum, gold or carbon are then deposited in a number of ways, including chemical vapour deposition (CVD), magnetron sputtering, or electron beam evaporation. A photocurable organic 'resist' layer is then deposited on top of the electrode by spin-coating, and cured in a pattern by means of exposure to UV radiation through a photomask. Two approaches can now be employed to create the final structure. The first, termed the 'lift-off procedure', involves the deposition of the conductive material (e.g. gold) which adheres strongly to the areas defined by the UV pattern. An organic solvent is then used to dissolve the 'resist' polymer, causing the unwanted material to fall away. In the second approach, the cured areas of resist protect the underlying metal layer during either a wet-etching (based on acid-base reactions), or dry-etching (based on reactive ions or plasma) process which remove unprotected materials from the surface. In both cases, after the electrode structures have been built, an insulating layer (e.g. SiO_2 or SiC) is patterned across the wafer to produce the finished electrode.

Sensors produced via microfabrication do suffer from drawbacks, however, particularly when used in electrolyte solutions where sensors can fail in minutes (Schmitt *et al*, 1999). Problems were generally attributed to film defects (pin-hole and particulate inclusion), adsorption and desorption processes, swelling, diffusion and the poor corrosion resistance of common passivation layers. However, by far the biggest barrier to the progress of microfabricated microelectrode arrays into the broader field of chemical analysis is their cost of production. Sensors for field analysis should ideally be disposable in nature (single use), preventing contamination and degradation from affecting reproducibility, and avoiding the cost and complication of cleaning procedures. This requirement currently precludes microfabricated sensors of this type from becoming more cost-effective than existing technologies allow. The development of an innovative method for the mass production of microelectrode arrays using low cost materials and production methods would allow this requirement to be met.

2.3 Electrochemical thin-film deposition

Electrochemical thin-film deposition forms an invaluable technique for sensor production (Osaka, 1997). Electrode substrates can be coated with a polymer via electropolymerisation with relative ease, generally requiring the anodic polarisation (potentiostatic, potentiodynamic or galvanostatic) of an electrode to give rise to a free radical, anionic or cationic polymerisation reaction mechanism. At one time, electrochemically initiated polymerisation was viewed as a hindrance, causing the inactivation of electrode surfaces (termed 'electrode poisoning'). The development of techniques enabling the coating of electrodes with polymers of pre-determined chemical and electrochemical properties is now considered a powerful tool in sensor design. In fact, electrochemistry offers a simple, clean, and efficient approach to polymer synthesis, and the deposition of insoluble polymeric material onto an electrode surface can provide both enhanced sensitivity and selectivity.

Historically, the first electrochemical polymerisation processes were *indirect*, as they involved the production of an initiator at the electrode surface while the remainder of

the process occurred in solution (Beck, 1988). It is also possible to modify a substrate with a polymer film by casting the polymer directly on to the electrode surface (Sittampalam & Wilson, 1983). However, this approach is less effective for complete and uniform coating of complex surface topographies (for example, of screen printed carbon-paste electrodes) and does not lend itself to repeatable mass production of miniaturised sensors. Chemical polymerisation, where the oxidising force is supplied by a chemical oxidant, is more suited to the bulk manufacture of polymers. Benzoyl peroxide, for example, is added to the reaction mixture in the manufacture of poly-(methylmethacrylate) (Wallace *et al*, 2002).

The electrochemical polymerisation of a polymer directly onto an electrode can offer a more suitable method of modification, providing complete coverage of the electrode surface on a molecular level (Sasso *et al*, 1990), (Castanón *et al*, 1997). In particular, the self-limiting nature of *insulating* polymers can allow electrochemically deposited films of minute thickness to be deposited consistently and reproducibly across electrode surfaces of any size or number. It is noted that deposition onto microelectrodes can sometimes be more difficult than for macroelectrodes. Although the enhanced rate of mass transport to the microelectrode prevents depletion of reactants, equally the rapid transportation of products from the electrode can remove polymer from the vicinity of the electrode surface before adsorption can occur (John & Wallace, 1990). Non-conducting films are self-limiting in thickness as their insulating properties electrically isolate the electrode from solution, thereby preventing further polymerisation. *Conducting* polymers are less self-limiting and can grow to thicknesses of micron dimensions (Yano, 1995), until the *iR* drop experienced from their finite resistance becomes significant. However, by measurement of the charge passed during polymerisation, it is still possible to accurately control the thickness of conducting polymers and this method is frequently used during the entrapment of enzymes for biosensor applications (Almeida & Mulchandani, 1993) (Yau *et al*, 1995) (Ryan *et al*, 1997) (Kelly *et al*, 2000). It is also possible to generate copolymers, which combine the benefits of different types of polymer films, simply by adding them into the reaction mixture (Malinauskas *et al*, 1998) (Li *et al*, 2001), or to greatly increase their conductivity by 'doping' (Section 2.3.1), as illustrated by Figure 2.33.

Electropolymerisation is also employed in the protection of metal surfaces from corrosion (Marsh *et al*, 2001).

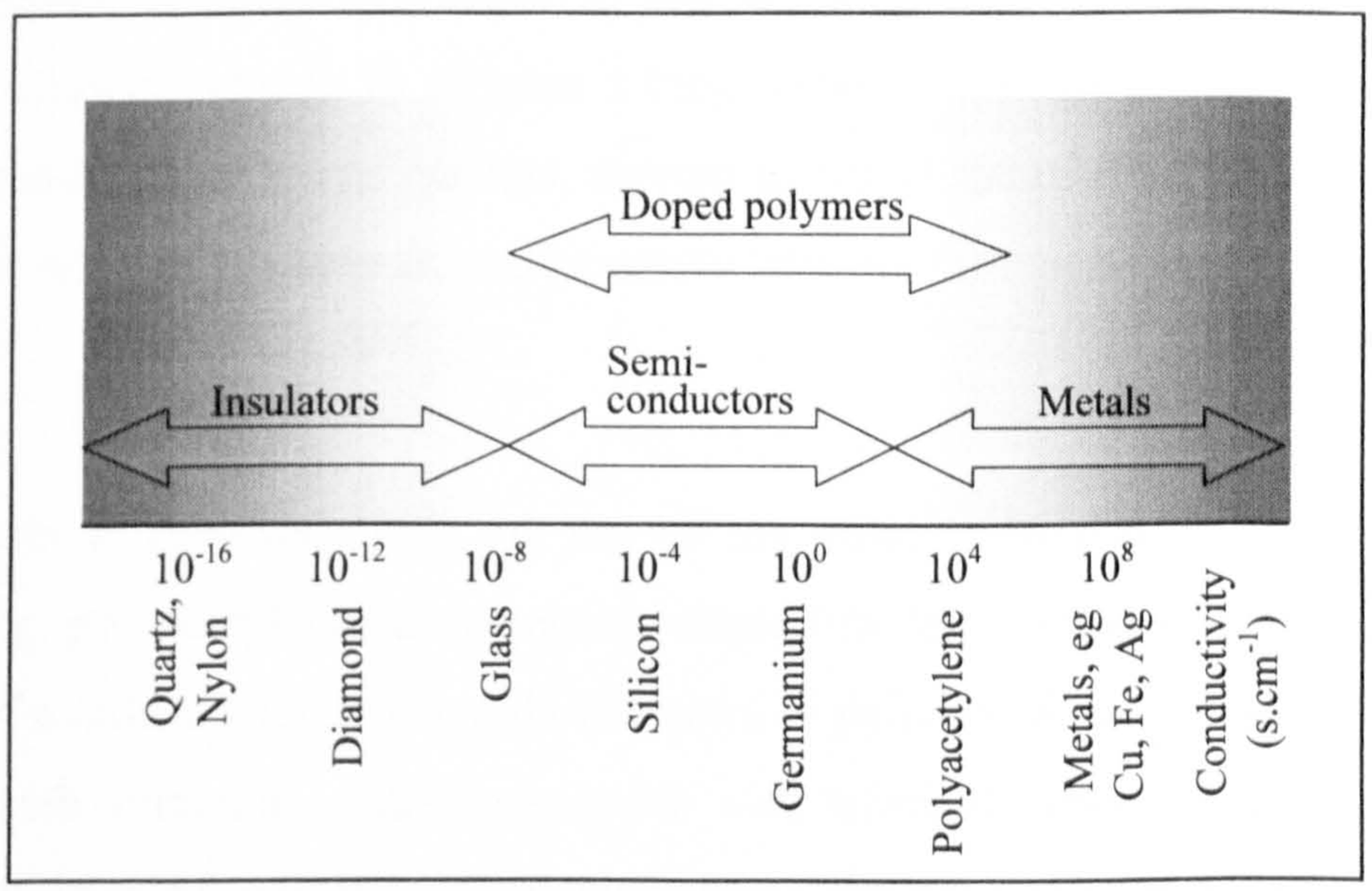

Figure 2.33: Conductivity of doped and undoped polymers

2.3.1 Electropolymerised poly(*o*-phenylenediamine)

Aniline, first known as aniline black (Fritsche, 1840), and its derivatives including poly-(phenylenediamine) have been known to scientists for over a century (Prochazka, 1880), (Fieser, 1930). However it was not until 1954 that the electrode filming properties of poly(*o*-phenylenediamine) produced via electropolymerisation in acidic solution were investigated using graphite electrodes (Lord & Rogers, 1954). In 1976, Yacynych and Mark investigated the nature of this film using infra-red, visible and ultra-violet spectroscopy, and speculated as to the nature of the conducting and non-conducting forms (Yacynych & Mark, 1976).

A key property of a conducting polymer is the presence of conjugated, i.e. alternating double and single bonds, along the backbone of the polymer. Each bond contains a localised *sigma* (σ) bond which results in a strong chemical bond. In addition, every

double bond also contains a less localised *pi* (π) bond which is weaker in nature. However, conjugation alone is not enough to make a polymer conductive. In addition, charge carriers in the form of electrons or 'holes' have to be injected in to the material, a hole being a position where an electron is missing. When such a hole is filled by an electron jumping in from a neighbouring position, a new hole (or *vacancy*) is created, and so on, allowing charge to migrate a long distance through the polymer thereby, becoming conductive. Charge carriers, serving to either add or remove electrons from the polymer, are termed *dopants*, and generally take the form of an acid or an inorganic molecule.

If an electron is removed from the top of the valance band of a semiconductive polymer, e.g. polyacetylene, the vacancy created in the carbon atom results in the formation of a radical cation. The radical cation, or *polaron*, is partly localised because of the coulomb attraction to the counter ion with which it formed. The addition of a high concentration of dopant to a polymer allows the polaron to move in the field of closely spaced counter-ions, thereby permitting the flow of current. If a second electron is removed from a previously oxidised section of the polymer, a second independent polaron may be created, or, if it is the unpaired electron from the first polaron that is removed, a bipolaron is formed which allows two positive charges to move as a pair. Charge transfer through the bulk of the polymer material occurs by electron transfer of localised charged states between polymer chains (Winokur *et al*, 1987). Although less common, a second mechanism for current flow involves the formation of *solitons*. These are solitary wave defects forming stable free radicals, created for example by the thermal isomerisation of a *cis* polyacetylene chain to the *trans* structure (a *neutral* soliton). Bulk conductivity through the polymer is permitted by *intersoliton hopping* between chains. Measurements of the electrical conductivity of a number of polyaniline derivates in acidic solution, including poly(*o*-phenylenediamine), referred to herein as P*o*PD, were carried out by Yano *et al* in 1985 (Yano *et al*, 1985). The conductivity of insulating P*o*PD polymerised in more neutral conditions was measured by Prasad et al to be approximately 3×10^{-9} S.cm^{-1} (Prasad *et al*, 1996), a million times lower than for P*o*PD polymerised under highly acidic conditions (1.2×10^{-3} S.cm^{-1}) (Yano, 1995).

Much research has been carried out into the possible uses of poly(*o*-phenylenediamine), for example sensor modification for the permselectivity against blood interferents such as ascorbic acid (Garjonte & Malinaukas, 1999), and to H^+ ions for the application of pH sensing (Cheek *et al*, 1983), (Rubenstein, 1984). Other applications reported include the protection against metal corrosion (D'Elia *et al*, 2001), electrochromic properties (Oyama *et al*, 1988), (Yano & Higuchi, 1990), (Yano *et al*, 1993), humidity sensing (Ogura *et al*, 1996), biomimetic molecularly imprinted polymers (Malitesta *et al*, 1999), plus a wealth of biosensor related applications (Malitesta *et al*, 1990; Diekers *et al*, 2000), (Ekinci *et al*, 2001), (Barton *et al*, 2004), (Pritchard *et al*, 2004).

The *o*-phenylenediamine monomer is an aromatic diamine which can be synthesised by nitration and reduction processes involving benzene (Figure 2.34)

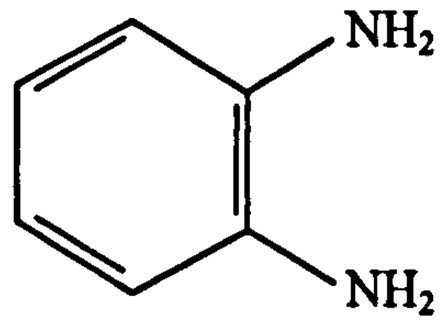

Figure 2.34: *o*-Phenylenediamine monomer (*o*PD)

Poly(*o*-phenylenediamine) can be deposited chemically (Bach, 1966), or electrochemically (Oyama *et al*, 1985) onto electrode surfaces. The benefits of electrochemical polymerisation noted earlier make it the method of choice for the modification of sensor surfaces by polymerisation. Despite the attention P*o*PD has received, there is relative uncertainty as to the precise structure of the polymer. Various analytical methods have been employed to elucidate its nature, including electrochemical techniques (Yano, 1995), quartz-crystal microbalance studies (Dai *et al*, 1998), Raman and UV-Vis spectroscopies (Wu *et al*, 1996), (Losito *et al*, 2001), radiometry (Martinusz *et al*, 1995) and scanning tunnelling microscopy (Ogura *et al*, 1995).

Two principle structures of P*o*PD have been suggested (Mederos *et al*, 1999). Oyama and co-workers used phenazine as a model compound, comparing the IR absorption spectra of P*o*PD with that of phenazine in KBr pellets (Chiba *et al*, 1987). They found that the IR spectra of P*o*PD was similar to that of phenazine, and that the absorption peak, indicated at 805 cm^{-1}, could be attributed to the skeletal vibrations of the phenazine rings. In contrast Yano found that electropolymerised P*o*PD films were soluble in common organic solvents and that a cast film of P*o*PD exhibited reversible redox behaviour which was accompanied by electrochromism, just as it did before being dissolved. This indicated that the polymer structure remained more or less unchanged and allowed a representative elemental analysis to be carried out via H FT NMR spectra. The polymeric backbone proposed by Yano was a 1,4-substituted benzoid-quinoid structure (Yano, 1995). Figures 2.35 and 2.36 illustrate these two suggested polymer configurations for polymerisation pH ranges 1-7 (Losito *et al*, 2001), (Wu *et al*, 1996):

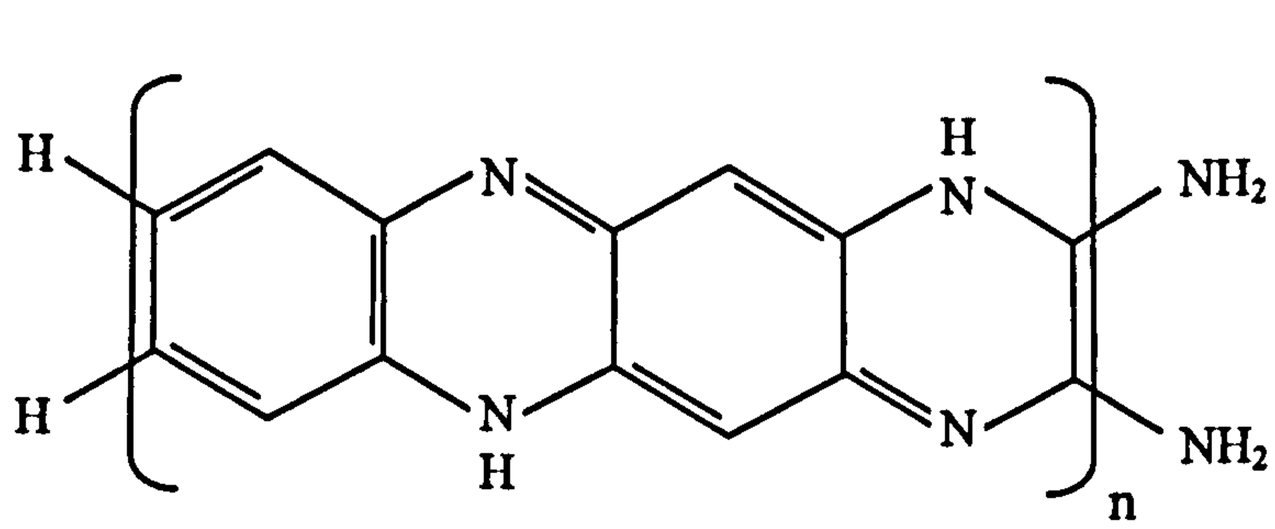

Figure 2.35: Phenazine type structure suggested by Oyama

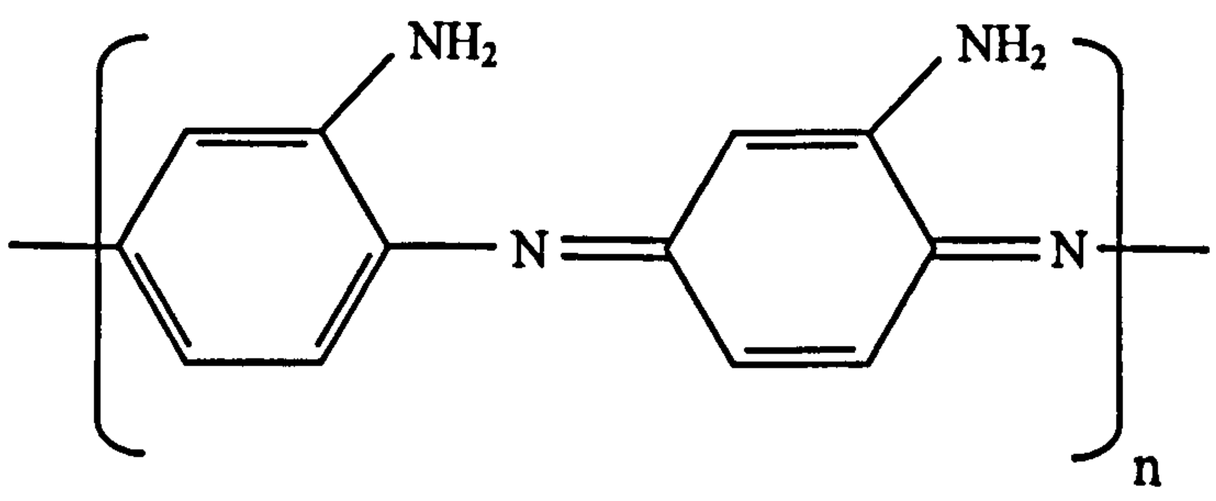

Figure 2.36: 1,4-substituted benzoid-quinoid structure suggested by Yano

The thickness of the film produced by the conducting form of PoPD has been reported to be as great as 850 nm (Yano, 1995). In contrast, the thickness of non-conducting P*o*PD assembled in more neutral conditions has been reported to be as little as 10 nm (Ohnuki *et al*, 1983), (Malitesta *et al*, 1990). However, more recent estimations based on scanning electron microscope (SEM) images in conjunction with charge transfer measurements and molecular modelling calculations report the film to be around 30 nm in thickness (Myler *et al*, 1997).

2.4 Sonochemistry

The physicochemical properties of ultrasound offer great potential to a wide range of applications. Neglecting the evolutionary development of ultrasound for the communication and navigation of creatures such as bats and dolphins, the generation of ultrasound was first established in the 1880's with the discovery of the piezoelectric effect (the generation of electricity through the movement of piezoelectric crystal) (Curie & Curie, 1880). Most modern ultrasonic devices rely on transducers, composed of piezoelectric material, which respond to the application of an electrical potential with a change in dimension (the inverse of the piezoelectric effect). If the potential is alternated at high enough frequencies, the vibration of the transducer will generate sound in the ultrasonic frequency range.

The earliest form of an ultrasonic transducer was a whistle developed by Francis Galton in 1883 to investigate the threshold frequency of human hearing (Galton, 1883). Sound frequencies are recorded in units of Hertz (cycles per second). The range of human hearing is from about 20 Hz to 20 kHz, where middle C is found at 256 Hz. Ultrasound itself is defined in terms of human hearing, being sound above the upper human hearing threshold, i.e. >20 kHz. The physical upper limit of ultrasound is not easily defined, but is thought to be around 5 MHz for gases and 500 MHz for liquids and solids. The uses of ultrasound within this range can be divided broadly into two categories.

The first area, termed *low power* or *high frequency* ultrasound, is concerned with the physical effects that the material of interest has upon the wave, and is sometimes called *diagnostic ultrasound* (3–20 MHz). The velocity and absorption coefficients of the medium are used for analytical purposes, such as medical imaging and deliberately avoids cavitational events (Gilmore, 1996). The second area, sometimes termed *power ultrasound*, involves *high energy* ultrasound with a range of 20–100 kHz and is generally used for cleaning applications. Sonochemical applications are now operated up to frequencies of 2 MHz, aided by the development of high power equipment capable of causing cavitation in this range.

Cavitation as a phenomenon was first described in 1895 by Sir John Thornycroft and Sidney Barnaby (Thornycroft & Barnaby, 1895). The discovery came as a result of an investigation into the unusually poor performance of a newly built destroyer, HMS Daring, whose top speed was well below design specifications. The problem was traced back to the propeller, where it was found that the rapid motion of the blades caused the surrounding water to rupture and the propeller to loose grip. This problem became of increasing concern to the Royal Navy, who commissioned Lord Rayleigh in 1917 to investigate the problem further. His research concluded that as well as wasting power, the enormous turbulence, heat and pressure produced when cavitation bubbles implode near to a propeller could quickly erode its surface (Lord Rayleigh, 1917). At the same time it was discovered that this was the origin of the familiar sound made when water approaches boiling point.

In the same year, the first commercial application of ultrasound appeared in the form of the 'echo sounder', invented by the Frenchman Paul Langévin. This device was designed to gauge the depth of water beneath a boat's keel and was later improved to detect the presence of enemy submarines, aptly named SONAR (SOund Navigation And Ranging).

Today, ultrasound is used in a wide range of industrial applications including the preparation of emulsion bases for sauces such as mayonnaise and tomato ketchup. A large proportion of ultrasonic equipment is also purchased for welding thermoplastic

components for high volume consumer markets (Rawson, 1987). Ultrasonic welding is carried out at a frequency of around 20 kHz on two pieces of thermoplastic held together under pneumatic pressure. The vibration travels easily through the solid top piece, but when it reaches the smaller contact area at the interface between the two sheets, the energy is concentrated and causes localised melting. When the ultrasound is stopped, heat is quickly dissipated into the bulk causing solidification of the joint. This process can also be applied to aluminium, whose tenacious oxide hinders normal welding operations. However, in this case the metal is not fully melted but instead material is simply made to diffuse between the two pieces.

A further major application of power ultrasound is ultrasonic cleaning. Ultrasound is particularly useful for surface decontamination since powerful microjets caused by cavitation can easily dislodge dirt or bacteria. The rapid cleaning action is also able to penetrate crevices which are inaccessible to conventional cleaning methods. Typical objects cleaned by ultrasound range from large crates used by the food industry, to the delicate surgical instruments used by dentists and surgeons. An interesting example of the advantages of ultrasonic cleaning lies in the raising of the Tudor warship, the 'Marie Rose'. Initially located using sonar, a large ultrasonic cleaning tank helped to quickly and gently clean the 17,000 organic and inorganic objects recovered from the wreck prior to preservation.

Aside from cleaning, power ultrasound is often used for microbiology and biochemistry, where cell walls are disrupted to release their contents for *in-vitro* studies. This process must be carefully controlled as the relatively tough cell wall is only a few microns in diameter and of a similar density to the surrounding medium, whereas the protein and nucleic acids contained within are macromolecules and can be easily denatured. In a similar manner it is also possible to destroy kidney stones (Brannen & Bush, 1984), blood clots (Shlamovitz *et al*, 2003), cancer cells (Shuqun *et al*, 2000), or even stem excessive bleeding (Vaezy *et al*, 1999) in the relatively new field of medicine called therapeutic ultrasound.

High frequency (diagnostic) ultrasound provides a non-invasive means for viewing the body. Typically applied at a high frequency (3-20 MHz), and at low power to avoid cavitation, the most well known example of diagnostic ultrasound is that of foetal imaging (Smith-Bindman *et al*, 2001). The origins of this technique extend back to the 18th century where physicians, who had always listened to the audible sounds of the heart and lungs, introduced a technique known as 'percussion'. Diagnosis of a number of medical conditions was made by tapping on the chest of a patient and listening for a resonant note emitted by an air or liquid filled space. Modern diagnostic methods operate by generating short pulses of high frequency ultrasound which propagate into the body. The pulses proceed in more or less straight lines, until they encounter tissue boundaries where they become scattered and returned to the transceiver. The time difference between launching and receiving the signal is proportional to the depth of the reflecting tissue and varies with its composition, compressibility and density. An image is generated line by line on a two-dimensional greyscale, providing the resolution of features as small as 1 mm.

Of great commercial interest is the use of ultrasound in chemistry. Despite there being reference to the use of ultrasound in polymer and chemical processes as far back as the 1940's (Mark, 1945), the major renaissance of *sonochemistry* did not occur until the last two decades of the 20th century. The reason for this was that ultrasonic baths were now common place in laboratories for the purpose of cleaning soiled glassware and dispersing immiscible organic materials into aqueous detergent. Scientists of all disciplines were now aware of the power of ultrasound and began to consider its role in chemical reactivity. Chemistry is fundamentally an interaction of energy and matter; chemical reactions require energy in one form or another to proceed, stopping altogether as temperature approaches absolute zero. The immense local temperatures and pressures, combined with ultra-fast heating and cooling rates associated with ultrasonic processes, offers a unique set of conditions for chemists to employ (Figure 2.37) (Suslick *et al*, 1999).

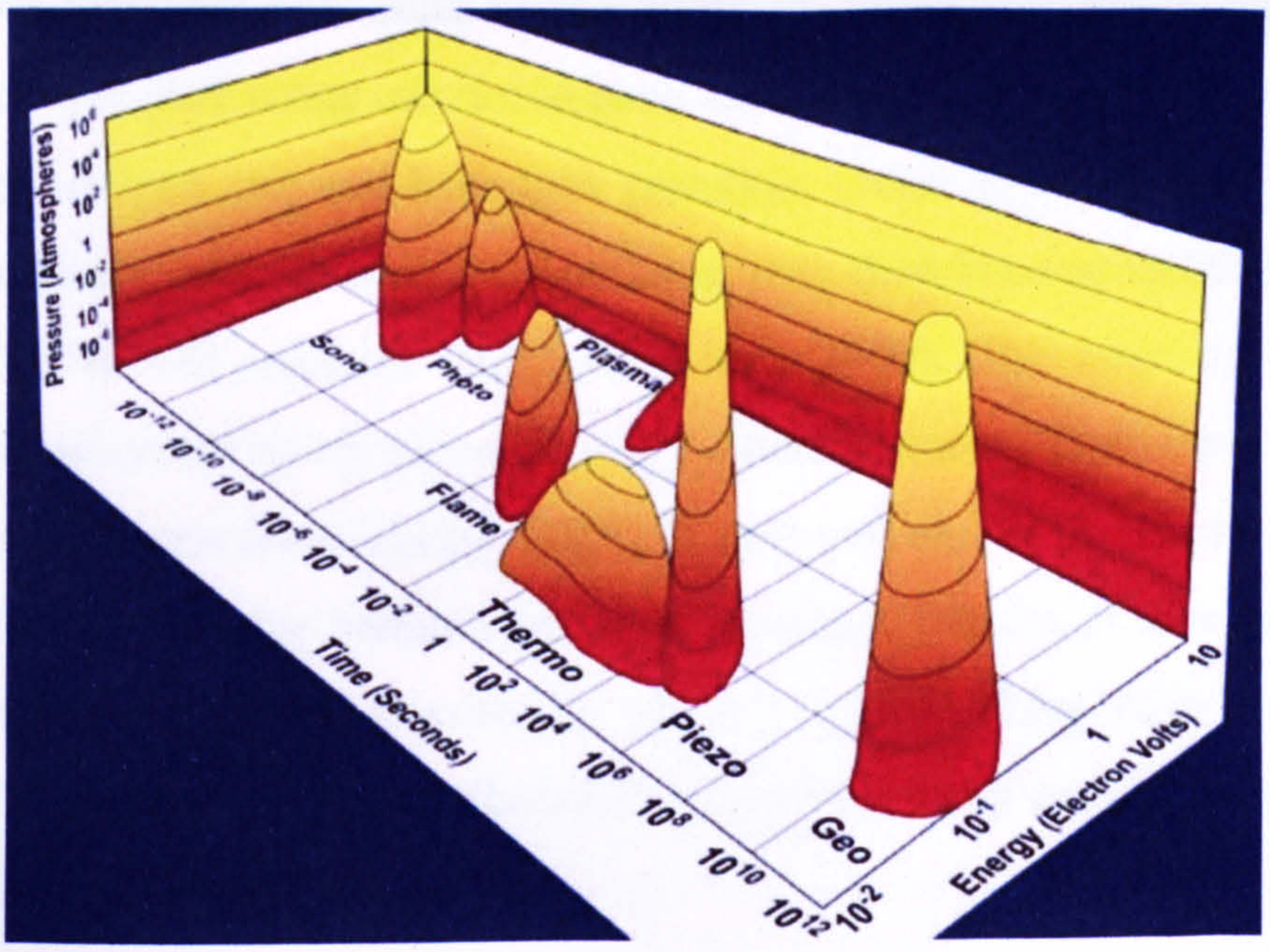

Figure 2.37: Chemistry: the interaction of energy and matter (Suslick *et al*, 1999)

The application of ultrasound to chemical reactions can be broadly divided into two areas: homogenous applications and heterogeneous applications (Figure 2.38).

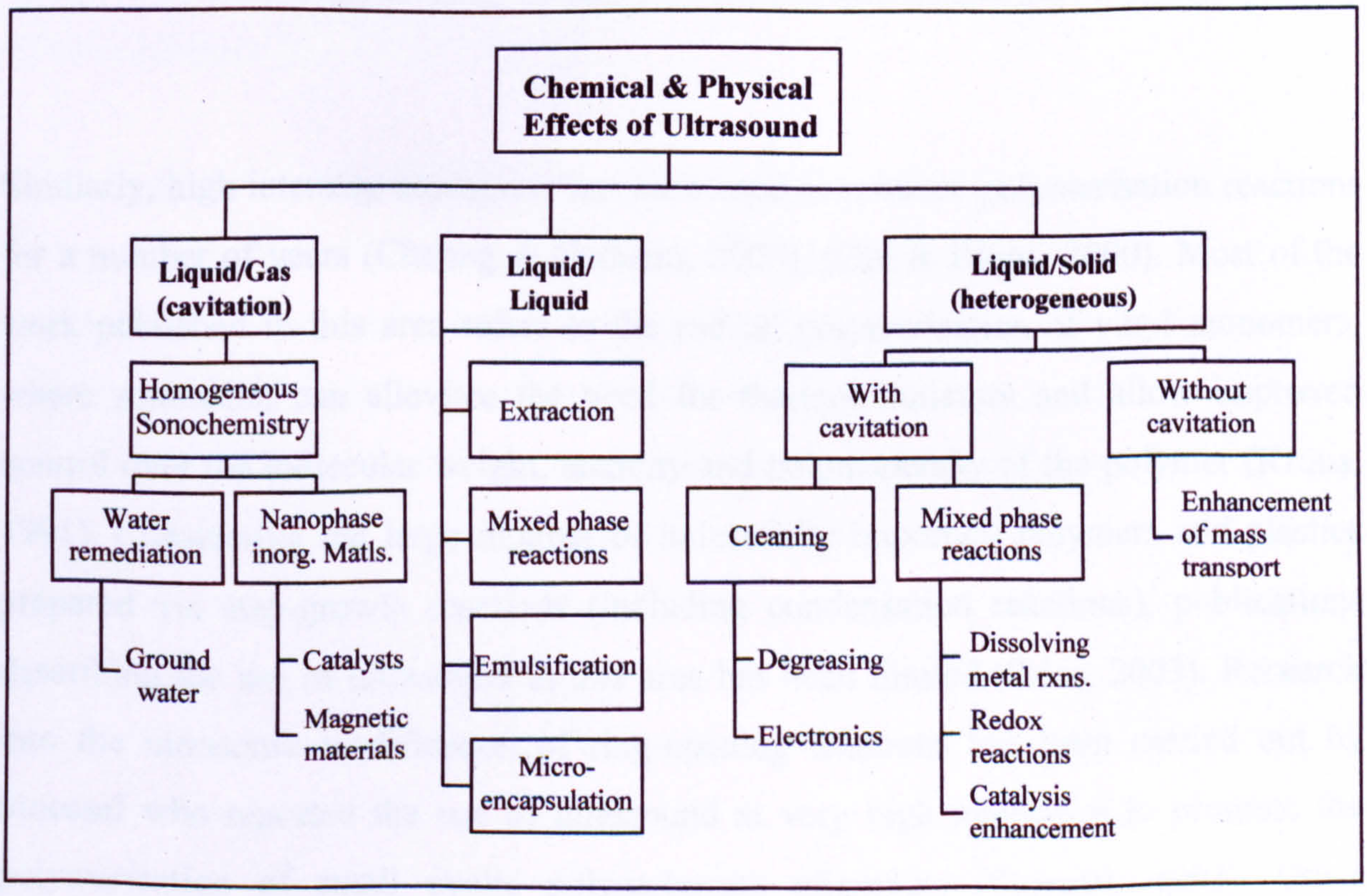

Figure 2.38: Chemistry: the interaction of energy and matter (Suslick *et al*, 1999)

Homogeneous reactions may refer to the effect of ultrasound on the liquid medium alone, for example pure water can decompose with the formation of radical species and production of oxygen gas and hydrogen peroxide. Other aqueous materials present, including inorganic molecules or hydrocarbons, may then become oxidised due to the presence of $H^{\cdot}$ or $OH^{\cdot}$ radicals (Misík & Riesz, 2000). The majority of reactions reported to be enhanced by ultrasound are of the heterogeneous type, involving organic and organometallic reactions (Luche, 1987), (Lindley *et al*, 1987), (Luche *et al*, 1990), (Yinghuai, 2004). Reactive metals such as magnesium, lithium or zinc are employed and reaction rates are often observed to increase tenfold along with a reduction in by-products. Equation 2.66 – 2.68 illustrate a few of the many such reactions enhanced by the application of power ultrasound.

$$C_6H_5Br + Li \xrightarrow{)))} C_6H_5Li + LiBr \qquad 2.66$$

$$C_6H_5CH_2Br + KCN \xrightarrow[Al_2O_3]{)))} C_6H_5CH_2CN \qquad 2.67$$

$$CH_3CH_2CHBrCH_3 + Mg \xrightarrow{)))} CH_3CH_2CH(MgBr)CH_3 \qquad 2.68$$

Similarly, high intensity ultrasound has been used to enhance polymerisation reactions for a number of years (Cheung & Gaddam, 2000), (Ooi & Biggs, 2000). Most of the work published in this area refers to the radical polymerisation of vinyl monomers, where sonication can alleviate the need for thermal initiators and allow improved control over the molecular weight, tacticity and polydispersity of the polymer (Kruus, 1991). Considering the large number of industrially important polymers and plastics prepared via step-growth reactions (including condensation reactions), publications describing the use of ultrasound in this area has been limited (Price, 2003). Research into the ultrasonic modification of ring-opening reactions has been carried out by Stoessel who reported the use of ultrasound at very high intensities to promote the polymerisation of small cyclic polycarbonate oligomers (Stoessel, 1993). Other

ring-opening reactions enhanced by ultrasound include the polymerisation of cyclic siloxanes to silicones (Price *et al*, 1996).

As an additional process parameter, ultrasound can be used to control the molecular weight distribution of polymers via degradation (the irreversible lowering of chain length caused by cleavage) without necessarily causing any chemical change. Although the precise details of the mechanism are not fully understood, this process has still been applied to a number of commercial applications (Mason & Lorimer, 2002). When a cavitation bubble collapses, the pressure wave which is emitted stretches the chain and causing it to break. Cleavage induced by thermal degradation methods results in random breaks along the chain length, whereas sonochemical methods are much more specific and have been shown to cause a preferential mid-chain cleavage providing a more controlled polydispersity (Van der Hoff & Glynn, 1974), (Nguyen *et al*, 1997). Furthermore, ultrasonic degradation occurs faster for higher molecular weights, yet stops almost completely for chains which are smaller than a limiting value for the particular system.

In summary, the application of ultrasound can offer a number benefits to chemical reactions (Mason & Lorimer, 2002):

- A reaction may be accelerated, or require less forcing conditions required
- Sonication allows use of cruder reagents than conventional techniques
- Reactions are often initiated by ultrasound without the need for additives
- In some situations a reaction can be directed to an alternative pathway, possibly reducing the number of steps required in a synthetic route
- Polydispersity can be controlled via ultrasonic degradation

2.4.1 Principles of ultrasound and acoustic cavitation

Sound energy can be transmitted through any substance, solid, liquid or gas, which possesses elastic properties. The movement of the vibrating body (the sound *source*) is transferred to the molecules of the medium, each of which transfers the motion to an adjoining molecule before returning to its original position. Sound takes the form of *longitudina*l waves, i.e. the alternating compression and rarefaction of material in the direction of the travel of the wave (Figure 2.39). In solid materials, atoms can vibrate in any direction creating *transverse* waves, perpendicular to the direction of travel. The inherent ability of a liquid to flow means that there is no restoring force in the transverse direction (i.e. *shear* elasticity), preventing the liquid from supporting shear waves; the liquid nature of the earth's core has been determined by the measurement of these two types of waves following seismic activity.

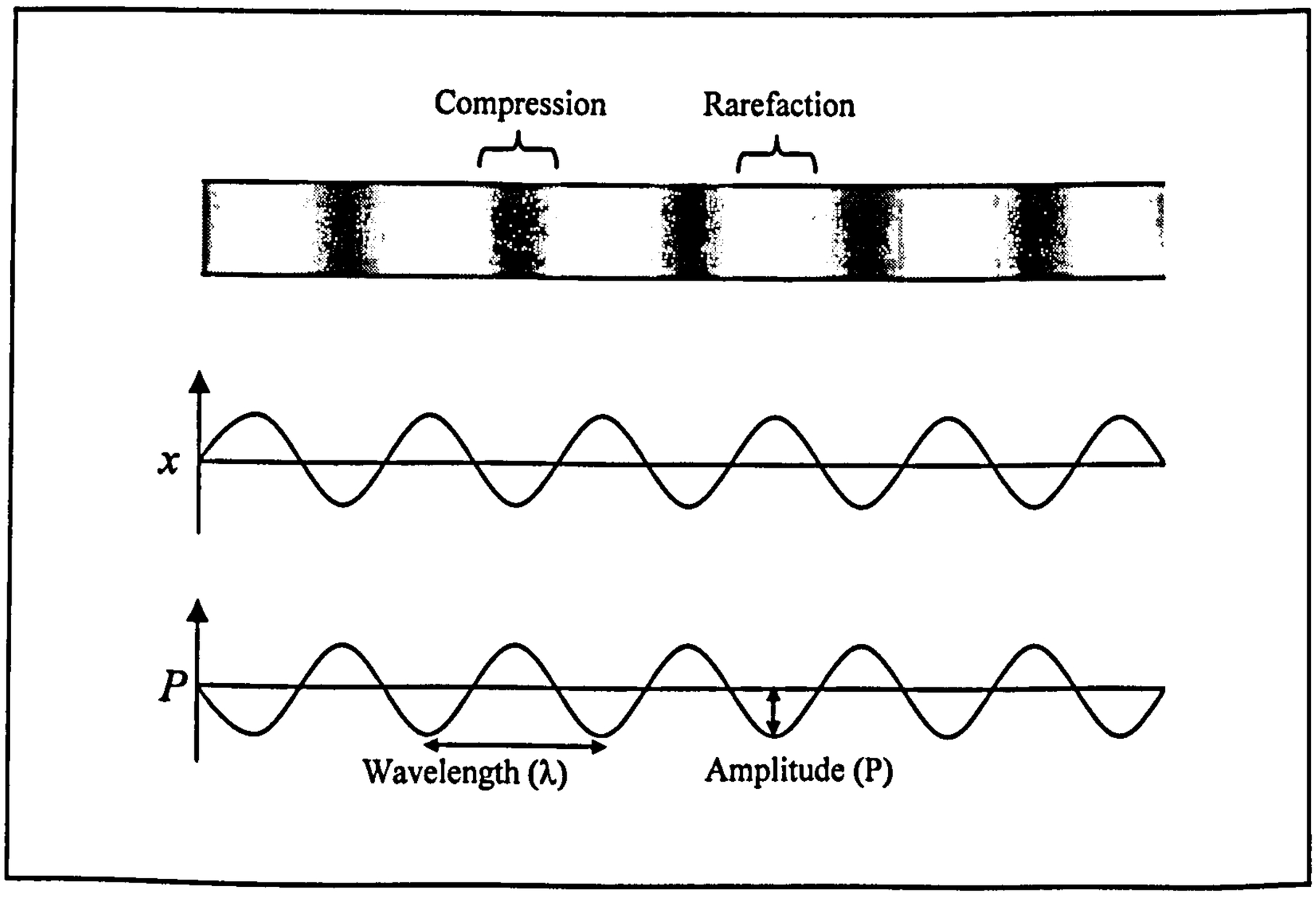

Figure 2.39: The displacement (x) and pressure variation (P) associated with a sound wave

When the frequency and amplitude of the longitudinal wave becomes sufficiently high, the rarefaction stage causes the molecules of a liquid (such as water) to become stretched too far apart too quickly, and the material tears apart, or 'cavitates', to form a bubble. This cavity will grow in size over a few cycles taking in some of the vapour or gas from the medium, a process termed 'rectified diffusion' (Crum, 1984). Because ultrasound passes through water in the form of a wave from a fixed source, positions of maximum and minimum amplitude will occur at multiples of the half wavelength of the frequency emitted. These distances may be easily calculated from the relationship between frequency, wavelength and the speed of a wave through a medium, such as water (Equation 2.69).

$$v = f\lambda \qquad 2.69$$

where v is the velocity of sound through water (~1500 m/s), f is the transducer operating frequency (Hz), and λ is the wavelength (cm).

Once formed, bubble growth will continue until an equilibrium size is reached which matches the frequency of the bubble resonance, a parameter controlled by the applied frequency of sound (Figure 2.40). However, the acoustic field experienced by an individual bubble is not stable because of the interference caused by other bubbles forming and resonating around it. The result is that some bubbles suffer sudden expansion to an unstable size and collapse violently. It is the fate of these cavities when they collapse which generates the energy for the chemical and mechanical effects experienced in an ultrasonic bath or tank.

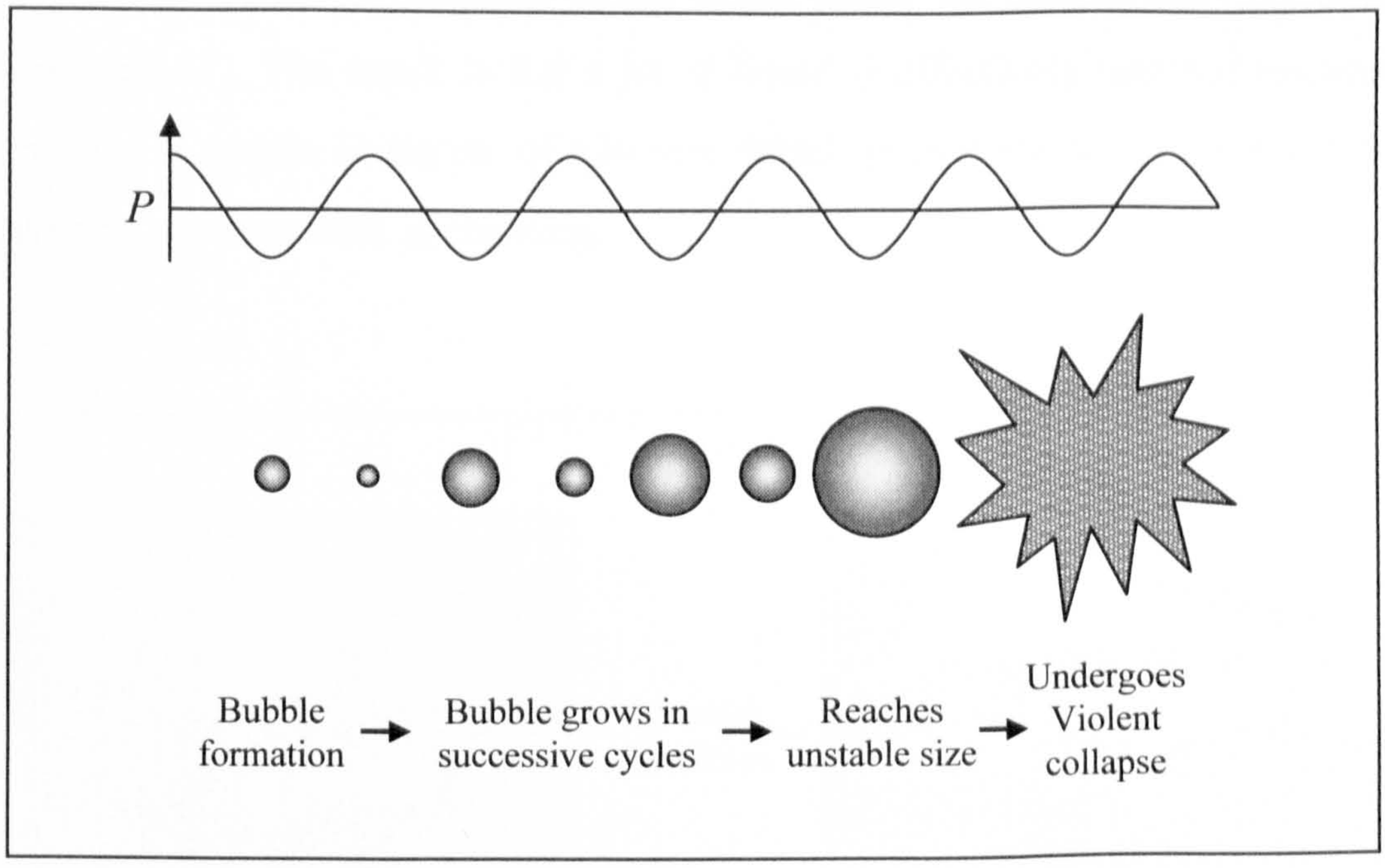

Figure 2.40: The development and collapse of cavitation bubbles

Theoretically, the negative pressure required to cause cavitation in pure water is of the order of 10,000 atmospheres. When an allowance is made for the cavitation bubble to be filled with vapour from the surrounding liquid, cavitation would still require around 1,500 atmospheres. However in practice cavitation can be produced at much lower applied acoustic pressures due to the presence of weak spots in the liquid, such as gas nuclei or suspended particles, which serve to lower its tensile strength (discussed further in Section 2.4.2). Several theories have been developed to explain the energy release involved with cavitation, of which the most understandable in a qualitative sense is the 'hot-spot' approach (Suslick *et al*, 1986). Each cavitation bubble acts as a localised microreactor, generating instantaneous temperatures of several thousand degrees and pressures in excess of one thousand atmospheres. Over the years, cavitation has been classified into types: *stable* and *transient cavitation*. Stable cavities are those bubbles which oscillate, often non-linearly, about some equilibrium size and have lifetimes of the order of tens of cycles. Transient cavities exist for no more than a few acoustic cycles, during which time they expand to at least double their initial radius before collapsing violently inwards within a few microseconds (Neppiras, 1984). When such an event occurs near to any large solid surface, bubble collapse is no longer symmetrical. The presence of a solid surface hinders the movement of liquid

from that side, and so the majority of the liquid enters the bubble from the opposite side (Figure 2.41). The result is that a jet of liquid is effectively targeted towards the solid surface at speeds in excess of 100 m/s, which goes some way in explaining the effectiveness of ultrasound at cleaning.

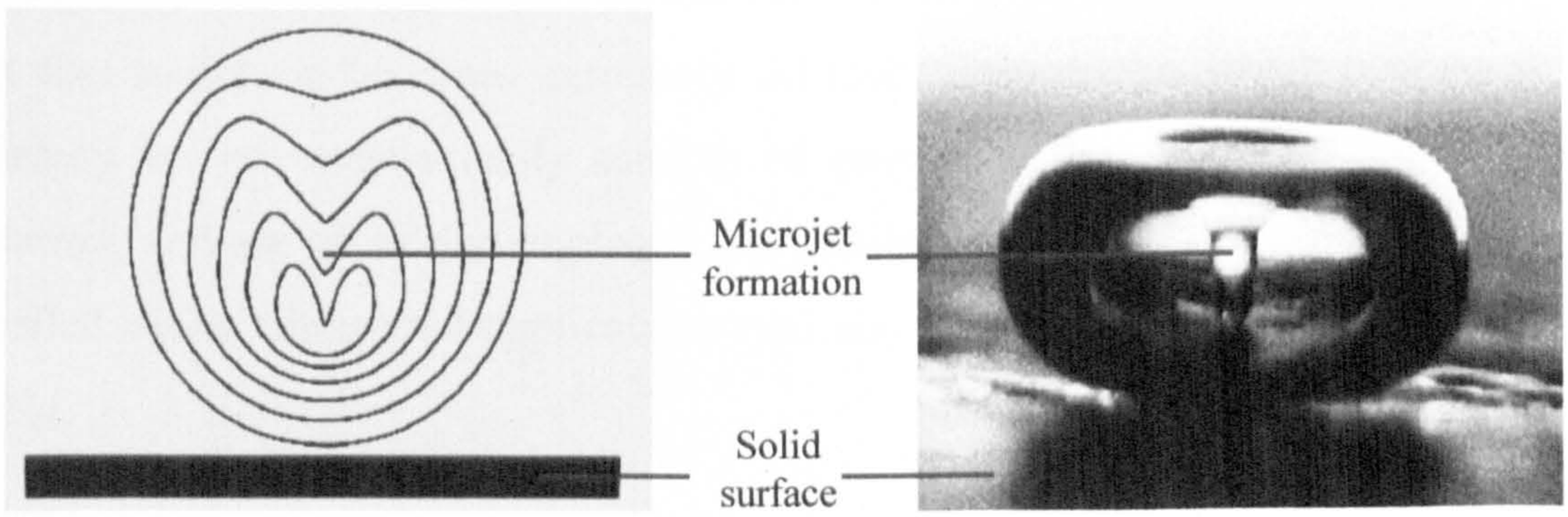

Figure 2.41: Cavitation bubble collapse near a solid surface

In addition to the tremendous forces experienced within a collapsing bubble (or the collision with a microjet), intermediate shear forces are experienced near to the liquid/bubble interface. To a lesser degree, stable cavitation will also contribute to sonochemical effects since the area immediately surrounding the bubble is subject to rapid expansion and contraction.

2.4.2 Factors affecting cavitation

In spite of the great amount of literature published in the field of sonochemistry, only a relatively small number of papers report the influence of reaction conditions on bubble formation and cavitational threshold. The key parameters controlling cavitational events are summarised as follows:

2.4.2.1 Frequency

As the frequency of ultrasound increases, so the rarefaction phase shortens. Consequently, it is necessary to increase the amplitude (power) of irradiation to maintain an equal level of cavitation in the system. In other words, more power is required at higher frequencies if the same cavitational effects are to be observed. When the frequency of the ultrasound reaches the MHz region, the rarefaction phase is so short that cavitation becomes extremely difficult. Transducers which operate at this frequency are not mechanically capable of generating the power required to cause cavitation, and are generally employed for non-invasive medical diagnostic purposes. So-called *power* ultrasound applications typically rely on frequencies between 20 and 40 kHz.

2.4.2.2 Intensity (Amplitude)

The intensity of ultrasonic cavitation is directly proportional to the square of the amplitude of vibration of the ultrasonic source (Mason, 1999). In general, an increase in intensity will provide an increase in cavitation, however, there are limits to the power that can be applied. The first key point is that for a given system, there is a minimum threshold of intensity, below which no cavitation will occur. Secondly, when a significant amount of power is entered into the system, a great number of cavitation bubbles are generated. Many of these will coalesce to form larger, longer lived bubbles which then act as a barrier to the transfer of energy through the liquid. Thirdly, at high vibrational amplitude, the source of the ultrasound will not be able to remain in contact with the solution throughout the entire cycle. Known as decoupling, this results in a great loss of efficiency in energy transfer to the liquid and is more pronounced when large numbers of cavitational bubbles are allowed to build up near the surface of the transmitter. Finally, the materials in the transducer begin to break down causing mechanical failure. An example of the variation of sonochemical efficiency with ultrasound intensity is given in Figure 2.42.

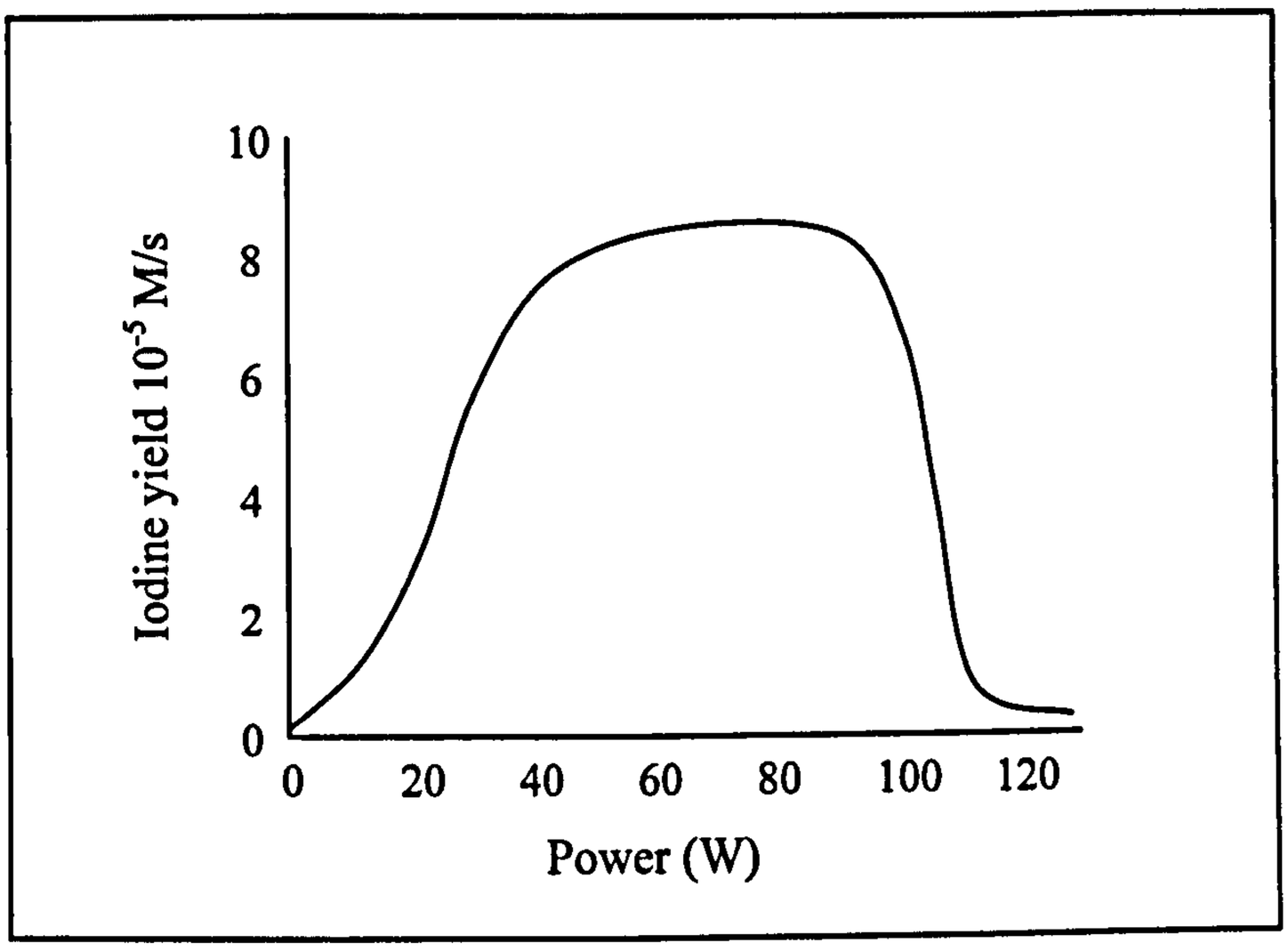

Figure 2.42: Iodine yield as a function of intensity (Mason, 1999)

The example above refers to the yield of iodine from the sonocation of aqueous potassium iodide. The initial reaction can be seen to increase proportionally with power, but the effect is reduced beyond 40 watts and drops dramatically above 100 watts where decoupling occurs. It is noted that this reaction will proceed in the absence of cavitation therefore the cavitational threshold of the solution is not obvious from the curve.

2.4.2.3 Viscosity, surface tension, vapour pressure, temperature and pressure

Cavitation bubbles are formed more easily in liquids of low viscosity, low surface tension and high vapour pressure. Since cavitation produces shear forces in the liquid, and viscosity is a measure of the resistance to shear, increased liquid viscosity makes cavitation more difficult. Bubble formation also requires the creation of a liquid-gas interface, and so a lower surface tension will facilitate the formation of cavitation bubbles and lead to a reduced cavitation threshold. Vapour pressure has two effects on

cavitation. When a cavity is formed, vapour released from the surrounding liquid permeates the interface and enters the bubble, reducing the energy required for cavitation and therefore reducing the cavitation threshold. However, once formed, the vapour present inside the bubble cushions its collapse causing a reduction in energy released. Viscosity, surface tension and vapour pressure are all affected by temperature. As temperature is increased cavitation becomes easier, but the energy released by bubble collapse is reduced. Conversely, increasing external applied pressure will raise the cavitation threshold while providing more energetic bubble collapse.

2.4.2.4 Dissolved gas and particulates

Atmospheric gases will normally be present in a liquid medium and serve to act a 'weak spots' reducing the cavitation threshold while simultaneously reducing power by cushioning bubble collapse. Similarly, suspended particles or impurities in the liquid can act as preferential nucleation sites for bubble formation. This effect may have been noticed when drinking a carbonated drink from a glass vessel. If a certain impurity is present at the surface of the glass, preferential nucleation of carbon dioxide will occur at that site and result in a stream of bubbles arising from the same spot even if the liquid is moved away intermittently. Furthermore, suspended particles often carry trapped vapour in the various recesses and crevices which themselves act as nucleation sites. Dissolved gas removes itself from a liquid during sonocation in the form of stable bubbles slowly rising to the surface (a process frequently carried out deliberately to maximise the cavitational energy in a process). However, it is almost impossible to remove all particulate matter from a system by normal purification methods. This was highlighted by experiments investigating the maximum experimental cavitation threshold of ultrafiltrated water, which achieved values of around 200 atmospheres compared to theoretical values of 1500 atmospheres (Greenspan & Tschiegg, 1967).

2.5 Detection of aqueous Chlorine

The world's population continues to grow, exceeding the six billion mark in the year 2000 (U.S. Census Bureau, 2004). To assist the planet in achieving a population compatible with its limited water supply, nature provides more and more waterborne pathogens such as *Cryptosporidium*, and the newer and more virulent *Giardia*. (Payment *et al*, 1997), (Emmerson, 2001), (Howe *et al*, 2002) (Hashimoto *et al*, 2002). Ever since the first epidemiology studies of cholera outbreaks in London during the 19th century, water quality has been seen as critical to human health across the world (Snow, 1849). Water suppliers use three key barriers to protect public health in this way: source protection, water filtration and disinfection. However, only disinfection can provide the final inactivation of disease-causing microbes.

Generally speaking, there are two methods for disinfection of water: chemical and physical. Physical methods including heating, sonocation (Hua & Thompson, 2000), irradiation with ultraviolet light (Craik *et al*, 2000), electron beam (Borrely *et al*, 1998b), and gamma-radiation (Borrely *et al*, 1998a). These methods are uniformly effective against all pathogens, however high energy demands or unfavourable materials, coupled with the inability to offer disinfection within the distribution network makes these methods less popular for large scale operations. Chemical disinfection methods provide a more suitable means for controlling pathogens in high volumes of water as well as providing a residual disinfection capability within the distribution network.

Historically, the most widely used chemical agent is chlorine, although other agents can be used, such as bromine (Westerhoff *et al*, 2004), iodine (Gottardi, 1999), hydrogen peroxide (Batterman *et al*, 2000), chlorine dioxide (Junli *et al*, 1997) and ozone (Chiang *et al*, 2003), which is often used in conjunction with chlorination. The goal of disinfection is to kill or render harmless the microbiological organisms that cause disease. Chlorine offers protection against a broad spectrum of pathogens and it is likely that a number of mechanisms suggested over the years contribute to its potency:

- *Protein precipitation:* Chlorine precipitates proteins and therefore deactivates essential enzymes

- *Oxidation*: Chlorine diffuses into the cell and oxidizes the cell protoplasm

- *Modification of cell wall permeability*: Chlorine may destroy the cell wall membrane, allowing vital solutes and nutrients, such as nitrogen and phosphorus, to diffuse out of the cell

- *Hydrolysis*: Chlorine hydrolizes the cell wall polysaccharides, weakening it and causing dehydration of the cell

In conjunction with its ability to offer excellent residual protection throughout a distribution system, chlorination is the most commonly employed water disinfection method and is likely to remain so for the foreseeable future (Russell, 1994), (White, 1999), (Binnie *et al*, 2002).

During the 1970's, attention was drawn to the existence of toxic disinfection by-products (DBPs), termed tri-halo methanes (THMs), the most dangerous of which being chloroform ($CHCl_3$), a known carcinogen (Epstein, 1974), (Richardson, 2003). Other disinfection by-products include those formed from the reaction between chlorine and ammonia, such as dichloramines ($NHCl_2$) and trichloramines (NCl_3) which are not particularly dangerous, but impart an unpleasant taste and odour to water. Monochloramine is tasteless and offers a reduced, but functional disinfection capability when compared to chlorine. It also is less likely to form poisonous THMs and is often employed as the method of residual disinfection in distribution networks. The presence of non-living organic material in water systems wastes chlorine and raises the level of unwanted by-products. Utilities companies who operate these systems have to meet both service-level obligations to the customer in terms of taste and odour, and the stringent legal obligations defined by the European Drinking Water Directive (98/83/EC, 1998) which is concerned with the dangers of excessive chlorine,

disinfection by-products, as well as microbial disease. It is little wonder that in 2003 the UK potable water industry modernised 5000 km of water mains, with a third of all capital expenditure invested in water quality enhancement programmes (Mintel, June 2004).

Further to the monitoring and control of potable water, industrial and domestic effluent is generally rich in chlorine. Even tiny amounts of chlorine entering surface water habitats can have disastrous consequences for aquatic life. Although current field measurement methods are inadequate to allow proper enforcement (being generally only accurate to ±0.02 mg/L) the European parliament stipulates a safe concentration of ≤0.005 mg/L total residual chlorine (78/659/EEC, 1997), (2000/60/EC, 2000) in surface waters such as rivers, lakes and estuaries. This creates a major market opportunity for an alternative portable analyser which could resolve to these ultra-low chlorine levels, as well as allowing the protection of our surface water environments. Accordingly the UK Environment Agency is sponsoring Microarray Limited in the development of such a sensor.

Other examples of applications requiring chlorine control include food processing, heating and cooling systems, swimming pools and the paper and textile manufacturing industries. In summary, the total global demand for chlorine in 2003 was 45.9 million metric tonnes, and with prices rising due to increasing energy costs, this exceeded a value of $12 billion (Chemical Market Associates Inc., 2003). Clearly the demand for chlorine tests will be reflected by the size of the chlorine market, and the Water Research Centre (WRc) have estimated that 20 million tests are carried out each day around the world leading to a total annual chlorine-test market value of over $300 million (Hall & Hyde, 1992).

2.5.1 Aqueous chlorine chemistry

As a result of the wide spread use of chlorine in water treatment, a number of comprehensive texts are available describing the chlorination of water (White, 1999), (Haas, 1999), (Binnie *et al*, 2002), (Sincero & Sincero, 2003); an overview focusing on the chemistry of aqueous chlorine disinfection will be presented here.

Chlorine in the form of a gas (Cl_2) can be used for chlorination. When added to water, chlorine rapidly forms a mixture of hypochlorous acid (HOCl) and dissolved hydrochloric acid (hydrogen ions and chloride ions), indicated by Equation 2.70.

$$Cl_{2(g)} + H_2O_{(aq)} \longleftrightarrow HOCl_{(aq)} + H^+_{(aq)} + Cl^-_{(aq)} \qquad 2.70$$

Alternatively, hypochlorite solution (typically sodium hypochlorite) can be added to form hypochlorous acid (Equation 2.71)

$$NaOCl_{(l)} + H_20_{(l)} \longrightarrow NaOH_{(aq)} + HOCl_{(aq)} \qquad 2.71$$

The hypochlorous acid produced is a weak acid ($K=2.8 \times 10^{-8}$) and can dissociate to release the hypochlorite ion (OCl^-) according to Equation 2.72.

$$HOCl_{(aq)} \longleftrightarrow H^+_{(aq)} + OCl^-_{(aq)} \qquad 2.72$$

At equilibrium, chorine can exist in any of these forms which are termed *free available residual chlorine* in proportions controlled primarily by pH, temperature and to some degree the ionic strength of the solution. The dependence of species equilibrium on pH is shown in Figure 2.43.

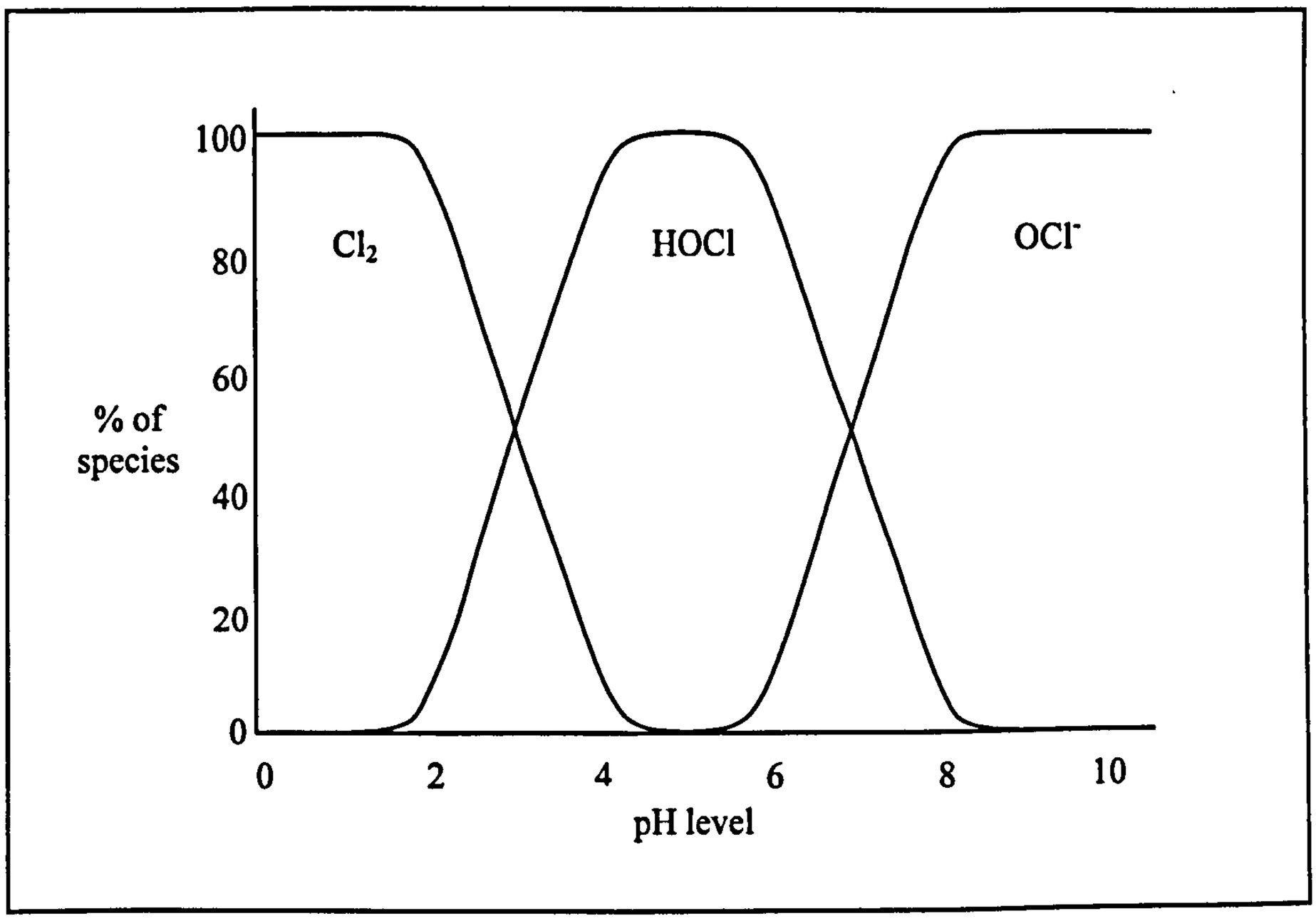

Figure 2.43: The effect of pH on the form of free chlorine in water

Hypochlorous acid has the greatest disinfection potency, thought to be a result of it neutral charge which allows it to more readily diffuse through cell membranes. As a relatively strong oxidising agent, chlorine will also attack molecules containing electron rich sites, such as ammonia, amino acids and nitrites (Palin, 1974). As a result, when free chlorine is added to water containing ammonia, hypochlorous acid will react to form monochloramine, dichloramine, or trichloramine depending on the ratio of chlorine to ammonia (Equations 2.73 to 2.75).

$$NH_3 + HOCl \longrightarrow NH_2Cl + H_2O \qquad 2.73$$
(5 : 1) (Monochloramine)

$$NH_2 + HOCl \longrightarrow NHCl_2 + H_2O \qquad 2.74$$
(7 : 1) (Dichloramine)

$$NHCl_2 + HOCl \longrightarrow NCl_3 + H_2O \qquad 2.75$$
(9 : 1) (Trichloramine)

Monochloramine has very little taste and possesses some disinfection capability. It is also more stable in transit and less likely to form dangerous THM by-products than hypochlorite, and so is frequently used in countries such as the USA and Australia as the main disinfectant carrier (Walker, 2002). Dichloramine and trichloramine contribute bad taste and odour to water, and as a result are considered unwanted disinfection by-products.

However, the majority of water treatment works rely on the more potent *free* chlorine to provide residual disinfection, and as such have to first overcome the organic loading in a system by dosing the water with chlorine beyond its *break point* (Figure 2.44) (Russell, 1994).

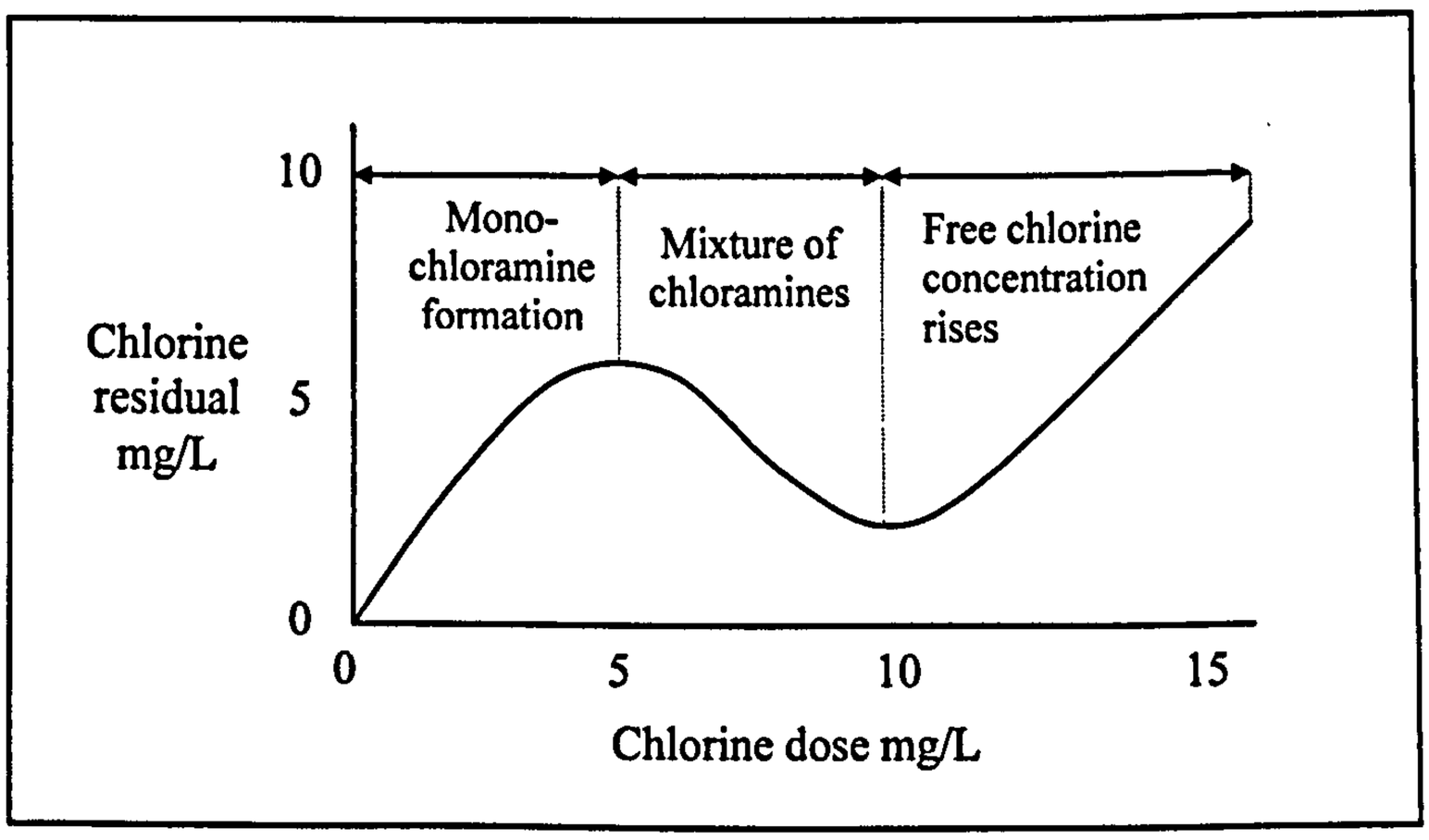

Figure 2.44: The breakpoint curve for disinfection chlorination of water

It follows that, in practice, any chlorine solution is likely to contain a mixture of different species of chlorine. These mixtures are described in terms of *free*, *total* and *combined* chlorine components, and their relationship is described by Equation 2.76:

$$[Total\ chlorine] - [Free\ chlorine] = [Combined\ Chlorine] \qquad 2.76$$

2.5.2 Contemporary methods of aqueous chlorine measurement

There are a number different laboratory and field-based methods used for the analysis of chlorine, each possessing its own particular set of advantages in terms of accuracy, sensitivity to interferents, range of detection and for portability.

2.5.2.1 Iodometric titration (starch-iodide method)

The starch-iodide titration method is one of the oldest methods for determining chlorine concentrations, and is relatively non-specific with respect to oxidising species. It is generally reserved for testing concentrations above 1 mg/L, with a detection limit of approximately 0.15 ppm. The method is based on an initial reaction of chlorine with potassium iodide, which in turn reacts with a thiosulphate solution at around pH 3.5 (Equation 2.77 and 2.78):

$$Cl_2 + 3KI \rightarrow I_3^- + 2Cl^- \qquad 2.77$$

$$I_3^- + 2Na_2S_2O_3 \rightarrow 3I^- + 4Na^+ + S_4O_6^{2-} \qquad 2.78$$

The titration end-point is indicated by the disappearance of the blue-coloured starch-iodide complex. Nowadays, this method is rarely used for the determination of chlorine, except for the assay of high concentration chlorine solutions, such as bleach or chlorine stock solutions (up to around 70,000 mg/L). Studies have shown that using this method, sample temperatures above 20°C can result in significant errors (Hatch & Yang, 1983).

2.5.2.2 Amperometric titration

Amperometric titration involves measuring the current change as a function of titrant added. The standard reducing agent for free chlorine determination is thiosulphate or phenylarsine oxide (PAO) at pH 7. Chlorine becomes reduced at the cathode from the reaction with the titrant (Equation 2.79).

$$PAO + Cl_2 + H_2O \rightarrow PAO(OH)_2 + 2Cl^- + 2H^+ \qquad 2.79$$

In order for current to flow, PAO is oxidised from the +3 to the +5 oxidation state at the anode. While free chlorine (the oxidant) remains present in the solution, a current flows through the cell. Upon consumption of all remaining free chlorine, the rate of change of current approaches zero, indicating the end point of the titration. The amount of titrant required is proportional to the chlorine concentration in the sample. The method can be modified for the determination of combined chlorine by the addition of acidified potassium iodide (pH 4). In this case, mono- and dichloramine liberates a triiodide ion for amperometric reduction (Equation 2.80 and 2.81). There is very little confirmed evidence that trichloramine species can be quantified by liberation with iodide (Gordon *et al*, 1992b).

$$NH_2Cl + 3I^- + H_2O + H^+ \rightarrow NH_4OH + Cl^- + I_3^- \qquad 2.80$$

$$NHCl_2 + 3I^- + H_2O + 2H^+ \rightarrow NH_4OH + 2Cl^- + I_3^- \qquad 2.81$$

The triiodide ion is then titrated with PAO and the current measured amperometrically:

$$PAO + I_3^- + 2H_2O \rightarrow 3I^- + PAO(OH)_2 + 2H^+ \qquad 2.82$$

Equation 2.76 can then be used to deduce the concentration of combined chlorine in the sample.

Various disadvantages exist with this method, primarily concerning the level of accuracy of detecting a titration end-point when dealing with very low concentrations. Although field methods for amperometric titration of chlorine do exist, a high level of required operator skill causes variability in results, and there is uncertainty over the effects of interferents (Harp, 1995).

2.5.2.2 Potentiometric electrode method

This method measures total residual chlorine and is suitable for natural, treated and waste water applications possessing a practical detection limit of approximately 0.05 ppm. The method is based on the potentiometric measurement of free iodine liberated by chorine in acidic conditions. There are known disadvantages to this method including sensitivity to oxidising species other than chlorine (e.g. manganese, bromine and cupric ions). Furthermore, potentiometric analysis equipment is too cumbersome to be used in the field and in a recent comparison with amperometric methods found to be inferior (Hernlem & Tsai, 2000).

2.5.2.3 Syringaldazine method

This method, commonly known as *FACTS* (free available chlorine testing with Syringaldazine), is based on the reaction of 3,5-dimethyl-1-4-hydroxybenzaldazine (syringaldazine) with hypochlorous acid (Figure 2.45) and was developed for the determination of free chlorine only (Cooper *et al*, 1975).

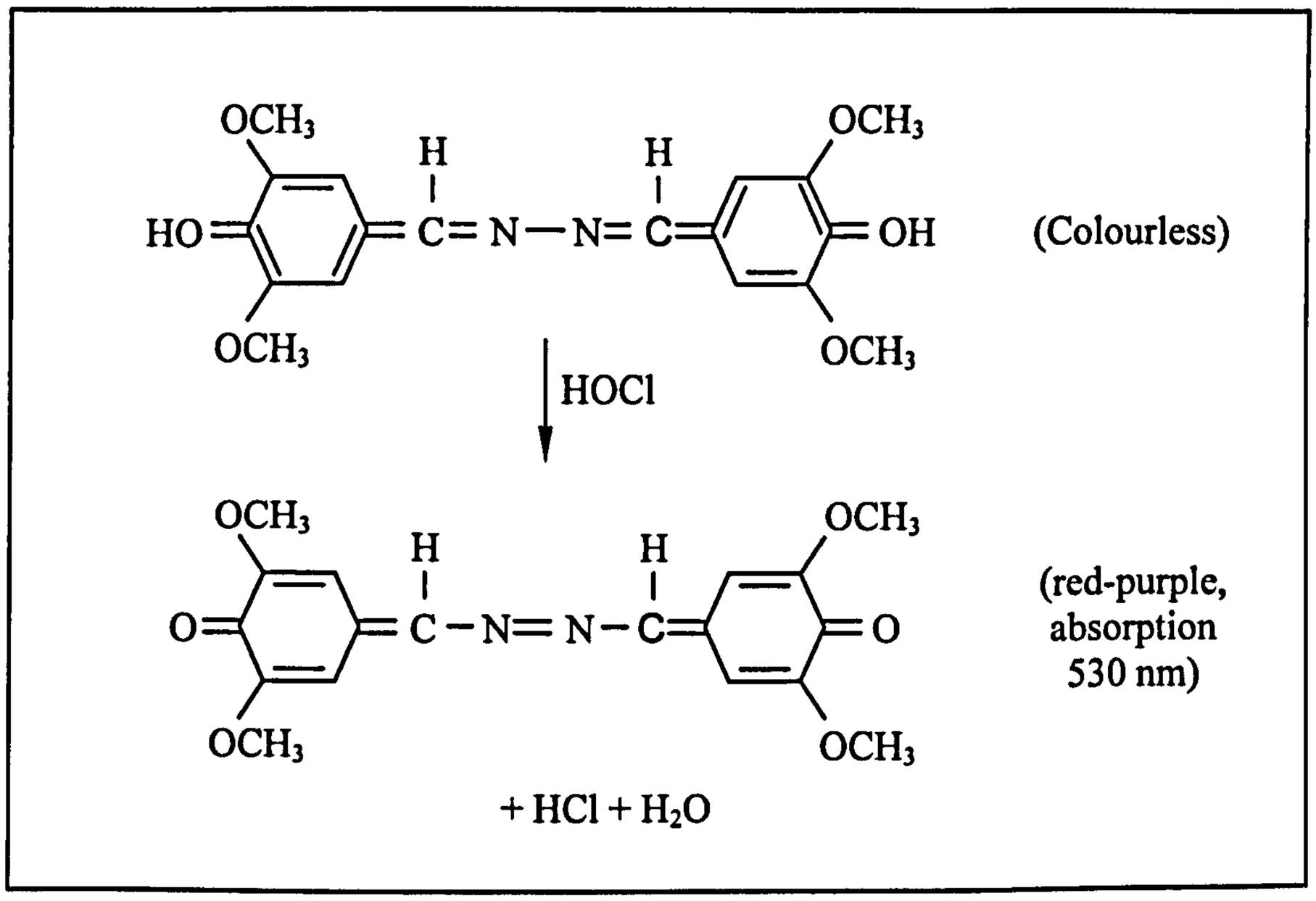

Figure 2.45: Oxidation of syringaldazine by hypochlorite

The sample is first buffered to pH 6.6 with a phosphate buffer and then the syringaldazine indicator, dissolved in propan-2-ol, is added. As the reaction proceeds, a colour change occurs which in turn is measured with a spectrophotometer to allow 0.1 to 10 ppm free chlorine to be measured. This method suffers from interference from strong oxidising agents such as bromine, iodine and ozone, although it suffers little interference from chloramines. However, the limited solubility of the indicator is problematic, and requires gentle heat and ultrasonic agitation for several hours before it will dissolve in the propan-2-ol solvent (which itself must be distilled prior to use to remove impurities). Furthermore, poor storage stability, fading of the indicator during use, and sensitivity to plastics has markedly reduced the popularity of the test method.

2.5.2.4 DPD colourimetric method

First introduced by Palin in 1957, DPD colourimetry is now the most widely used method for both field and laboratory determination of chlorine in water and wastewater

(Palin, 1957), (Wilde, 1991). Measurement is based on a colour changing reaction with DPD (N, N-diethyl-*p*-phenylenediamine) with free chlorine or iodine in the case of combined chlorine (Figure 2.46).

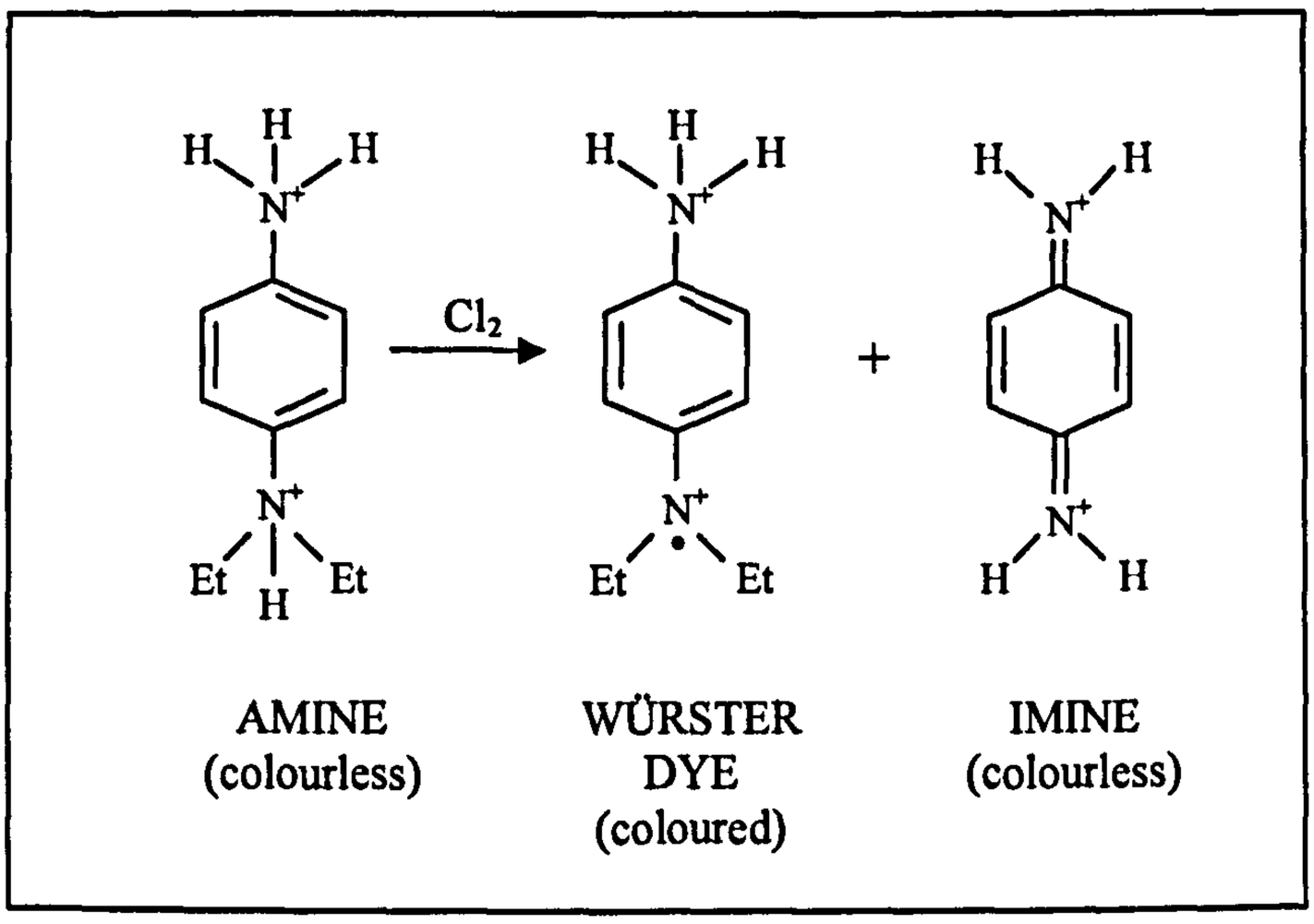

Figure 2.46: The reaction of DPD with chlorine

At approximately neutral pH, the primary reaction product is a stable, semi-quinoid cationic compound known as Wurster dye. It is this product which provides the pink/magenta colour in a DPD colourimetric test, and is proportional to the concentration of chlorine. Chlorine concentration can then be estimated via a colour reference chart (or comparator disc), or by photometric absorption, occurring at a wavelength of 490 to 555 nm. A number of commercial portable photometric colourimeters exist, common examples being the LaMotte™ 1200 Digital Chlorine Analyser Kit, or the Hach™ Chlorine Free & Total Pocket Colorimeter II, illustrated in Figures 2.47 (a) and (b) respectively.

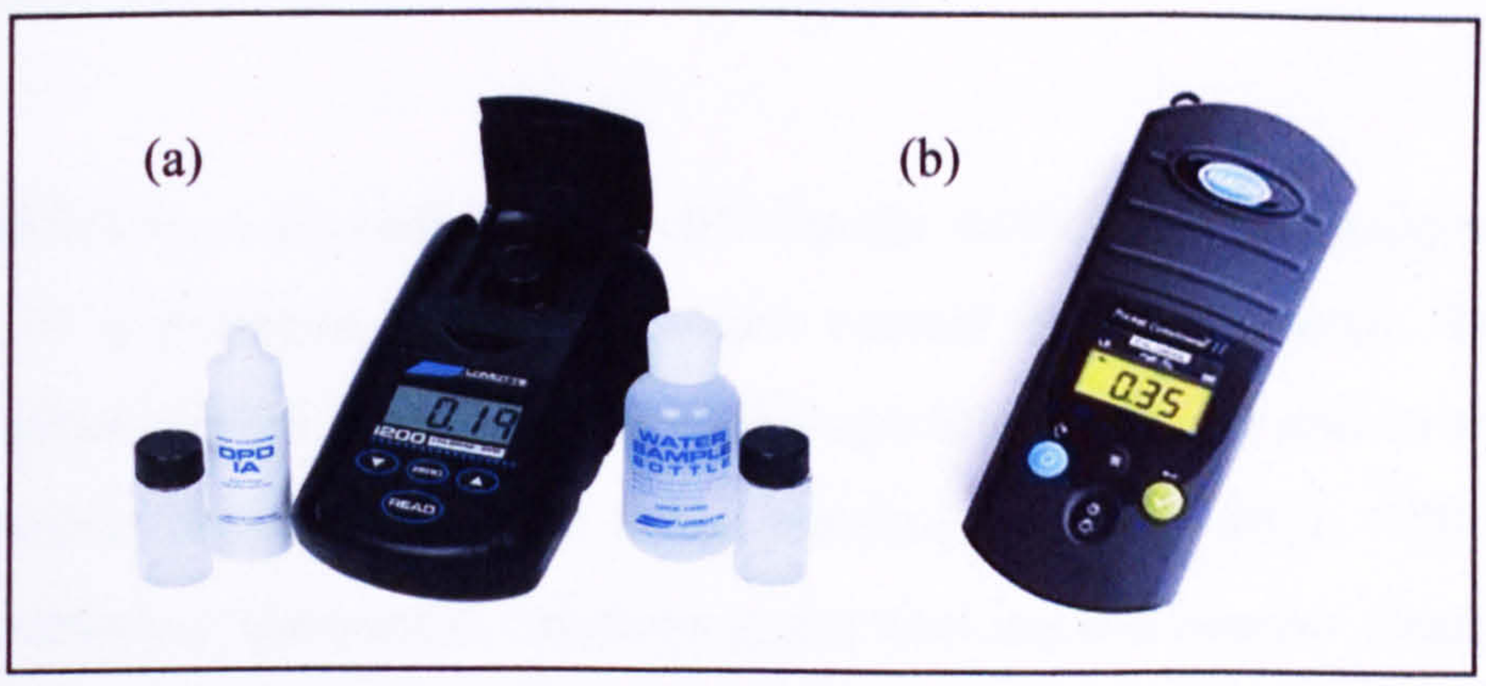

Figure 2.47: (a) the LaMotte™ and (b) Hach™ chlorine analyzer pocket colourimeter kits

These devices have typical ranges of around 0 to 2 ppm free and total chlorine, with accuracies of ±0.02 ppm. It is possible to measure concentrations up to 8 ppm with these devices; however accuracy of the result diminishes to approximately ±0.1 ppm. A drawback associated with DPD technology is that at higher concentrations of chlorine, the formation of the colourless imine product is favoured which causes fading of the solution and the impression of being of a low concentration. Consequently, this can lead to an over-dosing of chlorine which damages equipment and generates a significant health risk, a situation which is mostly likely too occur in privately owned swimming pools.

A further drawback of DPD, however, lies in its susceptibility to other oxidants such as manganese, copper, and iron. This can raise questions over the accuracy of any field measurement undertaken using this method. Furthermore, despite a blank being used prior to sample measurement, the very nature of photometric absorption makes it susceptible to the turbidity of natural waters.

A DPD titration method is also available for the determination of aqueous chlorine. Based on the same chemistry as the DPD colourimetric method, ferrous ammonium sulphate (FAS) is titrated into a DPD/chlorine mixture until the pink/magenta colour has fully disappeared, allowing the concentration to be deduced. This method does not offer any significant improvements over modern colourimetric methods and requires a more complex equipment and operator skill.

2.5.2.5 Potentiostatic amperometric measurement

This method involves the reduction of chlorine (or iodine) in a three-electrode cell by application of a potential and the resultant current being measured. The potential applied is optimised for the reduction of the species of interest and to minimise the effect from other substances present in the solution (typically -80 to -120 mV). In the case of free chlorine, the overall reactions at the working and counter electrodes can be described by Equations 2.82 and 2.84 respectively:

$$HOCl_{(aq)} + 2e^- \rightarrow Cl^-_{(aq)} + OH^-_{(aq)} \qquad 2.83$$

$$2H_2O_{(l)} \rightarrow O_{2(aq)} + 4H^+_{(aq)} + 4e^- \qquad 2.84$$

Combined chlorine will not directly reduce at the electrode surface, so acidified potassium iodide is added to the solution, preferentially oxidising both free chorine and combined chlorine according to Equations 2.85 and 2.86.

$$2I^- + Cl_2 \rightarrow I_2 + 2Cl^- \qquad 2.85$$

$$2H^+ + NH_2Cl + 2I^- \rightarrow NH_4Cl + I_2 \qquad 2.86$$

The iodine generated is then reduced at the working electrode to produce iodide, according to Equation 2.87.

$$I_2 + 2e^- \rightarrow 2I^- \qquad 2.87$$

Provided sufficient iodine is made available, the current measured is proportional to the concentration of total residual chlorine in the mixture. A number of factors will affect the magnitude of the current response. Primarily, as a consequence of the

mass-transport issues described in Section 2.2.4, movement of the solution by forced or natural convection will greatly influence sensor response. As a result of enhanced diffusion and reaction kinetics, temperature will also affect the measured current, increasing by approximately 3% per degree Celsius (at 20°C). A further important factor controlling the current signal is the pH of the cell. A typical response to pH change is shown in Figure 2.48.

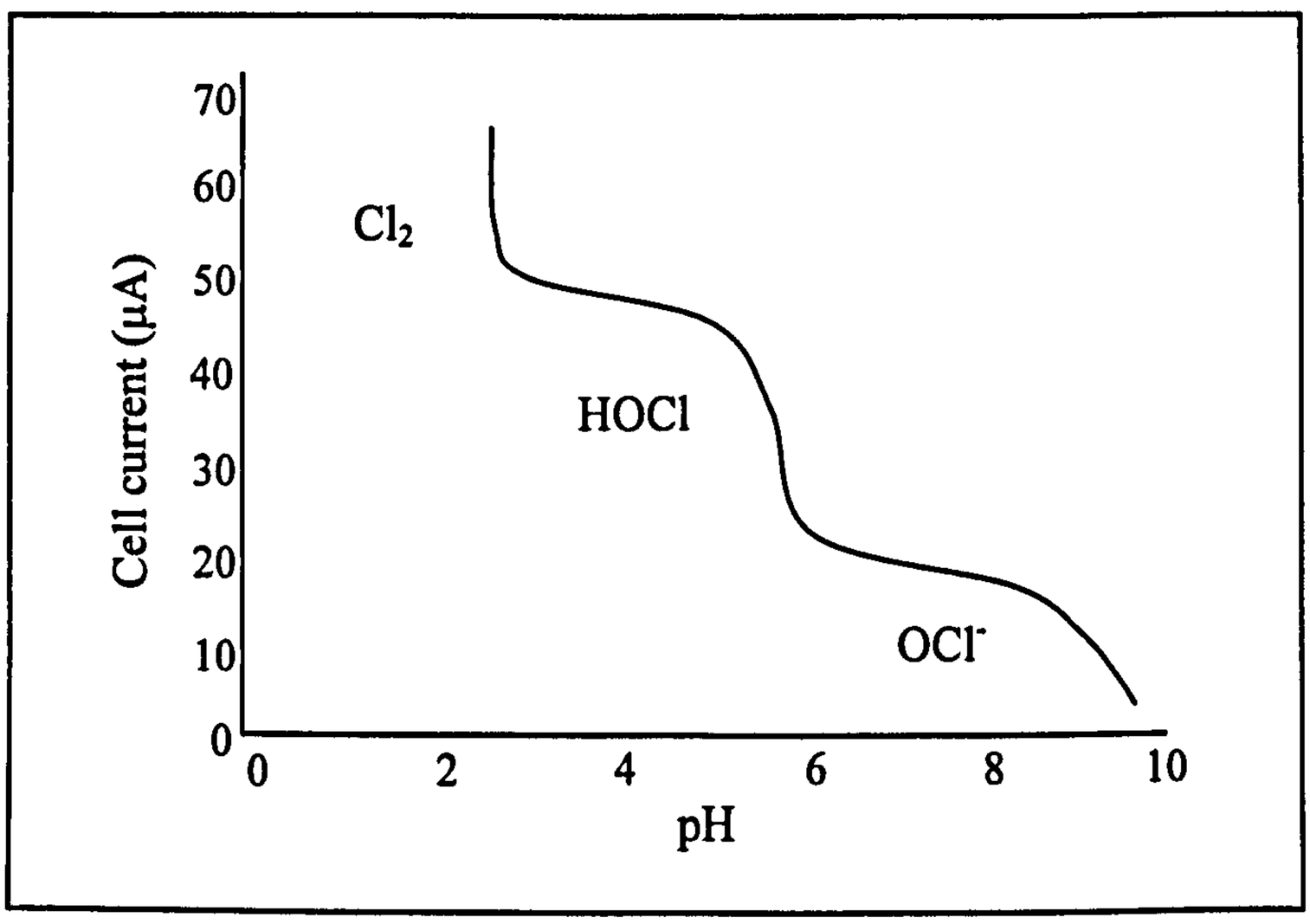

Figure 2.48: The effect of changing pH on amperometric current (0.5 ppm free chlorine)

The three parts of the curve correspond to the three forms of free available chlorine indicated previously Figure 2.43. Since the disinfection capacity of these species differs (for example hypochlorous acid has a greater disinfection capacity than the hypochlorite ion), it is important to be able to report the species of interest. For this reason pH control is an important aspect of potentiostatic amperometric chlorine determination. For free chlorine measurement, it is recommended to buffer the solution to pH 7 since this falls in the plateau region giving the most stable response as well as avoiding significant interference from monochloramine, which begins to occur below this value (Russell, 1994). In the case of total chlorine measurement, where the reaction with iodide is carried out in an acidified mixture containing both free residual

chlorine and iodine liberated via reaction with chloramines, pH 4 is selected, which corresponds to the hypochlorous acid species plateau.

It has been shown that there is currently no ideal method for chlorine detection available. The American Water Works Association have suggested fourteen idealised qualities for an aqueous chlorine analyser (Gordon *et al*, 1992a):

1. The method must be specific to the species (e.g. free and combined chlorine)
2. Possesses a selectivity of at least 500 times over possible interferences
3. Have a detection limit of 1 ppb as Cl_2
4. Possess a precision of ±0.1% or better
5. Have an accuracy of ±0.5% or better
6. Exhibit a linear working range of four orders of magnitude
7. Hold performance with any sample matrix
8. Have no requirement for sample dilution to minimise interferences
9. Work with both manual and automated modes
10. Have a maximum sensitivity with traditional laboratory instruments
11. Require no specialised skills required to perform the test
12. Have reagent stability in excess of one year
13. Exhibit performance of the test within one minute
14. Be cost effective

It is worth noting that, given the unstable nature of chlorine, the accuracy of a test will be enhanced if it is able to be carried out at the point of sampling. The valuable feature of *portability* appears to be missing from the ideal qualities of an aqueous chlorine analyser listed above by Gordon *et al*.

CHAPTER 3

Experimental Methodology

3.1 Reagents

Chloramine-T, orthophosphoric acid and sodium hypochlorite solution (all GPR grade), sodium thiosulphate solution 0.1 N, disodium hydrogen orthophosphate 12-hydrate, sodium acetate, sodium carbonate, sodium chloride, sodium dihydrogen orthophosphate 1-hydrate and zinc iodide/starch solution (all analytical grade) were purchased from BDH Laboratory Supplies (Poole, UK).

Acetic acid (glacial), ferrocenecarboxylic acid, gold(I) cyanide, hexaammineruthenium(III) chloride, Luminol, *o*-phenylenediamine dihydrochloride, potassium ferricyanide(III) (all analytical grade) were purchased from Sigma-Aldrich (Gillingham, Dorset, UK).

Potassium chloride, potassium hydroxide, potassium hydrogen phosphate and potassium iodide (all analytical grade) were purchased from Fisher Scientific (Loughborough, Leicestershire, UK).

3.2 Materials

Menzel® 'Superfrost' frosted microscope slides (76 x 26 mm) were purchased from Fisher Scientific (Loughborough, Leicestershire, UK) and were used for the construction of gold-sputter coated working and counter electrodes.

Epoxy resin (Araldite®) and Acheson Electrodag® (1415M) silver conductive paint were purchased from AGAR Scientific Ltd. (Stansted, Essex, UK) and was used for the construction of gold sputter-coated working and counter electrodes, and for the preparation of electron microscopy samples.

Aluminium pin stubs (12.5 mm diameter, 8 mm pin length) and carbon adhesive discs (12 mm diameter) were purchased from AGAR Scientific Ltd. (Stansted, Essex, UK) and used for the preparation of electron microscopy samples.

Multicore copper wire was purchased from Maplin Electronics (Luton, Bedfordshire, UK) was used for the construction of gold sputter-coated working and counter electrodes.

A silver/silver chloride (Ag/AgCl) reference electrode possessing an ion-selective frit was obtained for total chlorine investigations (silver/silver chloride reference type: REF321/XR300, Radiometer Analytical S.A., Villeurbanne, France).

Stainless steel gauze ('20 mesh, plain weave') was obtained from Fine Mesh Metals (Brierley Hill, West Midlands, UK) and was used as a counter electrode for a polymerisation cell.

Perforated stainless steel type 304 sheeting (hole diameter 3 mm hexagonal arrangement, pitch 5 mm, thickness 1 mm) was purchased from RM Perforating Ltd. (Warrington, UK) and was used for ultrasound baffling during sonocation.

Carbon paste electrodes (product code C2001222R5) were supplied by Gwent Electronic Materials Ltd. (Pontypool, Gwent, UK) for initial investigations into the amperometric response of carbon paste to chlorine (Figure 3.1). Working electrode area is 9 mm^2 if defined by dielectric (as shown).

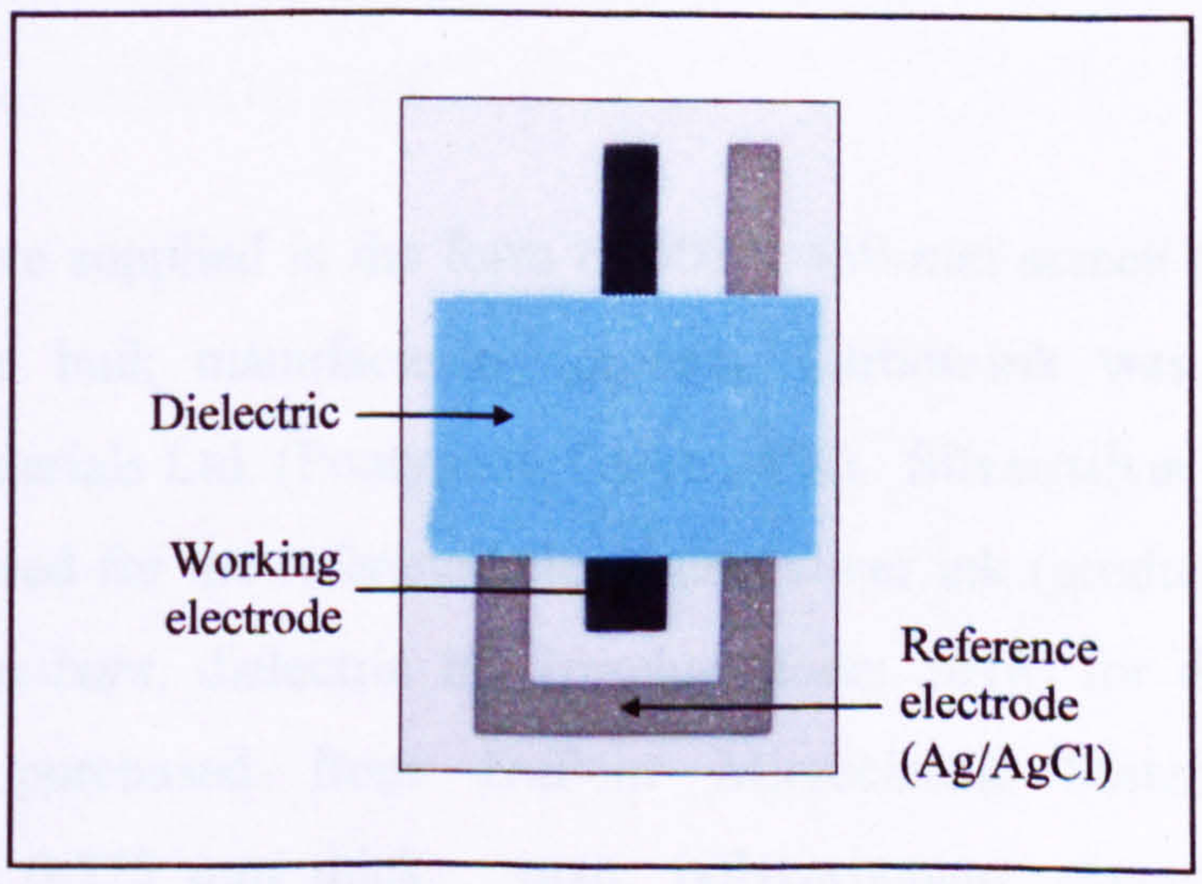

Figure 3.1: A GEM 'hockey stick' carbon paste electrode

Subsequent electrodes were screen printed at Polyflex Circuits Ltd. (Parlex Corporation, Newport, Isle of Wight, UK). Sensors are based on a 3-electrode construction and are suitable as generic disposable sensors for a range of applications (Figure 3.2). An additional working electrode was included to allow the measurement of both free and total chlorine.

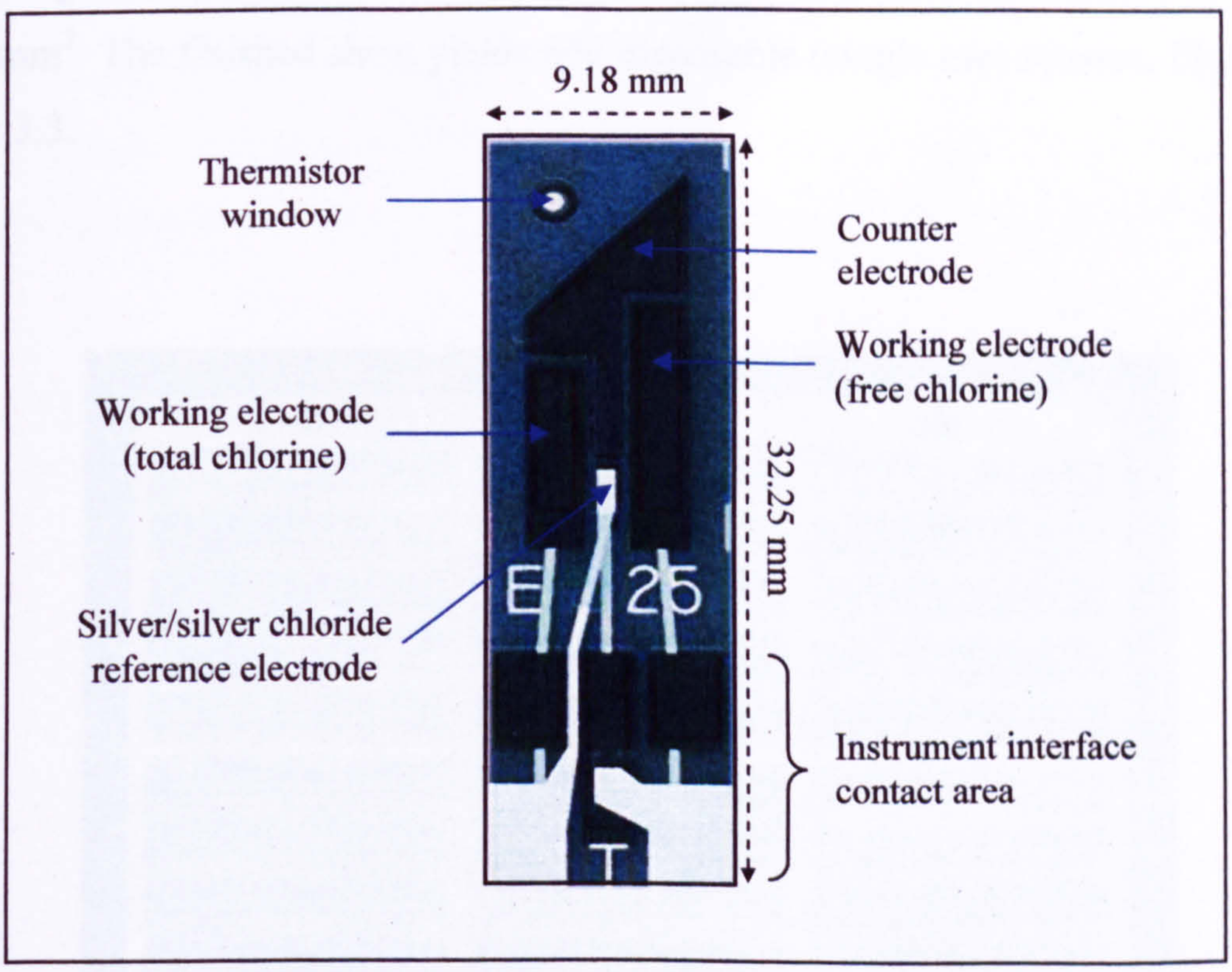

Figure 3.2: A single disposable sensor

Electrodes were supplied in the form of 600 x 450 mm screen printed sheets (Figure 3.4) from the bulk manufacturing process. Carbon-ink was supplied by Gwent Electronic Materials Ltd. (Pontypool, Gwent, UK). Silver/silver chloride ink (product code: 5874) used for the reference electrodes, silver ink (product code: 5028) for the conductive *bus-bars*, dielectric ink (product code: 5018) for defining the electrode areas were purchased from DuPont Microcircuit Materials (Bristol, UK). 600 x 450 x 0.375 mm thick matt polycarbonate sheets (Cadillac Plastics, Swindon, UK) were purchased to provide the substrate for electrode printing. Screen

printing was carried out by Polyflex Circuits Limited (Parlex Corporation, Newport, Isle of Wight, UK). Operational parameters, including silk screen mesh size, tension, and squeegee angle, pressure and speed will not be documented as they remain commercially confidential.

Working electrode geometries of finalised sensors are 8.82 mm^2 and 12.96 mm^2 for the total and free working electrodes respectively, providing a combined two-dimensional total working electrode area of 21.78 mm^2. The equivalent area of the counter electrode is 26.92 mm^2. The finished sheet yields 600 disposable (single use) sensors, illustrated in Figure 3.3.

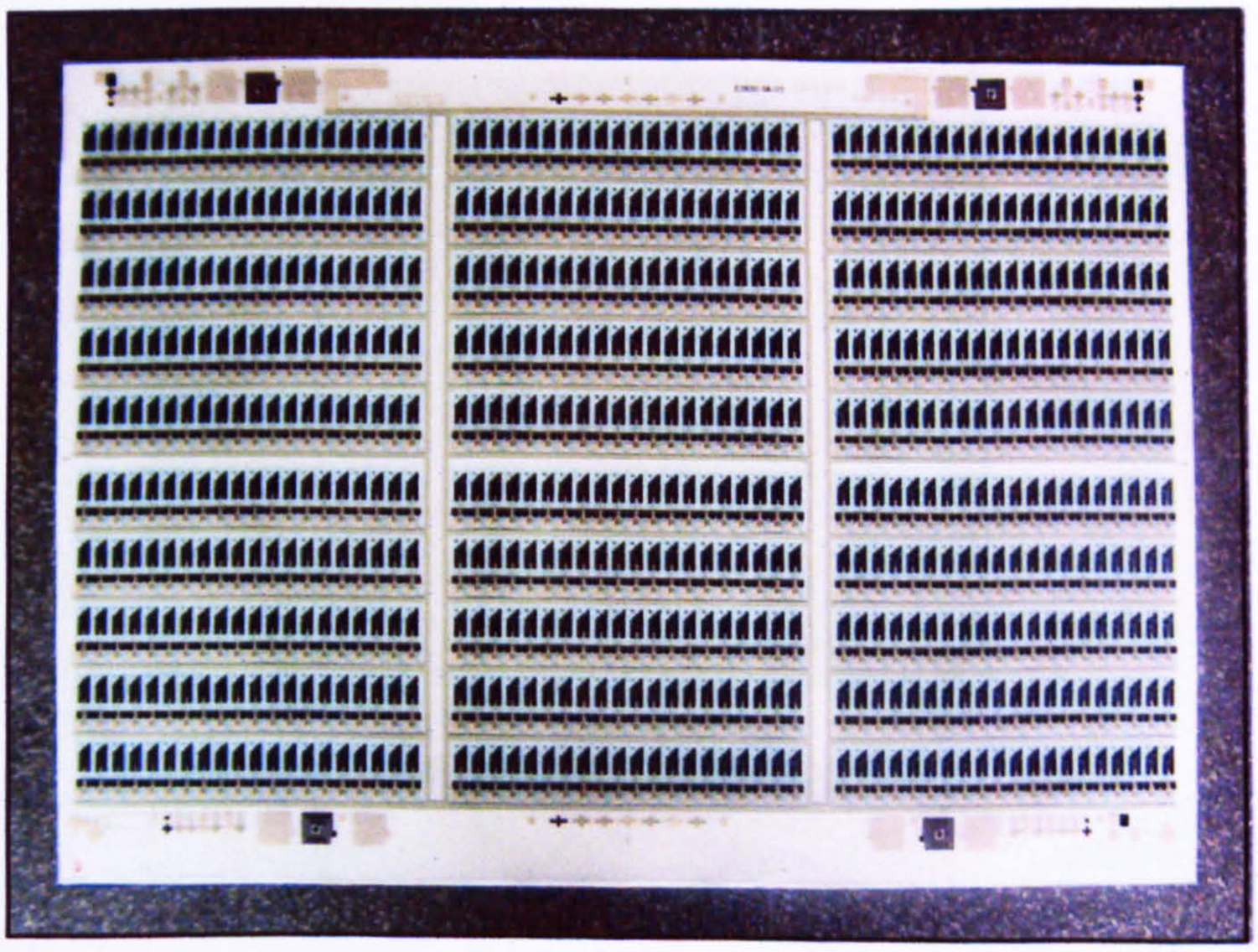

Figure 3.4: 600 x 450 mm sheet containing 600 disposable sensors

3.3 Experimental apparatus

In addition to standard laboratory equipment, the various apparatus used in the development of the chlorine sensor will now be discussed.

3.3.1 Gold sputter coating

An Agar B7341 Automatic Sputter Coater (Agar Scientific Ltd., Essex, UK), in conjunction with a Pfeiffer Rotary Vane Vacuum Pump (Pfeiffer Vacuum Ltd., Newport Pagnell, UK), was used for the preparation of gold sputter-coated working and counter electrodes and samples for investigation under SEM (Figure 3.5).

Figure 3.5: Agar scientific gold sputter coater

3.3.2 Potentiostats

A Sycopel Analytical Electrochemical Workstation Model AEW2-10 potentiostat (Sycopel Scientific Ltd, Washington, Tyne & Wear, UK) controlled by a PC equipped with an ECProg3 (version 3.60) software program was used for all laboratory scale electrochemical studies.

Figure 3.6: Sycopel AEW2-10 potentiostat

A custom-designed 40-channel potentiostat system (200 mA max per channel, single reference and counter electrode inputs), with an integrated PC control system was used for the electropolymerisation of sheets of sensors (Sycopel Scientific Ltd, Washington, Tyne & Wear, UK).

Figure 3.7: Sycopel multi-channel potentiostat

3.3.3 Ultrasonic Tanks

Sonication experiments were performed using a custom built 2 kW, 25.1 kHz ultrasound tank (Figure 3.8) with internal dimensions of 750 x 750 x 600 mm (working volume 750 x 750 x 500 mm) unless otherwise stated (Ultrawave Ltd., Cardiff, UK). The tank incorporates a frequency sweep of ± 1 kHz in 100 Hz steps three times per second, and a temperature control system allowing the temperature of the water to be maintained at 25°C. Software incorporated within the power generation system allows sonocation time to be varied between 1 and 99 seconds and for the power to be varied between 50 and 100 % of the maximum power output. The software also supports a square wave sonic pulse (50% duty cycle) to facilitate de-gassing of the water, which is carried out for 60 minutes prior to use.

Figure 3.8: Custom built 2kW ultrasound tank

As purity of the water is critical to the efficiency of the cavitation process, ultrasound tank water is continually purified via a 100 μm particulate filter, a 'CC9' carbon filter and a 'DC9' deioniser (Purite Ltd., Thame, Oxfordshire, UK), producing water with a conductivity of <0.1 μS.cm^{-}1 (>18 MΩcm^{-1}), confirmed by an integrated conductivity meter.

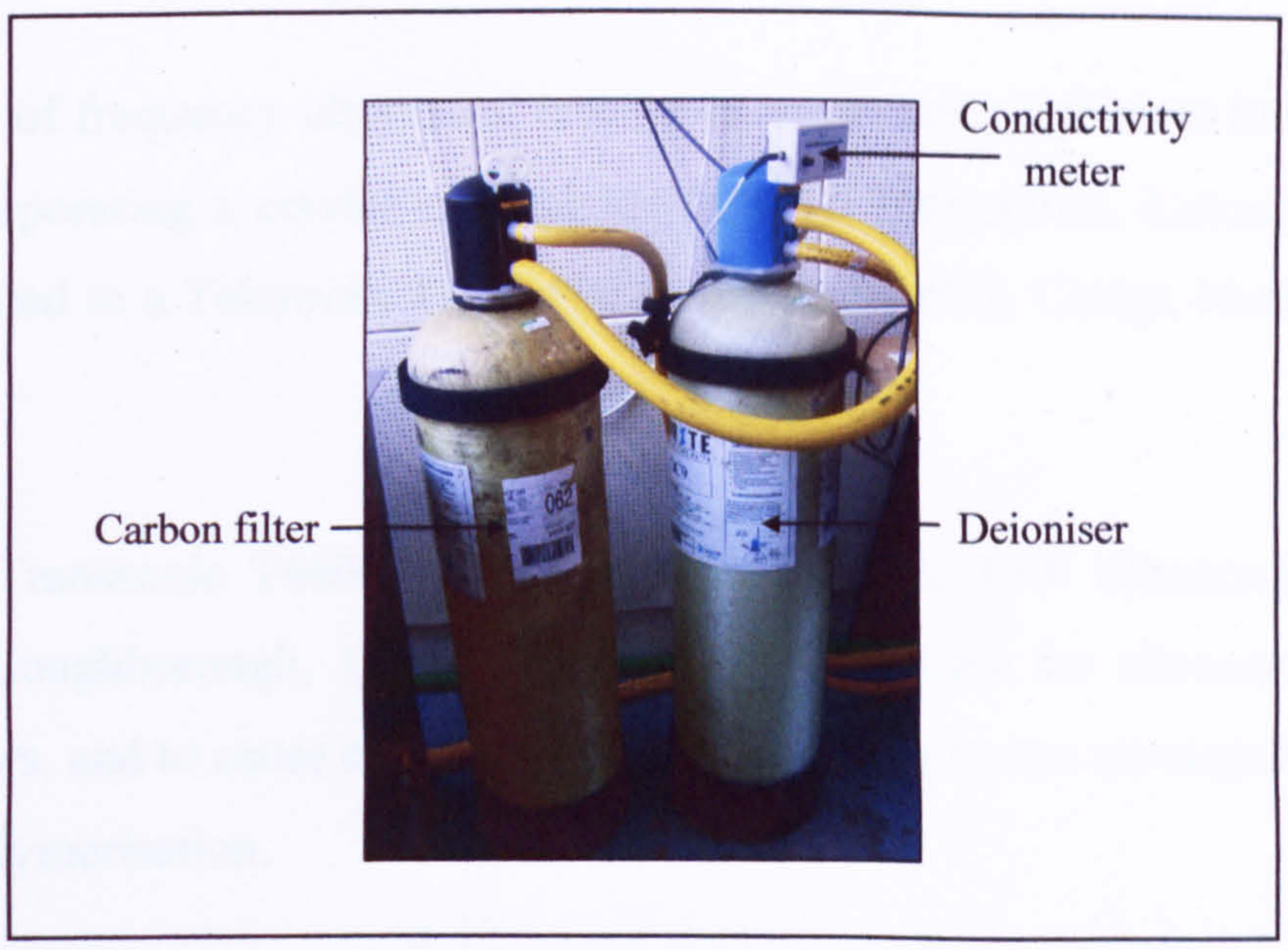

Figure 3.9: Water purification system for 2kW ultrasound tank

A perforated stainless steel baffle was also designed to reduce the formation of standing waves and wave reflections from the tank walls, thus improving ultrasound homogeneity (Figure 3.10). Baffle sides were set at a distance of 50 mm from tanks walls, including the base which was separated by vibration damping rubber feet. The baffling was employed during all sonocation procedures unless otherwise stated.

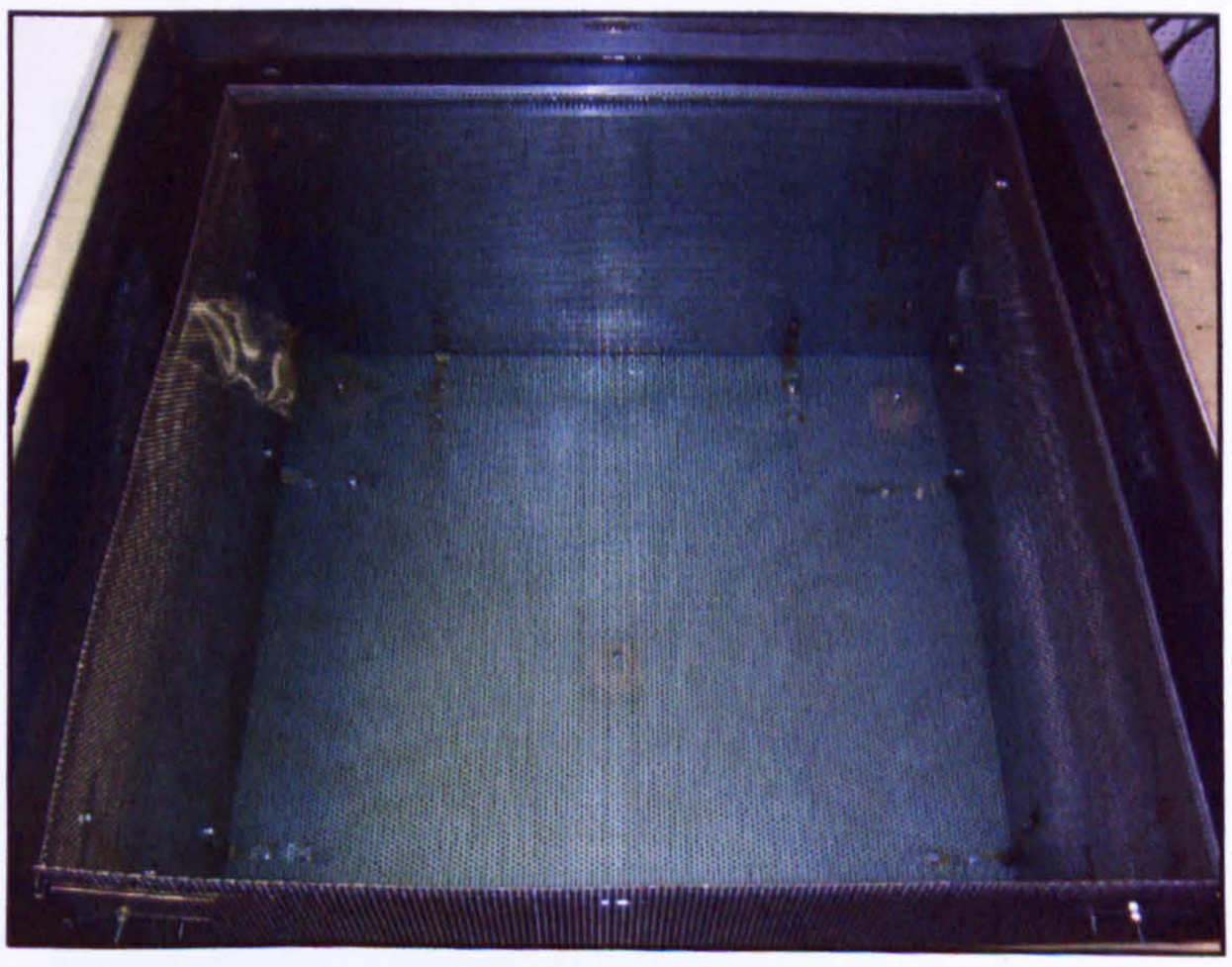

Figure 3.10: Ultrasound tank baffling

Verification of frequency ultrasound tank were made using a custom built hydrophone system incorporating a crystal microphone (Maplin Electronics, Luton, Bedfordshire, UK) connected to a Tektronix TDS 1002 oscilloscope (RS, Corby, Northamptonshire, UK).

A Camlab Transsonic T460, 4 litre capacity, 25 kHz, 30W ultrasonic bath (Fisher Scientific, Loughborough, Leicestershire, UK) was used for ultrasonic ablation of single sensors, and to cause complete wetting of sensors by the monomer solution prior to electropolymerisation.

3.3.4 Microscopy

An Olympus SZX12 bifocal microscope (max 90x magnification) incorporating a Schott KL1500 LCD light source, and a KPM1E/K CCD camera with Leutron Vision PicPort Color image frame grabber was used for all light microscopy analysis (Figure 3.12). A Philips XL30 FEG-SEM was used for all scanning electron microscopy. Atomic force microscopy was carried out on a Veeco Explorer AFM.

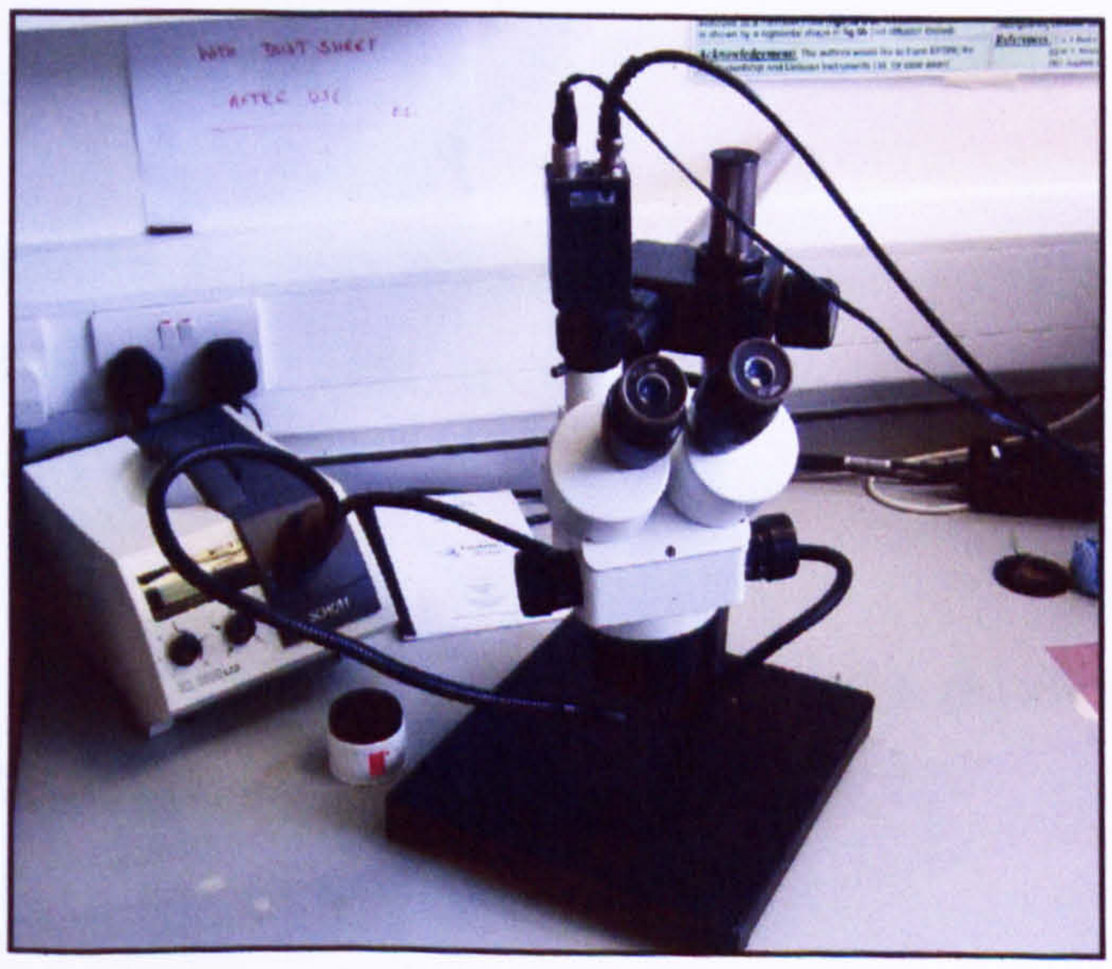

Figure 3.11: Olympus SZX12 microscope with Schott KL1500 light source

3.3.5 Chlorine concentration validation

A Hach® Pocket Colourimeter™ Chlorine Analysis System (cat no. 467000, Camlab, Over, UK) was used as a standard measurement for chlorine concentration (Figure 3.12).

Figure 3.12: Hach™ pocket colourimeter chlorine test kit

3.3.6 Chemical layer deposition

A BioDot Inc. AD3200™ dispense platform (350 x 425 x 800 mm range, 0.05 mm positioning repeatability) was used in conjunction with a BioJet Plus™ 3000 dispensing system (20 nL to 250 µL drop volume, ±7% accuracy) incorporating synQuad™ syringe pump technology, and controlled by PC driven AxSys™ software for the deposition of chemical modifying layers (Europe BioDot Ltd., Huntingdon, Cambridgeshire, UK).

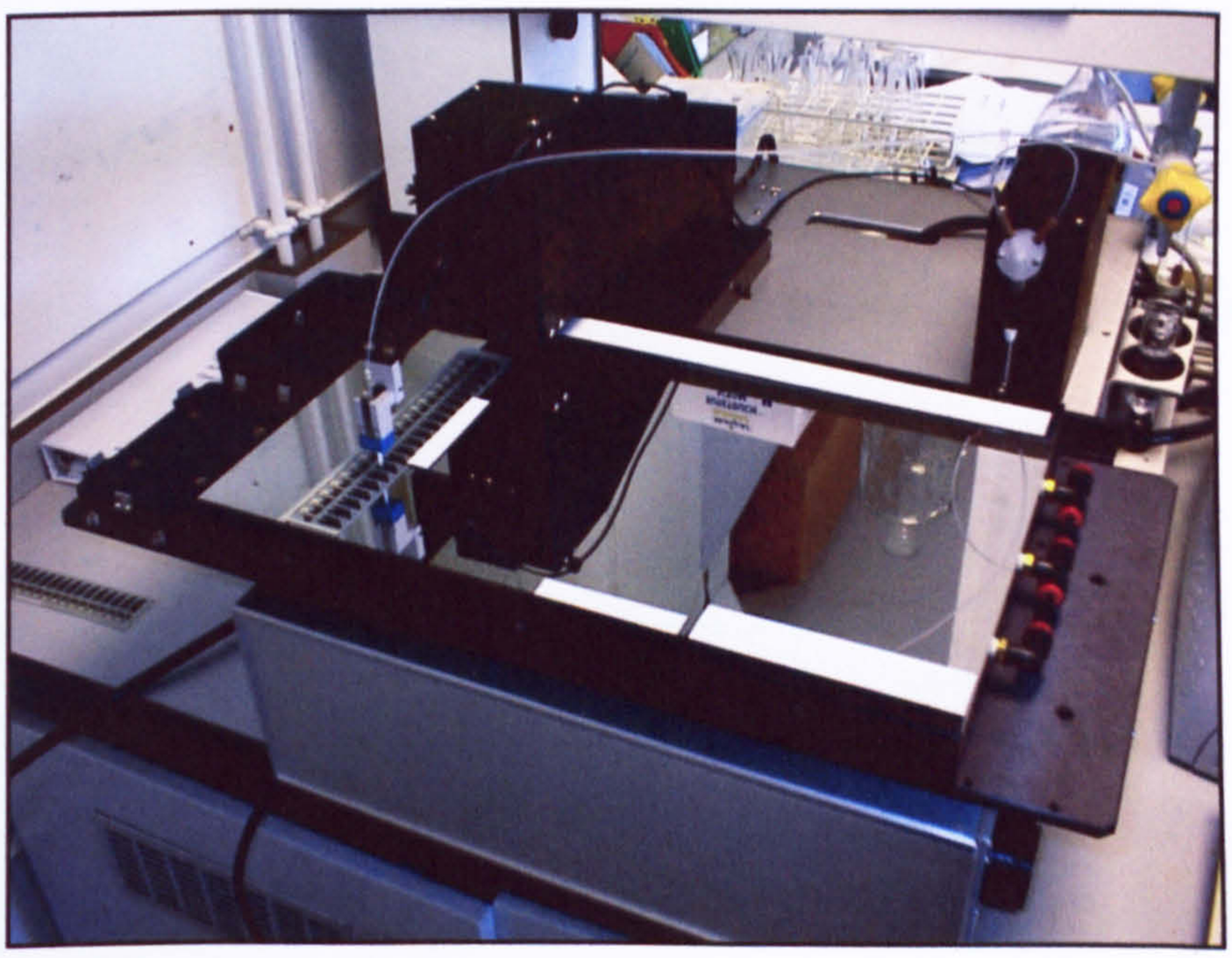

Figure 3.13: BioDot AD3200™ dispensing platform

A Carbolite PN120/200 convection oven was used to dry sensors immediately following the application of a chemical modifying layer (Carbolite Ltd., Hope Valley, UK).

3.4 Solutions

Unless otherwise stated, all solutions were prepared using deionised water (≥18 $M\Omega cm^{-1}$ resistivity) sourced from an Elga Purelab UHQ-II Water System (Vivendi Water Systems, High Wycombe, Buckinghamshire, UK).

3.4.1 *o*-phenylenediamine monomer solution for electropolymerisation

A 5.0×10^{-3} M *o*-phenylenediamine dihydrochloride solution was prepared in a pH 7.4 buffer comprising 5.28×10^{-2} M disodium hydrogen orthophosphate 12-hydrate, 1.30×10^{-2} M sodium dihydrogen orthophosphate 1-hydrate and 5.10×10^{-3} M sodium chloride.

3.4.2 Chlorine solutions for electrode performance analysis

All chlorine solutions were prepared according to Merck Analytical Quality Assurance standard procedures (Merck).

3.4.2.1 Total chlorine solutions

A 1000 ppm (1000 mg/l) stock solution of total chlorine was prepared by dissolving 4 grams of chloramine-T in 1 litre of deionised water. The stock solution is stable for 1 day when stored in a cool place (refrigerator).

A pH 4.0 buffer comprising 9.0 x 10^{-3} M orthophosphoric acid, 9.0 x 10^{-2} M sodium dihydrogen orthophosphate 1-hydrate and 0.5 M potassium chloride was used for the preparation of subsequent dilutions. Both the stock solution and serial dilutions are stable for one day if refrigerated. Amperometric reduction of the combined chlorine component of total chlorine solutions requires the addition of 1 M potassium iodide to liberate a species capable of reduction.

3.4.2.2 Free chlorine solutions

The highly reactive nature of free chlorine requires water used in its preparation to be purified to the highest possible standard. In order to achieve this, deionised water (obtained from the Elga Purelab UHQ-II Water System) was subsequently double distilled before use to prevent residual organic material from combining with free chlorine to form combined chlorine (Figure 1.14).

Figure 3.14: Water distillation set up

A stock solution of free chlorine (HOCl or ClO^-) was prepared by diluting 10 ml of sodium hypochlorite solution into 100 ml of distilled deionised water in a conformity checked 100 ml borosilicate glass volumetric flask. The unstable nature of free chlorine requires a precise assay of the stock solution each time a new stock solution is prepared. This was carried out via an iodine/thiosulphate titration, as follows: 5 ml of the stock solution was pipetted into a 250 ml ground-glass conical flask containing 30 ml of deionised water. 5 ml of acetic acid and 2 g of potassium iodide were added, and the vessel sealed, mixed thoroughly, and allowed to stand for 5 minutes to allow elimination of the iodine. The mixture was then titrated against 0.1 M sodium thiosulphate solution until a weak yellow colour developed. 2 ml of zinc iodide/starch solution was then added to form a deep blue colour and the titration was completed until the solution turned colourless. The procedure was repeated until concurrent results were obtained for each titration (±0.1 ml). The exact concentration of the stock solution was then calculated according to Equation 3.1:

$$ml\ sodium\ thiosulphate\ solution\ (0.1\ mol/L) \times 710 = mg/L\ free\ chlorine \qquad 3.1$$

A pH 7.0 buffer comprising 5.6 x 10^{-3} M disodium hydrogen orthophosphate 12-hydrate, 4.3 x 10^{-3} M sodium dihydrogen orthophosphate 1-hydrate, and 0.5 M potassium chloride was used for the preparation of subsequent dilutions. The stock solution is stable for 1 week if kept refrigerated, whereas dilutions are only stable for 2 hours.

3.4.3 Redox couples for microelectrode behaviour investigation

A 1.0 x 10^{-3} M ferrocenecarboxylic acid solution, a 1.0 x 10^{-3} M hexaammineruthenium(III) chloride solution and a 1.0 x 10^{-3} M potassium ferricyanide(III) solution were all prepared in pH 7.8 buffer comprising 3.18 x 10^{-2} M disodium hydrogen orthophosphate 12-hydrate, 4.35 x 10^{-3} M sodium dihydrogen orthophosphate 1-hydrate and 0.1 M potassium chloride.

3.4.4 Chemical modifying layer solutions

A nitrogen purged pH 4.0 solution comprising 9.0 x 10^{-3} M orthophosphoric acid, 9.0 x 10^{-2} M sodium dihydrogen orthophosphate 1-hydrate, 0.5 M potassium chloride and 1 M potassium iodide was used as principle components of a chemical modifying layer for the total chlorine working electrode. The solution was prepared in a borosilicate glass volumetric flask and applied straight away to minimise the oxidation of aqueous iodine.

A pH 7.0 solution comprising 5.6 x 10^{-3} M disodium hydrogen orthophosphate 12-hydrate, 4.3 x 10^{-3} M sodium dihydrogen orthophosphate 1-hydrate and 0.5 M sodium chloride was used as principle components of a chemical modifying layer for the free chlorine working electrode.

3.4.5 Solutions for sonoluminescence study

Finely ground Luminol was added to deionised water containing 1.5 x10^{-2} M Na_2CO_3, stirring to dissolve. The final concentration of Luminol in the ultrasonic tank was 5 x10^{-5} M, pH 10.7.

3.5 Experimental procedure

The following section describes principle experimental procedures utilised during the research.

3.5.1 Electrode preparation

Gold slide working and counter electrodes were fabricated from frosted microscope slides as follows. Slides were scored with a diamond-tipped blade and cut to produce ground glass sections of approximately 20 x 25 mm dimension. These were then sputter coated with gold for 2 minutes, producing an electrically conductive area. Multicore wires were then attached to this face using silver conductive paint, and the junction strengthened and insulated with epoxy resin (Figure 3.15).

Figure 3.15: Gold sputter coated glass slide electrode

3.5.2 Electropolymerisation of electrodes

For initial investigations into the electrodeposition of the insulating poly(*o*-phenylenediamine) layer, required for subsequent microelectrode array formation, gold sputter-coated ground glass slides were used as follows. pH 7.4 phosphate buffer solution was degassed by sonic pulsing for 60 minutes. 5 mM *o*-phenylenediamine dihydrochloride was added to provide a monomer mixture free of any dissolved atmospheric gases. A 3-electrode cell was prepared comprising a working electrode (to be coated), a gold sputter coated ground glass slide counter electrode, and a silver/silver chloride (Ag/AgCl) pseudo reference electrode. Electropolymerisation was carried out via potentiostatic cycling between 0 and +800 mV at 50 mVs^{-1} scan rate for 20 sweeps using a Sycopel AEW-2 potentiostat. The working electrode was removed, and excess monomer solution rinsed off with deionised water. The electropolymerised electrode must then be sonicated (Section 3.5.7) before the polymer has time to dry.

In the case of single carbon electrode polymerisation, 3 short pulses of ultrasonic energy (approximately 0.5 s, 25-35 kHz) are required prior to initialising the polymerisation step. This was to cause complete wetting of the carbon electrode surface by the monomer solution. Furthermore, the polymerisation process parameters were extended to 40 sweeps from 0 to +1000 mV at 50 mVs^{-1}. The procedure was then scaled-up to encompass sheets of 600 carbon electrodes which were electropolymerised using the custom built 40-channel Sycopel potentiostat. A 280 x 280 x 120 mm glass cell was selected as a reaction vessel for laboratory-scale electropolymerisation of up to 100 sensors (Figure 3.16). Stainless steel gauze was attached along one side to serve as a counter electrode

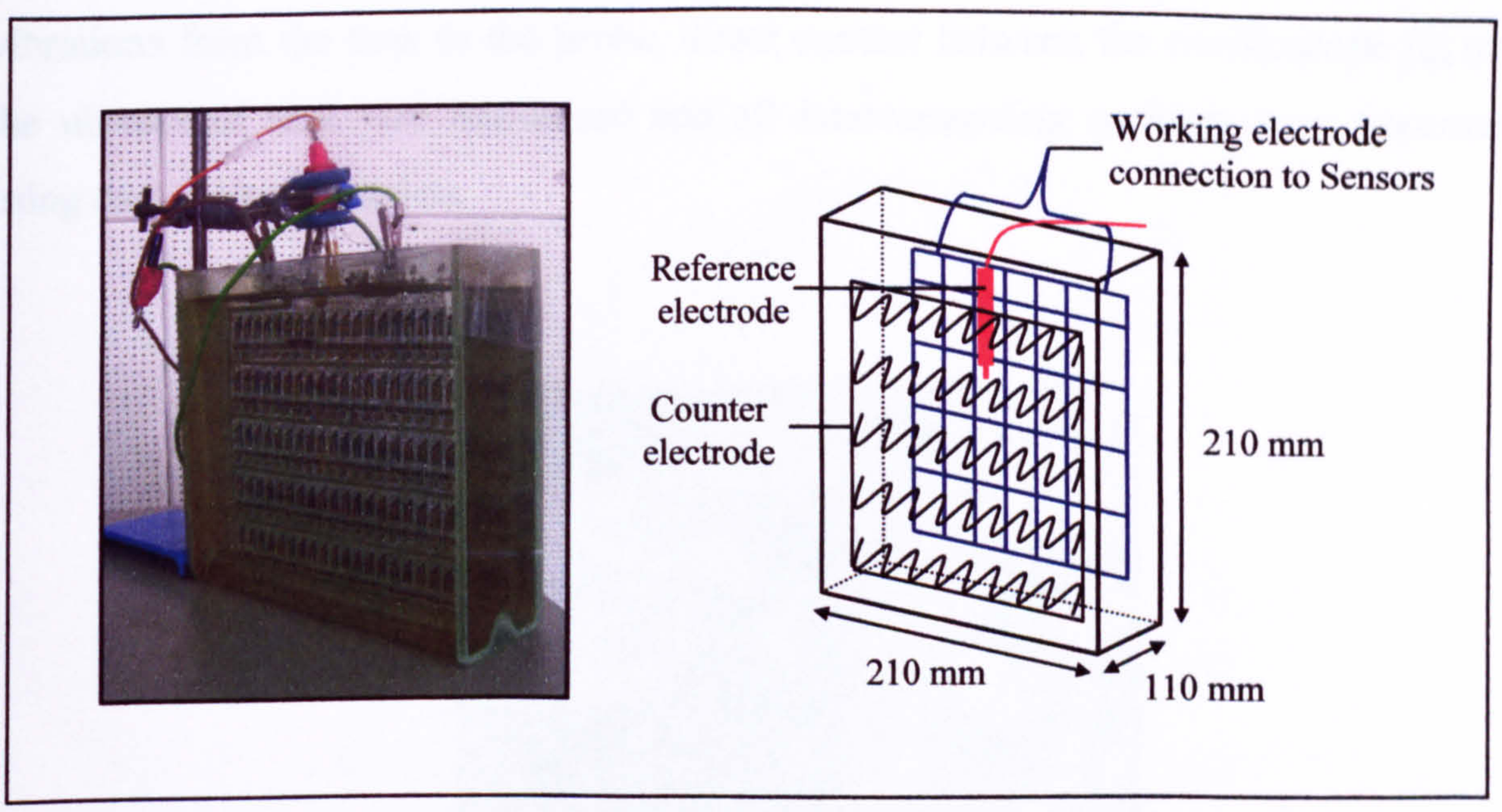

Figure 3.16: Electropolymerisation cell (up to 100 carbon-ink sensors)

Degassed monomer solution was added to a level such as to cover both the stainless steel gauze counter electrode and the sheets of 100 sensors. Three short pulses of ultrasound (required to permit complete wetting of the carbon-ink surface by the monomer solution) were provided by a Camlab Transsonic T460, in which the glass electropolymerisation cell was placed.

As part of the scale-up of the process a 500 x 600 x 25 mm internal diameter stainless steel container was employed as the polymerisation vessel for sheets of 600 sensors, again using a stainless gauze counter electrode affixed to one side of the vessel.

3.5.3 Ultrasonic energy mapping

Variation of ultrasonic intensity within the ultrasonic tank was measured using a custom built hydrophone monitored by a Tektronix TDS 1002 oscilloscope (RS, Corby, Northamptonshire, UK), with signal processing settings as follows: DC couple mode, high frequency reject, 32 bit sampling average. A jig was constructed to permit the placement of the probe at 50 mm intervals within the tank in three Cartesian directions (x, y, z). To limit any interference caused by the transmission of ultrasonic

vibrations from the tank to the probe, direct contact between the oscilloscope jig and the ultrasound tank was minimised and all interconnecting surfaces were separated using dampening materials.

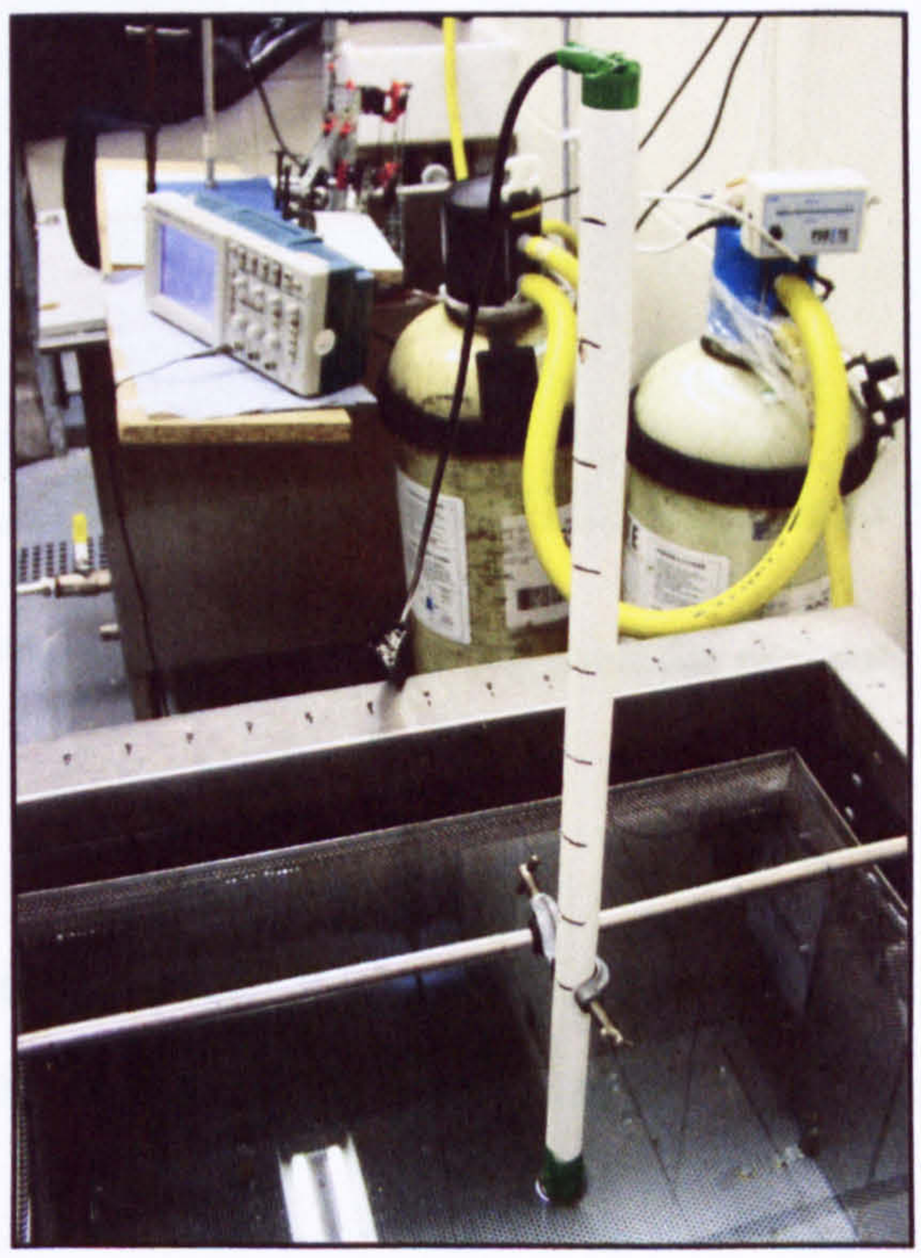

Figure 3.17: Custom-built hydrophone

By measuring the AC current induced in the piezoelectric microphone by the acoustic energy field (recorded as root mean square voltage, V_{RMS}), it was possible to assess the variation in acoustic amplitude throughout the tank.

3.5.4 Ultrasonic cavitation mapping using aluminium foil

The homogeneity of ultrasonic cavitation within the custom built 2 kW ultrasound tank was investigated using 'foil tests'. A clean piece of aluminium foil (40 cm x 53 cm) was weighted at the bottom by a thin steel rod and suspended vertically in the ultrasound tank to be sonicated at 75% power for 10 minutes (Figure 3.18).

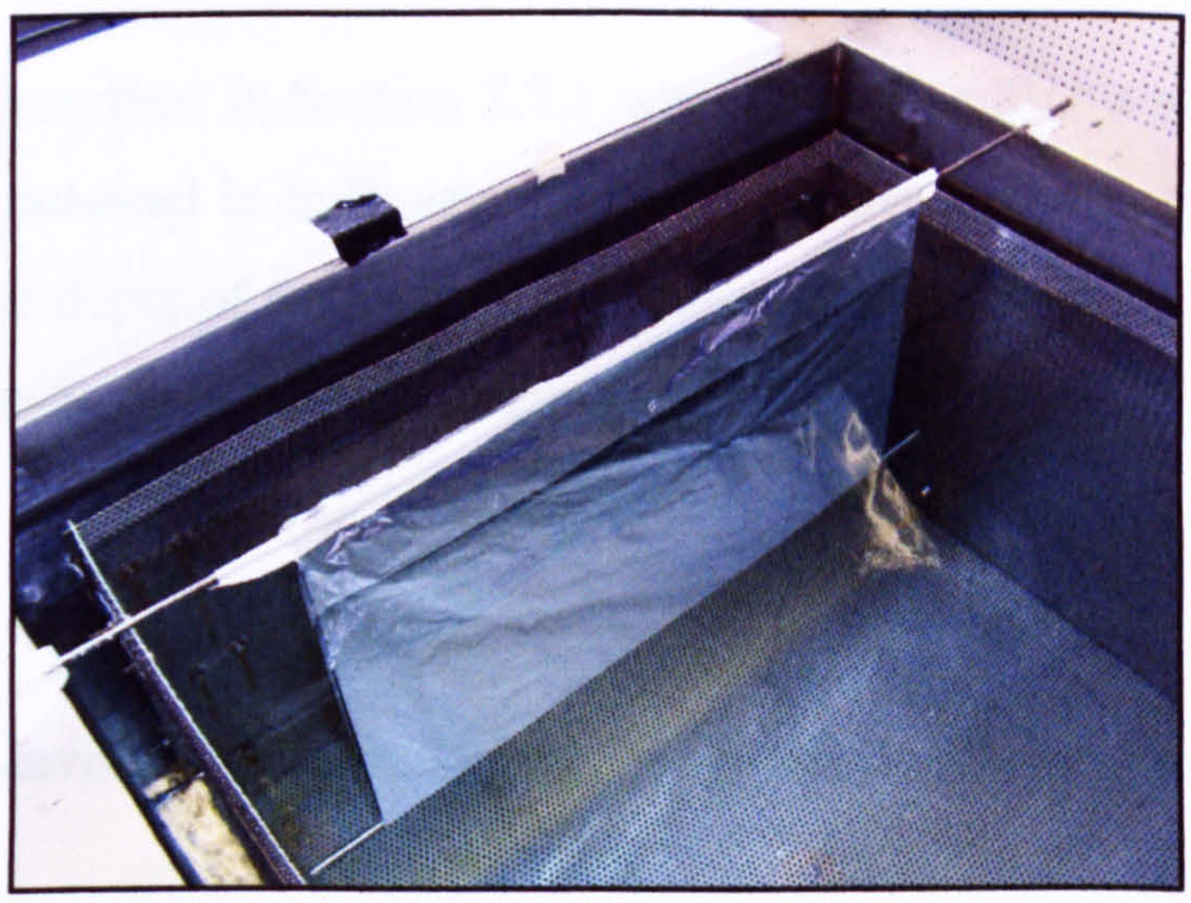

Figure 3.18: Vertical suspension of foil sheet for cavitation profiling

The process was repeated for positions A to F, as indicated in Figure 3.19, then carefully removed and photographed on a coordinate board for analysis.

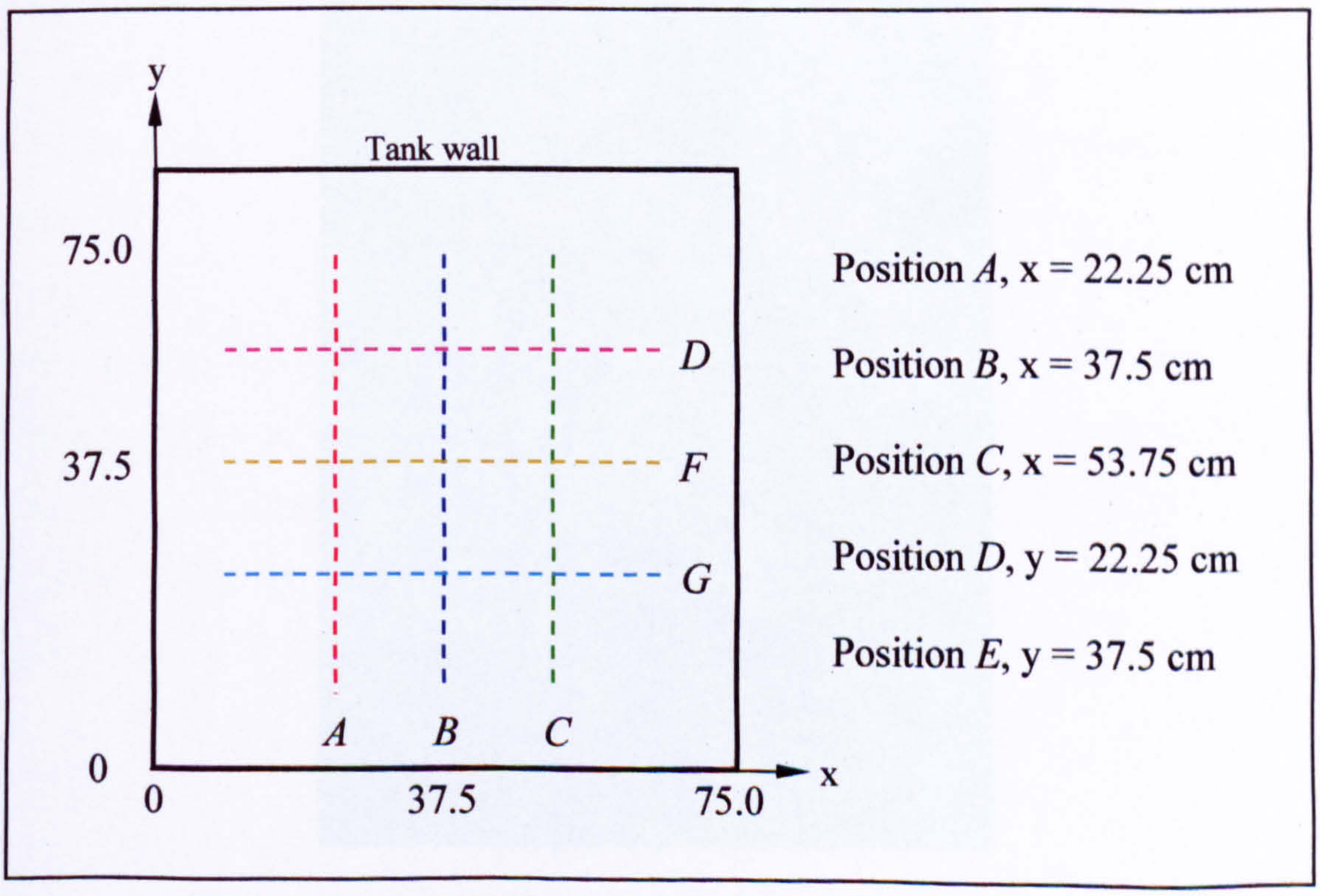

Figure 3.19: Vertical suspension of foil sheet for cavitation profiling

3.5.5 Ultrasound tank floor depth profiling

The mounting jig described in Section 3.5.3 was adopted to bear a stainless steel rod (diameter 5 mm) graduated in millimetres for the measurement of water depth in the ultrasound tank. The depth of the water, recorded at 7cm intervals in both the x and y plane, was used to indicate the profile of the tank floor.

3.5.6 Ultrasonic cavitation mapping using sonochemical luminescence

Homogeneity of the ultrasonic cavitation within custom built 2 kW ultrasound tank was also investigated by exploiting the sonochemical luminescence of Luminol. All sources of ambient light in the laboratory were blocked by means of extensive light-proofing and experiments were run during night-time hours. A tripod was assembled over the sonic tank to provide a fixed platform for photography (figure 3.20).

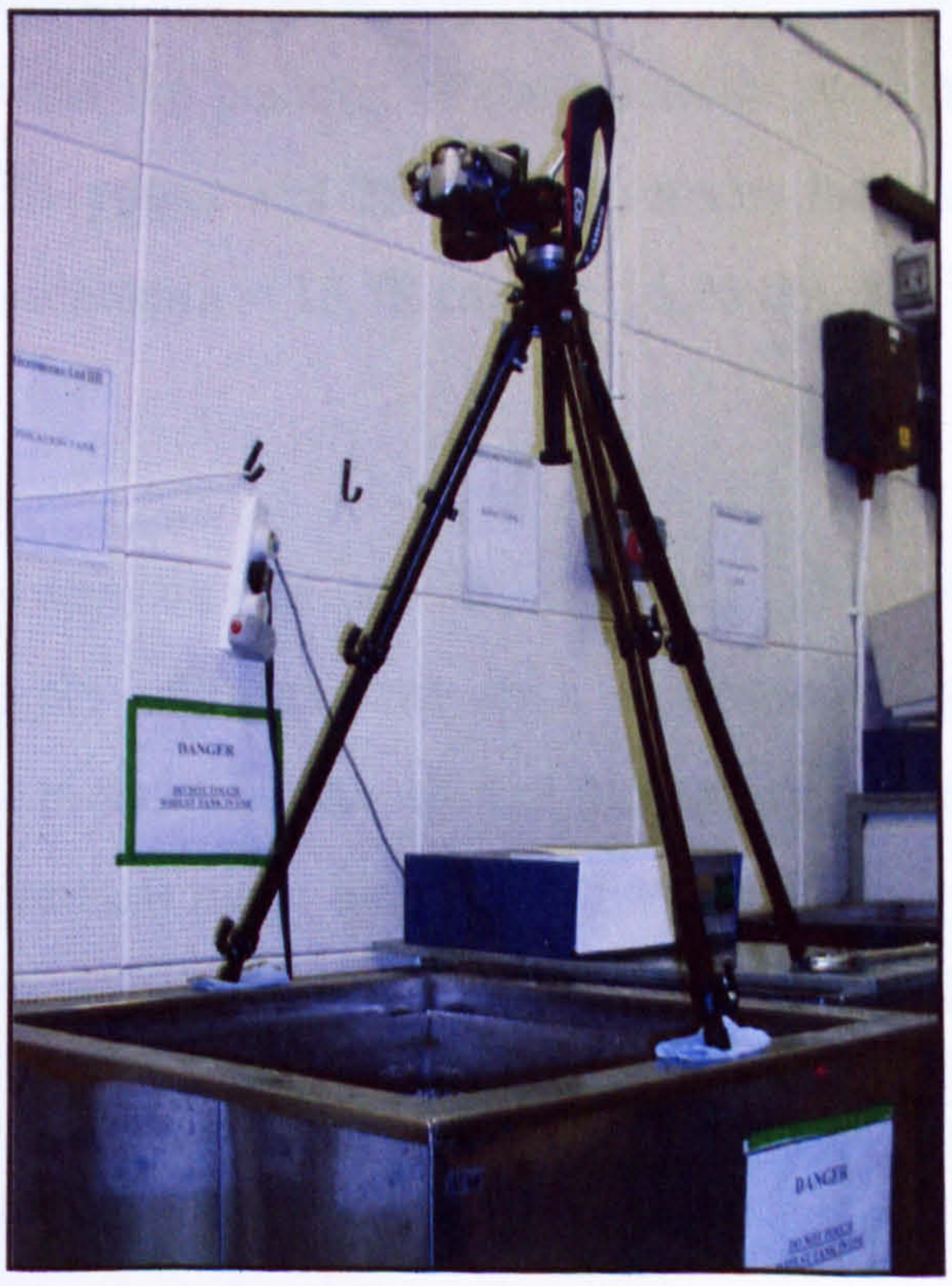

Figure 3.20: Tripod assembly for SLR camera

Images were captured on a Canon EOS 300V SLR camera using ISO1600 colour film. Maximum aperture size (setting 5.6) and exposure times of 25 minutes were required to capture images on film.

3.5.7 Ultrasonic ablation of poly(*o*-phenylenediamine film)

Initial studies involving single gold sputter-coated glass slides and single screen printed carbon electrodes were carried out using the Transsonic T460 bench-top ultrasound bath filled with 4 litres of deionised water. To prevent contamination from material entering solution from the bath, sensors were immersed in a beaker containing 100 ml deionised water. The beaker was then suspended at the centre point of the ultrasonic bath such that the water level within the beaker was in line with the water level of the bath and sonicated for 20 seconds (at 25 °C).

Ultrasonic ablation of sheets of 100 carbon electrodes was carried out in the 2kW Ultrawave Ltd. custom built ultrasonic tank. Sonocation parameters were optimised by adjusting time, power and the position of the electrodes within the tank; experiments were carried out at 75% power and 25°C, with sensors located facing the right-hand side of the tank at coordinates $x = 18.75$ cm, $y = 56.25$ cm, $z = 35$ cm unless otherwise stated.

Further investigations were carried out into the effect of moving the sensors during sonocation. Various types of movement were experimented with initially involving horizontal and vertical motion. Unidirectional movement was extended to a rotational movement within the vertical plane by means of a custom built jig system powered by a variable speed electric motor (shown schematically in Figure 3.21).

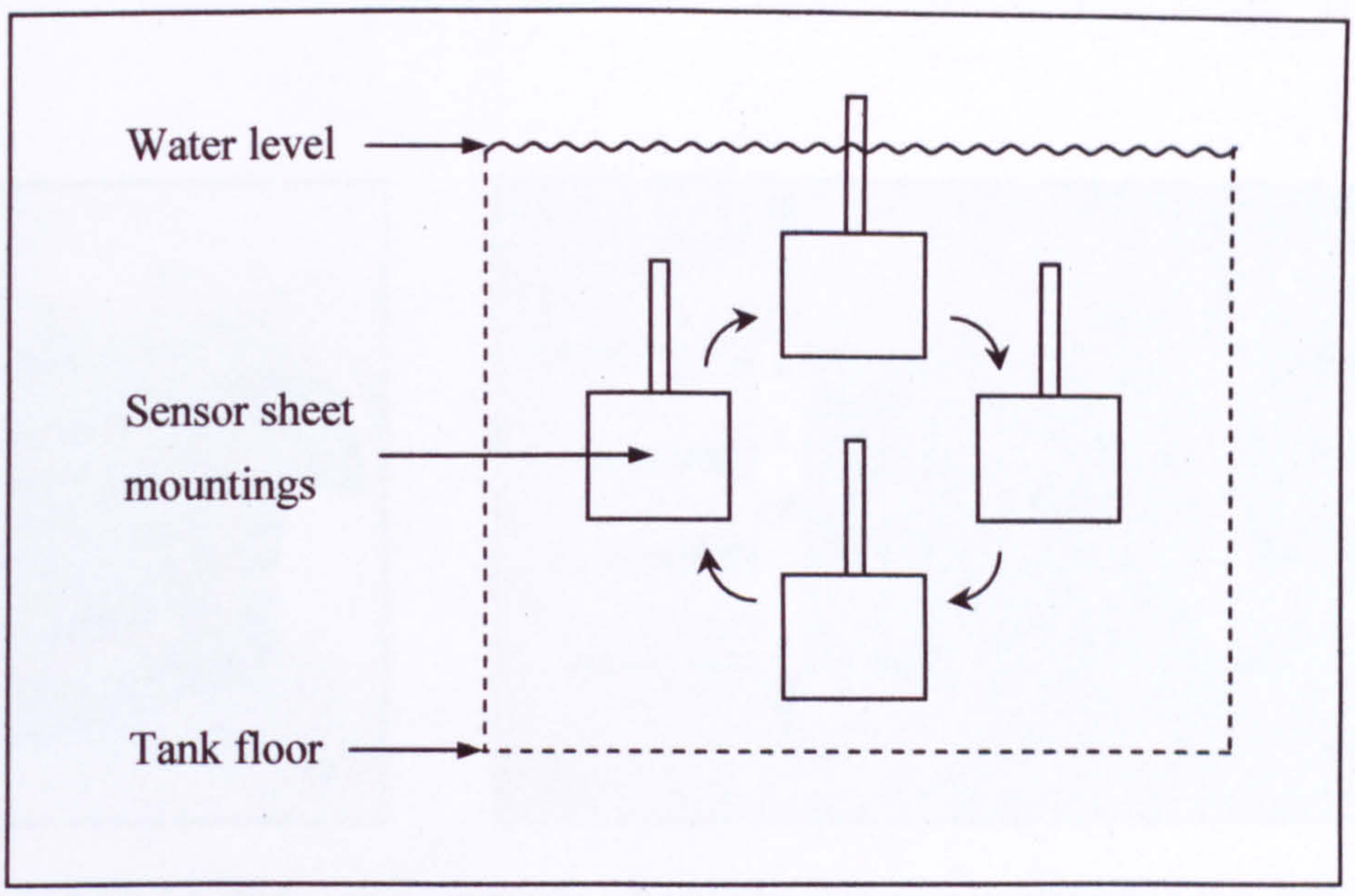

Figure 3.21: Schematic showing movement of sensor sheets during ultrasonic ablation

The rotation speed was such that one revolution was completed during ultrasonic irradiation (Figure 3.22a). The system was modified by incorporating an improved motor system (Kika Labortechnik RW28 electric motor system) (Figure 3.22b) and further modified to process multiple sheets of sensors, illustrated in Figures 3.23a and 3.23b).

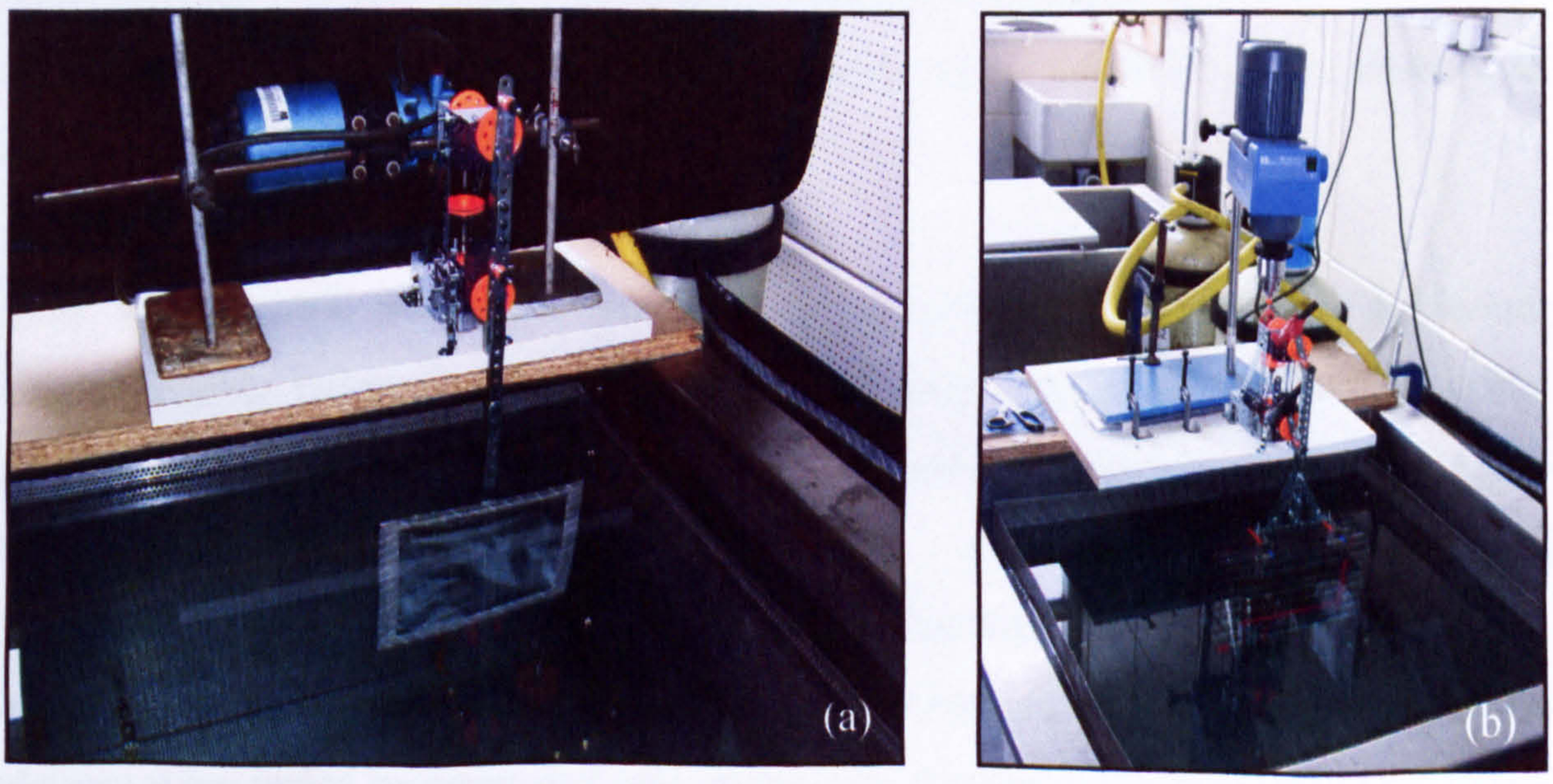

Figure 3.22: (a) Type 1 rotational system, (b) Type 2 rotational system

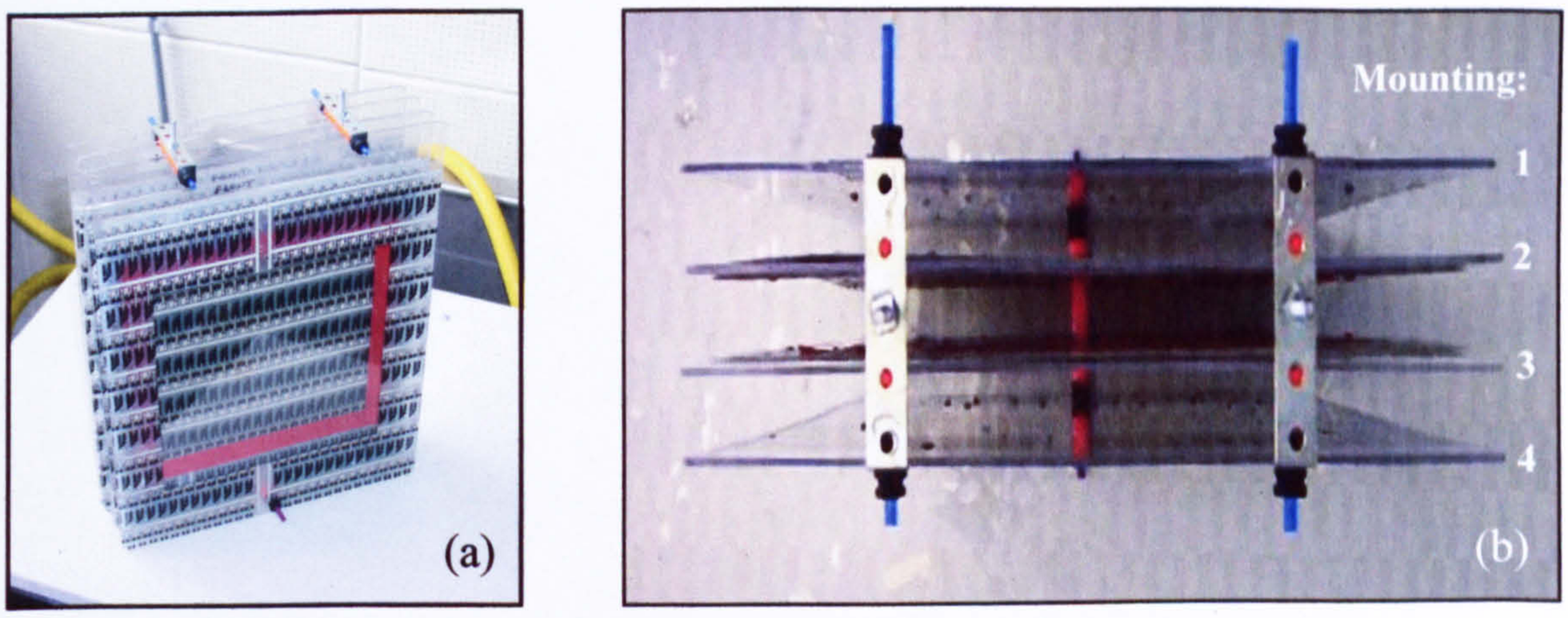

Figure 3.23: Multiple sensor mounting front view (a), sensor mounting top view (b)

3.5.8 Electrochemical characterisation of sensors

Unless otherwise stated, all electrochemical characterisation of planar and microelectrode array sensors was performed by connection to the Sycopel AEW-2 potentiostat.

Buffer solutions were checked for electroactive impurities via a cyclic voltammetric sweep between -1.0 and +1.0 V at 50 mVs^{-1}. Background signal contribution was also established for each test by polarising at the appropriate potential in the absence of analyte.

Cyclic voltammetric techniques were used to characterise microelectrode behaviour using reversible redox couples as follows: Electrodes characterised with potassium ferricyanide (III) solutions were interrogated between -0.2 and +0.6 V (vs. Ag/AgCl) initially sweeping in a cathodic direction, electrodes characterised with ferrocenecarboxylic acid solutions were tested between -0.3 and +0.55 V (vs. Ag/AgCl), and electrodes characterised with hexaammineruthenium (III) chloride solutions were tested between -0.7 and +0.2 V (vs. Ag/AgCl). Unless otherwise stated, characterisations were performed at a scan rate of 20 mVs^{-1}.

For chronoamperometric interrogation of electrodes in hexaammineruthenium (III) chloride solutions, a constant potential of -0.35 V (vs. Ag/AgCl) was applied for 90 seconds and the current-time transient was recorded. For characterising stir independent behaviour, after 30 seconds sensors were subjected to solution agitation via a Jenway 1100 magnetic stirrer (speed setting 5) with a 6 mm flea (Jenway Ltd., Dunmow, Essex, UK).

3.5.9 Analysis of chlorine

Electrodes were interrogated via voltammetric and amperometric methods using the Sycopel AEW-2 potentiostat connected. Voltammetric methods were used to determine the reduction potential of free and total chlorine species by cycling between +200 and -400 mV (vs. Ag/AgCl). In the case of total chlorine, the addition of potassium iodide immediately before testing required the use of a SCE or Ag/AgCl reference electrode protected by an integrated ion-selective frit to prevent contamination.

Voltammetric methods were also employed to characterise microelectrode performance by means of chronoamperometry and cyclic voltammetry. For example, for the chronoamperometric interrogation of total chlorine solutions, a three-electrode cell comprising the working electrode, a counter electrode and reference electrode (with ion-selective frit) was employed. A constant potential of -80 mV or -100 mV (vs. Ag/AgCl) was applied for 90 seconds for free and total chlorine solutions respectively, unless otherwise stated. Stir-independent properties can be assessed by applying solution agitation via a Jenway 1100 magnetic stirrer and 6 mm flea and comparing the steady state response to that of quiescent solution. Cyclic voltammetry was also used to assess microelectrode array performance by interpreting the voltammetric sensor response in quiescent solutions.

3.5.10 Chemical layer deposition

Various methods were employed for the deposition of a chemically modifying layer onto microelectrode array electrodes.

3.5.10.1 Screen printing of modifying emulsion

Emulsion-based chemical layer deposition was carried out at Polyflex Circuits Limited (Parlex Corporation, Newport, Isle of Wight, UK). Operational parameters, including silk screen mesh size, tension, and squeegee angle, pressure and speed will not be documented as they remain commercially confidential.

3.5.10.2 BioDot

A BioDot Inc. AD3200™ dispense platform incorporating a BioJet Plus™ 3000 dispensing system was used to dispense low-viscosity chemical modifying layer onto the electrode surface (Figure 3.14). Delivery of liquid occurred via 80 nL drops, at 0.3 mm pitch, to completely coat the electrode surface (20 drops for the total chlorine electrode, 28 drops for the larger free chlorine electrode). The operating steps for this process are controlled by PC driven AxSys™ software, pre-defined by BioDot Ltd., and incorporates priming and rinsing phases to ensure clean delivery.

A strip of 20 sensors was then placed in a fixed position on the dispense platform and the free chlorine electrodes were coated with the appropriate solution and convection oven dried for 10 minutes at 70°C. The process was repeated for the total chlorine electrodes, ensuring that the storage vessels and tubing used in the system were shielded with tin foil to minimise exposure of the iodide to light.

CHAPTER 4

Base sensor design

D. W. Mills

Cranfield University, Silsoe

4.1 Introduction

Initial studies into the production of ultrasonically fabricated microelectrode arrays were carried out within this research group using individual 'sputter-coated' gold slide electrodes (Myler, 2000). In order to develop a commercially viable, disposable aqueous chlorine sensor, it was necessary to design the base electrode in such a way so as to minimise materials used and their processing costs, whilst maintaining optimum functionality. In order for a new device to gain a major market advantage over existing technologies, it was critical that any improvements in product performance must not result in an unacceptable increase in unit cost.

Screen printing technology provides an ideal method for the inexpensive, mass-fabrication of sensors based on thick-film technology (Galán-Vidal *et al*, 1995), (Hart & Pemberton, 1997). Gold itself is a precious metal, and screen printable gold inks are, at approximately £5000 per kg, prohibitively expensive for the production of single-use, disposable sensors. Conductive carbon-inks offer a less expensive alternative for sensor production and are commercially available at around £300 per kilogram. For this reason, carbon screen printable inks were selected as the material of choice for sensor production.

Prior to the production of a three-electrode base sensor (comprising working, counter and reference electrode), it was necessary to establish the key geometric parameters required for sensor function. Further processing steps would then be required to prepare the base sensor for stir-independent aqueous chlorine detection.

This chapter will detail the design and function of the base sensor to incorporate the various functional features required as well as permitting a route to cost-effective manufacture.

4.2 Sensor overview

To allow the development of a disposable chlorine sensor having stir-independent response, it is necessary to understand the basic function of the proposed device. Detection of *free* chlorine will be achieved via direct amperometric reduction of hypochlorous acid / hypochlorite ions from aqueous solution (Equation 2.81). Similarly, the measurement of *total* chlorine, comprised of *free* and *combined* chlorine, will occur indirectly via the amperometric reduction of iodine, liberated by the reaction of aqueous potassium iodide with the chlorinated species in acidified conditions (Equations 2.83 and 2.84). It follows that the optimum potentials for the reduction of these species must primarily be established. As a means of preventing any fluctuation in response due to pH variation, free chlorine solutions were buffered to pH 7.0, corresponding to the amperometric current response plateau indicated in Figure 2.48, and minimising interference from monochloramine. Figure 4.1 exhibits a cyclic voltammogram obtained for a 20 ppm solution of free chlorine on a planar carbon-ink electrode.

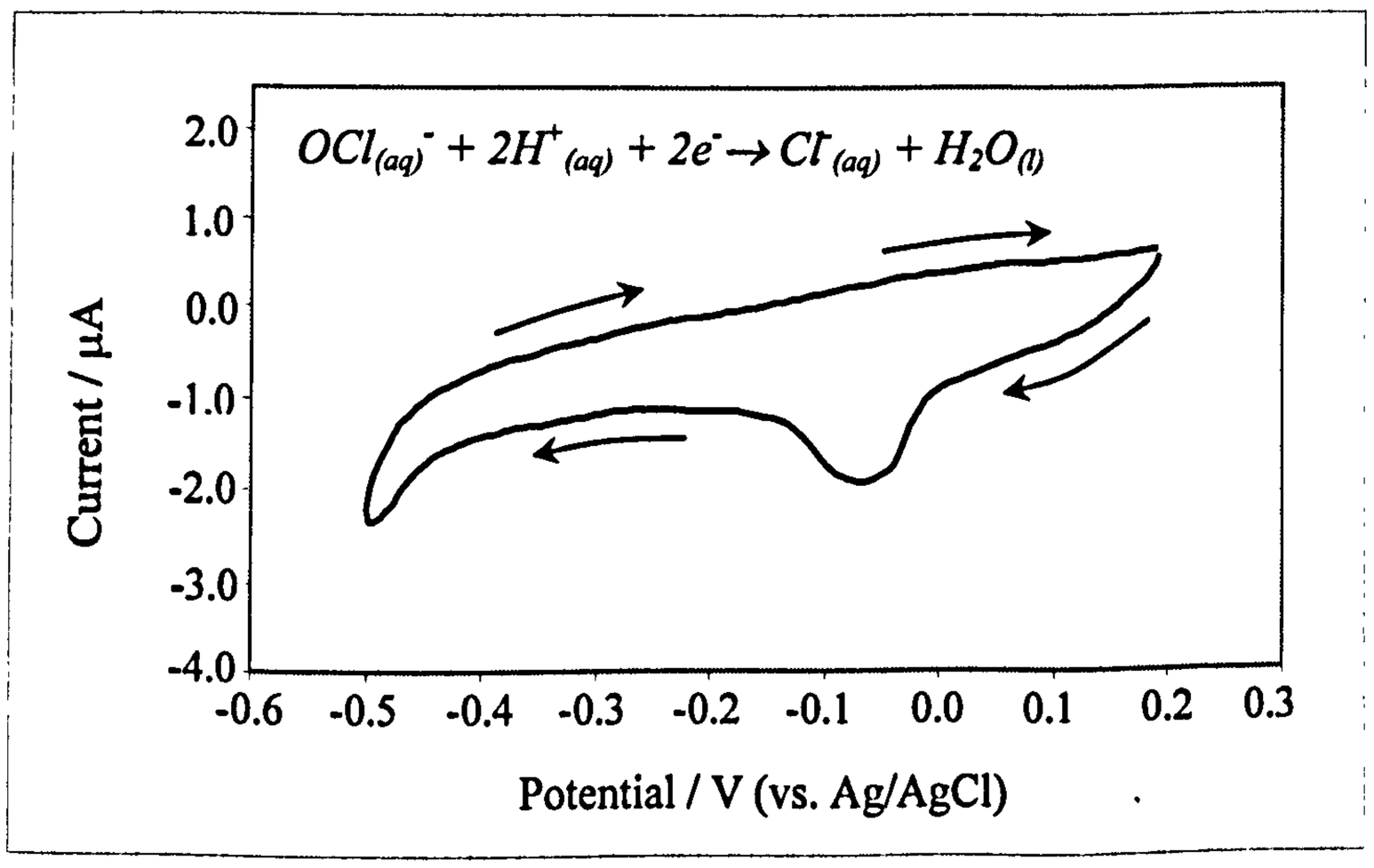

Figure 4.1: Cyclic voltammogram of 20 ppm free chlorine solution in pH 7.0 phosphate buffer (25 mVs^{-1})

It can be seen that the reduction peak of free chlorine ($HOCl/OCl^-$) occurs at approximately -80 mV (vs. Ag/AgCl). As the cathodic potential increases beyond

-300 mV, oxygen reduction can be seen to be beginning to commence. An optimal free chlorine working electrode polarising potential of -80 mV can therefore be selected; here the reduction of interferents (such as oxygen) is minimised, while maintaining a detectable signal corresponding to the reduction of the analyte of interest (free chlorine).

Cyclic voltammetry was also used to interrogate total chlorine solutions in the presence of excess potassium iodide (1 M). Solutions were buffered to pH 4.0 to provide the acidic conditions required for reaction of chloramines with iodide (Equation 2.83 and 2.84). Figure 4.2 exhibits the cyclic voltammogram obtained for the amperometric reduction of 20 ppm total chlorine with 1 M potassium iodide, on a planar screen printed carbon-ink electrode.

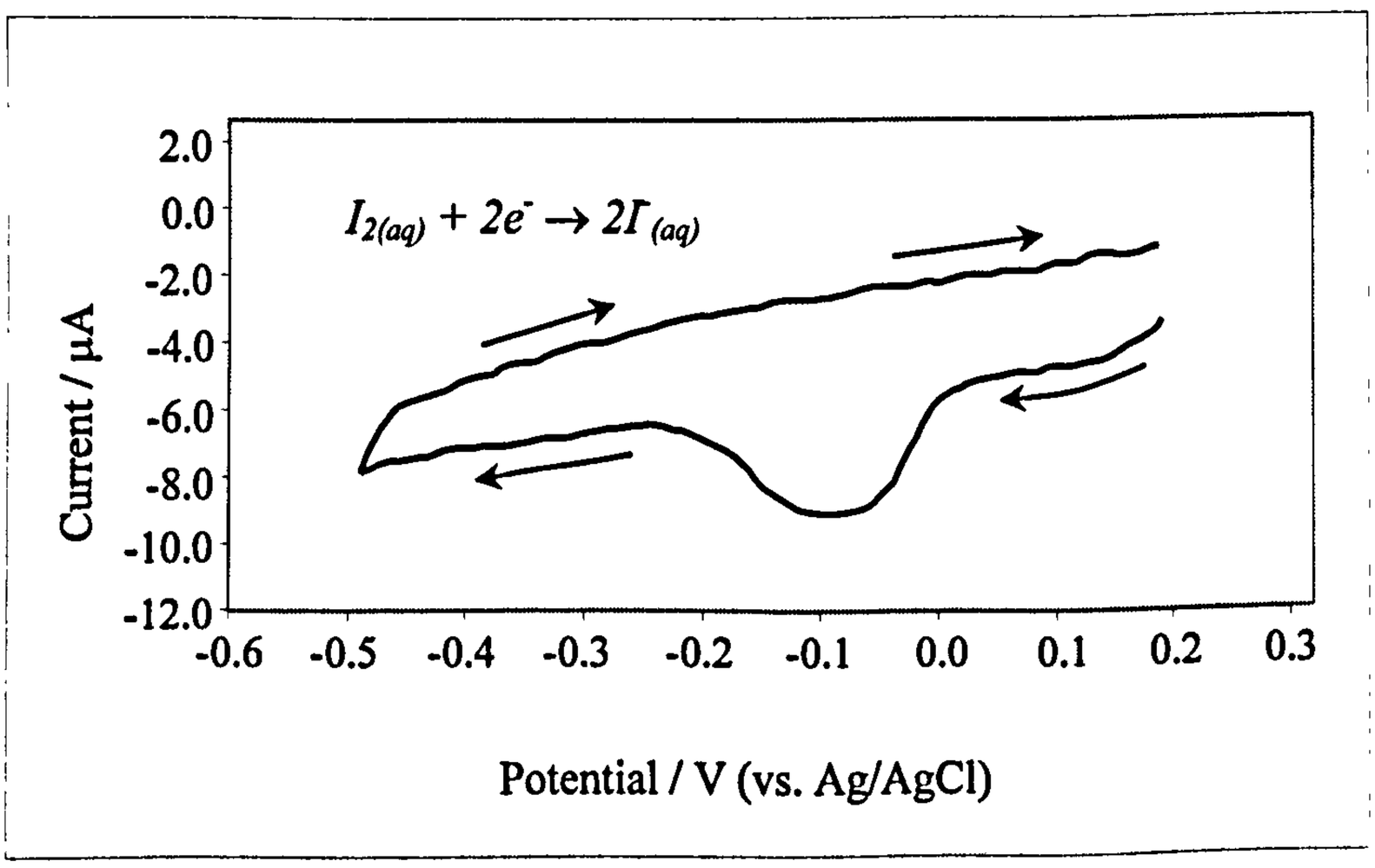

Figure 4.2: Cyclic voltammogram of 20 ppm total chlorine + 1 M potassium iodide in pH 4 acetate buffer (25 mVs^{-1})

This voltammogram indicates a reduction peak potential of approximately -100 mV (vs. Ag/AgCl) for the reduction of the total chlorine/iodine system. An optimal reduction potential for total chlorine analysis was therefore selected as -100 mV to avoid any signal contribution resulting from oxygen reduction, as well as interference from common metal ions (described in more detail in Section 7.4).

The amperometric detection of chlorine is to be carried out using a microelectrode array sensor, thus eliminating the disadvantages associated with a planar electrode surface, such as a stir-dependent signal response. The expense of manufacturing microelectrode array devices can be greatly lowered by exploiting the novel and patented manufacturing technology developed by Microarray Limited. As we have seen, screen printing technology can be used to mass produce planar sensors, using an inexpensive, carbon-based conductive ink.

The sensors so produced can be passivated by means of an ultra-thin electropolymerised film, such as poly(*o*-phenylenediamine) which serves to insulate the planar conducting surfaces from electroactive species in solution (Chapter 5). By submerging the sheets into an ultrasonic tank, cavitation events are able to puncture the relatively soft, ultra-thin film to reveal the harder conductive substrate beneath. Previous work within the research group has shown that the dimensions of the conductive pores are sufficiently small (<10 μm in diameter) to permit microelectrode electrochemical response behaviour (Myler, 2000). Furthermore, the continuous conductive layer beneath allows each pore to be electrically connected, resulting in a microelectrode array configuration. Figure 4.3 illustrates the formation of a microelectrode array by means of ultrasonic ablation.

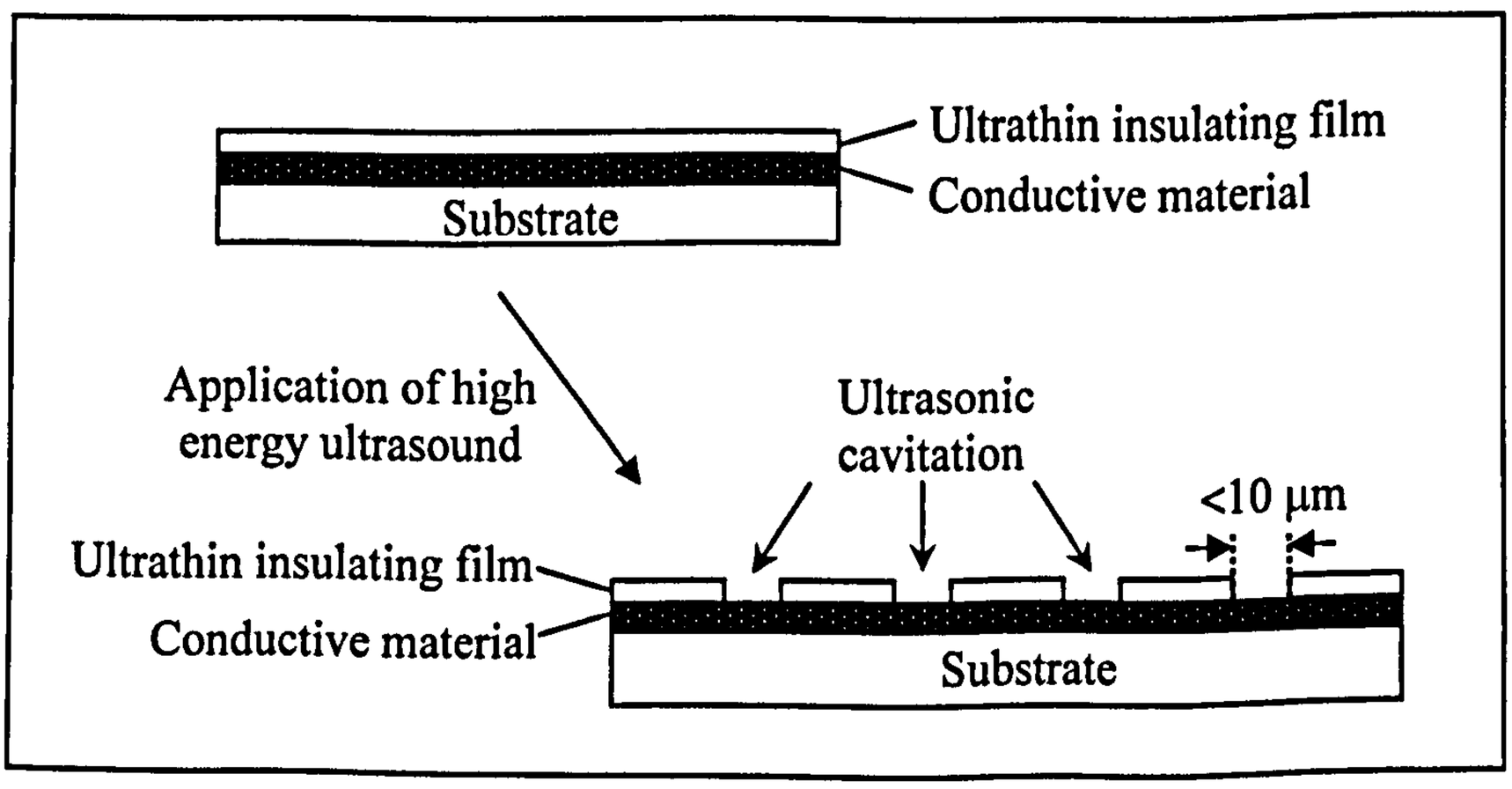

Figure 4.3: Microelectrode formation via ultrasonic ablation of a thin insulating film

This rapid and inexpensive manufacturing approach, under the ownership of Microarray Limited, provides an economical route for the mass production of disposable microelectrode array devices.

4.3 Electrode area requirements

An important aspect of the Microarray Limited aqueous chlorine measurement system is the ability to be able to measure free, total and combined chlorine concentrations in the same test. Since the combined chlorine concentration can be determined by the subtraction of the free chlorine concentration from the total chlorine concentration, all three components can therefore be measured via a two working electrode system (free and total chlorine). Current portable chlorine analysers have a detection limit as low as 0.01 ppm (free & total chlorine) and typically have an accuracy of ± 5% with a range of 0 to 4 ppm. The Microarray Limited system will aim to lower the detection limit further and improve the accuracy for total chlorine detection. In addition, the measurement range of both free and total chlorine may be extended to 20 ppm. A marketing decision was taken to produce a second type of sensor for the environmental monitoring market which requires a sensitivity of 0.005 ppm (2×10^{-9} M) for total chlorine. Detection at this level has, as yet, not been satisfied by standard field measurement methods but may be achieved by dedicating both working electrodes to the measurement of total chlorine, thereby cost-effectively addressing the market need. The concentration of free chlorine, which provides a smaller amperometric signal than total chlorine, will be measured with a resolution of 0.02 ppm. The Microarray Limited chlorine sensors will be interrogated using a portable instrument based on a simple potentiostatic system, able to resolve signal responses with an accuracy of 1 nA. It follows that for the equipment to measure such low concentrations, the sensor must provide a minimum of 1 nA signal size per unit concentration.

A batch of generic carbon paste electrodes (manufactured by Gwent Electronic Materials Ltd, Mamhilad, Gwent, UK), were modified into microelectrode array sensors via 20 sweeps electropolymerisation (0 to +800 mV vs. Ag/AgCl) and 10 seconds ultrasonic ablation (25kHz) (by means of a Camlab Transsonic T460). The sensors were used to determine current densities generated by free chlorine and total chlorine solutions on screen printed carbon-ink substrate microelectrode arrays, as depicted in Figures 4.4 and 4.5 respectively (buffers as detailed in section 3.4.2). Current magnitudes were determined by polarising 3 sequential sensors for 90 seconds in a range of concentrations of free (-80 mV) and total (-100 mV) chlorine. Error bars represent the standard deviation of the data obtained for each concentration.

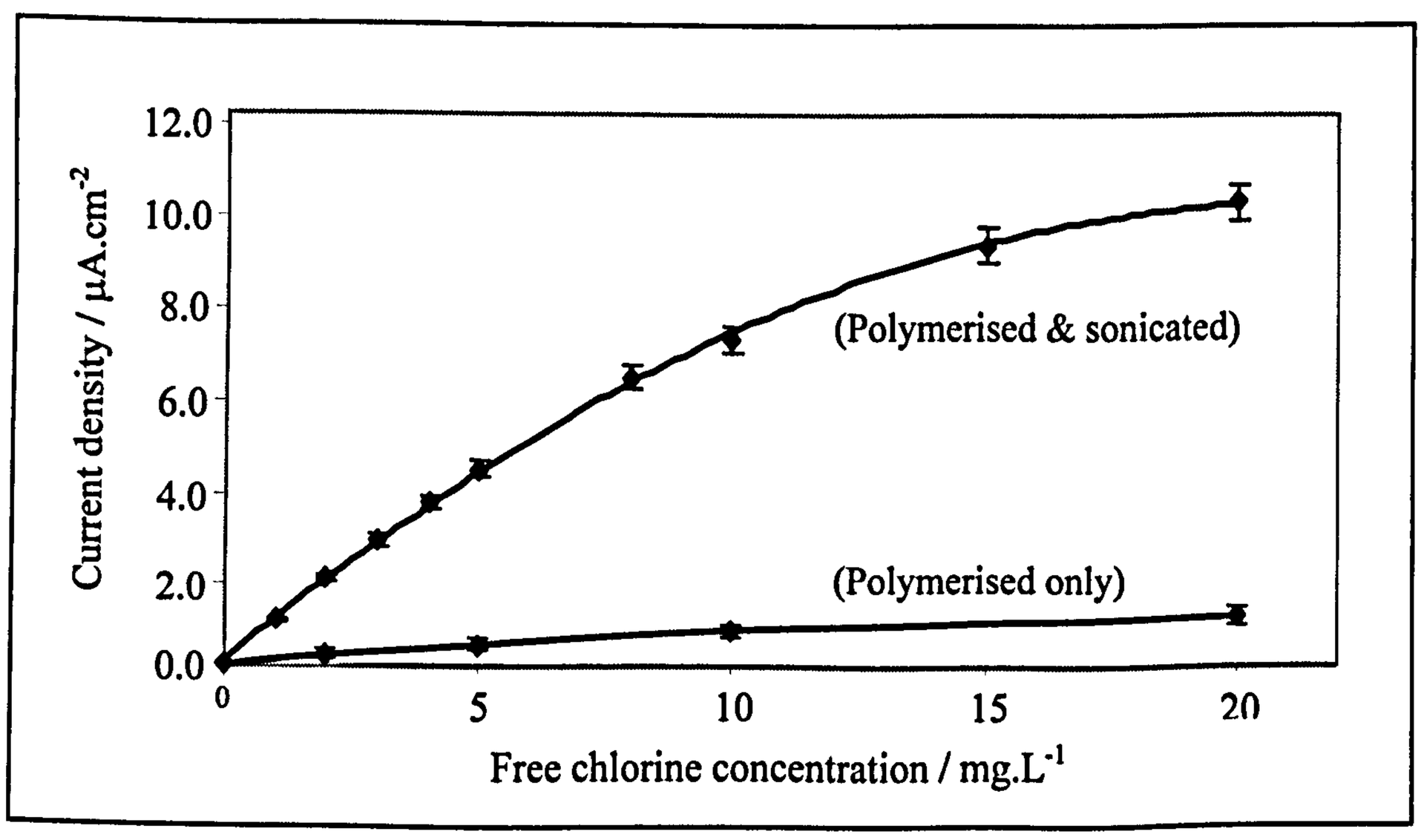

Figure 4.4: Calibration plot for free chlorine solutions on modified carbon electrodes

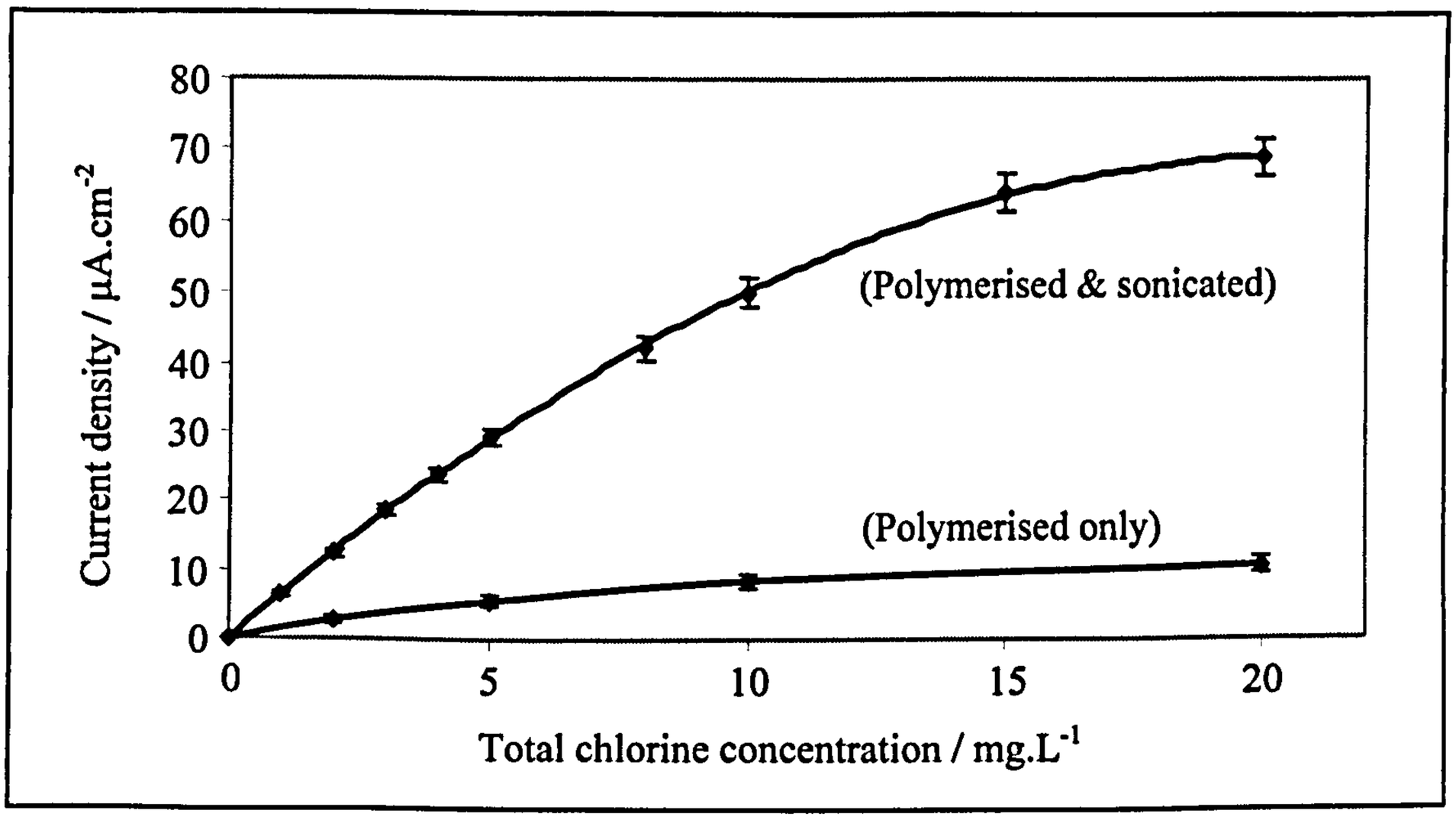

Figure 4.5: Calibration plot for total chlorine solutions on modified carbon electrodes

The calibration profiles indicate a quasi-linear response to both free and total chlorine solutions for electropolymerised and ultrasonically ablated microelectrode array sensors. As expected, the data indicates that the current response towards total chlorine is considerably greater than observed for free chlorine. From the data, the minimum electrode area required to provide a signal size of 1 nA for 0.02 ppm free chlorine can be calculated to be approximately 10 mm^2. Similarly, an electrode area of 6 mm^2 could be expected to enable a resolution of 5 ppb to be attained for total chlorine measurement.

Furthermore, to confirm the effectiveness of the insulating poly(*o*-phenylenediamine) film as a transport barrier to chlorine, electropolymerised sensors which had not been exposed to ultrasonic ablation (and therefore unperforated) were also interrogated in the free and total chlorine solutions (Figures 4.4 and 4.5). The much reduced currents obtained from these sensors confirm the suitability of poly(*o*-phenylenediamine) for the application as a transport barrier during the amperometric reduction of chlorine (discussed further in Section 5.4).

A three-electrode system for measuring the reduction of chlorine includes a counter electrode, which, since the rate of any reaction is controlled by its slowest,

rate-determining step, must be large enough to provide sufficient current. The size of the counter electrode required is related to the maximum current that will need to flow through the system and it is important to ensure that the counter electrode does not limit charge transfer at the working electrode, and so affect the response of the sensor at the higher concentrations. General electrochemical practice suggests a counter electrode size of approximately 2-10 times the area of the respective working electrode to eliminate any risk of it acting as a rate-limiting component. However, for the application of mass-produced, miniaturised sensors, it is important to consider the number of sensors that can be incorporated into each sheet as this affects unit cost. It therefore became necessary to determine the specific optimal counter to working electrode size ratio required for the Microarray Limited disposable chlorine sensor. To achieve this, a generic GEM carbon paste electrode was defined to an area of 12 mm^2 using a dielectric mask, and processed into an ultrasonically ablated microelectrode. Using a 2.54 mm PCB card 'edge connector', this working electrode was positioned next to a 40 mm^2 carbon counter electrode in the form of an unmodified generic GEM carbon-ink electrode; both sensors were trimmed to allow an inter-electrode distance of 5mm. A three-electrode cell was then constructed comprising an external silver/silver chloride (Ag/AgCl) reference electrode, and the two carbon-ink electrodes held in fixed positions in a 20 mg/L total chlorine solution (Figure 4.6). This concentration represents the upper limit required for detection, and as such the largest current demand that the system will have to support.

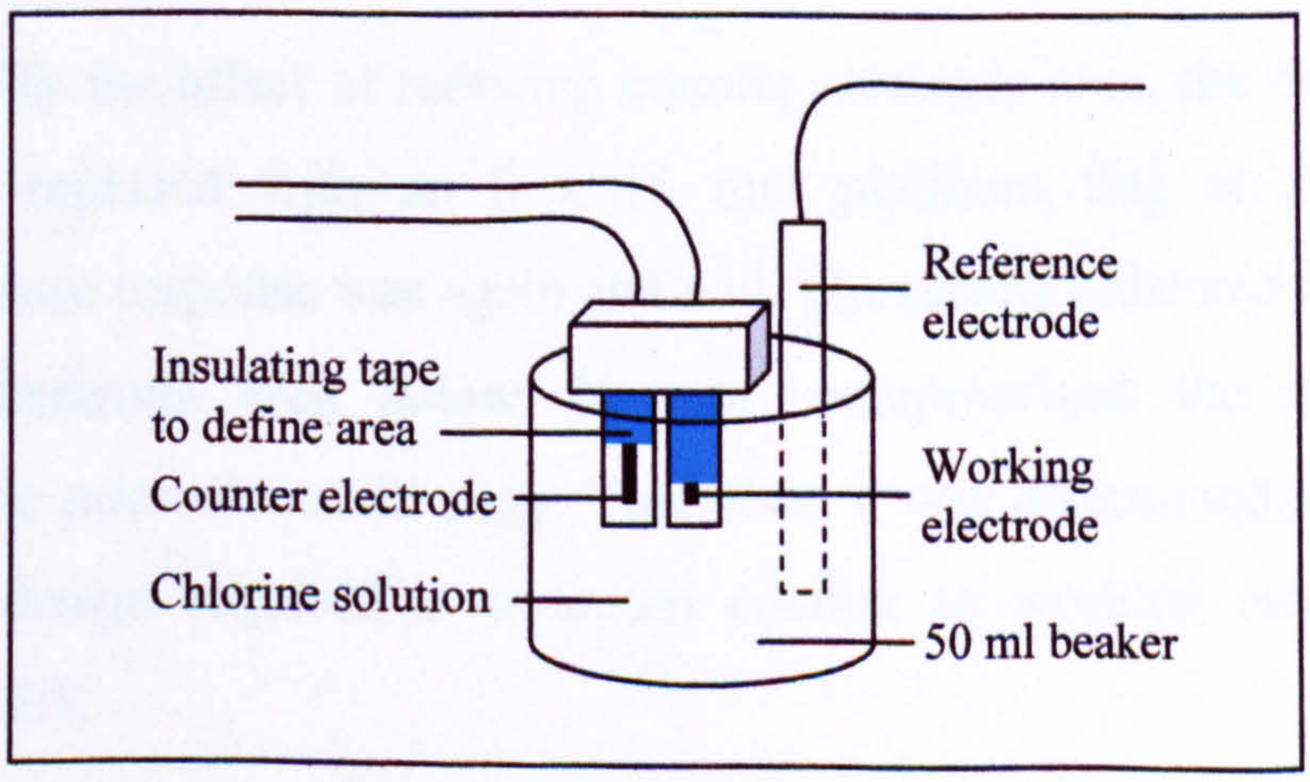

Figure 4.6: Three-electrode cell setup for determining counter electrode size

The working electrode was polarised at -100 mV and current flow in quiescent conditions recorded. A magnetic stirrer was then used to agitate the solution and cause current fluctuation. No change in current was observed when using a 40 mm^2 counter electrode size. The counter electrode size was then reduced by approximately 1 mm^2 in size using insulating tape until a signal fluctuation was observed when the solution was agitated (Figure 4.7).

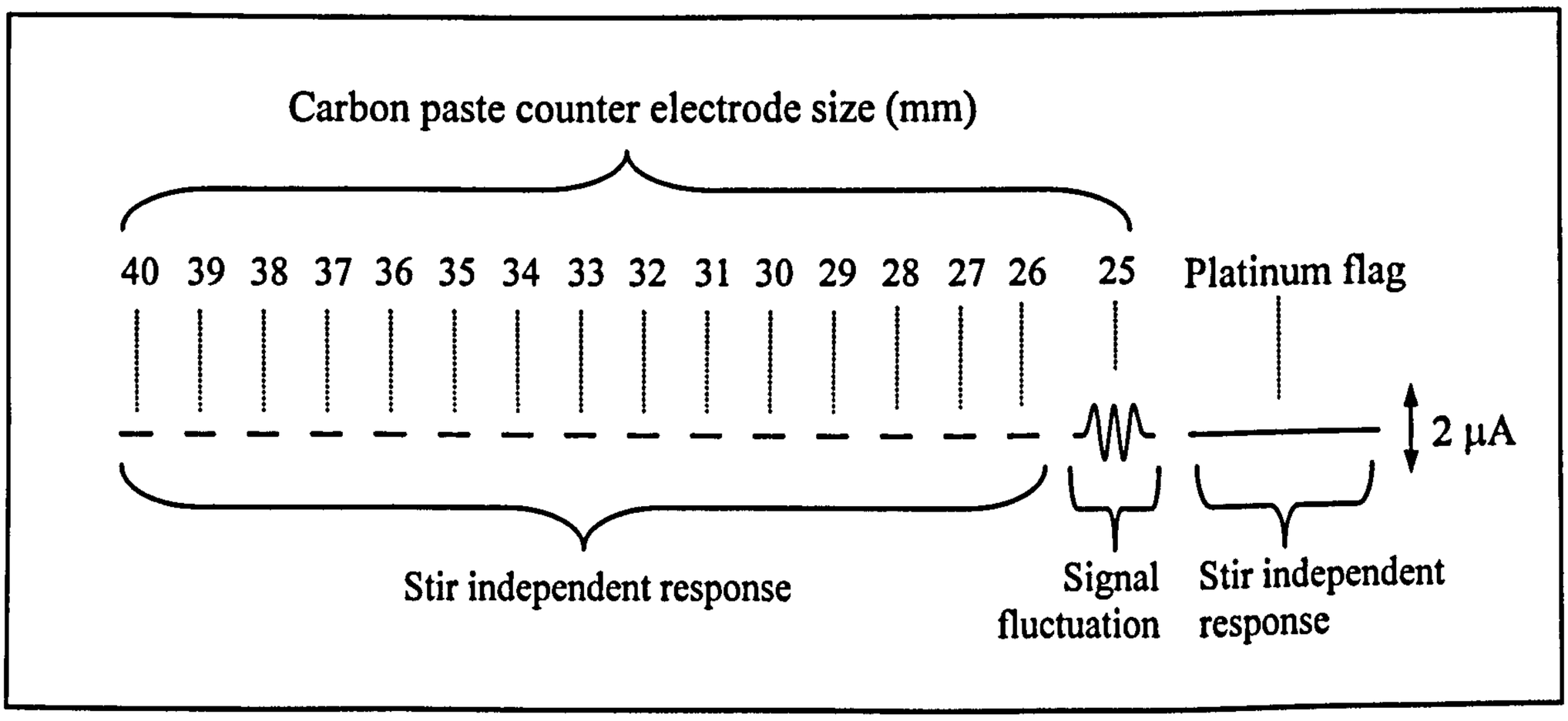

Figure 4.7: Determination of minimum counter electrode size

In order to verify the effect of reducing counter electrode area, the depleted counter electrode was replaced with an 8 x 15 mm platinum flag electrode, and stir independent sensor response was again attained. The results indicated that minimising the counter electrode area below 26 mm^2 compromised the stir-independent behaviour of the microelectrode array. Therefore, it was determined that the carbon-ink electrode design required a minimum counter to working electrode ratio of approximately 2:1.

4.4 Additional design considerations

It should be noted that the design of the sensor sheet for manufacture is as important as the design detail of the individual sensor. Therefore, in addition to current density considerations, further design features must be incorporated to facilitate *sensor production* and *sensor function*. It is important to note that the design of the sensor sheet as a whole is equally important as the design of the individual sensor. Base sensor production (via screen printing) must be as cost-effective as possible in terms of materials and production operations, while still allowing three primary down-stream requirements to be fulfilled:

1. *Quality control*. Since base sensor production will occur in high volumes via screen printing technology, appropriate quality control features must be considered in order to permit the simple and rapid assessment of print quality during production.

2. *Electropolymerisation*. Following screen printing, sensors undergo an electropolymerisation stage as part of sensor modification for microelectrode array formation (Section 5.3). This creates the requirement for the working electrodes of all sensors on a sheet to be electrically connected in order to allow for the polymerisation of a single sheet of sensors, or indeed the simultaneous parallel polymerisation of multiple sheets of sensors. The nature of this process, where sheets of sensors are suspended into a monomer solution for polymerisation, only allows for electrical connection at the top of a sheet. In order to guarantee the formation of an electrically insulating thin film, it was necessary to minimise the resistance path to all the sensors on a sheet.

3. *Packaging*. The ability for a disposable sensor and its delicate modifying layers to be protected from external abrasion and contamination during storage and transport is paramount to long-term sensor stability and performance. This will be achieved via a Microarray patented heat-seal

sensor packaging process (discussed in detail in Section 7.6). With similarity to the sensor / instrument connection requirement, this determined the need to devote some of the surface area in the sensor sheet design to heat-sealing.

Design considerations for base sensor functionality must also encompass the use of the sensor as a component of the instrument. For example:

1. *Confining solution to the sample chamber.* When water is placed into the sample chamber on the instrument, it must be prevented from escaping, especially into the contact pad area where it could disrupt the potentiostatic control of the cell.

2. *Interface with instrument.* In order for the sensor to be amperometrically interrogated, it must have some way of easily and reliably making a connection with the hand-held potentiostat-based instrument (Section 7.5). This can most cost-effectively be provided via means of a contact pad area designed for the familiar mobile phone SIM card interface.

3. *Removal of packaging.* It is important that at the point of use, the heat-seal layer is easily removed without causing any contact with the delicate sensor surface. This means that some of the sensor sheet area must be devoted to allow safer handling and easy removal of the protecting layer.

4. *Temperature correction.* As discussed in Section 2.5.2.5, amperometric response to chlorine varies to some degree with water temperature. Given the range of temperatures liable to be experienced in the field, it is necessary to incorporate a device such as a thermistor for measuring sample temperature and allowing a correction to be made.

5. *'Single use'.* To eliminate the possibility of a false result being provided by a sensor which has already been used, the design must incorporate a 'fuse' to prevent repeated use.

6. *Working electrode areas*. Every effort must be made at the design stage to ensure consistency of the size of the working electrode areas since this has a direct bearing on the amperometric signal size, and therefore sensor signal reproducibility.

4.5 Base sensor design

In order to maximise sensor performance and production efficiency, it was necessary to understand the screen printing production process and the basis of the production costs. Although specific prices and product details remain confidential, the main components of sensor design, including materials and processing operations, will be discussed.

It has already been mentioned that screen printable carbon-inks offer a less expensive alternative to more expensive conductive materials based on precious metals (Alvarez-Icaza & Bilitewski, 1993), and have become the substrate of choice for the manufacture of single-use (disposable) glucose sensors (Green & Hilditch, 1991), (Hart, 1994). Furthermore, carbon-inks exhibit lower background currents than metallic electrodes, so helping to yield higher signal-to-noise ratios (Niwa & Tabei, 1994). For these reasons carbon paste has been chosen as the main conductive surface for the working and counter electrodes. Work carried out in conjunction with Gwent Electronic Materials Ltd. (Mamhilad, Gwent, UK) allowed development of a low-cost, screen printable carbon-ink, suitable for measurement of aqueous chlorine. A matt polycarbonate material of 0.375 mm thickness (Cadillac Plastics Limited, Swindon, UK) was chosen for the printing substrate based on price, availability, good adhesion properties with carbon-inks and suitable rigidity for sensor handling. Standard off-the-shelf dielectric (insulating) and silver/silver chloride inks were also employed (DuPont Microcircuit Materials, Bristol, UK).

Given the selection of materials involved, it is clear that the production processes associated with screen printing are to have a relatively large influence on unit cost. Production costs are primarily based on the number of screen printing and drying operations required for production of a given batch of sensor sheets. For this reason it is necessary to design the production process in such a way that the number of steps required for production are minimised. This can be achieved by reducing the number of different materials required in the manufacture of each sensor sheet, and by only allowing only a single print operation for each one.

A further consideration for sheet design is the effect of electrical resistance of the conductive paths within a sheet of electrodes on the efficiency of the electropolymerisation process. Specific investigation was undertaken on this issue:

A screen printed carbon-ink (GEM) electrode (9 mm^2 area) was electropolymerised for 20 sweeps in 5 mM poly(*o*-phenylenediamine) solution (pH 7.4 phosphate buffer, 5 mM NaCl). The process was repeated with a range of resistors (0 to 100 kΩ) placed in series with the working electrode. The cyclic voltammograms for the electropolymerisation processes are illustrated in Figures 4.8 to 4.10. For clarity only voltammograms for resistances of 0, 1 and 3 kΩ are displayed here; the omitted results can be found in Appendix 1.

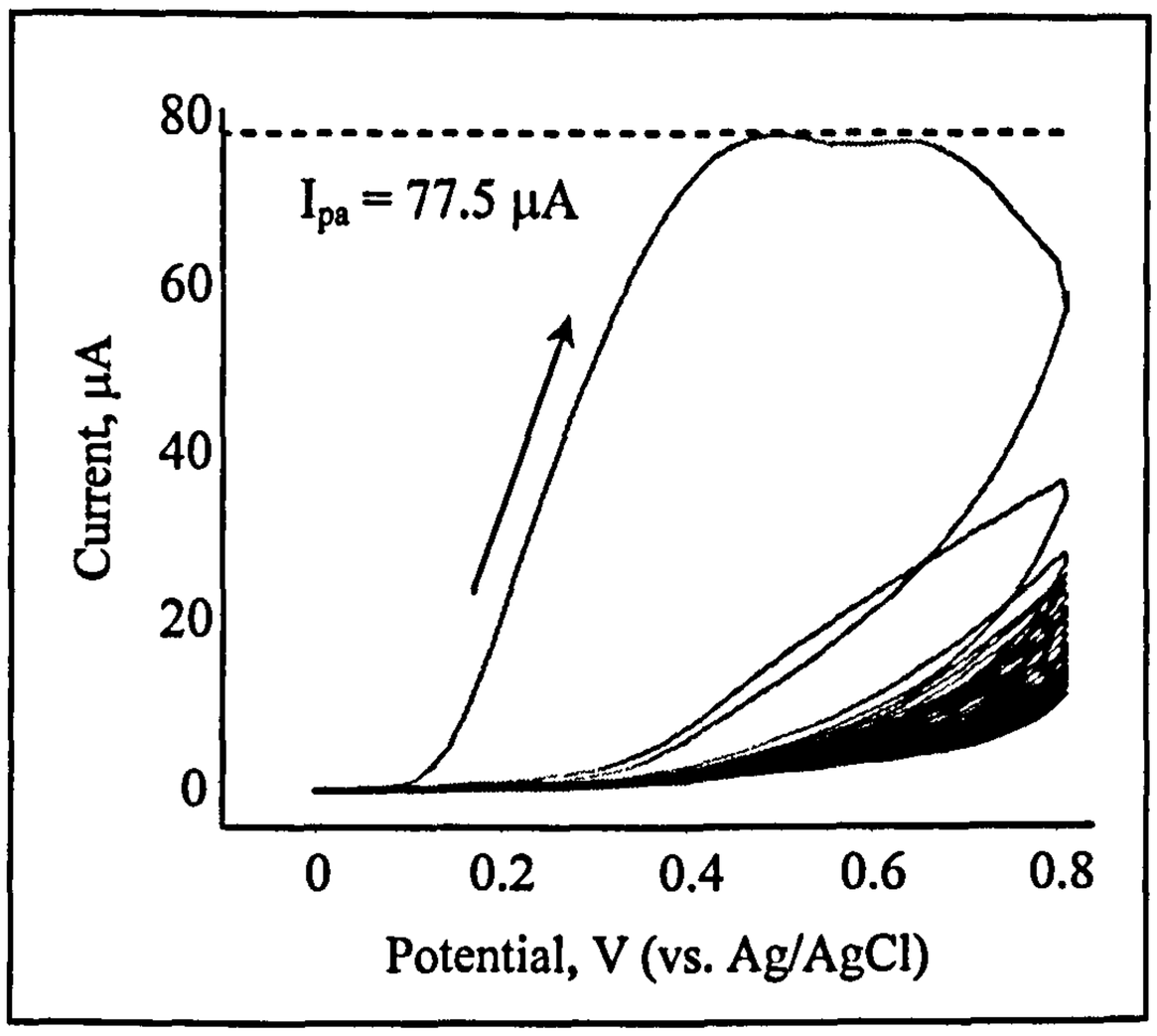

Figure 4.8: Electropolymerisation of 5 mM *o*PD (0 to +800 mV, 50 mVs^{-1}) on a 9 mm^2 screen printed carbon-ink host electrode

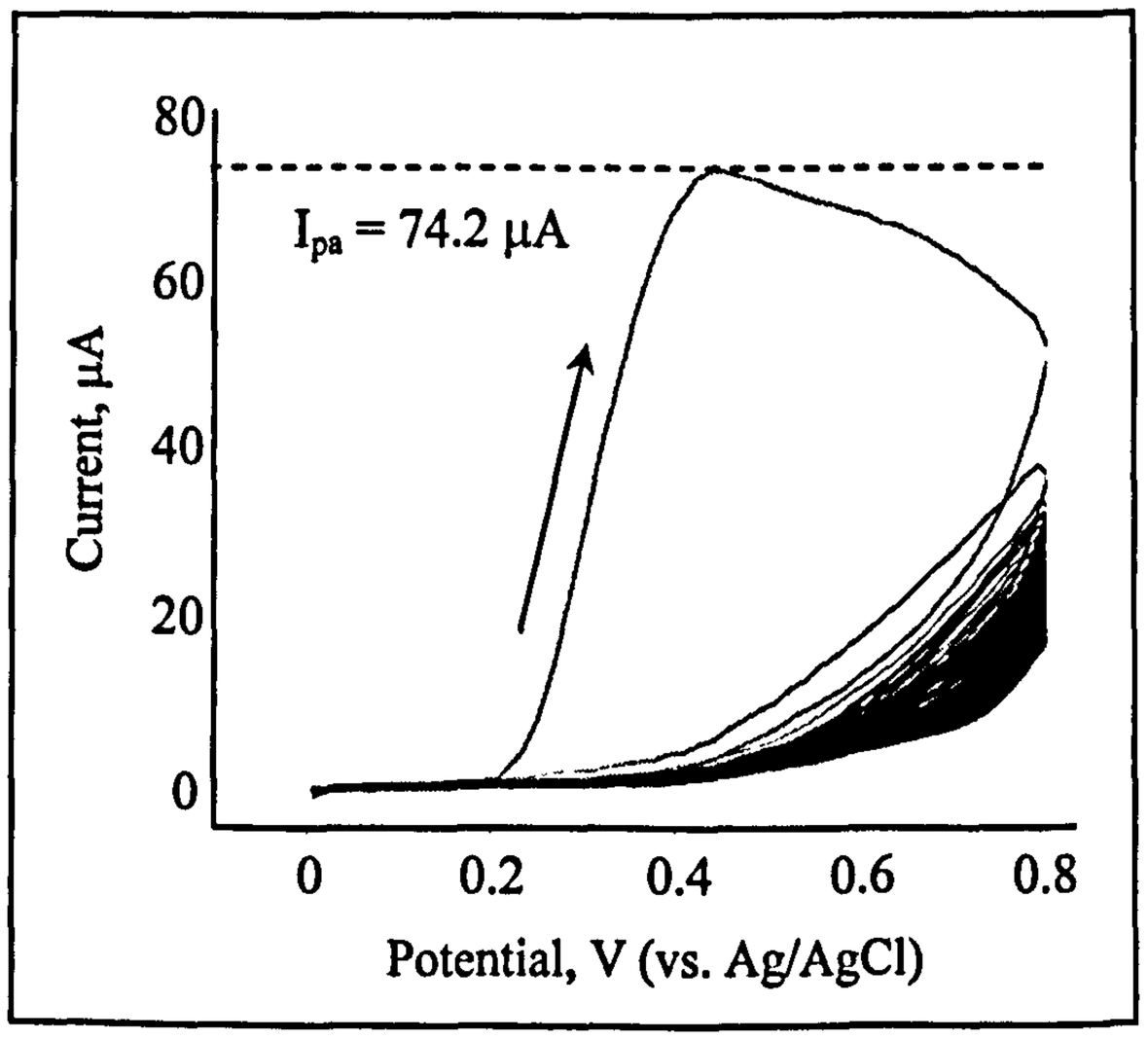

Figure 4.9: Electropolymerisation of 5mM *o*PD (0 to +800 mV, 50 mVs^{-1}), incorporating a 1 kΩ resistor in series

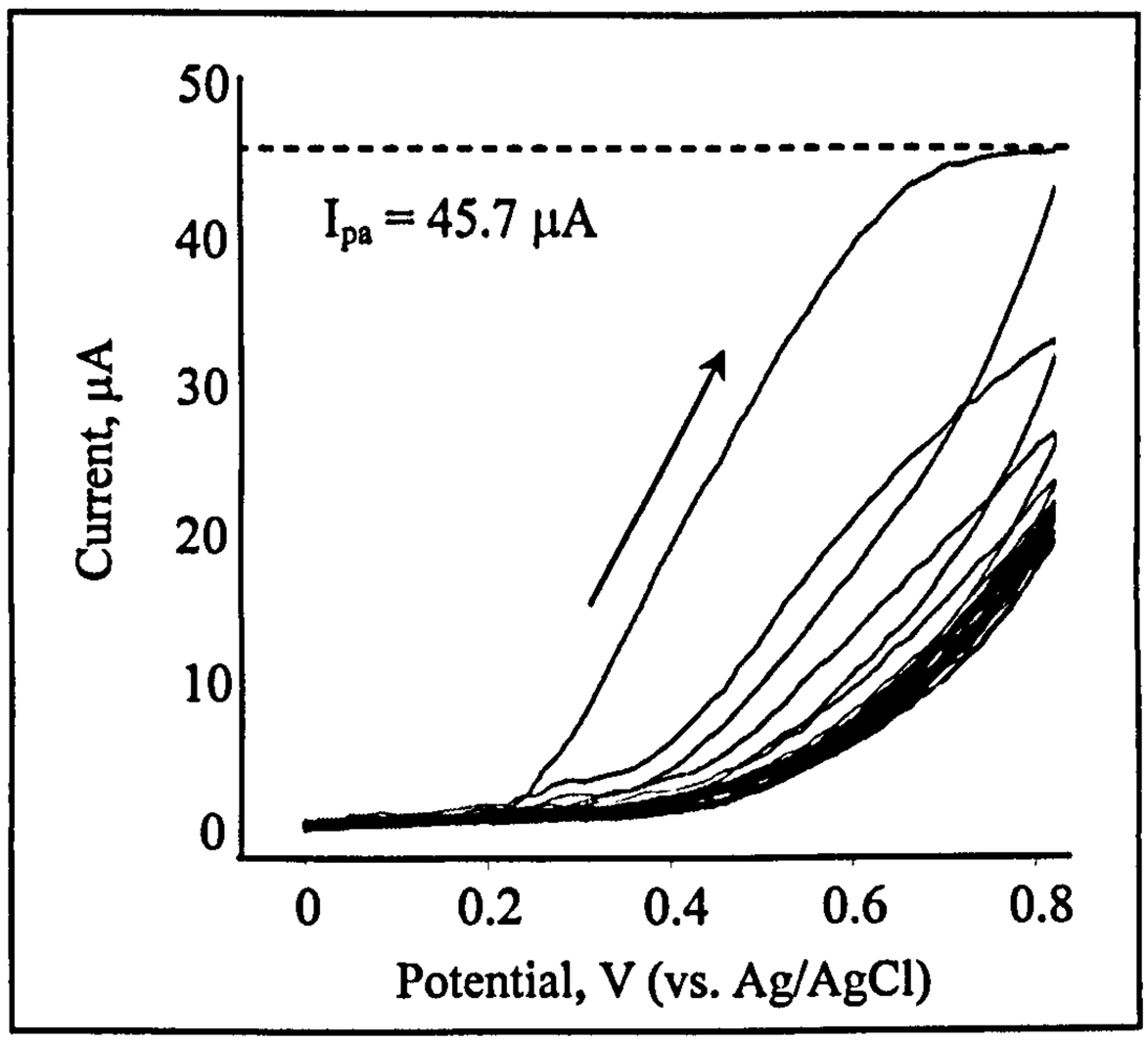

Figure 4.10: Electropolymerisation of 5 mM *o*PD (0 to +800 mV, 50 mVs^{-1}), incorporating a 3 kΩ resistor in series

From the data it can be seen that introducing a resistor in series with the working electrode results in a decrease in the magnitude of the initial peak currents. A large reduction in current (~40%) is observed with a 3 kΩ resistor, (Figure 4.7). Furthermore, the rate of electrode passivation is significantly reduced since the peak current on the final scan is approximately twice that for the case of no resistor (Figure 4.5). The decrease in current flow, together with the loss of the first anodic peak, suggests that resistance of this magnitude significantly limits the rate of charge transfer associated with the polymerisation process. Figure 4.6 exhibits the effect of a 1 kΩ resistor in series with the working electrode. The peak current for the initial scan can be seen to be reduced by only 4% when compared to Figure 4.5 (no resistor). Moreover, the first anodic peak on the first scan is still evident, and the decay in current exhibited by subsequent scans indicates an efficient rate of electrode passivation.

The significance of this data underlines the importance of the sensor sheet design in optimising the manufacturing process. Following screen printing, sensors undergo a

subsequent electropolymerisation stage as part of sensor modification for microelectrode array formation (Section 5.3). This creates the requirement for all the working electrodes present on each individual sensor to be electrically connected in order to allow their simultaneous electropolymerisation with poly(*o*-phenylenediamine). The nature of this process, where sheets of sensors are suspended into a monomer solution for polymerisation, only allows for electrical connection at the top of a sheet. From the data it was concluded that to permit efficient polymerisation, the design of the sensor sheet must provide a resistance path no greater than 1 kΩ from the top of the sheet to any one individual sensors working electrode.

Figure 4.11 shows a single Microarray Limited prototype sensor from the first trial-volume batch produced at Parlex UK Ltd. (Isle of Wight). The location of the working electrodes and the contact pads for the SIM interface have been highlighted in the photograph below (normally there would be a poor contrast between the exposed carbon and the remaining area of carbon, which is covered by a clear layer of insulating dielectric).

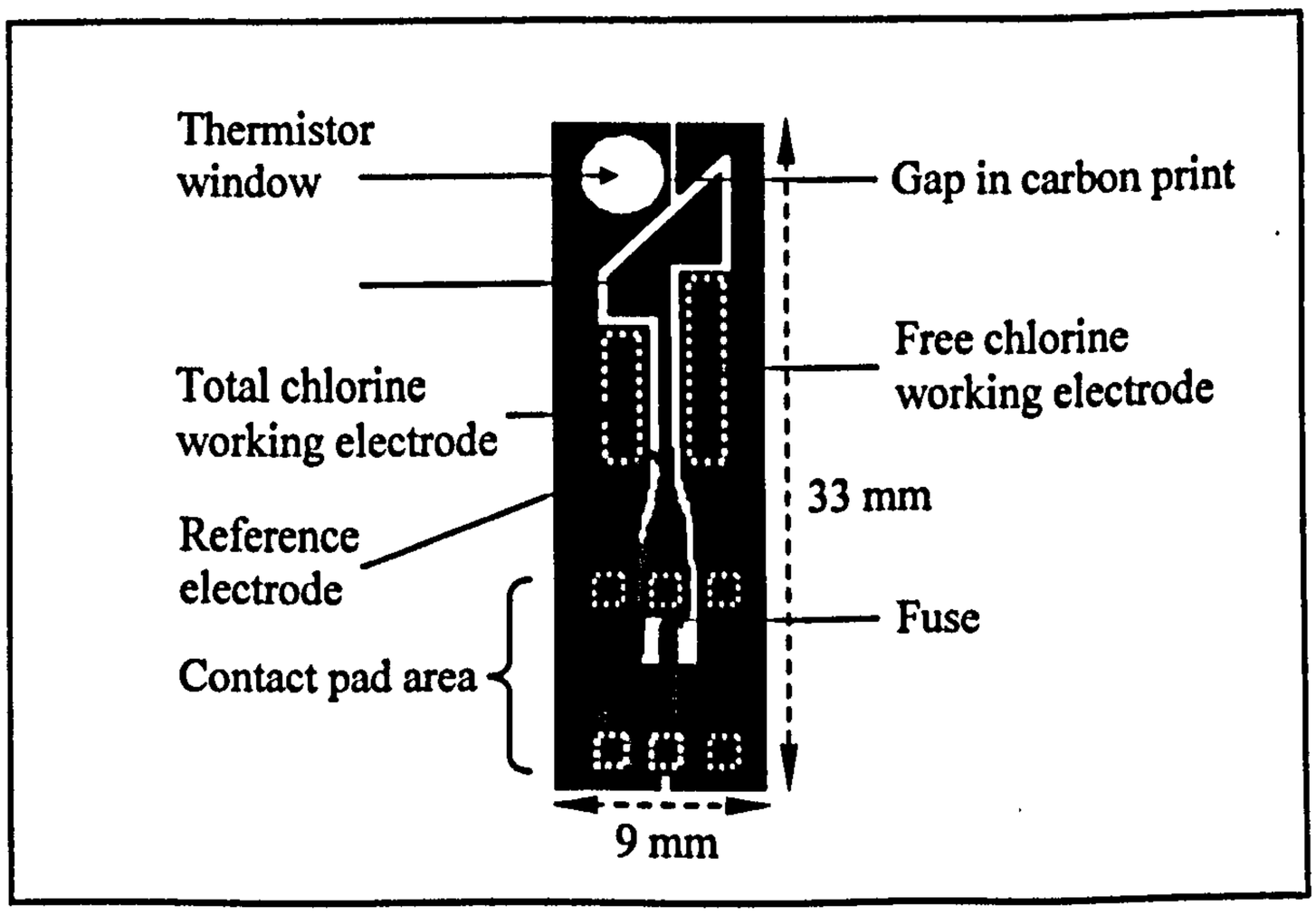

Figure 4.11: Microarray Ltd. prototype sensor from the industrial-scale production run

The prototype sensor design incorporated a *continuous* carbon layer across an entire sheet of electrodes. This was designed to facilitate the flow of current for the subsequent electropolymerisation sensor modification step, minimising the resistance experienced by any electrode to <1 kΩ. In this design, the two working electrodes become electrically isolated from each other following the separation of an individual sensor from a sheet. This occurs by means of a print gap within each sensor (indicated in Figure 4.11); the reference and counter electrodes are separated by a layer of dielectric material. There were a number of benefits to this system, for example, avoiding the need for more expensive conducting materials to carry the current for required electropolymerisation. In turn, this allowed the number of screen printing steps to be minimised to a single operation for each material used, namely carbon-ink, insulating dielectric material, and finally silver/silver chloride. A further advantage of the continuous carbon print design was the economical use of the sensor-sheet, since more of the area could be devoted to sensor production and so minimise sensor unit cost.

A key performance criterion of a *disposable* electrochemical sensor is the reproducibility of the size of the working electrode area, which directly affects the measured response. During screen printing production, a squeegee is used to force a viscous ink (such as carbon paste) through a silk-screen mesh onto the substrate below (Figure 4.12). Screen printing operational parameters, including the silk screen mesh size, tension and squeegee angle, pressure and speed will not be documented as they are remain commercially confidential.

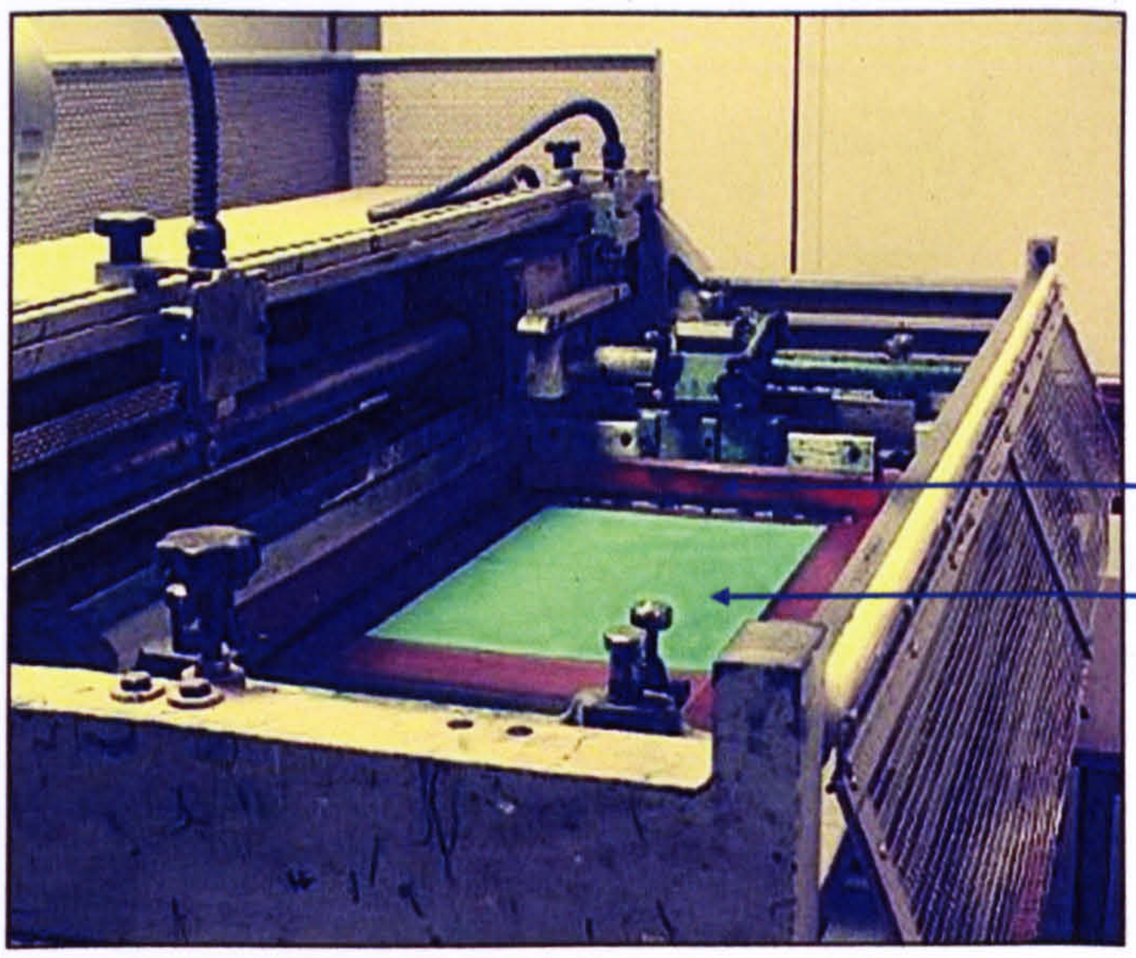

Figure 4.12: Screen printing machine showing squeegee and silk screen in place

Material is only able to pass through the 'open' area of the screen, i.e. the area of the screen which has not had the gaps between the threads sealed by a photoresist layer. The greatest factor affecting dimensional repeatability of a print operation is that of the location of the screen within the screen printer, and the position of the substrate placed underneath. The repeatability tolerances defined by Parlex Ltd. (Isle of Wight, UK) were given as ± 0.5 mm. This had important consequences for the electrode design. Given that a conductive track must lead from the bottom of each working electrode to the connective pad, this area must be insulated by dielectric material to prevent it contributing to the measured analyte signal. The variability of the position of this boundary would be detrimental for sheet-to-sheet signal consistency. In order to avoid this problem, working and counter electrode areas were defined on all sides by a single print of dielectric material, the 'dielectric window' (Figure 4.13).

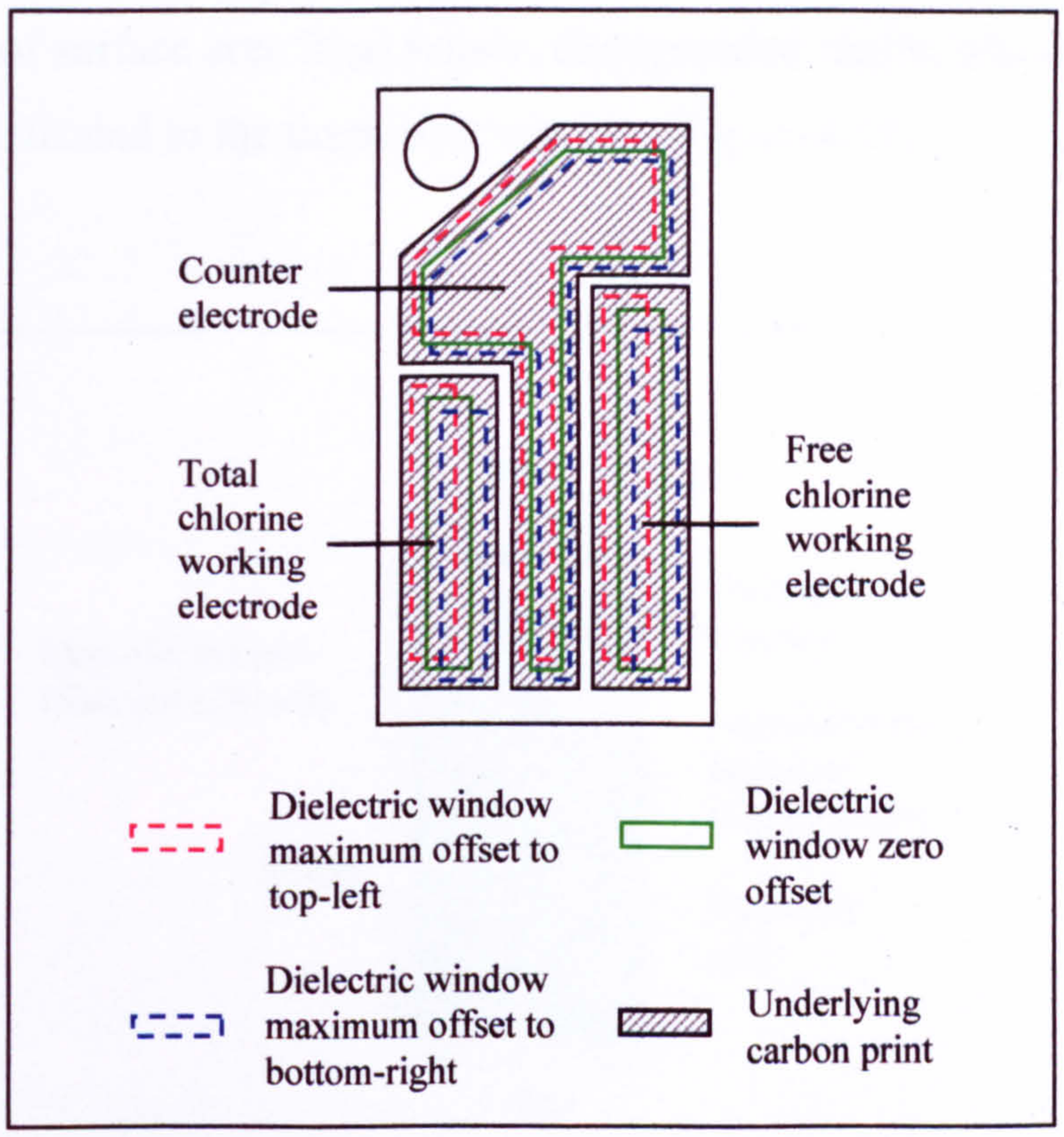

Figure 4.13: Schematic showing the definition of working and counter electrode areas by a single screen print dielectric window (not to scale)

It can be seen that using this design, even worst-case print alignment (for example, a 0.5 mm offset to the top-left or bottom-right) will not affect either the size of the working and counter electrodes, or their relative separation.

Further electrode design considerations had to be accounted for in order to create a functional sensor. For example, to allow interface with the hand-held instrument, a large area at the bottom of the sensor was devoted to the SIM contact pad area. In addition, the top left-hand corner was kept clear to allow the protrusion of a thermistor (mounted in the hand-held instrument) which permits the measurement of solution temperature as close as possible to the sensor surface.

As mentioned previously, in order to facilitate the safe removal of the protective packaging layer (Section 7.6) it was necessary to include an area of film which would not be adhered to the sensor surface. This provided the user with a point for easily

taking hold of the film to allow removal without damaging the sensor surface. To mitigate the loss of surface area from sensor, this unsealed region was combined with that of the area dedicated to the thermistor window (Figure 4.14).

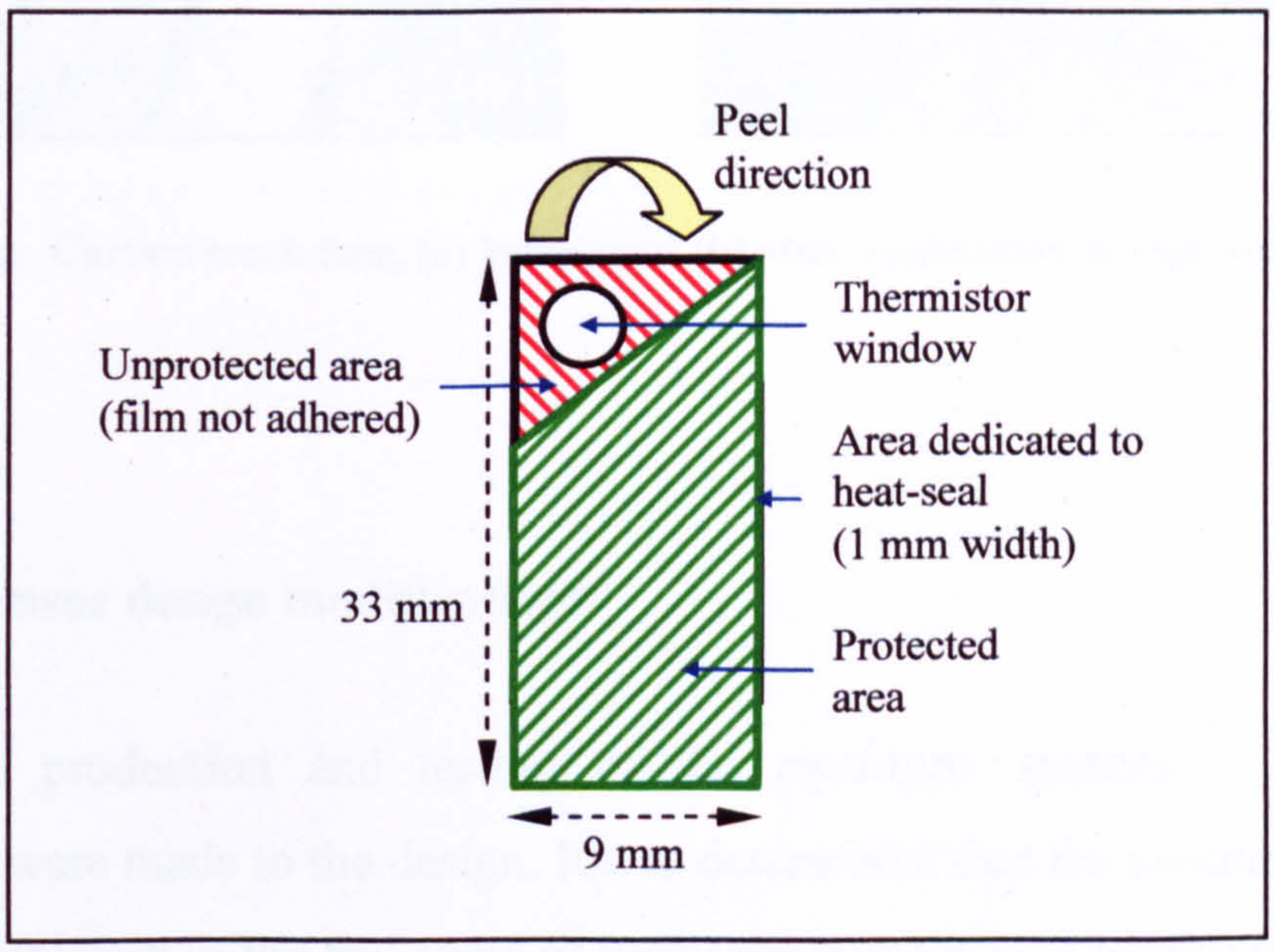

Figure 4.14: Schematic of sensor design indicating heat-sealed area and thermistor window (not to scale)

To prevent the repeated use of the same sensor, a fuse was incorporated into its design. When a sensor is inserted into the instrument for use, the instrument sends a short pulse through a thin carbon-track serving as a fuse, which 'blows' with an associated loss of electrical conductivity (Figure 4.15 (a) and (b) respectively). This indicates that the sensor has been used, and prevents repeated interrogation by the instrument. Tests were carried out on various widths of carbon track (0.4 to 1.0 mm) to determine the optimum dimension of carbon for the fuse design. The minimum width of carbon track able to be consistently screen printed was finally selected (0.4 mm). Below this dimension, inconsistent formation of the carbon track was observed on some sensors, in which the liquid paste reticulates (separates) as it wets the polycarbonate sheet. Using this dimension, a voltage of only 6 V was required for a period of 0.5 seconds to reliably blow the fuse, so helping to maintain the battery life of the instrument.

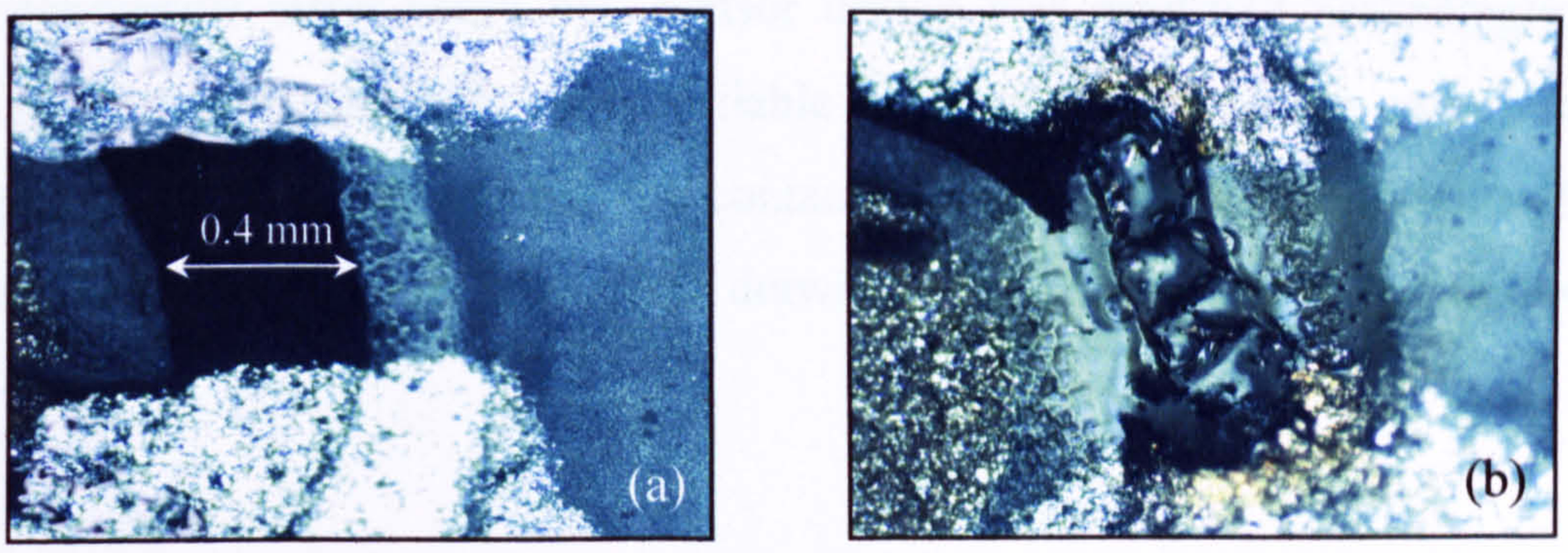

Figure 4.15: Carbon track fuse, (a) before and (b) after application of high voltage pulse

4.6 Base sensor design modifications

Following the production and testing of the prototype sensors, a number of improvements were made to the design. It was determined that the continuous carbon print design employed in the full sheet of prototype sensors was resulting in reduced sensor performance. When an individual sensor is cut from the sheet, a small area of carbon is exposed along the edges of the sensor. It was envisaged that the contribution of this area to the signal would be both negligible and reproducible, since the area exposed by cutting would be approximately the same for each sensor, and the thickness of the carbon print (~20 μm) satisfied the critical maximum dimension typically defined for microelectrode behaviour (Bard & Faulkner, 2001), (Zoski, 2002). However, when sensors were interrogated in the laboratory, it was observed that in stirred solutions, the signal contribution from the exposed edge was significantly compromising the sensors stir-independent response characteristics. This detrimental effect on sensor performance outweighed the cost-saving advantages of using a continuous carbon print, and a new design detail for maintaining low electrical resistance across a sheet was required.

An alternative method for minimising potential drop between different areas of the sensor sheet involves the printing of materials more conductive than carbon, dedicated for the role of carrying charge to the sensors for electropolymerisation (known as *bus-bars*). The least expensive material suitable for such a role was a

highly conductive silver-based ink. Sensor design was modified accordingly, and taking advantage of the additional available printing operation, the carbon tracks leading between the electrodes and the contact pad area were also replaced with the more conductive silver ink. The CAD drawing of a single sensor is exhibited in Figure 4.16.

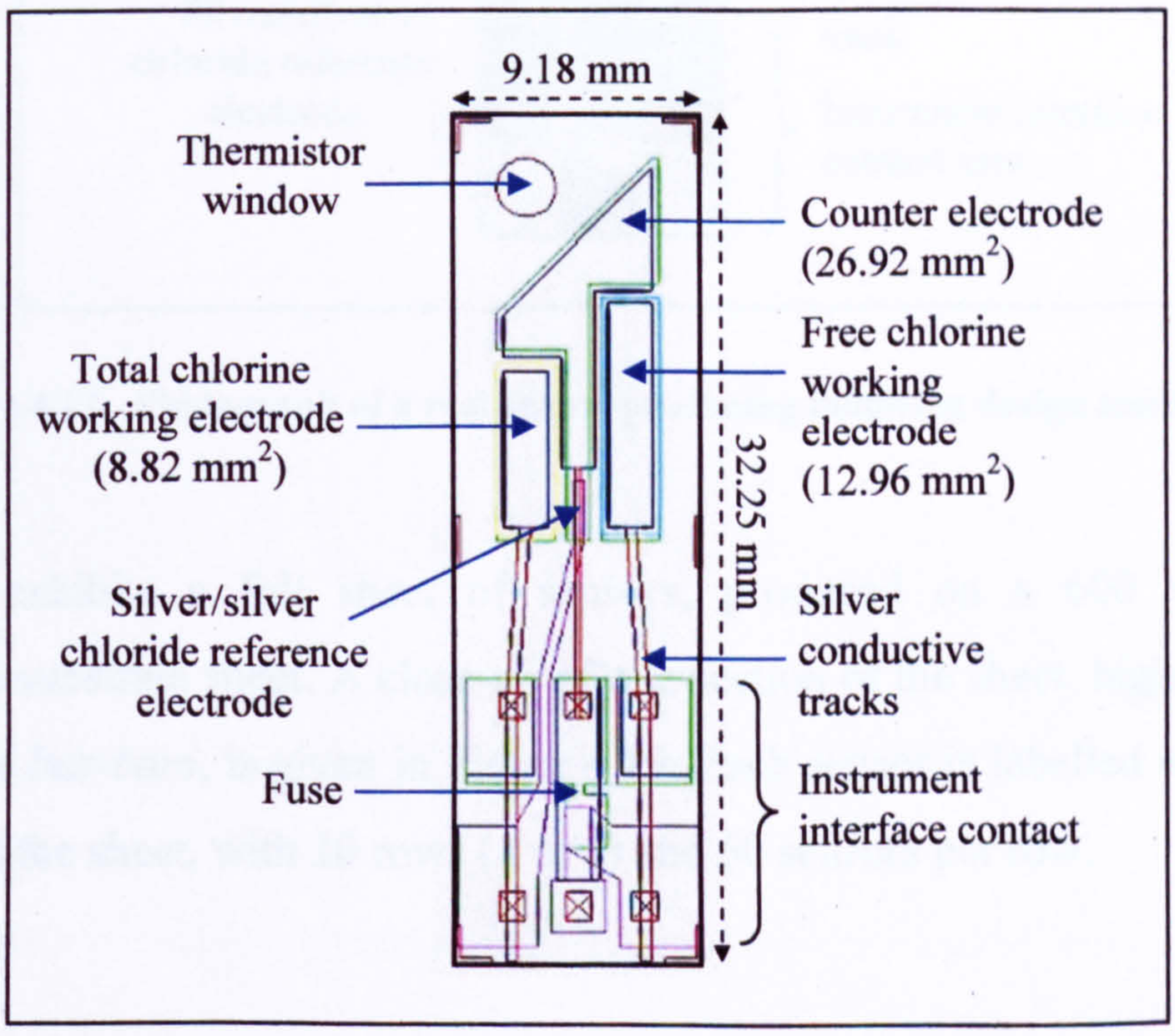

Figure 4.16: CAD drawing of finalised sensor

It can be seen that the areas of the working and counter electrodes exceed the minimum design requirements established in Section 4.2. This margin of excess is intended to guarantee sensor performance without adversely affecting unit cost.

A close-up photograph of a real sensor is exhibited in Figure 4.17. With the new sensor design, the limited use of carbon provides a natural contrast between the electrode areas and the rest of sensor (for example, the polycarbonate substrate), highlighting the design features. Subjectively, this is also more aesthetically pleasing when compared to the design shown in Figure 4.11.

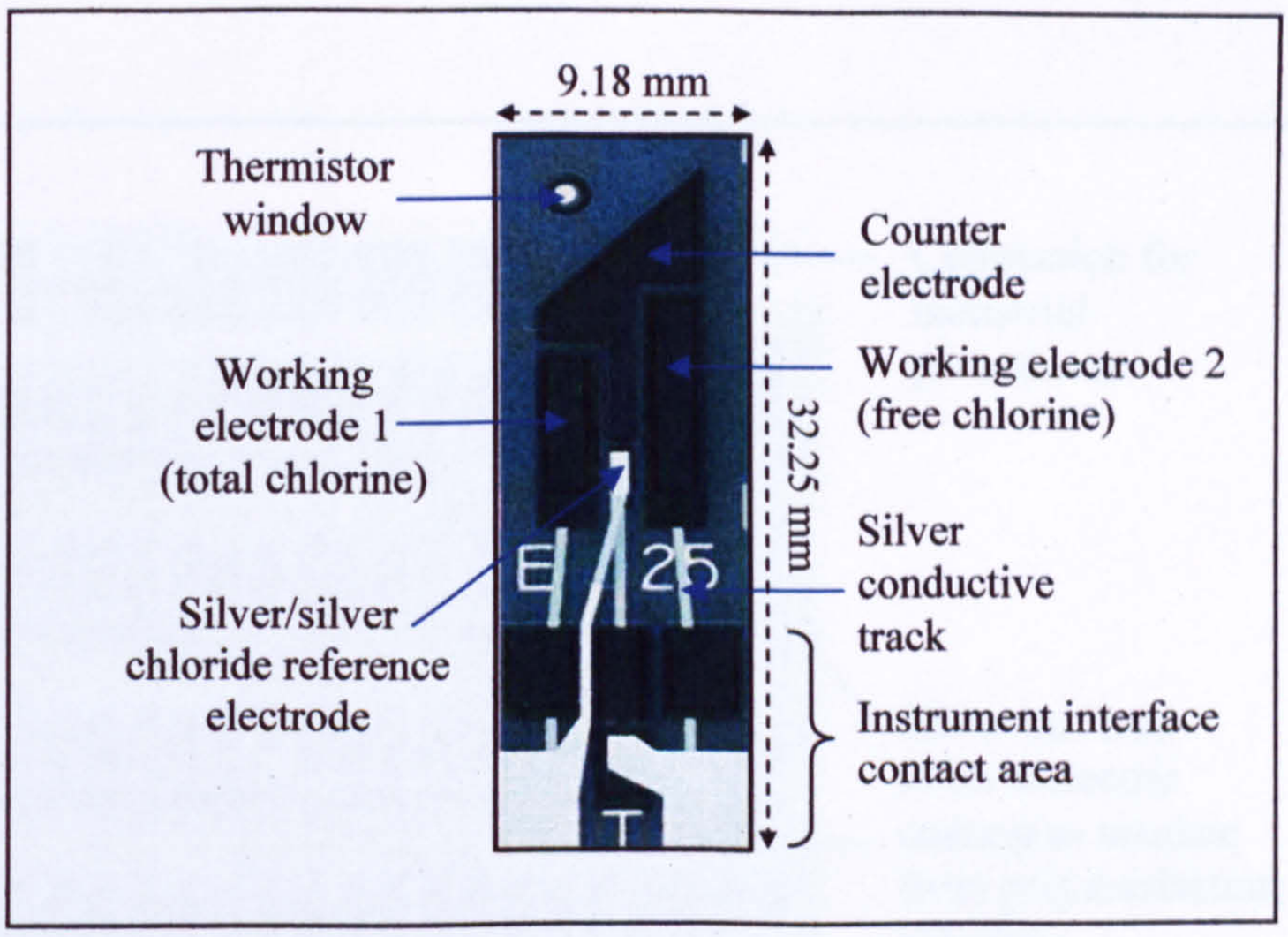

Figure 4.17: Photograph of a real sensor producing following design modifications

Figure 4.18 exhibits a full sheet of sensors, produced on a 600 x 400 mm polycarbonate substrate sheet. A close-up of one section of the sheet, highlighting the position of the *bus-bars*, is given in Figure 4.19. Each sensor is labelled according to its position on the sheet, with 10 rows (*A* to *J*) and 60 sensors per row.

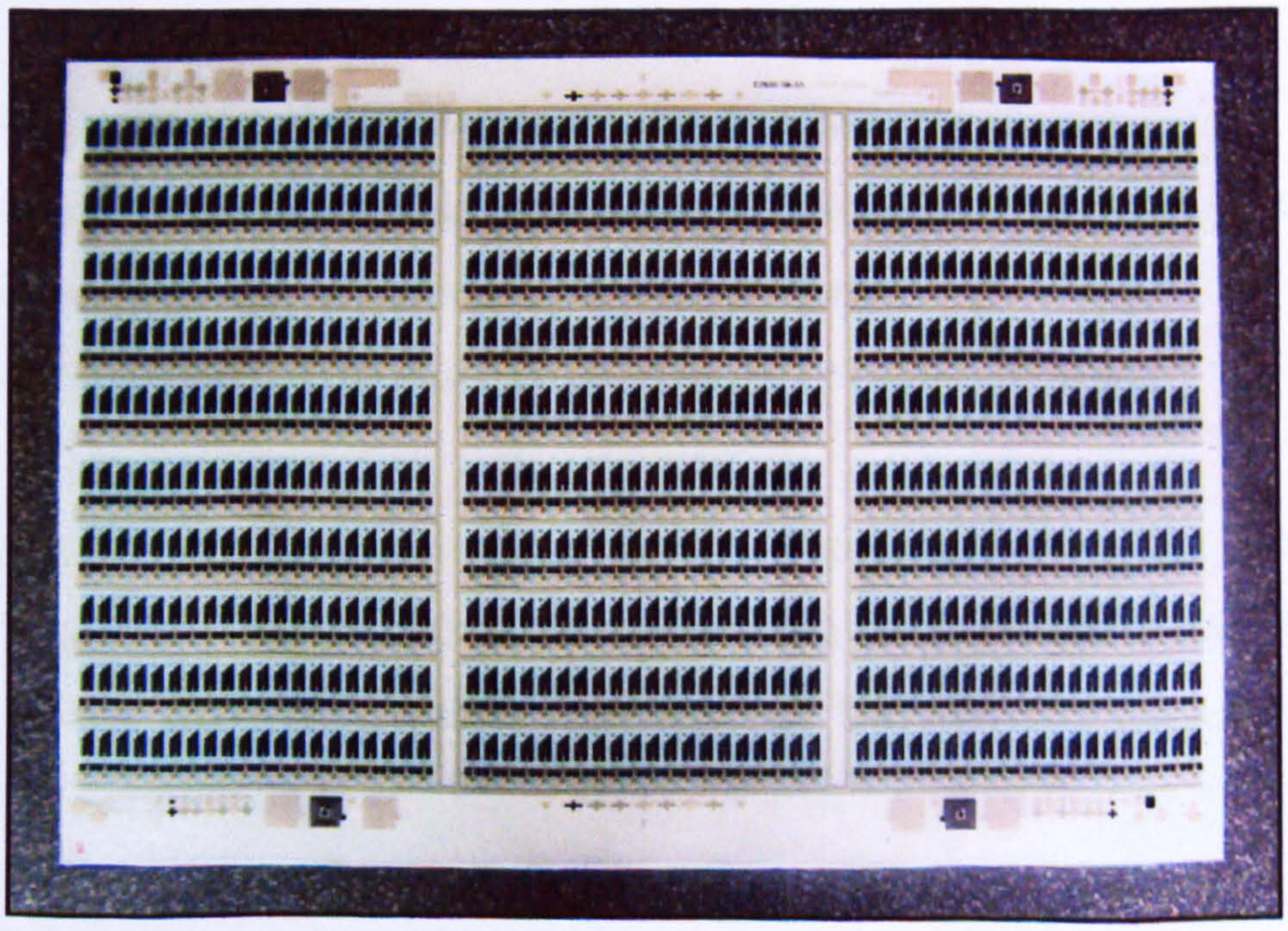

Figure 4.18: 600 disposable sensors, screen printed onto a 600 x 400 mm polycarbonate sheet

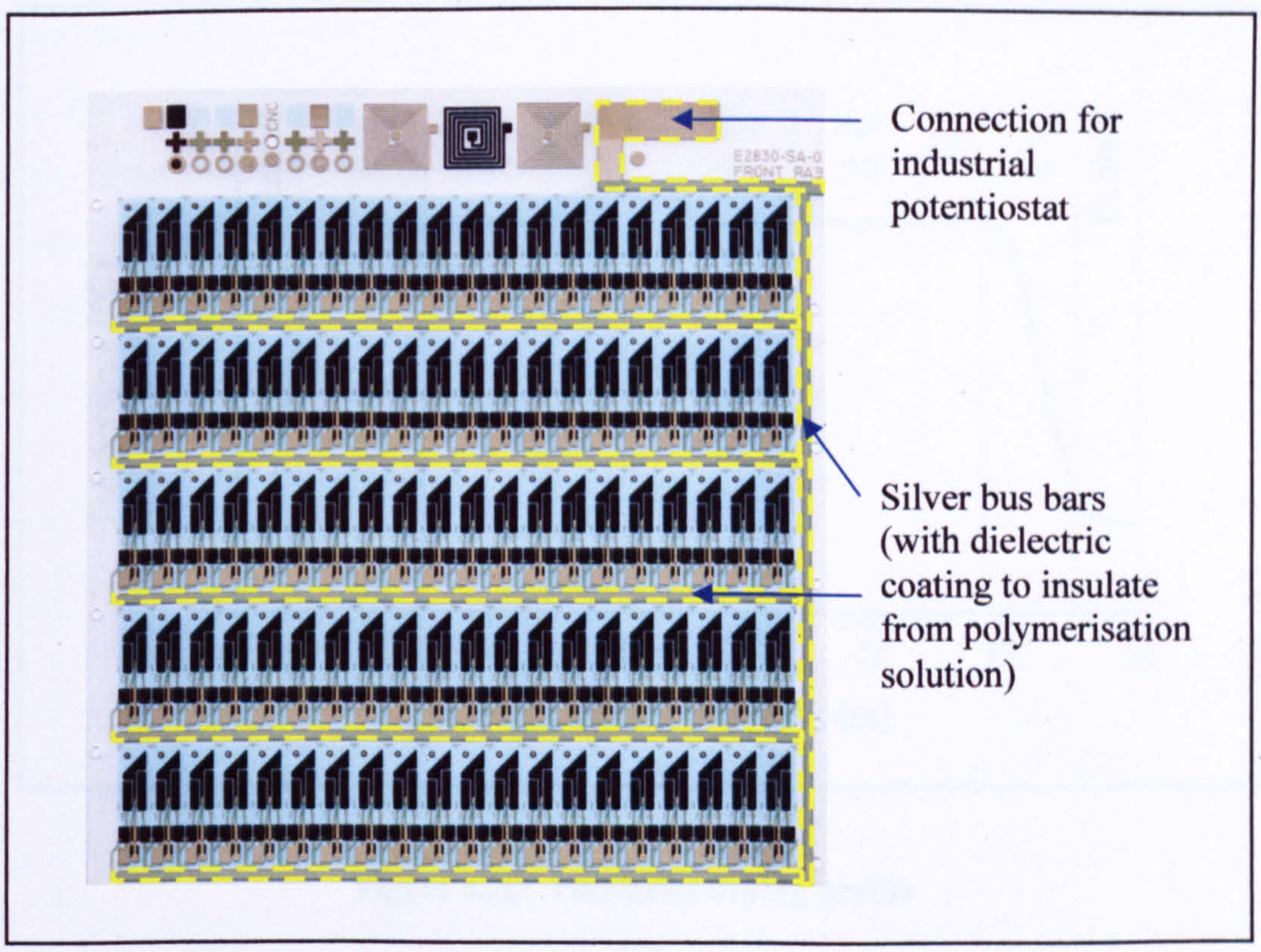

Figure 4.19: Close-up of sensor sheet illustrating bus-bars

The finalised screen printing process order is as follows, with each stage representing a single print operation:

1. Screen printing of the silver conductive bus bars
2. Screen printing of carbon paste electrode, contact pad and fuse components
3. Screen printing of an insulating dielectric layer
4. Screen printing of the silver/silver chloride reference electrode

Following every operation, a drying procedure was carried out using a controlled convection system (Figure 4.20). Following printing of the dielectric layer (stage 3), the sheets were also exposed to a short burst of UV radiation during the drying procedure to aid its curing.

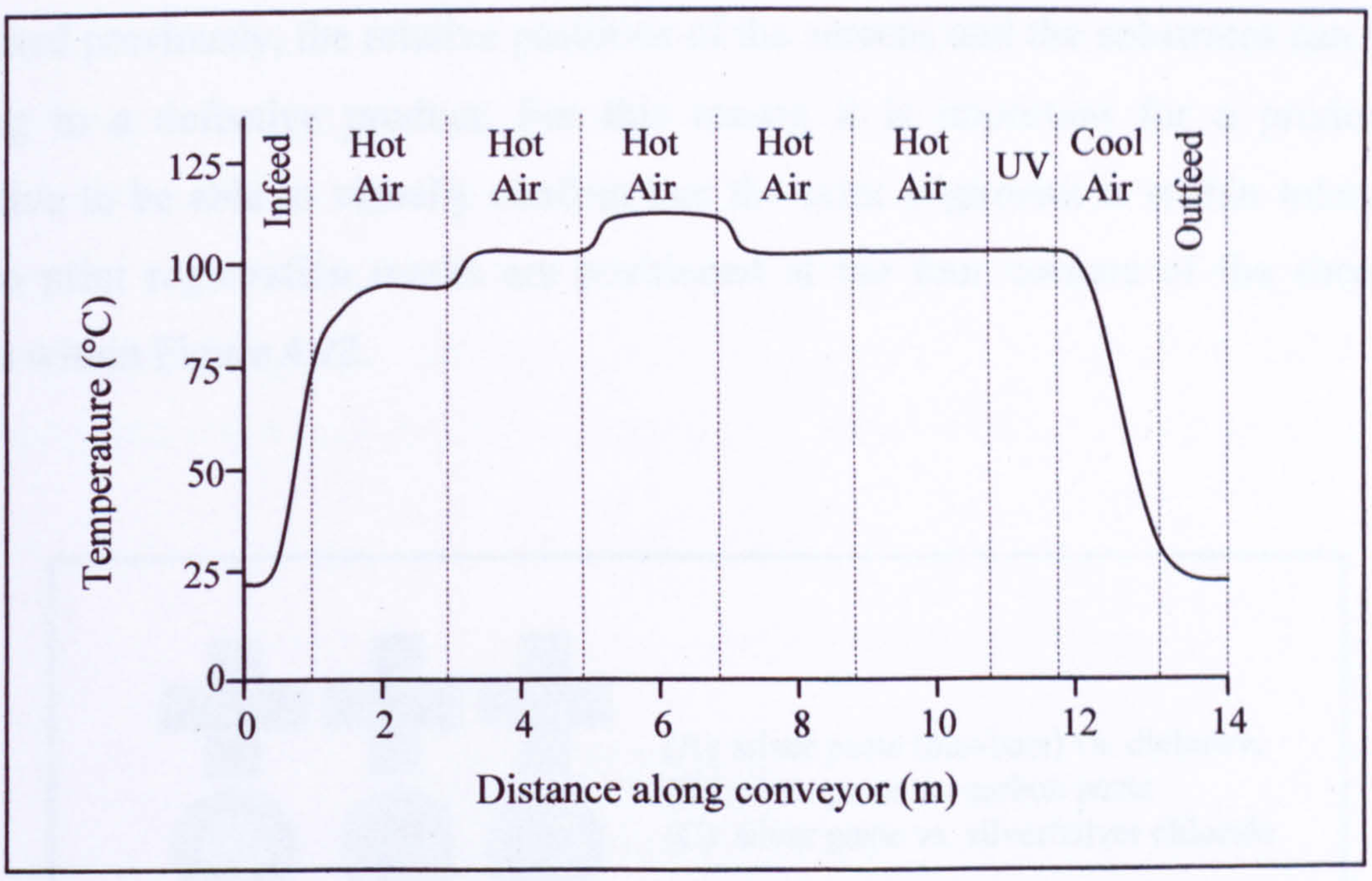

Figure 4.20: Post-print drying profile

Various design features were included on the sensor sheet to provide a method for verifying the quality of the screen printing process, located at the edges of the sensor sheets (highlighted in Figure 4.21).

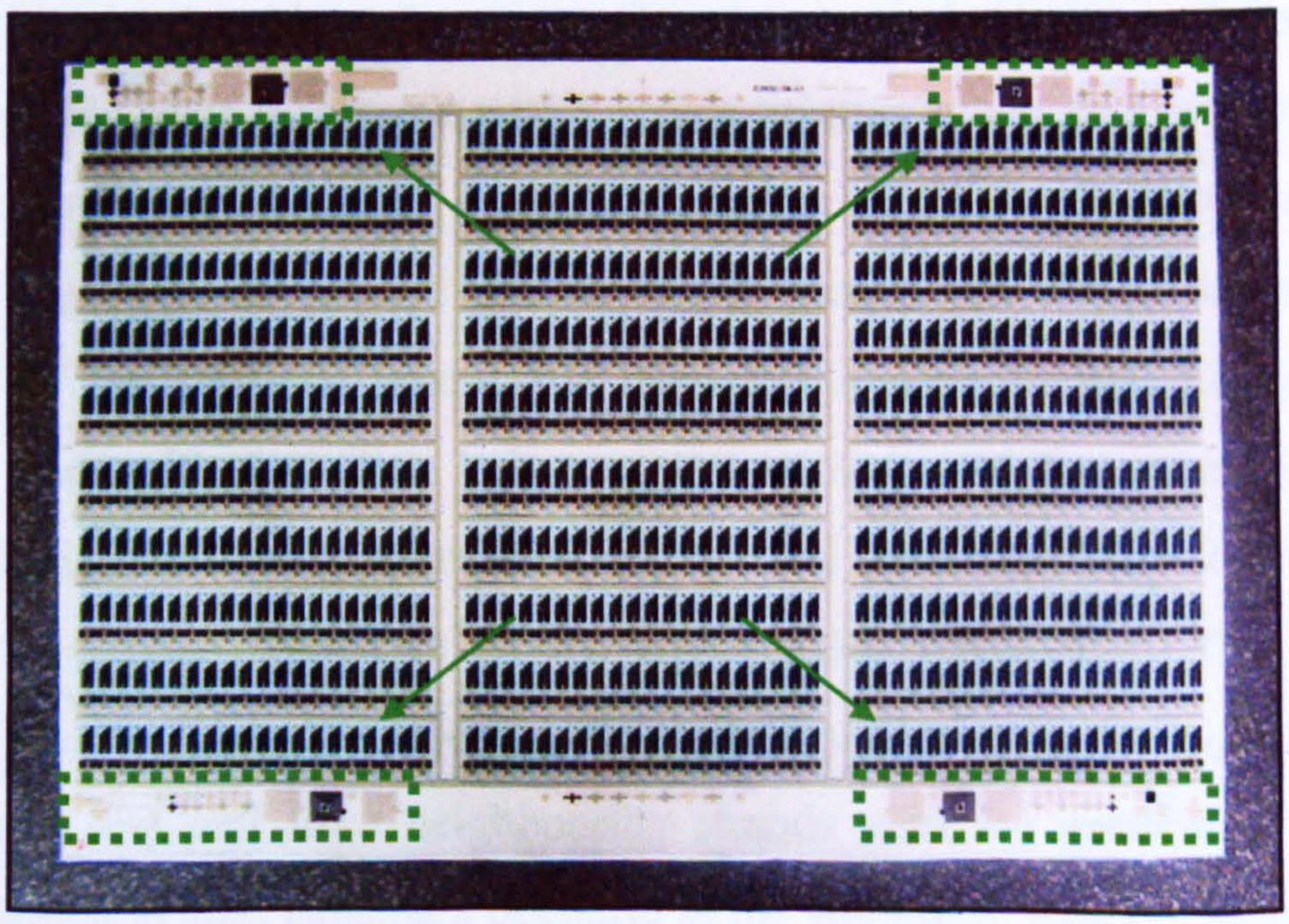

Figure 4.21: Location of screen print quality control design features

The primary concern relating to quality during screen printing is that of alignment. As discussed previously, the relative positions of the screens and the substrates can vary, leading to a defective product. For this reason it is important for a production operative to be able to visually confirm that the print alignment is within tolerance, and so print registration marks are positioned at the four corners of the sheet, as shown within Figure 4.22.

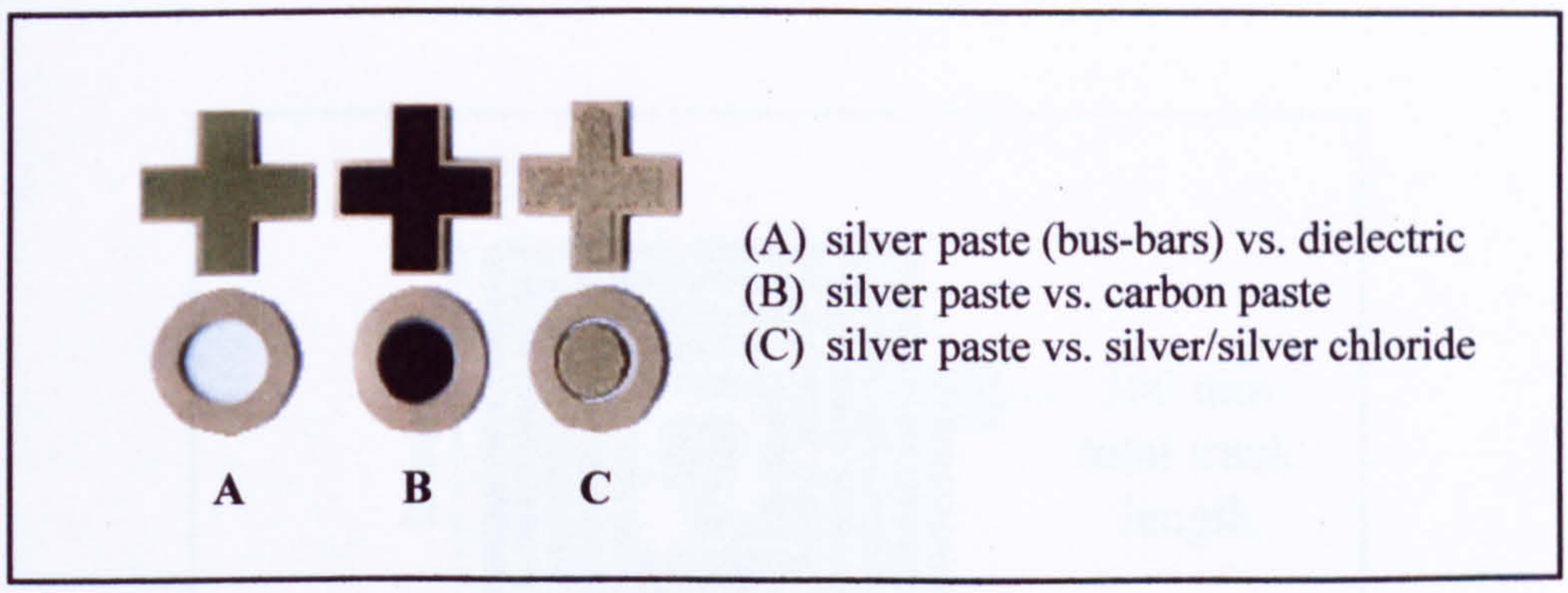

Figure 4.22: Screen print registration marks

This particular design feature allows the visual comparison of the relative positions of the printing operations. For example, in Figure 4.22 (c), the relative positions of the silver/silver chloride and silver bus-bars print can be seen. Although there is a slight off-set, registration is within tolerance as there is no over-lap between the two prints.

A further quality issue associated with a screen printing production process is related to variation in print-thickness. As a consequence of the screen printing process, whereby a squeegee is pressed against a silk screen and drawn across to force material onto the substrate below, the print-defining screen will naturally distort under the load, with the effect being more pronounced in the centre. Due to the repeated elastic deformation, combined with natural wear caused by friction, the silk screen fibres gradually undergo plastic (irreversible) deformation. This upsets the balance of tension across the screen, causing the fibres towards the edge of the sheet to experience less pull from neighbouring strands with the result that their pores become reduced in size, causing a decrease in the amount of material which can pass through during a printing cycle. Consequently, conductive tracks in these areas are prone to becoming excessively thinned, or even discontinuous, and the conductivity

of the printed tracks could be compromised to a point where it hinders the electropolymerisation process or simply prevents the electrochemical function of the sensor during use. Given the speed and volume of production, it was not feasible to rely entirely on visual inspection for this type of print quality assessment. Therefore, in order to allow a rapid, objective analysis, a spiral design motif possessing maximum track length for minimum area was included for each of the conductive inks, and again was positioned at the four corners of the printed sheet (Figure 4.23).

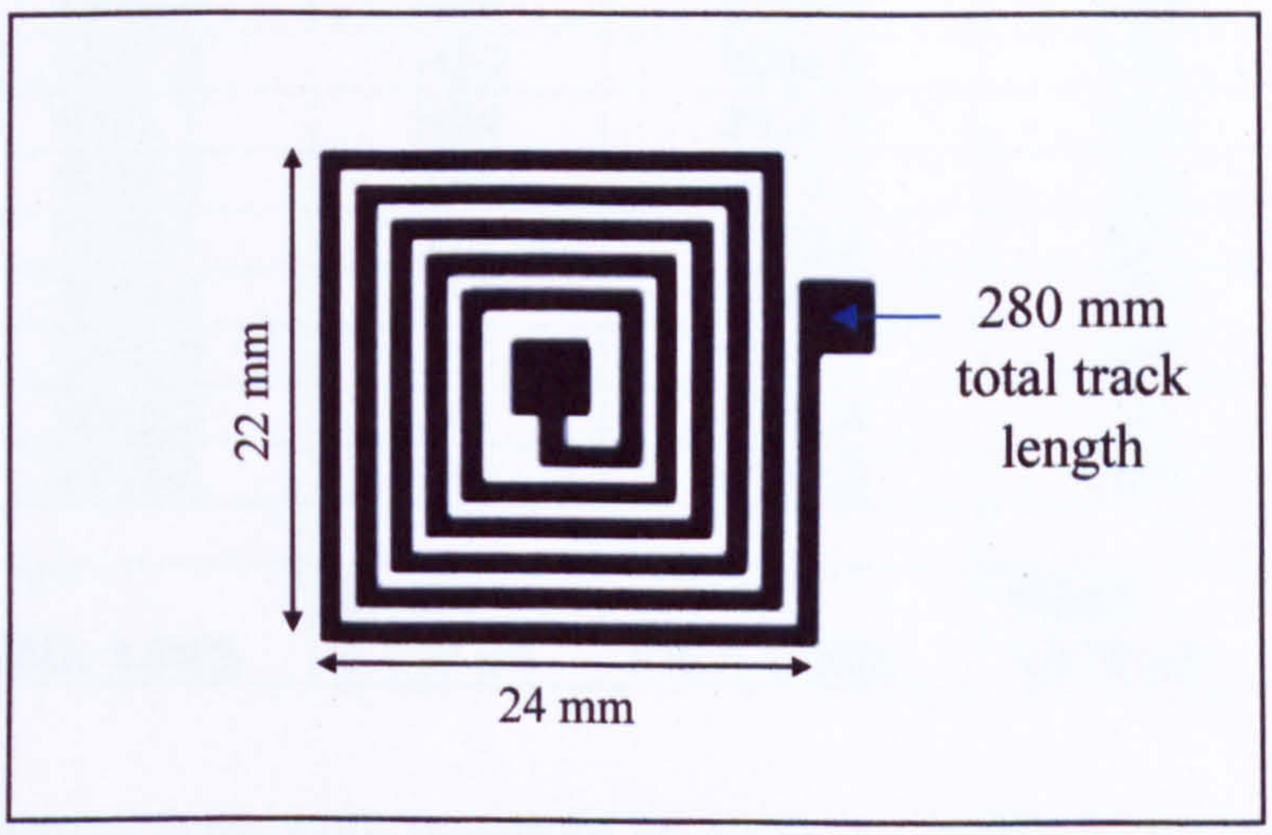

Figure 4.23: Spiral motif for confirming print quality of conductive inks

During full-scale manufacturing, an automated system will confirm the conductivity of the motif without interrupting production. A maximum resistivity of 25 kΩ, 500 Ω and 700 Ω indicates an acceptable print thickness for the carbon, silver and silver/silver chloride inks respectively.

Prior to further modification it was necessary to ascertain the reproducibility of the screen printed base sensor for chlorine detection. In order to achieve this, a random selection of 20 bare carbon sensors were taken from 3 sheets and interrogated amperometrically with 20 ppm total chlorine (pH 4.0 acetate buffer, 1 M KI, 50 mM NaCl). Signal magnitudes were taken from the mean current derived from the final 10 seconds of a 90 second polarisation period (-100 mV) in quiescent solution.

Sheet 1		Sheet 2		Sheet 3	
Sensor ID	**Current (nA)**	**Sensor ID**	**Current (nA)**	**Sensor ID**	**Current (nA)**
A1	9180.3	A5	9125.8	A1	9087.7
A20	9090.6	A28	9027.6	A20	9008.4
B48	9264.2	B48	9129.2	B48	9154.0
C12	8987.1	C12	9325.0	C12	9215.1
C32	9112.8	C32	9163.7	C32	8968.0
D28	8981.9	D28	9245.1	D28	9118.6
D52	9232.2	D52	8979.8	D52	9016.5
E19	9176.6	E19	9127.1	E19	9112.2
E60	8983.4	E60	9091.3	E60	9249.1
F23	9112.5	F23	9027.7	F23	9135.8
G9	9132.6	G9	9230.1	G9	8982.4
G49	9266.0	G49	9166.0	G49	9221.3
H26	8957.3	H26	9054.6	H26	9112.9
H24	9172.7	H24	9338.9	H24	9168.2
I32	9234.3	I32	9119.4	I32	9037.5
I55	9078.1	I55	9189.2	I55	9112.4
J10	9014.0	J10	9040.3	J10	9312.0
J30	9157.9	J30	9187.9	J30	9112.9
J41	9025.3	J41	9085.4	J41	8975.6
J60	9112.8	J60	9150.5	J60	9196.2
Mean: 9.114 µA	**RSD: 1.08%**	**Mean: 9.140 µA**	**RSD: 1.05%**	**Mean: 9.115 µA**	**RSD: 1.06%**

Table 4.1: Assessment of the reproducibility of signal response to 20 ppm total chlorine (pH 4.0 acetate buffer, 1M KI, 50 mM NaCl)

The results indicate a relative standard deviation (RSD) of approximately 1.1% for the unmodified screen printed carbon-ink base sensor, sufficiently low to permit further modification towards stir-independent aqueous chlorine detection.

4.8 Conclusions

A method for the amperometric detection of aqueous free, total and combined chlorine using a two-working electrode system has been established. As a means of minimising production costs (and ultimately unit cost) by careful sensor / sensor sheet design, working electrode and counter electrode area requirements were established using generic (GEM) screen printed carbon-ink electrodes

Additional sensor function and production requirements were then considered, such as the effective polymerisation of *o*PD onto screen printed carbon-ink electrodes, were it was established that a resistive path of no more than 1 kΩ should be experienced from the top of a sheet to any individual sensor. Furthermore, the inherent reproducibility of sensor responses was maximised by considering the nature of the screen printing production process and employing a single dielectric window to define the size and relative positions of the working and counter electrodes. This permitted the number of screen printing operations, and their associated production costs, to be minimised.

Sensors designed in this manner were manufactured at a specialist thick-film electronic materials screen printing facility (Parlex, UK) and shown to possess a base electrode reproducibility of approximately 1.1% (RSD), sufficiently low to permit subsequent modification towards stir-independent aqueous chlorine detection.

CHAPTER 5

Base electrode modification: Electropolymerisation of poly(*o*-phenylenediamine)

5.1 Introduction

A range of applications utilising electropolymerised poly(*o*-phenylenediamine) films have been investigated previously, including pH sensing applications (Cheek *et al*, 1983), synthesis of biomimetic molecularly imprinted polymers (Malitesta *et al*, 1999) and a wealth of biosensor related applications (Sasso *et al*, 1990), (Almeida and Mulchandani, 1993), (Castanón *et al*, 1997), (Ekinci *et al*, 2001), (Barton *et al*, 2004), (Pritchard *et al*, 2004).

The electropolymerisation of poly(*o*-phenylenediamine) can be exploited to electrically insulate a sensor surface with an ultra-thin layer of polymer. As described in more detail in Chapter 6, this film can then be ultrasonically ablated to create numerous microscopic pores exposing the underlying conductive substrate. As the conductive pores are electrically connected, this results in the formation of a microelectrode array sensor device.

Alternatively, it is possible to polymerise *o*-phenylenediamine via chemical polymerisation methods, employing a *chemical oxidant* as an initiator. These methods are often employed for industrial polymer syntheses, since the approach is highly appropriate for the bulk polymerisation of reaction mixtures. However, in the context of electrode surface modification, electrochemistry can provide a simple and efficient route to site specific polymerisations at electrode surfaces of any size or number (Imisides *et al*, 1991). The films produced can be easily controlled voltammetrically in terms of density and thickness (particularly for the case of self-limiting *insulating* polymers) and can provide complete coverage on a molecular level (Sasso *et al*, 1990) (Castanón *et al*, 1997). This chapter will detail the industrial scale-up for the electropolymerisation of *o*-phenylenediamine, from initial investigations up to industrial-sized sheets of screen printed carbon-ink electrodes.

5.2 Electropolymerisation of *o*PD onto gold substrates

Initial investigations into the electrodeposition of insulating films of poly(*o*-phenylenediamine) utilised gold sputter-coated ground glass slide electrodes. A 5 mM solution of *o*PD in pH 7.4 phosphate buffer was cycled 20 times between 0 and +800 mV at 50 mVs^{-1} (cyclic voltammogram illustrated in Figure 5.1). It is noted that unless otherwise stated, all potentials herein have been quoted with respect to Ag/AgCl.

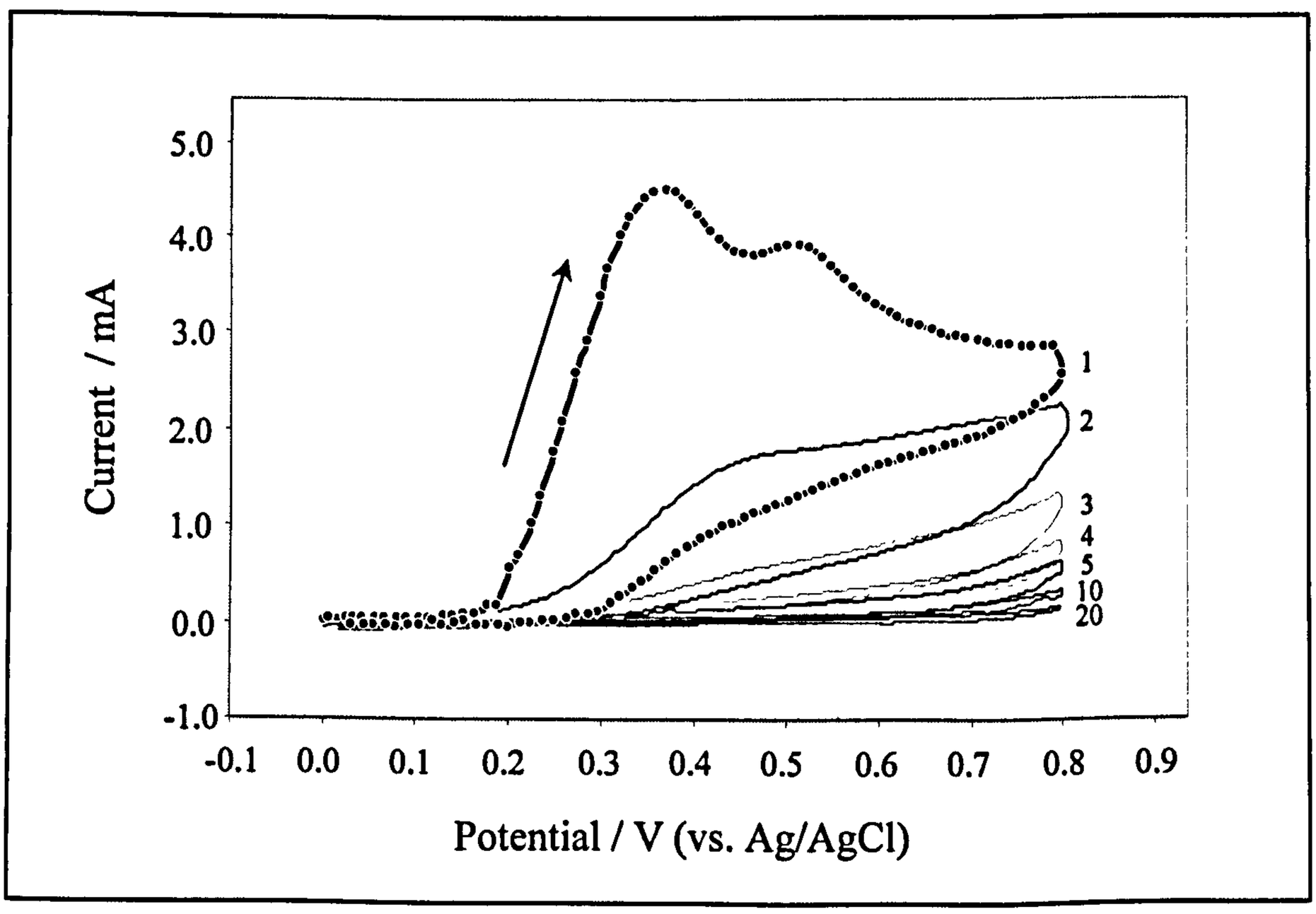

Figure 5.1: CV obtained during the polymerisation of *o*PD (at pH 7.4) on a gold slide electrode

A characteristic cyclic voltammogram for the electropolymerisation of *o*-phenylenediamine was obtained. Two anodic peaks are exhibited on the first sweep, at approximately +350 and +525 mV (vs. Ag/AgCl). Research by Jang *et al* investigated the nature of these peaks and showed that no complementary cathodic peaks can be found if the scan is reversed, indicating that the process is completely irreversible in nature (Jang *et al*, 1995). Using NMR spectroscopy, the first

voltammetric peak was identified as due to the oxidation of the *o*PD monomer to form a radical monocation (Figure 5.2).

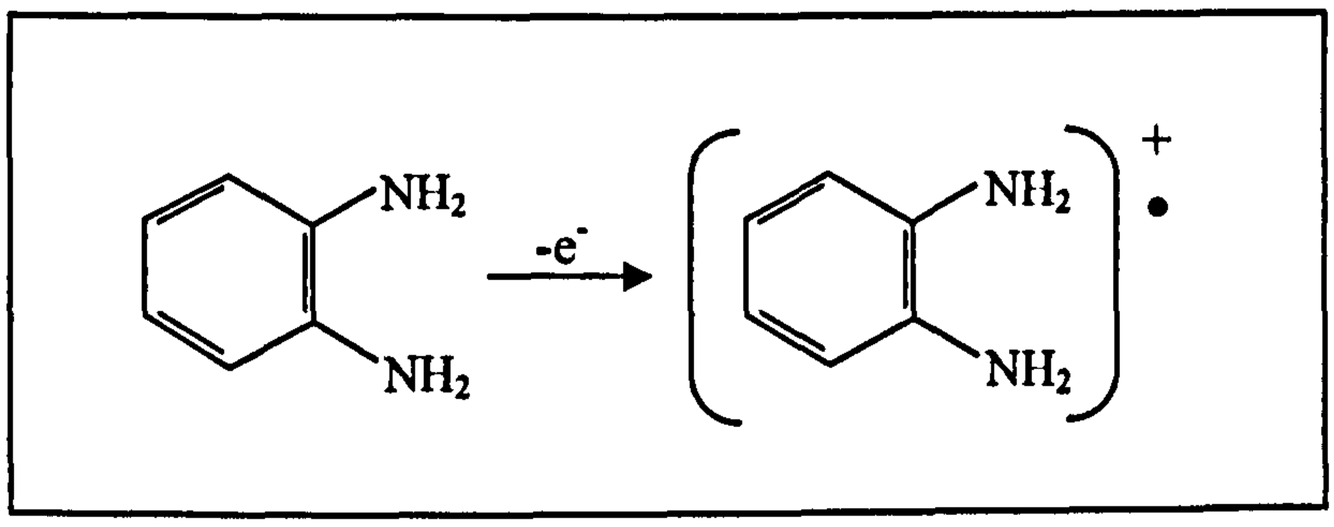

Figure 5.2: Initial oxidation of the *o*PD monomer to form a radical monocation

The monocation species immediately combines via radical coupling to form one of three possible dimers (Figure 5.3).

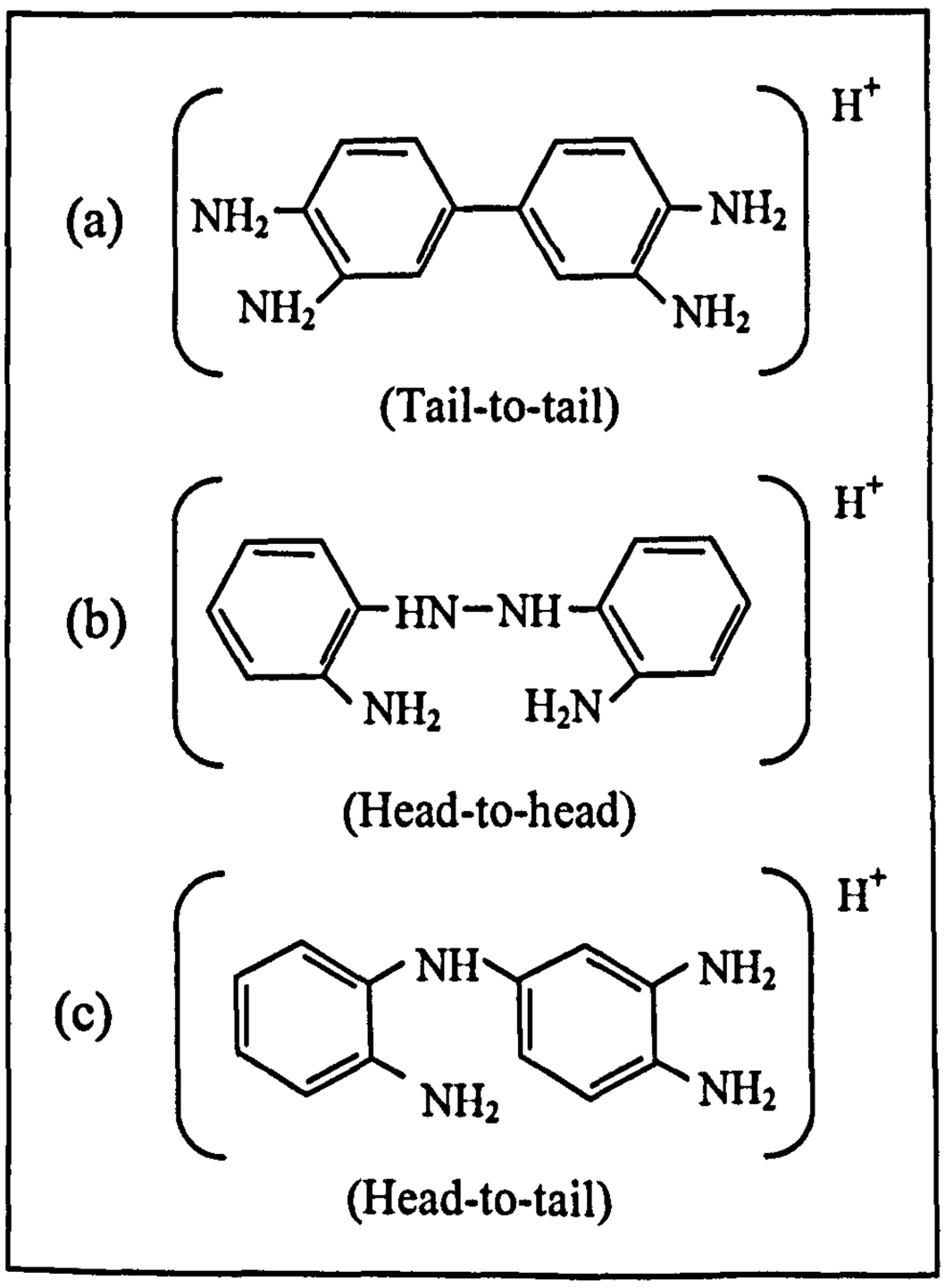

Figure 5.3: Dimerisation following oxidation of *o*PD

As C–N coupling has been shown to be dominant for the anodic oxidation of aromatic amines in aqueous solution (Volkov *et al*, 1980), (Deng & Van Berkel, 1999), the 'head-to-tail' dimer configuration is formed preferentially (Figure 5.3c). This structure is suitable for propagation, and the molecule can undergo further elongation to produce more (soluble) species (Figure 5.4).

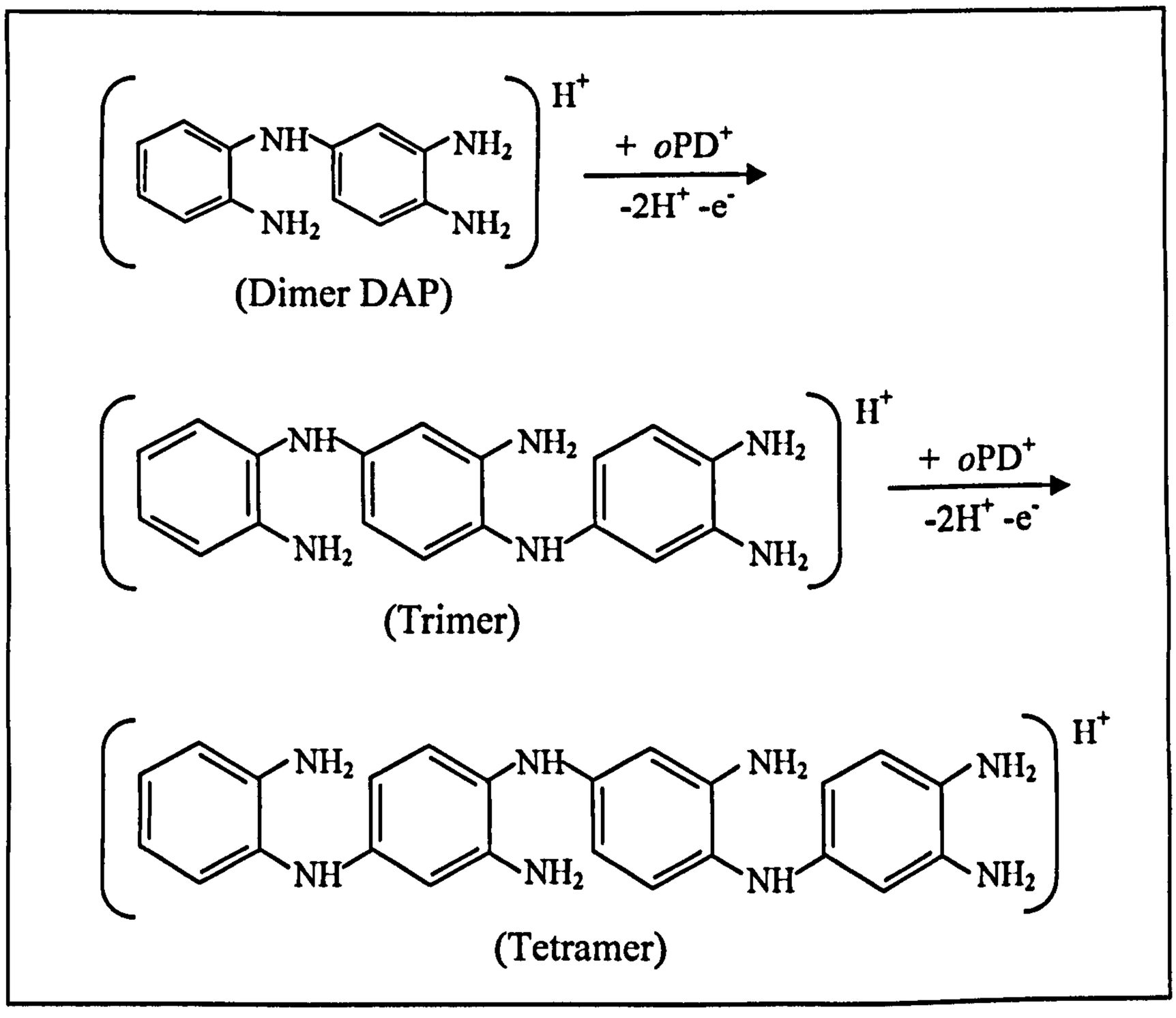

Figure 5.4: Chain propagation following dimerisation of *o*PD

Detailed work by Losito *et al* recently showed that chain propagation beyond tetramer length occurs only when the applied potential is increased by around +200 mV beyond that required for initial monomer dimerisation, and this gives rise to the second anodic peak seen in Figure 5.1 (Losito *et al*, 2003). At this point, more complex, pH-sensitive reactions take place, where competition exists between oxidative coupling (leading to chain propagation), and intramolecular oxidations with cyclization, so leading to the incorporation of phenazine and 1,4 benzoquinonediimine into the polymeric structure. In acidic conditions, the

oligomer formation favours phenazine-like subunits, whereas in more basic solutions, 1,4-benzoquinonediimine forming processes are preferred and this results in a less conjugated polymer structure (Figure 5.5).

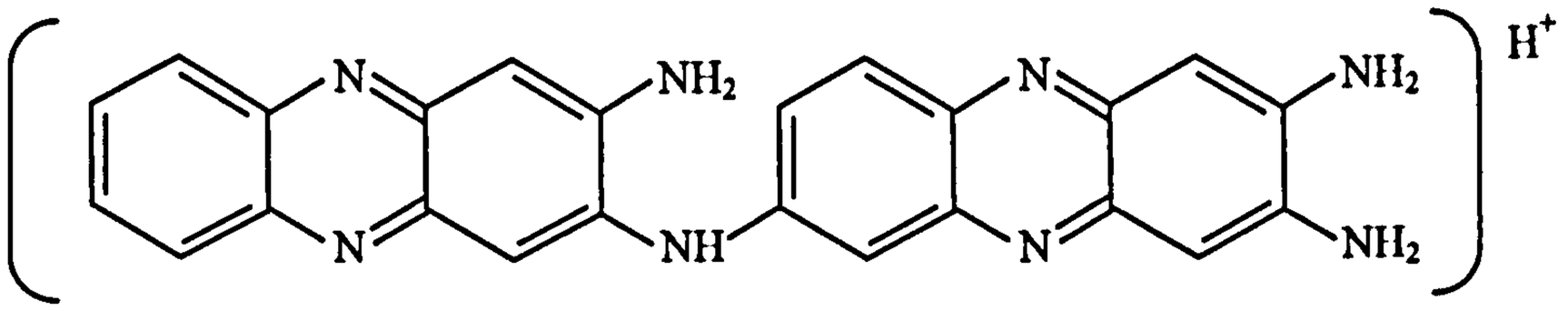

(a) P*o*PD oligomer incorporating phenazine sub-units

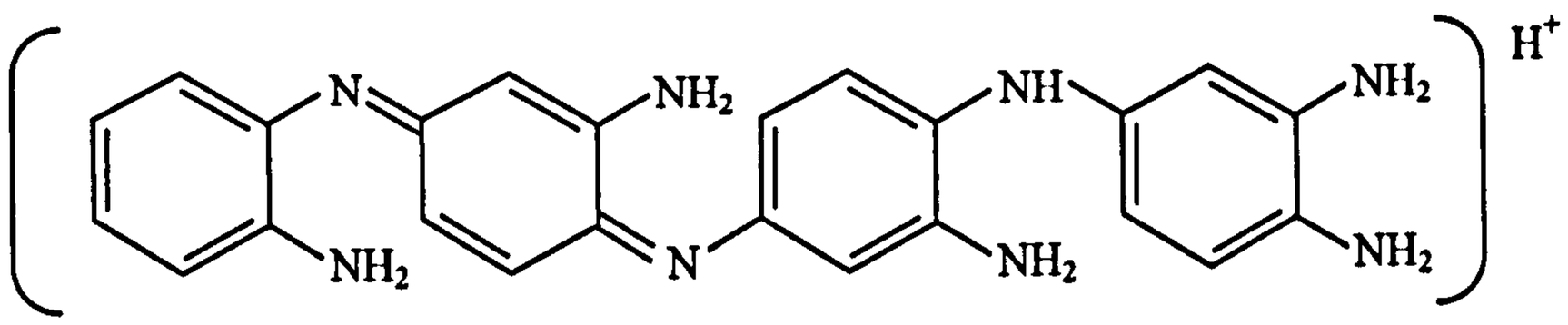

(b) P*o*PD oligomer incorporating 1,4-benzoquinonediimine sub-units

Figure 5.5: Schematic of P*o*PD oligomers formed in (a) acidic and (b) neutral conditions

The degree of π-conjugation greatly influences the conductivity of the film, and it follows that the poly(*o*-phenylenediamine) polymerised in neutral conditions (pH 7.4), utilised in this investigation, is non-conducting. This has two important consequences for sensor modification: firstly the film is not electroactive, thereby passivating the electrode, and it follows that for any further reaction to take place the electroactive species must first diffuse through the film (Emr & Yacynych, 1995). Secondly, the insulating nature of the polymer provides a film of uniform and self-limiting thickness. Wu & Chang showed through direct measurement via atomic force microscopy (AFM) that for 5 mM *o*PD polymerised on gold slide electrodes at pH 7.4, that film thickness was approximately 20 nm in all areas of the coated electrode (Wu & Chang, 2004). They compared the results with other techniques for

estimating film-thickness, illustrating that charge-transfer integration based methods (which first require the real surface area of the electrode to be established), do not account for the swelling of the hydrated polymer which increases film thickness by approximately three-fold.

It can be seen from figure 5.1 that the oxidation currents fall exponentially between subsequent scans, and that after 20 cycles a current plateau has been reached. This is in agreement with observations by Wu & Chang, who showed that for the same conditions, 96.5% of charge had passed after 7 scans. It is the deposition (adsorption) of the insoluble, higher oligomers onto the electrode surface which results in electrode-passivation with an ultra-thin film, readily suitable for ultrasonic ablation. Figures 5.6 and 5.7 illustrate a scanning electron-microscope (SEM) image of a gold sputter-coated slide electrode unmodified and electropolymerised with *o*PD respectively.

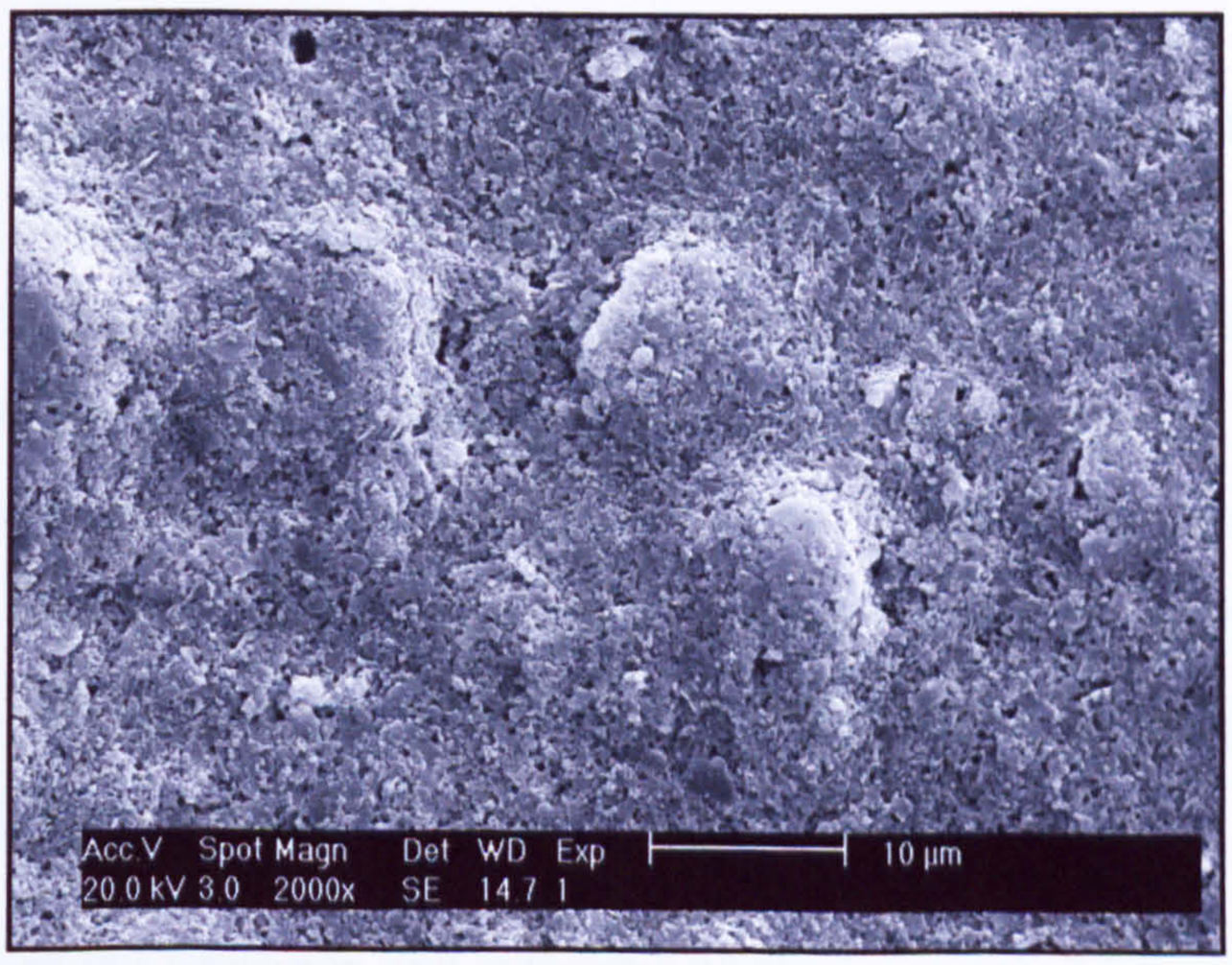

Figure 5.6: SEM image of the surface of an unmodified gold glass-slide electrode

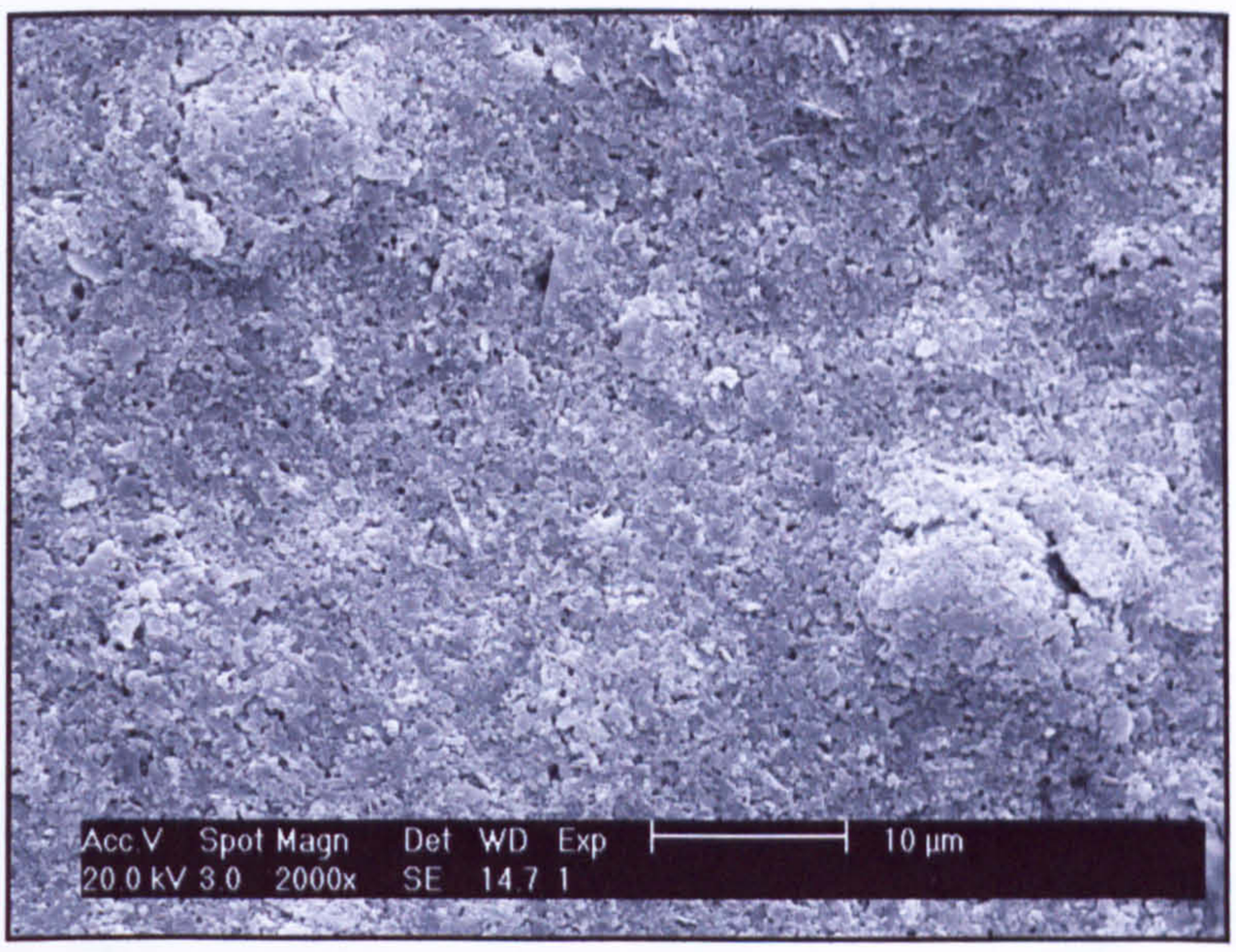

Figure 5.7: SEM image of a gold slide electropolymerised with *o*PD (pH 7.4, 20 scans, 50mVs^{-1})

The surface roughness of the thin polymer film conforms to that of the gold sputter-coated ground glass slide, indicating that the polymer forms an ultrathin film, self-limiting in thickness. Given the electrically insulating nature of the film, it was necessary to coat the sample exhibited in Figure 5.7 with a second layer of gold across the surface to allow examination by SEM. Although sputter-coated gold deposition does not produce an atomically smooth finish, the size of the gold agglomerates do not exceed 100 nm and so maintain an accurate depiction of the surface beneath (Schug *et al*, 1999).

In order to confirm the presence and integrity of the poly(*o*-phenylenediamine) film, polymer coated gold slide electrodes were interrogated via cyclic voltammetry in 1 mM potassium ferricyanide solutions (pH 7.8). The experiment was repeated with uncoated bare gold electrodes to compare signal response and voltammetric profiles. Equation 5.1 indicates the reduction-oxidation (redox) couple of potassium ferricyanide:

$$[Fe^{(III)}(CN)_6]^{3-} + e^- \leftrightarrow [Fe^{(II)}(CN)_6]^{4-} \qquad 5.1$$

Figure 5.8 illustrates the cyclic voltammograms obtained; the initial sweep is in the cathodic direction in order to reduce Fe^{3+} to Fe^{2+}.

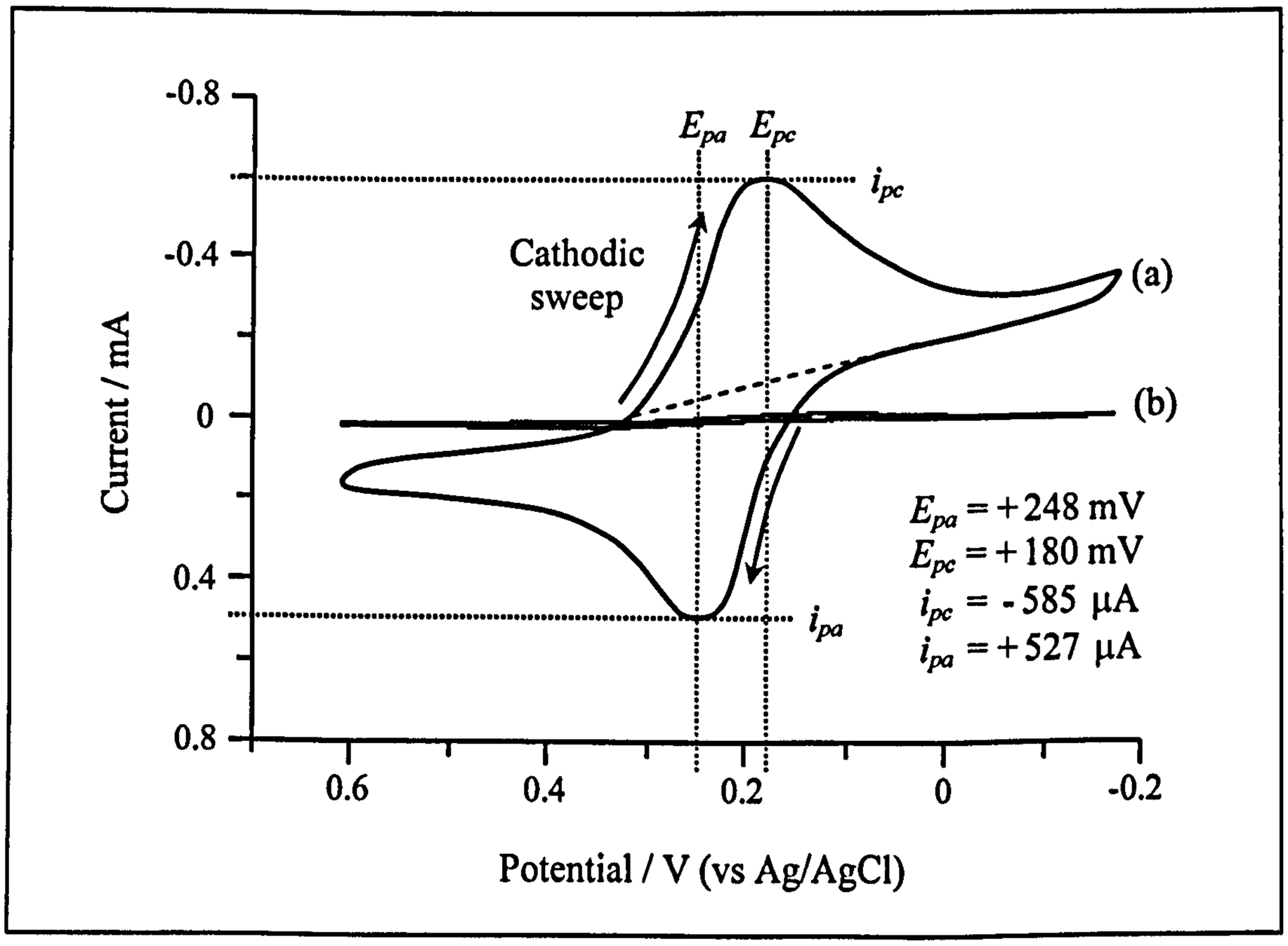

Figure 5.8: Cyclic voltammogram of (a) bare gold, and (b) poly(*o*-phenylenediamine) coated gold-slide electrode in a 1 mM potassium ferricyanide (15 mVs^{-1})

The cyclic voltammogram yields a peak separation (E_{pa}-E_{pc}) of approximately 68 mV, which is close to the value of 59 mV expected for a reversible, diffusion-controlled single electron transfer reaction. It is likely that the source of this discrepancy can be attributed to solution resistance and surface topography leading to non-ideality. Furthermore, it has been shown that this redox couple is prone to causing the formation of a passivating film of Prussian blue on platinum electrodes (Pharr & Griffiths, 1997), (Granger & Swain, 1999), which also is possible in this instance. Even low levels of electrode passivation can cause a decrease in the rate of

electron transfer, which in turn results in a decrease in peak potentials and an increase in peak separation.

A reversible reaction is also indicted by the ratio of i_{pc} and i_{pa}, which is approximately equal to one. Since the solution consisted mainly of ferricyanide, the reaction product from the cathodic sweep (ferrocyanide) experiences a diffusion gradient away from the electrode, causing it to move out of the diffusion layer and resulting in a charge bias in favour of reduction.

If the diffusion coefficient of ferricyanide is known, the Randles-Sevcik equation can be used in conjunction with data obtained from the cyclic voltammogram to allow the real electrode surface area to be calculated (Equation 5.4).

$$i_p = (2.69 \times 10^5)\, n^{3/2} A D^{1/2} C v^{1/2} \qquad 5.4$$

for a reversible system at 25°C, where i_p is the peak current (A), n is the number of electrons, A is the surface area (cm^2), D is the diffusion coefficient ($cm.s^{-1}$), C is the concentration of the electroactive species ($mol.cm^{-3}$) and v is the sweep rate (Vs^{-1}).

The diffusion coefficients for ferricyanide in solutions of 0.1 M KCl have been previously measured to be 7.26 $\times 10^{-6}$ $cm^2 s^{-1}$ (Konopka & McDuffie, 1970). The concentration of ferricyanide was 1 $\times 10^{-3}$ M, the sweep rate was 15 mVs^{-1} and the peak cathodic current (i_{pc}) can be measured from the cyclic voltammogram in Figure 5.7 as 585 $\times 10^{-6}$ A.

From this data, the real electrode surface area was calculated to be approximately 6.6 cm^2. The insulated adhesive wire junction on the surface of the gold slide electrode is not accurately defined, however it masks approximately 0.5 cm^2 of the available 5 cm^2 gold slide area. Therefore, although an accurate comparison of geometric and real electrode surface area cannot be made, it is clear that the surface topography of the ground-glass slide substrate significantly increases the available surface area.

Since the real electrode area is now known, it becomes possible to estimate film thickness via charge integration methods (Myler *et al*, 1997) for comparison with polymerisations on carbon paste substrates. The total charge passed for the sputter-coated gold electrode polymerisation illustrated in Figure 5.1 was 102.642 mC (≅ 15.620 $mCcm^{-2}$). If it is assumed that each monomer unit lies flat on the surface of the electrode, and possesses cross-sectional dimensions of 3 x 5 Å, then the density of a monolayer can be approximated to 6.66 $x10^{14}$ monomer units per cm^2. Given that the polymerisation of *o*-phenylenediamine occurs via a 2 electron transfer process, the charge associated with the polymerisation of a single monolayer can be approximated to 0.21 mC/cm^2. For the charge passed, it can therefore be estimated that following 20 cycles, approximately 74 monolayers are formed. If each monolayer is assumed to have a thickness of 1.4 Å, the diameter of the largest atom, carbon (Stafström *et al*, 1987), then the thickness of the film can be calculated to be approximately 10.4 nm.

It has been mentioned previously that film thickness estimations based on charge integration methods are inaccurate for the case of hydrated polymer (i.e. when immersed in aqueous medium) (Wu & Chang, 2004). However, this method still provides an effective tool for the comparison of polymer thickness on different substrates.

5.3 Electropolymerisation onto screen printed carbon substrate

In order to produce a sensor at a commercially viable unit cost, it is required to replace sputter-deposited gold substrates with screen printed carbon-ink, and therefore, it is necessary to the suitability of carbon-ink to accept comparative electropolymerisation of poly(*o*-phenylenediamine). Initially, single disposable carbon paste electrodes were subjected to the same electropolymerisation regime used for gold substrates. Figure 5.9 exhibits the cyclic voltammogram obtained for the electropolymerisation of 5 mM *o*PD (0 to +800 mV, 50 mVs^{-1}, pH 7.4) onto an 8.82 mm^2 carbon-paste electrode (Microarray Ltd).

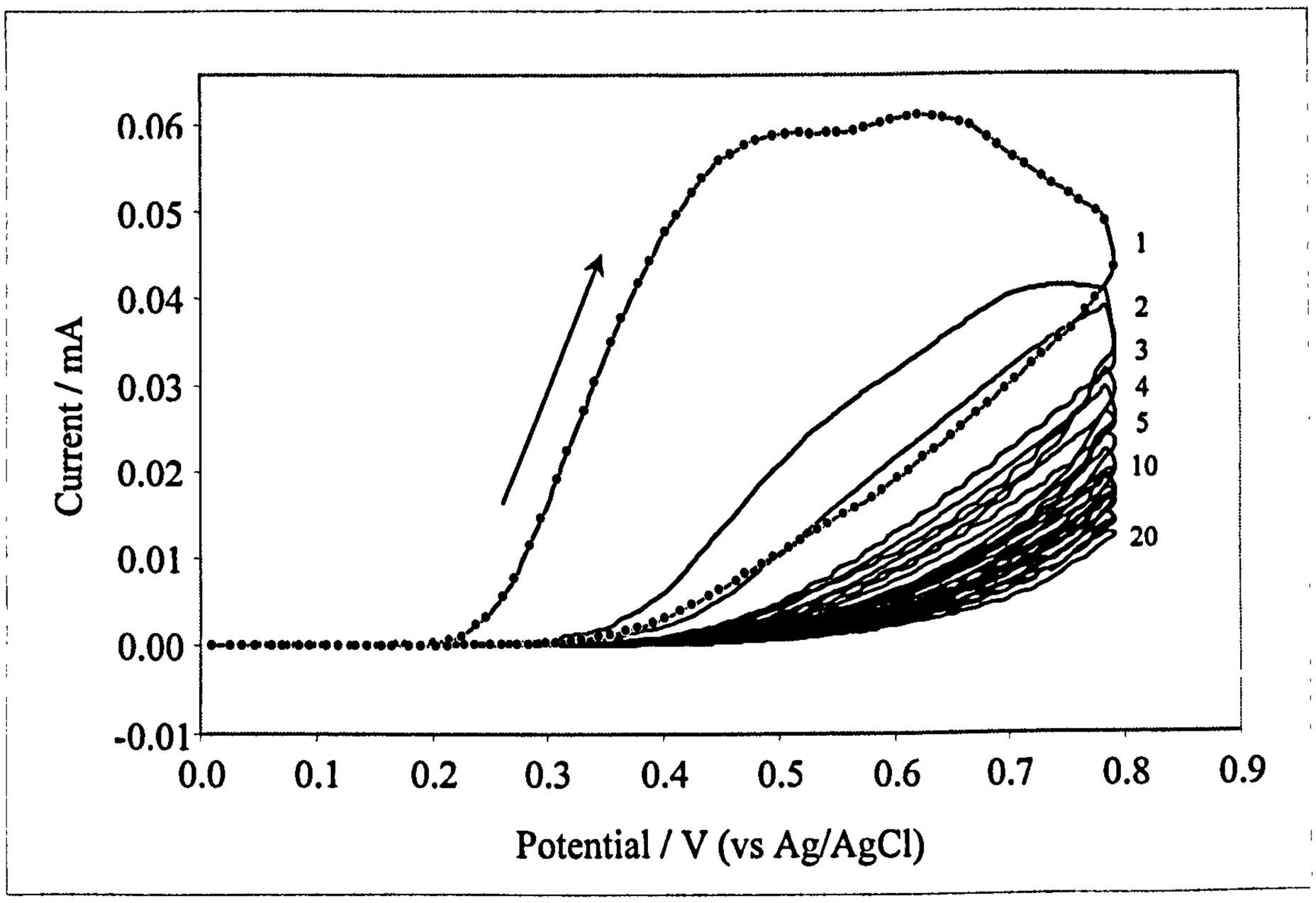

Figure 5.9: Electropolymerisation of 5 mM *o*PD at a screen printed carbon electrode (0 to +800 mV, 50 mVs^{-1}, pH 7.4 phosphate buffer)

The cyclic voltammogram obtained indicates two less pronounced anodic peaks at approximately +480 and +625 mV. When compared to the equivalent voltammogram obtained for gold electrodes (Figure 5.1), it can be seen that the peak potentials have been shifted anodically by approximately +150 mV, indicating that the screen printed carbon surface is less electroactive when compared to gold. Therefore it can be said that the electron transfer associated with the oxidation of the *o*PD monomer and subsequent chain propagation is less kinetically favourable across the carbon / solution interface than that for gold. Furthermore, in comparison to Figure 5.1, the second anodic peak appears to be less prominent and the rate of decrease of the anodic current appears to be diminished, suggesting the incomplete polymerisation of the oxidised monomer. This agrees with data provided by Losito *et al*, who showed that by limiting the anodic switching potential, or making the polymerisation stage less kinetically favourable by reducing the pH, that the formation of soluble dimers, trimers and tetramers exceeded the rate formation of

insoluble, passivating *o*PD *n*-mers (Losito *et al*, 2003). Consequently, for the case of electropolymerisation on carbon-paste electrodes, it was decided to extend the anodic potential sweep to +1000 mV in order to increase the thermodynamic favourability of chain propagation. Figure 5.10 indicates the cyclic voltammogram of *o*PD polymerised on the carbon-paste electrodes for this increased potential range.

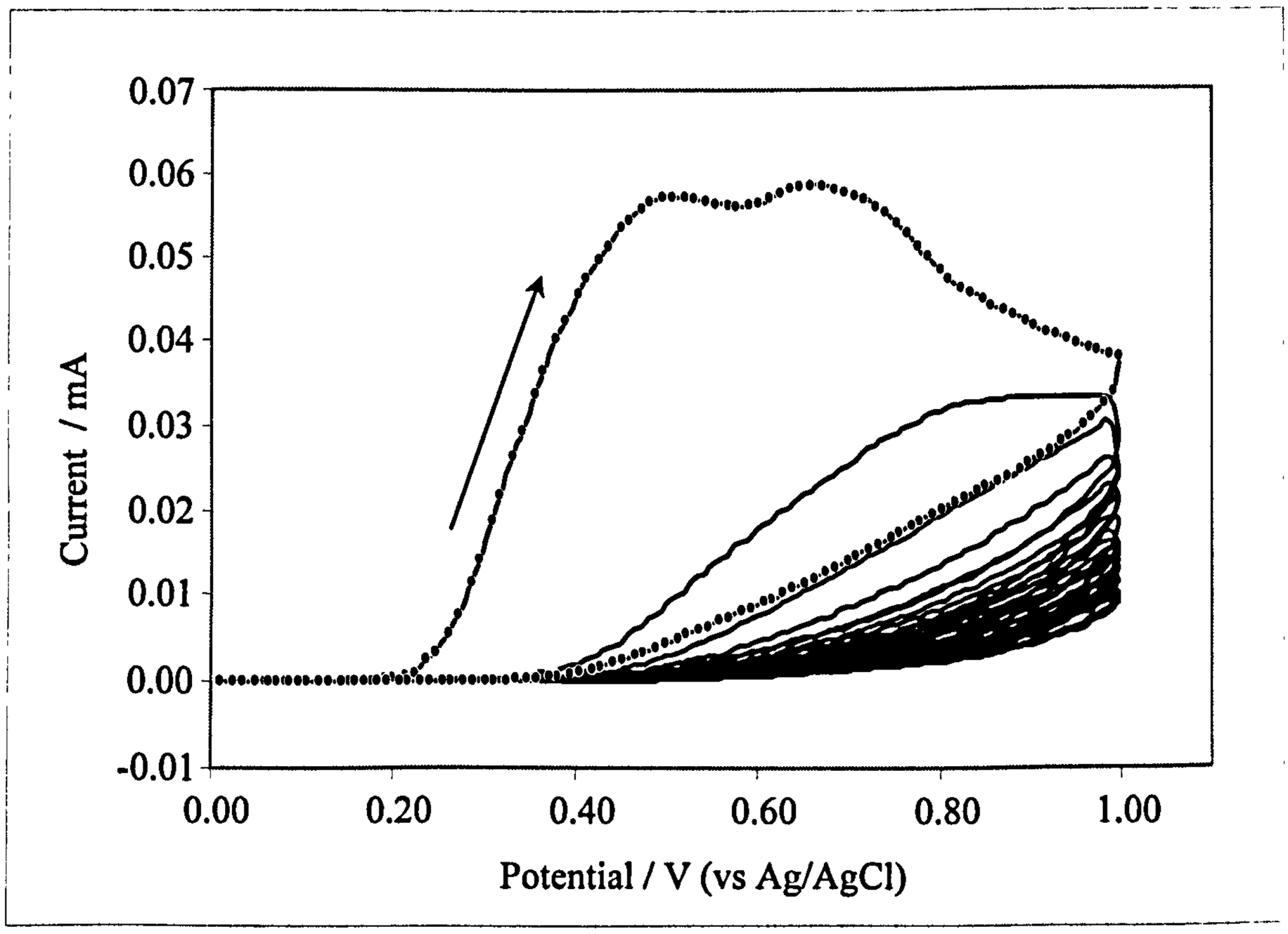

Figure 5.10: Electropolymerisation of *o*PD at a screen printed carbon electrode (0 to +1000 mV, 50 mVs^{-1}, pH 7.4 phosphate buffer)

It can be seen that there is a more rapid decrease in the current flow between each scan, indicating a more efficient chain propagation phase and resulting in the enhanced passivation of the electrode surface. Figure 5.11 compares the charge passed per sweep during the polymerisation of *o*PD from 0 to +800 and 0 to +1000 mV.

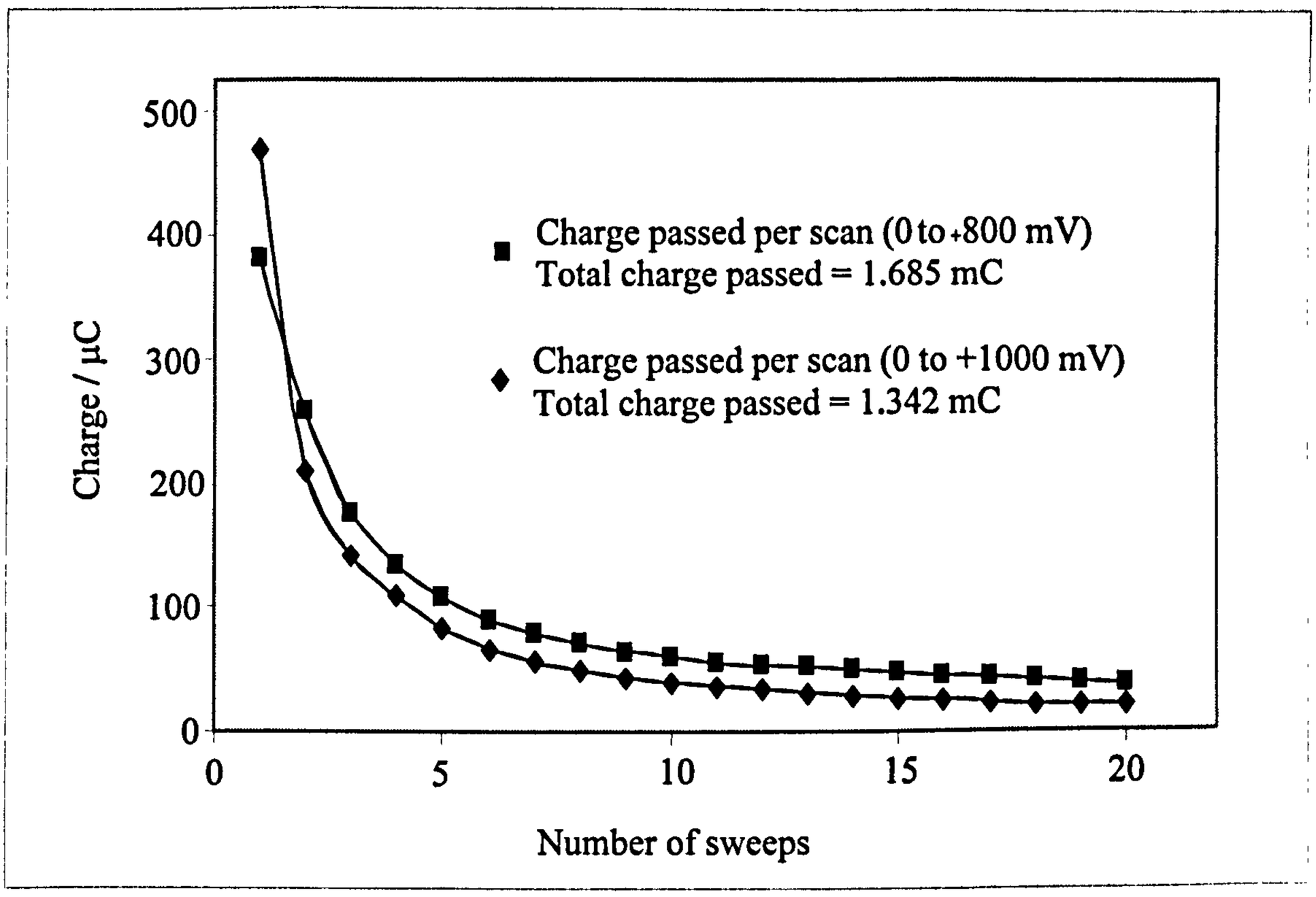

Figure 5.11: Charge passed for the polymerisation of *o*PD at a single carbon electrode for scans between: ■ 0 to +800 mV, and ♦ 0 to +1000 mV (50 mVs^{-1}, pH 7.4 phosphate buffer)

Figure 5.11 indicates the charge passed per scan for both polymerisation potential ranges. In both cases the charge passed can be seen to decay exponentially, however, from this figure it is evident that the potential range of 0 to +1000 mV results in a more effective insulation of the electrode. More charge can be seen to pass on the first scan, as would be expected due to the anodic sweep being extended. However, for the remaining scans less charge flows, suggesting improved electrode passivation and so insulation. The larger net current flow exhibited for the original regime (0 to +800 mV) can therefore be attributed to the successful oxidation of chains up to tetramer size (which are soluble and can migrate away without passifying the electrode), but the inadequate production of longer, insoluble polymer chains, which occurs at the higher potentials. Although the charge passed appears to achieve a plateau, a very small current may still be observed if the polymerisation is extended to many hundreds of cycles. This has been attributed to cross-linking reactions taking place within the film which even in its 'insulating' form still posses a finite

conductivity, especially when hydrated (Centonze *et al*, 1994). Scanning electron micrographs were taken of bare carbon (Figures 5.12) and at an *o*PD electropolymerised carbon surface (Figure 5.13) respectively.

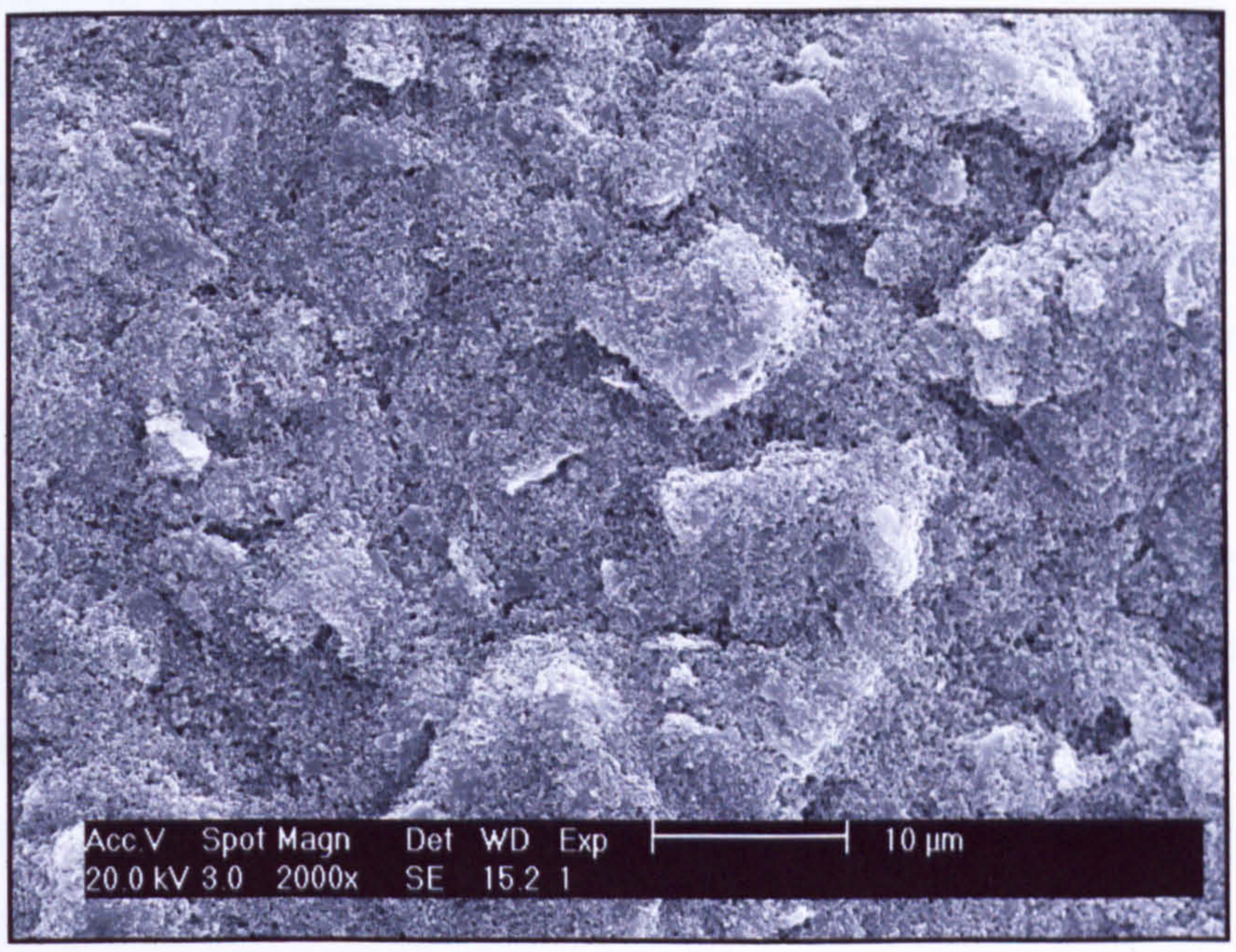

Figure 5.12: SEM image of the surface of a bare carbon-paste electrode

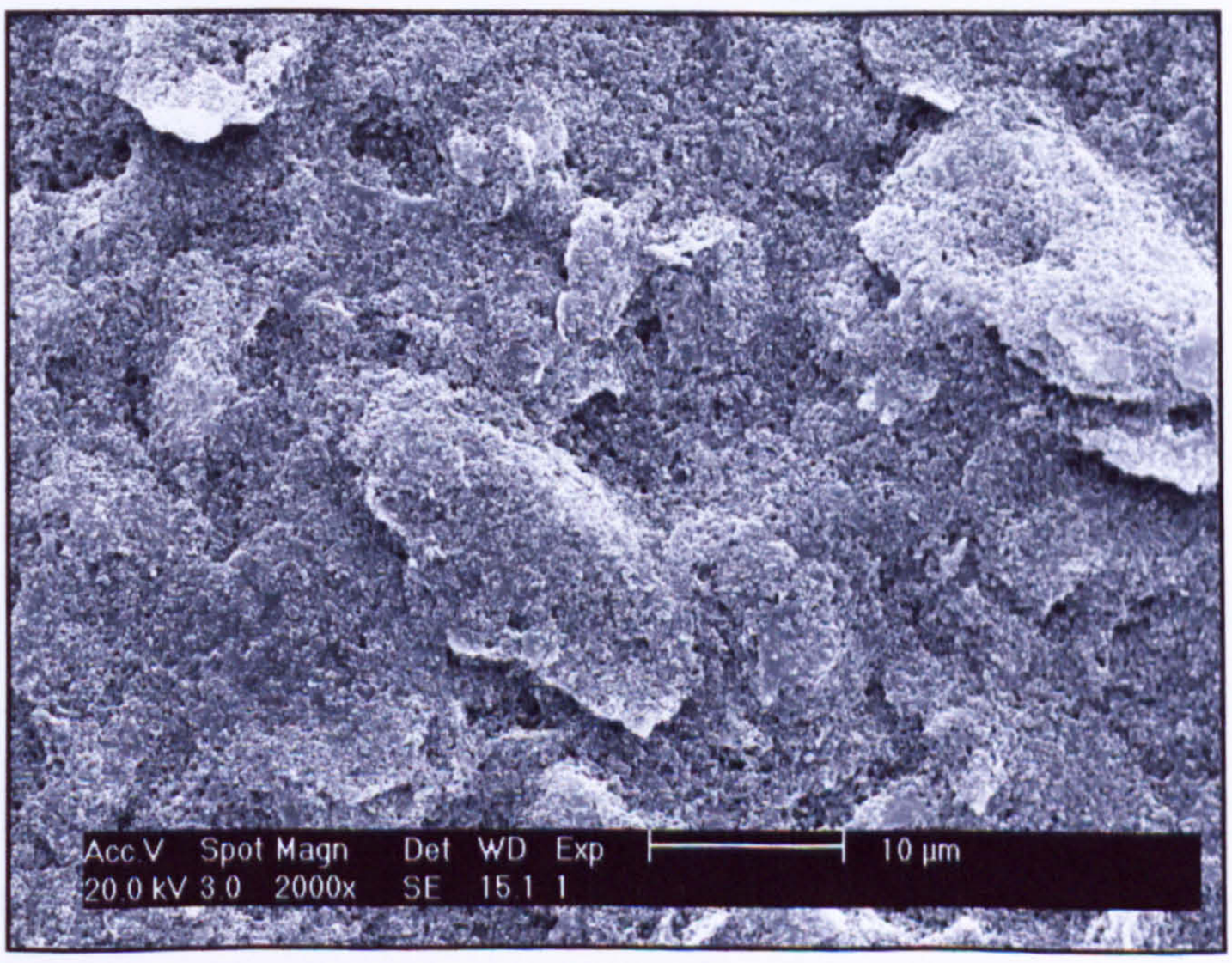

Figure 5.13: SEM image of an *o*PD polymerised carbon-paste electrode

The micrographs indicate that the film formed by the electropolymerisation of *o*PD is again extremely thin, faithfully replicating the surface beneath it. The insulated surface requires to be coated with a conductive layer to allow examination via SEM (in this instance surfaces were sputter-coated with gold). As a result, information concerning material conductivity by contrasting the level of brightness of the two images is lost. However, the insulating properties of the *o*PD film were confirmed when an electropolymerised electrode without a conductive coating was examined, and was seen to cause rapid saturation of the micrograph image. It may be possible, however, to circumvent this problem by use of a microscope capable of employing a lower accelerating voltage.

The thickness of the polymer film formed on carbon-paste can be compared to that of gold by using charge integration methods, although once again the real surface area of the electrode must first be calculated. Figure 5.14 exhibits the cyclic voltammogram obtained for a bare carbon electrode interrogated using a 1 mM potassium ferricyanide redox couple.

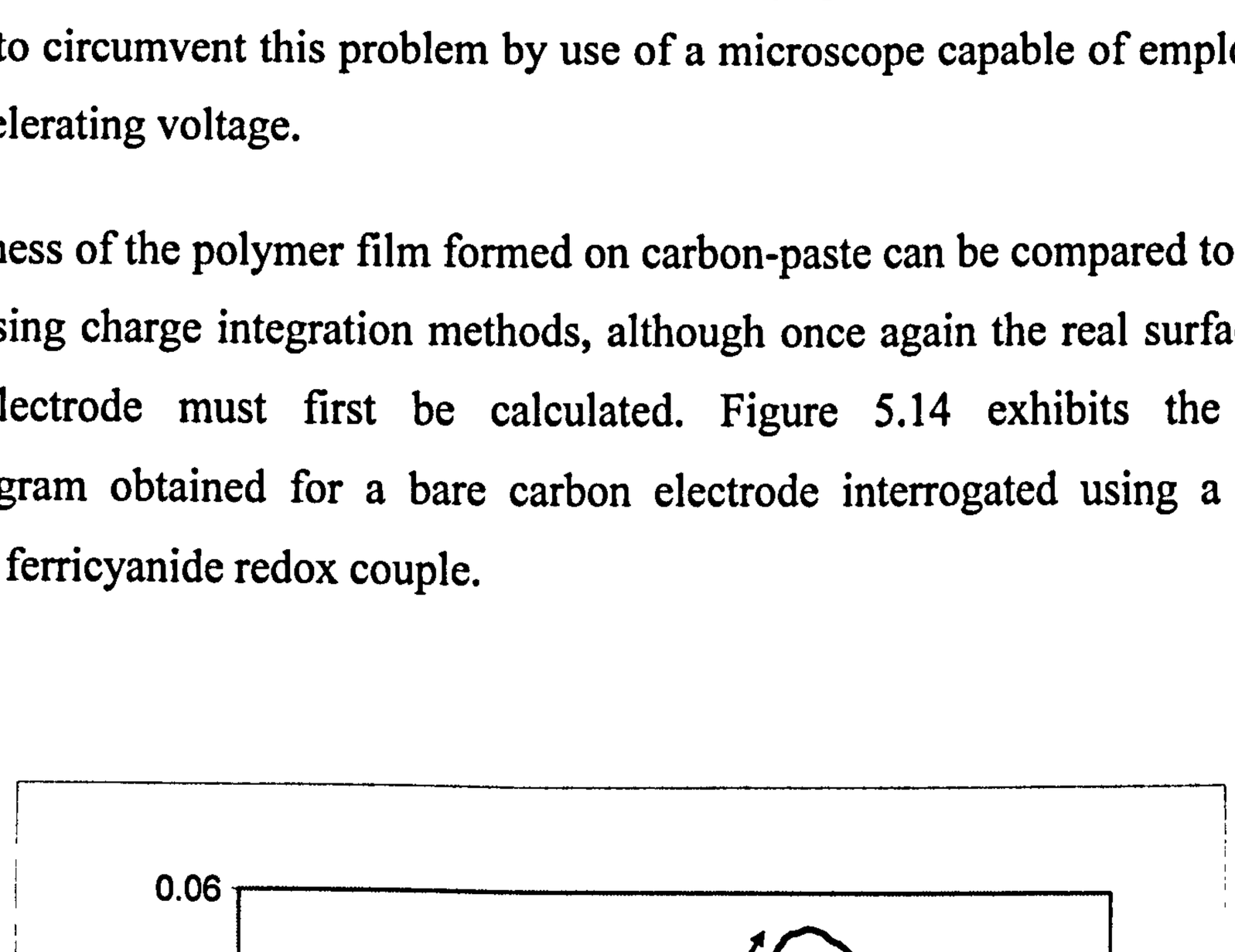

Figure 5.14: Cyclic voltammogram of bare carbon sensor interrogated from (a) +0.6 to -0.2 V, and (b) +0.6 to -0.5 V in 1 mM $Fe(CN)_6^{3-/4-}$ solution

Cyclic voltammetry reveals very poor reaction kinetics of potassium ferricyanide with the carbon-paste substrate. It can be seen that when the voltammetric scan was undertaken using the potential range originally employed for a gold electrode (-0.2 to +0.6 V), no clear peak cathodic current was observed, and so the reductive sweep was therefore extended to -0.5 V. ΔE_p is considerably larger than for the gold surface (~465 mV compared to 68 mV), which agrees well with work carried out by Deakin *et al* who measured redox peak separation to be around 450 mV (Deakin *et al*, 1985). This data indicates poor reaction kinetics and corroborates the shift in oxidation potentials expressed during the electropolymerisation of *o*PD on carbon-paste (Figure 5.10). Furthermore, the shape of the scan is distorted as the rate of electron transfer relative to the rate of mass transport is decreased.

Quasi-reversible and irreversible redox processes are commonly experienced with screen printed carbon electrodes (Dock & Ruzgas, 2003), whose electrochemical behaviour can be explained by their heterogeneous construction. The precise composition of the carbon-ink formulation used cannot be reported in this work for commercial reasons. However, screen printed carbon-inks typically comprise a mixture of graphite powder, a polymeric binder (typically vinyl or epoxy based), and other chemical additives to aid dispersion and printing (Adams, 1958), (Grennan *et al*, 2001), (Svancara *et al*, 2001). The resultant paste is a composite of randomly oriented graphite particles, suspended in an insulating matrix of polymer. Electrical conductivity within the bulk system is believed to be provided by points of physical contact between graphite particles, providing a conductive path through the polymeric medium, (Svancara *et al*, 1996). An alternative mechanism involving indirect electron tunnelling between particles in close proximity has also been suggested (Svancara & Vytras, 2000).

Graphite itself is a natural arrangement of flat layers of hexagonal rings of carbon, held closely together by strong, hybridised sp^2 covalent bonds. Consecutive layers of the ring structures are only held together via 'Van der Waals' forces, resulting in a weak and more distant association (Figure 5.15).

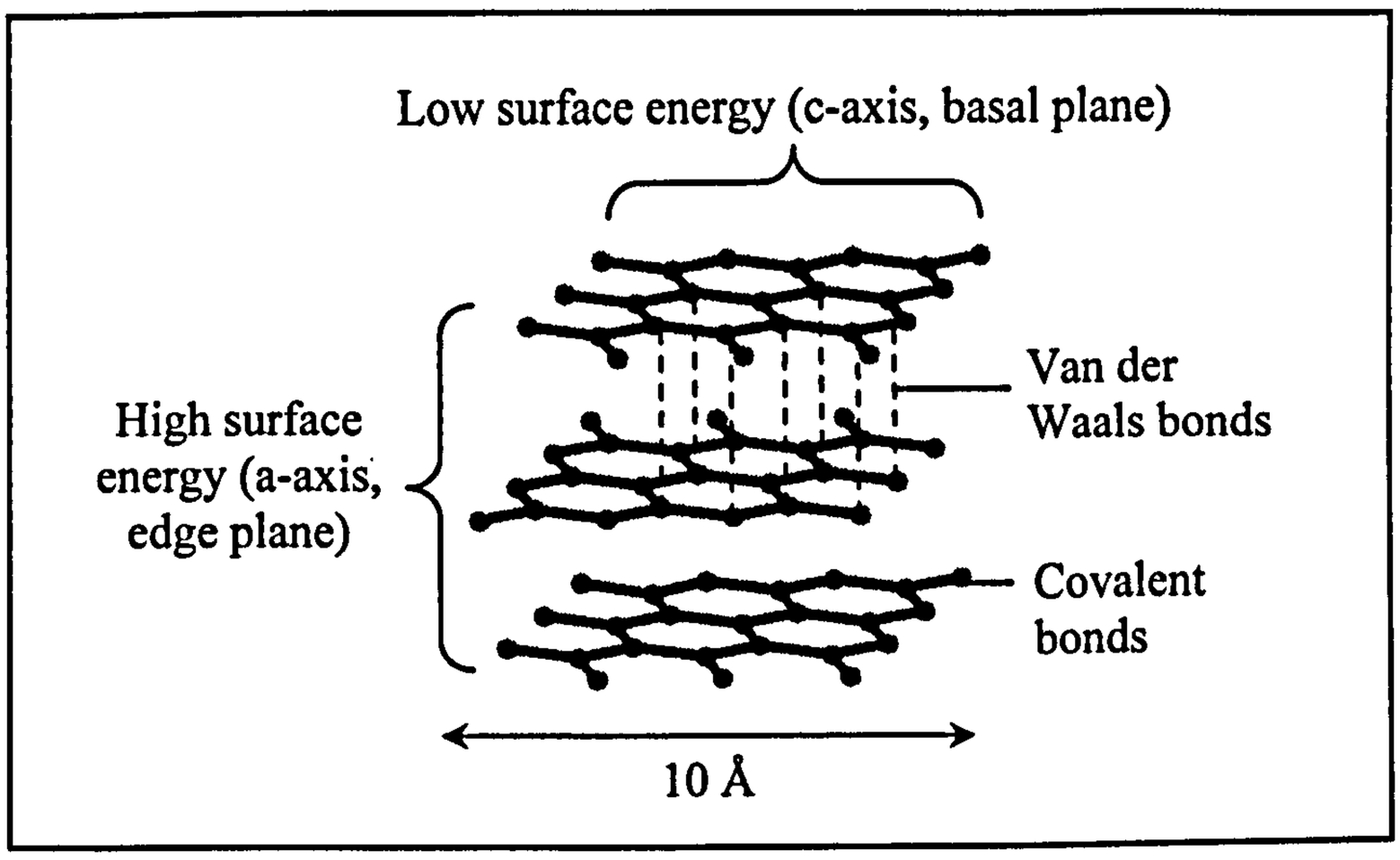

Figure 5.15: Structural arrangement of carbon graphite

This structure leads to anisotropic physico-chemical properties. Firstly, the large difference in bond strength within the plane of the carbon rings (known as the *basal* plane) compared to the strength between the basal plane layers, results in a macro-molecular 'flake-like' structure, formed during processing. Secondly, the close atomic spacing, and electron mobility in the extended π system found within the carbon rings, leads to excellent conductivity parallel to the basal plane (~0.1 Ωcm). In contrast, a much more resistive path exists between the layers (~1 x 10^{-4} Ωcm) (McCreery, 1991). Furthermore, the surface energies at the face of the basal plane are much lower than that of the edge plane, and offer varying wettability and electroactivity (Rice & McCreery, 1989), (McCreery, 1991). The result is a complex heterogeneous surface with differing physical and chemical characteristics, in which the main electroactive component (graphite) is almost entirely coated, even at the surface, by a film of non-conducting pasting liquid whose presence is essential for printing processes (Kalcher, 1990). The polymer membrane causes hydrophobicity and reduces the electroactivity of the entire surface, including the areas containing exposed edge-planes of graphite. Consequently the electrochemical properties of a carbon-ink are sensitive to the ratio of graphite to pasting liquid. The edge plane of dry graphite will exhibit near Nernstian behaviour, even with a potassium ferricyanide redox couple, while in contrast the basal plane shows extremely low

activity (McCreery, 1991). As the proportion of polymer binder increases in the carbon-paste mixture, so the conductivity and electrode kinetics decrease accordingly (Rice *et al*, 1983), (Hu *et al*, 1985).

The description of the carbon paste given above and within the literature is of a two-phase mixture of graphite and polymer binder. However, in addition to the graphite, examination of the carbon-paste sensors used in this work under higher magnifications indicates the presence of a smaller particulate material (Figures 5.16 and 5.17).

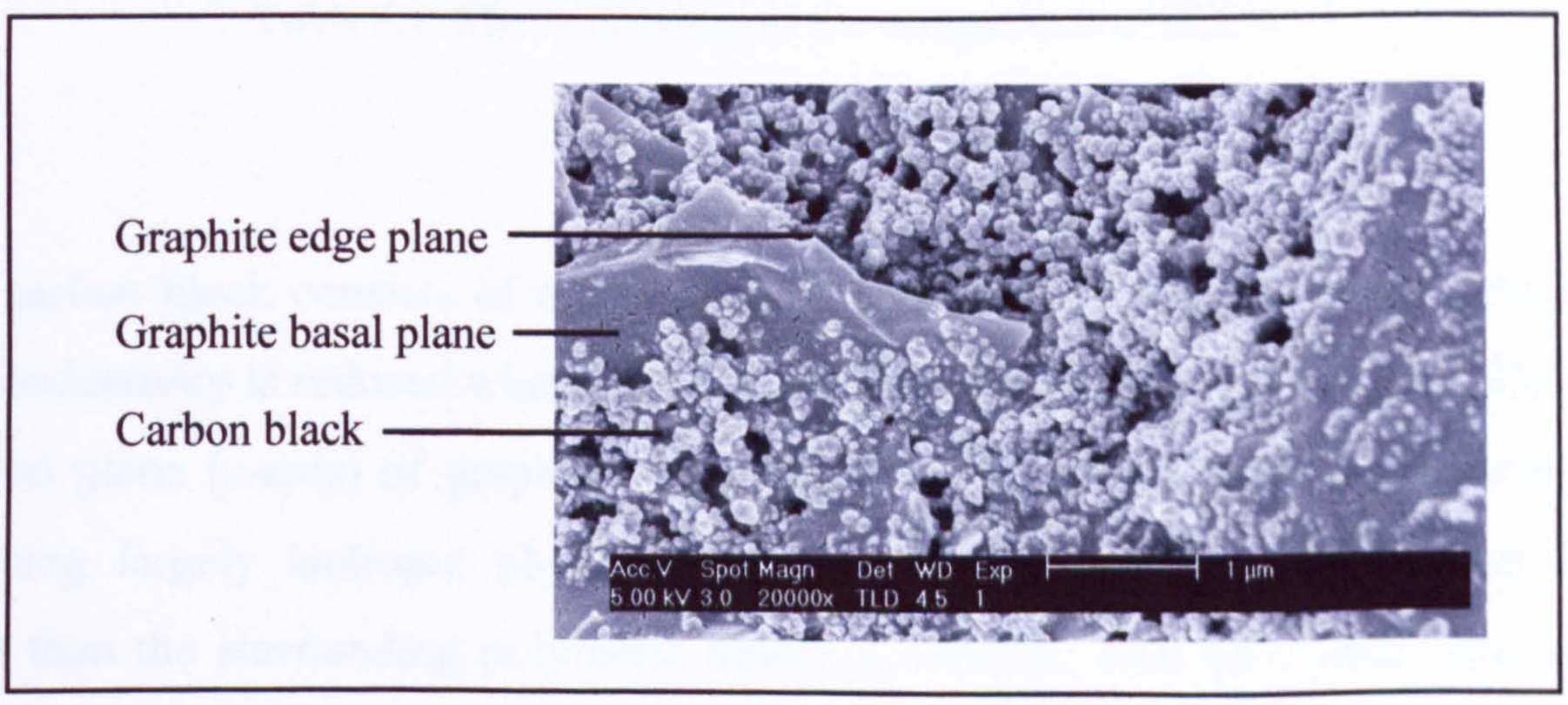

Figure 5.16: 20,000 x magnification of the carbon-paste surface electrode surface

The particles are likely to be carbon black, spherular agglomerates of disordered graphite 10-3000 Å in size, and have been previously described as a constituent of screen printed carbon-inks by Cui *et al* (Kinoshita, 1988), (Cui *et al*, 2001). The approximate resistivities of graphite, carbon black, and the polymeric binder can be seen in Table 5.1 (McCreery, 1991), (www.matweb.com).

Material	Resistivity (Ω.cm)
Graphite (a-axis)	4×10^{-5}
Graphite (c-axis)	0.17
Carbon black	1×10^{-2}
Vinyl & phenolic resins	$\sim 1 \times 10^{13}$
Epoxy resins	$\sim 1 \times 10^{14}$

Table 5.1: The resistivities of the components of SCE's

Since carbon black consists of microcrystals of graphite in a random arrangement, their conductivity is reduced when compared to that of a direction which is parallel to the basal plane (c-axis) of graphite. However, this also results in the agglomerates possessing largely isotropic physico-chemical properties, with conductivities far greater than the surrounding polymeric binder. Combined with their small size and round shape, carbon black must act as conductive 'filler' within the insulating polymer matrix. Furthermore, carbon black possesses a higher density of exposed edge planes at the surface when compared to the a-axis of a single graphite crystal. Since the high surface energy of exposed edge planes (and defects) allows an enhanced rate of electron transfer and wettability by a polar solvent, this makes carbon black a more suitable interface for aqueous solutions than a graphite crystal presenting its basal plane. Figure 5.17 exhibits the extensive coating of the electrode surface by carbon black.

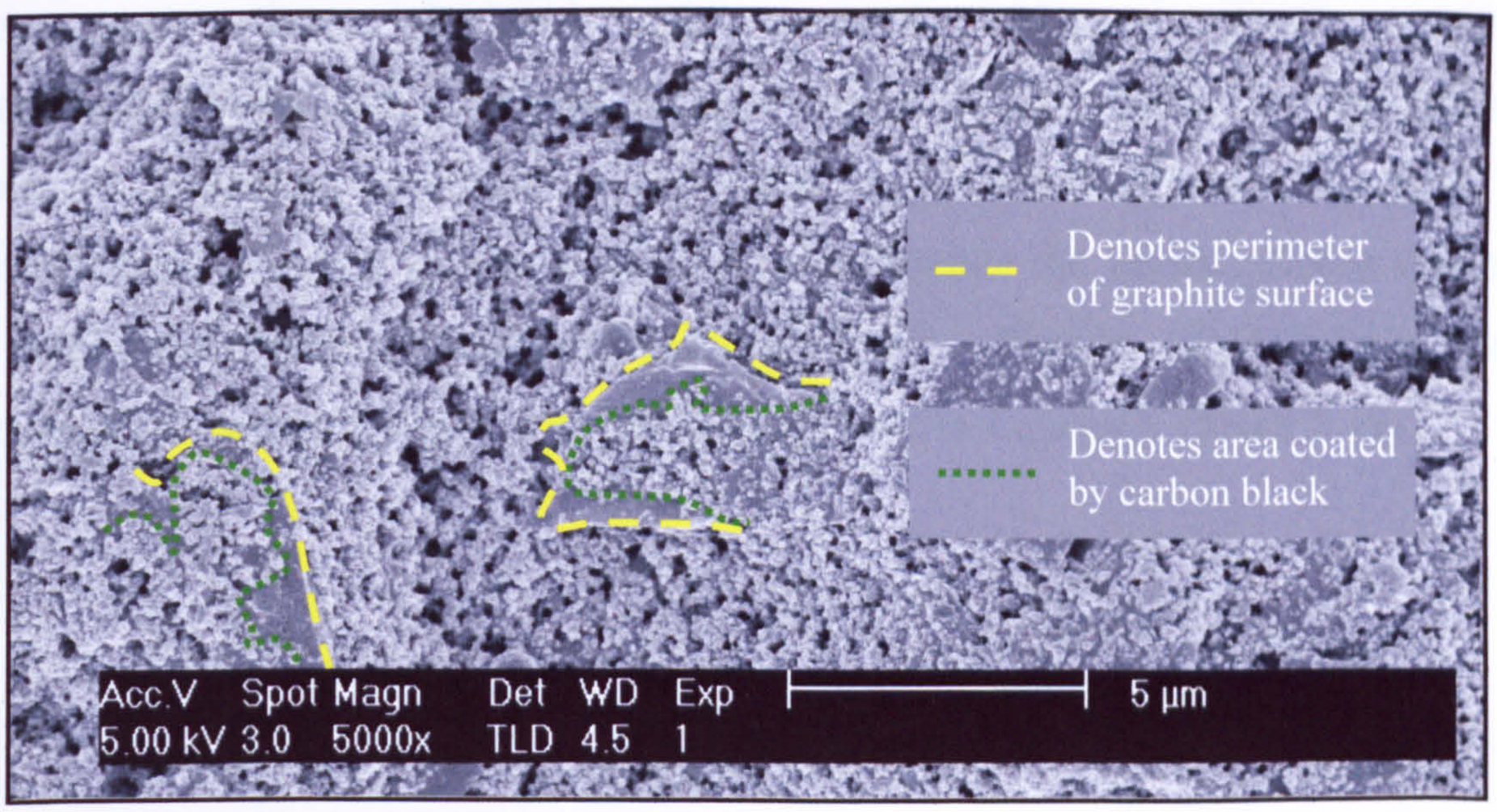

Figure 5.17: The partial coating of graphite crystals at the electrode surface with carbon black

During processing, the carbon-ink mixture will contain graphite particles aligned in every direction. However, the SEM images indicate that the large graphite particles generally adopt a 'flattened' orientation as the ink dries, at least at the visible surface. While benefiting the application of printed circuitry by maximising ink conductivity, this does not enhance electrochemical activity of the electrode surface. Carbon black can be seen across a large portion of the electrode surface, including the exposed low energy graphite basal planes where it provides a conductive path back to the matrix. The result is a surface which is more electrochemically active and homogeneous than that of a mixture of graphite and binder alone. However, cyclic voltammetry with a ferricyanide redox couple indicated poor reaction kinetics (Figure 5.14). Cui *et al* investigated a number of screen printed carbon-inks using techniques such as ac impedance and cyclic voltammetry (Cui *et al*, 2001). They found that, since the electrodes had all been produced in-house by the same method, variations in behaviour could only be attributed to differences in the proprietary polymeric binders and types of graphite employed. They too noted a poor response by carbon-inks to the potassium ferricyanide redox couple, and refer to a report by Deakin *et al*, who describe a negatively charged carbon-paste / solution interface, responsible for slow

reaction kinetics with negatively charged redox couples (Deakin *et al*, 1985). In the same paper they identified the positively charged redox couple, hexaammineruthenium(III) chloride to show excellent reversibility on unmodified carbon-ink substrates. Consequently two redox couples which dissociate in water to form positively charged species were used to interrogate the screen printed carbon-ink substrates, namely hexaammineruthenium(III) chloride, $Ru(NH_3)_6Cl_3$, and ferrocenemonocarboxylic acid, $Fc(CO_2H)$ (illustrated in Figures 5.18 and 5.19).

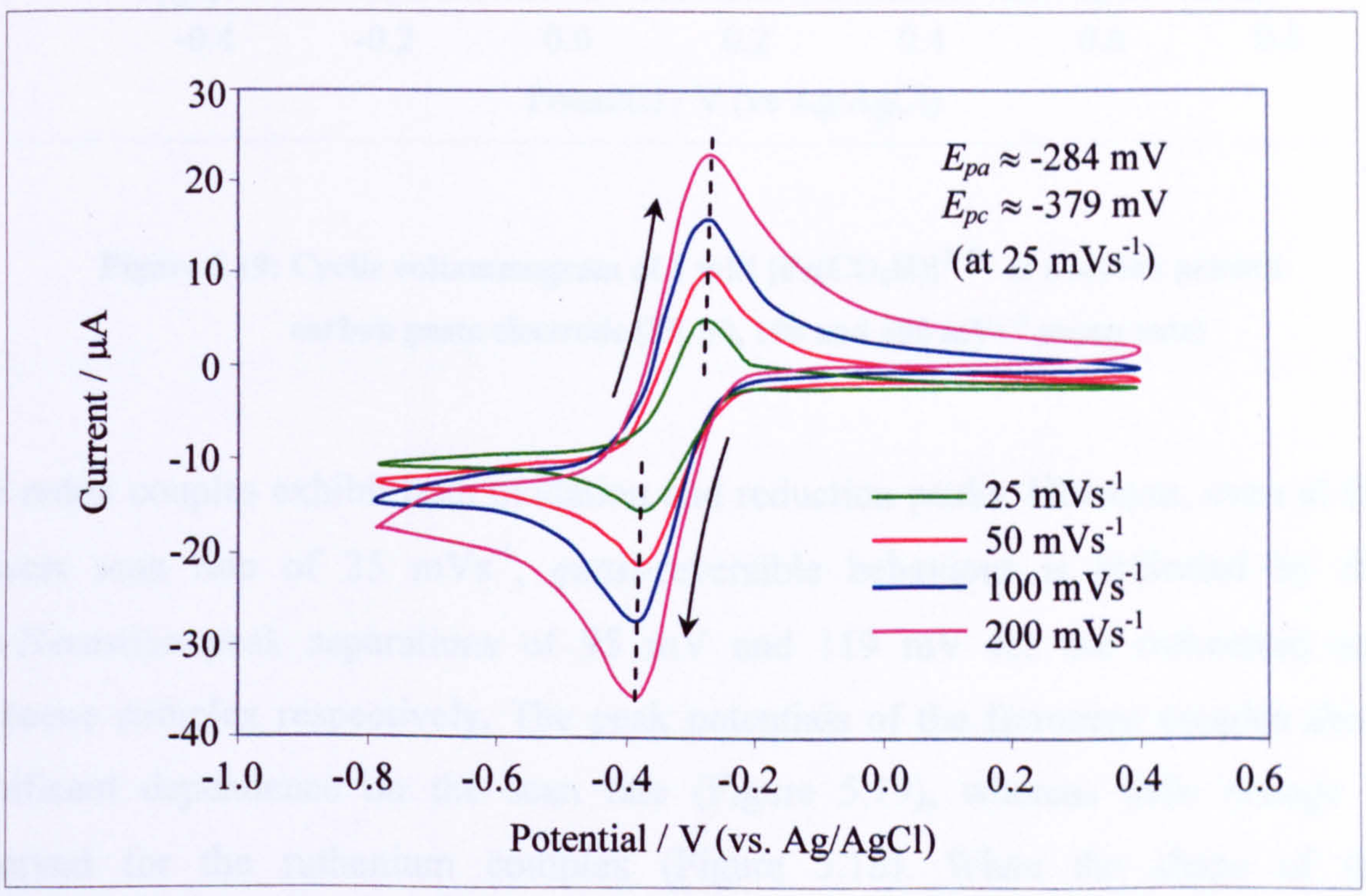

Figure 5.18: Cyclic voltammogram of 1 mM $[Ru(NH_3)_6]^{3+/2+}$ at a screen printed carbon paste electrode (25, 50, 100 and 200 mVs^{-1} sweep rate)

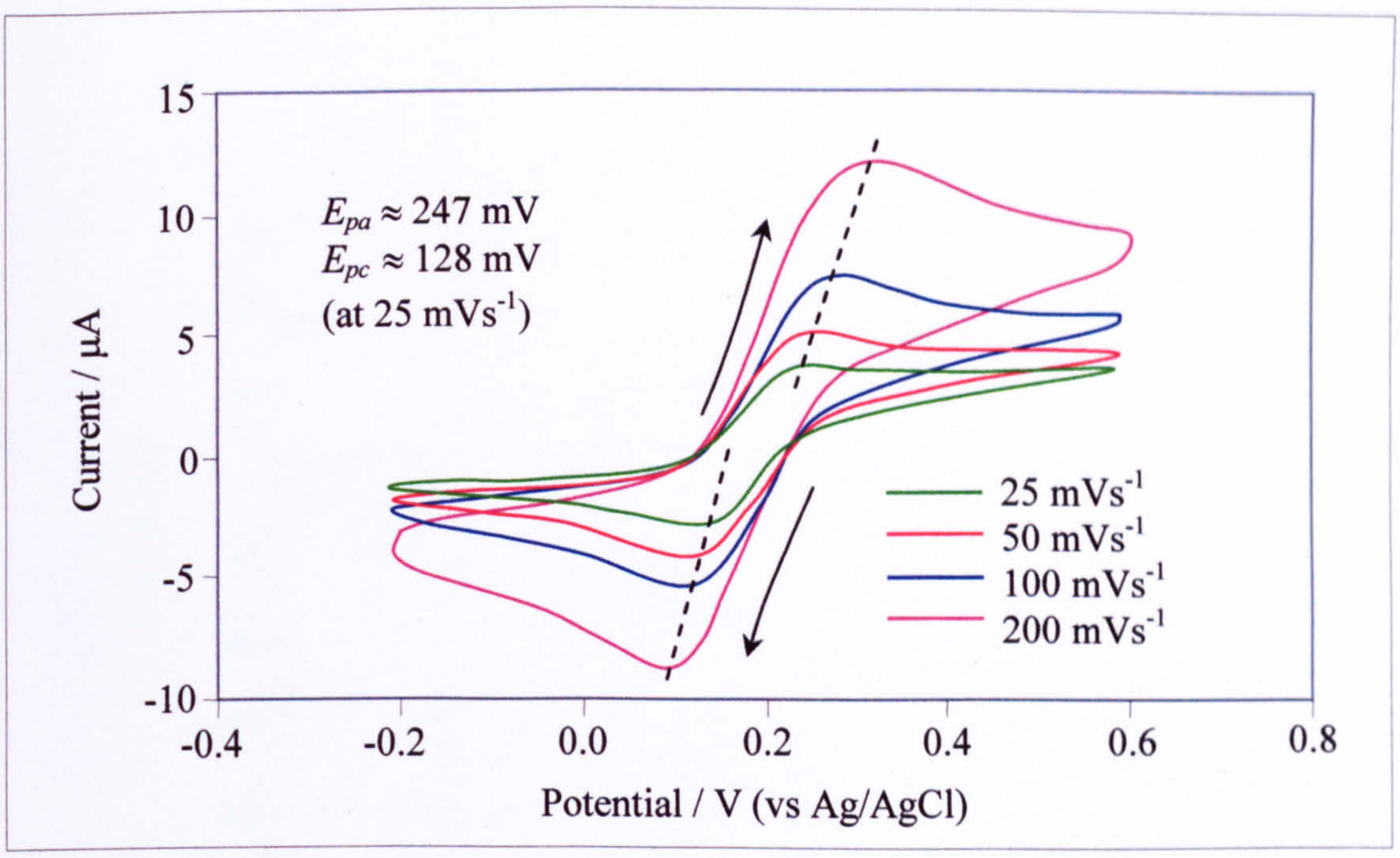

Figure 5.19: Cyclic voltammogram of 1 mM $[Fe(CO_2H)]^{2+/3+}$ at a screen printed carbon paste electrode (25, 50, 100 and 200 mVs^{-1} sweep rate)

The redox couples exhibit both oxidation and reduction peaks. However, even at the slowest scan rate of 25 mVs^{-1}, *quasi*-reversible behaviour is indicated by the non-Nernstian peak separations of 95 mV and 119 mV for the ruthenium and ferrocene complex respectively. The peak potentials of the ferrocene couples show significant dependence on the scan rate (Figure 5.19), whereas little change is observed for the ruthenium complex (Figure 5.18). When the shape of the voltammograms are also considered, it can be concluded that the hexaammineruthenium(III) chloride exhibits superior electron transfer kinetics with a carbon-ink electrode surface than either ferrocenemonocarboxylic acid or potassium ferricyanide. The high reversibility of a $[Ru(NH_3)_6]^{3+/2+}$ solution on screen printed carbon is also suggested when the peak anodic and cathodic currents are plotted as a function of the square root of the sweep rate (Figure 5.20).

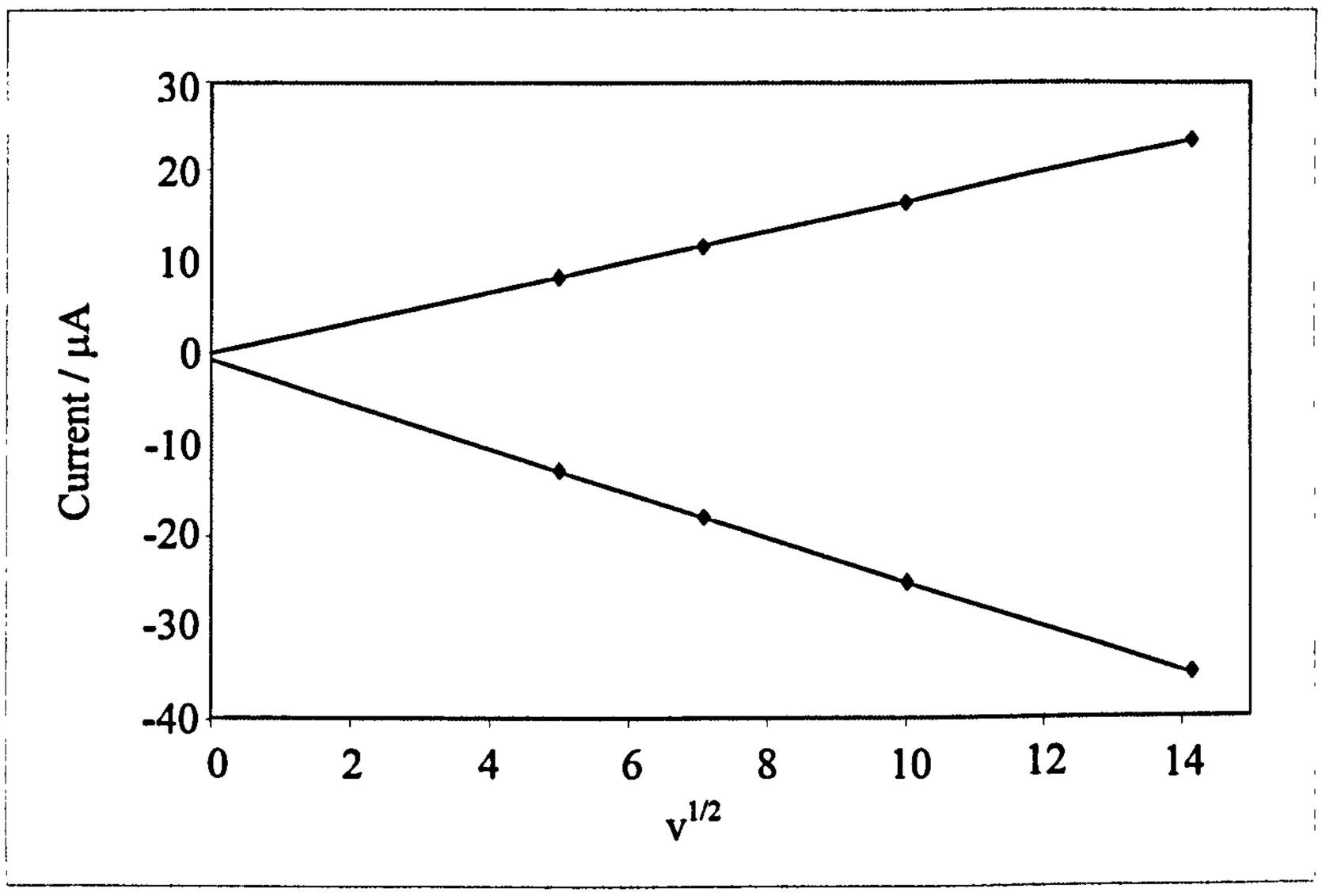

Figure 5.20: i_{pa} and i_{pc} as a function of $v^{1/2}$ for 1 mM $[Ru(NH_3)_6]^{3+/2+}$ on a carbon-ink electrode

In a perfectly reversible system, the plots of i_{pa} and i_{pc} against v are both linear and pass through the origin. This is closely mirrored by the hexaammineruthenium system above, and further suggests that it is a suitable redox couple for the interrogation of screen printed carbon paste sensors.

If the diffusion coefficient of $[Ru(NH_3)_6]^{3+}$ is assumed to be 8.6 x10^{-6} cm^2s^{-1} (Barker *et al*, 1998), then the real surface area of the carbon-ink electrode can be calculated using the Randles-Sevcik equation to be approximately 11.1 mm^2. This is slightly larger than the geometric area of 8.82 mm^2 which can be attributed to the rough topography of the sensor surface. The electroactive area can be used to estimate the thickness of the poly(*o*-phenylenediamine) film using charge integration methods. If depositing a single monolayer results in a charge density of 2.1 x10^{-4} $C.cm^{-2}$, then the total charge measured for the polymerisation of a single carbon-ink working electrode (1.342 x10^{-3} C) indicates a film thickness of approximately 8.1 nm. This is slightly thinner than that of the film deposited on a sputter-coated gold electrode (~10.2 nm),

and may reflect the less favourable electron transfer kinetics of a carbon ink surface when compared to gold.

It was necessary to confirm the effectiveness of an ultrathin P*o*PD film formed on Microarray Limited screen printed carbon-ink electrodes as a transport barrier for the application of amperometric chlorine detection. The potentiostatic responses of P*o*PD 5 coated sensors (20 sweeps, 0 to +1000 mV) were compared to those of 5 bare carbon electrodes by polarising at -80 and -100 mV in 20 ppm free (Figure 5.21) and 20 ppm total chlorine solutions (Figure 5.22) respectively. Error bars represent the standard deviation at 10 second intervals for the data acquired.

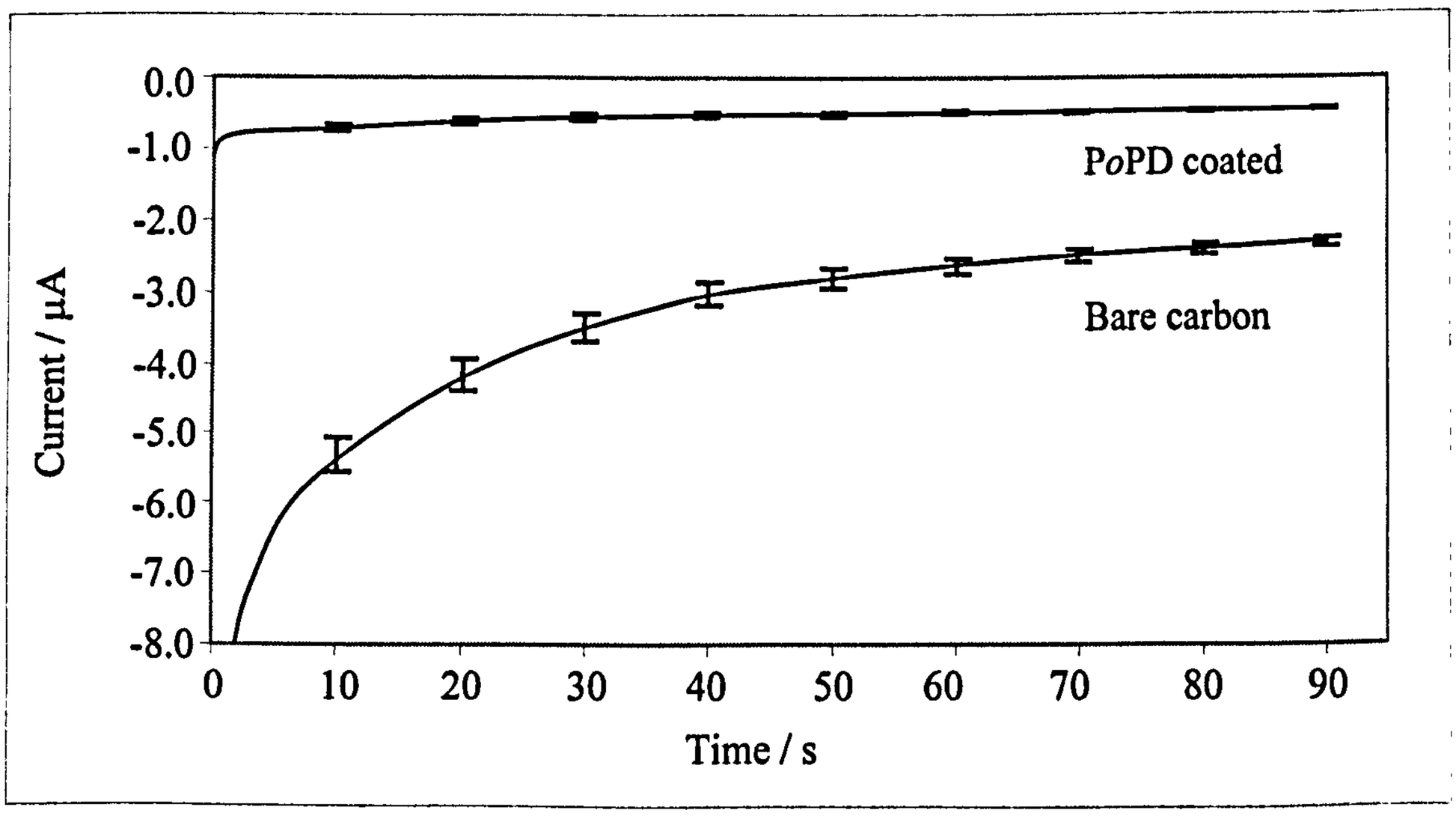

Figure 5.21: Current-time transients for bare carbon and P*o*PD polymer coated carbon electrodes in 20 ppm free chlorine solutions (-80 mV, pH 7.0 phosphate buffer, 50 mM KCl)

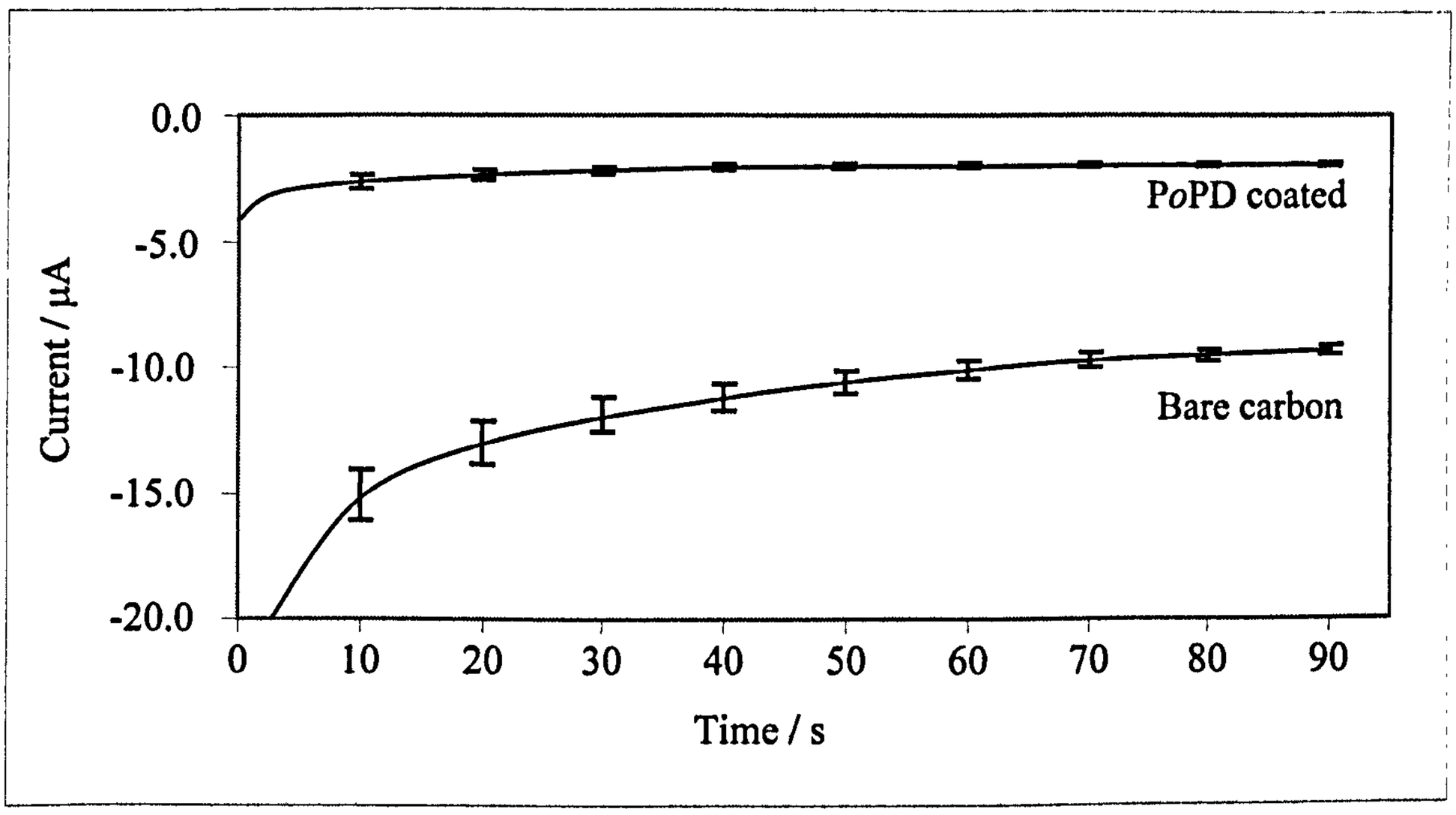

Figure 5.22: Current-time transients for bare carbon and P*o*PD polymer coated carbon electrodes in 20 ppm total chlorine solutions (-100 mV, pH 4.0 acetate buffer, 1M KI, 50 mM KCl)

It can be seen that despite the minute thickness of the electropolymerised film (an essential feature for subsequent microelectrode pore fabrication), when polymerised electrodes are exposed to both free and total chlorine the magnitude of the signal is reduced by approximately 90%. Given the electroinactive nature of P*o*PD films fabricated in neutral conditions (as is in this case), signal response obtained for the coated electrode must almost entirely result from the direct reduction of the analyte at the metal/polymer/solution interface. Since the nature of the electropolymerisation process yields a pristine, defect free layer (at least compared to the size of a monomer), then the electrochemistry of the analyte must involve its permeation through the polymer film (Centonze *et al*, 1994).

Yano *et al* investigated the permeability of P*o*PD films to iodine and bromine ions (Yano *et al*, 1992a). Although the films employed in their research were in the conducting form (i.e. polymerised in acidic conditions), and the analytes being determined were the halogenide ions I^- and Br^-, the paper still provides evidence in the support of non-conducting poly(*o*-phenylenediamine) films as diffusional barriers in free and total chlorine systems. They reported that the incorporation of

benzoquinone moieties into the conducting polymer film resulted in a major decrease in the permeability of the films to I^- and Br^-. Benzoquinone sub-units have been shown to be present in non-conducting P*o*PD films (Section 5.2) and it follows that a similar interaction may cause the low permeability of the P*o*PD film to free chlorine when in the form of the small, negatively charged hypochlorite ion (OCl^-).

Centonze *et al* showed that the permselectivity of P*o*PD films does not simply occur via a molecular size and charge basis, but is also the result of more complex chemical interactions between probe and film, such as hydrogen bonding or hydrophobic interactions (Centonze *et al*, 1994), (Murphy, 1998). Selectivity of this nature is clearly beneficial in providing a barrier to the transport of small, electrostatically neutral molecules and may explain the resistance to permeation of free chlorine species such as Cl_2, HOCl, or in the case of total chlorine systems, I_2. It is noted that irrespective of the type of analyte, some decrease in signal size will be attributed directly to the reduction of the effective electrode area caused by the adsorption of the polymer film to the electrode surface (Yano *et al*, 1992b).

5.4 Further optimisation of the electropolymerisation process

Previous investigations into the electropolymerisation of *o*PD at screen printed carbon-ink surfaces (Section 5.3) described an extended polymerisation potential range of 0 to +1000 mV, required to permit efficient film formation in comparison to films formed on gold surfaces. Other variables controlling film formation have been largely optimised in the literature. For example, the pH of the monomer solution affects the structure of the polymer film, and has been shown to produce ultrathin, insulating films in more neutral conditions. (Centonze *et al*, 1994), (Losito *et al*, 2003). Once formed, the integrity of P*o*PD films of this type have been shown to be stable over a wide pH range (3-11) (Heineman *et al*, 1980), (Cheek *et al*, 1983).

Increasing the concentration of *o*PD monomer does not necessarily benefit the rate of electrode passivation, as concentrations of up to 25 mM have been shown to cause a decrease in the density of the polymer film (Malinauskas *et al*, 1998), (Li *et al*, 2002). Throughout the literature, and in this research, a concentration of 5 mM *o*PD has been used for the application of producing ultrathin, low permeability, insulating films. Further optimisation of *o*PD monomer concentration will be carried out when the cost constraints associated with environmental waste regulation, pertaining to the disposal of high volumes of *o*PD monomer solution, are defined by the location of the production facility.

Deoxygenation of the buffer solution with nitrogen gas prior to addition of the monomer is required, since *o*PD is easily oxidised by dissolved oxygen, which can be observed by a solution colour change from clear to yellow within a few minutes of preparation (Yao *et al*, 1994). This is thought to result in the formation of 2,3-diaminophenazine, which in turn disrupts the polymer structure and increases its permeability to electroactive species (Murphy, 1998). Atmospheric gases also pose a problem specific to the case of electropolymerisation of screen printed carbon-ink electrodes. As a result of the rough topography and hydrophobic nature of the carbon-ink surface, sensors that are submerged into an aqueous monomer solution prior to polymerisation, suffer from air entrapment at the interface, visible in the form of a 'sheen' at the carbon surface. Consequently, incomplete wetting of the electrode surface occurs, translating into a disrupted polymeric layer. To overcome this problem, 3 short pulses of ultrasonic energy (approximately 0.5 s, 25-35 kHz) are applied to the system prior to commencing electropolymerisation. This causes the air to become displaced by the solution, and permits intimate contact across the electrode surface.

The electropolymerisation of the sensor sheets will be carried out as a batch process. Therefore, costings must be established with respect to polymerisation batch size and duration. This creates the requirement for the design of the industrial-scale process to focus on the primary time-dependent factors, namely the number of cycles and the sweep rate employed. Since the application of the film formed is to function as a diffusional barrier to the migration of chlorine to the electrode surface, it follows that

chlorine probes must be used in assessing the effectiveness of various polymerisation regimes.

Microarray Limited screen printed carbon-ink sensors (8.82 mm^2) were electropolymerised at 25, 50, and 100 mVs^{-1}, with the number of sweeps relating to the time-frames of approximately 15, 20, 30, 40 and 60 minutes respectively. The responses of the polymer-coated electrodes were measured potentiostatically in concentrations of 20 ppm free and total chlorine, which represents the upper limit required for chlorine detection. The magnitudes of the signals were derived from the mean current recorded over the final 10 seconds of a 90 second polarisation time (-80 mV and -100 mV vs. Ag/AgCl for free and total chlorine respectively). Figures 5.23 and 5.24 indicate the mean current responses obtained for 5 sensors polymerised under each different polymerisation regime in free and total chlorine solutions respectively. Error bars represent the standard deviation calculated from each data set.

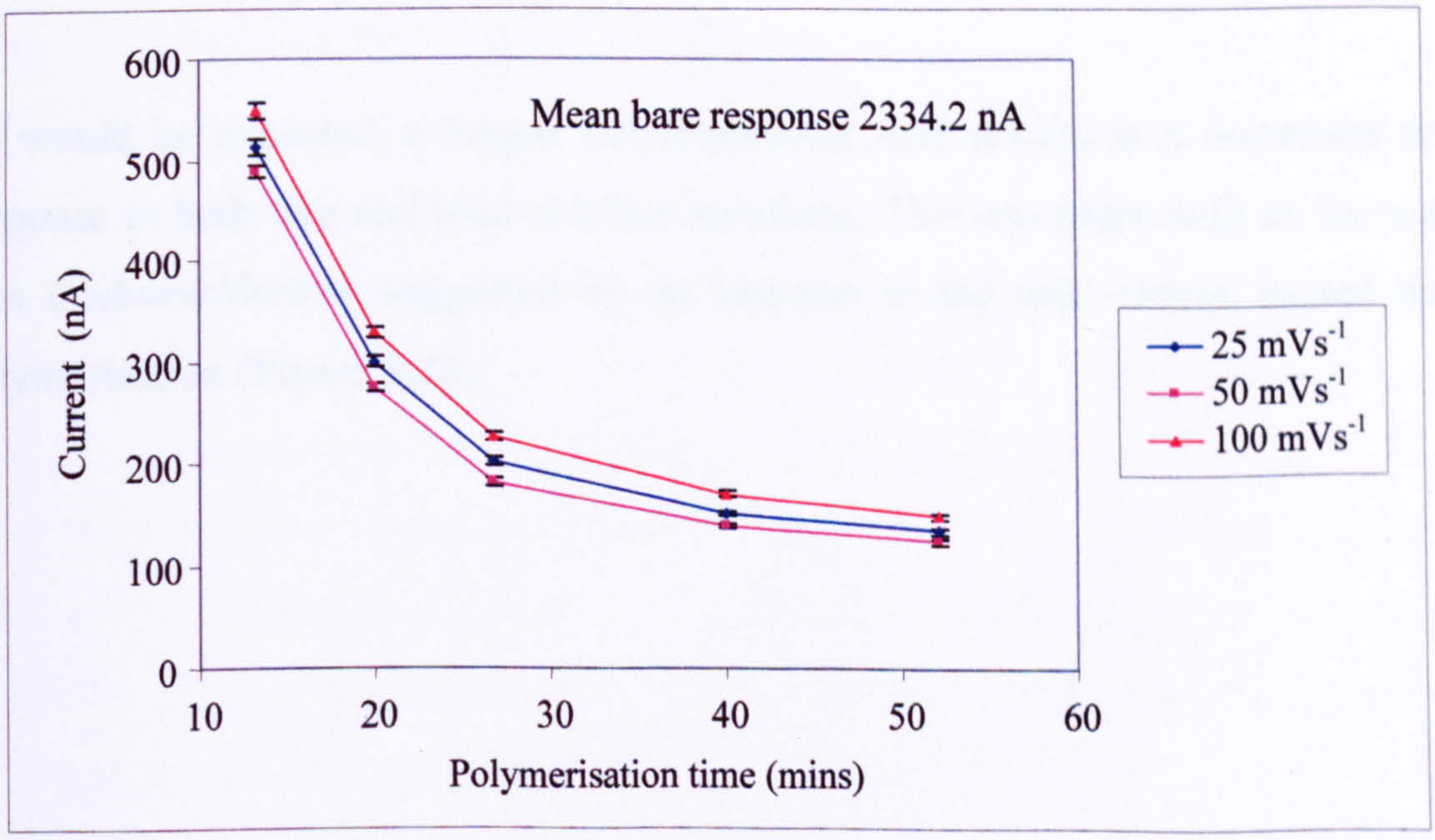

Figure 5.23: Effect of *o*PD polymerisation regime on response to 20 ppm free chlorine solutions

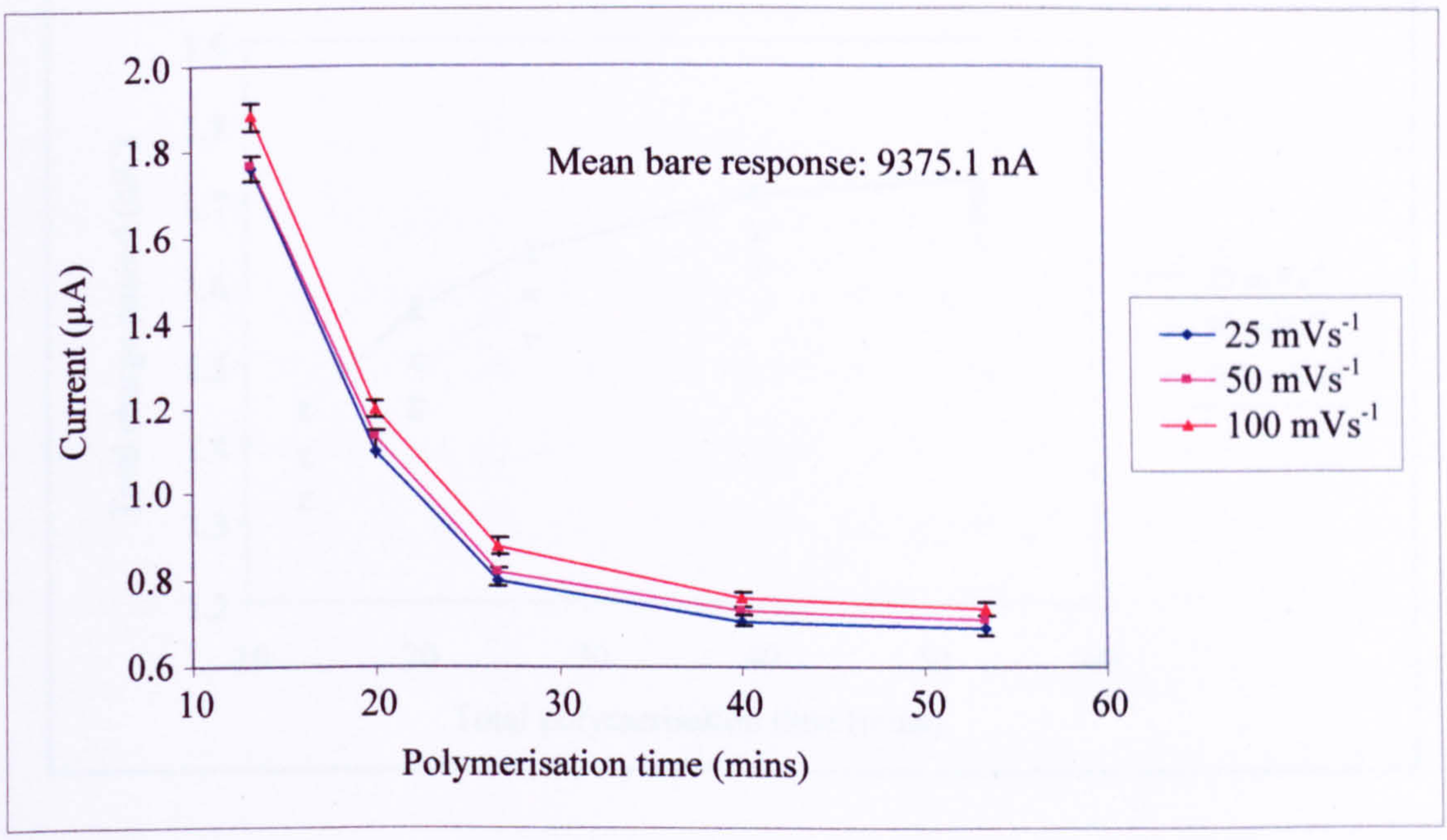

Figure 5.24: Effect of *o*PD polymerisation regime on response to 20 ppm total chlorine solutions + 1M KI

As would be expected, a longer polymerisation time results in a decreased sensor response to both free and total chlorine solutions. This correlates with an increase in film thickness/density suggested by an increase in the total charge passed during polymerisation (Figure 5.25).

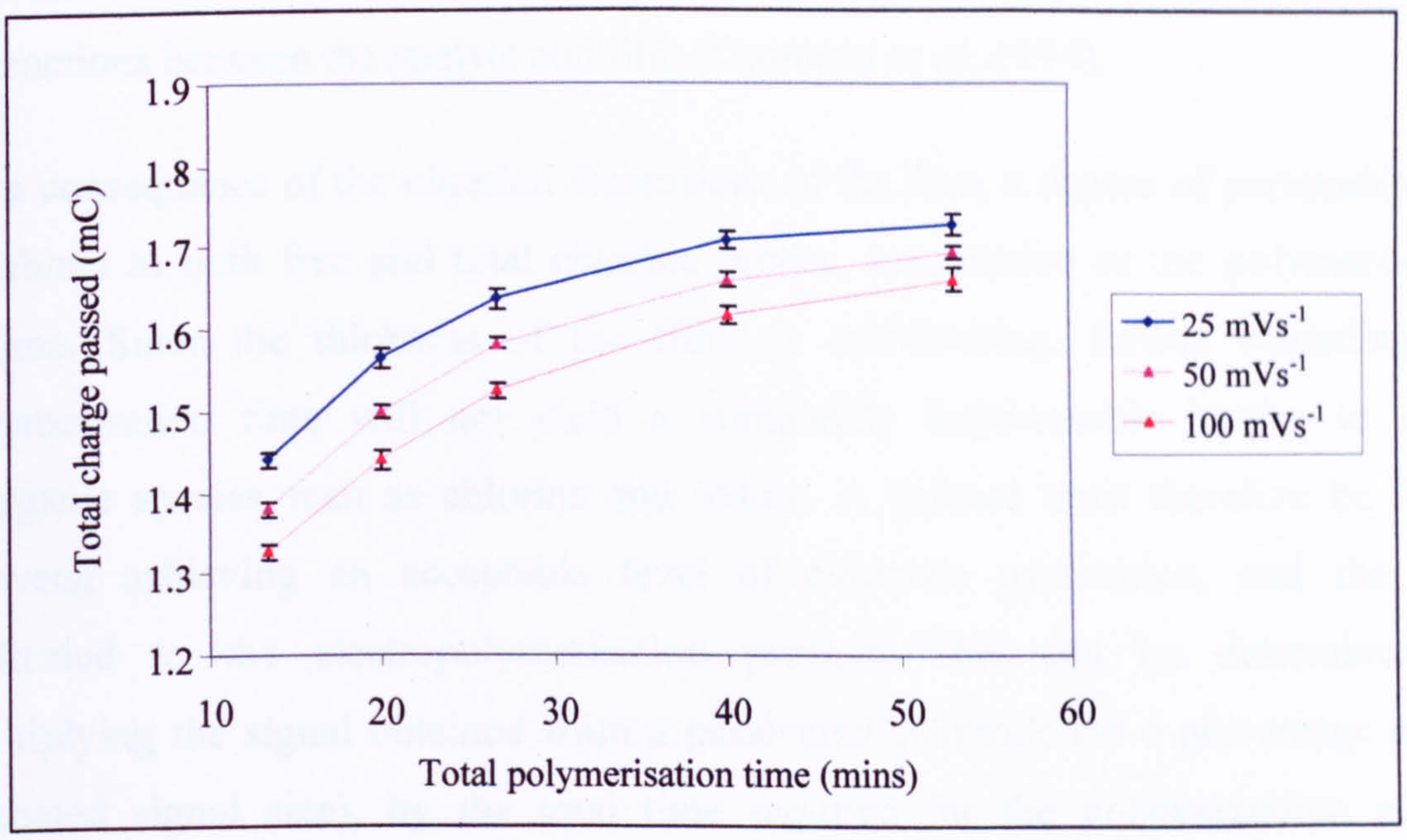

Figure 5.25: Total charge passed for various polymerisation regimes

The sweep rate employed can be seen to have a significant effect on the permeability of the polymer film. For a given polymerisation time, electrodes polymerised at sweep rates of 100 mVs^{-1} consistently show greater current responses to free and total chlorine probes than those coated at slower scan rates (25 and 50 mVs^{-1}). This is possibly related to the dependency of the polymerisation reaction kinetics on the applied potential, since the higher potentials, which favour chain termination, are reached sooner. In turn, the polymer structure will be affected, and may result in a lower density, higher permeability film (Curulli *et al*, 1998). The trend was continued when sensors polymerised at slower scan rates (25 and 50 mVs^{-1}) were interrogated with total chlorine solutions, whereby the slower scan rate produced a marginally decreased current response.

However, the permeability of P*o*PD film to free chlorine exhibited a more complex dependency upon scan rate. The data indicated that films produced at a scan rate of 50 mVs^{-1} presented a more effective barrier than those polymerised at the slower potential sweep of 25 mVs^{-1}. Since Figure 5.25 indicates that more polymer is laid down for 25 mVs^{-1} than for 50 mVs^{-1}, this supports the hypothesis suggested by Centonze *et al* (described in Section 5.3) that the diffusional hindrance caused by the

ultrathin P*o*PD film depends to a large extent on its structure and specific chemical interactions between the analyte and film (Centonze *et al*, 1994).

As a consequence of the ultrathin dimensions of the film, a degree of permeability is exhibited to both free and total chlorine probes, irrespective of the polymerisation regime. Since the thickness of the films is self-limiting, further extending the polymerisation time will not yield a completely impermeable barrier to small inorganic species such as chlorine and iodine. A balance must therefore be found between achieving an acceptable level of electrode passivation, and the time dedicated to the electropolymerisation process. This can be determined by multiplying the signal obtained from a passivated electrode (as a percentage of the uncoated signal size), by the total time required for the polymerisation regime (Figure 5.26).

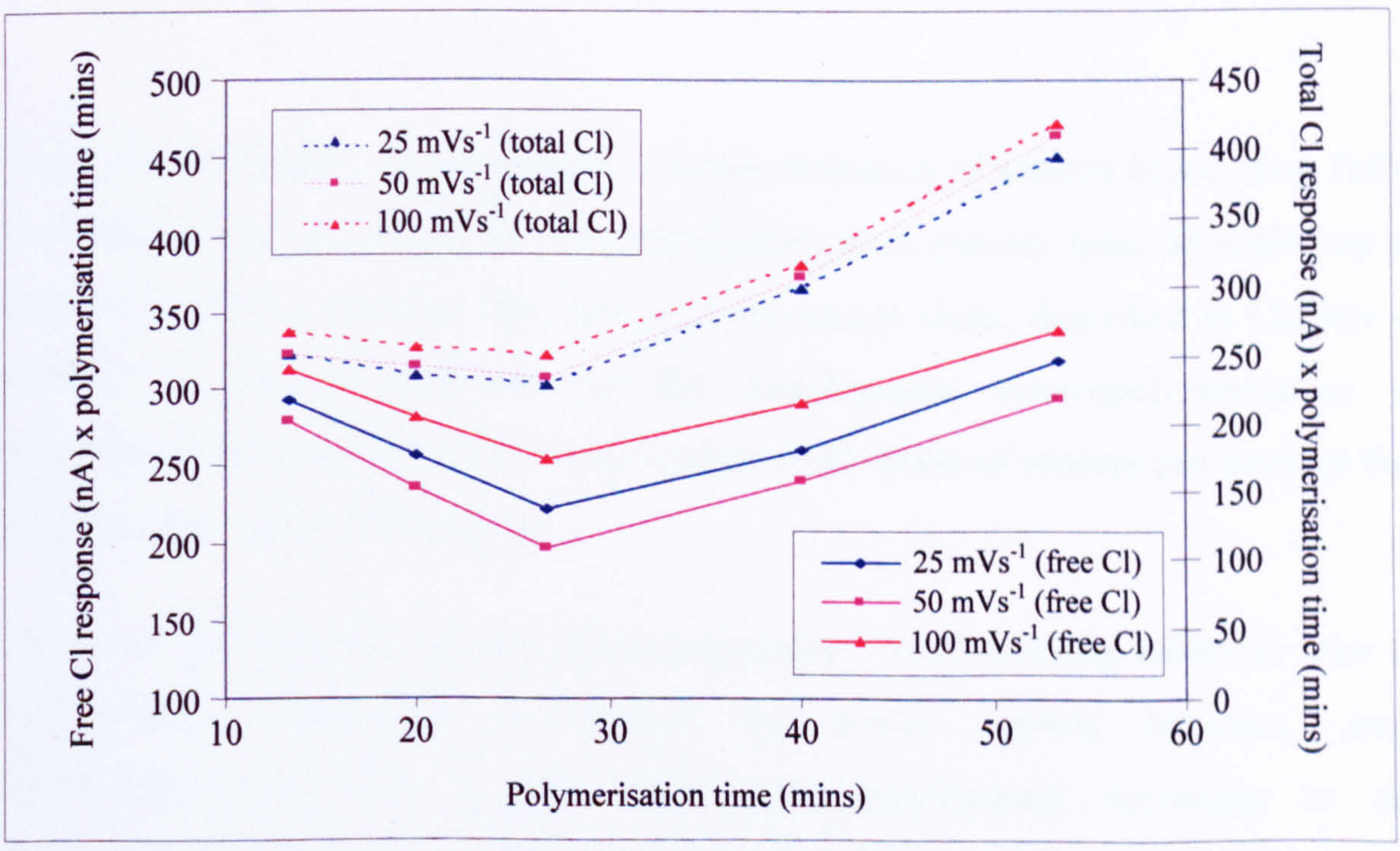

Figure 5.26: Determination of optimal polymerisation regime

In can be seen that for free chlorine, the optimal polymerisation regime (i.e. where the most effective insulation is attained for the least time) occurs for a polymerisation time of 26.7 minutes (0 to +1000 mV, 40 cycles at 50 mVs^{-1}). This arrangement

reduces the response to free chlorine by around 92.5% when compared to that of a bare carbon electrode. Sensors interrogated using total chlorine solutions also indicated an optimal polymerisation time of 26.7 min, although a slower sweep rate of 25 mVs^{-1} appeared to offer a marginally better passivation (8.7%) than for a sweep rate of 50 mVs^{-1} (8.5%). However, since the difference between the passivation provided by the two methods is small, and since only one polymerisation regime can be employed during commercial production, the optimal polymerisation regime was determined to be 40 cycles (0 to +1000 mV) at 50 mVs^{-1} relating to a process batch time of 26.7 minutes.

5.5 Upscale of the polymerisation process

To in order to achieve the successful commercialisation of sensors based upon P*o*PD modified carbon electrodes, the electropolymerisation process must be scaled-up as cost effectively as possible. The design of the sensor sheet, described in Chapter 4, provides a suitable platform for the simultaneous electropolymerisation of 600 sensors; the parallel polymerisation of up to 40 sheets of sensors can increase this number to the order of thousands.

A group of 20 and 100 sensors (each possessing a total working electrode area of 21.78 mm^2), connected in parallel by screen printed bus-bars, were electropolymerised with 5 mM poly(*o*-phenylenediamine) according to the polymerisation regime previously determined in Sections 5.3 and 5.4. The cyclic voltammograms from each process are displayed in Figures 5.27 and 5.28.

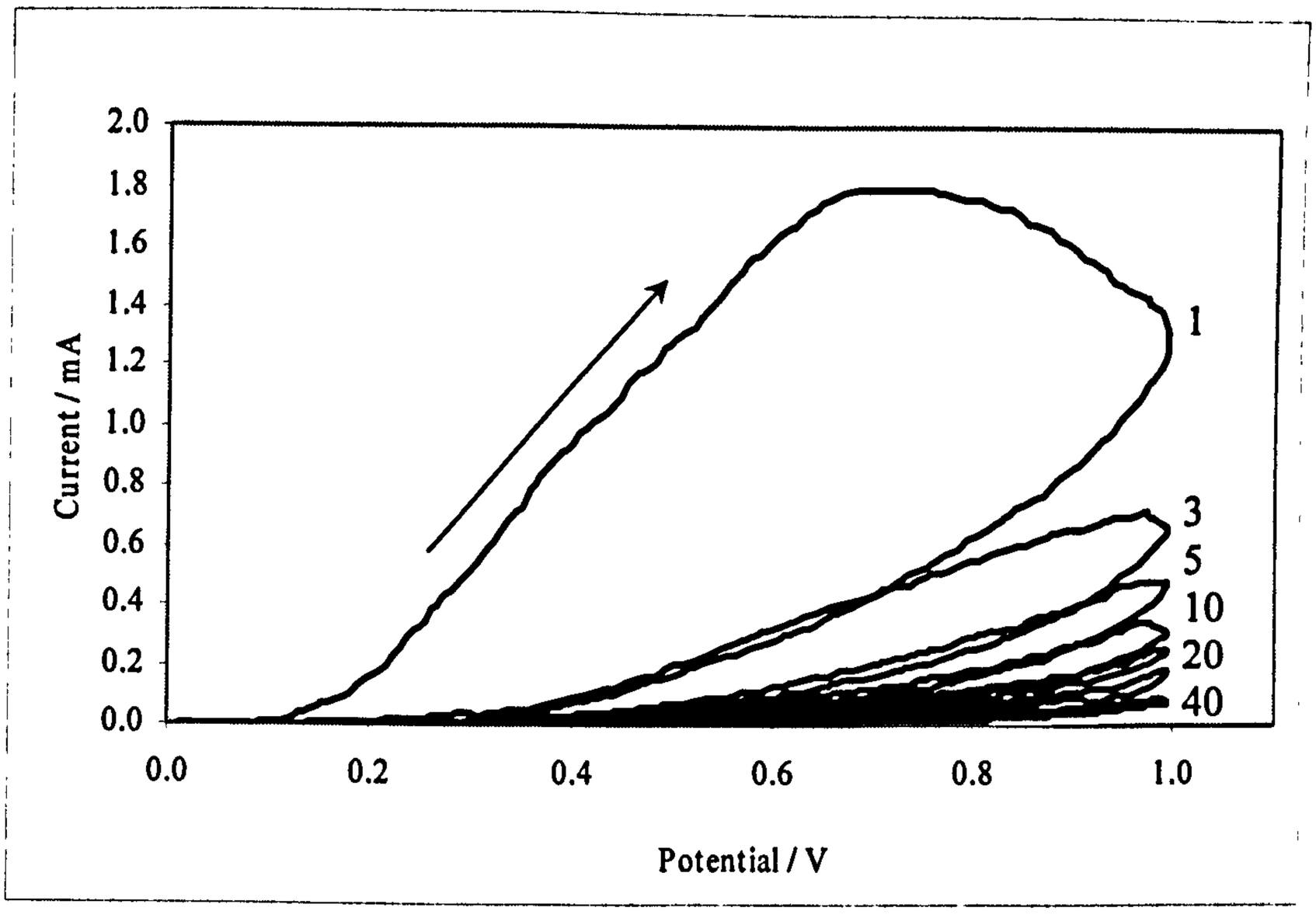

Figure 5.27: Cyclic voltammogram displaying the simultaneous polymerisation of 20 screen printed carbon-ink sensors electrodes (5 mM *o*PD, 40 sweeps, 0 to +1000 mV, pH 7.4 phosphate buffer, 50 mM KCl)

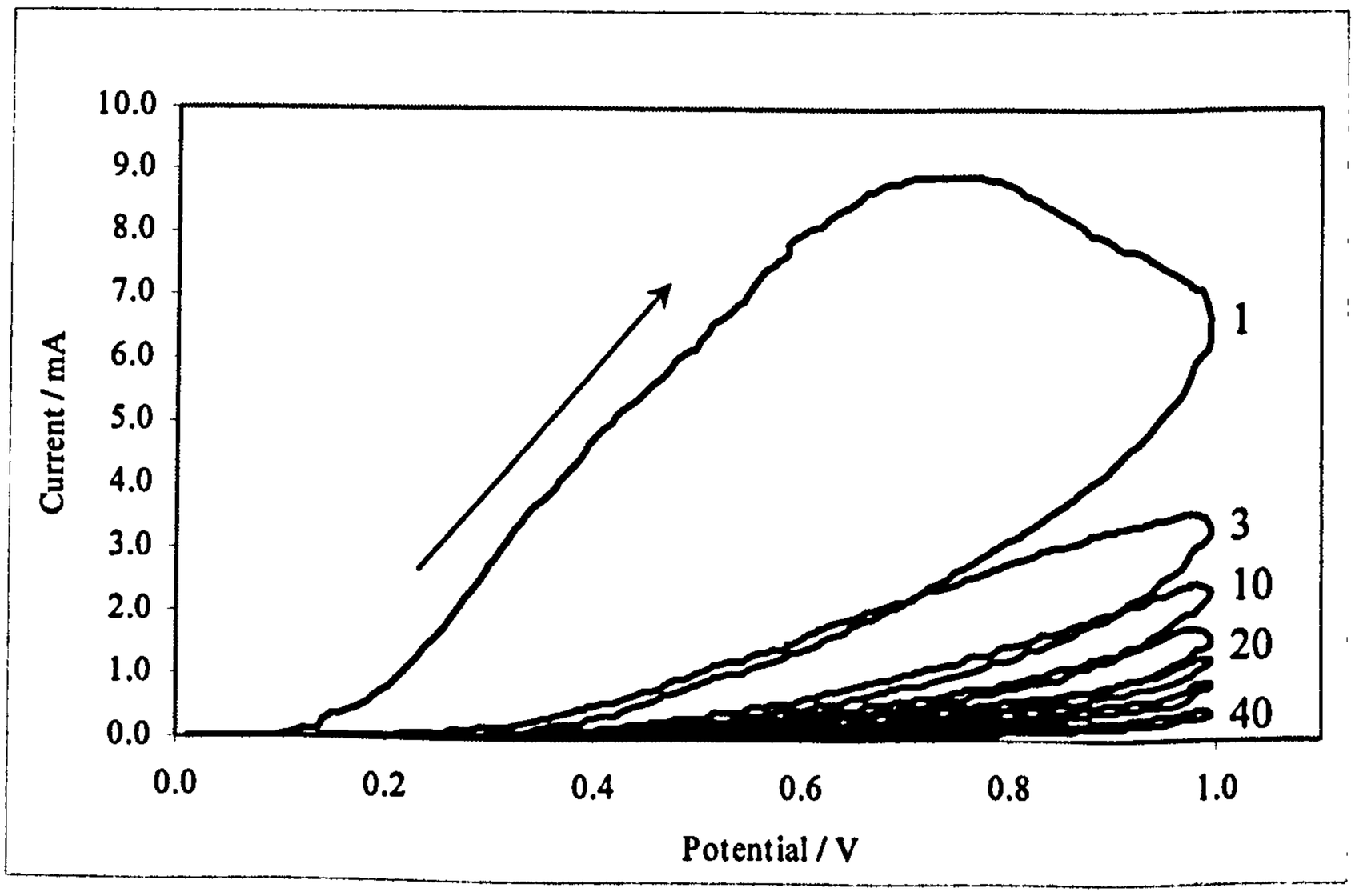

Figure 5.28: Cyclic voltammogram displaying the simultaneous polymerisation of 100 screen printed carbon-ink sensors electrodes (5 mM *o*PD, 0 to +1000 mV, 40 sweeps, pH 7.4 phosphate buffer, 50 mM KCl)

The cyclic voltammograms indicate the deposition of insulating poly(*o*-phenylenediamine) onto the surfaces of both 20 and 100 sensors simultaneously. Furthermore, the magnitude of the anodic peak currents observed closely corresponds to 20 and 100 times that recorded for a single carbon sensor (Figure 5.10). However, it can be seen that the two anodic peaks evident for the polymerisation on single electrodes have merged, forming a single anodic peak at approximately +750 mV. This difference can be attributed to the resistance introduced by the screen printed bus-bars, which serve to connect the electrodes to the potentiostat. Since the measured current is a cumulative response across all electrodes, the definition of the separate oxidation peaks is lost. Importantly, the peak current generated for the simultaneous polymerisation of 100 sensors (indicated in Figure 5.28) approaches that of the maximum output of the laboratory potentiostat (10 mA). In order to permit the simultaneous polymerisation of sheets of 600 sensors, a design specification was written for the acquisition of a purpose-built potentiostat (a draft of which is displayed in Appendix 2). Since the equipment is to be used for the commercial production of sensors, a number of design considerations relating to equipment operation had to be considered.

Firstly, the system must initiate an ultrasonic pulse to allow any air trapped against the screen printed carbon-ink electrode surfaces to be displaced by monomer solution, as previously described. Only then can the electropolymerisation sequence be activated, whereby the system must be able to provide the necessary charge for the simultaneous polymerisation of 40 sheets of electrodes. For quality assurance reasons, it must be possible to verify the successful polymerisation of each sheet of 600 electrodes. This can be achieved by means of an automated assessment of initial peak currents and total charge transfer recorded for individual sensor sheets, thereby necessitating a multi-channel system configuration. A simple, colour-coded go/no-go software interface was envisaged to permit operatives to quickly and easily determine whether a polymerisation batch was running correctly (Figure 5.29).

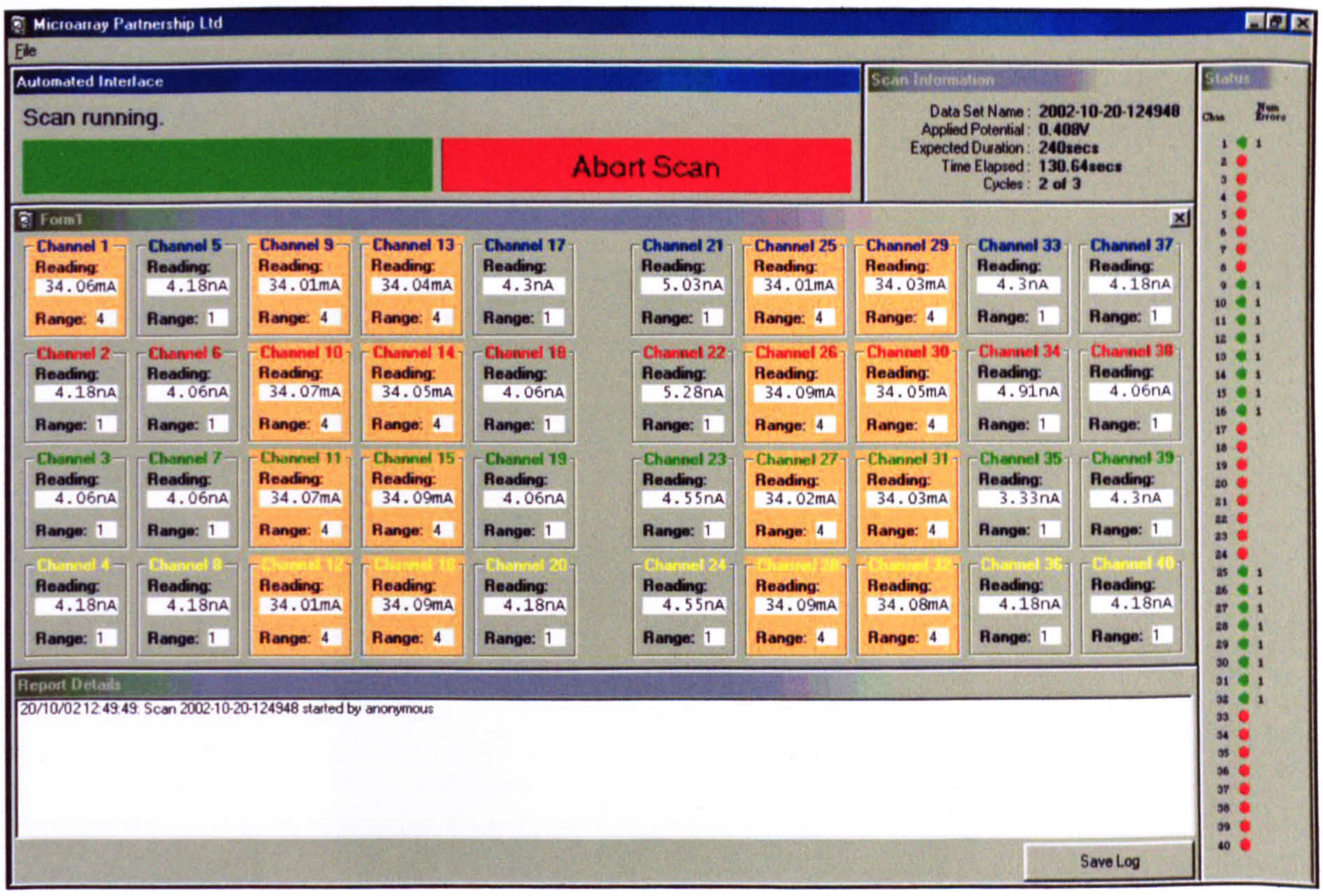

Figure 5.29: Industrial polymerisation potentiostat front-end user interface

In the screen-shot above, 17 of the 40 channels are active (indicated by the orange colouring), with currents displayed in real time. The status bar on the right-hand side indicates to the operator that each of the active sheets returned an initial anodic peak current of between 50 and 55 mA (green colour coding). This in turn indicates that each sheet is correctly connected and that the polymerisation reaction is progressing as intended. In addition, an integrated graphical software package permits the visual inspection of each channel in terms of time vs. current, potential vs. time and current vs. potential. For manufacturing traceability, each polymerisation operation requires a user log-in which is recorded along with data from the polymerisation process. This approach also prevents unauthorised users from making changes to the polymerisation regime.

Figure 5.30 illustrates the Microarray Limited custom designed 40-channel industrial potentiostat.

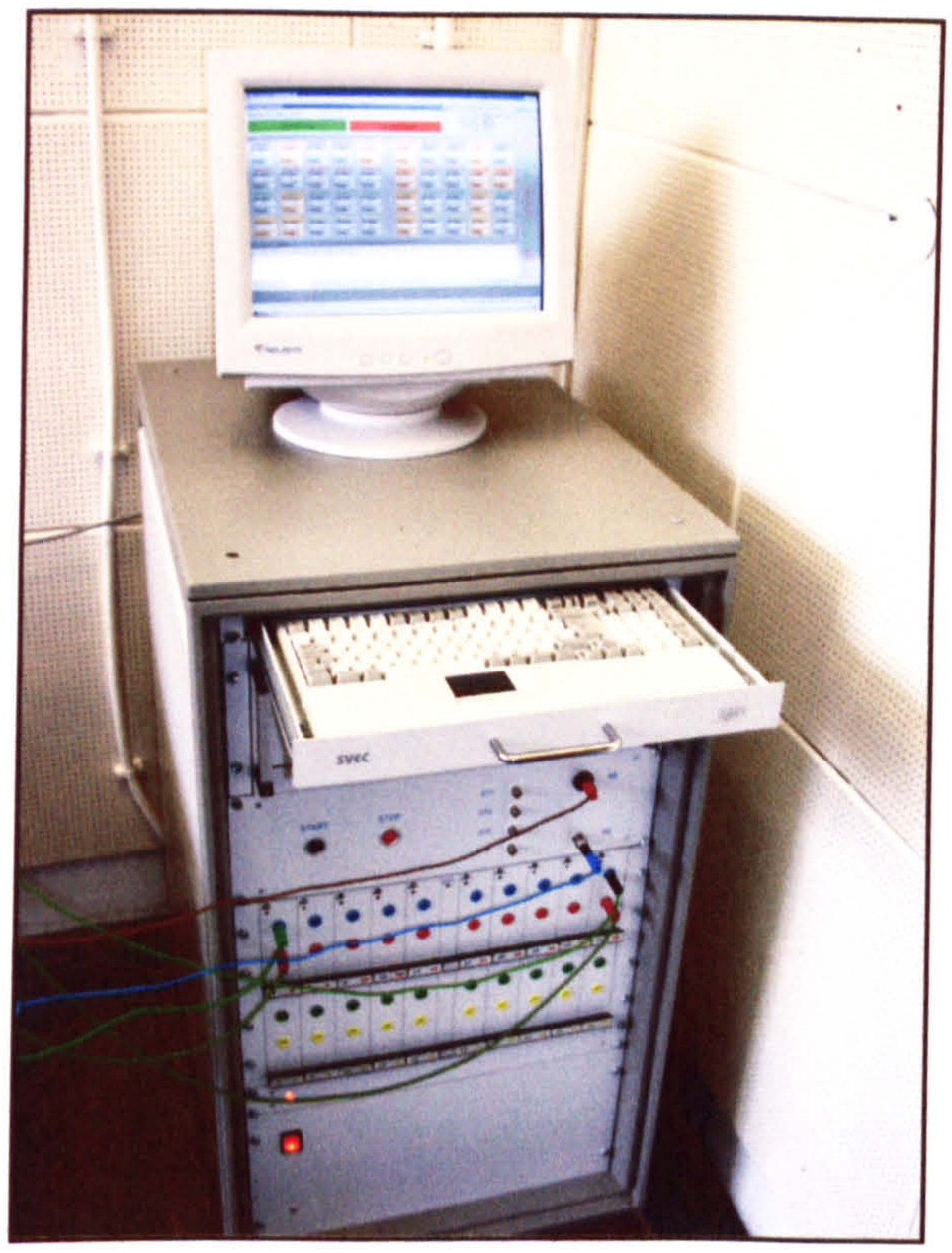

Figure 5.30: Microarray Limited custom built 40-channel industrial potentiostat

A two-stage validation of the industrial polymerisation system was carried out. In the first instance, each channel was confirmed to be operating correctly by means of mounting a purpose-built dummy cell (comprising a resistor board construction) onto the front of the potentiostat, allowing each channel to be simultaneously assessed in terms of potential output and measured current. The system was then used to electropolymerise full-sized (400 x 600 mm) sheets of 600 electrodes to confirm that all sensors are successfully insulated with poly(*o*-phenylenediamine) using the polymerisation regime determined and optimised in Sections 5.3 and 5.4. A 500 x 600 x 25 mm internal diameter stainless steel container was employed as the polymerisation vessel, with a 400 x 600 mm section of stainless gauze attached along one side to serve as the counter electrode. Sensor sheets were attached to the opposite side, facing into the chamber, such that the width of the container allowed a constant separation of 25 mm between the sensor sheet and the counter electrode to be maintained. A typical voltammogram from the electropolymerisation of a full sheet of sensors is displayed in Figure 5.31.

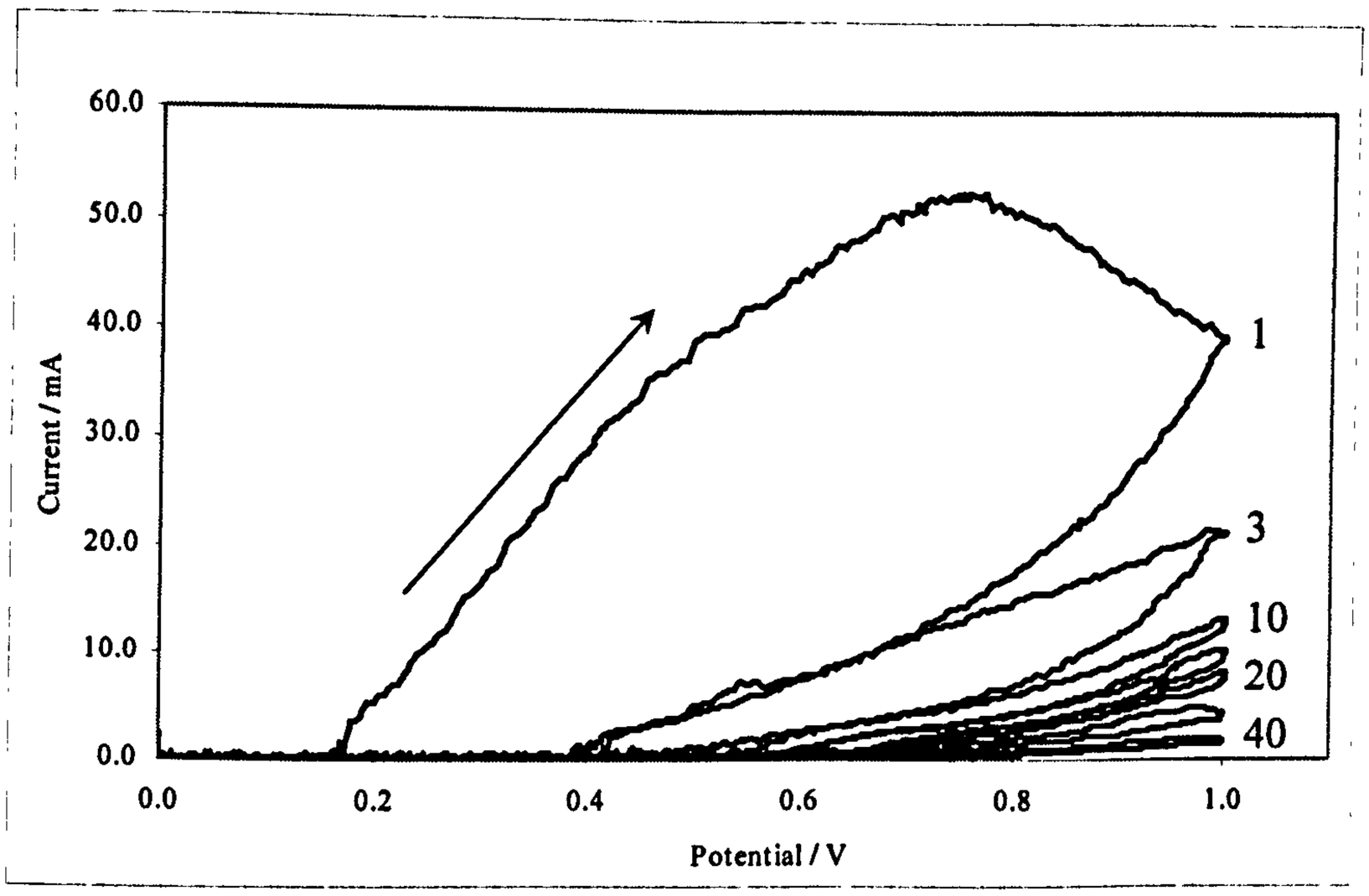

Figure 5.31: Cyclic voltammogram displaying the simultaneous polymerisation of 600 screen printed carbon-ink sensors electrodes (5 mM *o*PD, 0 to +1000 mV, 40 sweeps, pH 7.4 phosphate buffer, 50 mM KCl)

The decay in current observed for successive sweeps indicated in Figure 5.31 depicts the passivation of a full sheet of screen printed carbon-ink sensors with poly(*o*-phenylenediamine). Furthermore, the magnitude of the peak anodic currents displayed corresponds to the number of sensors undergoing electropolymerisation when compared to previous polymerisation scans for 1, 20 and 100 sensors. The increased noise exhibited when compared to Figures 5.27 and 5.28 is most likely a consequence of the heavy-duty design of the electronics, which must cope with currents far beyond that experienced during normal electrochemical investigations.

However, to be certain that sensors undergo an equal degree of passivation via polymer deposition, it was necessary to analyse the response of sensors taken from a wide range of positions to a 20 ppm total chlorine probe. In addition, adjacent sensors were interrogated using a 1 mM hexaammineruthenium probe, previously identified to show favourable reaction kinetics with screen printed carbon-ink surfaces. Tables 5.2 and 5.3 indicate the amperometric electrode responses obtained for 20 ppm total chlorine (-100 mV vs. Ag/AgCl) and 1 mM hexaammineruthenium

(-375 mV vs. Ag/AgCl) probes respectively. Signal magnitudes were obtained from the mean current from the final 10 seconds of a 90 second polarisation period.

Sensor ID	Current (nA)	Sensor ID	Current (nA)	Sensor ID	Current (nA)
A1	820.1	A30	830.1	A60	839.0
B10	822.1	B26	834.8	B50	810.2
C20	831.6	C36	818.1	C41	826.3
E1	836.0	E30	828.0	E60	817.5
F10	810.0	F30	805.1	F50	832.9
H20	808.7	G40	811.1	H41	820.3
I10	818.1	I21	828.4	I50	834.1
J1	831.4	J30	822.8	J60	825.8

Mean: 823.4 nA Bare mean: 9.19 μA Signal reduction: 90% RSD: 1.17%

Table 5.2: Response of *o*PD electropolymerised screen printed carbon-ink sensors to 20 ppm total chlorine (pH 4 acetate buffer, 1 M KI, 0.5 M NaCl)

Sensor ID	Current (nA)	Sensor ID	Current (nA)	Sensor ID	Current (nA)
A2	106.1	A31	108.4	A59	109.5
B11	107.1	B27	106.9	B51	107.8
C19	105.9	C35	104.2	C42	104.7
E2	108.6	E31	105.6	E59	110.6
F11	107.0	F31	110.5	F51	107.8
H19	108.0	G39	109.3	H42	106.6
I11	104.7	I22	108.4	I51	105.1
J2	109.2	J31	110.5	J59	108.0

Mean: 107.5 nA Bare mean: 6.57 μA Signal reduction: 98% RSD: 1.77%

Table 5.3: Response of *o*PD electropolymerised screen printed carbon-ink sensors to 1 mM hexaammineruthenium(III) chloride (pH 7.8 phosphate buffer, 0.1 M NaCl)

Analysis of the above data-set indicates that the relative standard deviation obtained for current responses to the total chlorine probe (1.17%) is similar to that previously determined for unmodified screen printed carbon-ink electrodes in Section 4.6 (1.06%). This suggests that there is good consistency of polymer film structure, thickness and density across a sheet of 600 electrodes. The P*o*PD film exhibits

considerably less permeability to the hexaammineruthenium probe, likely to be a result of cationic repulsion between the larger, positively charged (cationic) ruthenium couple and positively charged sites (such as protonated amine/imine groups) present within the polymeric film (Yano *et al*, 1992b). Consequently, the measured variation in sensor response shows more sensitivity to defects in the film, such as pin-holes, since there is a much lower permeation through the surrounding polymer. A relative standard deviation of 1.77% is observed for the hexaammineruthenium couple, suggesting a relatively defect-free film obtained by the parallel polymerisation of 600 screen printed carbon-ink sensors.

In order to assess the effect of bulk sensor polymerisation, the data presented above was translated into a two-dimensional representation of the sensor sheet (Figure 5.32).

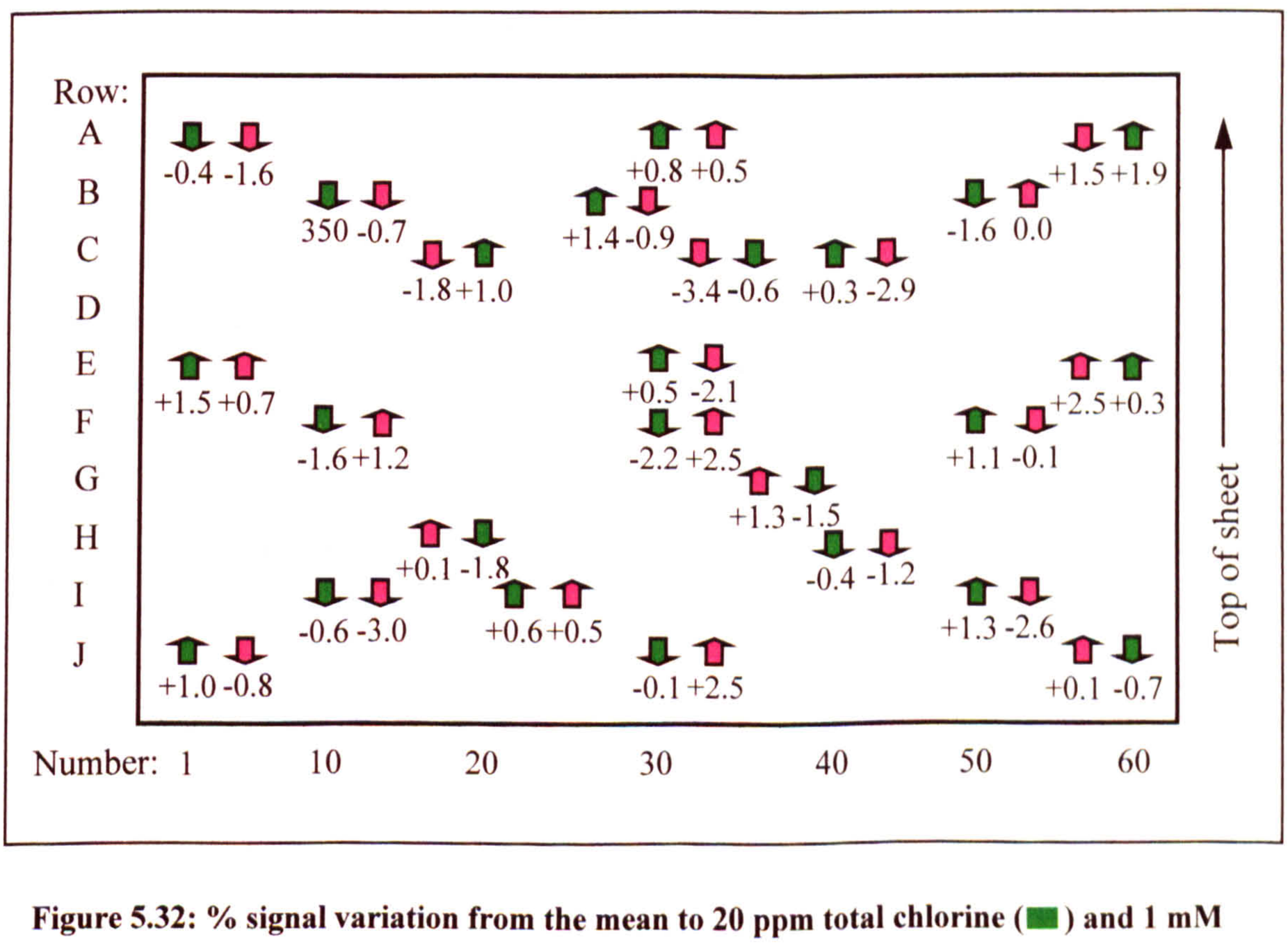

Figure 5.32: % signal variation from the mean to 20 ppm total chlorine (■) and 1 mM hexaammineruthenium(III) chloride (■)

The data in Figure 5.32 suggests that that there is no correlation between the position of the sensor within the sheet and the efficiency of the P*o*PD film formation. Given

adequate electropolymerisation conditions (40 sweeps at 50 mVs^{-1}, from 0 to +1000 mV vs. Ag/AgCl), this in turn suggests that the self-limiting growth of the P*o*PD film allows for a substantially even coating to be deposited across the sheet, irrespective of position or distance from the potentiostat connections.

5.6 Conclusions

The electropolymerisation of poly(*o*-phenylenediamine) onto gold sputter-coated ground glass slide electrodes was characterised in neutral conditions to show a two electron transfer mechanism for the formation of a non-conducting, ultrathin film. This was then applied to screen printed carbon-ink electrode surfaces, which offer a less expensive route to the mass production of disposable aqueous chlorine sensors. As a consequence of the decreased electron transfer kinetics associated with carbon-ink host electrodes, the electropolymerisation process was refined by extending the polymerisation potential window from 0 to +800 mV to 0 to +1000 mV (vs. Ag/AgCl), allowing the more anodic reactions to take place and so a more efficient passivation of the electrode surface to occur. A pre-polymerisation sonocation step (three 0.5 s pulses of ultrasonic energy) was identified as being required to remove trapped air from the electrode surface, thereby permitting intimate contact with the monomer solution and preventing disruption of the polymer layer.

Film thickness of P*o*PD on gold (10.2 nm) and on screen printed carbon-ink electrodes (8.1 nm) were shown to be similar. Estimations of film thickness required interrogation by cyclic voltammetry, and an appropriate redox couple for screen printed carbon-ink surfaces was identified as hexaammineruthenium(III) chloride. The passivation of screen printed carbon-ink electrodes via electropolymerisation of non-conducting poly(*o*-phenylenediamine) was confirmed to show an approximately 90% decrease in response to free and total chlorine solutions.

In order to minimise the impact of production upon unit cost, the polymerisation batch process was optimised as a function of time. A polymerisation regime of 0 to +1000 mV, with 40 sweeps at 50 mVs^{-1} was shown to produce the most effective barrier in the shortest time (approximately 27 minutes). Polymerisation batch size was successfully increased from single screen printed carbon-ink electrodes, up to sheets of 600 sensors by means of a custom-built industrial potentiostat, possessing an appropriate user interface for commercial production. This equipment has the capability to electropolymerise up to 40 sheets of sensors simultaneously, equating to a batch size of 24,000 sensors.

CHAPTER 6

Formation of microelectrode arrays via the ultrasonic ablation of poly(*o*-phenylenediamine) modified screen printed carbon-ink electrodes

6.1 Introduction

The use of ultrasonic techniques in manufacturing processes extends through a variety of applications, including chemical synthesis, wastewater treatment (for the degradation of biomolecules and complex chemicals), textiles processing and biotechnology (primarily for biological cell disruption) (Mason & Lorimer, 2002). Ultrasonics are most widely used in the manufacturing industry for the purpose of cleaning, where the intense heat and pressures associated with cavitational bubble collapse greatly increase the efficiency of surface contamination removal (Mason *et al*, 1989). However, ultrasonics have now been utilised in a novel approach for the fabrication of microelectrodes by means of the ultrasonic ablation of thin polymer films (Higson, Filed 19th November 1996; publication date October 1996). Previous work within this research group has shown that the electropolymerisation of poly(*o*-phenylenediamine) onto gold sputter-coated ground glass slide electrodes results in a largely featureless, insulating polymer layer of less than 100 nm thickness (Myler *et al*, 1997) (Figure 6.1). This process has been extended to a less expensive, screen printable carbon-ink substrate, which offers a commercially viable route suitable for disposable sensor manufacture (Chapter 5).

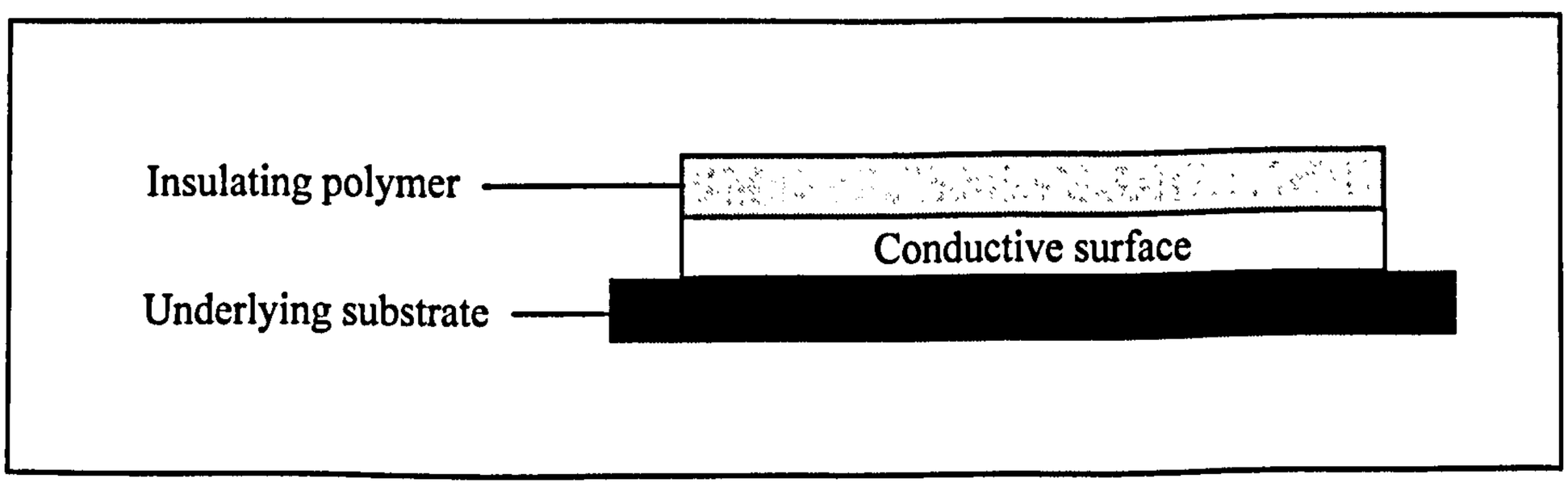

Figure 6.1: Schematic of a polymer insulated electrode

Ultrasound (in the kHz range) passing through a solvent such as water induces cavitation, whereby localised hotspots of up to several thousand degrees Kelvin are created in the form of super-heated vapour bubbles (Suslick, 1990), (Taleyarkan *et al*,

2002). The surrounding medium, which is of ambient temperature, very rapidly cools the vapour bubbles, and causes them to collapse upon themselves. When these events occur close to a solid surface, the movement of water is hindered by the presence of the object and so the majority of the liquid enters the bubble from the opposite side (Figure 2.41). This results in an asymmetric bubble collapse, which produces a high velocity jet of liquid targeted towards the solid surface. The velocity of these microjets (hundreds of metres per second) may cause the shattering of hard, brittle solids, and have been exploited for many years within medicine as a means of breaking up kidney stones (Brannen and Bush, 1984), (Suslick, 1990). Softer, more ductile materials receive surface ablation from the impact of such jets. In the case of soft, ultrathin polymer films, such as poly(*o*-phenylenediamine), the extent of this surface ablation is sufficient to cause perforation through to the harder underlying conductive surface, as depicted in Figure 6.2.

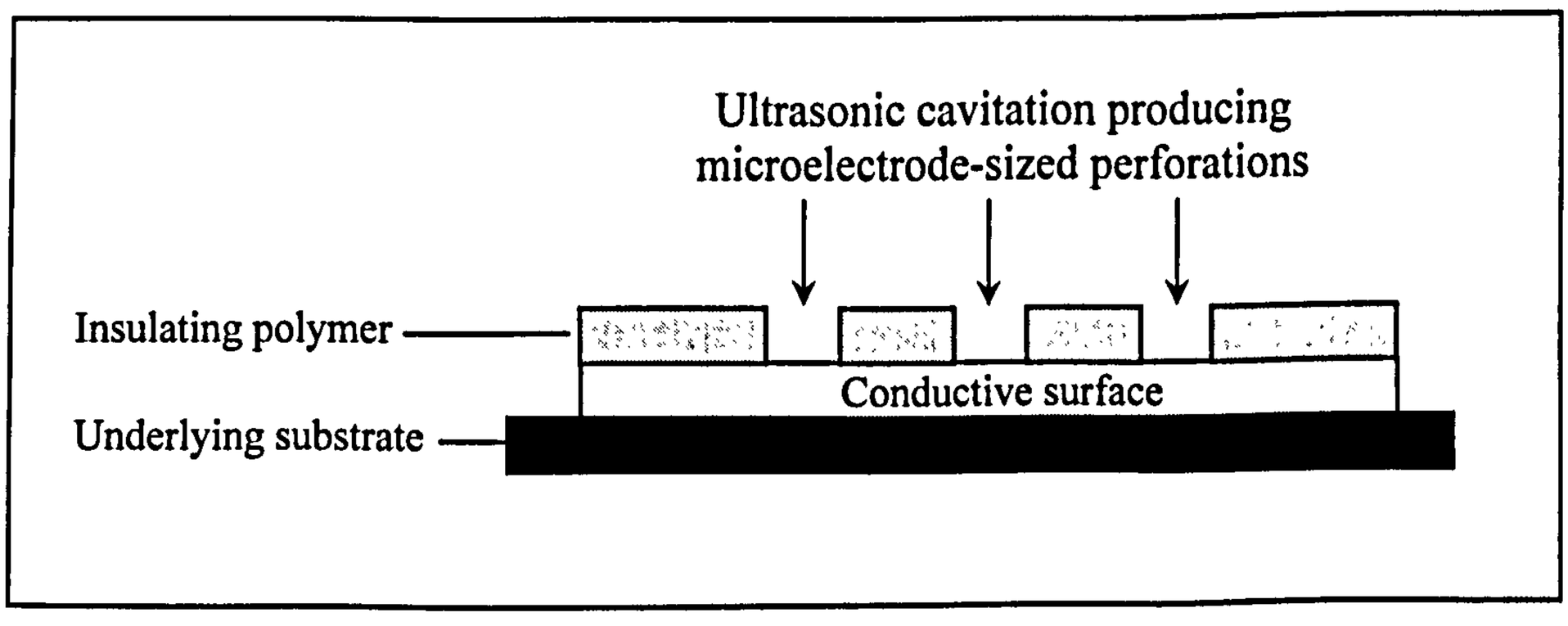

Figure 6.2: Ultrasonic ablation of a thin polymer layer revealing conductive substrate beneath

The small size of the perforations formed (<10 μm diameter) and the minute thickness of the surrounding polymer (<100 nm) permits a hemispherical diffusion profile to the conductive substrate beneath (Figure 6.3). Furthermore, since the ablation process exposes a single, continuous piece of conductive material (such as gold or carbon), each perforation forms part of a microelectrode array construction, with an inherent stir independent electrochemical response characteristic.

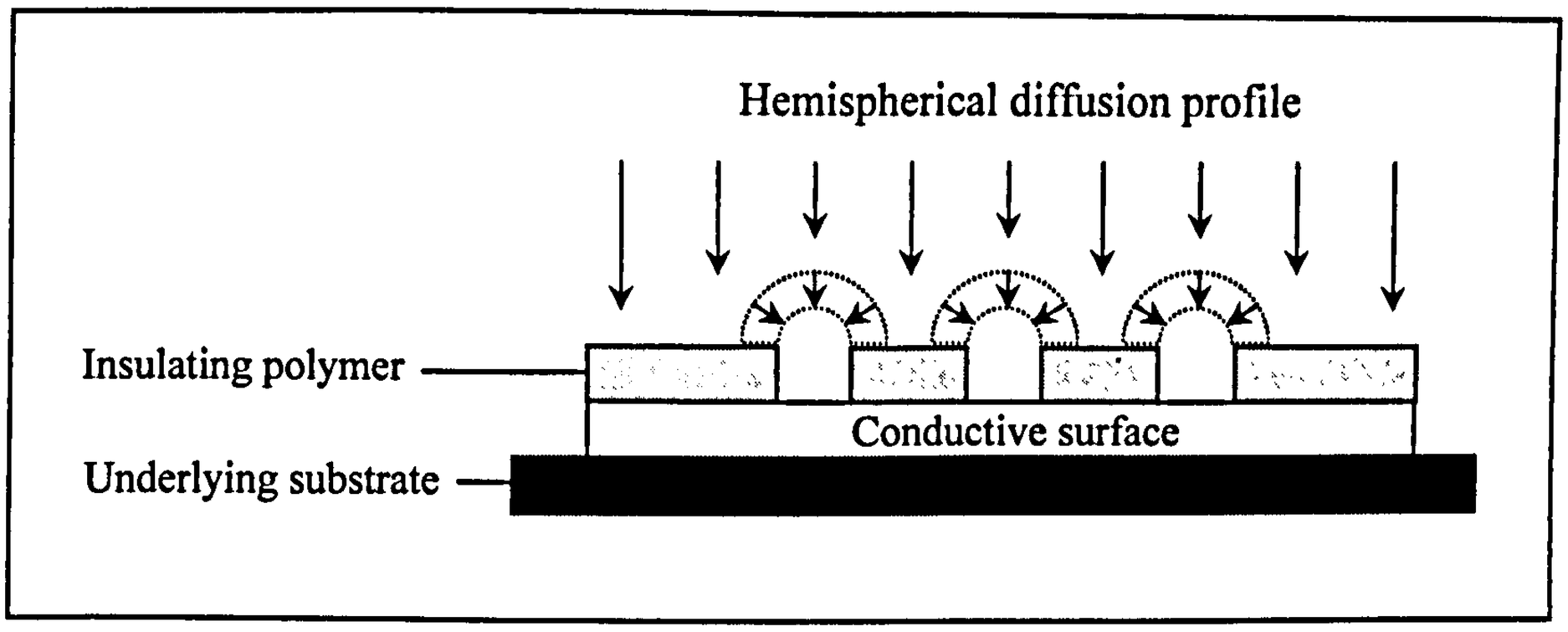

Figure 6.3: Hemispherical diffusion profile resulting from ultrasonic ablation of an ultrathin polymer film

The mass production of microelectrode array devices using existing microfabrication technologies, such as photolithography (Cunningham *et al*, 2001) or laser ablation (Fofonoff *et al*, 2004) have to date proved cost prohibitive for application to large-scale commercial manufacture of single-use sensors. However, the novel manufacturing approach described above lends itself well to rapid, large scale, and importantly low-cost fabrication of disposable microelectrode array sensors. Furthermore, the generic nature of this technology allows it to be applied to virtually any electroanalytical application. Microarray Limited, an R&D company specialising in developing and exploiting new intellectual property for sensor applications, has selected the aqueous chlorine detection market as a vehicle for demonstrating the capabilities and performance of this new manufacturing technology.

Reasons for this selection include the large size of the aqueous chlorine measurement market (over $300 million) (Hall & Hyde, 1992), which is currently dominated by wet-chemical colourimetry-based methods, first introduced in 1957 (Palin, 1957), (Wilde, 1991). There is now a growing dissatisfaction relating to the skill and time required to conduct one of these tests, the effect of common interferents present in natural waters on response validity, and also the carcinogenicity of the principle chemical involved, (N, N-diethyl-*p*-phenylenediamine), commonly known as DPD (Boswell, 2001). When compared to other potential applications, for example pesticide detection (Trojanowicz, 2002), chlorine offers a relatively simple chemistry

and does not require the use of enzymes or other such additional biological reagents for measurement. Furthermore, most people in the developed world are familiar with chlorine, since it is ubiquitous with the treatment of water. Consequently, Microarray brand value may benefit from such an association.

This chapter will detail the development and industrial upscale of microelectrode array sensors based upon this new and innovative manufacturing technology. Screen printed carbon-ink sensors developed in Chapter 4, further modified by the methods described in Chapter 5, form precursors to this ultrasound-based research designed to create working sensing devices.

6.2 Initial investigations into the ultrasonic fabrication of microelectrode arrays on gold sputter-coated ground glass slide electrodes

Previous work within this research group reported the production of microelectrode array sensors via the ultrasonic ablation of poly(*o*-phenylenediamine) passivated gold sputter-coated ground glass slide electrodes (Myler, 2000). As part of the industrial scale-up of the process, investigations were carried out into the fabrication of individual microelectrode array sensors based on this technique.

As a precursor to developing the technique on carbon-ink based substrates, gold sputter-coated ground glass slide electrodes were insulated with 20 sweeps of poly(*o*-phenylenediamine) (5 mM P*o*PD, 0 to +800 mV vs. Ag/AgCl, 50 mVs^{-1}, pH 7.4 phosphate buffer, 5.1 M NaCl) prior to ultrasonic exposure. To prevent contamination by material present in the ultrasound bath, the passivated electrodes were suspended vertically in a flat-bottomed 50 mL glass beaker, containing de-gassed, distilled, deionised water (Mason *et al*, 1989). The beaker was then positioned in the centre of a 25 kHz Transsonic T460 bench top ultrasonic bath, with the water level of the beaker matching that of the surrounding medium to facilitate transfer of acoustic energy between the two liquid bodies. P*o*PD insulated electrodes

were then exposed to ultrasonic energy emitted from a single, fixed position transducer attached to the base of the ultrasound bath (Figure 6.4).

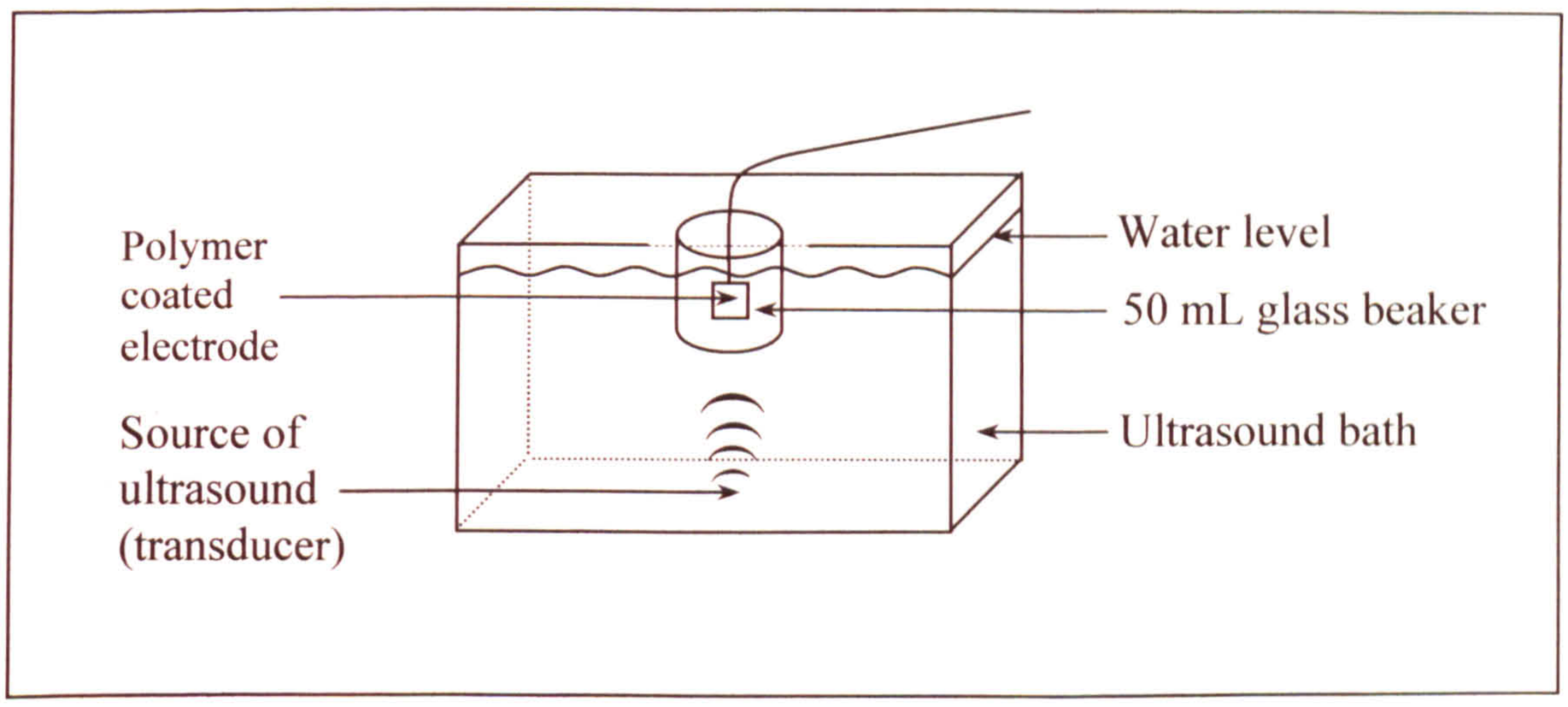

Figure 6.4: Laboratory-scale microelectrode array fabrication via ultrasonic ablation

Figures 6.5 and 6.6 exhibit scanning electron micrographs obtained for a *Po*PD insulated gold sputter coated glass slide electrode exposed to 20 seconds sonication.

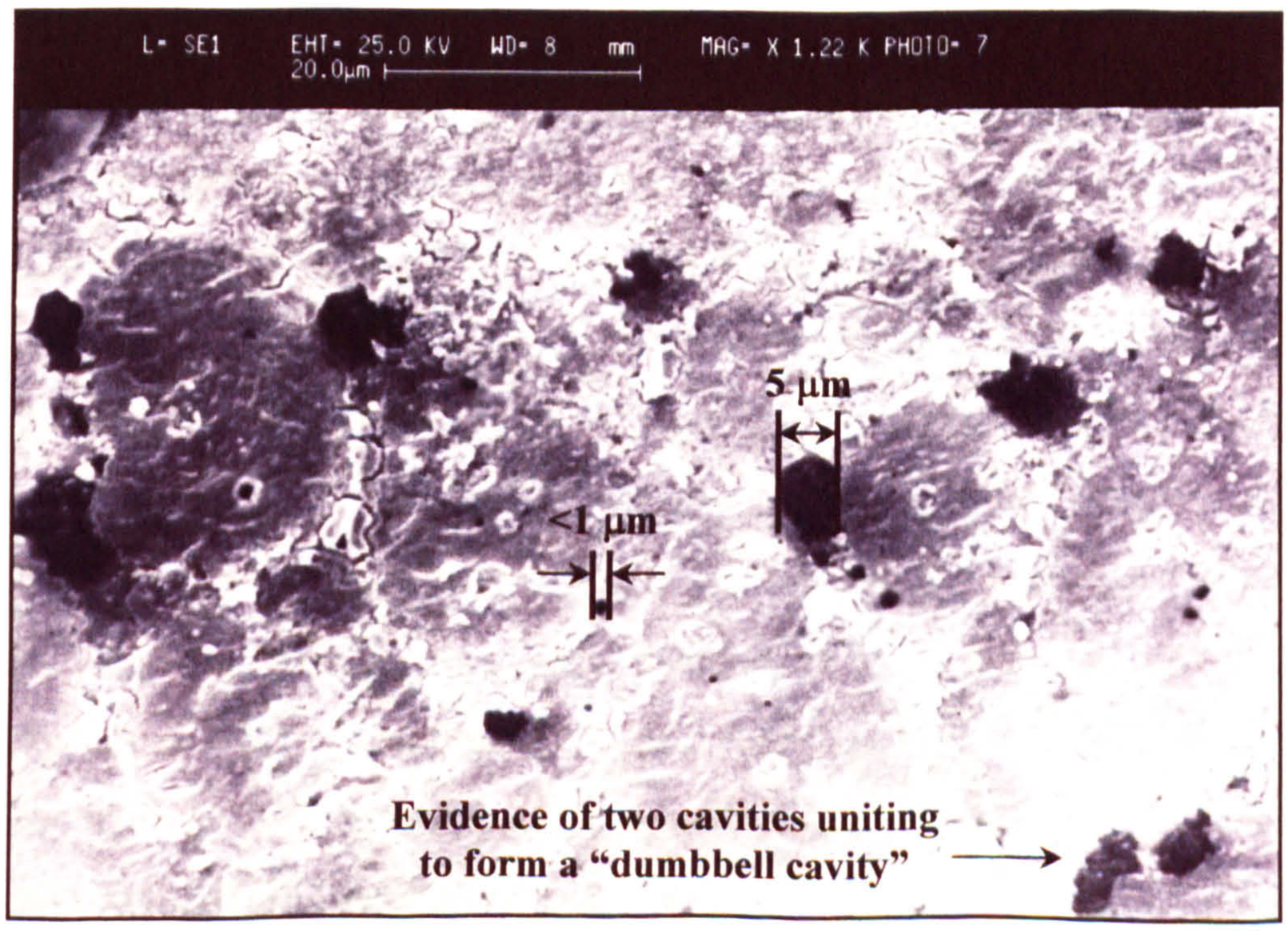

Figure 6.5: Electron micrograph of sonochemically fabricated microelectrode array

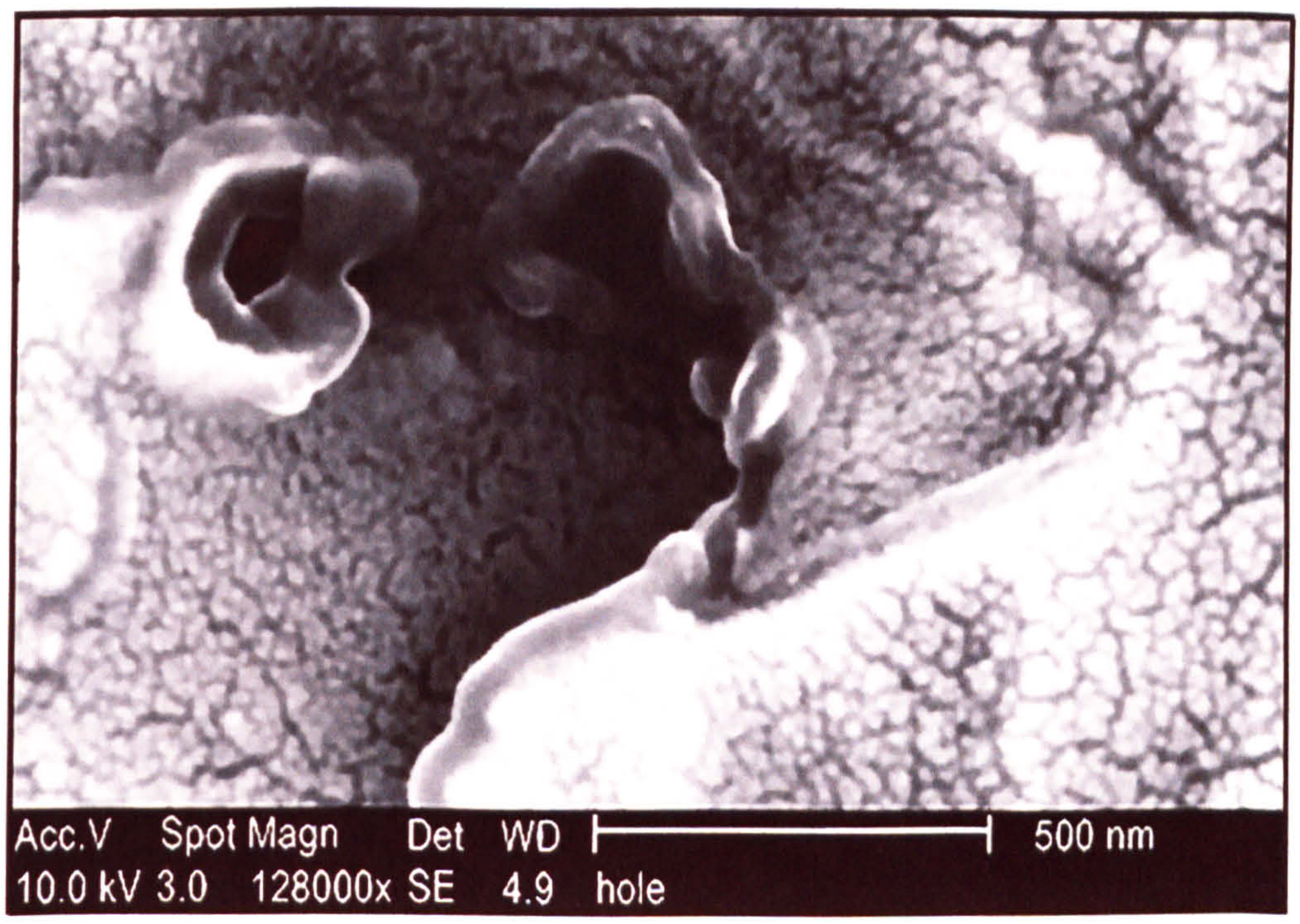

Figure 6.6: Close up of a sub-micron microelectrode showing pore structure

There are a number of features of interest displayed within the micrographs. It can be seen that as a result of the chaotic nature of the cavitation process, the spatial distribution of pores over the polymer surface is random. In some instances this results in two pores forming in close proximity, eventually uniting to form a 'dumbbell' shaped cavity (Barton *et al*, 2004). It is also evident that almost all of the pores are bimodal in size, possessing either 4 μm (± 1 μm) or sub-micron diameters. The smaller cavities may result from the initial impact of the micro-jets of fluid, and it is thought that these pores may then act as nucleation sites for further bubble formation (Suslick, 1990), giving rise to a quantum enlargement in the diameter of the cavity. Since there is no evidence of pores with diameters above 5 μm, it is believed that this is the threshold size beyond which a pore ceases to function as a nucleation site. A higher magnification micrograph of an ultrasonically fabricated microelectrode is exhibited in Figure 6.6, and indicates that the initial impact of the cavitation micro-jet has caused the polymer to become thermoplastically distorted around the perimeter of the pore.

Electrochemical characterisation of electrode assemblies was carried out via cyclic voltammetric interrogation of a 1 mM potassium ferricyanide(III) solution. Voltammograms of unmodified (planar) electrodes were compared to both *Po*PD insulated, and microelectrode array sensors produced on polymerised and sonicated gold sputter coated glass slide electrodes (Figures 6.7 and 6.8 respectively). Microelectrode arrays were produced individually using a sonication period of 20 seconds, consistent with previous methodologies which determined the optimum conditions for obtaining stir independent response characteristics (Myler, 2000).

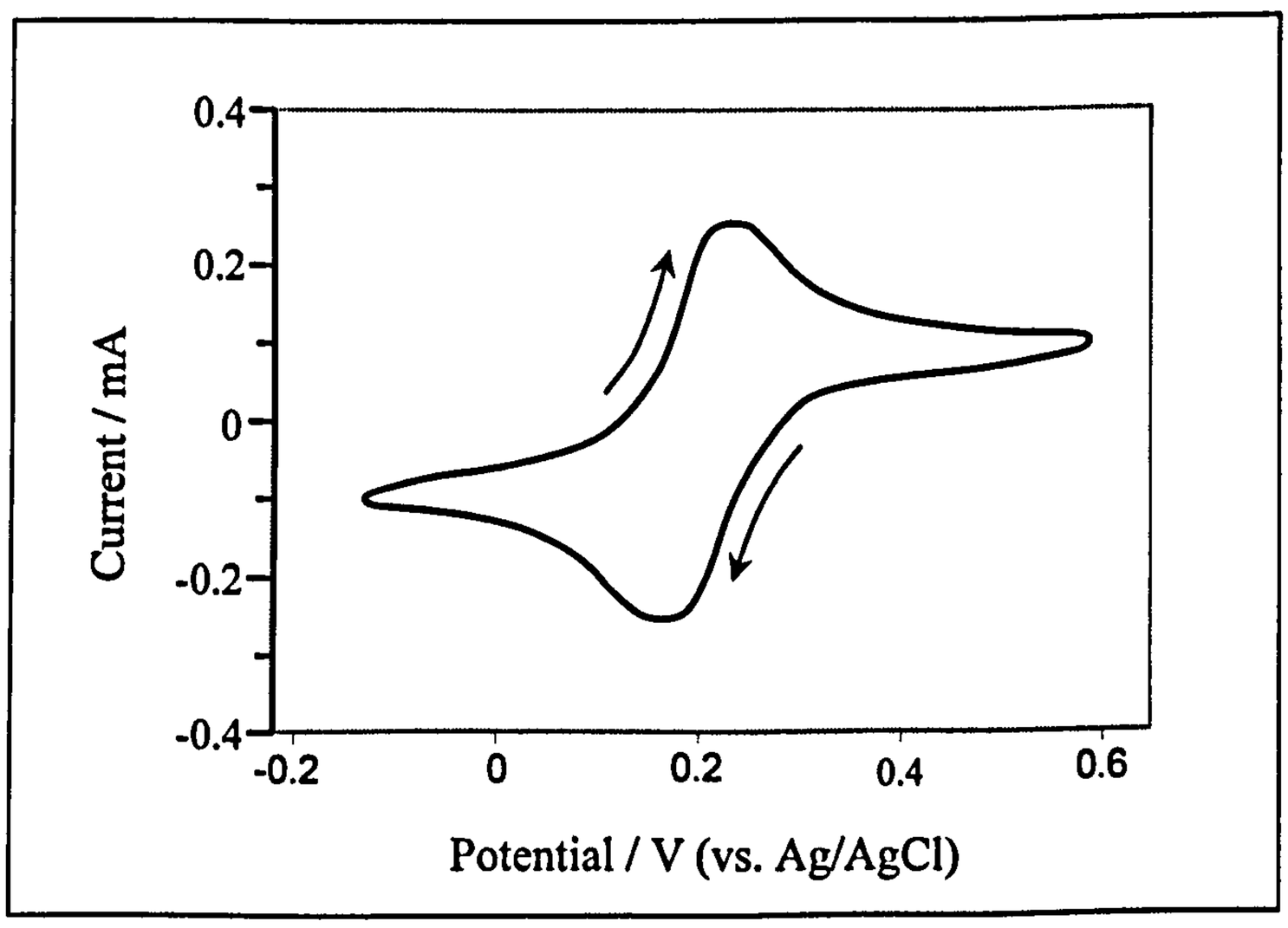

Figure 6.7: Cyclic voltammogram of ferri/ferrocyanide couple at a planar gold sputter-coated glass slide electrode (scan rate 50 mVs^{-1}, 1 mM $Fe(CN)_6^{3-}$, pH 7.8, 0.1 M KCl)

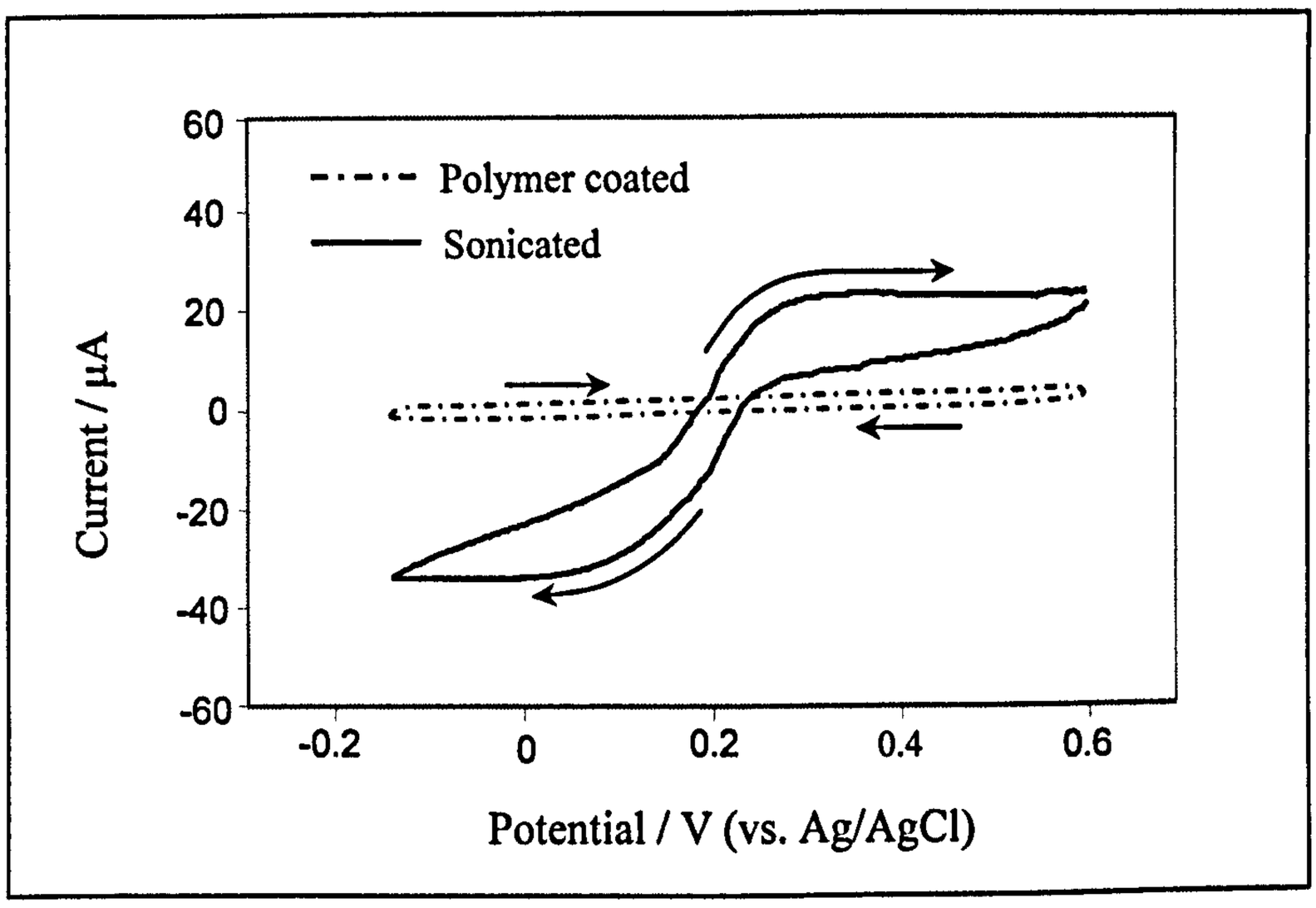

Figure 6.8: Cyclic voltammetry of ferri/ferrocyanide couple at an unsonicated P*o*PD coated gold slide electrode compared to that exposed to 20 s ultrasonic ablation (scan rate 50 mVs^{-1}, 1 mM $Fe(CN)_6^{3-}$, 0.1 M KCl)

The voltammograms corresponding to the planar (uncoated) electrodes (Figure 6.7) indicate a Nernstian peak separation of approximately 59 mV, as would be expected for a reversible, diffusion controlled single electron transfer process. In contrast, very little faradaic response is observed for the unsonicated, P*o*PD coated electrode, confirming the presence of a pristine, insulating polymeric layer (Figure 6.8). Interrogation of the ultrasonically ablated microelectrode array sensors revealed a sigmoidal response, suggesting a non-linear (hemispherical) diffusion profile typically associated with microelectrode constructions (Southampton Electrochemistry Group, 1985). Theory predicts that for an ideal microelectrode, the oxidative and reductive sweeps will overlay perfectly, however it can be seen that in Figure 6.8 there is some separation of the forward and reverse sweeps. This is a consequence of the chaotic nature of the cavitation process, whereby microelectrode pores are positioned randomly across a sensor surface. Inevitably, some of the microelectrodes formed will be in such close proximity (for example, the dumbbell cavity displayed in Figure 6.5) that there is an overlap of the diffuse parts of their

double layers resulting in a charging capacitance. The overall stir dependence of the sensors was examined by means of chronoamperometric interrogation in unstirred (quiescent) and artificially convected solutions. Electrodes were polarised at -300 mV vs. Ag/AgCl using a 1 mM potassium ferricyanide solution and their responses recorded for 90 seconds in quiescent solution before stirring was applied (Jenway 1100 magnetic stirrer, 300 rpm, 6 mm flea). Typical current-time transients obtained for the convectional dependency of unmodified (planar) gold sputter-coated glass slide electrodes and those modified to form microelectrode array constructions are illustrated in Figures 6.9 and 6.10 respectively.

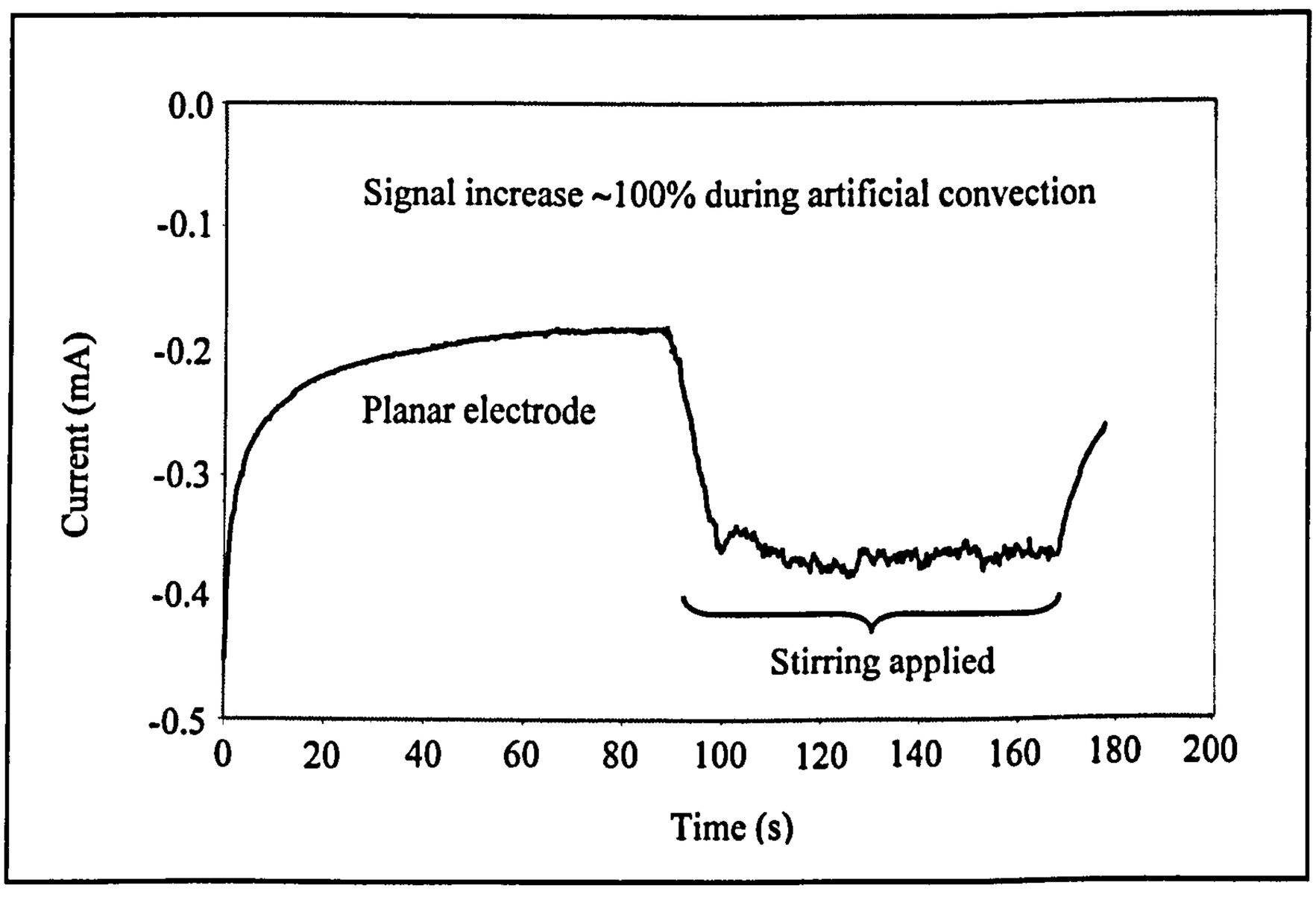

Figure 6.9: Current-time transient of a planar gold sputter-coated ground glass slide electrode polarised at -300 mV in quiescent and stirred 1 mM $Fe(CN)_6^{3-}$ solution (pH 7.8 phosphate buffer, 0.1 M KCl)

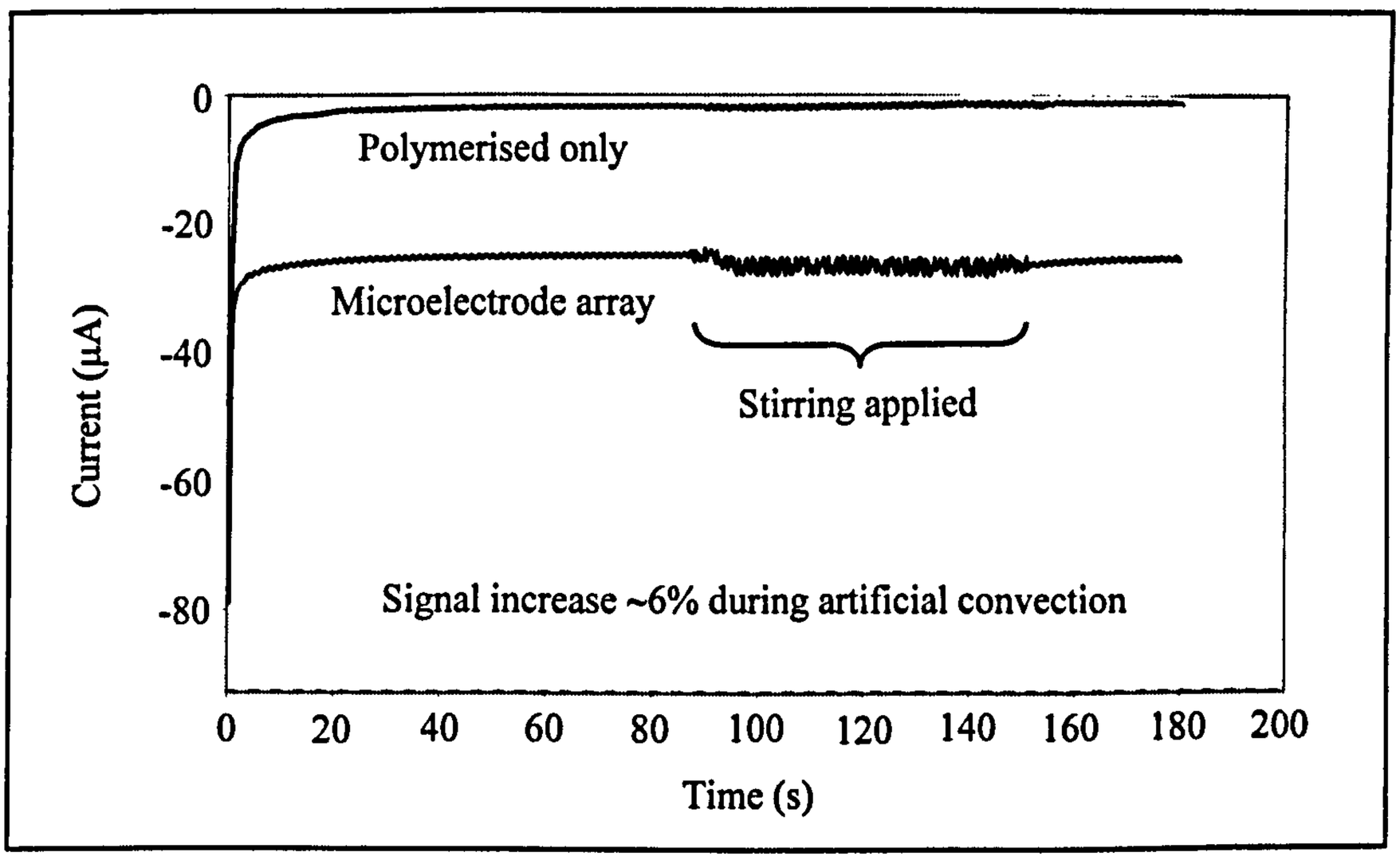

Figure 6.10: Current-time transient of gold sputter-coated ground glass slide microelectrode array fabricated via 20 seconds ultrasonic ablation polarised at -300 mV in quiescent and stirred 1 mM $Fe(CN)_6^{3-}$ solution (pH 7.8 phosphate buffer, 0.1 M KCl)

It can be seen in Figure 6.9 that for a planar gold sputter-coated glass slide electrode, the amperometric sensor response in artificially convected solution increases by approximately 100 % when compared to the response obtained in quiescent solution. This can be expected for macroscopic electrode surfaces which experience linear diffusion profiles. In contrast, the current responses for gold sputter-coated glass slide microelectrode array assemblies exhibited very little change in amperometric response when convection was introduced (<6%) (Figure 6.10). This is a consequence of the hemispherical diffusion profiles associated with microelectrodes, whose characteristic dimension is smaller than the diffusion layer thickness under the conditions applied (Štulík *et al*, 2000). The eight-fold decrease in the magnitude of the current response in quiescent solution (when compared to unmodified planar sputter-coated gold glass slide electrodes) is a reflection of the decreased active area of the electrode surface following passivation with P*o*PD and subsequent ultrasonic ablation (Fletcher & Horne, 1999).

Unsonicated P*o*PD polymerised gold sputter-coated glass slide electrodes were also interrogated amperometrically as a control to determine the function of the insulating polymeric film (Figure 6.10). Very little response could be seen for unsonicated electrodes, once again indicating the presence of an essentially defect free layer of insulating poly(*o*-phenylenediamine). It is noted that for both the insulated and the ultrasonically ablated microelectrodes, increased noise is observed for the period in which stirring was applied. The most likely source of this interference can be attributed to inductance caused by the action of the electro-magnetic stirrer.

6.3 Commercial upscale and enhancement of ultrasonic microelectrode fabrication equipment

As a means of achieving economically viable manufacture of microelectrode array-based disposable aqueous chlorine sensors, the scale of production must be increased from single gold sputter-coated glass slide electrodes to multiple screen printed carbon-ink electrodes. To achive this, the ultrasonic ablation equipment was subject to further development, as outlined below.

Bench top ultrasound baths such as the Camlab Transsonic T460 possess a single ultrasonic transducer attached to the base resulting in a focus of acoustic energy through the centre of the sonication vessel (depicted in Figure 6.4). Consequently, the degree of acoustic cavitation experienced when multiple sensors are sonicated simultaneously varies considerably at differing positions within the tank. For this reason it was necessary to design an industrial sized ultrasound tank suitable for the ultrasonic ablation of large numbers of sensors. Working in conjunction with Ultrawave Limited (Cardiff, Wales), a customised ultrasonic tank with internal dimensions 750 x 750 x 600 mm (working volume 750 x 750 x 550 mm) was fabricated (Figure 6.11). In this design, 10 transducers are attached to the base of the tank to permit the even spread of acoustic energy throughout the volume of water contained (Figure 6.12). The transducers are powered by an external amplifier, generating a 2 kW, 25.1 kHz frequency signal, and can provide similar power/volume

ratios to the Transsonic T460 used for laboratory-scale microelectrode array fabrication. Since temperature can affect the energy associated with cavitational activity, the ultrasound bath includes a heating system to maintain the temperature of the water at 25°C ±1°C. As a liquid approaches its boiling point, vapour pressure increases and bubble formation occurs more readily. However, the energy associated with bubble collapse decreases since more rapid movement of vapour into the bubbles cushions their collapse (Mason *et al*, 1989). For simplicity, the temperature control system employed here served to raise the temperature of the water to 25°C by means of integrated electrical heating elements; cooling of the water is attained by dissipation of heat into the surroundings, which themselves must not exceed 25°C.

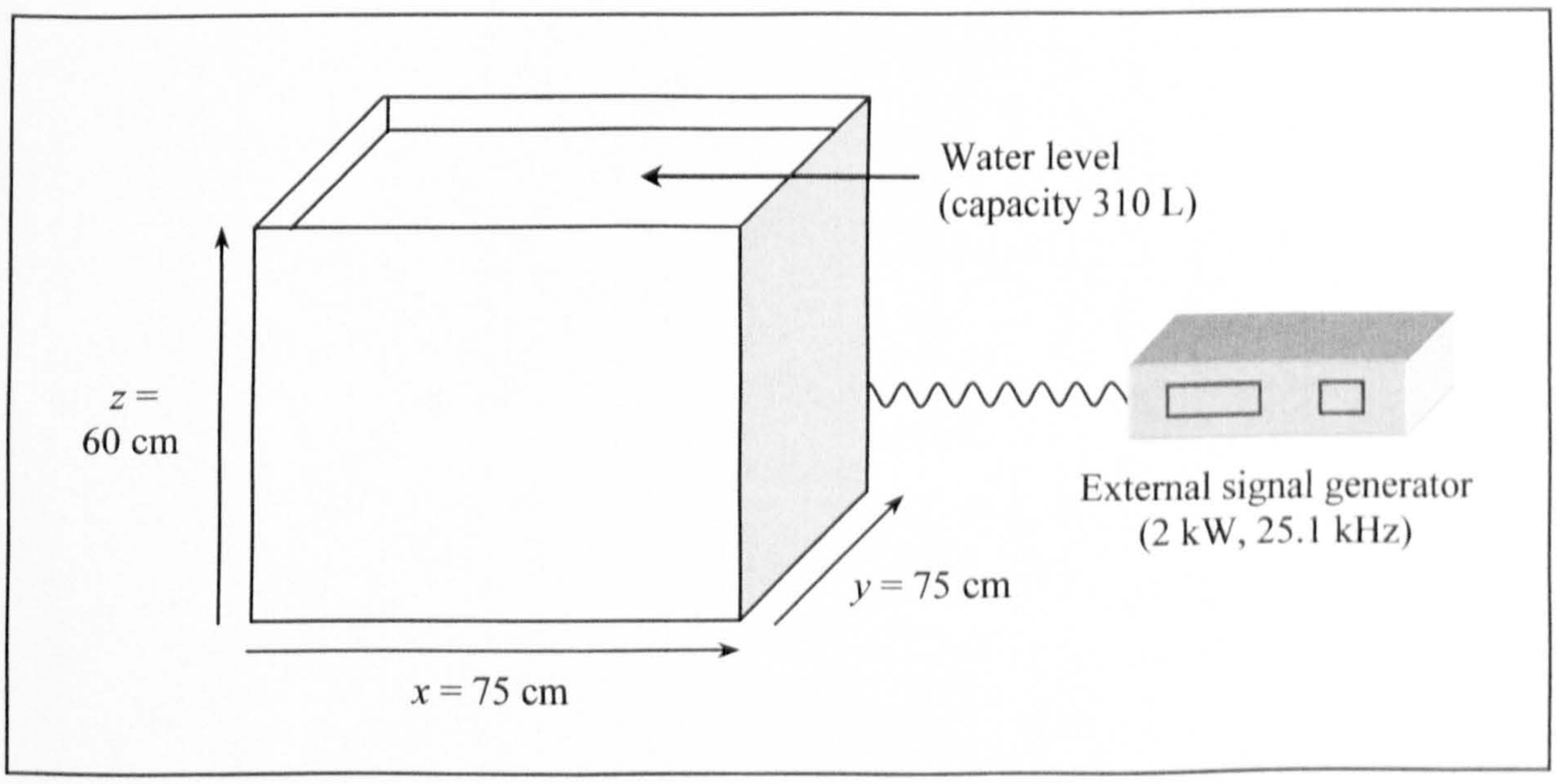

Figure 6.11: Schematic of industrial scale ultrasonic tank

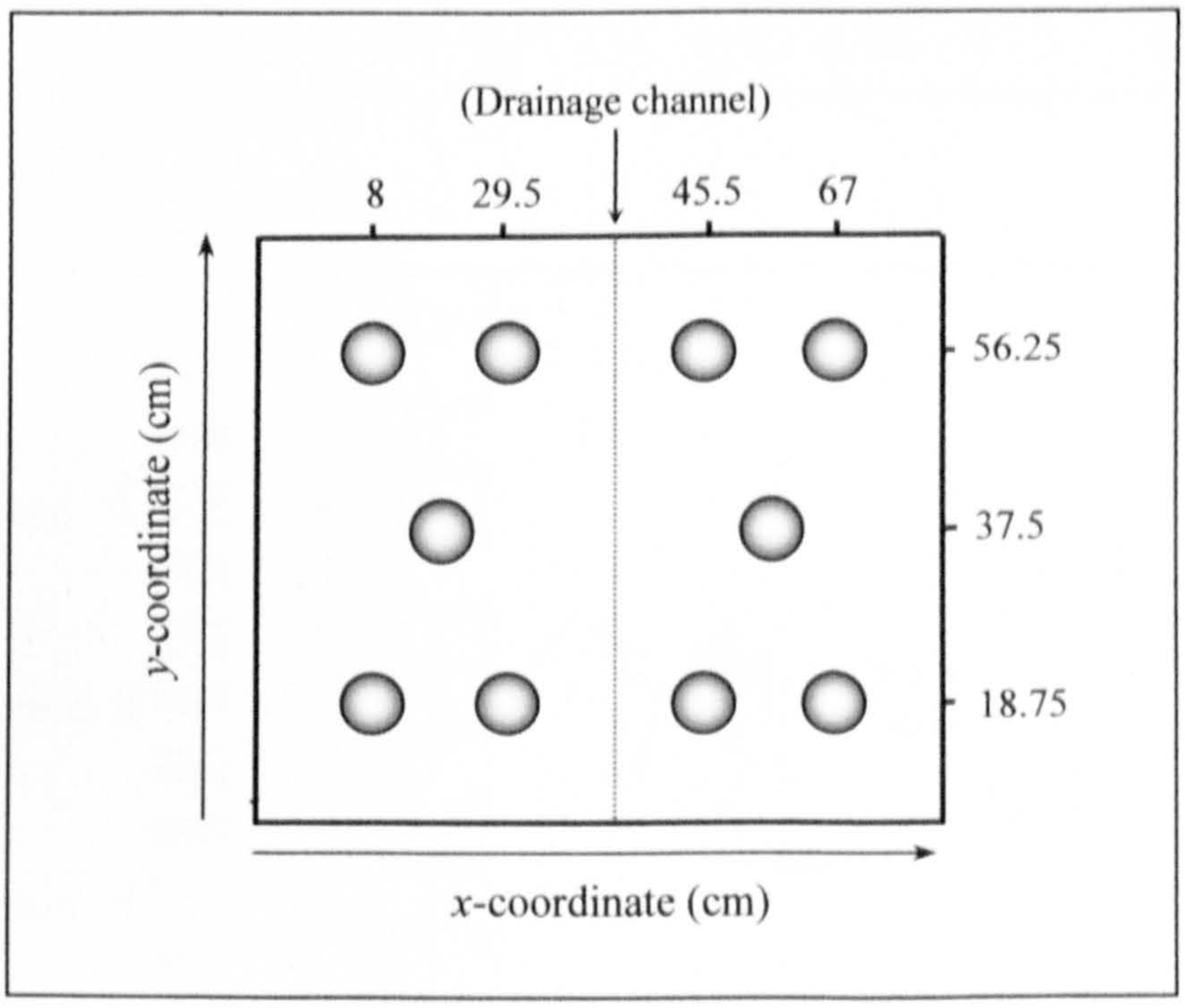

Figure 6.12: Positioning of ultrasonic transducers (◯) at base of ultrasound tank

An important aspect of mass production of microelectrode array sensors via ultrasonic ablation is the spatial homogeneity of the cavitation experienced by each sensor during production. In order to provide a uniform exposure of sensors to ultrasonic cavitation, it is necessary to understand the factors controlling its distribution. In a fixed transducer ultrasonic tank (such as the prototype above) an ultrasonic standing wave field is generated inside the liquid (Hepher *et al*, 2000), (Yasui *et al*, 2005). As the wave propagates through the medium, some regions experience high amplitude pressure variation (termed *antinodes*) and others experience very little pressure change (termed *nodes*). Nodal positions correlate to multiples of the wavelength (λ) of the ultrasonic wave, while antinodal positions relate to multiples of half wavelength ($\lambda/2$), illustrated in Figure 6.13.

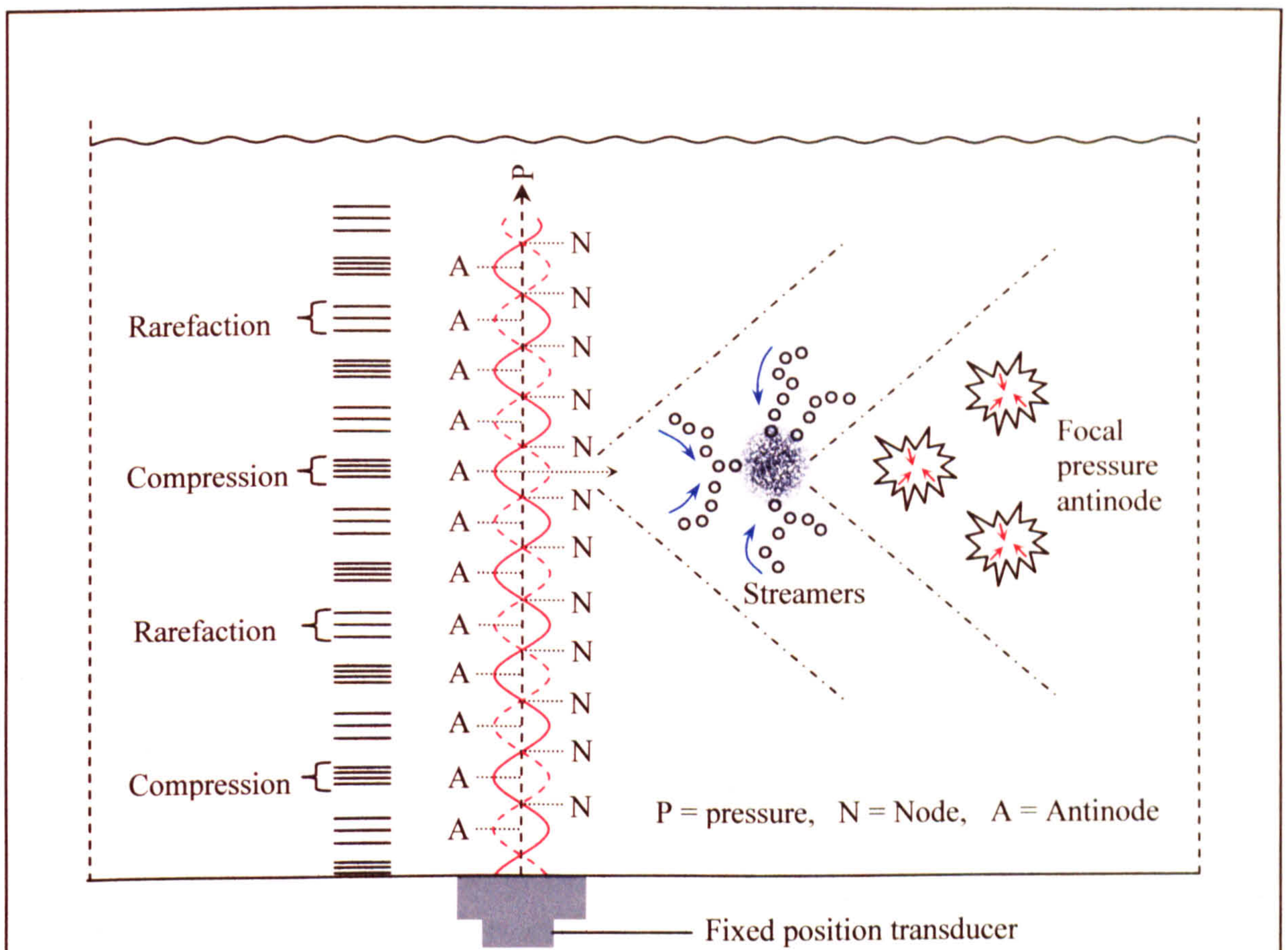

Figure 6.13: Schematic representation of ultrasonic wave propagation and acoustic cavitation

Assuming sufficient acoustic amplitude during the rarefaction stage, a liquid medium will tear apart in the region around the *antinode*, producing cavitation bubbles. Two classes of cavitation exist, known as *stable* and *transient* cavitation (Leighton, 1994), (Mason & Lorimer, 2002). Stable cavitation, or *noninertial cavitation*, refers to bubbles generated at lower acoustic pressures (or higher frequencies) and which exist over many acoustic cycles (Church & Cartensen, 2001). During this period, the stable cavitation bubble oscillates with (although slightly behind) the surrounding pressure field. Throughout the rarefaction phase, the radius of the bubble increases in size, and as a result of a lower internal vapour pressure when compared to that of the surrounding medium, dissolved gases diffuse across the interface into the bubble cavity. Over the lifetime of the oscillating stable cavitation bubble, surface area is

greater during the tension phase than during the compression period, and so dissolved gas tends to diffuse into the bubble at a faster rate than it can diffuse out during compression (termed *rectified diffusion*) (Dendy, 1988). At some point, non-linear conditions created by, for example, the super-imposition of compression maxima, or the interaction with a neighbouring bubble, results in the collapse of the bubble. The presence of non-condensable gas which has diffused across the interface from the surrounding medium cushions the collapse. Consequently, the energy released is greatly reduced, preventing a significant contribution to the process of ultrasonic ablation caused by the microjets of water (Leighton, 1994).

Transient cavitation, or *inertial cavitation*, refers to those cavities which exist over a much shorter time scale (1-3 cycles). If the acoustic pressure is great enough during the rarefaction stage, the cavity will expand to many times its equilibrium size (Leighton, 1995). Flynn determined that if the ratio of the expanded bubble size (R_{max}) to the equilibrium bubble size (R_0) is sufficiently large ($R_{max}/R_0 \geq 2$), then the compressive phase will cause an instantaneous adiabatic collapse of the cavity (Flynn, 1964), (Apfel, 1981). Since the bubble has only existed for an extremely short time (typically only one cycle), there is no time for heat exchange or the diffusion of dissolved gases into the cavity. The cavity will contain some vapour from the surrounding medium, but the vapour remains at or near its equilibrium pressure and can evaporate or condense freely at the cavity wall (Neppiras, 1984). The result is that in the absence of cushioning residual permanent gas, the collapse of transient cavities is extremely energetic, generating temperatures of several thousand degrees Kelvin, pressures of around 1000 atm, cooling rates of over 10^{10} Ks^{-1} and generating the powerful microjets of fluid associated with asymmetrical bubble collapse near a solid surface (Tuziuti *et al*, 2005). It is these microjets of fluid which are responsible for the mechanical effects of ultrasonic cavitation and are required for the perforation poly(*o*-phenylenediamine) films in the fabrication of microelectrode array constructions.

Of further consideration towards achieving uniform exposure of P*o*PD insulated sensors to transient cavitation is the localised spatial distribution of cavitation bubble

clouds. The formation of cavitation bubble structures is a common feature in fixed position transducer ultrasound tanks, where standing waves create the localised pressure fields termed *nodes* and *antinodes* (Figure 6.13) (Mettin *et al*, 1999), (Yanagida *et al*, 2000). Instead of being homogeneous, cavitation bubbles form clusters (described by Lauterborn *et al* as 'acoustic Lichtenberg figures) consisting of streams of bubbles moving towards a common centre (at the focal pressure antinode) to form a dense cloud containing cavitating bubbles (Figure 6.13) (Lauterborn & Ohl, 1997), (Lauterborn *et al*, 1999). The streams of small bubbles, termed 'streamers', appear to follow specific paths from their nucleation sources, known as 'motes', driven towards the pressure antinode at speeds of up to 1 ms^{-1} (Leighton, 1994), (Mettin *et al*, 1999). The bubbles are moved by primary Bjerknes forces, whereby acoustic pressure gradients couple with bubble oscillations to produce a translational force (Bjerknes, 1906), (Leighton *et al*, 1990), (Mettin *et al*, 1999). Conversely, larger bubbles formed through stable cavitation or bubble coalescence experience a repulsive force and are driven towards the pressure nodes (regions of low acoustic amplitude). The distinction between large and small bubbles is defined by Equation 6.1, a transposition of the Minnaert resonant frequency equation (Minnaert, 1933), (Irvine, 1979), (Ghiotto &Penrose, 2000).

$$R_0 = \frac{1}{\omega}.\sqrt{\frac{3kp_0}{\rho}} \qquad 6.1$$

Where $\boldsymbol{R_0}$ is the equilibrium bubble radius (cm), $\boldsymbol{k}$ is a constant (the *polytropic index*), $\boldsymbol{P_0}$ is the hydrostatic liquid pressure outside the bubble (dynes.cm^{-2}), $\boldsymbol{\rho}$ is the medium density (g.cm^{-3}) and $\boldsymbol{\omega = 2\pi f}$.

Typical values for aqueous solutions at 25°C are $\boldsymbol{k}$ = 1.3, $\boldsymbol{P_0}$ = $1x10^6$ dynes.cm^{-2}, $\boldsymbol{\rho}$ = 1 g.cm^{-3} and equate to a resonant equilibrium bubble radius ($\boldsymbol{R_0}$) of approximately 0.0125 cm for an input frequency of 25.1 kHz (Pierce, 1989), (Dunn, 2001). It follows that bubbles with equilibrium radii ($\boldsymbol{R_0}$) which exceed this value migrate to

the pressure nodes, while smaller bubbles migrate to the pressure antinodes through the action of primary Bjerknes force.

From the preceding discussion it is clear that an inherent spatial inhomogeneity of cavitational intensity exists due to a presence of standing waves with their associated pressure gradients. In other words, focal antinodes (regions of consistently high acoustic amplitude) host more pronounced cavitational activity than pressure nodes. As a means of further enhancing the uniform distribution of acoustic energy, a modulated frequency sweep was incorporated into the output of the signal generator. This technique is often employed in the role of cleaning delicate semiconductor or other microelectronic devices. In these circumstances, uneven rates of surface ablation may cause permanent damage to the component, and a varying frequency of ultrasound can enhance the spatio-temporal homogenisation of the node and antinode positions.

Ideally, the frequency modulation would be used to regulate the wavelength sufficiently to cause the complete overlap of node and antinodal foci. However, this is impractical since the transducers used to generate the ultrasonic field only operate efficiently at their resonant frequency. For example, in a 25.1 kHz ultrasound tank, the amplitude of the acoustic wave emitted decreases rapidly as the applied frequency deviates from this value. Consequently, a maximum frequency variation of around ±5% of the resonant transducer frequency can be employed to vary the wavelength and the antinodal foci as much as possible without greatly compromising power output (Frederick, 1965).

The incorporation of a ±1 kHz frequency sweep (~5% of 25.1 kHz) into the signal generator output for the industrial scale tank provided a total frequency range of 24.1 to 26.1 kHz. In a simple standing wave model, this causes the spread of the antinodal energy peaks, demonstrated graphically in Figure 6.14.

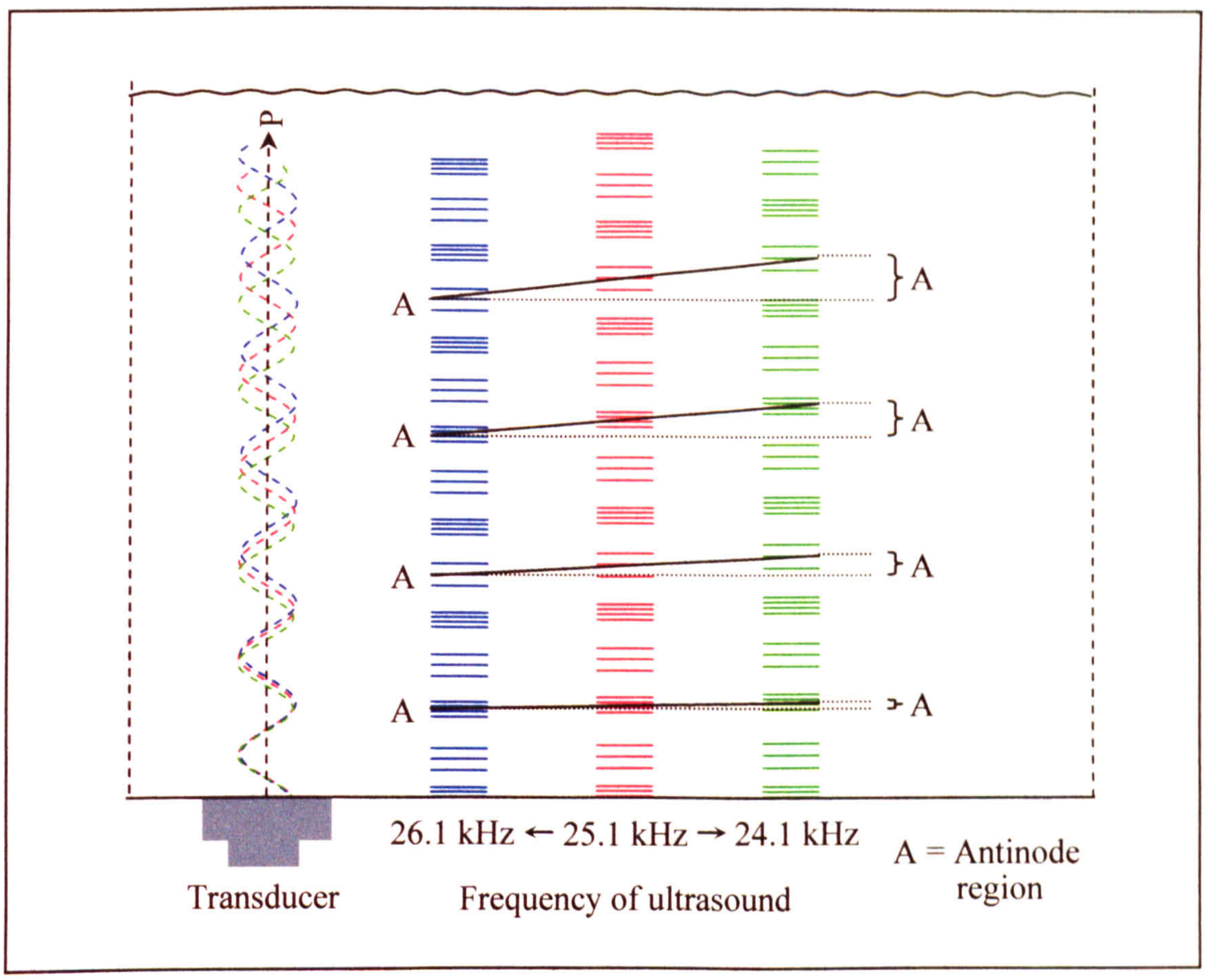

Figure 6.14: Spread of antinodal foci with distance, *z*, resulting from frequency modulation (not to scale)

It can be seen that as the wavefront advances through the liquid, the spread of antinodal foci increases with distance from the source, yet is insufficient to cause the complete overlap of the nodes and antinodes, particularly towards the base of the tank. When an acoustic wave reaches a boundary with a medium possessing significantly different acoustic impedance, for example a liquid / air interface, a proportion of energy becomes reflected according to the amplitude reflection coefficient, ***R*** (Equation 6.2).

$$R = \frac{\left(z_2 / z_1\right) - \sqrt{1 - [n-1]\tan^2 \alpha_i}}{\left(z_2 / z_1\right) + \sqrt{1 - [n-1]\tan^2 \alpha_i}} \qquad 6.2$$

where z, the acoustic impedance of a material, is the product of material density (ρ) and speed of sound (c) in the medium (kg/m^2/s), $n = (c_2/c_1)^2$, and α_i is the angle of incidence of the wave.

For the case of waves normally incident to a boundary, the reflection coefficient equation may be simplified to the following, Equation 6.3 (Pope & Winter, 1985).

$$R = \frac{(z_2 - z_1)}{(z_2 + z_1)} \qquad 6.3$$

The acoustic impedance values for fresh water, air, aluminium and steel are indicated below in Table 6.1.

Material	Impedance, z (Rayles)
Air	415
Fresh water	1,480,000
Aluminium	17,000,000
Steel	47,000,000

Table 6.1: Acoustic impedance values for air, fresh water and metals (Pierce, 1989)

Acoustic reflection coefficients have values ranging between -1 and +1, with the median (0) indicating no reflection of the incident energy wave. For the case of the liquid / air interface encountered by the ultrasonic wave at the tank surface, an acoustic amplitude reflection coefficient (R) of approximately -1 is obtained, indicating that virtually all incident acoustic energy is reflected back into the volume of the tank. Furthermore, since the acoustic impedance of air is many orders of magnitude less than water (denoted by the negative value), the interface is considered

a *soft* or *pressure release* boundary (Etter, 2003). Consequently, as the waveform is reflected from the surface it undergoes a 180° phase change, limiting any destructive interference at the liquid / air boundary and continuing the homogenisation of node and antinodal pressure regions (exhibited to scale in Figure 6.15).

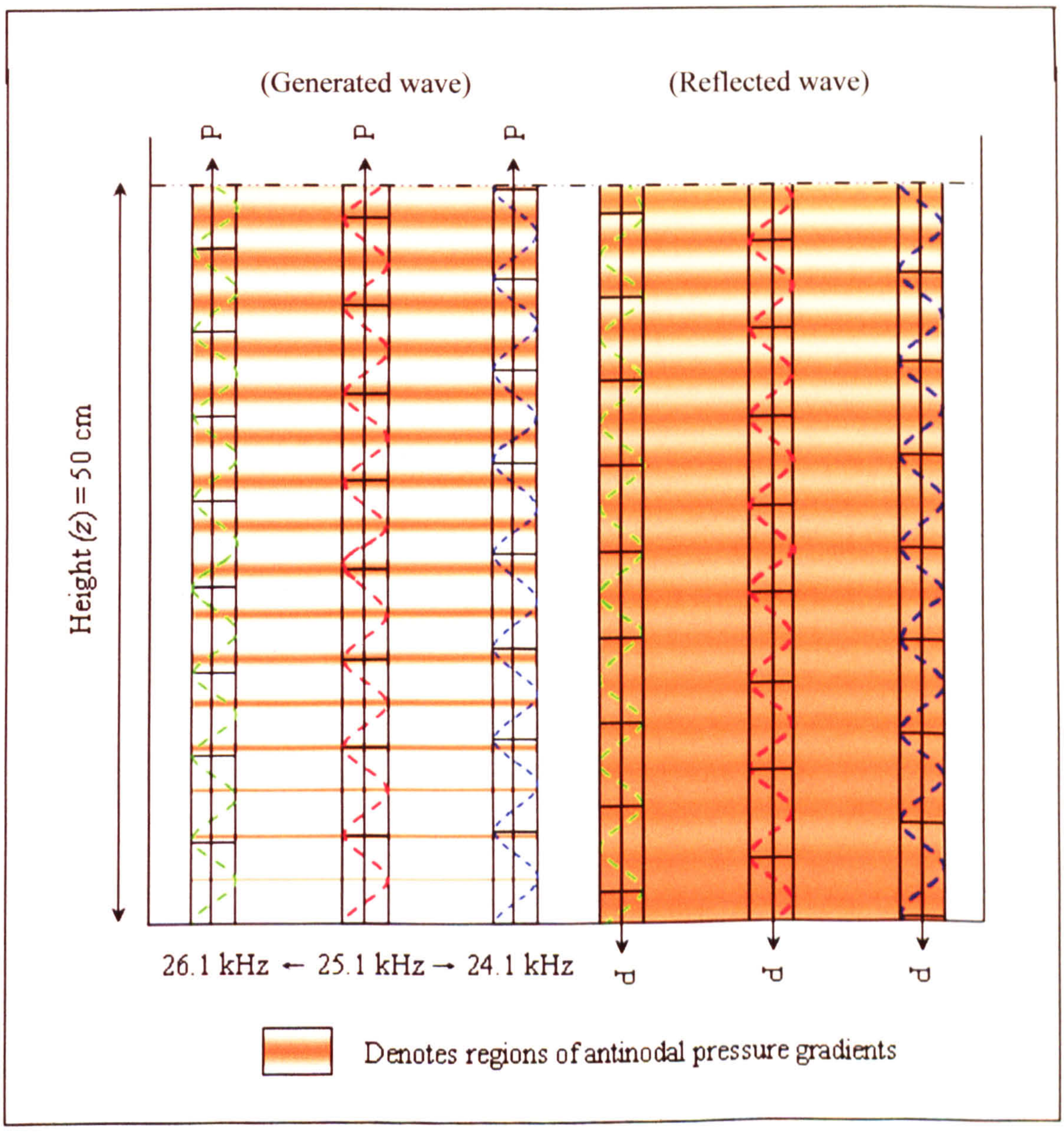

Figure 6.15: Reflection of an ultrasonic wavefront at liquid / air interface permitting the spread of antinode pressure regions (Scale 1:5)

From the diagram it can be seen that the distance between the base of the tank and the surface is critical to the positioning of the reflected wave, for which a depth of 50 cm

permits maximum overlap of the antinodal foci. The reflected wave can be seen to travel back down through the medium towards the tank floor, where the high acoustic impedance of the steel surface compared to water permits approximately 96% of incident acoustic energy to be reflected back into the medium (Equation 6.3). Increased homogenisation of the node and antinodal foci is then achieved, as the range of wavelengths produced by the frequency sweep (25.1 ±1 kHz) is further enlarged by interaction with the oscillating tank floor. Acoustic energy incident upon a moving surface becomes subject to Doppler shift, according to Equation 6.4 (Doppler, 1843).

$$F_L = F_s \frac{(v + v_l)}{(v - v_s)} \qquad 6.4$$

where F_L is the frequency of the reflected waveform, F_s is the frequency of incident sound, v is the speed of sound (in water), v_l is the relative speed of the observer (zero in this case), and v_s is speed of movement of the reflecting surface. Assuming a peak deflection of ±0.5 mm, the frequency modulation of the reflected sound wave is extended to 25.1 kHz ± 1.8 kHz, corresponding to maximum and minimum wavelengths of approximately 6.44 cm and 5.58 cm respectively.

Further benefit of having a range of ultrasonic frequencies is derived from the interaction of bubbles with the radiating sound field. Cavitation bubbles with equilibrium radii close to that defined in Equation 6.1 for a particular frequency absorb energy from the incident sound field more effectively than others; by sweeping the frequency, a range of cavitation bubble sizes become resonant. For example, for a frequency sweep of 24.1 to 26.1 kHz, bubbles with radii ranging between 0.012 and 0.013 cm are maximally excited, compared to only those which are close to an equilibrium radius 0.0125 cm for a fixed frequency of 25.1 kHz.

6.4 Assessment and optimisation of ultrasonic field

As a means of assessing the homogeneity of the acoustic field produced, a hydrophone analysis system was designed for measuring acoustic amplitude profiles throughout the tank. A probe housing was constructed from a 25 mm diameter polypropylene tube which offered a minimal perturbation of the ultrasound field when compared to harder materials, such as steel, often employed for hydrophone construction (Devaraju *et al*, 2002). A piezoelectric crystal microphone (frequency response range 0 – 50 kHz) was positioned within the tubing and connected by screened coaxial cable to an oscilloscope (Hodnett & Zeqiri, 1997). Initial experiments showed very poor response to the ultrasonic energy field resulting from the presence of an air gap between the receptive surface of the microphone and the ultrasonically irradiated water. Consequently, a custom designed liquid/liquid hydrophone interface was constructed to permit efficient propagation of the acoustic waveform to the microphone (Figure 6.16).

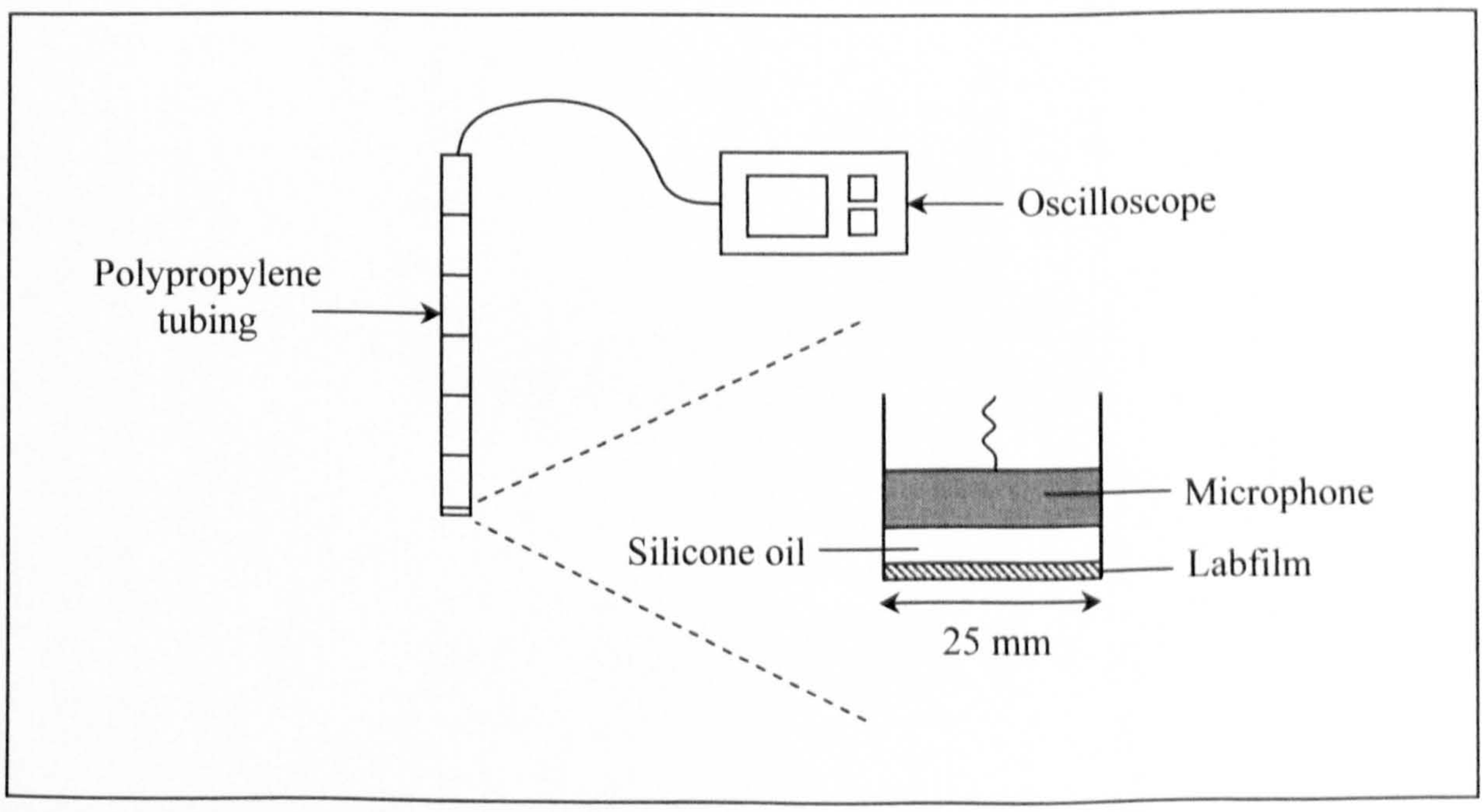

Figure 6.16: Schematic showing construction of custom-made hydrophone

Silicone oil was selected as the intermediary material for its electrical insulating properties and also for its high cavitation threshold which prevents transient bubble formation and collapse from occurring and causing damage to the delicate microphone surface (Moholkar *et al*, 2000). A thin layer of lab-film was used to contain the silicone oil within the microphone construction.

To limit any interference caused by the transfer of ultrasonic vibrations in the form of surface acoustic waves ('Rayleigh waves'), direct contact between the oscilloscope jig and the ultrasound tank was minimised and all interconnecting surfaces were separated by dampening materials (Lord Rayleigh, 1885), (Frass *et al*, 2001). Utilising the settings described in Section 3.5.3, an oscilloscope was used to record the sinusoidal acoustic waveform at 5 cm intervals within the tank in three Cartesian directions (x, y, z). Figure 6.17 depicts a typical response obtained.

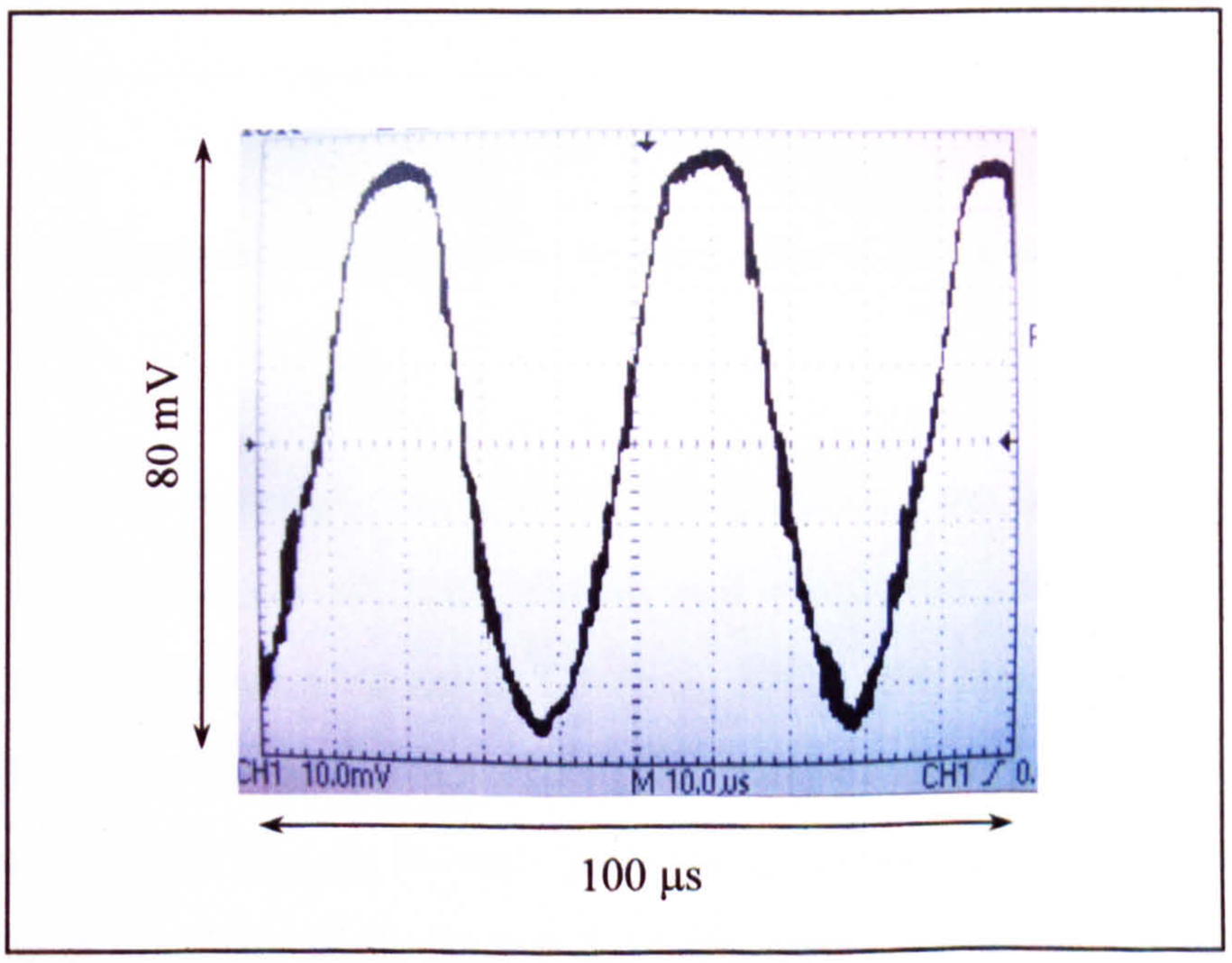

Figure 6.17: Screen shot of acoustic waveform

The recorded waveform confirms the output frequency of transducers to be 25.1 kHz and was found to be consistent throughout the tank except for a peripheral zone within approximately 5 cm of any wall or the water/air interface wherein acoustic

reflections and harmonics caused significant interference, disrupting the oscilloscope's trigger function and preventing clear signal characterisation, as depicted in Figure 6.18.

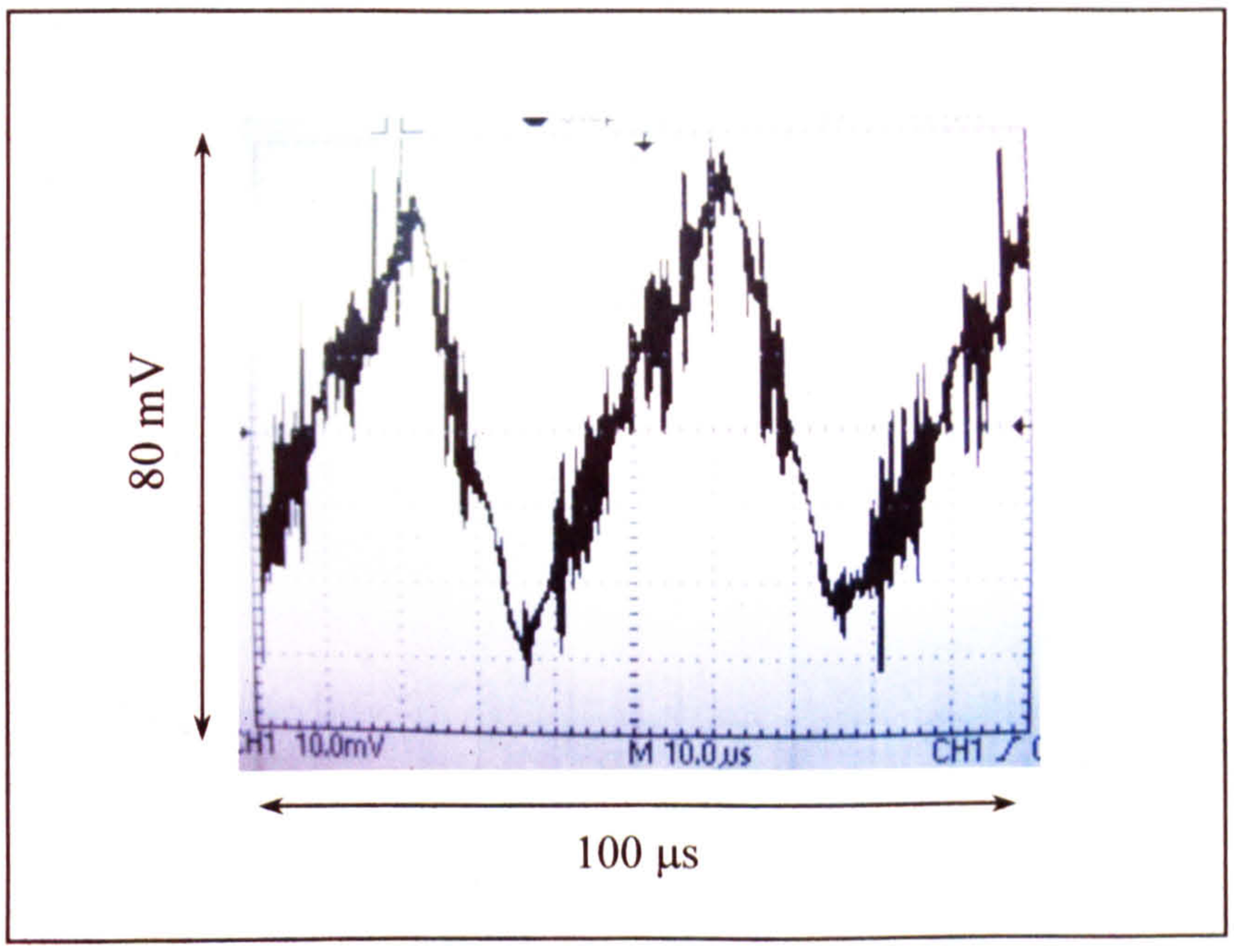

Figure 6.18: Screen shot of acoustic waveform close to tank walls or water surface

The intensity of the ultrasonic wave propagating through the tank is of interest since the greater the magnitude of compression and rarefaction, the greater the energy associated with cavitation (Mason & Lorimer, 2002). By measuring the AC current induced in the piezoelectric microphone by the acoustic energy field (recorded as root mean square voltage, V_{RMS}), it was possible to assess the variation in acoustic amplitude throughout the tank. Figure 6.19 illustrates the variation of the acoustic amplitude measured at three depths (z = 15, 30 and 45 cm) at intervals of 5 cm across the horizontal plane (x, y). This spacing can be considered to provide a reasonably accurate spatial resolution since it is twice the width of the receiving device.

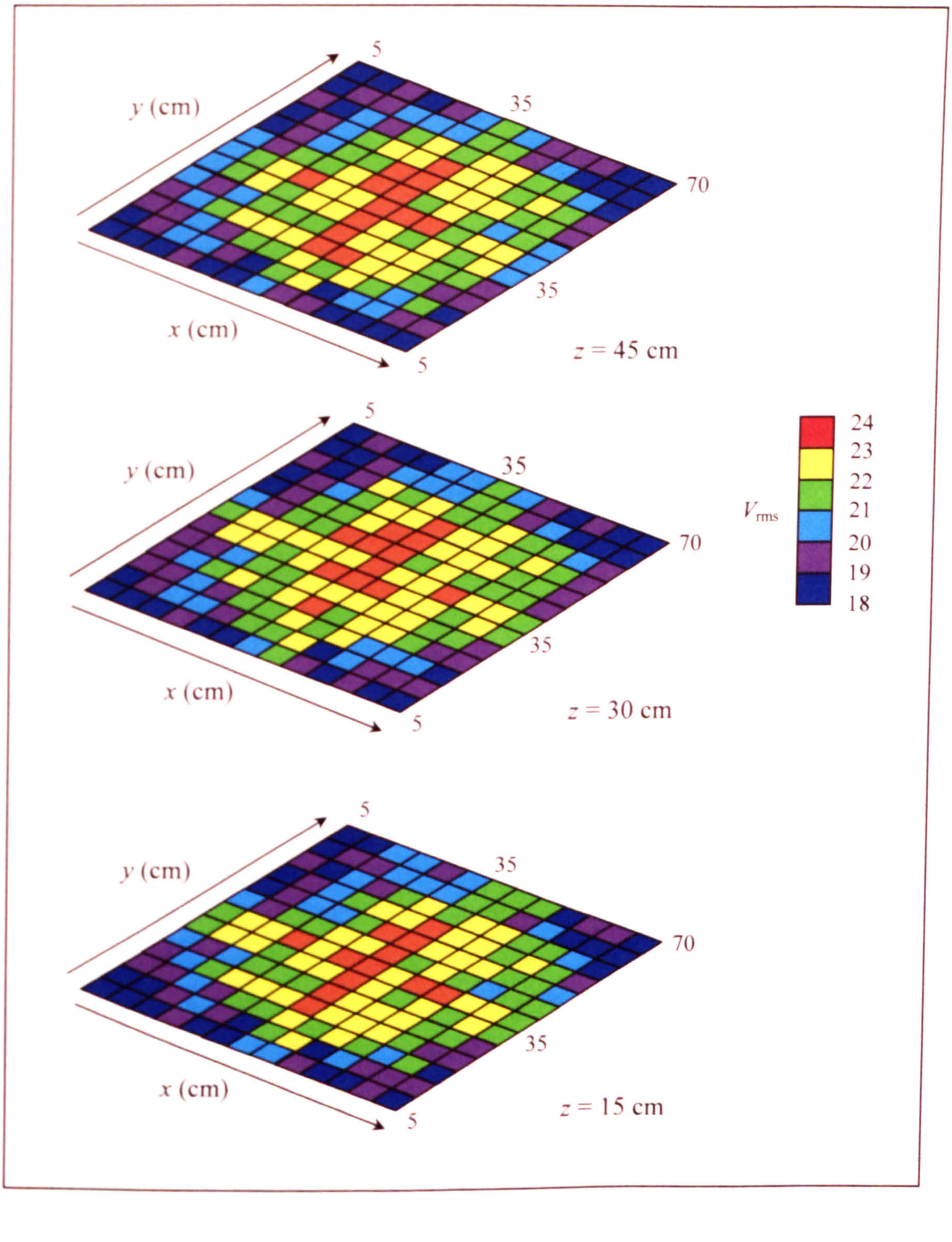

Figure 6.19: Variation of acoustic wave amplitude through the industrial-sized ultrasonic tank

The results indicated a concentration of the acoustic energy towards the centre of the ultrasonic tank, and did not indicate the positions of the ultrasonic horns as shown in

Figure 6.12. One possible explanation for this is that in a multiple transducer construction as described in this case, each horn vibrates in-phase and causes the entire surface to act as a single source of emission. Since the steel base to which they are attached is connected at the edges to the tank body, movement in that region is inhibited, contributing towards the reduced acoustic intensity indicated towards the tank edges in figure 6.19. Very little attenuation of the acoustic energy field is observed with increasing distance from the transducers, *z*, as expected for a low viscosity liquid medium such as water (Moholkar *et al*, 2000). Moreover, the large number of transducers reduces the effect of geometric energy dispersion with increasing distance, *z*, when compared to single transducer constructions (Horst *et al*, 1996). It was not possible to observe regions of high and low acoustic amplitude with variation of height (distance, *z*). This suggested a disruption of node and antinodal pressure foci by the modulated frequency sweep, although it is likely that perturbation of the ultrasonic wavefront through the vertical plane by the probe itself, as well as resolution limitations, prevents the disclosure of acoustic 'hot-spots'.

6.4.1 Mapping of cavitational activity via erosion of aluminium foil

Since the formation of microelectrode arrays occurs via the ultrasonic ablation of thin poly(*o*-phenylenediamine) films, it was necessary to assess the mechanical effects of cavitation induced by the radiating acoustic field. Aluminium foil is quickly eroded by transient bubble collapse and can be used to indicate regions of high and low activity within low frequency ultrasound tanks (Crawford, 1964), (Krefting *et al*, 2004). For this reason, clean pieces of aluminium foil (40 x 53 cm) were suspended at various coordinates within the tank and subjected to 10 minutes sonocation time at 100 % power (described in Section 3.5.7).

The submerged aluminium sheets degraded rapidly upon exposure to ultrasound. Within around 30 seconds, most of the surface experienced a shallow dimpling, followed by pinhole formation in localised regions. Once formed, the high surface energy of the exposed edges became preferential sites for cavitation bubble

nucleation, and caused an enlargement of the pinholes to form clear voids in the material (Figure 6.20).

Figure 6.20: Coalescence of pin holes to form large voids in the foil sheet

Following sonocation, the aluminium sheets were placed on a matt black coordinate board for assessment. Examples of the sheets obtained are displayed in Figure 6.20.

x = 18.75 cm

y = 18.75 cm

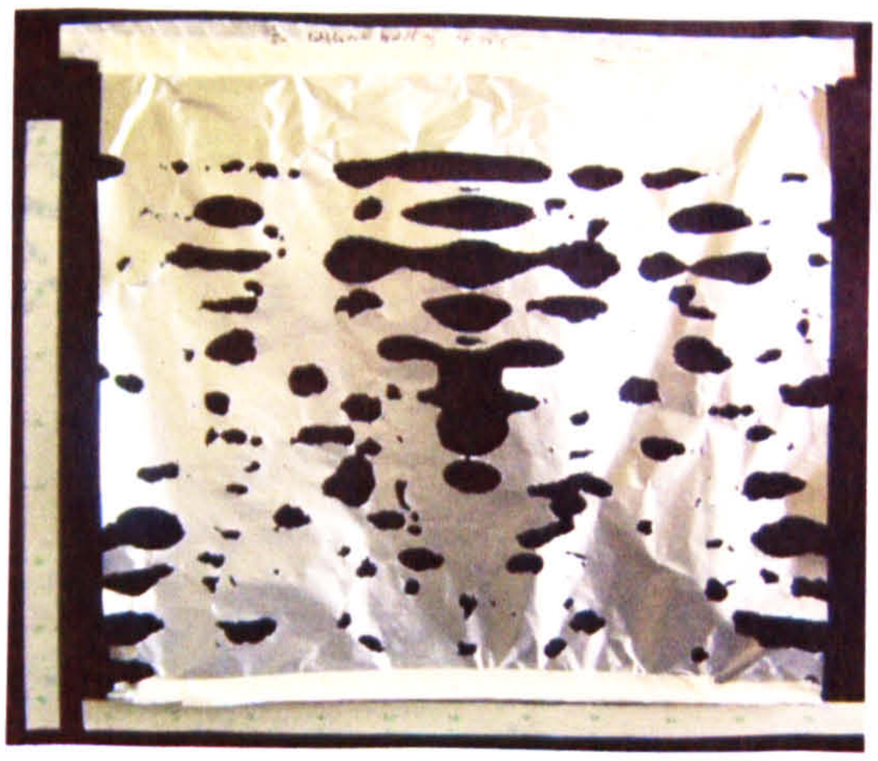

x = 37.5 cm

y = 37.5 cm

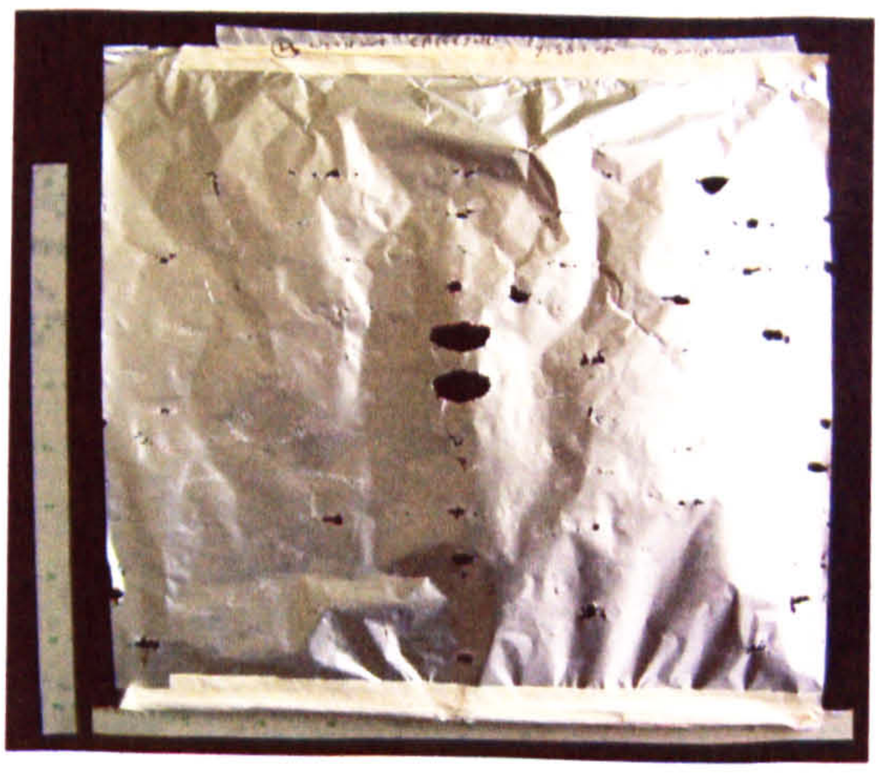

x = 56.25 cm

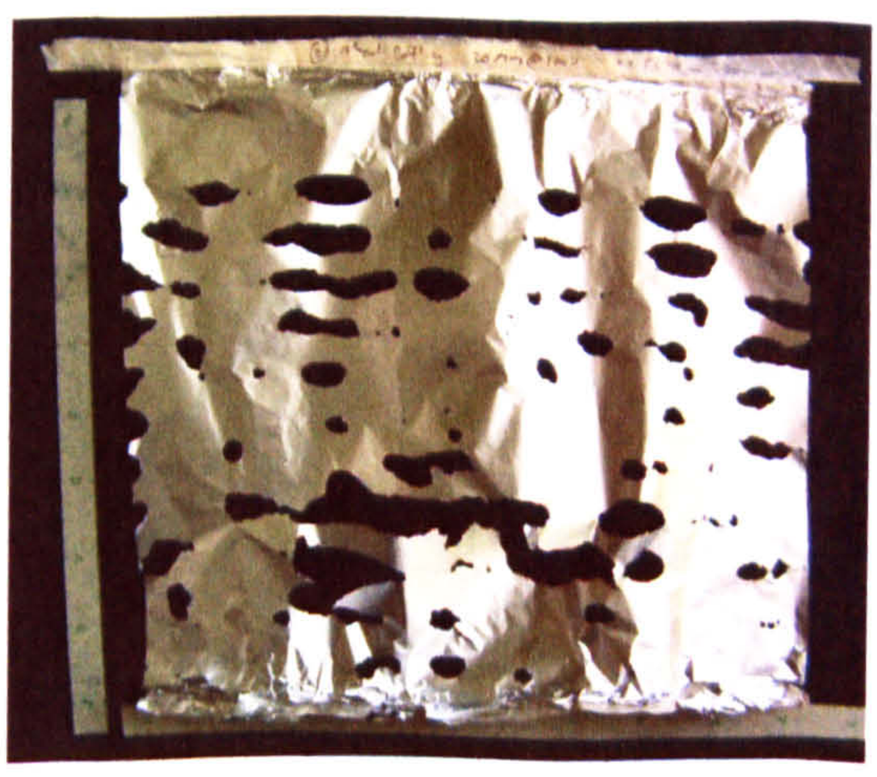

y = 56.25 cm

Figure 6.20: Aluminium foil tests illustrating variation in cavitational intensity

It can be seen that a greater cavitational intensity is indicated for the centre of the ultrasound tank (x = 37.5 cm, y = 37.5 cm), correlating the acoustic intensity data indicated in Figure 6.19. The greater degree of ultrasonic ablation experienced for sheets at positions y = 18.75 cm and y = 56.25 cm when compared to the equivalent positions in the x-coordinate is most likely to result from the positioning of two sets of transducers which lie along the y = 18.75 cm and y = 56.25 cm (Figure 6.12). A semi-ordered distribution of heavily eroded regions can be observed, suggesting a relatively poor uniformity of cavitation processes. Although the fresh edges exposed from initial pin-hole formation then become preferential nucleation sites which cause an acceleration of destruction in that region, closer inspection of the foil sheets reveal some order to their distribution. Figure 6.21 displays a close-up of the aluminium foil sheet sonicated at position y = 37.5 cm.

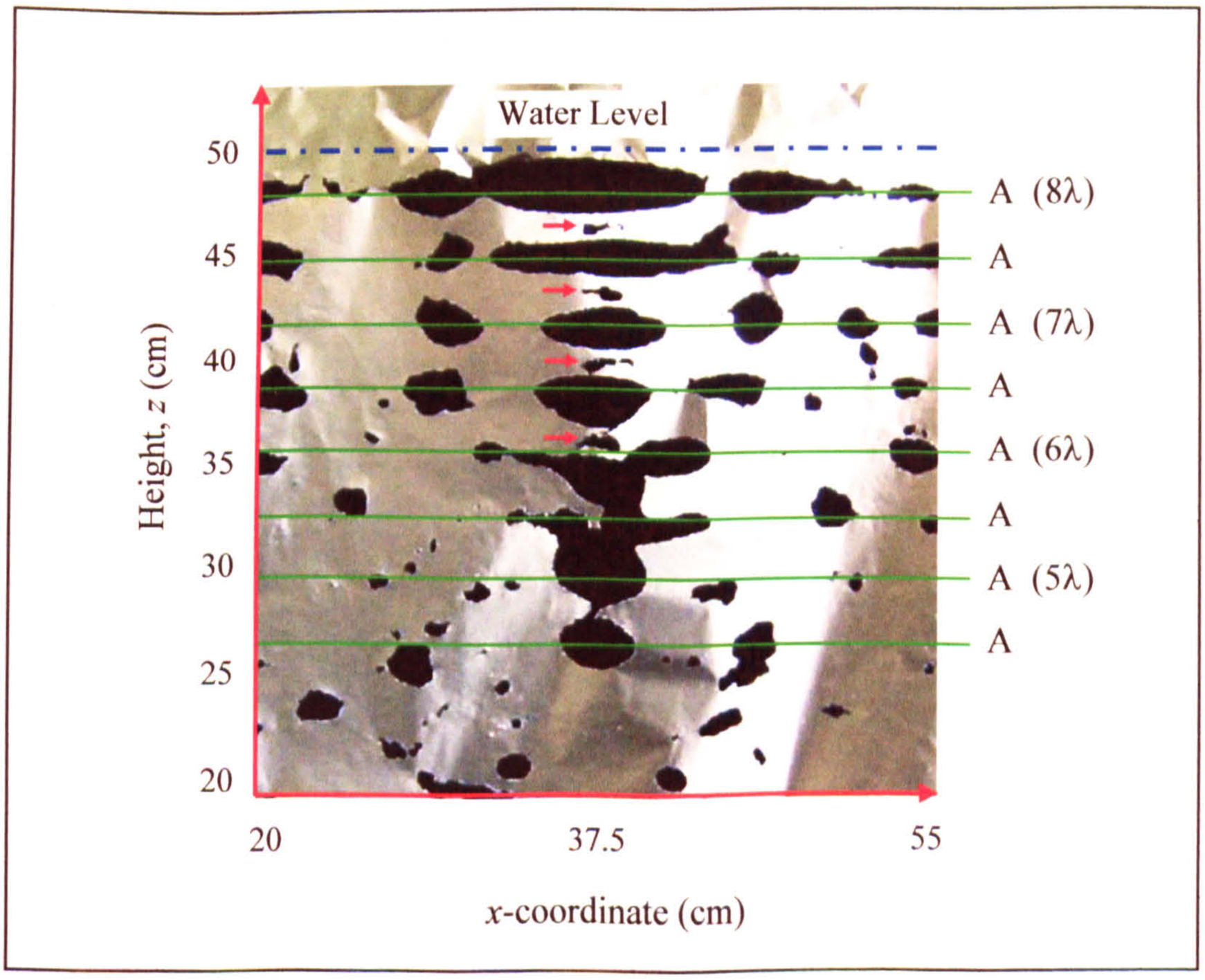

Figure 6.21: Close up of aluminium sheet exposed to 10 minutes sonocation at position y = 37.5 cm (A = antinode)

A strong correlation exists between the locations of the ultrasonically eroded holes in the aluminium film and the theoretical positions of the antinodes shown in Figure 6.15. This confirms the presence of standing waves with their associated variation in cavitational activity. There is some evidence of erosion caused by the wave reflected from the liquid / air interface (indicated by the red arrows), again correlating well to those antinodal positions depicted for the reflected wave in Figure 6.15. However, the degree of erosion caused by the reflected wave appears to be markedly reduced compared to that caused by the incident waveform. This is in contradiction to the theoretical prediction that virtually all of the incident energy is reflected from the surface (Equation 6.3). Furthermore, there is no clear evidence of holes formed at the reflected wave antinodal positions in other regions of the sheet. In order to establish the cause of this deviation, the source of emission (the tank base) was accurately profiled, according to the method described in Section 3.5.5. In order to enhance the smoothness of the surface illustration whilst minimising the number of measurements required, the data was interpolated in both the *x* and the *y* planes (Figure 6.22).

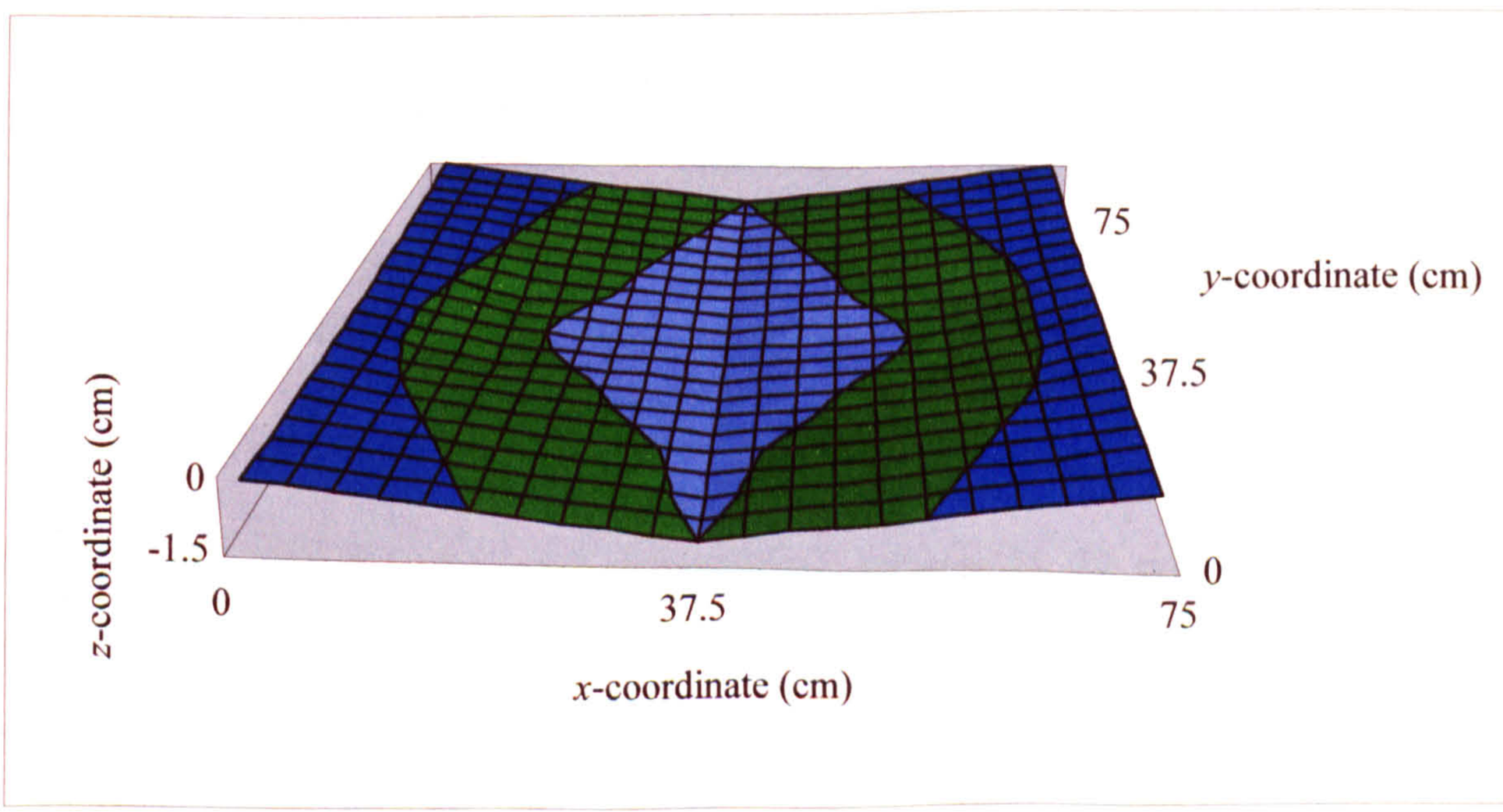

Figure 6.22: Depth profile of ultrasonic tank floor

The analysis showed that, in addition to a drainage channel running along the centre of the *x*-axis, a deflection in the tank floor was also present along the centre of the

y-axis. The source of this distortion can be attributed to residual fabrication stresses: the high temperature welding processes involved in construction of the tank cause the steel sheets to expand, leading to a permanent distortion upon cooling to room temperature. Figure 6.23 exhibits a close-up of the ultrasonically ablated aluminium foil sheet, sonicated along the plane $x = 37.5$ cm.

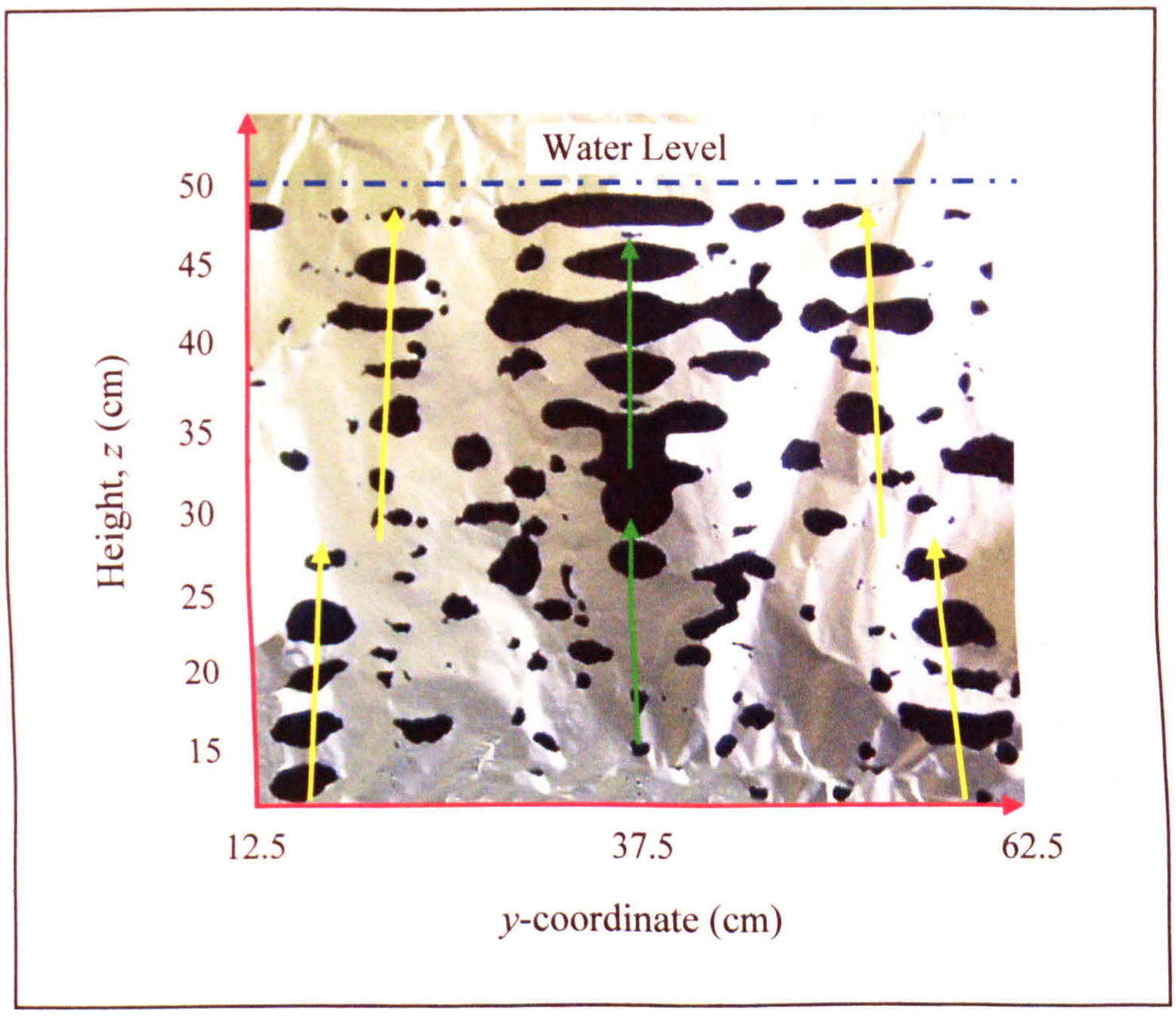

Figure 6.23: Close-up of aluminium foil sheet exposed to 10 minutes ultrasonic ablation along the plane $x = 37.5$ cm

It can be seen that away from central positions, indicted by the green arrows, that the direction of the antinodal perforations follow a path inclined towards the centre of the tank by an offset of approximately 2.5° from the normal (indicated by the yellow arrows). This corresponds to the angle at which transducers placed at $y = 18.75$ cm and $y = 56.25$ cm face according to the tank floor profile data, presented in Figure 6.22. The presence of reflected wave antinodal erosion at central locations in Figures 6.21 and 6.23, and their absence in adjacent areas may therefore be attributed to the focusing of ultrasonic energy towards the centre of the tank by the deflection in

the base. Moreover, as the direction of acoustic energy emitted from central positions experience the least deviation from the normal (green arrows *cf.* red arrows in Figure 6.23), the wave returns along its original path since the angle of incidence equals the angle of reflection.

However, this explanation alone is not sufficient to account for either the apparent reduction in cavitation intensity at the central reflected wave antinodal positions, or the absence of antinodal positions from regions were the reflected wave could be expected to travel. As there is a large difference in the acoustic impedance between water and air, small deviations in the angle of incidence would result in very little energy loss during reflection at the surface (Equation 6.2). By observing the ultrasonic tank during the de-gassing phase (described in more detail section 6.4.4), were sonics are applied under a 50% duty cycle, it was observed that during sonication small waves spread from the sides to form a continuous disruption of the water surface. Consequently, acoustic energy reaching the surface experiences a dynamic interface, scattering the reflected energy in different, continuously changing, directions. Furthermore, since the angle of incidence of acoustic energy at the interface can be greatly increased depending on the shape of the surface wave at that point, there is a simultaneous reduction in the efficiency at which energy is reflected, according to Equation 6.2. These effects provide an explanation for the limited evidence for reflected wave antinodal positions.

6.4.2 Mapping of cavitational activity via sonochemical luminescence and the enhancement of ultrasound tank acoustics

In the previous section, the distribution of cavitational activity was mapped by assessing the mechanical damage incurred on a solid aluminium foil surface placed into the cavitating liquid. Aluminium has a high acoustic impedance (Table 6.1) and as such may cause significant perturbation of the ultrasound field. Furthermore, once perforated, freshly exposed metal edges become preferential sites for subsequent transient bubble formation, thereby causing the localisation of cavitation in that

region. The use of an aqueous probe to reveal the natural distribution of cavitational intensity throughout the tank will be clearly beneficial.

The enormous energies associated with transient cavitation bubble collapse have for many years been known to cause the emission of light (termed *sonoluminescence*). Although invisible to the naked eye, Frenzel and Schultes observed in 1934 the bleaching of photographic film when experimenting with ultrasound to speed up the development process. Sadly, little information was obtained from the experiments since the effect was extremely slow acting and the weak, scattered light emissions associated with multibubble sonoluminescence provided virtually no spatial resolution (Frenzel & Schultes, 1934).

Sonoluminescence is a third-order process, stemming from the second order effect of high frequency sound in water, namely cavitation. Thermal hydrolysis of water vapour contained within collapsing cavitation bubbles is believed to give rise to high energy free radicals, which in turn react with surrounding bodies, releasing light as a by-product (Equation 6.5) (Sehgal *et al*, 1980), (Riesz *et al*, 1985).

$$H^{\bullet} + OH^{\bullet} + M \rightarrow H_2O + M + h\nu \qquad 6.5$$

where M represents a third body (such as a gas or water molecule) that assists the above process by providing a stabilised intermediate complex, h is Plank's constant and ν is the speed of light.

For more than 50 years after its discovery, very little research into phenomenon of sonoluminescence was carried out, until in 1989 Felipe Gaitan and Lawrence Crum developed a technique to trap a single bubble in an ultrasonic resonator and cause it to emit light of an intensity many orders of magnitude greater than previously experienced. Termed 'single bubble sonoluminescence' it was now possible to witness directly the light produced by ultrasonic cavitation in a liquid medium, and became known as 'the star in a jar' (Gaitan *et al*, 1992). Less than a decade later,

sonoluminescence gained notoriety amid claims that, under certain experimental conditions, the enormous energies associated with transient bubble collapse were capable of initiating nuclear fusion (Taleyarkan *et al*, 2002), (Shapira & Saltmarsh, 2002).

Unfortunately, light emission experienced during *multi-bubble* sonoluminescence (which exists in ultrasonic tanks) is too weak to provide useful data on the spatial distribution of ultrasonic cavitation (Verrall & Sehgal, 1987). In order to enhance the intensity of light emitted from transient bubble collapse, so permitting the visualisation of cavitation intensity, a handful of researchers have added the fluorescent chemical *Luminol* (3-aminophthalhydrazine) to the cavitating liquid medium (Renaudin *et al*, 1994), (Yanagida *et al*, 2000), (Birkin *et al*, 2003). Luminol, ordinarily employed for detection in molecular biology or for the forensic detection of blood at a crime scene, is a di-cyclic oxygenated amine which can decompose to release blue light of a characteristic wavelength of 430 nm. Hydroxyl radicals generated during transient cavitation bubble collapse (Equation 6.5) are able to react with Luminol under alkaline conditions, producing light of an intensity many orders of magnitude greater than that experienced in ordinary multibubble sonoluminescence (Figure 6.24).

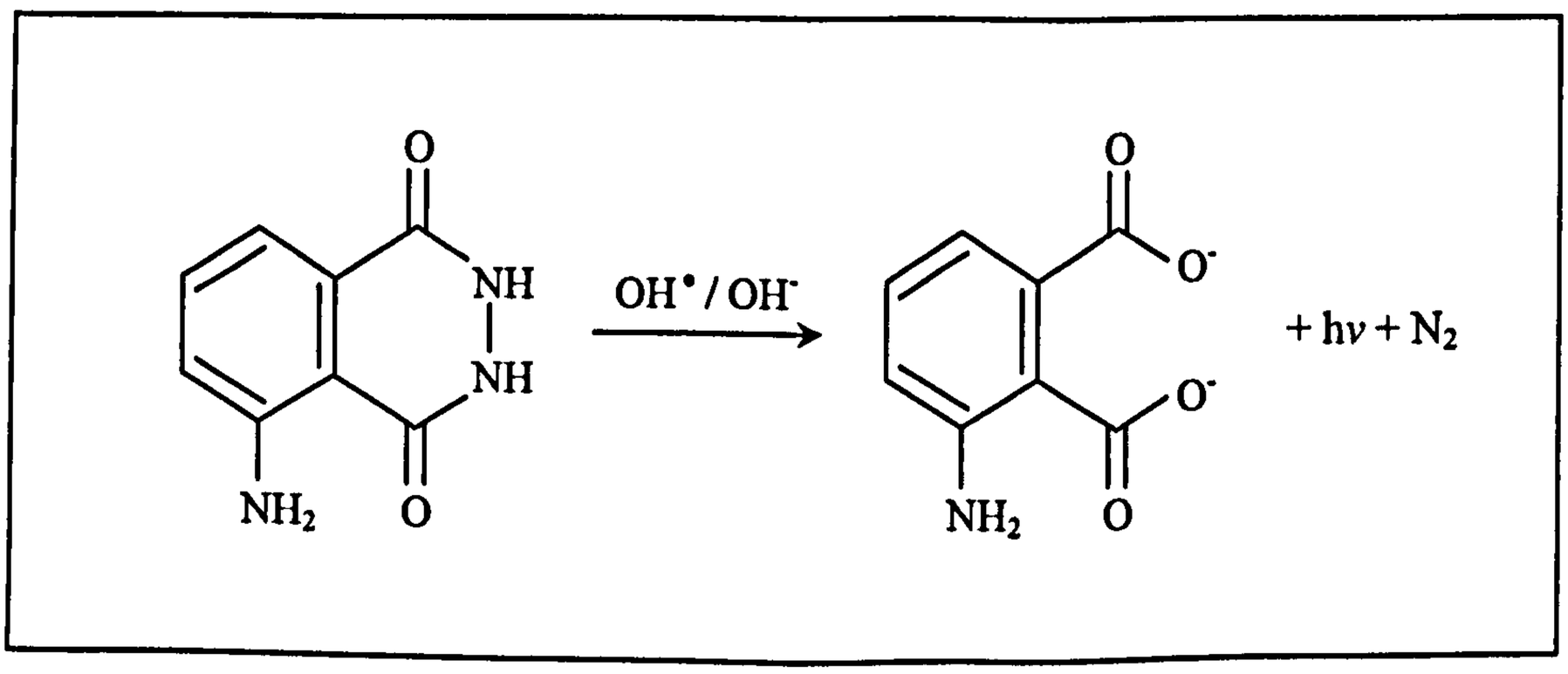

Figure 6.24: Decomposition of Luminol in aqueous alkaline conditions (Renaudin *et al*, 1994)

To permit the visualisation of cavitational homogeneity throughout the industrial-sized ultrasonic tank, Luminol was added to the volume of water and adjusted to pH 10.7 according to the method described in Section 3.5.6. The light emitted by the mixture upon exposure to ultrasound was barely visible to the naked eye and in addition to conducting the experiments at night, it was necessary to take extensive measures to prevent any source of light from penetrating the laboratory area. A range of exposure times, aperture settings and photographic film speeds were employed in order to attain a reasonable image. A qualitative summary of the variables used to determine the optimal procedure is displayed in Table 6.2.

Variable	Minimum	Maximum	Optimal
Film speed	ISO 200	ISO 3200	ISO 1600
Aperture size	27	5.6	5.6
Exposure time	1/1000 second	40 minutes	25 minutes

Table 6.2: Determination of the optimal procedure for capturing sonochemical luminescence on photographic film

Figure 6.26 (a) exhibits the pattern of light emission successfully captured from the decomposition of Luminol induced by acoustic cavitation. It can be seen that a significant variation in cavitational intensity exists across the ultrasonic tank, where bright areas represent regions of high intensity, and dark areas indicate low cavitational activity. The positions of the transducers attached to the tank floor are indicated and, since the deflection in the tank floor partially directs the ultrasound towards the centre of the tank, it is possible to associate some of the brighter regions on the picture with transducer locations. However, it can also be seen that regions of the tank that are not directly above a transducer also experience intense cavitation, suggesting multiple reflections and spread of acoustic energy within the body of water. Interestingly, two lines of symmetry exist in the pattern created (along $x = 37.5$ cm and $y = 37.5$ cm), matching that of the profile of the tank floor and again suggesting that large areas of the floor oscillate to act as emitting surfaces.

With the intention of establishing a homogeneous cavitational distribution throughout the tank, an internal ultrasonic baffling system was developed. Various materials were employed during the development process and the aggressive environment present inside the ultrasonic tank was found to be unsuitable for many polymeric materials, such as polyester and poly vinylchloride, which were found to degrade and cause fouling of the water purification system. Similarly, the zinc coating present in galvanised steel was found to react with water during cavitation to form a white powder (zinc hydroxide), in turn exposing the unprotected steel beneath. Consequently, samples of stainless steel sheets of the type employed in the main tank construction were obtained, and perforated with regularly spaced round holes of various pitch and diameter. Initial investigations into the disruption of the sound field based on the small-scale microelectrode manufacture indicated that the steel with the smallest and most closely packed perforations available provided the best disruption of the ultrasonic waveform while maintaining cavitational intensity. Consequently, a full-sized ultrasound baffle was constructed using 1 mm thickness grade 307 stainless steel, perforated with 3 mm diameter and 5 mm pitch round holes (illustrated in Figure 6.25).

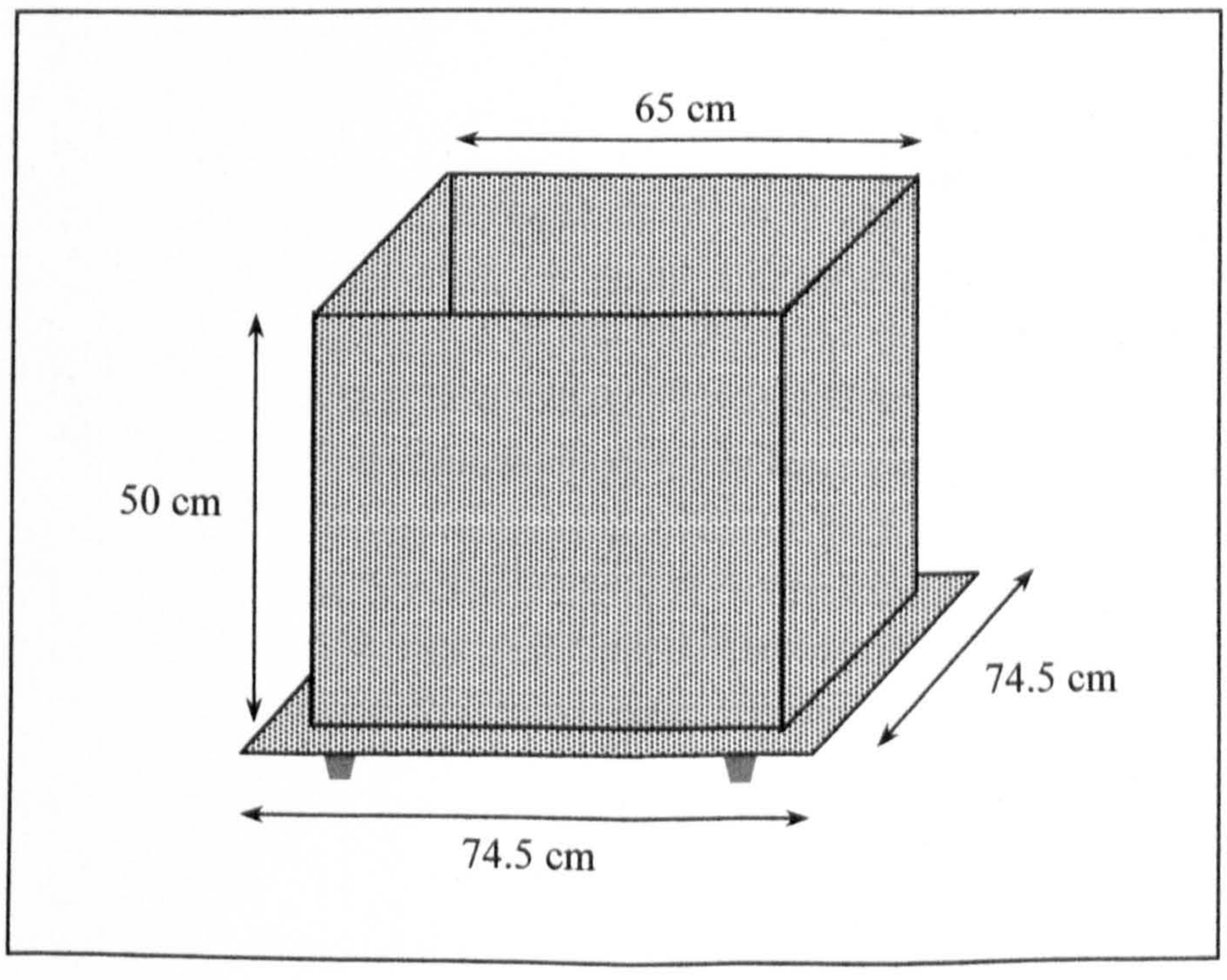

Figure 6.25: Schematic of ultrasonic tank baffling design

The baffle construction was placed on rubber feet to separate it from the tank floor by a distance of 5 cm. This served to prevent the cage from hindering the motion of the tank floor or disrupting the formation of the acoustic wave at the emitting surface. The use of rubber feet also served to dampen the direct transmission of vibrational energy from tank body to the interior of the baffle cage. Furthermore, the lengths of the supports were adjusted to compensate for the dip in the tank floor, creating a flat base within the confines of the cage. Following the construction of the baffle, the distribution of cavitation within the tank was once again assessed using sonochemical luminescence, displayed in Figure 6.26 (b).

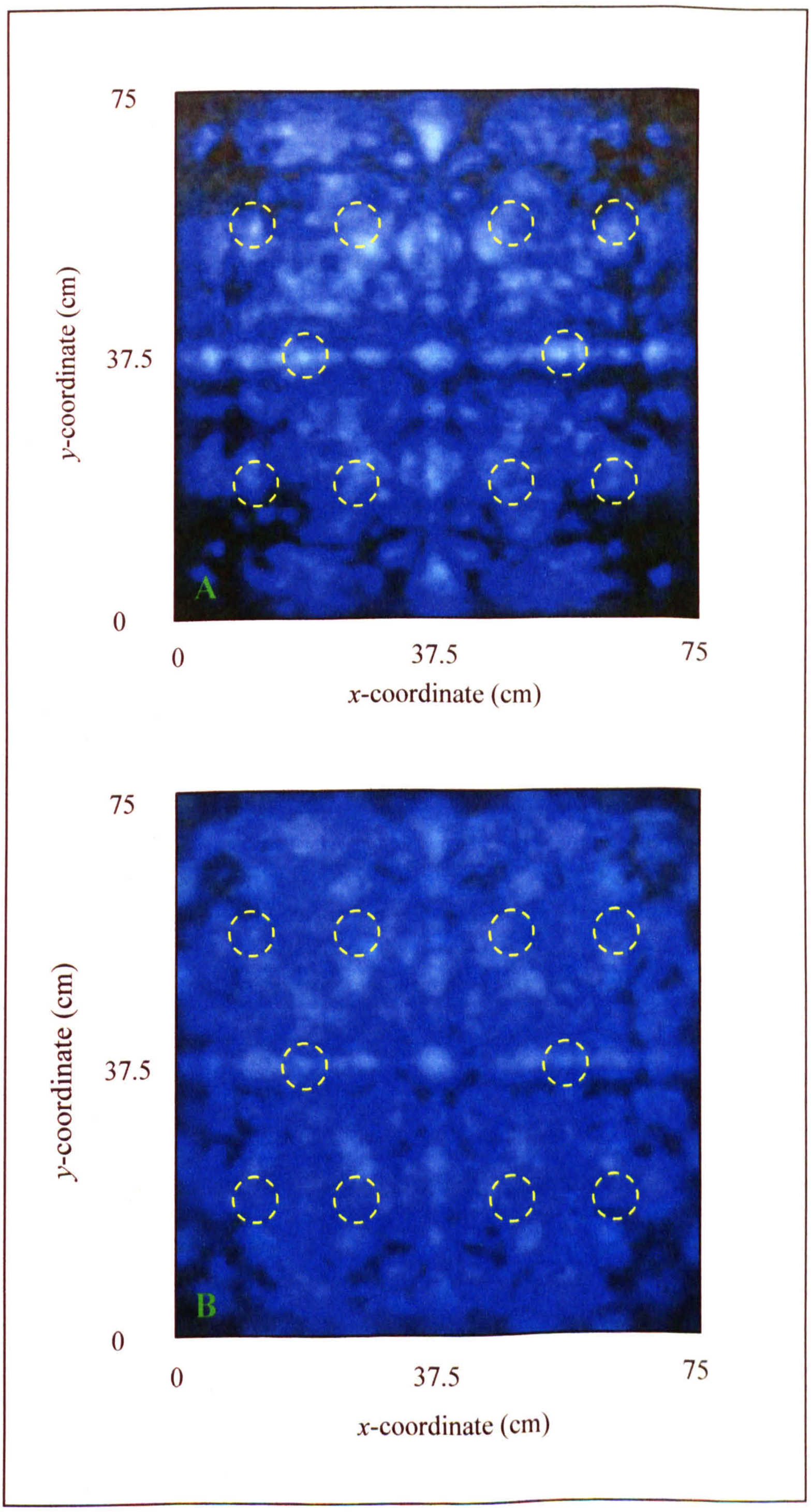

Figure 6.26: Variation of cavitational intensity (a) without baffling and (b) with baffling, ( ) indicates position of ultrasonic transducer

It can be seen that the presence of the baffling significantly improved the uniformity of cavitational intensity throughout the tank since the numerous, regularly spaced perforations act as point sources of acoustic emission. Importantly, since the diameter of the perforations in the steel baffling are much smaller than the range of incident wavelengths, the sound wave is diffracted as it passes through the gap, resulting in an increased homogeneity of node and antinodal positions (Figure 6.27). In addition, the flattened base of the ultrasound cage permits a more even distribution of acoustic energy when compared to emissions from the tank floor.

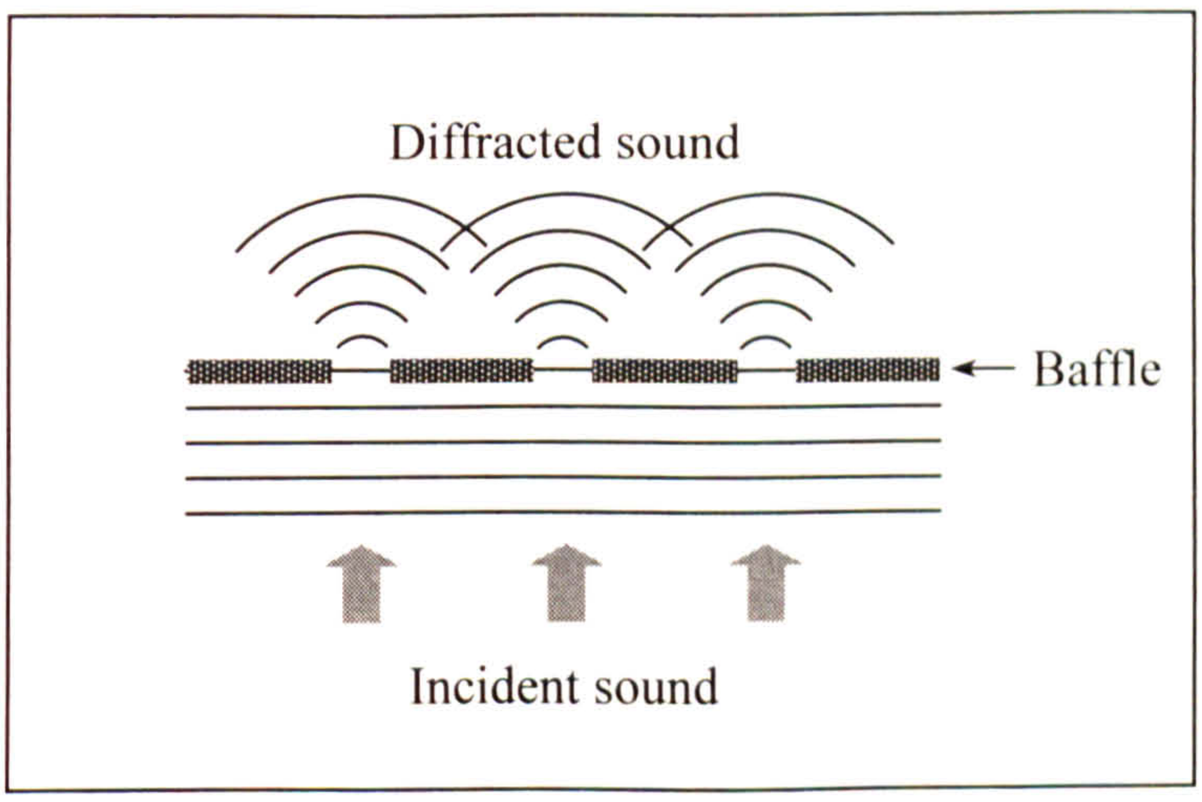

Figure 6.27: Schematic representation a sound wave passing through a narrow gap

6.4.3 Process development for large scale microelectrode sensor production

In order to achieve the successful commercialisation of microelectrode array sensors based on polymer modified screen printed carbon-ink electrodes, it is necessary to increase the process batch size from that of individual sensors to many hundreds. Initially, 18 x 18 cm blocks of 100 sensors (illustrated in Figure 4.19) were separated from the main sheet and modified with poly(*o*-phenylenediamine) as described in Section 5.5. Sensors were suspended by the top of the sheet facing towards the right-hand side of the tank with centre at coordinates x = 18.75 cm, y = 56.25 cm, z = 35 cm which corresponded to a cavitationally homogenous region observed in

Figure 6.26. Three batches of sensors were exposed to 10 seconds ultrasonic ablation and were then interrogated potentiostatically using a 1 mM hexaammineruthenium(III) chloride redox couple using the procedure detailed in Section 3.5.8. The mean currents of the middle rows of the sensor sheets (recorded over the final 10 seconds of a 60 second polarisation time) are displayed in Figure 6.28. For comparison, error bars indicate the relative standard deviation (RSD) of 1.77 %, recorded for the response of screen printed carbon-ink electrodes coated with poly(*o*-phenylenediamine) to 1 mM hexaammineruthenium(III) chloride in Section 5.5.

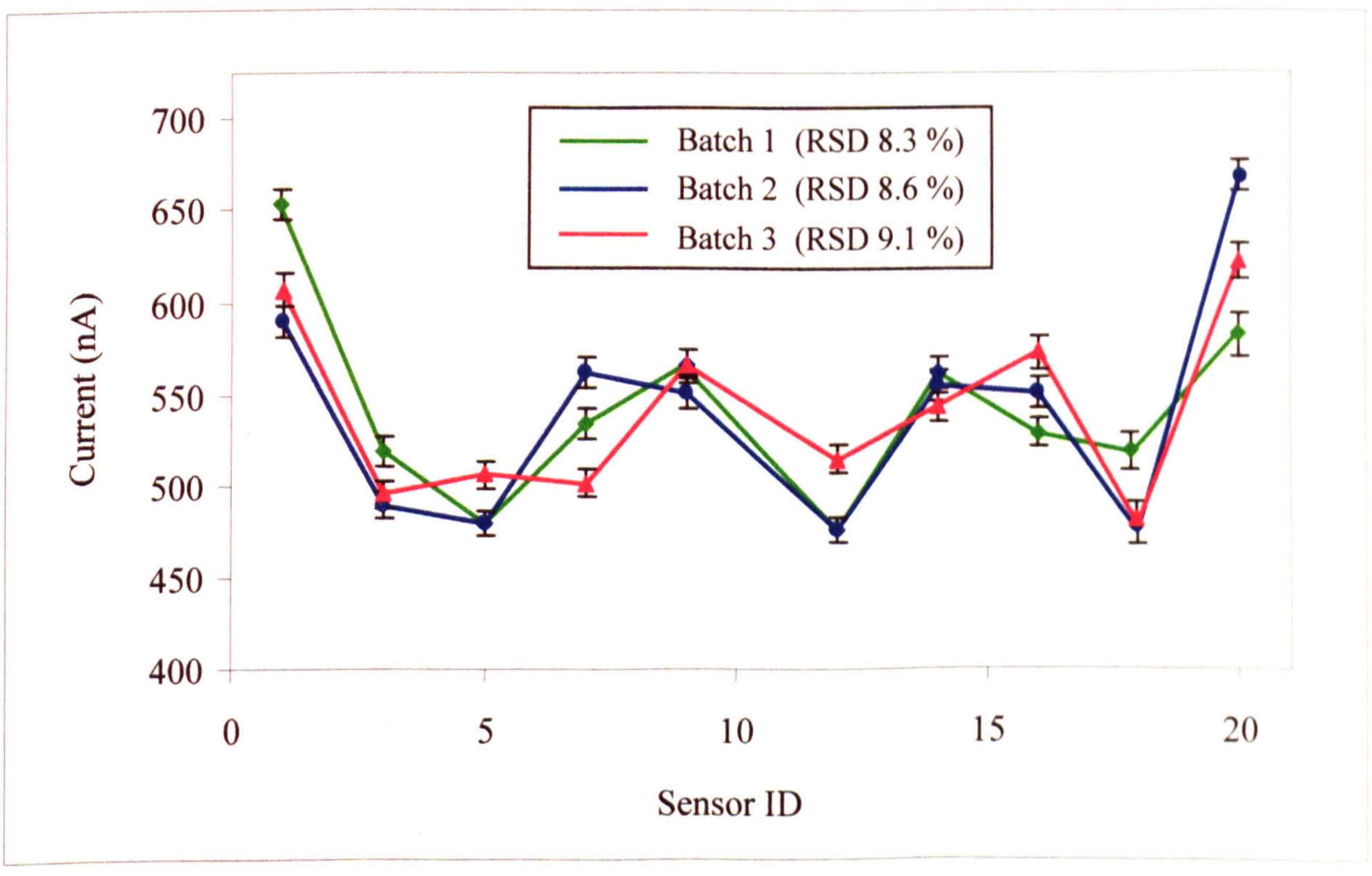

Figure 6.28: Variation in mean current response to 1 mM $[Ru(NH_3)_6]^{3+/2+}$ for three batches of 20 screen printed carbon-ink sensors sonicated at the same locations in the industrial-sized ultrasonic tank.

The results indicate that despite the improvements in the uniformity of the acoustic field provided by the baffling system, localised cavitational 'hot-spots' still exist at certain locations within the horizontal plane. This level of variation would not be of

any consequence in ordinary ultrasonic cleaning applications, but for the fabrication of microelectrode array sensors, differences in cavitational intensity on this scale are detrimental to sensor performance. The relative standard deviation for each batch of sensors was calculated and can be seen to greatly exceed the variation measured for the same redox probe during the interrogation of unsonicated, P*o*PD electropolymerised screen printed carbon-ink electrodes. This confirms that the variation is a direct result of inhomogeneities in the sonocation process.

It can also been seen from Figure 6.28 that sensors towards the edge of the sheet exhibit the greatest current responses, indicating that they have experienced a greater degree of ultrasonic ablation than sensors away from the sheet edge. This effect was observed consistently during experimentation for sensors located at all edges of the sheet and appeared to be relatively independent of the positioning of the sensor sheet in the tank. Figure 6.29 displays a photograph obtained following investigations into the cause of this phenomenon using sonochemical luminescence.

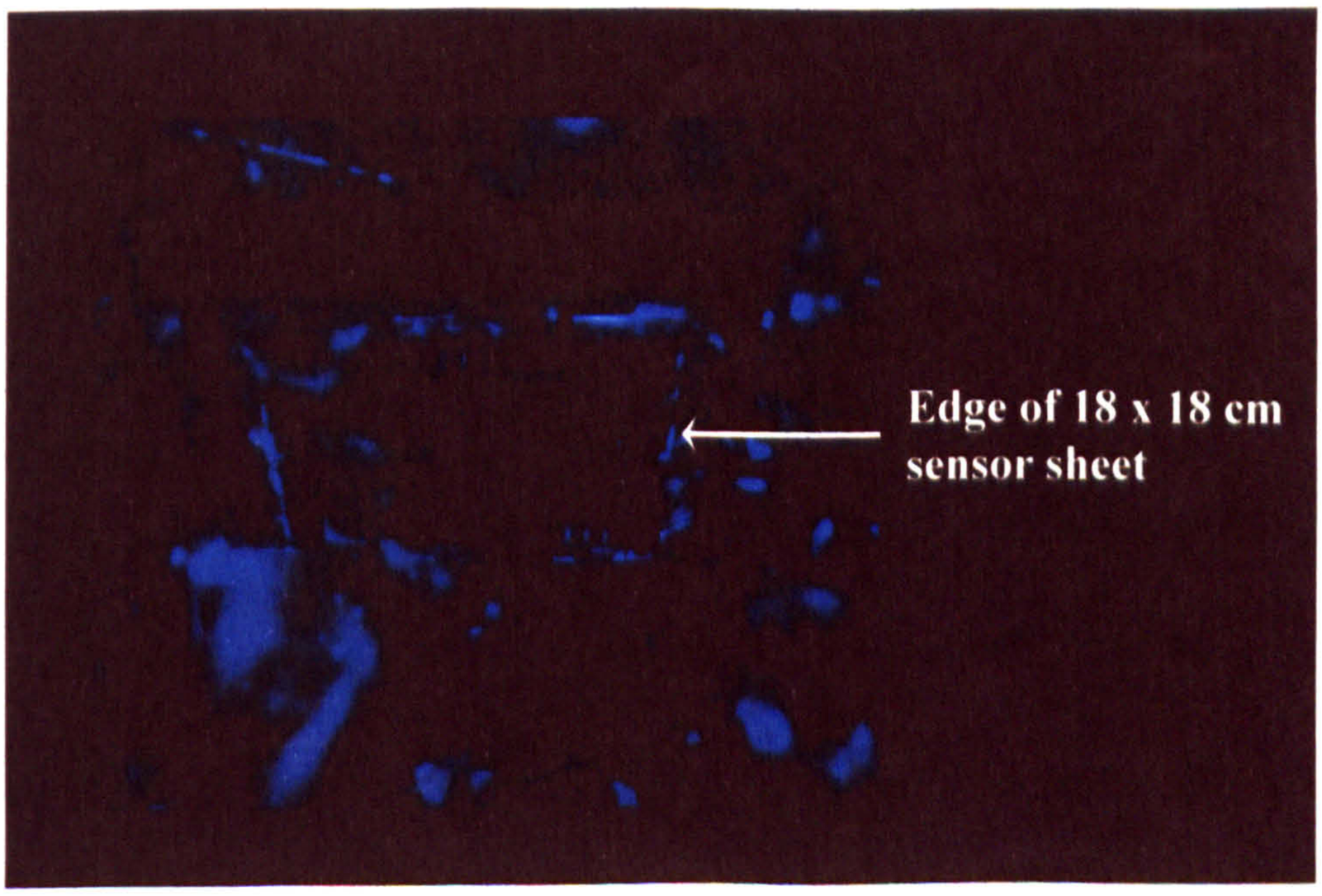

Figure 6.29: Sonochemical luminescence investigations into elevated signal responses from sensors located at the sheet edge

The image revealed that the sharp edges of the 0.375 mm polycarbonate sensor sheets appeared to be causing preferential nucleation of transient cavitation bubbles. Consequently sensors around the edge experienced more intensive ablation than sensors located elsewhere. To avoid this problem, a mounting device was constructed to shield the outer edges of the sensor sheet from exposure to the cavitating liquid (Figure 6.30).

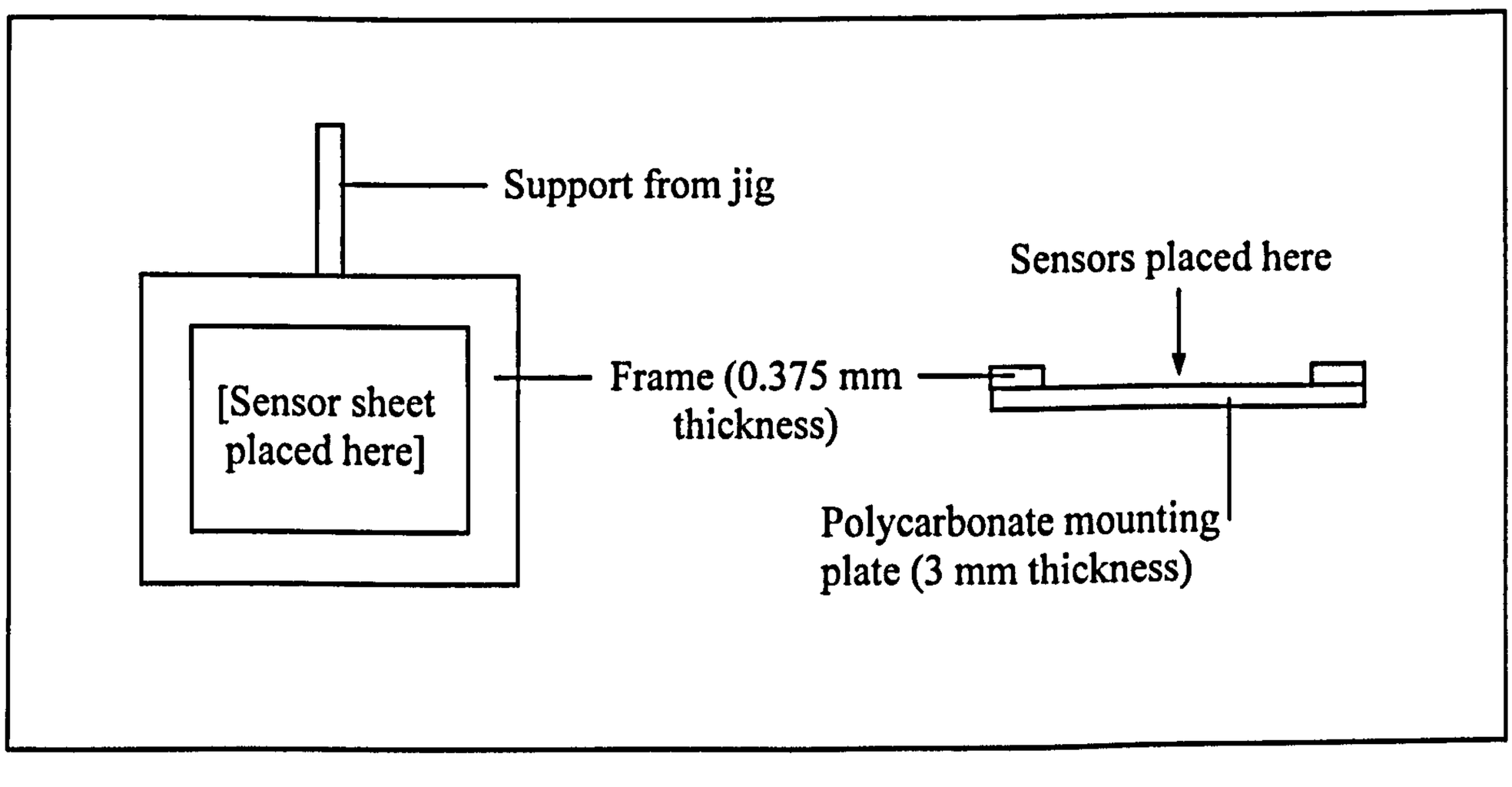

Figure 6.30: Sensor sheet mounting system to eliminate preferential bubble nucleation

The fluctuation in signal magnitude exhibited in Figure 6.28 (i.e. current amplitude maxima and minima varying within the horizontal plane) corresponds to a distance of around 3 cm, close to the natural variation of acoustic amplitude experienced in the vertical plane which results from antinodal positions in a 25.1 kHz standing wave field. Consequently, a method for providing electrodes with a uniform exposure to cavitation was conceived, based on the controlled movement of sensors within the sound field. A prototype robotics system was constructed to permit the movement of sheets of 100 sensors in a circular vertical plane of radius 3 cm (Figure 6.31).

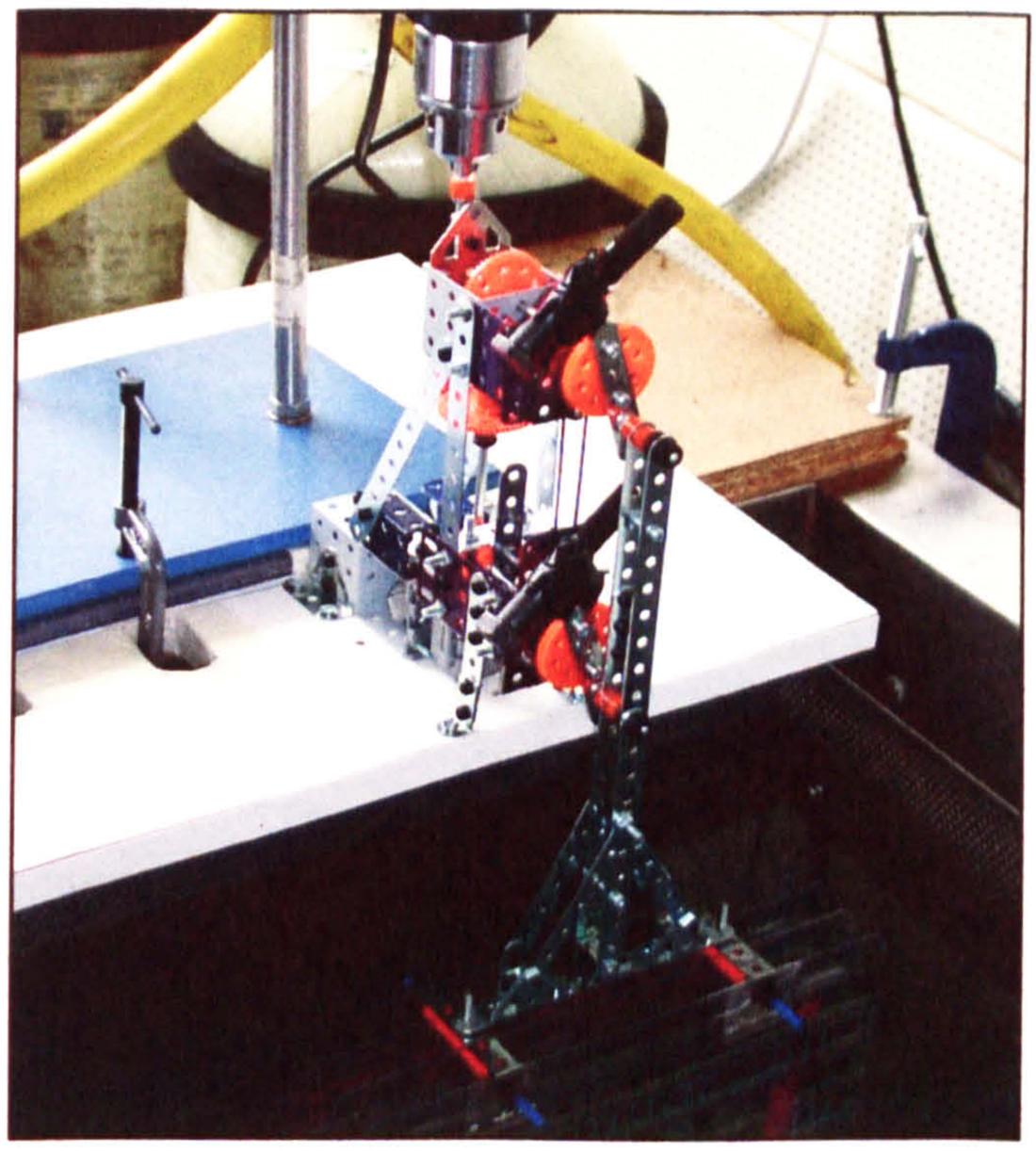

Figure 6.31: Robotics movement for the ultrasonic ablation of sensors

Three batches of 100 sensors were mounted in the frame described above and connected to the robotics movement system (described in Section 3.5.7). Sensors were set in motion then exposed to 10 seconds ultrasonic ablation during a single rotary cycle (6 rpm). 20 sensors from random positions within each batch were interrogated potentiostatically using 1 mM hexaammineruthenium(III) chloride. Figure 6.32 exhibits the current-time transients obtained for a polarisation time of 60 seconds. Error bars represent the highest and lowest current values measured across all three batches for that time period.

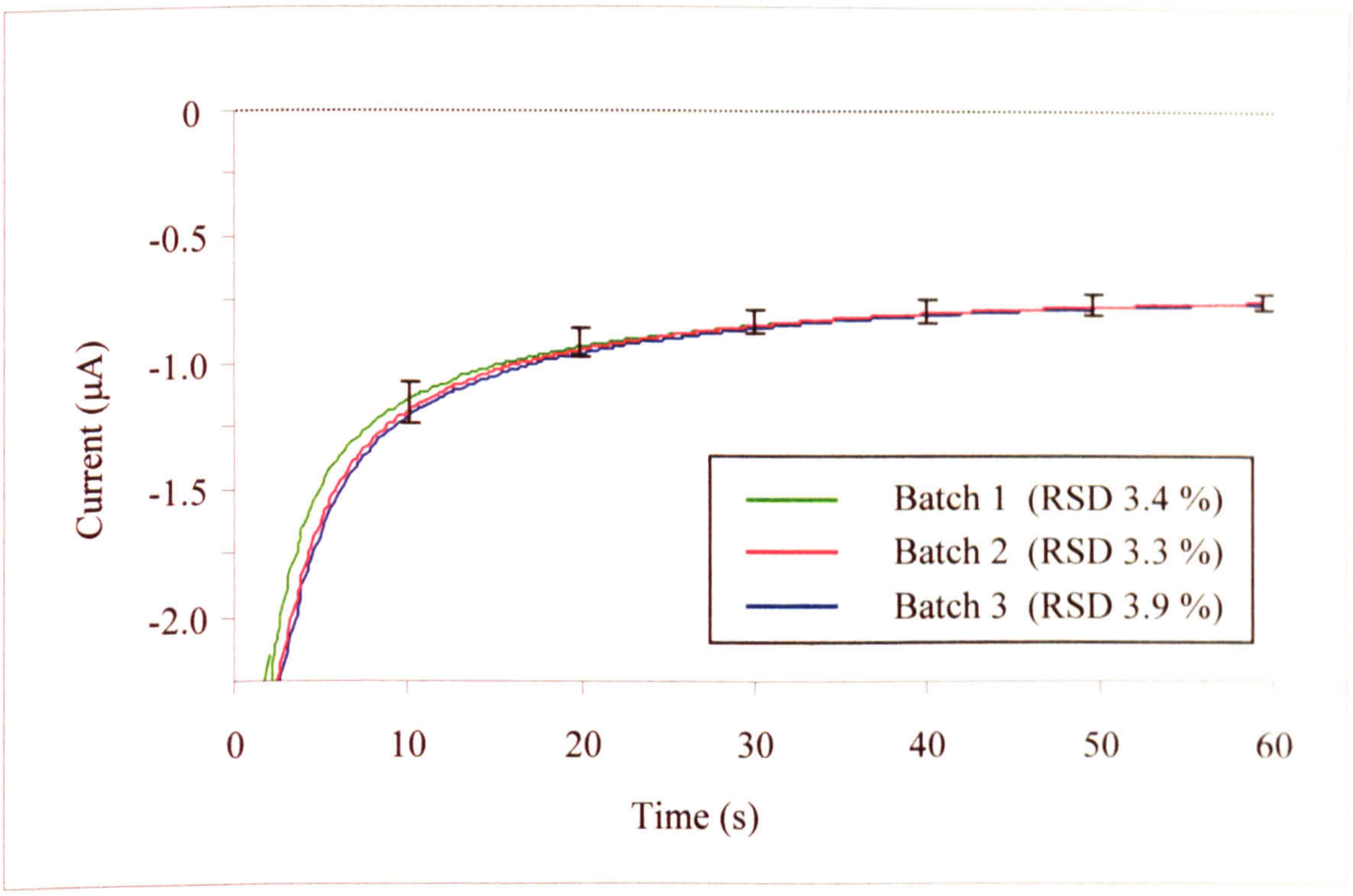

Figure 6.32: Current-time transients obtained during sensor interrogation with 1 mM hexaammineruthenium(III) chloride redox probe

A mean relative standard deviation of 3.6 % was obtained across all three production batches, confirming that the controlled movement of the sensors through the cavitating liquid medium permits each electrode to be exposed to the same degree of ultrasonic ablation. Following the success of the robotic movement system, it was necessary to continue to upscale the process in order to permit multiple sheets of sensors to be sonicated simultaneously. Based on the previous design, a custom-built steel jig was obtained which offered smoother rotational control and was capable of bearing the heavier loads associated with multiple sensor sheets and their mountings (Figures 6.33 and 6.34)

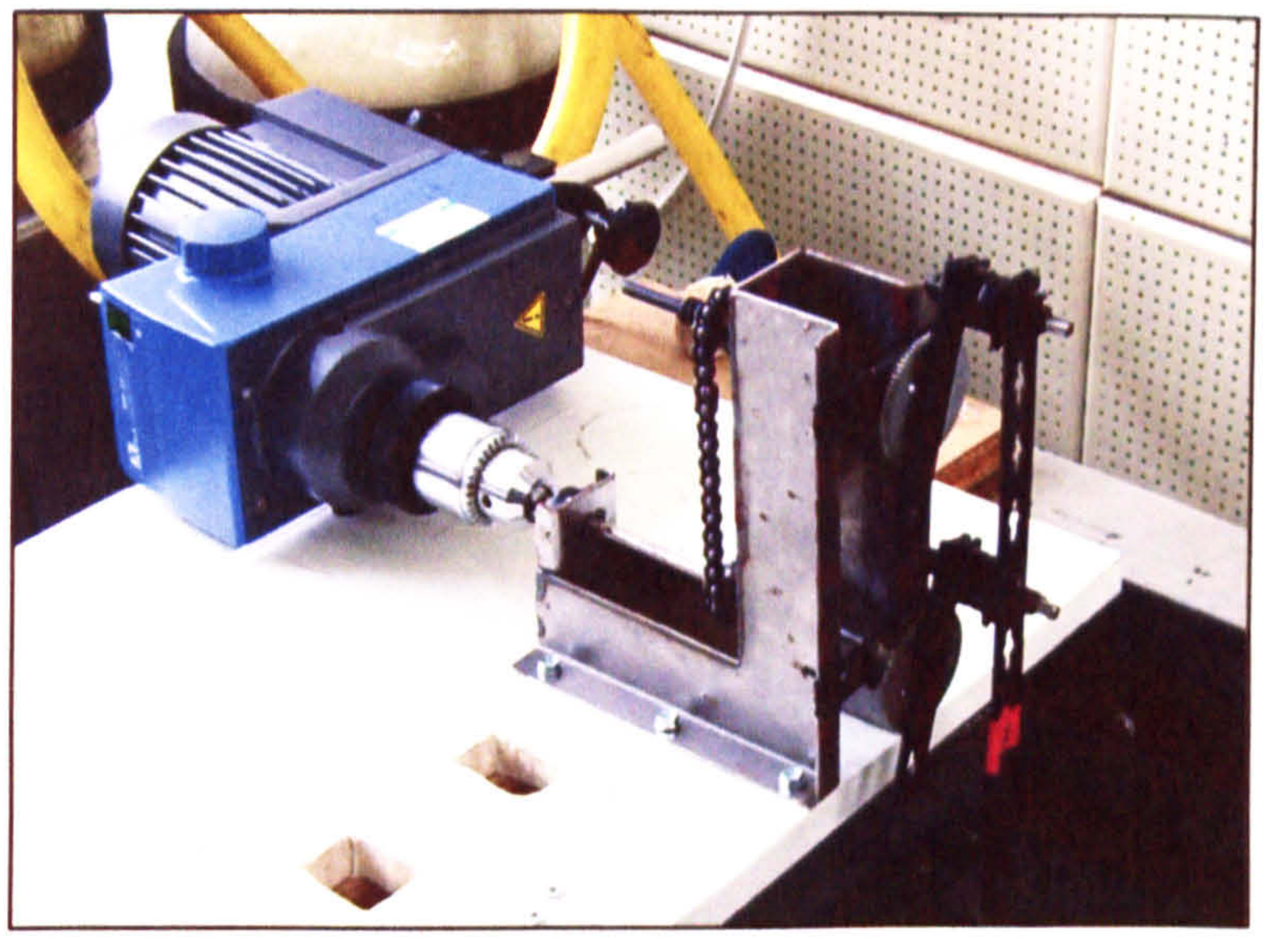

Figure 6.33: Heavy duty robotics movement system suitable carrying for multiple sensor sheets

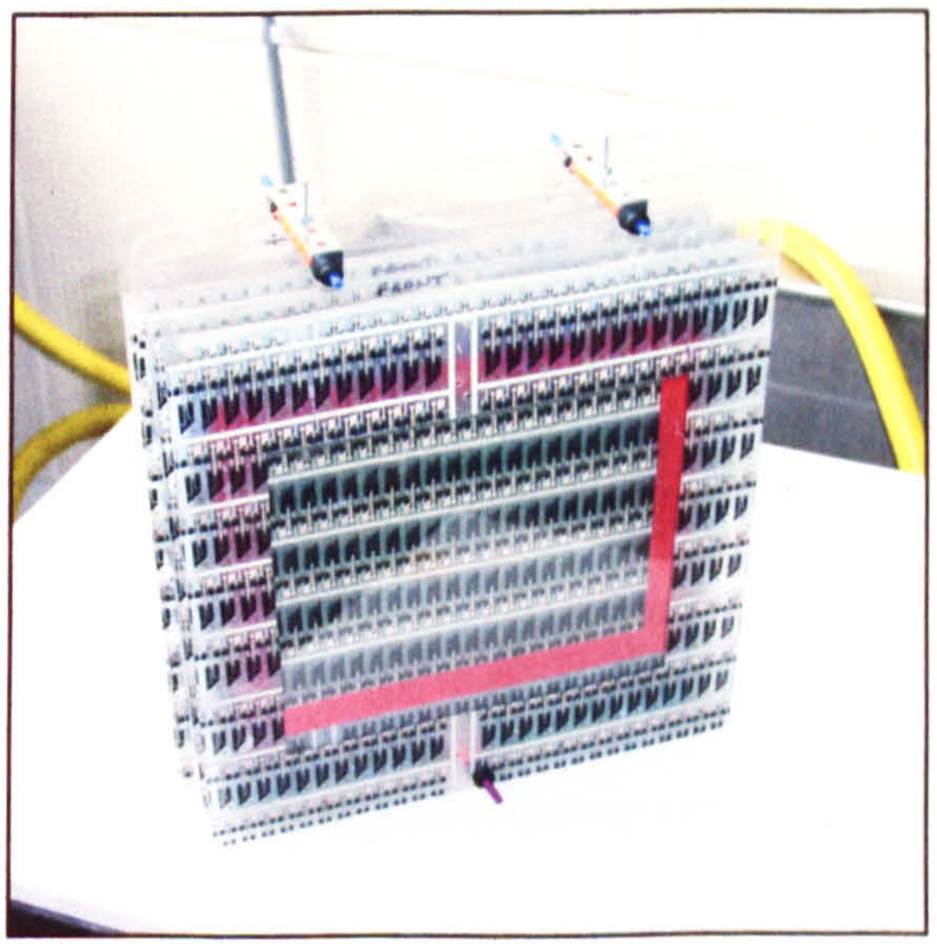

Figure 6.34: Multiple sensor mounting

Initial investigations were carried out into the simultaneous ultrasonic ablation of multiple sheets of sensors using various configurations of sheet position and separation. Using the robotics movement system and mounting jig pictured above, 4 x 100 sensors sheets were exposed to 10 seconds ultrasonic ablation at 75% power, central to coordinates x = 18.75 cm, y = 56.25 cm, z = 35 cm. Sensors were interrogated amperometrically for 60 seconds at -350 mV (vs. Ag/AgCl) using a 1 mM hexaammineruthenium redox probe. The current magnitudes of 20 sensors,

taken from equivalent positions in each sheet, were recorded as an average over the last 10 seconds of polarisation time to assess the effect of multiple sheets (and their mountings) on the uniformity of the cavitational activity experienced. The data presented in Table 6.3 summarises the values obtained from a test configuration simulating a possible sheet arrangement for production, displayed in Figure 6.35. Green arrows represent the direction in which the sensor sheets face and although none were attached to mountings 1 and 4, they remained in place to create an equal environment for sensor sheets A to D.

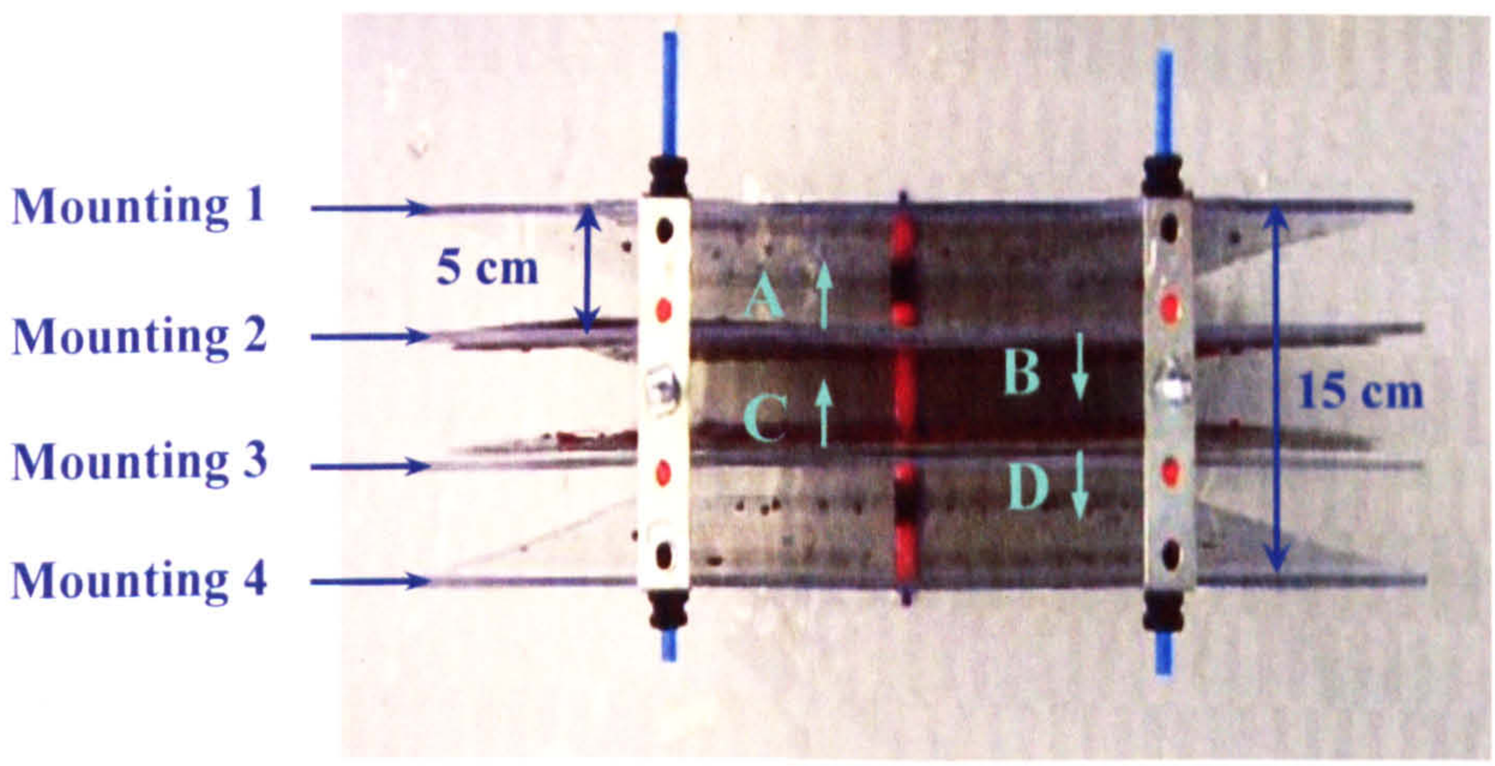

Figure 6.35: Configuration of sensor sheets during simultaneous ultrasonic ablation, (arrows indicate the direction in which the sheets face)

Sheet	Mean current (nA) across sheet	RSD (%)
Sheet A	-728	9.83
Sheet B	-842	9.41
Sheet C	-743	6.79
Sheet D	-919	10.29
Total average:	**-808**	**11.09**

Table 6.3: Amperometric signal variation of 4 sheets of sensors sonicated simultaneously

The results indicated a significant deterioration in the spatial homogeneity of the ultrasound field caused by the local presence of sensor sheets and their mountings. No correlation in the data could be seen pertaining to current response and the relative horizontal and vertical positions of the electrodes within the sensor sheet. One possible explanation for the disruption is the interaction of incident acoustic waves with the range of materials (of varying hardness) present on the sensor sheets. Due to the distortion present in the ultrasound tank floor the direction of the acoustic wave is not normal to the surface, therefore the incident wave will inevitably intrude upon the sheets and their mountings to a greater extent than if the wave could propagate unhindered vertically between the four mountings.

6.4.4 Process optimisation for microelectrode fabrication

In addition to the acoustic baffling cage, the customised sensor mounting frame and robotic sensor movement system, a number of other ultrasonic tank parameters have been optimised for enhancing the exposure of sensors to cavitational activity for the purpose of ultrasonic ablation (listed in Table 6.4).

Parameter	Effect	Action
Gas loading of cavitating liquid medium	Prevents reduction of energy released in bubble collapse due to cushioning of transient bubble collapse	1 hour degassing prior to use via 50% sonics duty cycle
Purity of cavitating liquid medium	Prevents foreign materials from reducing the energy associated with transient bubble cavitation	100 μm particulate filter, carbon filter and deioniser used for purity <0.1 $\mu S.cm^{-1}$
Temperature of the cavitating liquid medium	The closer that a liquid approaches its boiling point, the less energetic the collapse of cavitating bubbles	Maintain temperature of the water to 25°C
Frequency sweep	Homogenisation of regions of high and low acoustic amplitude	Frequency = 25.1 ± 1 kHz
Water level	Permits favourable positions of reflected wave antinodes	Depth of water = 50 cm

Table 6.4: Summary of parameters for optimal cavitational exposure

For the production of stir-independent electrochemical sensors two further key parameters must be optimised in order to control microelectrode pore size and density, namely sonocation power and time. Both variables can be accurately controlled via integrated software, with sonocation time controllable from 0 to 99 seconds in one second increments and power ranging from relative intensities of between 50% (minimum) and 100% (maximum). Sheets of 100 poly(*o*-phenylenediamine) coated screen printed carbon-ink electrodes were mounted on the robotic sensor movement system and ultrasonically ablated using a range of sonication power and time settings at tank coordinates x = 18.75 cm, y = 56.25 cm, z = 35 cm. Sensors were then polarised at -350 mV for 360 seconds in a 1 mM hexaammineruthenium(III) solution for characterisation of stir-independent behaviour. Quiescent solution conditions were maintained for the first 90 seconds of polarisation, followed by 90 seconds of solution convection introduced by a Jenway magnetic stirrer and 6 mm flea set to speed setting level 4. The rate of convection was then increased to stir level 6 for a further 90 seconds, and the experiment then concluded with a return to quiescent solution conditions. Figures 6.35 to 6.37

illustrate the current-time transients obtained for 5, 10 and 15 seconds sonocation times respectively. Mean sensor responses were calculated from the middle 30 seconds for each solution condition, i.e. unstirred (quiescent) was recorded as the average current between 30 and 60 seconds, stir level 4 between 120 and 150 seconds and stir level 6 between 210 and 240 seconds.

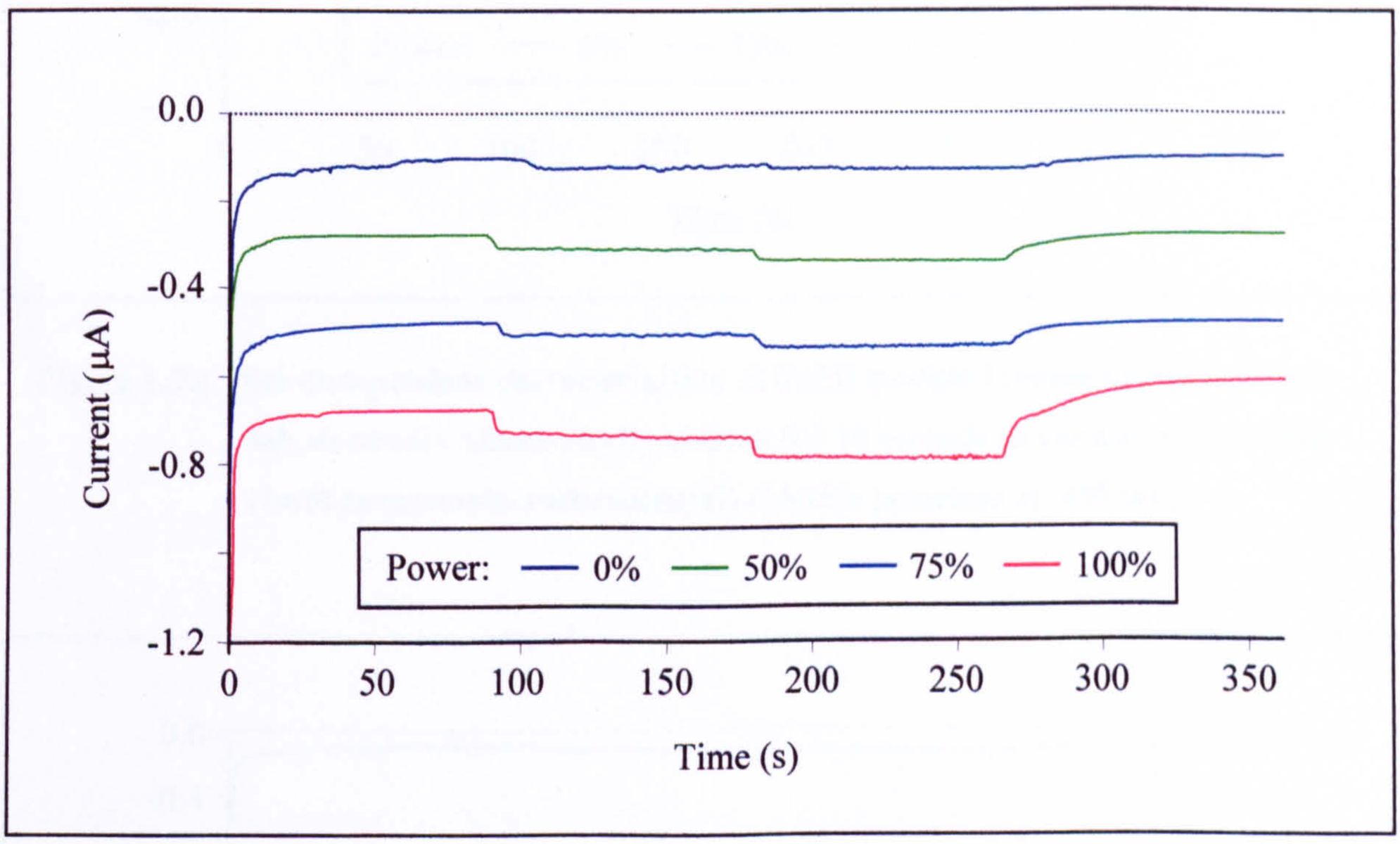

Figure 6.35: Stir-independent characterisation of PoPD modified screen printed carbon-ink electrodes ultrasonically ablated for 5 seconds at various power levels (1mM hexaammineruthenium(III) chloride polarised at -350 mV)

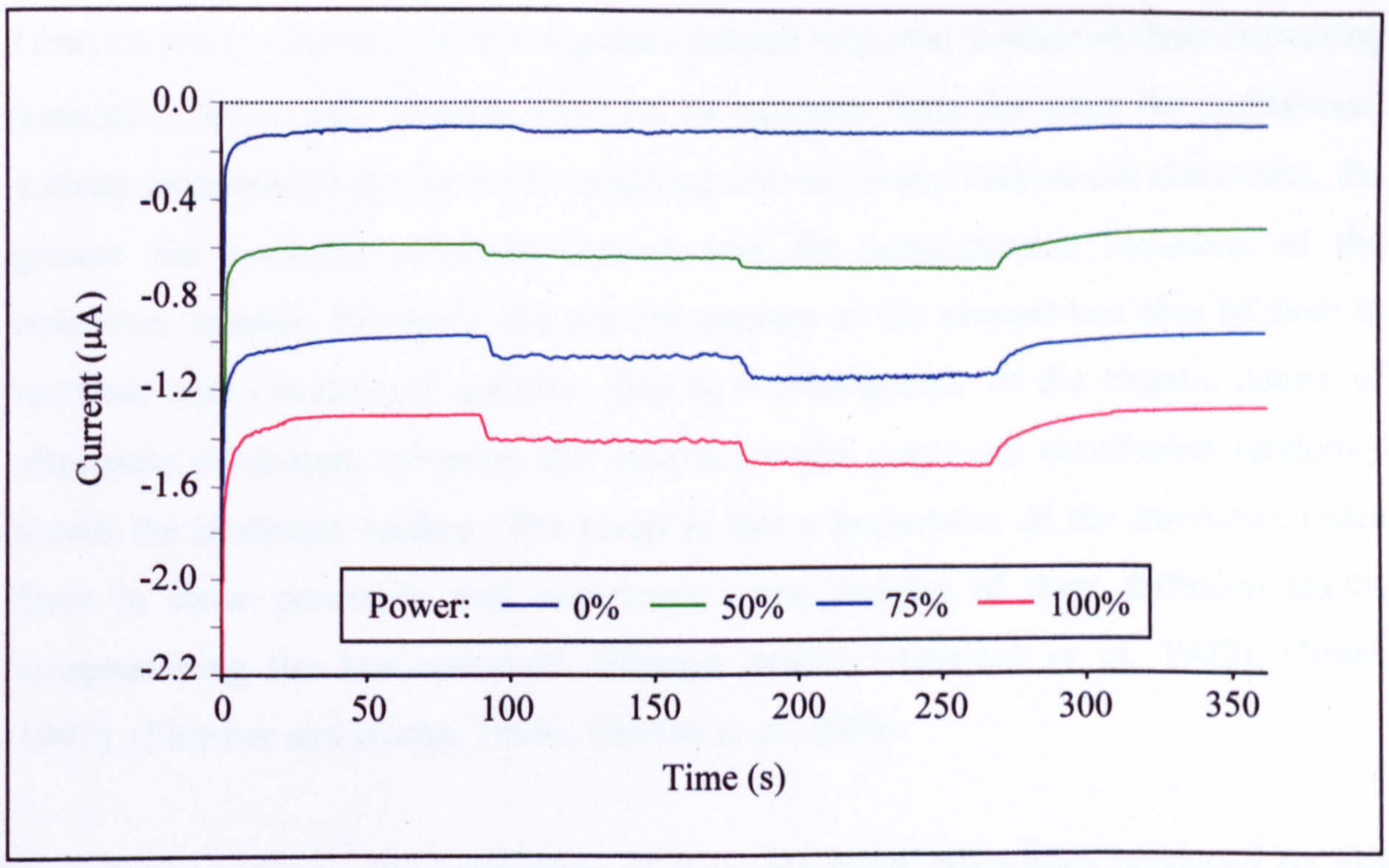

Figure 6.36: Stir-independent characterisation of PoPD modified screen printed carbon-ink electrodes ultrasonically ablated for 10 seconds at various power levels (1mM hexaammineruthenium(III) chloride polarised at -350 mV)

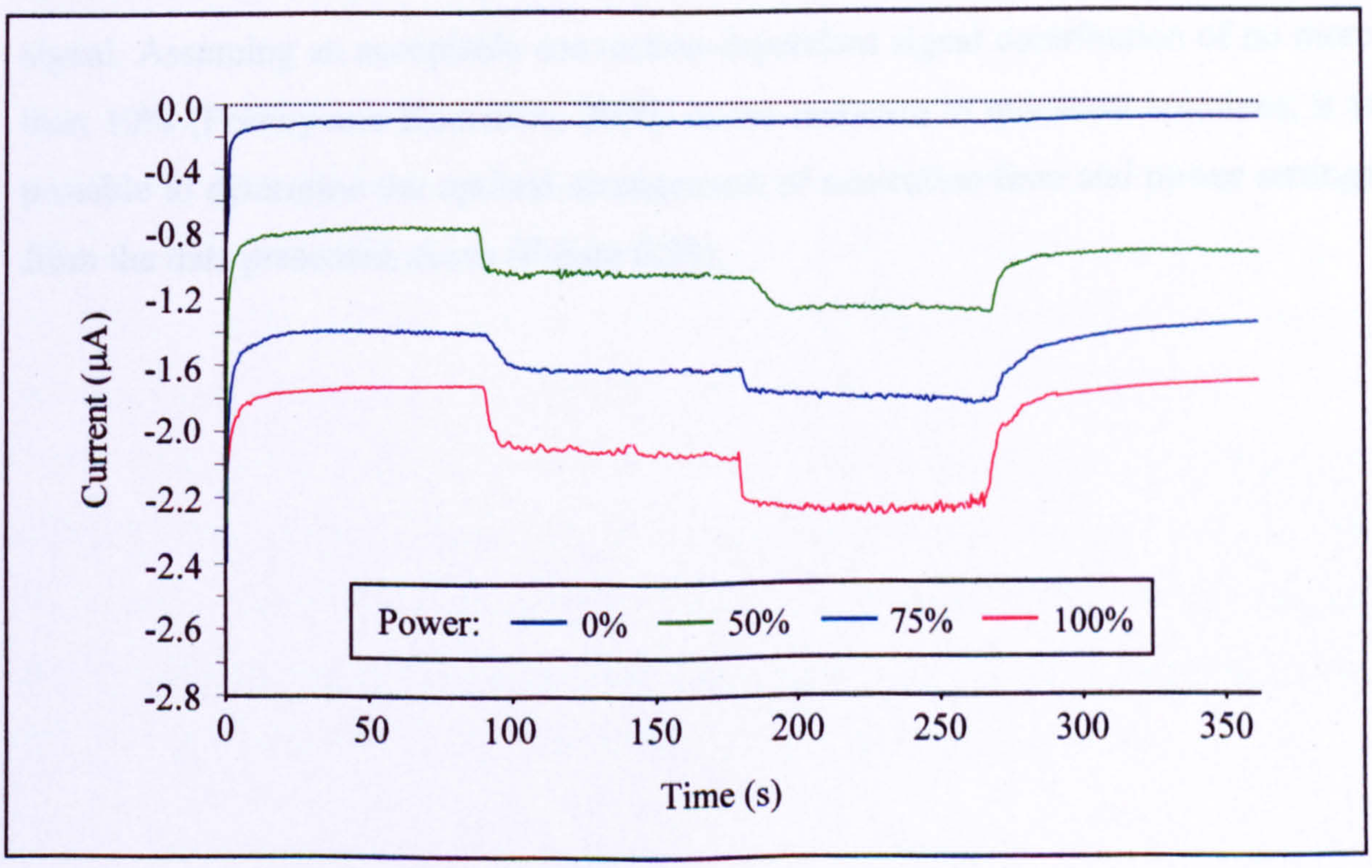

Figure 6.37: Stir-independent characterisation of PoPD modified screen printed carbon-ink electrodes ultrasonically ablated for 15 seconds at various power levels (1mM hexaammineruthenium(III) chloride polarised at -350 mV)

From the data it can be seen that a greater current response is attained from increasing sonication power and duration. This can be expected since the more the cavitational activity experienced by the P*o*PD modified screen printed carbon-ink electrodes, the greater the available electrode surface area for amperometric reduction of the ruthenium species. Similarly, the stir-dependency of the sensors can also be seen to increase with cavitational activity. This is a consequence of the chaotic nature of ultrasonic cavitation, whereby the microelectrode pores are distributed randomly across the electrode surface. The result is that a proportion of the microelectrodes form in close proximity and experience some overlap of their diffusion shells, compromising the hemispherical diffusion profile (Amatore *et al*, 1983), (Morf, 1997), (Fletcher and Horne, 1999), (Barton *et al*, 2004).

In order to optimise the production of microelectrode assemblies produced by this method, a balance must be found between the magnitude of the current response, and its dependency upon solution convection. To permit the practical detection of aqueous analytes such as chlorine, a satisfactory level of stir-dependence must first be defined in order to optimise process parameters and achieve the maximum attainable signal. Assuming an acceptable convection-dependent signal contribution of no more than 10% (Feeney and Kounaves, 2000) of the response in quiescent solutions, it is possible to determine the optimal arrangement of sonication time and power settings from the data presented above (Figure 6.38).

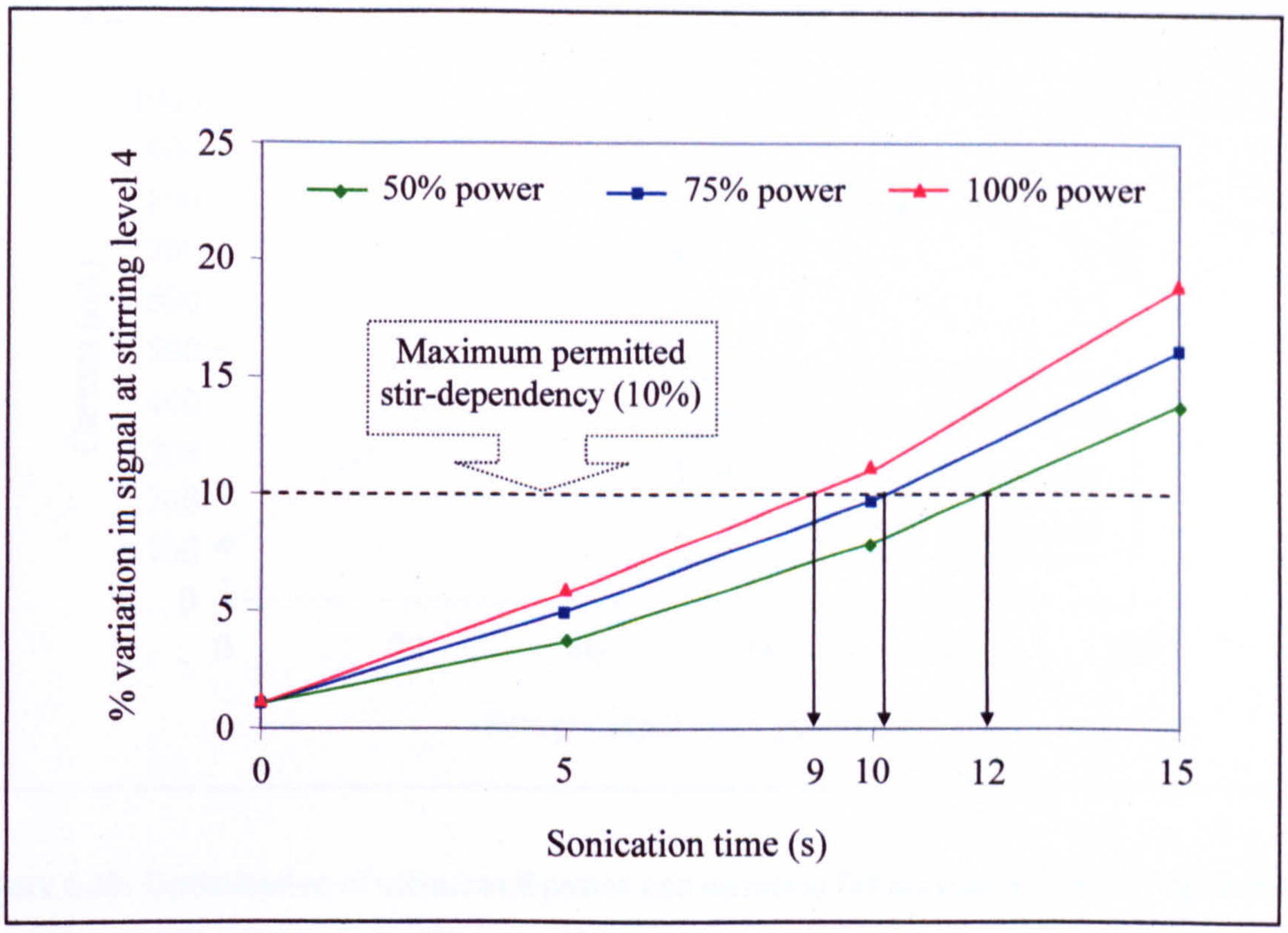

Figure 6.38: Comparison of convection-dependent signal contribution for various sonication times and powers

It can be seen that stir-dependent response increases in a linear manner with sonication time, correlating with data previously recorded within this research group (Myler, 2000), (Barton *et al*, 2004). The upper limit permissible for convection-dependent signal contribution is indicated, revealing the maximum ultrasound exposure times allowable for sonocation power ratings of 50%, 75% and 100%. These times are approximated to the nearest whole second, since at present the ultrasonic tank control software only permits the accurate regulation of exposure time from between 0 and 99 seconds in integers of one second. Figure 6.39 exhibits the current response to 1 mM hexaammineruthenium(III) chloride of sensors exposed to 50%, 75% and 100% relative power for the times identified in Figure 6.38.

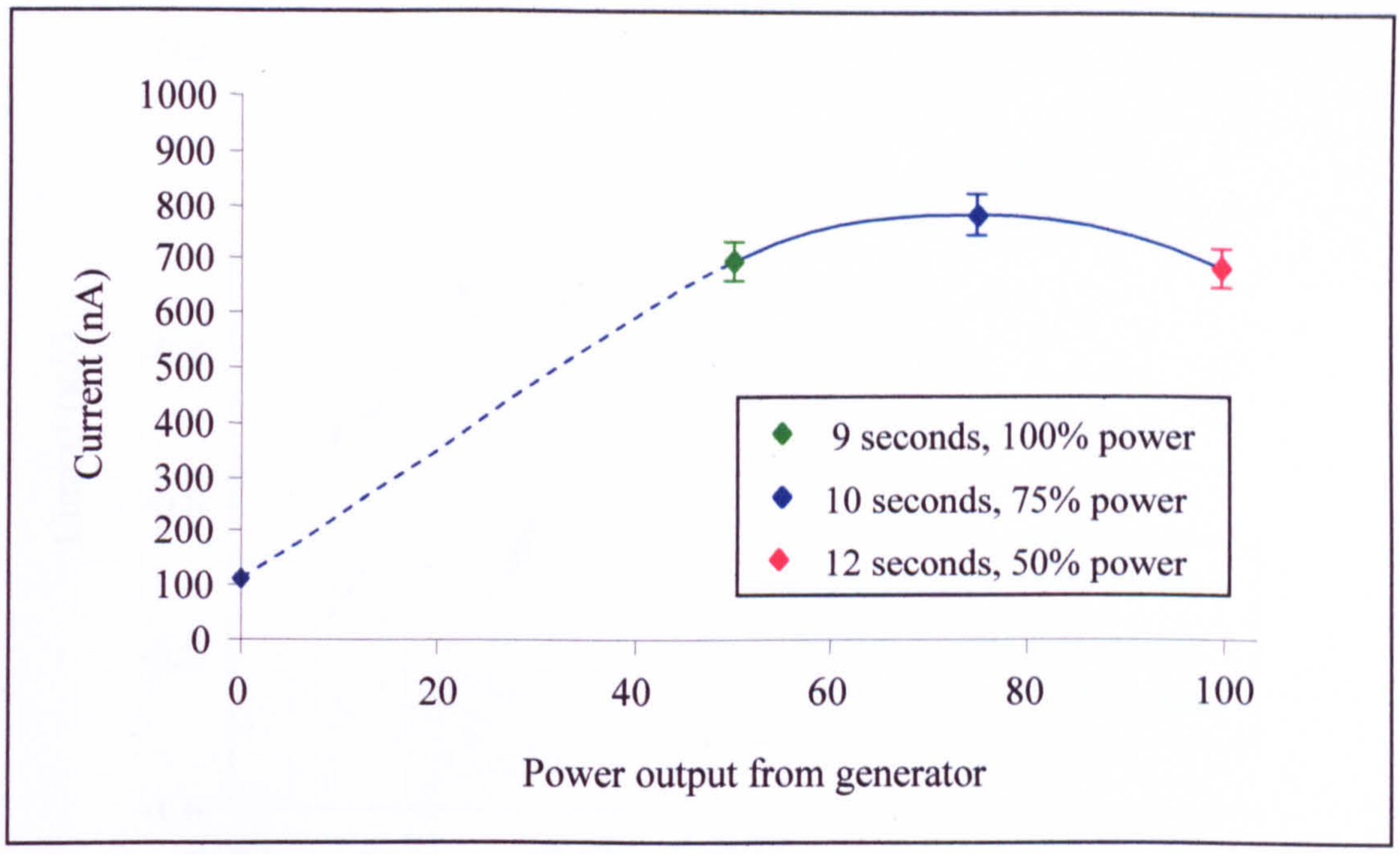

Figure 6.39: Optimisation of ultrasound power and duration for maximum sensor response at -350 mV (vs. Ag/AgCl) to 1mM hexaammineruthenium(III) chloride solution

The data indicates that 10 seconds sonication time at 75% power provides the maximum attainable signal size for an upper stir-dependent signal contribution limit of 10%. Although marginal, the differing effects of sonication power and time (whereby a longer sonication period at a lower power is not necessarily equivalent to a shorter exposure time at a higher power) relates to differences in the size and distribution of the microelectrode pores. This is because varying the acoustic amplitude not only results in a change in the strength and number of cavitational events for a given time, but also a change in the localised distribution of transient cavitation, for example bubble clustering (Crum, 1994), (Matula *et al*, 1997), (Mettin *et al*, 1999). Figure 6.40 illustrates the response to the voltammetric interrogation of microelectrode array sensors (produced via 10 seconds ultrasonic ablation at 50%, 75% and 100% power) in a 1mM hexaammineruthenium solution.

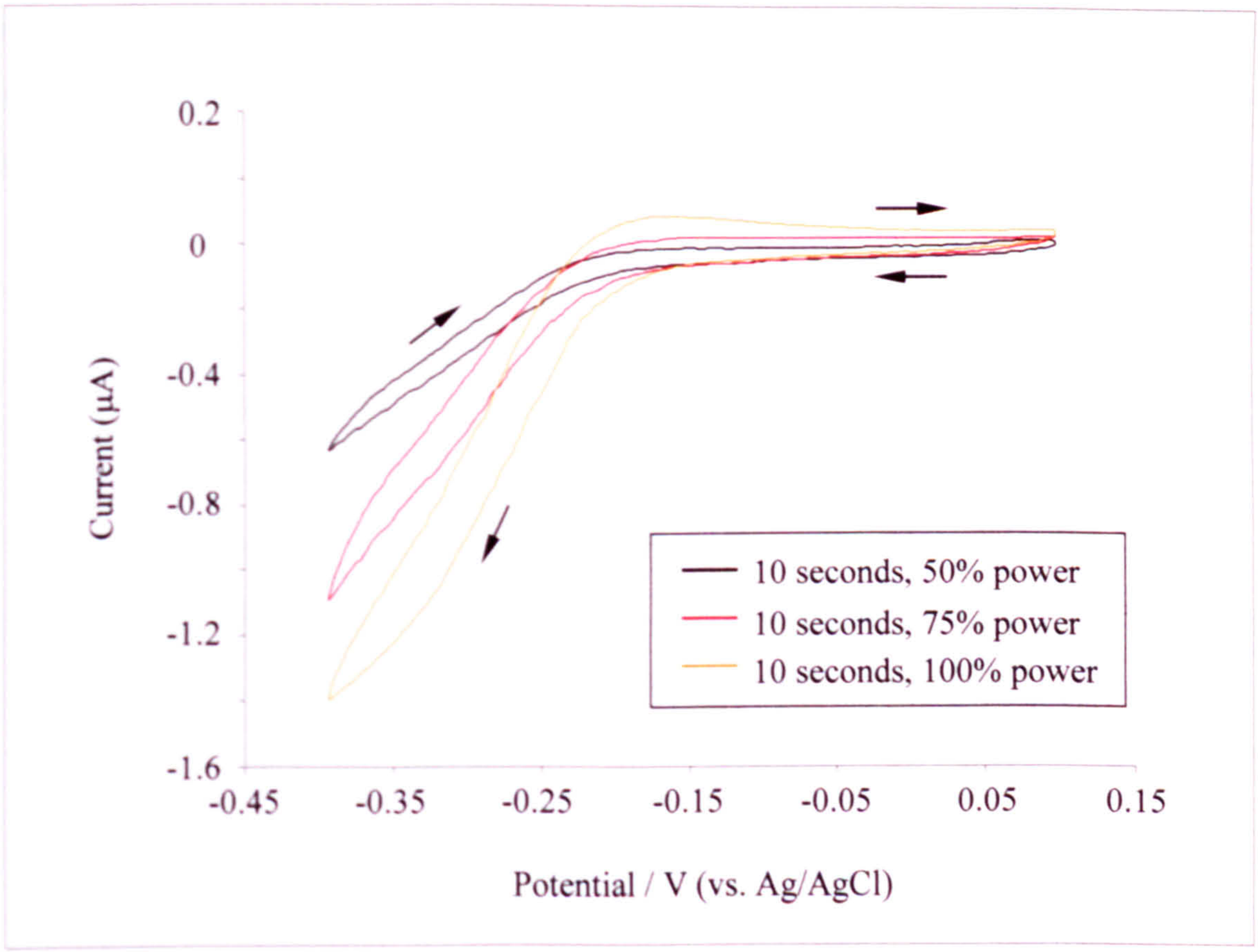

Figure 6.40: Interrogation of microelectrode array sensors via cyclic voltammetry of a 1 mM hexaammineruthenium(III) chloride solution (25 mVs^{-1})

The results display a characteristic sigmoidal sensor response for microelectrodes fabricated using 10 seconds ultrasonic ablation at 75% power. In contrast, sensors exposed to 10 seconds sonication time at 100% power exhibit a peaked response associated with diffusion-controlled mass transport. The response of sensors produced by 10 seconds sonication at 50% power also exhibit a sigmoidal response, however the current magnitude is noticeably decreased when compared to the more powerful acoustic intensities. Evidence towards the presence of a functional microelectrode array configuration is also provided by the sigmoidal current response of sensors interrogated using 1 mM hexaammineruthenium(III) chloride solution with varying sweep rates (Figure 6.41). The shapes of the voltammograms obtained were compared to those recorded using a single polished 25 µm diameter platinum microelectrode in a degassed 1 mM hexaammineruthenium solution (pH 7.8 sodium phosphate buffer, 0.1 mM KCl) (Figure 6.42). As a consequence of their extremely small surface area, the faradaic current response of single microelectrodes is easily

swamped by electrostatic noise, and so it was necessary to eliminate airborne mains interference by means of a faraday cage - with all circuits wired in a common ground plane.

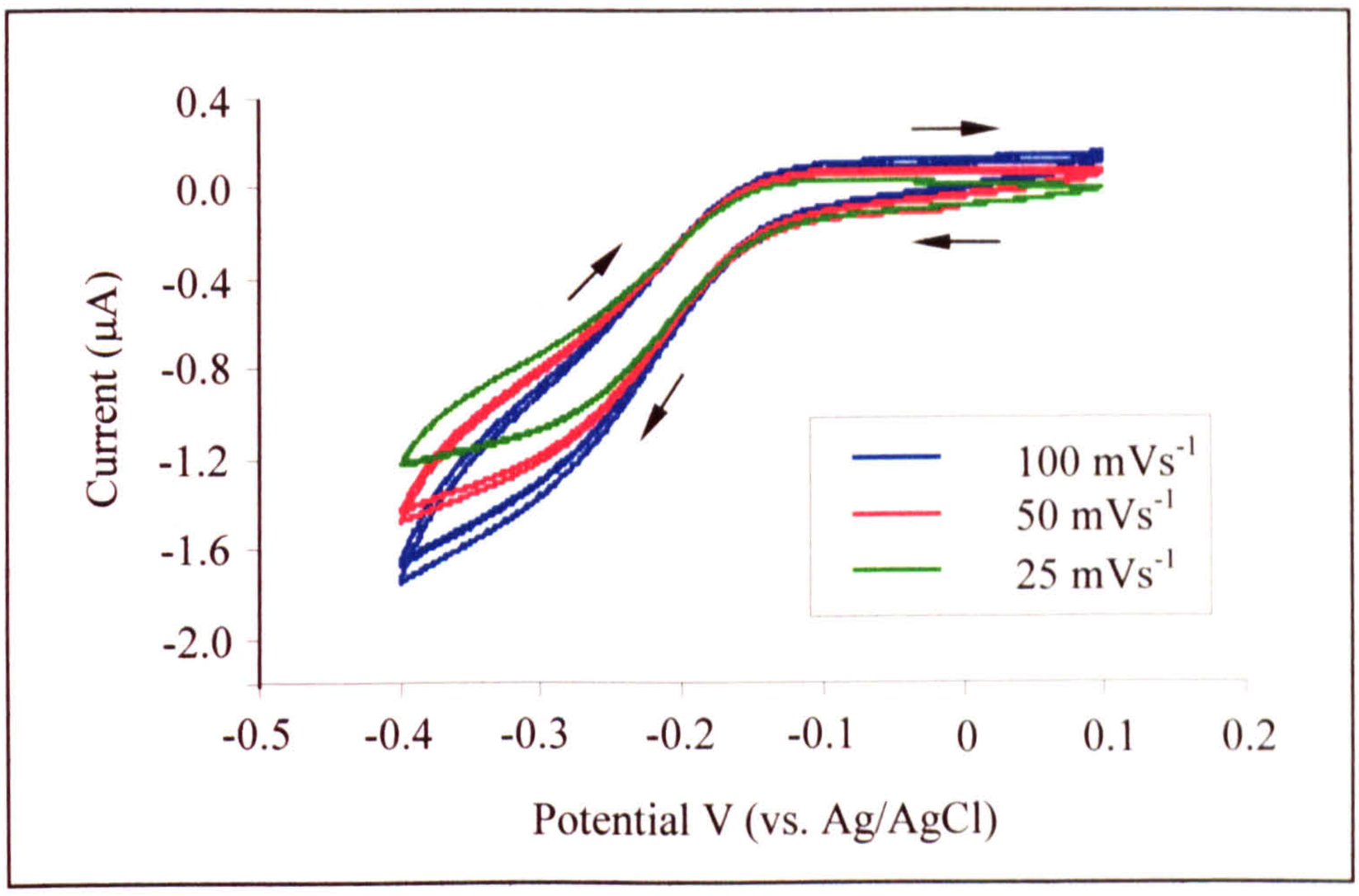

Figure 6.41: Cyclic-voltammetry of microelectrode array sensors in a range of sweep rates in 1 mM hexaammineruthenium(III) chloride

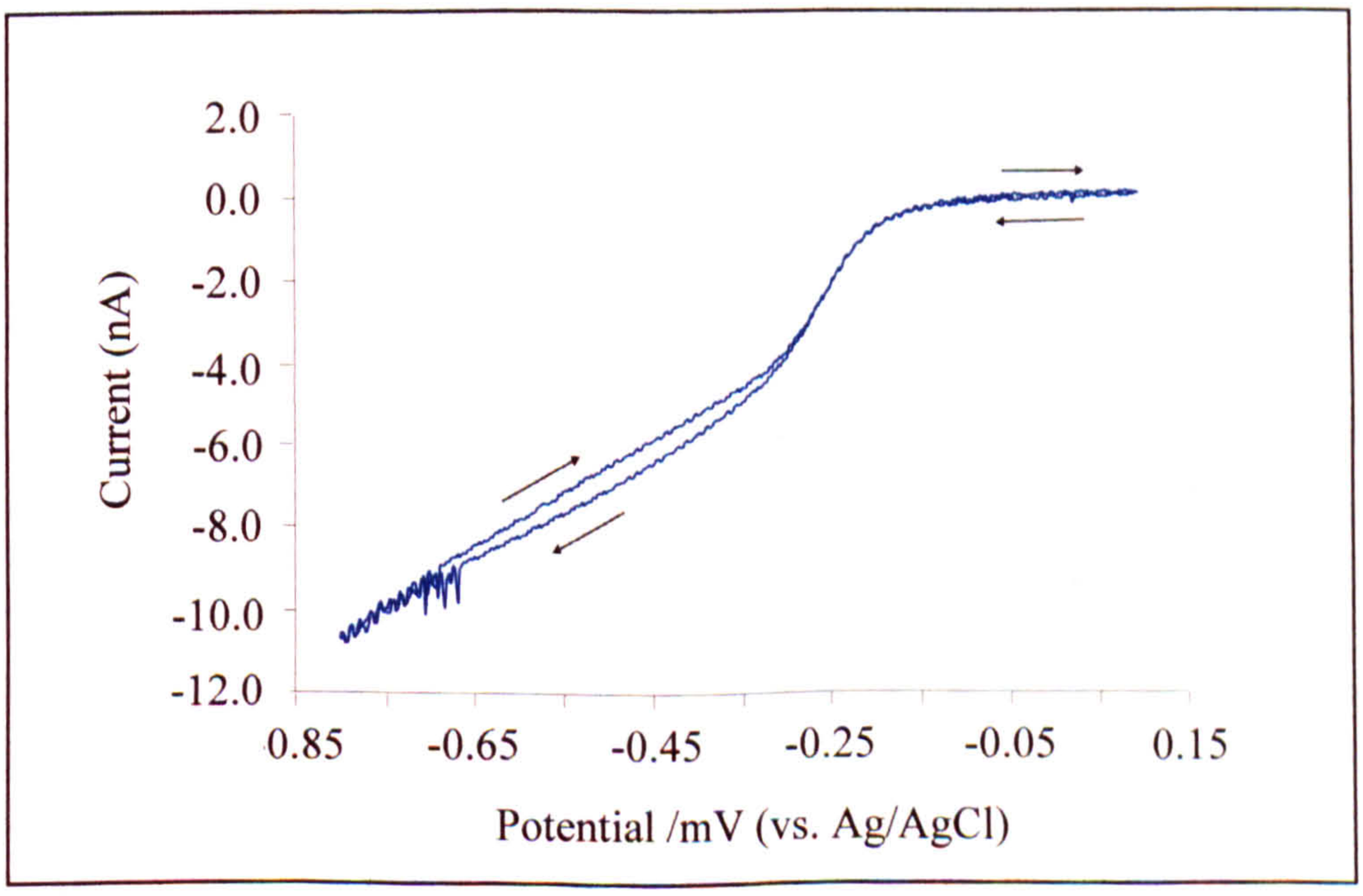

Figure 6.42: Cyclic-voltammetric response of a 25 μm diameter platinum microelectrode to 1mM hexaammineruthenium(III) chloride

It can be seen that the sigmoidal shape of the voltammogram recorded for a single platinum wire microelectrode is similar to those obtained for microelectrode array sensors manufactured via ultrasonic ablation. The separation of the forward and reverse sweeps exhibited for the case of the microelectrode array assembly is an indication of double layer charging capacitance caused by the very large numbers of microelectrode pores with our arrays (Barton *et al*, 2004). For both cases very little oxidative current can be seen to pass. The presence or lack of a reverse faradaic current relates to the concentrations of the predominant and generated redox species, their diffusion rates, the thickness and geometry of the diffusion layer and the scan rate. Therefore in this case, the greatly reduced reverse faradaic signal is indicative of good microelectrode behaviour (Lee *et al*, 2001).

6.5 Conclusions

Microelectrode array assemblies were produced on the laboratory scale via the ultrasonic ablation of poly(*o*-phenylenediamine) modified gold sputter-coated ground glass slide electrodes. Sensors were interrogated using cyclic voltammetry and chrono-amperometry in a ferri/ferrocyanide redox couple to show sigmoidal behaviour and a convection-dependent signal contribution of <6%.

As part of the scale-up for production, an industrial-sized ultrasonic tank was procured and a modulated frequency sweep introduced to enhance the uniformity of the ultrasonic field. Acoustic amplitude within the tank was then assessed using a custom-designed hydrophone, which showed some concentration of acoustic energy towards the centre of the tank. Variation in the intensity of ultrasonic cavitation was then mapped using aluminium foil test sheets and revealed the presence of node and antinodal positions associated with a standing wave field. The tank base (which acts as the emitting surface) was profiled and data shown to correlate with particular geometrical features present in the aluminium foil test sheets. A procedure for analysing the distribution of cavitational activity via the sonochemical luminescence of Luminol was developed and used to successfully expose regions of high and low

cavitational activity within the ultrasound tank, these relating to energy focused by the positioning of the ultrasonic transducers and the asymmetry in the profile of the tank base. The uniformity of the distribution of acoustic energy was then further enhanced through the development of an acoustic baffling system.

Investigations were carried out into the variation in the degree of ultrasonic ablation received by sheets of 100 poly(*o*-phenylenediamine) modified screen printed carbon-ink electrodes exposed to 10 seconds ultrasonic ablation in a fixed position (tank coordinates x = 18.75 cm, y = 56.25 cm, z = 35 cm). A significant variation in response (~8.5% RSD) was observed, indicating residual inhomogeneities in the distribution of cavitation. Furthermore, preferential transient bubble nucleation at the sharp edges of the sensor sheet was discovered, which required the construction of a mounting frame to improve the cavitational homogeneity in proximity to the edge of the sensor sheet.

To facilitate the equal exposure of the polymer modified electrodes to ultrasonic ablation, a robotics movement system was constructed which enabled the controlled movement of sensor sheets around a 30 mm radius at a rate of one revolution per sonication period. Multiple batches of 100 sensors produced with 10 seconds sonication at 75% power were shown to exhibit a low variation in amperometric response (~3.6% RSD), indicating a relatively uniform exposure to cavitational activity.

Following the success of the prototype robotics movement system, a heavy-duty steel replacement was obtained with the capability of supporting the simultaneous ultrasonic ablation of multiple sensor sheets. Initial investigations carried out into the properties of sensors produced in this environment indicated a non-ideal distribution of cavitational activity. However, future development of this aspect of sensor production, including for example a more refined ultrasonic tank construction, should permit a sufficiently uniform cavitational exposure.

The optimisation of sonication process parameters for sheets of 100 poly(*o*-phenylenediamine) modified screen printed carbon-ink electrodes for the purpose of microelectrode array production was carried out by means of electrochemical analysis. Following chronoamperometric interrogation of sensors produced at range of sonication times and powers, an upper limit for the convection-dependent signal contribution was identified (10% at stir level 4) to permit the optimisation of process variables for attaining the highest possible amperometric current response. A sonication exposure time of 10 seconds at a relative power of 75% was determined as the optimal arrangement of ultrasonic power and duration for the purpose of microelectrode sensor production. Sensors produced in this manner were then characterised via cyclic voltammetry and shown to offer good microelectrode array performance.

CHAPTER 7

Commercialisation of a new class of sensor

7.1 Introduction

To allow for the successful commercialisation of the electrochemical sensors, developed throughout the preceding chapters, consideration must be given to the marketing environment in which they will be situated. Following the identification of a primary application for Microarray Limited's generic microelectrode array manufacturing technology, key performance characteristics and value-adding features can be identified to provide a valuable competitive edge over existing colourimetry-based products. Growth in sales will raise revenue and develop brand equity, in turn encouraging successful commercialisation in other electrochemical applications.

7.2 Commercialisation of a new class of sensors: market selection and the environmental relationship

In order to successfully exploit intellectual property pertaining to the rapid, low-cost production of disposable microelectrode array sensors, it is necessary to identify a primary market to which the product should be applied. The aqueous chlorine detection industry is an attractive option, since besides offering a globally expanding market (an estimated $300 million annually), it has distinct attributes relating to the readiness for companies to adopt a new measurement technology (Hall & Hyde, 1992), (Mintel, September 2003). One aspect of particular importance is that tailoring a microelectrode base sensor towards the amperometric detection of chlorine is technically uncomplicated and does not require the use of any biological sensing elements, such as enzymes or antibodies, which would present discrete problems in terms of production, cost and sensor storage found in the pursuit of other analytical markets. Furthermore, current technologies are acknowledged as outdated by users and suppliers alike, who are at present actively seeking new technologies for portable aqueous chlorine detection (Boswell, 2001). In fact, the performance limitations of existing colourimetry based methods provide the greatest opportunity for market penetration by an electrochemical-based system, previously restricted by response

stir-dependency issues. The application of environmental monitoring of aqueous chlorine in the field, for which there is currently no cost-effective approach available to permit the enforcement of the stringent environmental regulations (now commonplace in most developed countries), is a pivotal component of the strategy to realize disposable microelectrode array sensors in their first commercial application (78/659/EEC, 1997), (2000/60/EC, 2000).

The relationship between industry and the environment is changing rapidly, and provides an excellent incentive for companies to overcome the inertia associated with their established systems for aqueous chlorine monitoring, and to adopt a new approach based on Microarray Limited sensor technology. Business expert Michael Porter suggested that stricter environmental regulation may have a positive effect on a company's performance by stimulating innovations (Porter, 1991), (Porter & van der Linde, 1995a), (Porter & van der Linde, 1995b). He argues that properly designed environmental regulation can trigger innovation that may partially or more than fully offset the costs of complying with them, and may even lead to absolute advantages over foreign competitors. This relationship is based to some degree on pollution being a manifestation of economic waste. Energy and materials, which have an associated cost, are lost into the environment during production. This may then go unnoticed, or ignored, until environmental regulation associates a value to the waste, prompting companies to innovate their processes and become more efficient. In the context of the aqueous chlorine analyser proposed by Microarray Limited, this reflects the savings a company could make by being able to more carefully control their use of chlorine, the price of which has been seen over recent years to increase annually due to an energy-intensive production process.

Other researchers of the period were quick to adopt the concept, that is, in some circumstances, companies can simultaneously improve their environmental performance along with their competitive position (Gore, 1992), (Walley & Whitehead, 1994). The notion of a 'win-win' scenario contradicts the traditional adversarial view of a fixed trade-off between the environment and the economy. On one side there are the social benefits gained from stricter environmental standards,

and on the other, the company's profits will suffer in sustaining prevention and cleanup costs, resulting in higher prices and reduced competitiveness. Furthermore, critics liken the proposed savings to money lining the streets, inferring that any rational company will take steps to make these profitable changes without external prompting. However, Porter argues that generally firms do not fit into a static optimisation framework. If technology, products, processes and customer needs were all fixed, then environmental regulation would certainly raise costs. In fact, companies operate in a reality of dynamic competition, constantly finding innovative solutions to pressures from customers, competitors as well as external forces such as regulation. This situation is further compounded by the continual acceleration of technology.

Key arguments proposed by Porter for the availability of potential cost savings by the adoption of innovative technologies with environmental benefit can be summarised as follows:

- Companies fail to be fully aware of potential savings; traditionally environmental protection is not a key business driver, so they won't have undertaken extensive research in this area.

- Regulation raises corporate awareness, promoting higher level and company-wide thinking.

- Regulation reduces uncertainty that environmentally favourable investments will be valuable.

In accordance with modern philosophy, chlorine regulation is following a predictable path to greater stringency, while existing technologies can already be assumed to be inadequate. In the future, the requirement for low concentration chlorine measurement is likely to increase, and as such, the risk associated with committing to a new technology which provides increased sensitivity will diminish.

Modern regulation tends to focus on outputs rather than technologies. This takes into account the likelihood that a new or emerging technology has not yet established itself as the industry *best practice* utilising *best available technology* (BAT). Sizable development grants have been generated by European and environmental regulatory bodies for the development of technology to fulfil these demands, and for the application of aqueous chlorine detection, such funds have formed a significant contribution towards Microarray Limited's start-up capital. The ability for regulation to focus upon an output requires that output to be measurable; in the case of the measurement of aqueous chlorine a lack of sensitivity in existing portable chlorine measurement instrumentation provides a window of opportunity for the Microarray Limited aqueous chlorine detection system.

Organisations that successfully anticipate the trend of environmental regulations will gain a competitive advantage. Most companies today understand the value of the "first mover's" advantage, recognising that their environmental policy contributes significantly towards their strategic position. Anticipating the speed and direction of government regulation requires an awareness of how environmental policy is changing with the times. The government, and associated regulatory bodies, are evolving towards a 'goal setting approach' rather than a driver of specific policy responses (Esty & Chertow, 1997). In fact, with the popularity of regulatory 'guidelines', product differentiation based on environmental variables becomes ever more effective. The increased perceived value of 'environmentally friendly' products and services is often enough to considerably outweigh any additionally incurred production costs and cause a permanent change to the marketing environment, familiar examples being those of 'dolphin-friendly' tuna or 'bleach free' (low chorine) paper-based products (Lewis, 1992), (Van Dam & Apeldoorn, 1996).

Environmental considerations have therefore played an integral role in Microarray Limited's market selection, project funding, and ultimately the sensor development. The analytical technology being developed offers a powerful, cost-effective solution to the problems traditionally associated with electrochemical sensors, namely a sensitivity to the flow, or movement of the analyte. The generic sensor technology

developed here can be applied to a range of substances including alcohol, ammonia, ascorbic acid and many other significant analytes (Barton *et al*, 2004), (Myler *et al*, 2004), (Pritchard *et al*, 2004), (Myler *et al*, *Article in press*). However, the opportunities existing for a low-cost, enhanced method of aqueous chlorine detection has focused attention towards this substantial market. As such, commercial development of Microarray Limited's new class of sensor has, from the outset, been tailored towards the application of aqueous chlorine detection. Figure 7.1 illustrates some important aspects considered during the design the chlorine sensor (Brett, 2001).

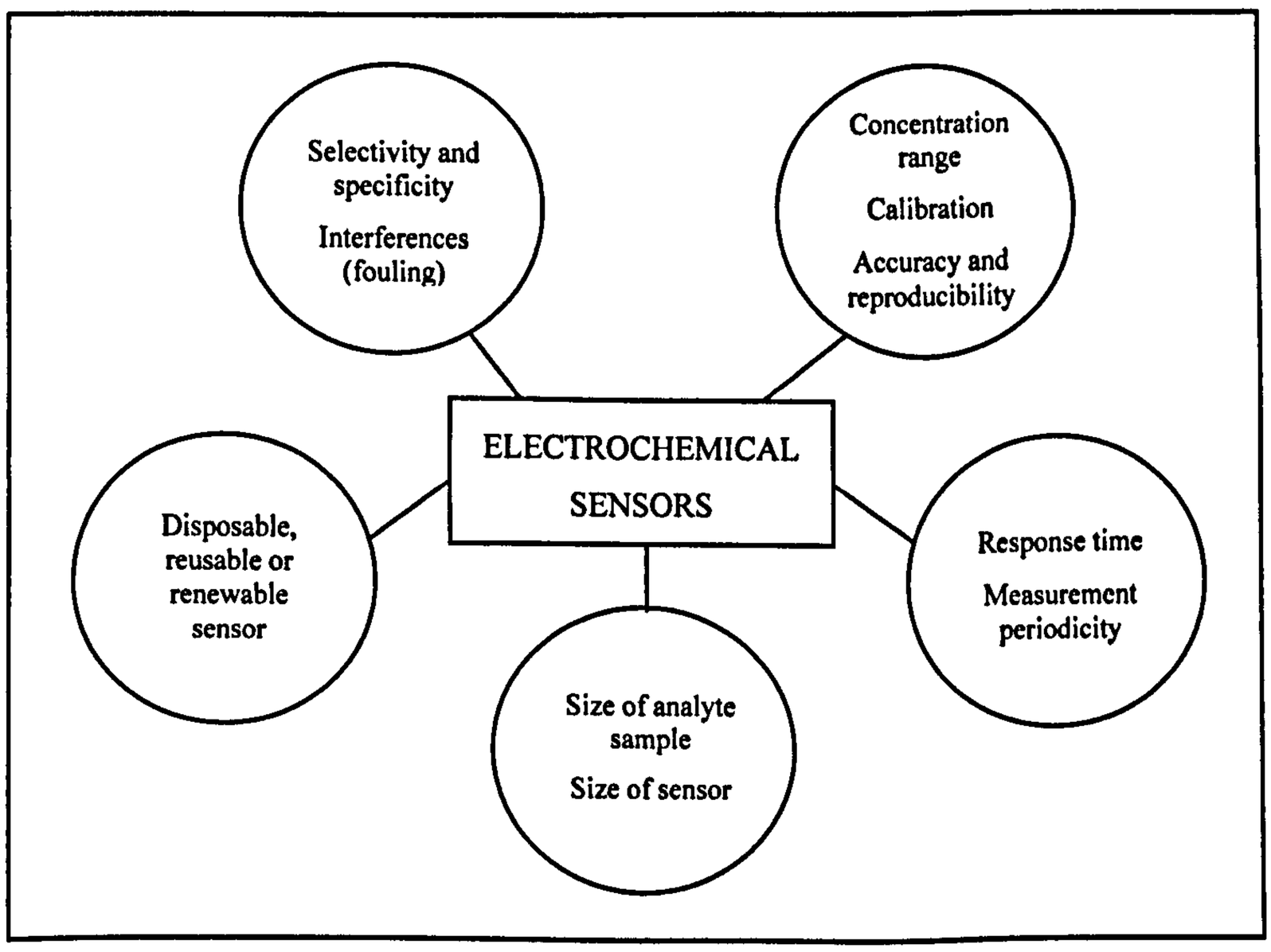

Figure 7.1: Important aspects pertaining to electrochemical sensor design (Brett, 2001)

Chlorine monitoring has been identified as an ideal vehicle for demonstrating the capabilities of this new approach for the manufacture of microelectrode array devices. Accordingly, environmental considerations have been recognised as being key to the successful commercialisation of the product, which, whilst avoiding the use of harmful chemical reagents, must also be able to provide the practical detection limit of total chlorine as low as 5 ppb.

7.3 Chemical modification layer development and sensor performance

Throughout the preceding chapters, chemical control required for the reduction of free and total chlorine (namely solution pH and the liberation of combined chlorine by reaction with potassium iodide) has been achieved by means of dispersing the relevant chemical reagents into the test solution mixture (chemistry detailed in Section 2.5, solutions detailed in Section 3.4.2). For the successful commercialisation of a rapid, reduced operator-skill portable aqueous chlorine analysis system, it is vital that all necessary chemical reagents are 'on-board' the sensor. This required the development of a depositable chemical modification layer suitable for low-cost, high volume manufacturing.

Initially, as a means of minimising production costs, a chemical modification layer to be applied in the form of a concluding screen printing operation was envisaged. Work was carried out in conjunction with Gwent Electronic Materials Limited (Pontypool, Gwent, UK) to develop a water-based emulsion layer, sufficiently viscous to enable application to sensors via screen printing methods and to confine the chemical layer at the electrode surface during use. Two types of emulsions were developed, relating to the free and total chlorine working electrodes (as depicted in Figure 4.17). The formulations of the emulsion layers developed cannot be documented as they remain confidential.

Following a number of trials it was determined that in order to permit application by screen printing, while guaranteeing reliable surface coverage, the thickness of the printed layer caused significant loss of sensor performance in terms of signal response. Consequently it was necessary to conceive a new approach for the application of an 'on-board' sensor chemical modification layer. From the previous investigations it was concluded that a low-viscosity compound would permit the deposition of a sufficiently thin layer of compound, thereby facilitating mass transportational diffusion of chlorine to the electrode surface. Following initial trials based on dip-coating and spray-coating methods, work was carried out in association with BioDot Limited (Huntingdon, Cambridgeshire, UK) to develop a unique, low

viscosity, electrode surface chemical modification system suitable for rapid, low-cost and high-volume manufacturing.

Although the exact formulations of the chemical modification layer solutions remain commercially sensitive, principle components and their functions are listed in Tables 7.1 and 7.2 for free and total chlorine formulations respectively.

Reagent	Concentration	Function
$Na_2HPO4.12H_2O$	5.6×10^{-3} M	Acid component of buffer
$NaH_2PO_4.H_2O$	4.3×10^{-3} M	Basic component of buffer
KCl	0.5 M	Electrolyte for conductivity

Table 7.1: Principle components of free chlorine chemical modification layer (pH 7.0)

Reagent	Concentration	Function
H_3PO_4	9.0×10^{-3} M	Acid component of buffer
$NaH_2PO_4.H_2O$	9×10^{-2} M	Basic component of buffer
KCl	0.5 M	Electrolyte for conductivity
KI	1 M	Liberation of combined chlorine species

Table 7.2: Principle components of total chlorine chemical modification layer (pH 4.0)

A BioDot AD3200 dispensing platform, incorporating a BioJet Plus™ 3000 dispensing system, was acquired and used to deposit the modifying layers as described in Section 3.5.10.2. An important aspect in the deposition of the total chlorine chemical layer was to minimise the oxidation of potassium iodide which occurs naturally upon dissolution in the presence of oxygen or other oxidising species. This was achieved by purging the total chlorine chemical modification mixture with argon gas for 1 hour before the addition of potassium iodide. Sensors are then processed immediately, followed by an accelerated drying period

in a convection oven for 10 minutes at 70°C. Once dried, potassium iodide regains stability. Schematic representation of the BioDot dispensing system and a photograph of the equipment during operation can be seen in Figures 7.2 and 7.3 respectively.

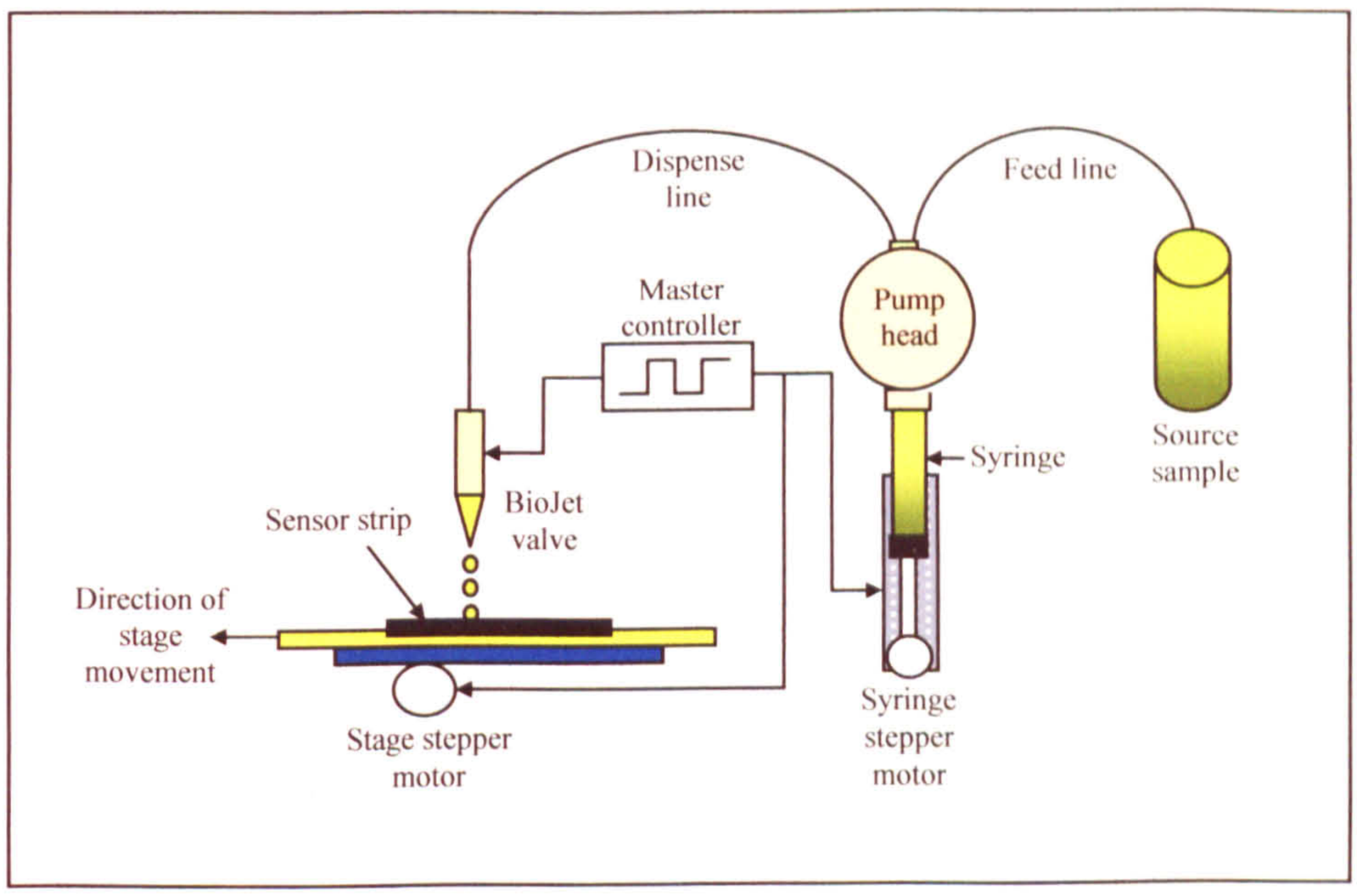

Figure 7.2: Schematic of BioDot dispensing system

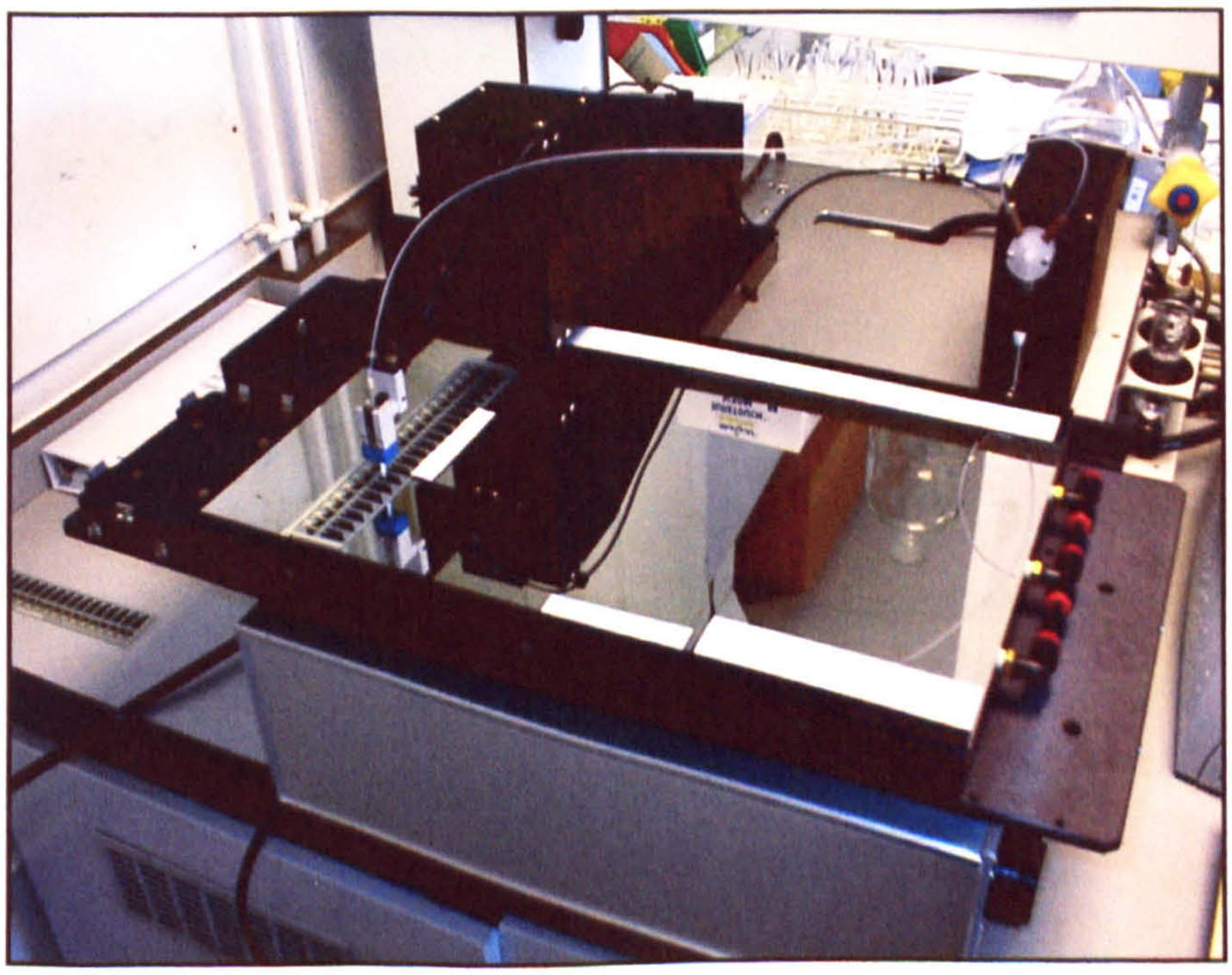

Figure 7.3: BioDot AD3200™ dispensing platform

In contrast to DPD colourimetry based methods, no toxic reagents are required to be included in the chemical modification solutions, whose role is to regulate acidity at the electrode surface and facilitate the electrochemical reduction of the species of interest. A schematic of the final sensor construction is displayed in Figure 7.4.

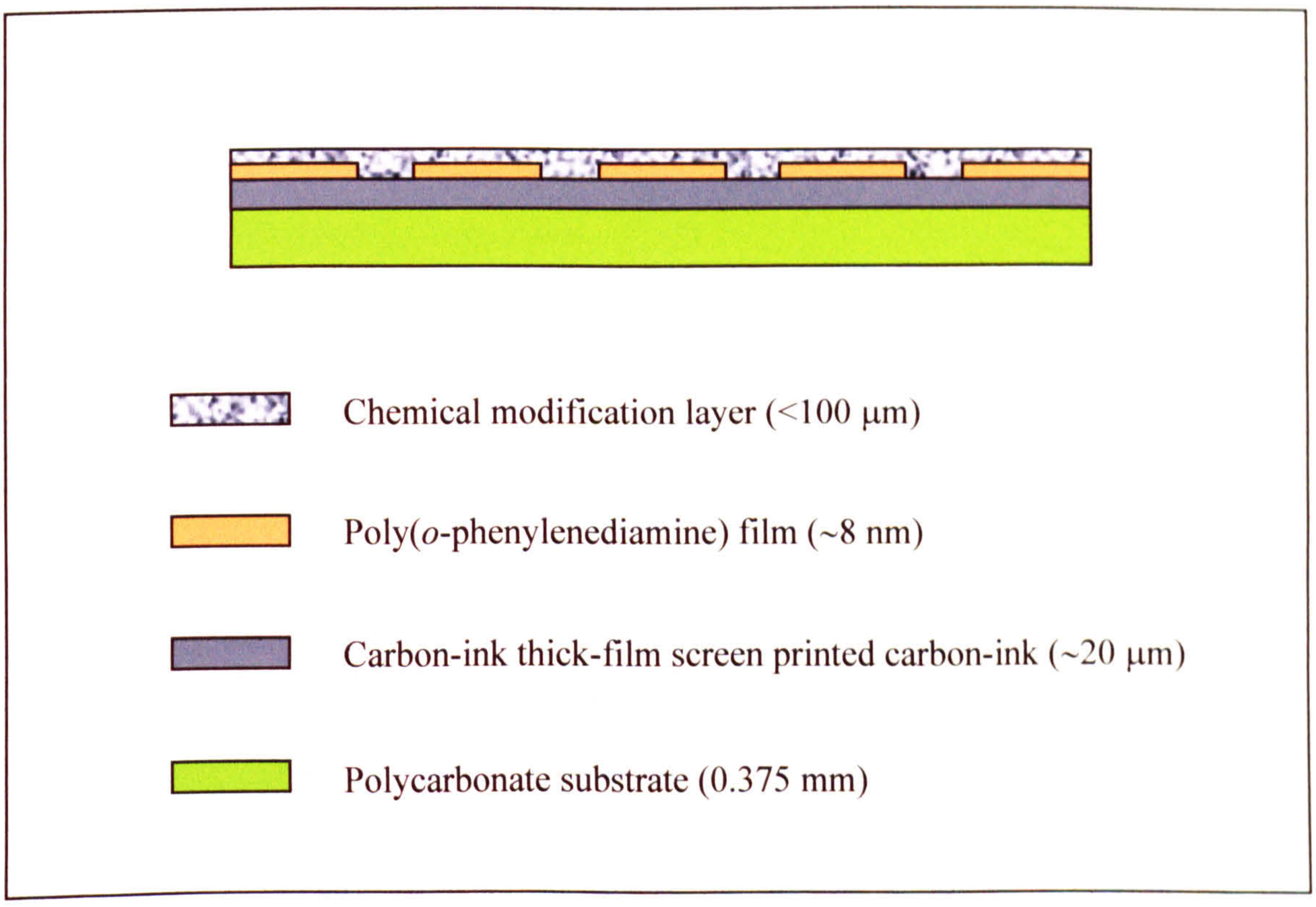

Figure 7.4: Schematic of final sensor construction

Following the finalisation of sensor construction it became necessary to determine the range of amperometric responses from 0 to 20 ppm free and total chlorine in order to provide calibration data for the Microarray Limited portable chlorine measurement instrument (described in Section 7.4). Figures 7.5 and 7.6 exhibit calibration profiles obtained for total chlorine solutions interrogated with BioDot modified microelectrode array sensors (concentrations of 0, 0.01, 0.02, 0.03, 0.05, 0.1, 0.2, 0.5, 1, 2, 5, 10 and 20 ppm). Given the range of the current responses obtained, data is presented in low- and high-range calibration curves. Error bars represent the relative standard deviation (RSD) from the 5 sensors taken at each chlorine concentration.

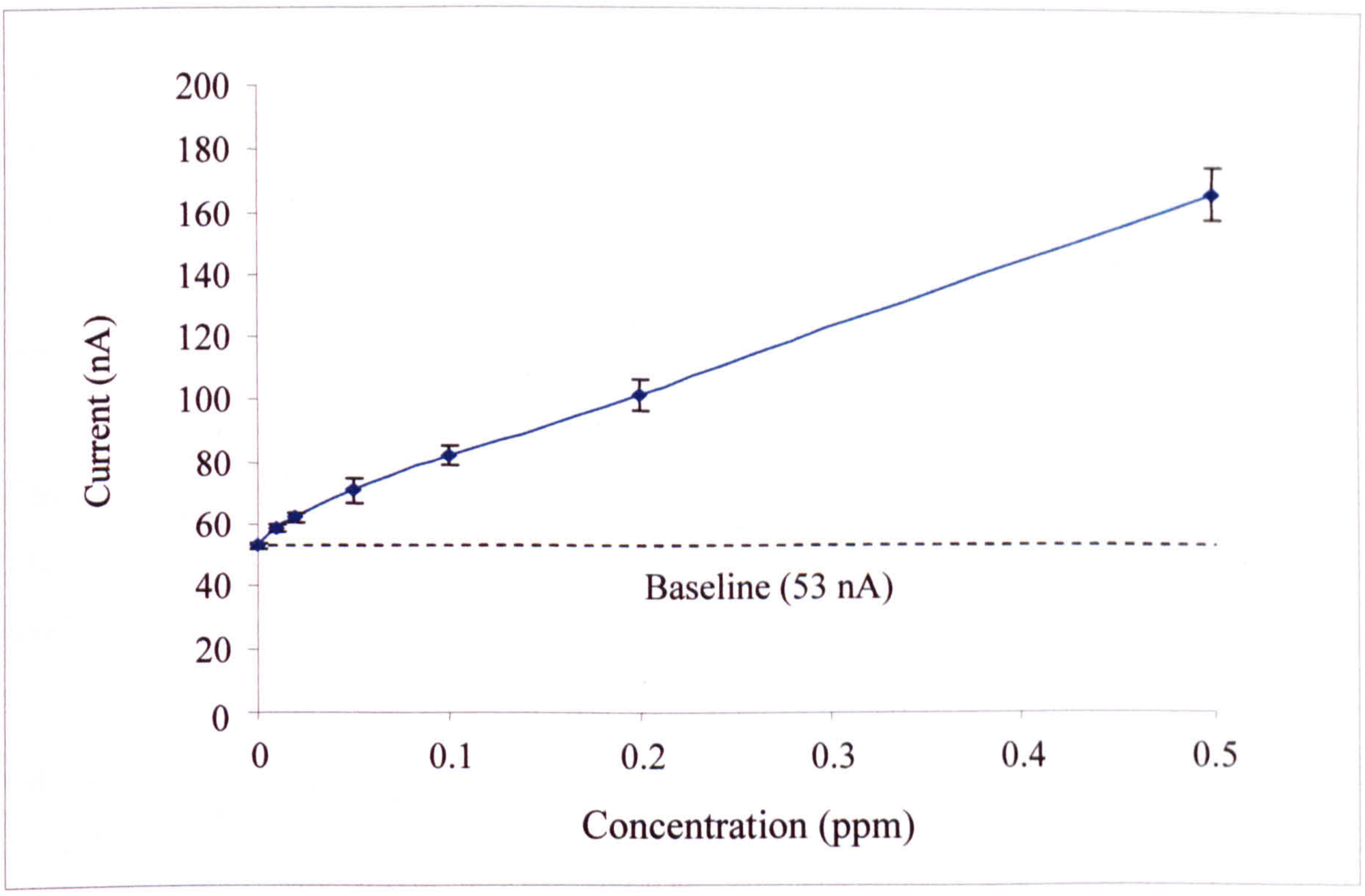

Figure 7.5: 'Low' range total chlorine calibration curve from 0 to 0.5 ppm (mean RSD 4.1%)

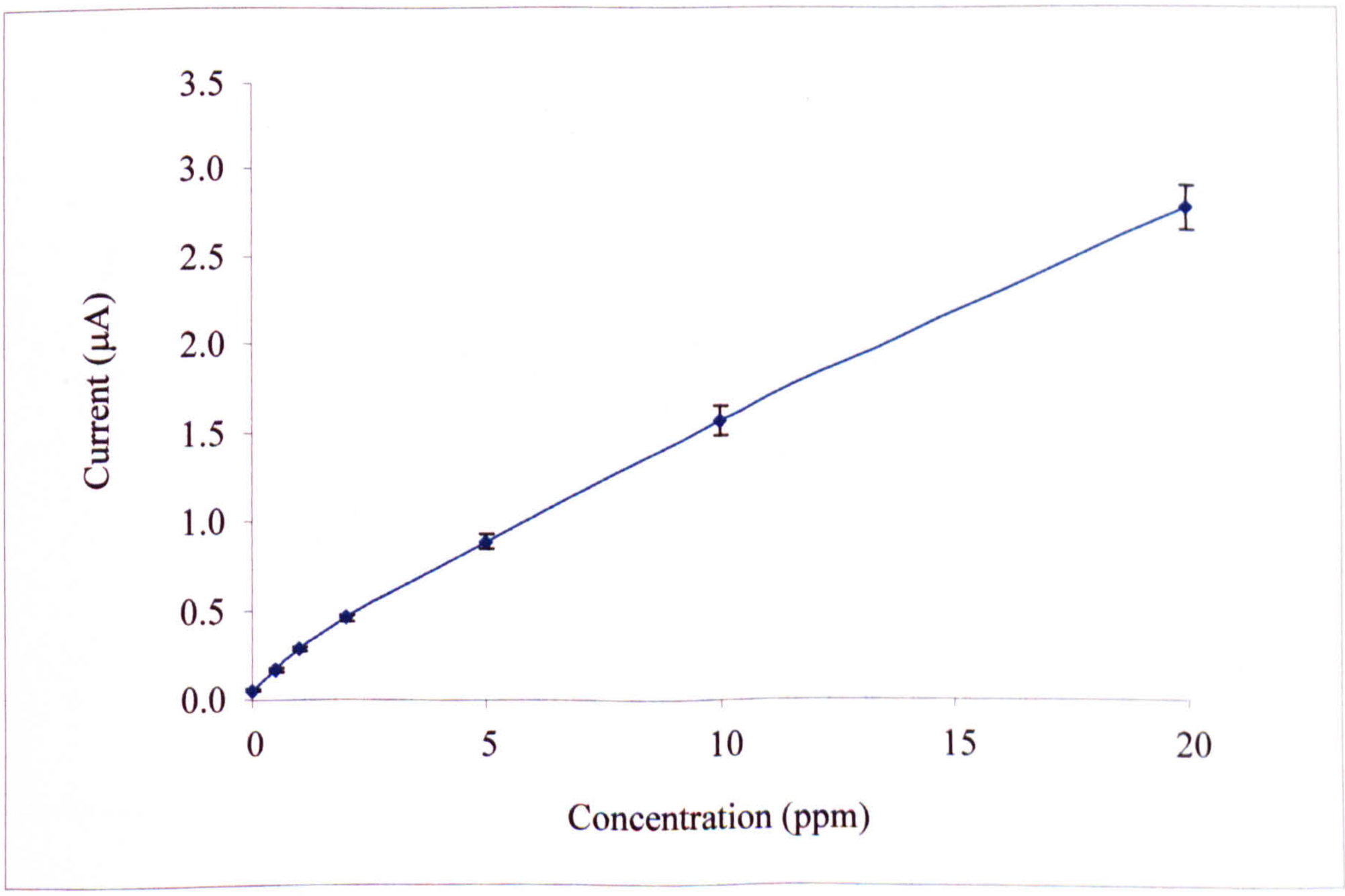

Figure 7.6: 'High' range total chlorine calibration curve from 0 to 20 ppm (mean RSD 4.3%)

The full sensor calibration data exhibits a quasi-linear response to total chlorine solutions, resulting in diminishing escalation in response with increasing concentration. A response of approximately 3 nA per 0.01 ppm for low range total chlorine and 1 nA per 0.01 ppm for high range concentrations was obtained, sufficiently large to permit the differentiation of 0.01 ppm total chlorine resolution as specified in Section 4.3.

The unusually large baseline signal of approximately 53 nA indicated for the 0 ppm total chlorine is the result of oxidised iodide present in the chemical modification layer, formed during processing.

Figures 7.7 and 7.8 exhibit calibration profiles for concentrations of 0, 0.02, 0.05, 0.1, 0.2, 0.3, 0.5, 1, 2, 5, 10, and 20 ppm free chlorine interrogated with modified screen printed carbon-ink based microelectrode array sensors.

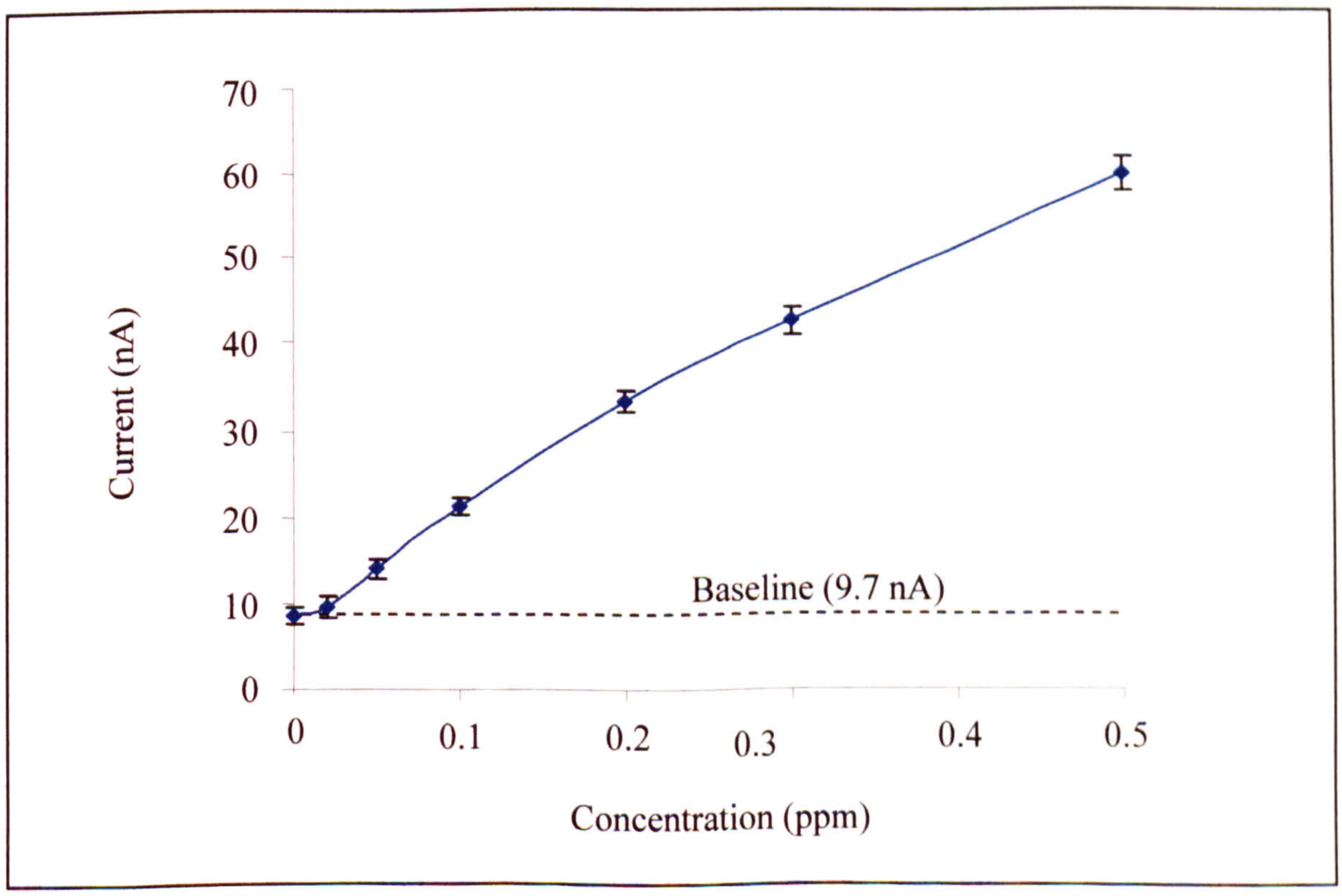

Figure 7.7: 'Low' range free chlorine calibration curve from 0 to 0.5 ppm (mean RSD 3.8%)

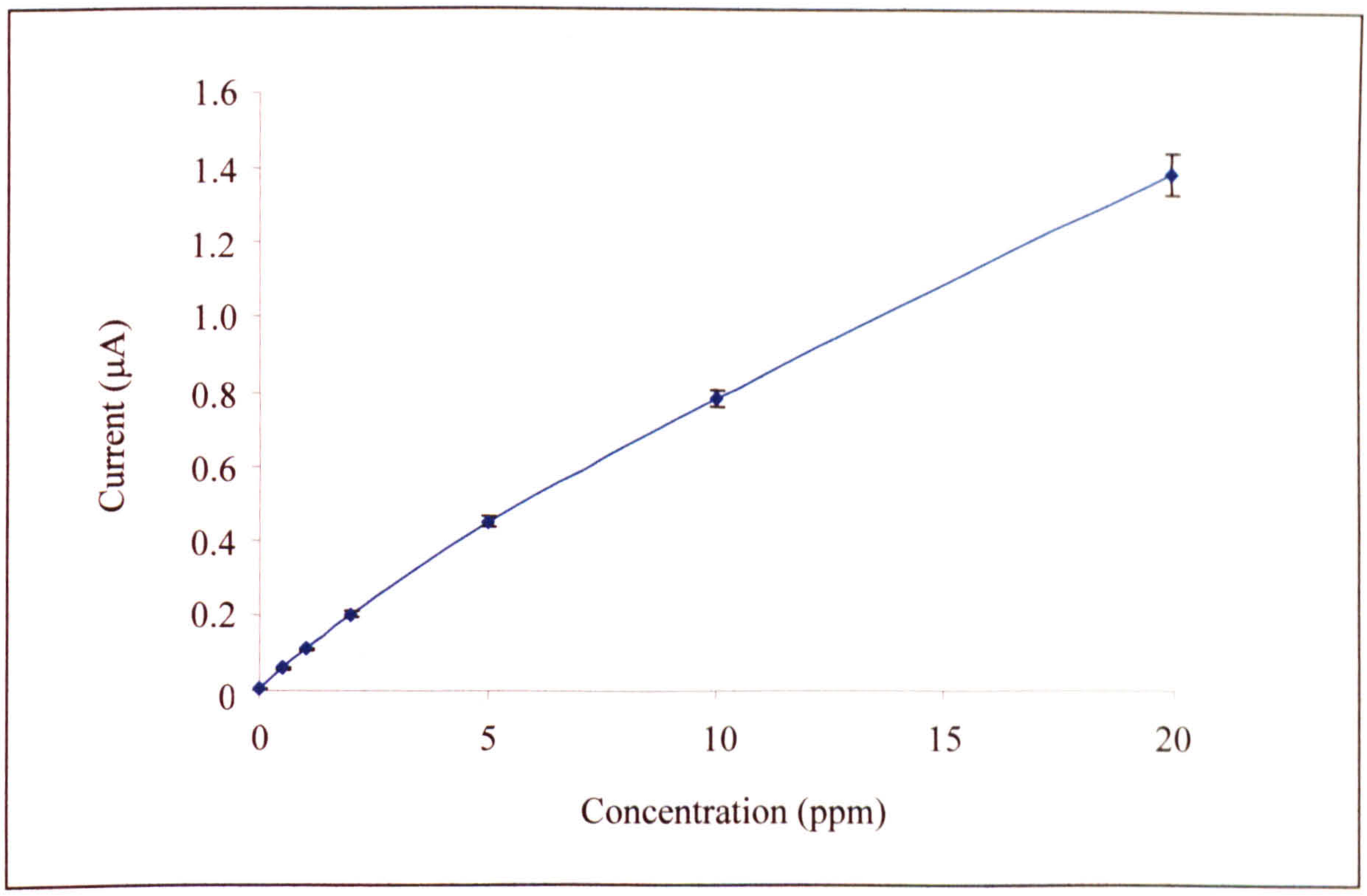

Figure 7.8: 'High' range free chlorine calibration curve from 0 to 20 ppm (mean RSD 4.2%)

Once again, a quasi-linear calibration profile is obtained for the BioDot modified microelectrode arrays sensors with a response of approximately 2 nA per 0.02 ppm increment for low range free chlorine and 1 nA per 0.02 ppm for high range concentrations. A much lower background current of approximately 10 nA is obtained in this case since there are no electroactive constituents present in the free chlorine chemical modification layer. As expected, there is a considerably smaller amperometric response for free chlorine when compared to the total chlorine response (Section 4.3). However, for the case of chemically modified microelectrode array sensors being interrogated in this instance, the decrease is greater than that predicted during determination of the electrode area requirements (Section 4.3) and may require further sensor development to attain the necessary sensor responses to remain competitive in the aqueous chlorine detection marketplace.

The signal deficiency for free chlorine detection is confirmed by the calculation of the minimum detection limit, x_L (Equation 7.1) (IUPAC, 1997b).

$$x_L = \overline{x_{bl}} + ks_{bl} \qquad 7.1$$

where x_{bl} is the mean background current recorded for 10 replicate measurements of 0 ppm free chlorine, s_{bl} is the standard deviation of the values obtained and k represents the confidence level desired. Assuming a satisfactory confidence interval of 0.95 (which assumes an accuracy of 5% relative standard deviation), k can be approximated to 1.95996 (Townend, 2002).

The results indicate a limit of detection of approximately 10.5 nA, equating to a free chlorine concentration of 0.03 ppm and falling short of the original target for a free chlorine detection limit of 0.02 ppm. In comparison, a limit of detection of approximately 56 nA can be calculated for total chlorine measurement, which permits the reliable detection of a concentration of 0.01 ppm. This can be extended to 5 ppb for environmental monitoring applications by combining both working electrodes for the pursuit of total chlorine measurement. It is noted that following the amalgamation of the chemically modified microelectrode array sensors with the finalised Microarray Limited portable chlorine analysis instrument, limits of detection will be re-defined using the 'method detection limit' approach, which encompasses all operational variables associated with sample preparation, operating technicians and equipment involved in attaining a measurement (EPA-821-R-03-005, February 2003).

7.4 Sensitivity to electrochemical interferents

A central component towards the validation of a portable chlorine analyser system is the effect of interferents on the sensor response. Electrochemical methods of analysis possess inherent advantages to the detection of analyte when compared to photometric (colourimetric) based approaches. Current portable aqueous chlorine

analysers require the addition of a reagent (known as DPD) which reacts with chlorine to produce a colour change. Photometric absorption of a light-source passing through the sample is used to quantify the degree of colour change and estimate chlorine concentration. Natural waters invariably contain suspended solid materials (termed *sample turbidity*), influencing photometric absorption and so affecting the measured output. Electrochemical methods remain unaffected and so are essentially 'blind' to sample turbidity, offering a fundamentally superior approach to the accurate measurement of aqueous chlorine. However, in order to gain a competitive advantage over existing products, it is important that the new system is not adversely affected by other, potentially electroactive, materials present in the water sample. Of primary interest are the common metal species present in natural waters, listed in Table 7.3 (Stumm & Morgan, 1996), (Rúriková & Kunáková, 1999), (Muñoz & Palmero, 2004).

Metal	Common species
Zinc(II)	ZN^{2+}, $ZnCO_3$
Cadmium(II)	Cd^{2+}, $CdCO_3$
Cobalt(II)	Co^{2+}, $CoCO_3$
Nickel(II)	Ni^{2+}, $NiCO_3$
Lead(II)	Pb^{2+}, $PbCO_3$
Copper(II)	$CuCO_3$, $Cu(OH)_2$
Mercury(II)	$Hg(OH)_2$
Aluminium(III)	$Al(OH)_{3(s)}$, $Al(OH)^{2+}$, $Al(OH)^{4-}$
Iron(III)	$Fe(OH)_{3(s)}$, $Fe(OH)^{2+}$, $Fe(OH)^{4-}$
Manganese (IV)	$MnO_{2(s)}$
Arsenic(V)	$HasO_4^{2-}$
Selenium(VI)	SeO_4^{2-}

Table 7.3: Metal species in natural fresh waters

The reduction of these species at the electrode surface would constitute a false signal and affect the reliability of the final reading displayed by the chlorine analyser. The standard electrode potentials for free metal ions present in natural waters are listed in Table 7.4.

Reaction	Standard Potential, E^0 (vs. Ag/AgCl)
$Zn^{2+} + 2e^- = Zn_{(s)}$	-0.98 V
$Cd^{2+} + 2e^- = Cd_{(s)}$	-0.62 V
$Co^{2+} + 2e^- = Co_{(s)}$	-0.50 V
$Ni^{2+} + 2e^- = Ni_{(s)}$	-0.47 V
$Pb^{2+} + 2e^- = Pb_{(s)}$	-0.35 V

Table 7.4: Standard electrode potentials (ionic strength of 1 M at 25°C)

It can be seen that the electrochemical reduction of common metal ions present in water is thermodynamically unfavourable at the reduction potentials employed for free and total chlorine analysis (-80 and -100 mV vs. Ag/AgCl respectively). Similarly, the overpotential required to reduce metal complexes (including carbonates, phosphates and hydroxides) are greater than those employed for free and total chlorine analysis.

In addition to the presence of metals, non-metallic species could act as interferents during the electrochemical detection of chlorine. As such, it was necessary to test for the effects of monochloramine, nitrate, nitrite and ammonia on signal response to both free and total chlorine (Figures 7.9 to 7.12 respectively). In each case, 10 sensors were used for both the untreated solutions and those with interferents introduced to them. Error bars represent the standard deviation for each data set.

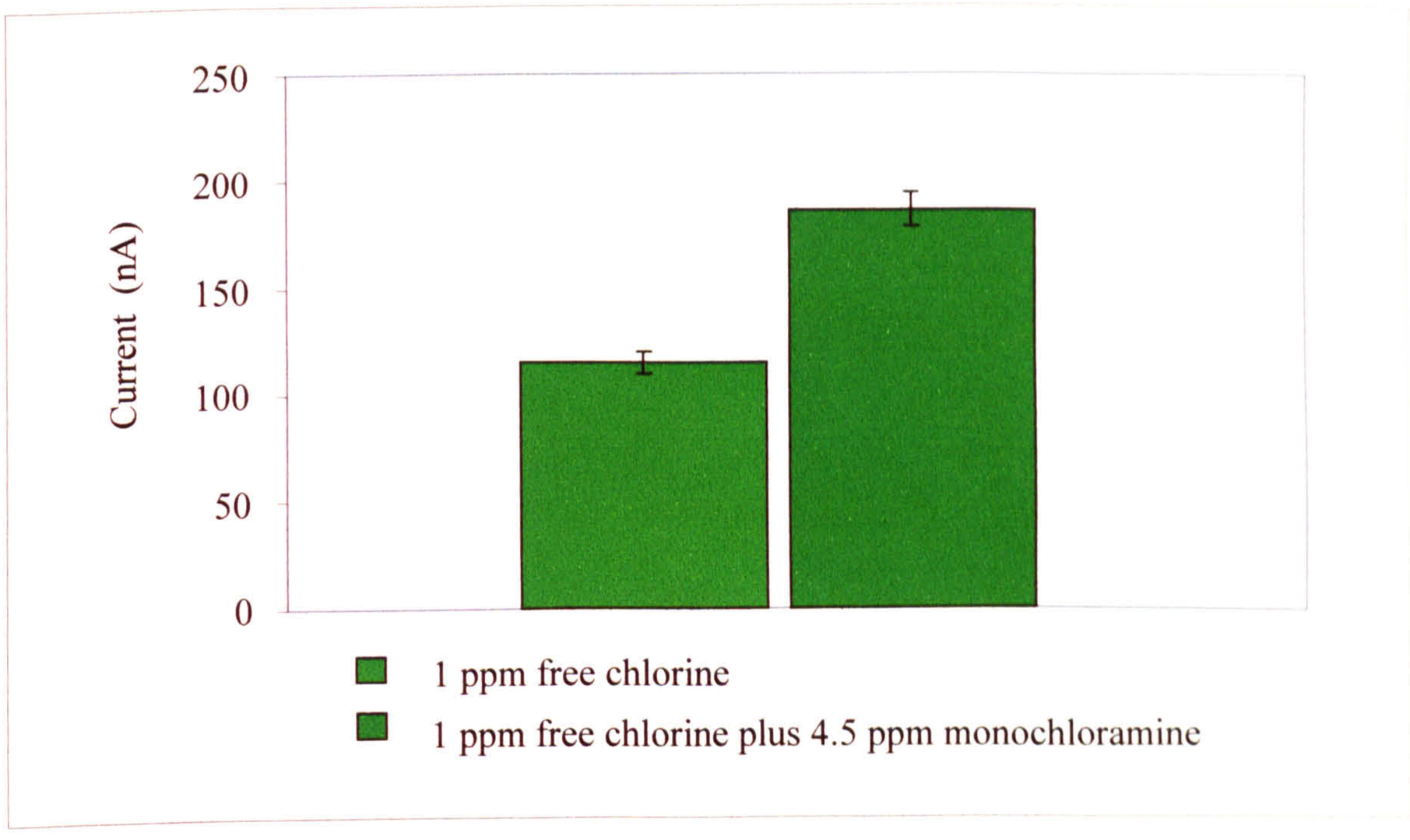

Figure 7.9: Amperometric response to free chlorine with and without monochloramine (NH_2Cl)

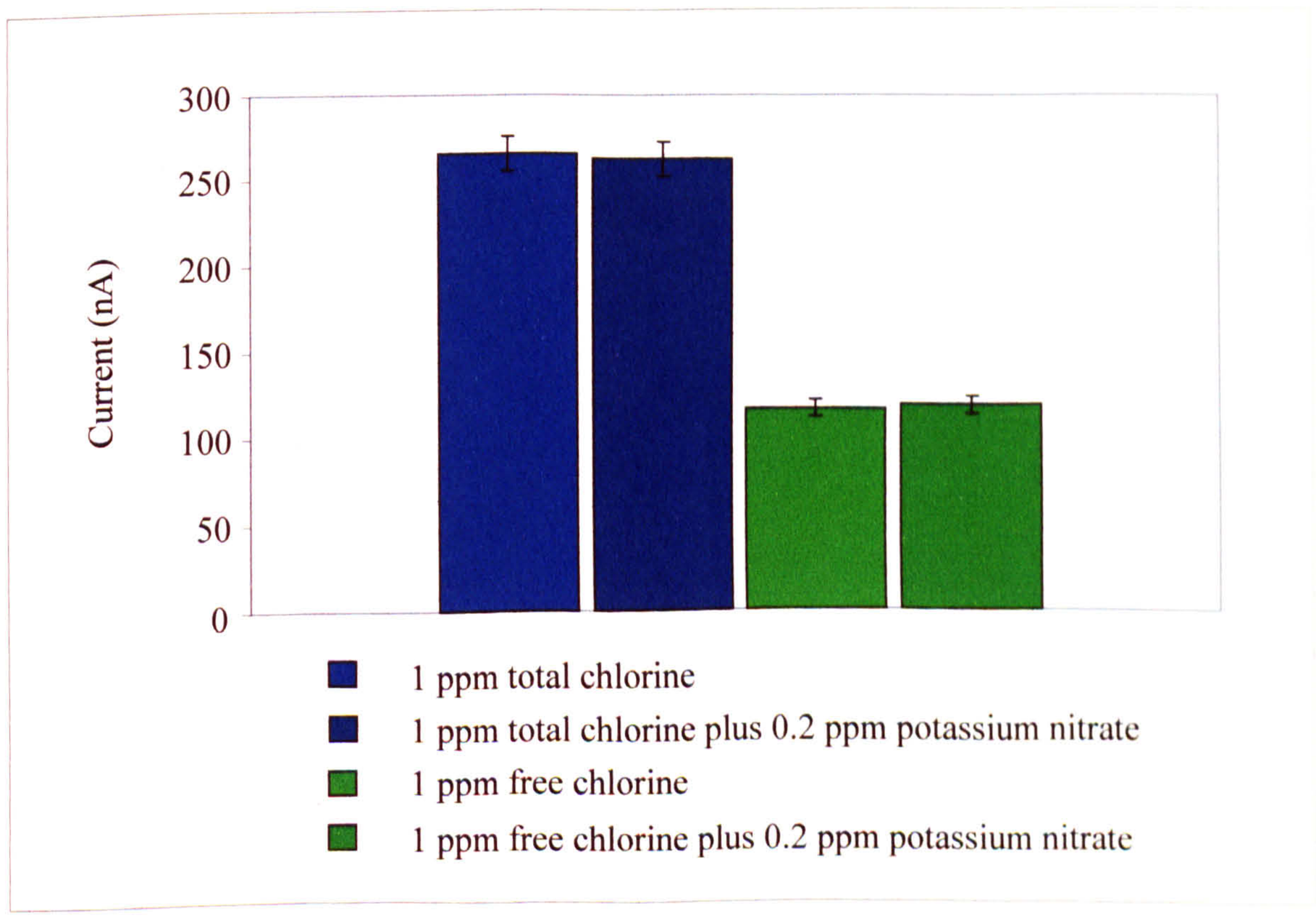

Figure 7.10: Interferent effect of nitrate (NO_3) on the measurement of free and total chlorine

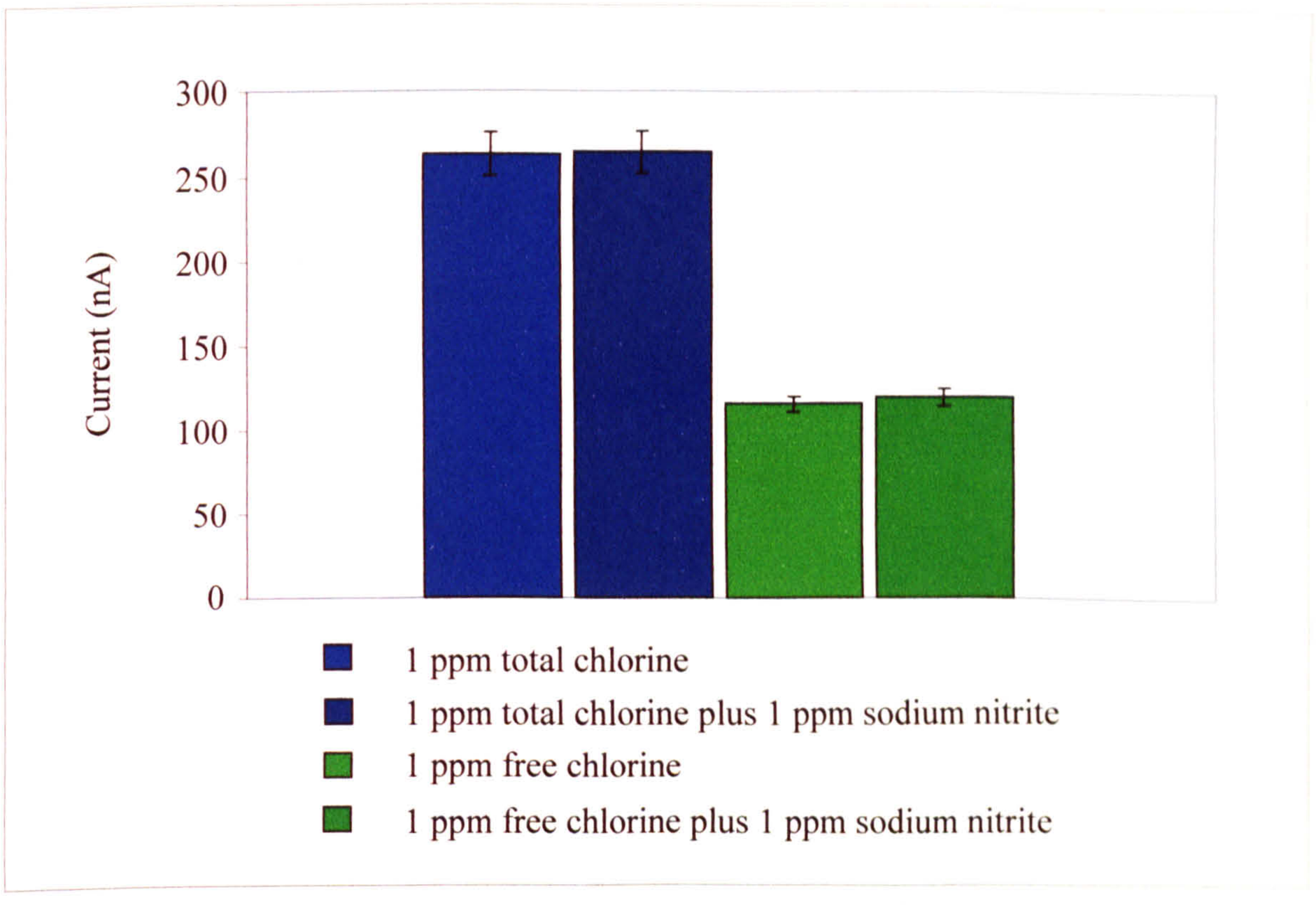

Figure 7.11: Interferent effect of nitrite (NO_2) on the measurement of free and total chlorine

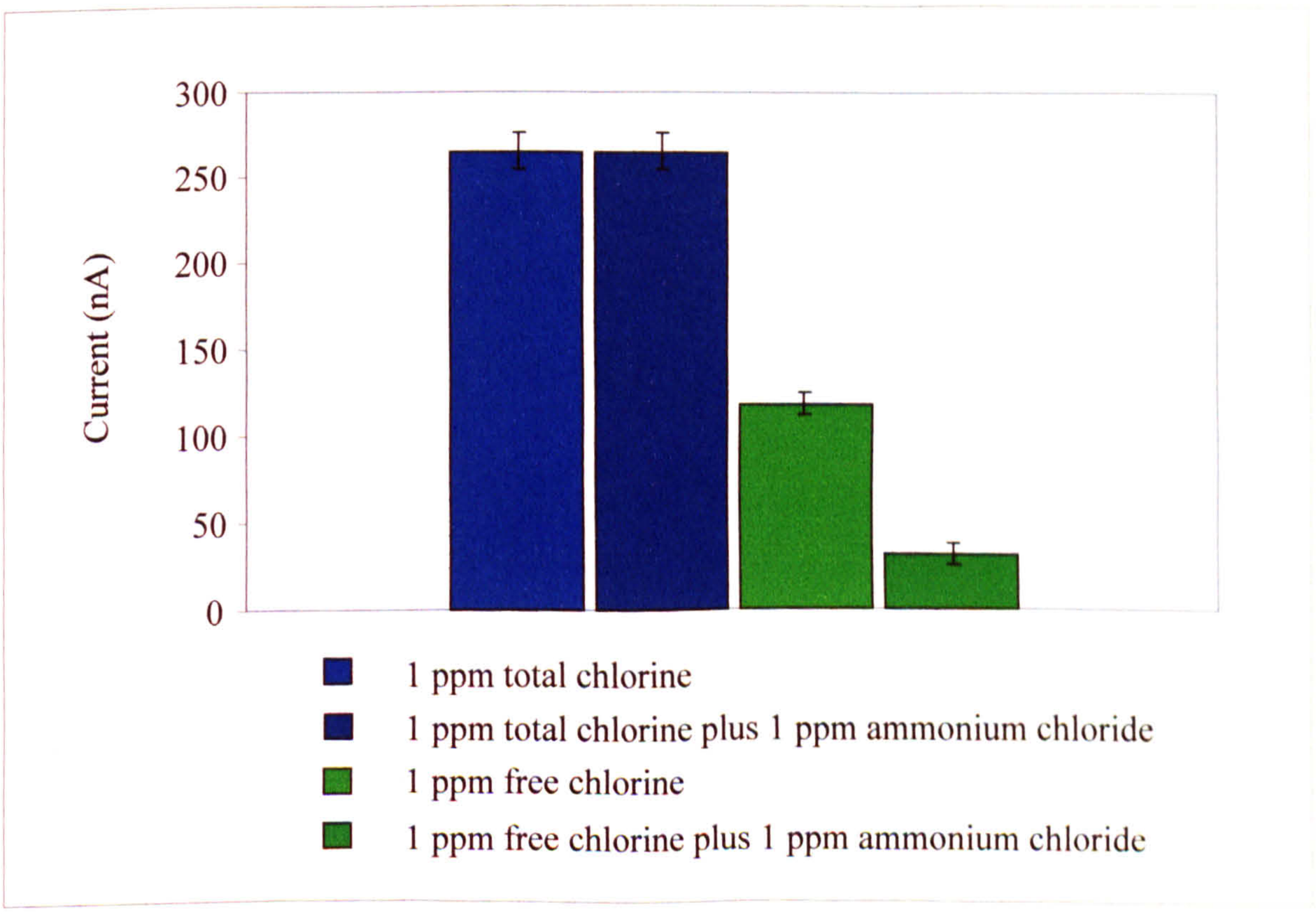

Figure 7.12: Interferent effect of ammonia (NH_3) on the measurement of free and total chlorine

The results are summarised below, in Table 7.5. As a means of assessing the susceptibility of Microarray Limited chlorine sensors to interferents, readings are compared with two conventional portable aqueous chlorine detection systems (a Hach® Pocket Colourimeter and the Aqueous Chlorine Analyser 1200 by LaMotte®).

Interferent	Microarray Limited sensors				'Hach' system reading	'Lamotte' system reading
	Total		Free			
	Total Cl Only	**Total Cl & Interferent**	Free Cl Only	**Free Cl & Interferent**		
Monochloramine ***4.5 ppm per 1 ppm free chlorine solutions***	N / A	N / A	**115 nA** SD ± 5.4 RSD 4.7%	**186 nA** SD ± 10 RSD 5.3%	**1.97 ppm** SD ± 0.12 RSD 6.1%	**2.08 ppm** SD ± 0.09 RSD 4.3%
Nitrate ***0.2 ppm per 1 ppm total/free chlorine solutions***	**265 nA** SD ± 10.3 RSD 3.8%	**262nA** SD ± 9.5 RSD 3.6%	**116 nA** SD ± 5.2 RSD 4.5%	**118 nA** SD ± 6.5 RSD 5.5%	N / A	N / A
Nitrite ***1 ppm per 1 ppm total/free chlorine solutions***	**263 nA** SD ± 11.7 RSD 4.4%	**264 nA** SD ± 13.1 RSD 5.0%	**113 nA** SD ± 5.2 RSD 4.7%	**117 nA** SD ± 6.5 RSD 5.5%	N / A	N / A
Chlorite ***0.3 ppm per 1 ppm total/free chlorine solutions***	**263 nA** SD ± 11.7 RSD 4.4%	**42 nA** SD ± 12.7 RSD 30.2%	**115 nA** SD ± 5.4 RSD 4.7%	**255 nA** SD ± 31.6 RSD 12.4%	Off Scale	Off Scale
Ammonia ***1 ppm per 1 ppm total/free chlorine solutions***	**263 nA** SD ± 11.7 RSD 5.1%	**260 nA** SD ± 12.6 RSD 4.8%	**115 nA** SD ± 5.4 RSD 4.7%	**30 nA** SD ± 6.3 RSD 21.0%	**0.12 ppm** SD ± 0.04 RSD 33%	**0.13 ppm** SD ± 0.03 RSD 23%

Table 7.5: Summary of values for free and total chlorine interference

From the results it can be seen that nitrate and nitrite have no effect on the amperometric response of free and total chlorine, since their reduction potentials in the pH range 4-7 exceeds the maximum potential applied during testing, -100mV (vs. Ag/AgCl) for total chlorine.

The addition of 4.5 ppm monochloramine to a 1 ppm free chlorine solution resulted in a 60% increase in sensor response. This is a result of the partial dissociation of monochloramine (NH_2Cl) in neutral solutions to release free chlorine species. Consequently, the increase in measured response is a true representation of the free chlorine concentration in the solution and is therefore not an active interferent. Since monochloramine is a form of combined chlorine and is intentionally detected during total chlorine measurement, the test was not repeated for total chlorine sensors. The decrease in measured response to free chlorine with the addition of ammonia also reflects the true value since free chlorine naturally combines with certain nitrogen-containing compounds to form combined chlorine species (Section 2.5.1).

7.5 Penetration of the established aqueous chlorine detection market: Attaining market position

Microarray Limited is an R&D company specialising in developing and exploiting new intellectual property for electrochemical sensor applications. Microarray Limited maintains international patent protection for its core technology, which offers a commercially viable route to the mass-production of low-cost, disposable microelectrode array sensors. The aqueous chlorine detection market has been selected by Microarray Limited as a vehicle for proving its technology, primarily because of the short-comings of existing products based on outdated DPD colourimetry-based methods, as well as the large size of the market which will benefit from Microarray Limited's high volume, low-cost manufacturing capabilities.

The aqueous chlorine detection market is currently controlled by a few select corporate giants who have led the industry for decades. Devoid of significant innovations, each product in the marketplace is essentially the same whereby incremental augmented features such as extended measurement range, increased battery life or decreased test duration provide product differentiation in a largely cost-oriented market. Every test requires the addition of a chemical reagent (DPD) to

the test sample, which turns a shade of purple proportional to the concentration of chlorine in the solution. A hand-held instrument then probes the sample by shining light of wavelength 490 – 555 nm through the solution to measure absorbance and in turn gauge the concentration of chlorine. This method of analysis has a number of short-comings, one of which is progressively becoming more of a concern to suppliers and customers alike. The principle chemical behind the current technology, DPD, is known to be harmful to humans and may even possess carcinogenic properties (Hanna, 2004). In an effort to minimise unit cost in current products, the chemical indicator is packaged into small foil pouches which are torn open by the operator during each test for dispensing. Regular users are obliged to wear protective gloves and must be careful not to inhale any of the powder, which can spray into the air when the pouch is opened. Careful or otherwise, no operator likes this aspect of their daily routine and there is always the risk of law suites being filed if regular operators suffer from related health problems in the future.

An additional drawback to the current approach to portable aqueous chlorine analysis relates to the cumbersome operating procedure it requires. As a result of the sensitivity of photometric absorbance methods to sample turbidity, every analysis requires two separate tests to be performed. The first establishes the natural absorbance of the water sample, which is then used as a reference for the second test, where the sample is probed with the reagent, DPD. Both stages have an associated waiting time, since DPD must be allowed to react with the sample for a period of up to 4 minutes prior to the measurement of absorbance and estimation of chlorine concentration. Moreover, the reliance of the transmission of light through sample chambers (which become exposed to external contamination between tests) results in the need for regular system calibration, raising time costs and operator skill levels yet further. The proposed Microarray Limited portable aqueous chlorine analyser can measure both free and total chlorine in the same test, requires no addition of chemical reagents, produces a test result within 90 seconds and does not require post-production calibration.

All data can be obtained in three steps:

1. Place new sensor tip into instrument
2. Fill chamber with water sample
3. Press 'Go' button

Current portable chlorine analysers offer a limited measurement range of approximately 0 – 4.5 ppm. Should the concentration of chlorine exceed this, DPD can become bleached and the solution becomes transparent, falsely indicating that the concentration of chlorine is low. This has been experienced on numerous occasions for applications requiring chlorine control, in particular swimming pools where the problem is only exposed by the harmful effects experienced by swimmers. The Microarray Limited system offers a considerably wider measurement range (0 to 20 ppm free and total chlorine), which if exceeded will not give rise to a false negative reading. By dedicating both working electrodes to the measurement of total chlorine, detection limits of 0.005 ppm (5 ppb) can be achieved to satisfy environmental monitoring applications. The proposed appliance also has a value-adding feature permitting greater traceability of data through the use of an infrared communications port. Table 7.6 provides a method comparison summary for the two approaches to aqueous chlorine analysis.

Feature	Colourimetric method	Microarray method
By-products	Hazardous chemicals and by-products	Reagentless operation and no harmless by-products
Measurement range	Typically 0-2 ppm for ±0.01 ppm accuracy, 0-4.5 ppm for ±0.05 ppm accuracy. Suffers from bleaching effect.	0-20 ppm range ±0.01 ppm, detection limit as low as 0.005 ppm (5 ppb) for environmental monitoring applications
Sample turbidity	Affected by solution colour	Unaffected
Skill requirement	Relatively high skill/training requirement for test	Minimal skill required – quality of the test is principally governed by the reproducibility of the manufacturing process
Drift and calibration	Can suffer from drift and requires calibration	Zero drift and requires no calibration
Analytes	Separate tests for free and total chlorine	A single sensor can perform both tests
Test logistics	Wet chemistry / chemical mixing	Simple dip test
Time per test	Each test takes several minutes	Complete test within 90 seconds

Table 7.6: Method comparison for two aqueous chlorine analysis systems

Microarray Limited has chosen to focus on the inherent disadvantages of colourimetry based methods to gain a foothold, and eventually dominate the aqueous chlorine measurement industry. Technology based on DPD colourimetry has represented the only widely used method of detection since the 1950's (Palin, 1957), (Wilde, 1991). In the marketing microenvironment, Microarray Limited poses a threat as a new entrant to the chlorine measurement industry, as observed in Porter's Five Competitive Forces model (Figure 7.13) (Porter, 1980).

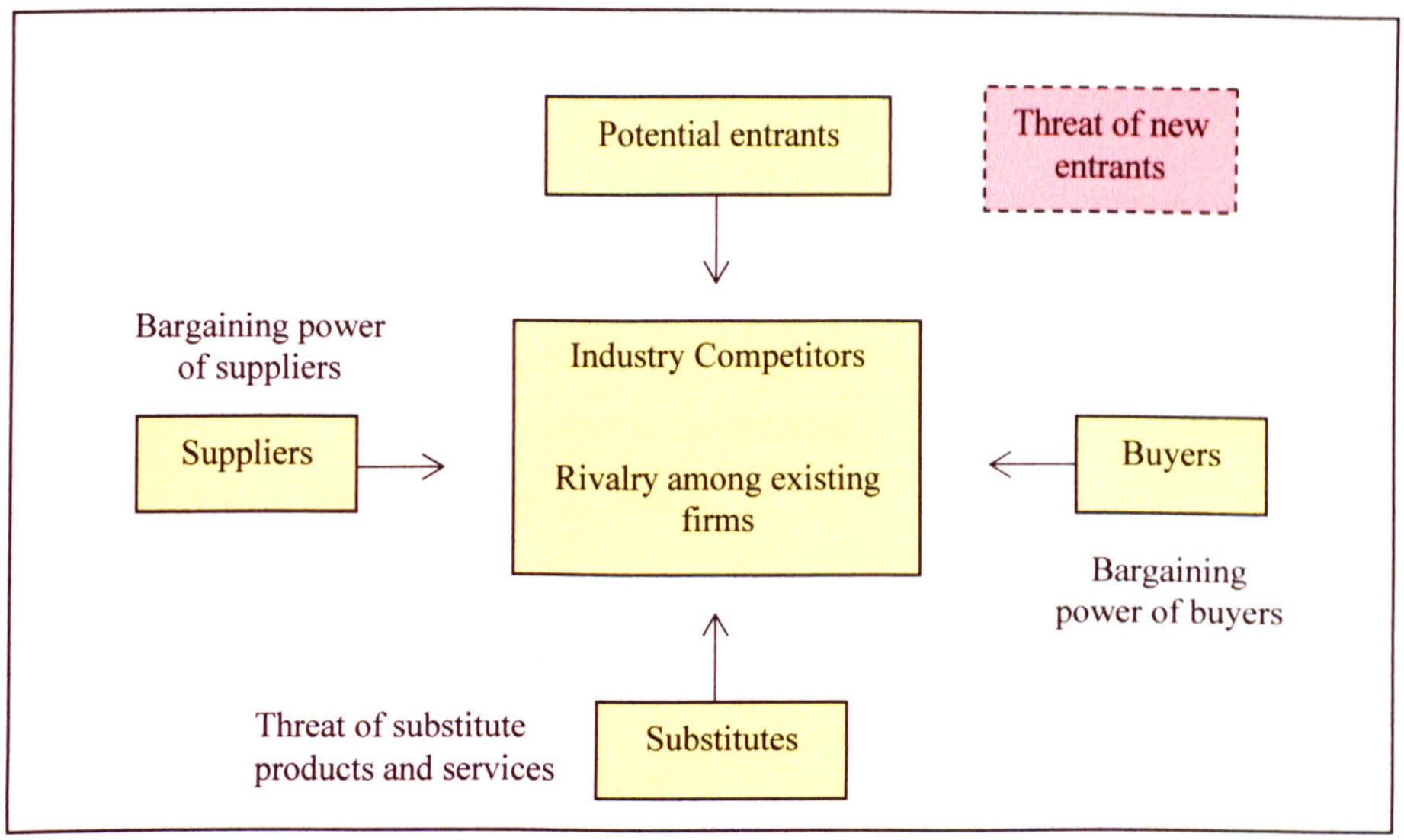

Figure 7.13: Porters Five Competitive Forces model (Porter, 1980)

With respect to the current photometric aqueous chlorine detection market, Microarray Limited's portable analyser can be considered a substitute good, since it measures chlorine but is based on different technology to current products.

In the marketing macroenvironment various forces exist which can drastically alter the competitive market within which an organisation operates, for example political, legal, regulatory, economic, societal, environmental and technological forces. *Environmental* and *regulatory forces* highlight the inadequacy of current technologies, which cannot offer the reliable detection of ultra-low concentrations of chlorine required to enforce regulation. However, with respect to the development of cost-effective manufacture for microelectrode array sensors, it is *technological forces* which are to change the entire market. The advance towards practical microelectrode based measurement of aqueous chlorine, with its inherent advantages, will dramatically change the marketing environment. In fact, there is growing consensus that technological advancement is causing ever-shortening product life cycles for all

products and industries and it is believed that the majority of products available today will not be available in ten years time (Ford & Saren, 2001).

The concept of the product life cycle has become an accepted part of marketing theory, providing a valuable analytical and strategic tool. Symbolically linked to familiar junctures in life, namely gestation, birth, adolescence, maturity and death, the product life cycle describes changes in product sales as a function of time (Figure 7.14) (William & McCarthy, 1997).

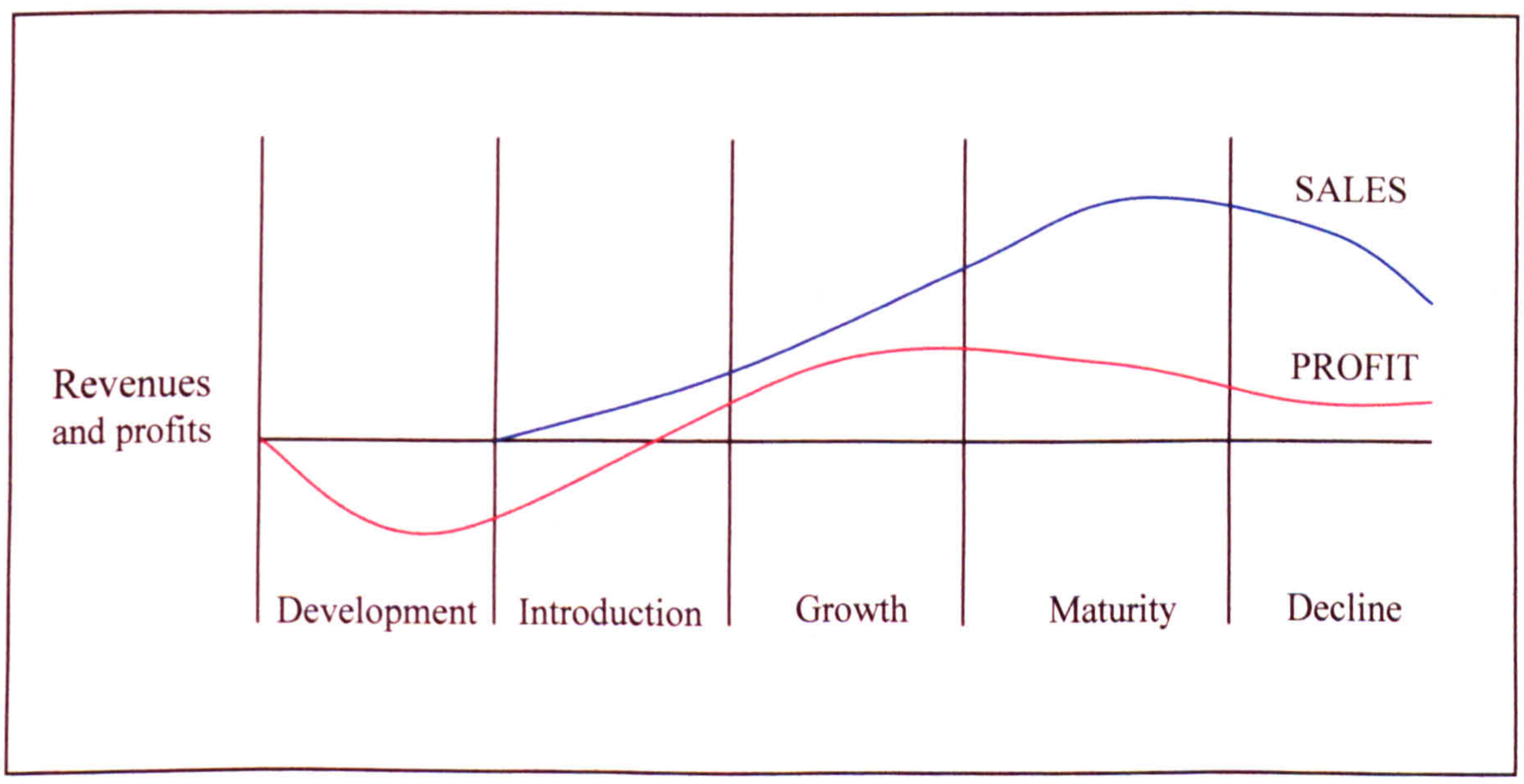

Figure 7.14: The product life cycle model (William & McCarthy, 1997)

In the case of portable aqueous chlorine analysers, the same type of product has been generating profits for decades simply because there has not been anything superior in terms of function and/or cost to cause a decline in the product form. Using three-level life cycle analysis, it is possible to analyse the outcome of new products in the aqueous chlorine detection industry as a whole. This method looks at product class (portable aqueous chlorine measurement), product form (DPD vs. electrochemical) and specific product or brand (for example, Hach Limited versus Microarray Limited) (Figure 7.15).

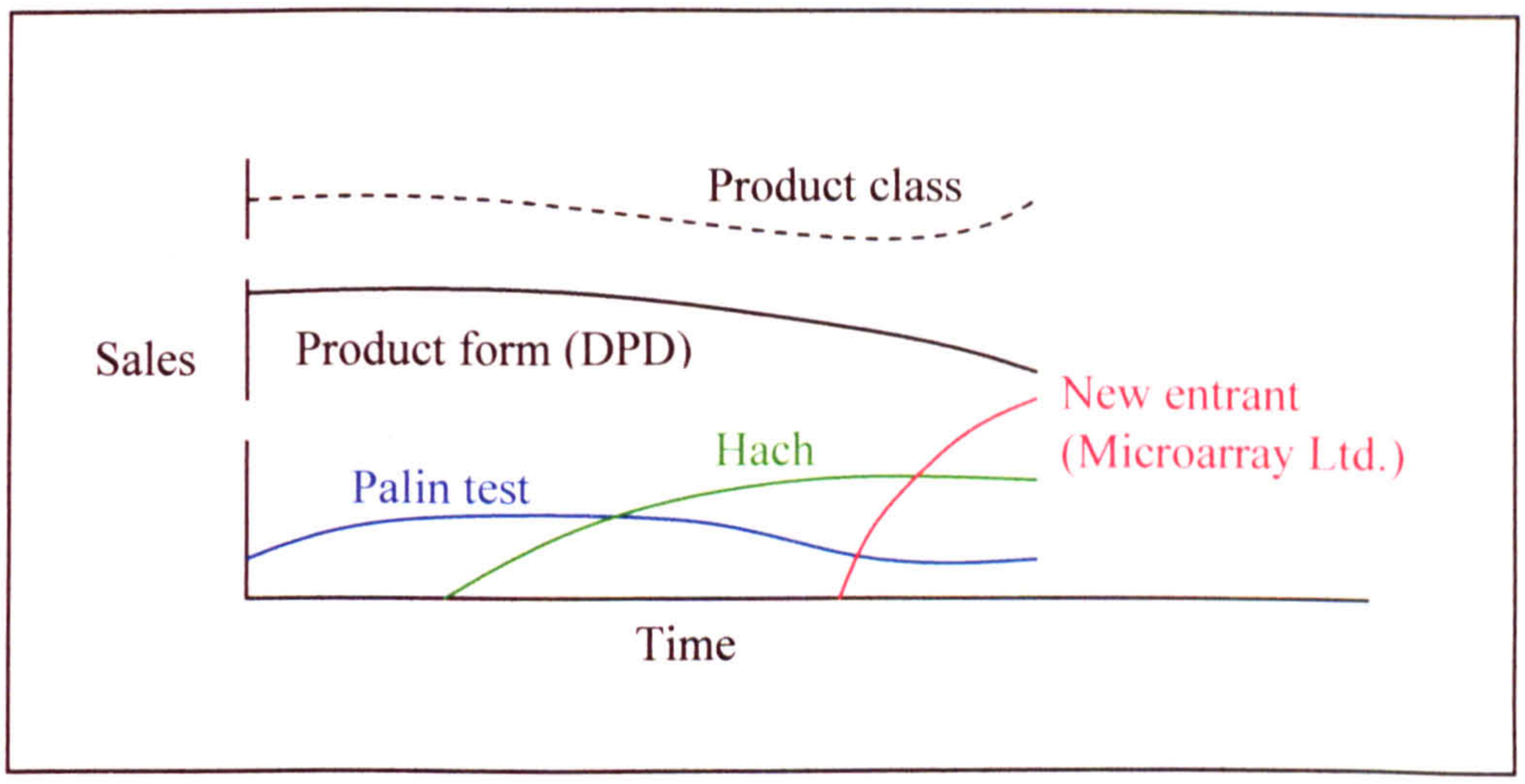

Figure 7.15: Three-level life cycle analysis of the aqueous chlorine measurement market

Clearly a new product form in the portable aqueous chlorine measurement marketplace is long overdue and both users and suppliers acknowledge current technologies as being outdated and unsatisfactory. In order to attain a market position within the industry it is first necessary to identify the customer. The aqueous chlorine measurement industry is unusual in some ways, as single product lines target both *consumers* and *business customers*; furthermore it does so through similar channels (generally catalogue wholesalers and their websites). For example, most people who own private swimming pools measure and control their own chlorine levels. These people are ordinary consumers purchasing the kits for their own personal benefit. However, the greater market segment is held by industrial customers. An industrial product is one bought for use by a company providing a product or service. Unlike consumer goods they are bought not for their own sake or for personal consumption, but in order to contribute to an organisational objective. The cost of attracting a new customer is many times greater than for keeping an existing one. To reach the thousands of companies using traditional methods of aqueous chlorine measurement, a comprehensive business-to-business promotional mix must be employed to win over the decision making units, or 'buyer units'. Critical to early market position, the drive for awareness must utilise as many channels as possible, including sales

personnel, specialised press advertising, direct mail to technical employees, sales literature, trade exhibitions, internet websites, seminars, demonstrations and word of mouth as well as favourable product placement within the usual wholesale catalogues. However, product performance data alone may not be enough to persuade companies to purchase the new technology, particularly considering the inertia associated with industrial validation procedures and the perceived risk associated with an unfamiliar product.

Accordingly, business customers must initially be persuaded on the basis of unit cost for the consumable component of the system. Based on volume batches of 250,000, Microarray Limited sensors can be manufactured for a unit cost of approximately 2.5 pence. This compares favourably to current colourimetric-based products which sell for approximately 5-12 pence per test depending on discounts. When managers see the vastly reduced testing times, elimination of toxic reagents, and the enhanced performance of the Microarray aqueous chlorine measurement system, they will realise the considerable inadequacies of their existing choice; this should be a one-way step.

Like existing products, the Microarray Limited system will also require a one-off instrument purchase which may at first be sold at a loss in order to generate demand for the disposable sensors. Figure 7.16 exhibits the prototype hand-held instrument; CAD drawings illustrate how the sensor is placed into the device using a hinged section.

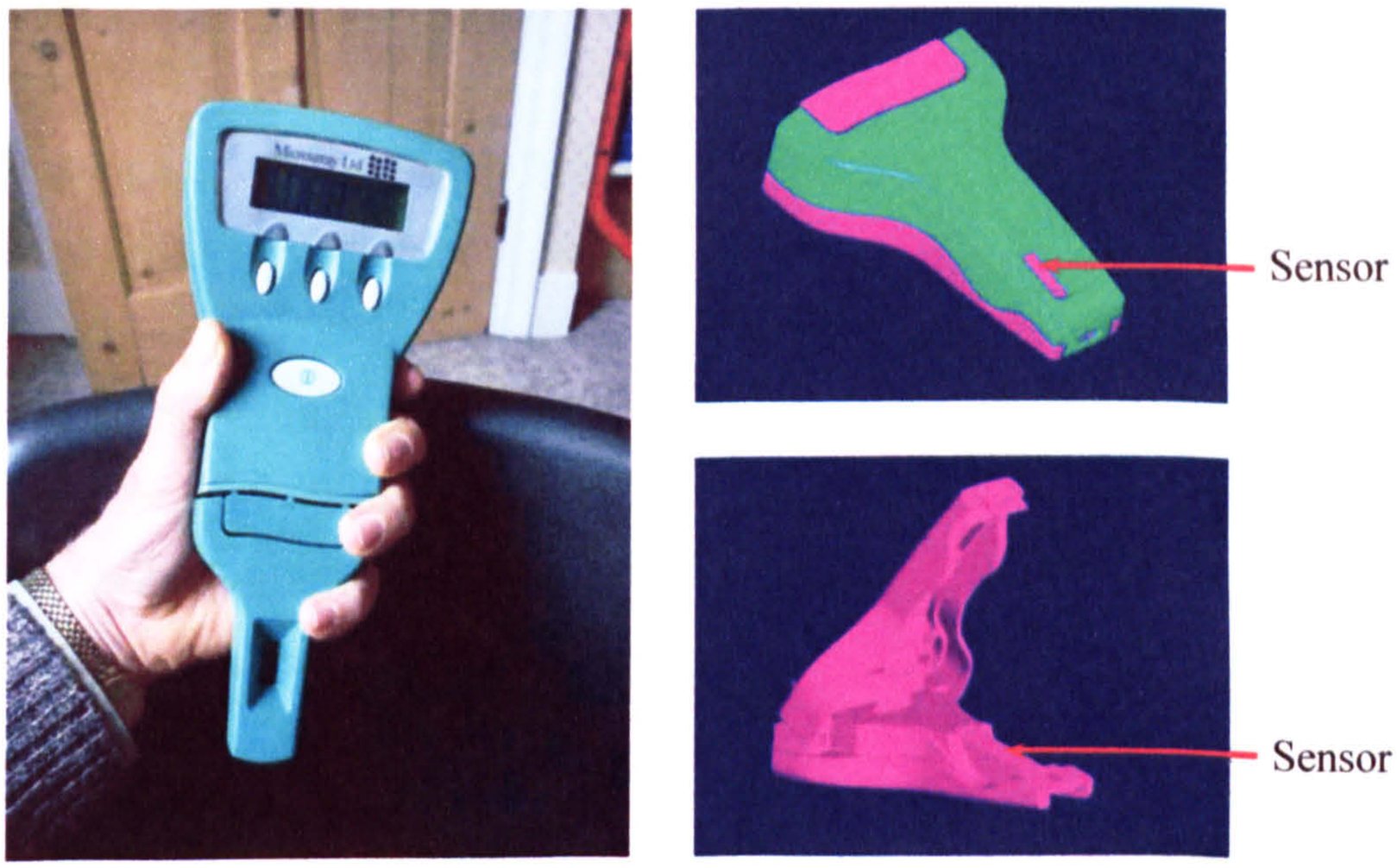

Figure 7.16: The Microarray Limited prototype aqueous chlorine analysis system

Human nature often results in people becoming loyal to a brand, and crucially until they actually use the Microarray Limited chlorine analyser, they will not be fully aware of their need for it. In the context of business-to-business ('B2B') marketing, brand loyalty was previously considered to be far less important than for retail consumers (Egan *et al*, 1992). However, in more recent times the importance and value of industrial branding has become more widely recognised (Mudambi *et al*, 1997), (Wood, 2000), (Knox & Bickerton, 2003). The decision-making unit, or buyer unit responsible for procuring technology on behalf of a company are subject to similar psychological processes that they experience as consumers in the high street. In this situation, the buyer exhibits 'brand awareness' and their purchasing decision becomes affected by various subjective aspects that they associate with a particular manufacturer. Familiarity with an existing product or brand represents a lower risk,

whilst a new company has to create an image to instil confidence in their product range image without any previous experience from customers. For example, in addition to functional statistics and price competitiveness, instrument aesthetics, product artwork and value-adding features would be very significant in the initial sales effort.

The technological advancements behind the Microarray Limited aqueous chlorine analyser permit major performance advantages over existing products. With the launch of the new analyser, Microarray Limited, will cause a repositioning of the portable aqueous chlorine analysis market, simultaneously compromising the security of the established brands and facilitating market penetration (Ries & Trout, 2001). It is possible to analyse the various levels of the Microarray Limited corporate image using the Kotler analysis of brand meaning (Table 7.7) (Kotler, 1999).

Meaning	Description	Example
Attributes	A brand brings to mind certain attributes	Microarray suggests reliable, rapid, reagentless chlorine measurement
Benefits	Attributes must be translated into functional and emotional benefits	The attribute 'reliable' could translate into the functional benefit of a long lasting measurement system.
Values	The brand says something about the producer's values	Microarray stands for innovation and low cost value adding performance
Culture	The brand may represent a certain culture	Microarray represents innovation, quality
Personality	The brand can project a certain personality	Microarray may suggest a friendly, knowledgeable and efficient technician
User	The brand suggests the kind of customer who buys or uses the product	Microarray technology will be first adopted by forward-thinking, dynamic companies.

Table 7.7: Levels of brand meaning described by Kotler

In order to maximise the potential of brand awareness, image and ultimately brand equity, great attention has been paid to the brand elements of Microarray Limited. Currently, all equipment produced by the market leaders, Hach®, is manufactured in a particular colour, Hach 'blue', which builds an image in the customers mind suggesting that Hach are *the* water experts. Most competitors to Hach in the marketplace also adopt a similar blue colour, implying that their product is just as good as the market leaders. However, in order to contest the brand image, Microarray Limited has adopted an equally transferable colour (Figure 7.17).

Figure 7.17: Comparison of the Hach® and Microarray Limited colour schemes

The alternative green colour represents a fresh, environmentally friendly and user friendly alternative to existing technologies. Differentiating itself in this manner also makes a bold statement to the industry about Microarray Limited's intentions to cause significant changes in the marketing environment. Importantly, the brand name 'Microarray' serves to highlight the technological difference behind the company.

Many people working within the sensor industry will understand the performance difference of a microelectrode array system and will associate it with the Microarray brand name. In this respect the Microarray Limited brand name is superior to the market leaders, Hach, which has become synonymous with water analysis only through time and market share. The Microarray brand is also supported by a logo, which through an attractive simplicity once more highlights the company's technological distinction (Figure 7.18).

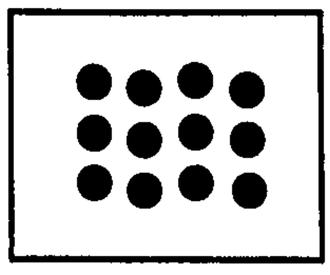

Figure 7.18: A simple representation of a microelectrode array provides a useful branding tool for Microarray Limited

By creating perceived differences among products through branding and developing loyal consumers, marketers can create value translating into financial profits for the firm. A successful brand must combine an effective product, distinctive identity and added values as perceived by the customer. Brand equity is therefore the total value of the brand to the core product (Doyle, 1994).

In addition to reducing the perceived risk associated with purchasing a branded product, the customer also experiences an increase in anticipated satisfaction. It is therefore important that the product lives up to the customers expectations from the outset or the brand image created will be a negative one. Market research following the launch of the Microarray Limited portable aqueous chlorine analyser will determine the level of customer satisfaction, which can be represented using the Kano model of customer satisfaction (Figure 7.19) (Kano, 1984).

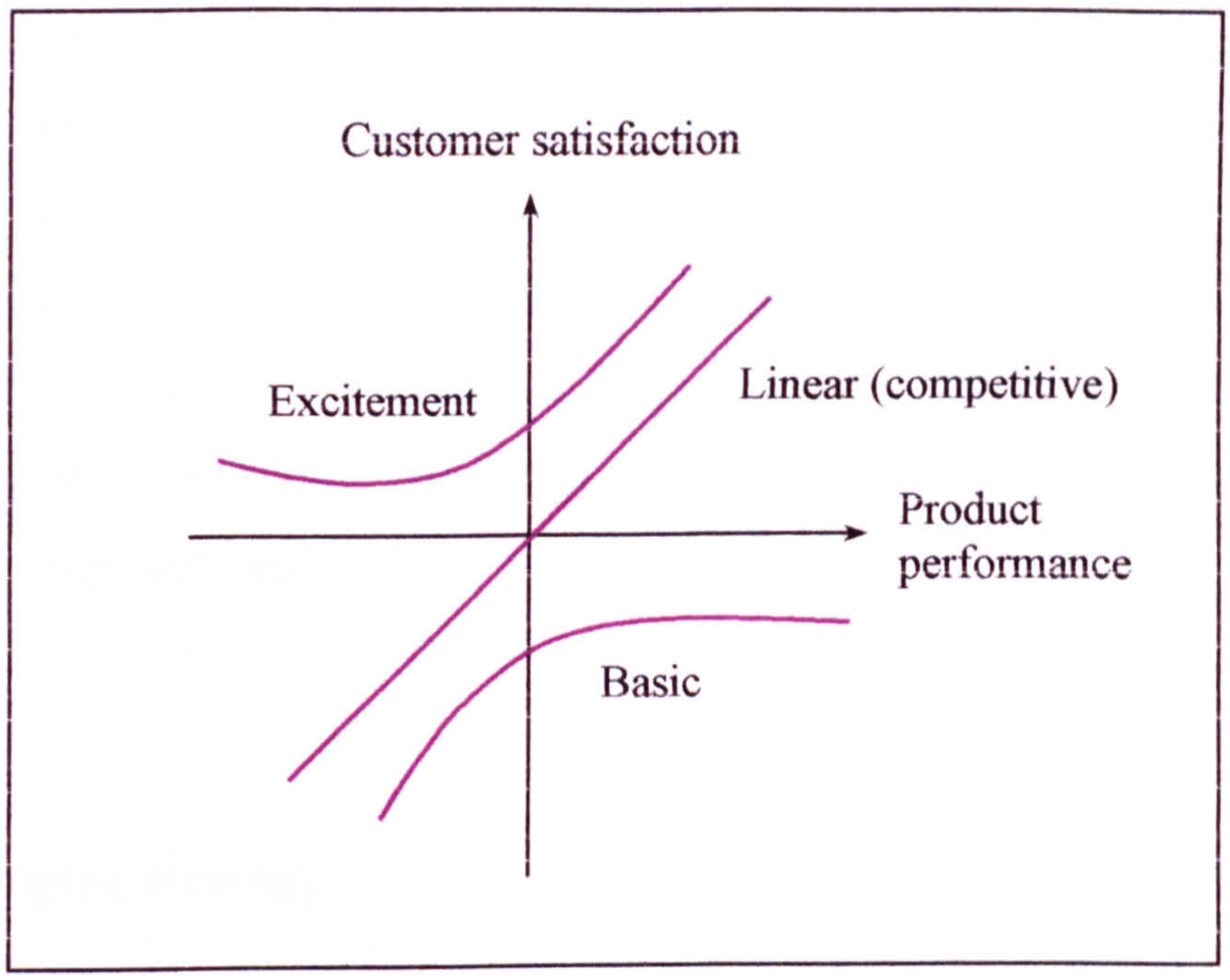

Figure 7.19: The Kano model of customer satisfaction (Kano, 1984)

Once market position has been attained it will need to be defended and improved. Intellectual property pertaining to the commercially viable fabrication of disposable microelectrode array sensors is protected through an international patent and prevents unauthorised sales in the following countries:

- UK
- USA
- Japan
- Australia
- Germany
- Italy
- Spain
- France
- Netherlands
- Sweden

Patent protection is set to expire in May 2016, and it is important that in the preceding time Microarray Limited develops key skills and knowledge in its core production technology, optimising manufacturing processes and establishing themselves as market leaders. The company must continue to foster a culture of technical innovation

and focus its business strategy on future markets (Abell, 1995). Around two thirds of the worlds population (approximately 4 billion people) drink chlorinated water, making aqueous chlorine detection a product that everyone can relate to. The Microarray brand image, having established a reputation for quality and performance on this scale, will permit ease of entry into many other sensing applications which can benefit from low-cost microelectrode array manufacturing technology, including the detection of pesticides, herbicides, sensors in drug manufacture, DNA screening and *in vitro / in vivo* biosensors.

7.6 Packaging strategy

In order to achieve successful commercialisation of a new product, a packaging strategy must be designed for the sensor strip to contain the product from the point of manufacture, to the point of operation. The *European Packaging and Packaging Waste directive* defines packaging as 'any material, container or wrapping, used for or in connection with the containment, transport, handling, protection, promotion, marketing or sale of any product or substance' (94/62/EC, 1994). The functions of packaging can be broadly divided into three areas as discussed below. Primary functions are concerned with the technical nature of the packaging, and involve protecting the contents from the environment and vice versa; this includes withstanding static and dynamic forces experienced during transport, storage and handling operations. Secondary functions relate to communications, for example, gaining added value through displaying the company brand, or satisfying legislation by displaying important information. Tertiary function relates to the extent to which the packaging materials may be re-used once the package contents have been used, the most common example being that of recycling paper and cardboard packaging. It is important that the cost and performance of the packaging, process and materials is optimised without causing adverse effect on the come at a price, and there is only so much that can be taken out of a packaging process before it adversely affects the product itself in terms of increased damage through distribution, or adverse customer perception. This trade-off generates the need to develop a packaging strategy which is

unique to the application, and not necessarily following the same approach employed by similar products already in the market place.

Firstly it was necessary to understand the requirements for the packaging system, then to incorporate it into the product design from the earliest stage in order to minimise overall costs. Business analyst Michael Hammer warns established companies that in order to survive in today's global economy, companies must focus and reorganise themselves around their processes (Hammer, 1996). For a new company with a new product the opportunity presents itself for a process-focused product design to include and optimise packaging requirements from the earliest stage.

Firstly it was necessary to understand the requirements for the packaging system, then to incorporate them into the product design at minimum overall cost. In order to guarantee consistent sensor performance, the product packaging must provide protection from mechanical damage (such as abrasion), and prevent contamination by dirt and atmospheric gases (including moisture). At the point of operation, the packaging must allow the sensor to be quickly and easily employed by the user, whilst reducing the risk of incurring damage. Above all, production costs must be minimised as far as possible, otherwise an over-engineered packaging solution will simply result in an uneconomical product.

A novel packaging strategy was conceived whereby rather than separating each sensor prior to wrapping it, they are instead packaged *simultaneously* before being cut up and separated. By incorporating packaging into the principle product design, instead of treating it as a separate component, a packaging system was developed based on heat-sealing a flexible polymer or foil film directly onto the sensor substrate as a final production step (Figure 7.20).

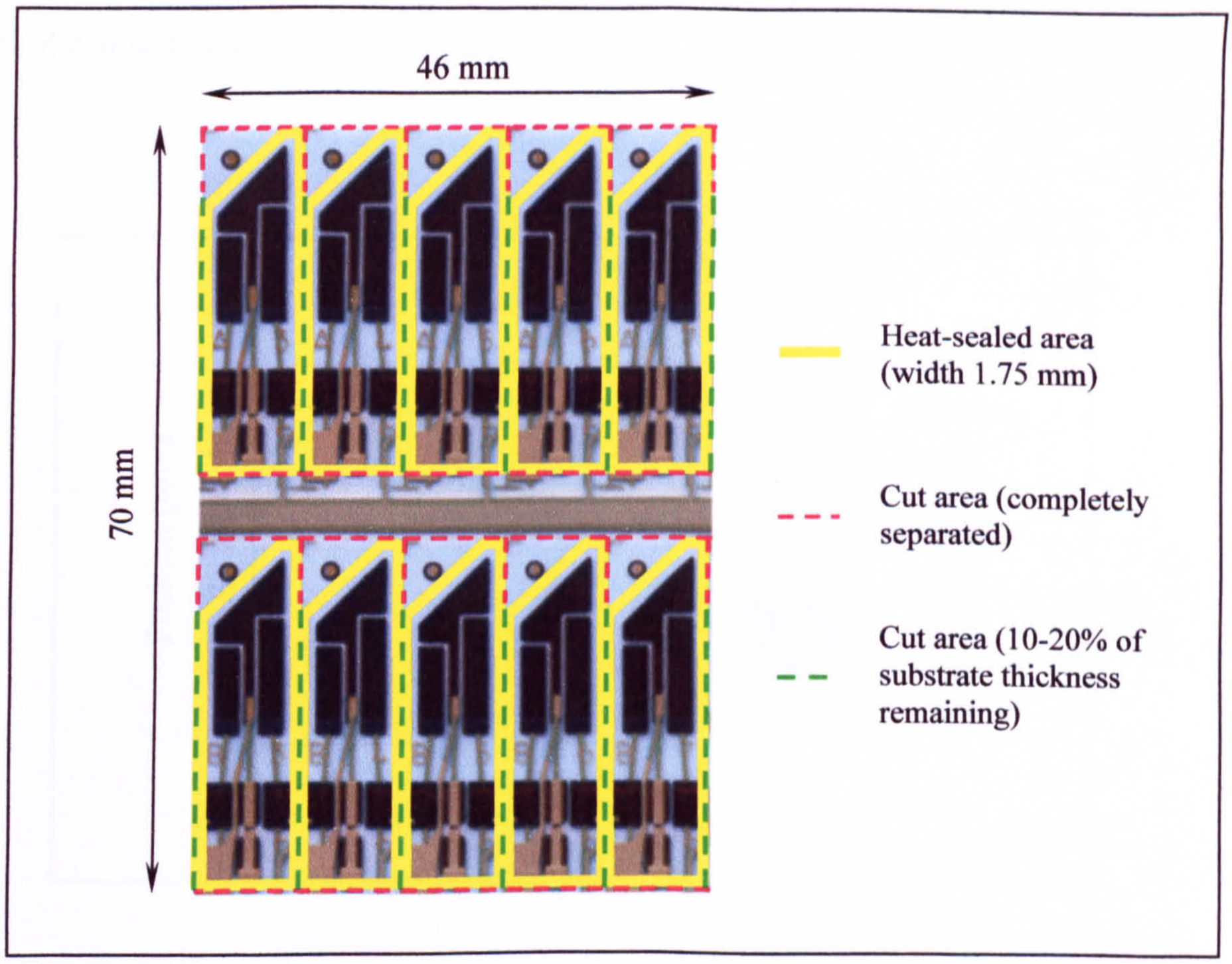

Figure 7.20: Diagram indicating the area of heat-seal for primary packaging of sensor

Investigations into the development of the heat-seal process were carried out in conjunction with Cadillac Plastic Ltd (Swindon, UK) and ProSeal UK Ltd (Macclesfield, UK), specifically to develop a film layer possessing a peel-force of 1 to 5 N and affording appropriate protection from the surrounding environment. A selection of Melinex® (DuPont) and polymer coated foil films were used in the trials, which focused on variations in the time, temperature and pressure of the heat-sealing process for producing a hermetic seal, yet allowing for a simplified and reliable removal process. However, specific details of the production equipment along with materials and processing parameters investigated and subsequently employed remain commercially sensitive, and as such cannot be documented here. Information on the mechanical properties of film / sensor seal were principally derived from peel forces measured by means of an Instron model 5565 universal testing rig (High Wycombe, Buckinghamshire, UK) used to determine seal strength and consistency via a

180° peel angle. Figure 7.21 displays a typical force-position curve obtained for the peel of a single sensor wall (peel rate 1 $cm.s^{-1}$).

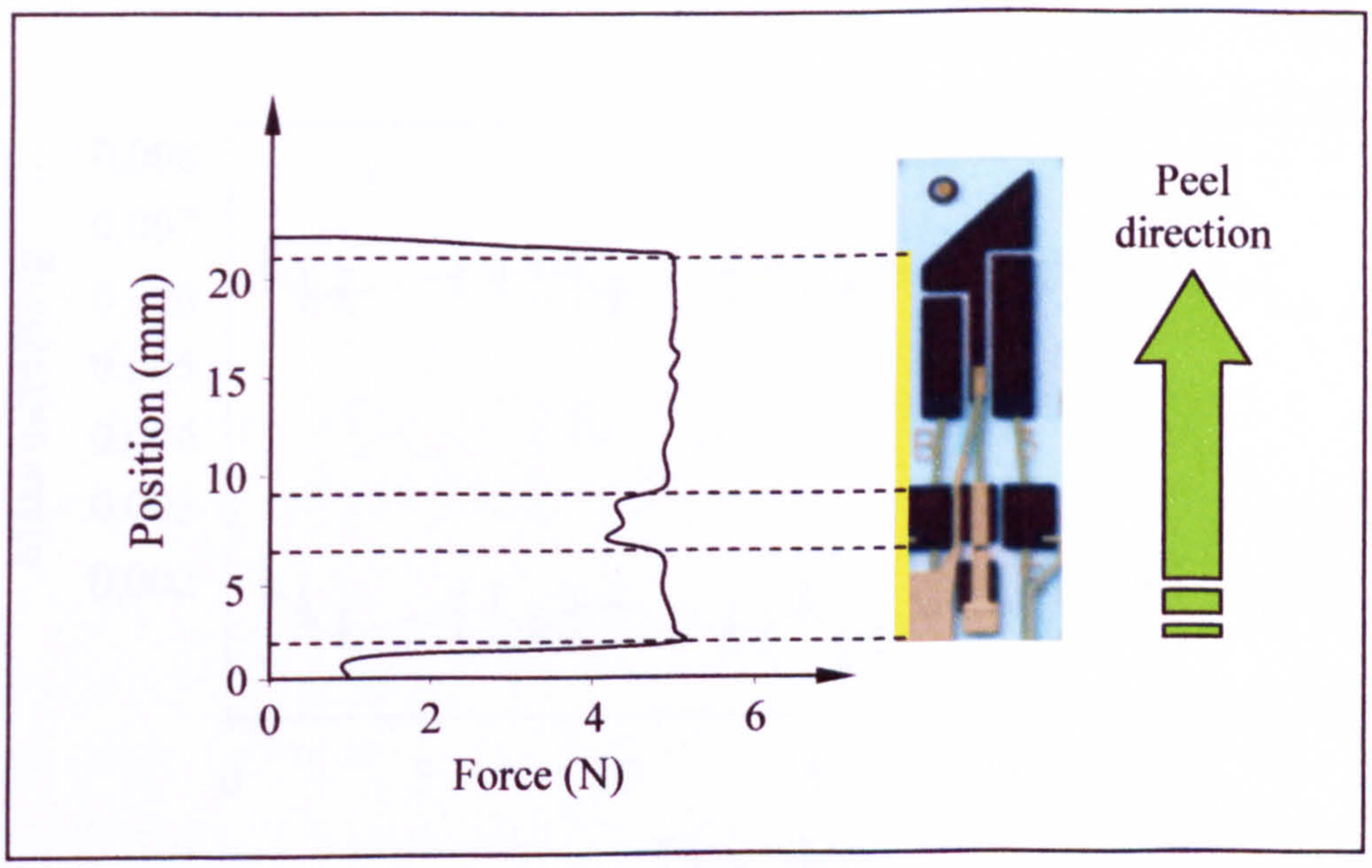

Figure 7.21: Example of a typical force-position curve obtained for a single sensor seal

From the investigations undertaken, a number of polyester films were identified as providing appropriate seal strengths under certain heat-seal process settings. Importantly, adhesion of the film to the substrate showed good consistency, remaining at approximately 5 N throughout, including the area of carbon-ink comprising a SIM contact pad which falls partly into the sealing region (approximately 6-9 mm in Figure 7.21).

Initial investigations were carried out to confirm the effectiveness of the film packaging system to form an effective barrier against atmospheric moisture. Finely ground, desiccated, copper sulphate crystals were positioned onto the electrode surface and sealed in place using a low water-vapour permeability polyester film. Groups of three sensors were stored both in ambient conditions and at 38°C / 90% relative humidity for accelerated life-time testing. Each day, the groups of sensors were weighed together, and the mass increase resulting from moisture ingress was

recorded. Figure 7.22 indicates the average daily mass increase corresponding to the rate uptake of transpired water from the atmosphere by the copper sulphate crystals; error bars represent the spread of data obtained from the weighings.

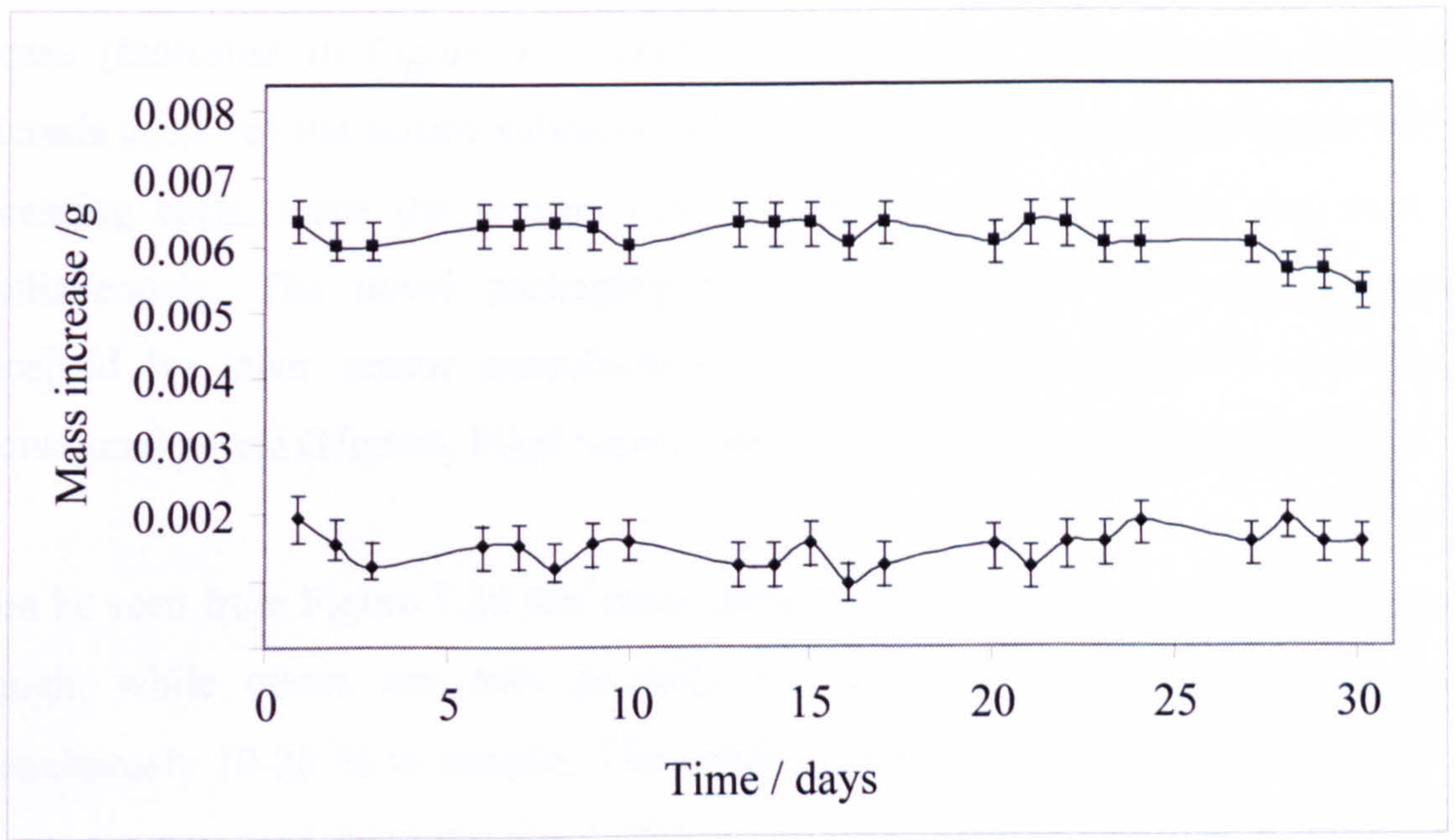

Figure 7.22: Total mass of water absorbed each day by 3 sensors stored under ambient (♦) and 90% RH / 38°C atmospheric conditions (■)

The material properties data supplied by the manufacturer pertaining to the film moisture-vapour transmission rate (8 $g/m^2/24$ hrs) was compared to the data obtained for sensors stored under the same conditions. Assuming a two-dimensional profile for the film layer, then the available area for moisture permeation is approximately 2.4×10^{-4} m^2, and a moisture-vapour permeation rate of approximately 8.5 $g/m^2/24$ hours is obtained. This correlates well with the materials property data for the film, indicating that good seal integrity is obtained for sensors packaged by this method. The hermetic nature of the film/heat-seal packaging system also suggests that the permeability to other atmospheric gases (such as oxygen) will remain consistent with materials properties provided by the film manufacturers.

The decrease in water absorption, noted towards the end of the 30 day experiment for the case of elevated temperature and humidity, may be an indication that the copper

sulphate crystals were partially saturated with water and had become less efficient at absorbing moisture. A marginal colour change was also observed for some of the copper sulphate crystals, which turn from blue to pink upon moisture uptake.

Following the heat-sealing operation, sensors are separated by a die-cut or laser-cut process (indicated in Figure 7.20 above). This method of packaging minimises materials costs (as the sensor substrate acts as one half of the packaging) as well as processing costs, since the sensors can be sealed in one operation and then cut simultaneously. The novel packaging approach described here, not previously conceived by other sensor manufacturers, now forms the basis of a published international patent (Higson, Filed September 2002; publication date April 2004).

It can be seen from Figure 7.20 that some parts of the sensor sheet are cut all the way through, while others are only partially cut to allow a substrate thickness of approximately 10-20 % to remain. The result is that during production, strips of 20 sensors are removed from the sheet and placed in secondary and tertiary packaging for shipment. This method of dissemination facilitates convenient handling and counting of sensors by both the manufacturer and the user. Sensors can be individually separated by tearing a single unit from the strip of 20 electrodes, and the protective layer can be easily removed by taking hold of the un-adhered corner of the film and peeling away immediately prior to use.

A strip of sensors manufactured in this format is exhibited by in Figure 7.23.

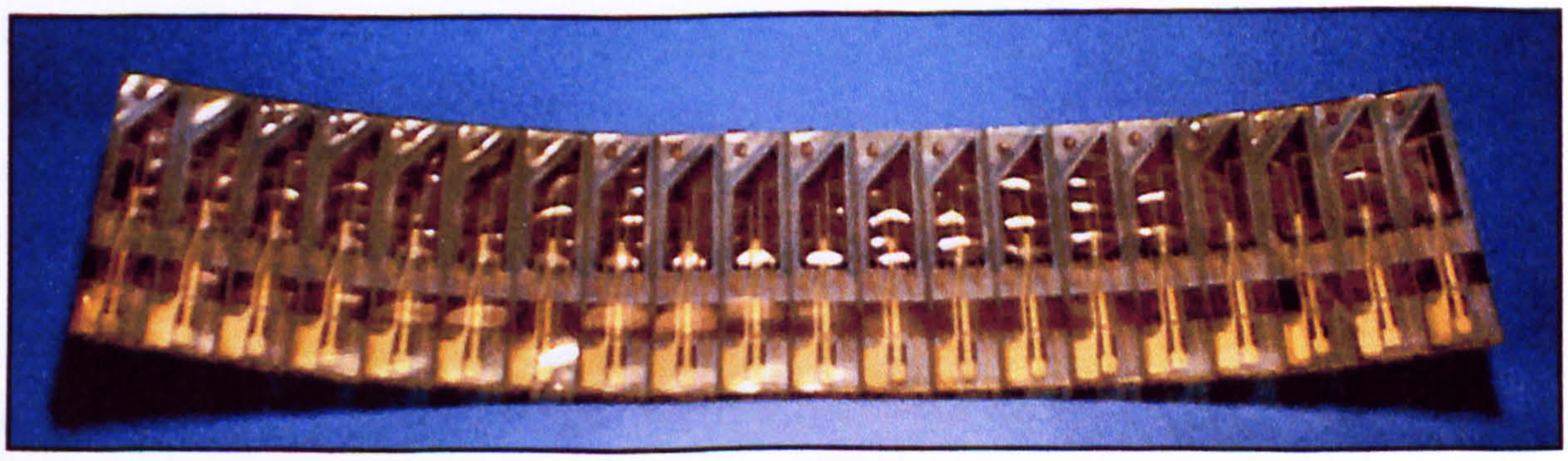

Figure 7.23: A strip of 20 Microarray Ltd. chlorine sensors, packaged beneath a protective film

It follows that in addition to savings on materials and processing, this unique packaging system adds further value to the product. Packaging is, after all, the first stage of customer interaction, and allows the Microarray Limited product to be positively differentiated from other products on the market, thereby enhancing brand value.

7.7 Considerations towards an effective marketing strategy

In order for Microarray Limited to successfully commercialise a disposable aqueous chlorine sensor, careful planning in the development of a comprehensive marketing strategy is first required to establish a profitable business plan.

An effective marketing strategy begins with conducting market research. This will provide relevant data for the targeting of potential customers and the key benefits which they will receive through the adoption of the product or service in question.

Typically, the three most pragmatic ways to conduct market research are by means of direct mail survey, telephone survey, or by conducting a focus group. Importantly, to prevent existing preconceptions of those already close to the business leading to the acquisition of bias or deficient market data, this research should be largely undertaken by a reputable independent third party (Hague, 2002). Secondary data is also imperative to a successful marketing plan. Reports and studies carried out by government agencies, trade associations or other businesses concerned with aqueous chlorine detection have provided important statistics on the growth and direction of this industry (Boswell, 2001), (Mintel, September 2003), (Mintel, June 2004).

Central to the successful market penetration of any product is the issue of unit cost. Market research has shown that current suppliers of DPD colourimetric based equipment typically sell at a price of around 5-10 pence per test, dependent on the provision of buyer discounts. In order to provide a realistic alternative to existing

methods on a price basis, all aspects of sensor development and industrial upscale previously described have focused on attaining market leading performance at a competitive price. Based on volume batches of 250,000, it has been calculated that Microarray Limited sensors can be manufactured for a unit cost of approximately 2.5 pence, sufficiently low to provide scope for a competitive yet profitable sale price. Market research has suggested that although the DPD-based aqueous chlorine detection industry is a mature market, domination by a few select giants has permitted the establishment of a partially collusive pricing strategy, with potential for tenacious price-based competition. For this reason Microarray Limited will strive to communicate the benefits to customers of using its technology.

Having gained a comprehensive understanding of the aqueous chlorine detection market, it is imperative to develop an effective marketing strategy. In order to be truly successful, it is necessary for Microarray Limited to maximise its marketing by using at least ten primary ways of promoting its flagship aqueous chlorine detection system, for example by exploiting avenues such as direct mail, advertising, using the telephone, referral systems, the internet, email marketing, public relations and strategic alliances.

Table 7.8 illustrates the primary advantages and disadvantages associated with the most common components used in a promotional mix (Kotler, 2005).

Mix Element	Advantages	Disadvantages
Advertising	Good for building awareness Effective at reaching a wide audience Repetition of main brand and product position helps build customer trust	Impersonal – cannot answer all of a customers questions Not good at getting customers to make a final purchasing decision
Personal Selling	Highly interactive - lots of communication between the buyer and seller Excellent for communicating complex / detailed product information and features Relationships can be built up - important if closing the sale make take a long time	Costly - employing a sales force has many hidden costs in addition to wages Not suitable if there are thousands of important buyers
Sales Promotion	Can stimulate quick increases in sales by targeting promotional incentives on particular products Good short term tactical tool	If used over the long-term, customers may get used to the effect Too much promotion may damage the brand image
Public Relations	Often seen as more "credible" - since the message seems to be coming from a third party (e.g. magazine, newspaper) Cheap way of reaching many customers – if the publicity is achieved through the right media	Risk of losing control - cannot always control what other people write or say about your product

Table 7.8: Advantages and disadvantages of the promotional mix (Kotler, 2005)

Central to Microarray Limited's marketing strategy is an understanding of customer needs and product differentiation. Since people will *only* buy a product when they have explicitly understood the benefits which they could enjoy, it is important to communicate the advantages of the Microarray Limited aqueous chlorine detection system in every word of promotional material used. By directly contrasting key

aspects of the Microarray Limited aqueous chlorine detection system against traditional wet-chemical based technologies, potential customers can immediately understand the benefits available to them (as shown in Table 7.9)

Feature	Colourimetric method	Microarray method
By-products	Hazardous chemicals and by-products	Reagentless operation and no harmless by-products
Measurement range	Typically 0-2 ppm for ±0.01 ppm accuracy, 0-4.5 ppm for ±0.05 ppm accuracy. Suffers from bleaching effect.	0-20 ppm range ±0.01 ppm, detection limit as low as 0.005 ppm (5 ppb) for environmental monitoring applications
Sample turbidity	Affected by solution colour	Unaffected
Skill requirement	Relatively high skill/training requirement for test	Minimal skill required – quality of the test is principally governed by the reproducibility of the manufacturing process
Drift and calibration	Can suffer from drift and requires calibration	Zero drift and requires no calibration
Analytes	Separate tests for free and total chlorine	A single sensor can perform both tests
Test logistics	Wet chemistry / chemical mixing	Simple dip test
Time per test	Each test takes several minutes	Complete test within 90 seconds

Table 7.9: Method comparison for two aqueous chlorine analysis systems

Pivotal to the performance of an electrochemical sensor technology in comparison to wet-chemical photometric absorption methods is the ability to overcome signal variation resulting from forced or natural convection experienced an electrochemical cell. This would normally be exasperated in the case of field-based analysis, where physical movement of the system during testing, and escalated temperature gradients between the sample solutions and the measurement equipment would cause an erratic sensor response. However, the Microarray Limited aqueous chlorine analyser

circumvents these intrinsic problems by means of its patented low-cost, high volume microelectrode array production process.

Market research data can be combined with promotional channels and product performance data to produce a tailored product and marketing mix for each individual market segment. In the case of the Microarray Limited aqueous chlorine analyser, this can be principally divided into three areas, namely environmental surface water monitoring, drinking and industrial process water control and pool and spa monitoring.

Each of the market segments identified will require their own set of promotional channels, highlighting the individual benefits that each type of customer will receive, whilst presenting a specific pricing strategy (Table 7.10).

Application	Primary customers	Key value-adding features offered	Focused promotional mix	Relative sale price
Drinking water and industrial process water	Utility companies, food industry, b2b buyers	Reduced operator skill, reduced testing time, data traceability	Catalogues, conferences, direct sales, email marketing	Low
Environmental and surface water applications	Environmental protection agencies, b2b buyers	Ultra-low detection limit (5 ppb), no toxic reagents	Environmental publications, direct communication with regulatory bodies	Medium
Pool and Spa	Private swimming pool owners, Recreation centres	Rapid, easy use Aesthetically pleasing, sophisticated digital instrument	Web advertising, email marketing, mail shots	High

Table 7.10: Identification of market segments

In order for Microarray Limited to maximise its marketing, it will need to test and measure all aspects of its primary marketing methods to appreciate exactly what level of response is achieved by each approach; how many of those response are converted to sales; and what the value is to the company when compared to the costs incurred. It is noted that in the case of web advertising, Google, Yahoo and MSN account for 95% of search engine visitors to all websites, and as such listings should be concentrated on these (Sweeney, 2004). Alternatively, following a former demise in the favourability of website advertising, pay-per-click promotions now offer a cost-effective approach to reaching potential customers. In the case of the Microarray Limited aqueous chlorine detection system, a punchy advert describing how chlorine measurement has changed (and the key benefits which this provides) could be placed on a webpage which already sells pool and spa consumables. This would quickly draw the attention of numerous potential customers, their very presence at the website revealing that they are prepared to make a purchase of some kind.

Personal referral is unsurpassed as an advertising tool. It costs nothing and is the most 'believable' of all (Ries & Trout, 2000). This is therefore a positive reason for Microarray Limited to sustain excellent customer service and relations. Central to Microarray Limited's business plan is to continually exploit new intellectual property for electrochemical sensor applications. With the right level of re-investment into its research and development program, enjoying enhanced brand equity for its generic microelectrode array production technologies and with a proven track record, Microarray Limited will possess all the requirements for sustaining long-term growth and real achievements in a range of analytical markets.

7.8 Conclusions

Portable aqueous chlorine detection has been selected as the primary market for the commercialisation of an innovative microelectrode array manufacturing technology. Environmental monitoring sensor applications possess a number of attractive features, including reduced barriers entry resulting from higher performance demands

and an increased willingness for companies to adopt new technologies. Furthermore, aqueous chlorine detection is relatively straight forward and avoids many of the cumbersome trails and evaluation periods associated with the commercialisation of medical products.

In order to achieve performance advantages over existing products, a method was developed for localising chemical reagents required for chlorine detection at the electrode surface. Formulations excluded harmful chemicals and calibration profiles determined the suitability of the sensor construction for the measurement of 0.01 ppm total chlorine. By dedicating both working electrodes to the measurement of total chlorine, this will satisfy requirements for the detection of 5 ppb total chlorine in surface waters. Sensor response for the detection of free chlorine using the final sensor construction was found to be marginally short of the required specification for a detection limit of 0.02 ppm free chlorine. Further optimisation of production and analysis methods will permit the necessary signal magnitude to be obtained. Principle organic and inorganic materials present in natural waters were shown to be of little threat to the electrochemical detection of aqueous chlorine since the overpotentials required for their reduction exceed those required for free and total chlorine analysis.

Based on the analysis of current technologies for the detection of aqueous chlorine and a comparison with the Microarray Limited approach, a marketing strategy was described disclosing the penetration of the aqueous chlorine detection industry. The development of brand equity was shown to facilitate entry into other analytical markets, safeguarding the future success of the company. By adopting a holistic approach to sensor production, down-stream supply chain was benefited by the development of a novel packaging strategy permitting both a reduction in packaging costs and the facilitation of end-of-line use in the form of strips of 20, individually sealed, and partially separated sensors. Since this innovative packaging strategy may be advantageous to many other sensor manufacturing processes, the concept has been protected through an international patent application (Higson, Filed September 2002; publication date April 2004).

Central to Microarray Limited's business plan, the primary considerations for a marketing strategy have been proposed. Market research undertaken by a reputable third party has been shown to be an invaluable precursor for a profitable marketing strategy. Ten primary marketing tools have been suggested, and it is imperative that these methods be tested and measured for their effectiveness to allow focus of the future marketing effort. Elements of the promotional mix have been combined with a method comparison between the Microarray Limited aqueous chlorine detection system and existing technologies based on wet-chemical photometric absorption. Analysis of principle market segments and ther respective needs was then used to suggest an individually focussed promotional mix. The execution of an effective marketing strategy will provide enhanced brand equity for Microarray Limited's generic microelectrode array production technologies. By incorporating an appropriate level of re-investment into its research and development program, Microarray Limited will possess all the requirements for sustaining long-term growth and real achievements in a range of analytical markets.

CHAPTER 8

Summary conclusions

The commercial development of a disposable aqueous chlorine sensor based on an innovative, low-cost microelectrode array manufacturing process has been described. Focus has been drawn towards the optimisation of production processes for enhancing sensor performance whilst minimising unit cost at the design stage. Chapter 4 identified screen printing technology as an inexpensive method for base sensor production since it is well-suited to high volume manufacture. Low-cost materials were selected and a screen printable carbon-ink was utilised for the primary electrode substrate (developed in conjunction with Gwent Electronic Materials Limited). The amperometric detection of free and total chlorine solutions was determined to occur at -80 and -100 mV (vs. Ag/AgCl) at the screen printed carbon-ink surface, and current densities were used to estimate the required electrode areas for sensor design. Moreover, the number of screen printing operations required for sheet production was minimised to reduce production costs.

Additional design considerations addressed sensor *production* requirements including the connectivity of working electrodes for modification via the electrochemical polymerisation of poly(*o*-phenylenediamine) and the inclusion of redundant surface area to satisfy downstream packaging requirements. Quality control features were included in the sheet design to permit assessment of screen printing consistency by means of visual print registration marks and spiral design motifs to permit the automated assessment of ink conductivity. Sensor *function* design considerations led to the incorporation of a SIM connector contact area to permit interrogation of sensors by an instrument, a single dielectric print defining working and counter electrode areas and positions (thereby minimising sensor-to-sensor signal variation) and the inclusion of a fuse to prevent the same sensor being used more than once.

Following trial screen printing production (Parlex UK), sensor sheet design revisions were undertaken to prevent the loss of stir-independent response caused by regions of carbon-ink being exposed after cutting. This was achieved by replacing the continuous carbon-ink print design with screen printed silver ink *bus-bars* to facilitate the flow of current during the electrochemical polymerisation production step.

The revised sensor design was employed in a trial screen printing production run and sensors manufactured in this manner were shown to possess a base sensor variability of approximately 1.1% RSD in 20 ppm total chlorine, sufficiently low to permit subsequent sensor modification towards stir-independent aqueous chlorine detection.

As a prerequisite to the production of microelectrode arrays via ultrasonic ablation, an electrode surface must first be coated with a thin insulating film of poly(*o*-phenylenediamine). Chapter 5 described the electropolymerisation of poly(*o*-phenylenediamine) in neutral conditions at gold sputter-coated ground glass slide electrodes, showing a two electron transfer mechanism for the formation of a non-conducting, ultrathin film. To permit the cost-effective production of disposable aqueous chlorine sensors, this was then applied to screen printed carbon-ink electrode surfaces were it was discovered that the decreased electron transfer kinetics associated with carbon-ink host electrodes required an extension of the polymerisation potential range from 0 to +800 mV to 0 to +1000 mV (vs. Ag/AgCl). A pre-polymerisation sonocation step (three 0.5 s pulses of ultrasonic energy) was also identified as being required to remove trapped air from the electrode surface, to facilitate intimate contact with the monomer solution, in turn allowing a defect free polymer layer to be formed.

Film thickness of poly(*o*-phenylenediamine) on gold (10.2 nm) and on screen printed carbon-ink electrodes (8.1 nm) were shown to impart similar insulating properties. Estimations of film thickness required interrogation by cyclic voltammetry, and hexaammineruthenium(III) chloride was identified as an appropriate redox couple for screen printed carbon-ink surfaces. Screen printed carbon-ink electrodes passivated via electropolymerisation of insulating poly(*o*-phenylenediamine) were confirmed to show an approximately 90% decrease in response to free and total chlorine solutions. In order to reduce production costs, the polymerisation batch process was optimised as a function of time. A polymerisation regime of 0 to +1000 mV, with 40 sweeps at 50 mVs^{-1} was shown to produce the most effective barrier in the shortest time period (approximately 27 minutes).

Polymerisation batch size was successfully increased from single screen printed carbon-ink electrodes, up to sheets of 600 sensors by means of a custom-built industrial potentiostat, possessing an appropriate user interface for commercial production. This equipment has the capability to support the electropolymerisation of up to 40 sheets of sensors simultaneously, equating to a batch size of 24,000 sensors.

Chapter 6 described the laboratory-scale production of microelectrode array assemblies via the ultrasonic ablation of poly(*o*-phenylenediamine) modified gold sputter-coated ground glass slide electrodes. Sensors were interrogated using cyclic voltammetry and chrono-amperometry in a ferri/ferrocyanide redox couple to show sigmoidal behaviour and a convection-dependent signal contribution of <6%.

With a view to the cost-effective scale-up of microelectrode sensor production, an industrial-sized ultrasonic tank was procured and a modulated frequency sweep was introduced to enhance the uniformity of the ultrasonic field. Acoustic amplitude was then assessed using a custom-built hydrophone, which revealed a concentration of acoustic energy towards the centre of the tank. Variation in the intensity of ultrasonic cavitation was then mapped using aluminium foil test sheets and revealed the presence of node and antinodal positions associated with a standing wave field. The topography of the tank base (which acts as the emitting surface) was profiled and data shown to correlate with particular ablation patterns present on the aluminium foil test sheets. A procedure for analysing the distribution of cavitational activity via the sonochemical luminescence of Luminol was developed to exposed regions of high and low cavitational activity within the ultrasound tank, which in turn related to the focusing of energy by the positioning of the ultrasonic transducers and the asymmetry in the profile of the tank base. The distribution of acoustic energy was then enhanced by means of an acoustic baffling system

Investigations were carried out into the variation in the degree of ultrasonic ablation across sheets of 100 poly(*o*-phenylenediamine) modified screen printed carbon-ink electrodes exposed to 10 seconds of ultrasonic ablation in a fixed position (tank coordinates x = 18.75 cm, y = 56.25 cm, z = 35 cm). When sensors were interrogated potentiostatically using a 1mM hexaammineruthenium(III) chloride

solution, considerable variation in response was observed (~8.5% RSD), indicating that inhomogeneities in the distribution of cavitation remained. Furthermore, preferential transient bubble nucleation at the sharp edges of the sensor sheet was discovered, which required the construction of a mounting frame to improve the cavitational homogeneity in proximity to the edge of the sensor sheet.

To facilitate the equal exposure of the polymer modified electrodes to ultrasonic ablation, a robotics movement system was then constructed to enable the controlled movement of sensor sheets around a 30 mm radius at a rate of one revolution per sonication period. Multiple batches of 100 sensors produced with 10 seconds sonication at 75% power were shown to exhibit a low variation in amperometric response (~3.6% RSD), indicating a relatively uniform exposure to cavitational activity.

Following the success of the prototype robotics movement system, a heavy-duty replacement was obtained with the capability of supporting the simultaneous ultrasonic ablation of multiple sensor sheets. Initial investigations carried out into the properties of sensors produced in this environment indicated a non-ideal distribution of cavitational activity. However, future development of this aspect of sensor production, including for example a more refined ultrasonic tank construction, we believe will permit a sufficiently uniform cavitational exposure.

The optimisation of sonication process parameters for sheets of 100 poly(*o*-phenylenediamine) modified screen printed carbon-ink electrodes for the purpose of microelectrode array production was carried out by means of electrochemical analysis. Following chronoamperometric interrogation of sensors produced at range of sonication times and powers, an upper limit of 10% convection-dependent signal contribution was identified to permit the optimisation of process variables for attaining the highest possible amperometric current response. A sonication exposure time of 10 seconds at a relative power of 75% was determined as the optimal arrangement of ultrasonic power and duration for the purpose of microelectrode sensor production. Sensors produced in this manner were then

characterised via cyclic voltammetry and shown to offer good microelectrode array performance.

Broader perspectives towards the commercialisation of the microelectrode array devices fabricated via ultrasonic ablation are described in Chapter 7. Portable aqueous chlorine detection has been selected as the primary market for the commercialisation of an innovative microelectrode array manufacturing technology. Environmental monitoring sensor applications possess a number of attractive features, including reduced barriers to entry resulting from increasing performance demands and a willingness for forward-thinking companies to adopt new technologies. Furthermore, aqueous chlorine detection is relatively straight forward and avoids many of the cumbersome trails and evaluation periods associated with the commercialisation of medical products.

In order to achieve performance advantages over existing products, a method was developed for localising the chemical reagents required for chlorine detection at the electrode surface. Formulations excluded harmful chemicals and calibration profiles determined the suitability of the sensor construction for the measurement of 0.01 ppm total chlorine. By dedicating both working electrodes to the measurement of total chlorine, this will satisfy requirements for the detection of 5 ppb total chlorine in surface waters. Sensor responses for the detection of free chlorine using the final sensor construction was found to be marginally short of the required specification for a detection limit of 0.02 ppm free chlorine. Further optimisation of production and analysis methods will permit the necessary signal magnitude to be obtained. Principle organic and inorganic materials present in natural waters were shown to present little threat to the electrochemical detection of aqueous chlorine since the overpotentials required for their reduction are greater than those required for free and total chlorine analysis.

Based on the analysis of current technologies for the detection of aqueous chlorine and a comparison with the Microarray Limited approach, a marketing strategy was described to gain penetration of the aqueous chlorine detection market. Brand equity

was developed to facilitate entry into other analytical markets, safeguarding the future success of the company. By adopting a holistic approach to sensor production, downstream supply was benefited by the development of a novel packaging strategy permitting both a reduction in packaging costs and facilitating end-of-line use in the form of strips of 20, individually sealed, and partially separated sensors. This innovative packaging strategy may be exploited by virtually any electrochemical sensor manufacturing process and the concept has accordingly been protected through an international patent application.

In summary, the production of microelectrode array devices fabricated on an individual basis via the ultrasonic ablation of polymer-insulated gold-sputter coated surfaces has been extended towards the cost-effective, large-scale manufacture of a stir-independent aqueous chlorine sensor. Product development has been described from initial concept to the pre-production phase and Microarray Limited are currently negotiating licensing agreements prior to transfer of the chlorine analysis technology to existing bodies. Microarray Limited will retain control of the generic microelectrode array fabrication process and aim to further build its portfolio focusing on innovate electrochemical sensor technology.

CHAPTER 9

Suggestions for further work

Future research relating to microelectrode array manufacture will benefit from further enhancement in the uniformity of cavitational activity in the ultrasound tank. This may be achieved through a number of routes. Primarily, the design of the ultrasound tank must be improved to provide more accurate control over variables (such as power, time and temperature), eliminate asymmetry in the final construction and to include a motorised transducer base which will extend the artificial homogenisation of node and antinodal positions to the *x,y* plane. Further enhancement may be achieved by employing low 'Q-factor' ultrasonic transducers in the construction of the tank. These devices are less dependent than conventional transducers on their resonant frequency, and so a broader frequency sweep can be applied without loss of power.

Following the implementation of ultrasound tank modifications, further work can be carried out into the scale-up of the ultrasonic ablation process in order to permit the the simultaneous sonication of 40 sheets of 600 sensors, corresponding to a batch size of 24,000 sensors.

In addition to company confidential investigations and the data presented in Chapter 7, more detailed research into the effects of possible interferents on the reliability of measurements from the Microarray Limited portable aqueous chlorine analyser will be undertaken as part of a system validation procedure.

Other electrochemical sensor applications benefiting from low-cost microelectrode array manufacture can be pursued. Numerous opportunities exist including for example those of pesticide / herbicide detection in environmental monitoring or *in vitro* / *in vivo* point-of-care testing in healthcare diagnostics. These applications may require further innovations on sensor construction, for example involving growing conducting polymer 'mushroom' protrusions containing bio-recognition molecules within the ultrasonically fabricated microelectrode arrays.

CHAPTER 10

References

2000/60/EC (2000), *EU Water Framework Directive*, EEC, Brussels.

78/659/EEC (1997), *The Surface Waters Regulations*, EEC, Brussels.

94/62/EC (1994), *EU Packaging and Packaging Waste Directive*, EEC, Brussels.

98/83/EC (1998), *Drinking Water Directive: Quality of water intended for human consumption*, EEC, Brussels.

Abell, D.F. (1995), *Marketing Strategy: Strategic Windows*, Butterworth-Heinemann Limited, Oxford.

Adams, R.N. (1958), 'Carbon Paste Electrodes', *Analytical Chemistry,* Vol. 30, p. 1576.

Almeida, N.F. and Mulchandani, A.K. (1993), 'A mediated amperometric enzyme electrode using tetrathiafulvalene and L-glutamate oxidase for the determination of L-glutamic acid', *Analytica Chimica Acta,* Vol. 282, p. 353-361.

Alvarez-Icaza, M. and Bilitewski, U. (1993), 'Mass production of biosensors', *Analytical Chemistry,* Vol. 65, No. 11, p. 525A-533A.

Amatore, C. (1995), *Physical Electrochemistry*, Marcel Dekker, New York, USA.

Amatore, C., Savéant, J.M. and Tessier, D. (1983), 'Charge transfer at partially blocked surfaces', *Journal of Electroanalytical Chemistry,* Vol. 147, p. 39-51.

Anderson, J.L., Coury, L.A.J. and Leddy J. (1998), 'Dynamic electrochemistry: methodology and application', *Analytical Chemistry,* Vol. 70, p. 519R-589R.

Aoki, K., Morita, M., Niwa, O. and Tabei, H. (1989), 'Fabrication and characteristics of vertically separated interdigitated array electrodes', *Journal of Electroanalytical Chemistry,* Vol. 267, p. 291-297.

Apfel, R.E. (1981), *Methods in Experimental Physics, Volume 19*, Academic Press Limited, New York, USA.

Bach, H.C. (1966), 'Polymer preparation', *American Chemical Society Division of Polymer Chemistry,* Vol. 7, p. 576-581.

Bakker, E. (2004), 'Electrochemical sensors', *Analytical Chemistry,* Vol. 76, No. 12, p. 3285-3298.

Bakker, E. and Pretsch, E. (2002), 'The new wave of ion-selective electrodes', *Analytical chemistry A-pages,* Vol. 74, No. 15, p. 420A-426A.

Bard, A.J. and Faulkner, L.R. (2001), *Electrochemical Methods: Fundamentals and Applications* (2nd edition), John Wiley & Sons Limited, New York, USA.

Barton, A.C., Collyer, S.D.C., Davis, F., Gornall, D.D., Law, K.A., Lawrence, E.C.D., Mills, D.W., Myler, S., Pritchard, J.A., Thompson, M. and Higson, S.P.J. (2004), 'Sonochemically fabricated microelectrode arrays for biosensors offering widespread applicability: part I', *Biosensors and Bioelectronics,* Vol. 20, p. 328-337.

Batterman, S., Zhang, L. and Wang, S. (2000), 'Quenching of chlorination disinfection by-product formation in drinking water by hydrogen peroxide', *Water Research,* Vol. 34, No. 5, p. 1652-1658.

BCC Research (2002), *Worldwide Diabetes Market,* available at: http://www.bccresearch.com/editors/RB-158.html (accessed 10th June 2004).

Beck, F. (1988), 'Electrodeposition of polymer coatings', *Electrochimica Acta,* Vol. 33, p. 839-850.

Bilitewski, U. and Turner, A.P.F. (Eds.) (2000), *Biosensors for Environmental Monitoring,* Harwood Academic Publishers, Amsterdam, The Netherlands.

Binnie, C., Kimber, M. and Smethurst, G. (2002), 'Basic Water Treatment', (3rd edition), Thomas Telford Publishing, London, UK, p. 211-228.

Birkin, P.R., Power, J.F., Vinçotte, A.M.L. and Leighton, T.G. (2003), 'A 1 KHz resolution frequency study of a variety of sonochemical processes', *Physical Chemistry Chemical Physics,* Vol. 5, p. 4170-4174.

Bjerknes, V.F.K. (1906), *Fields of Force*, Columbia University Press, New York, USA.

Bockris, J.M., Devanathan, M.A. and Muller, K. (1963), 'On the structure of charged interfaces', *Proceedings from the Royal Society,* Vol. A274, p. 55-79.

Borrely, S.I., Cruz, A.C., Mastro, N.L., Sampa, M.H.O. and Somessari, E.S. (1998a), 'Radiation processing of sewage and sludge. A review.', *Progress in Nuclear Energy,* Vol. 33, No. 1-2, p. 3-21.

Borrely, S.I., Mastro, N.L. and Sampa, M.H.O. (1998b), 'Improvements in municipal wastewaters by electron beam accelerator in Brazil', *Radiation Physics and Chemistry,* Vol. 52, No. 1-6, p. 333-337.

Boswell, J. (2001), *Investigations into discrepancies between E.A. Wales (EAW) and DCWW in measuring free chlorine in the field*, Trem y Dyffryn, Wales.

Brannen, G.E. and Bush, W.H. (1984), 'Ultrasonic destruction of kidney stones', *Western Journal of Medicine,* Vol. 140, No. 2, p. 227-232.

Brett, C.M.A. (2001), 'Electrochemical sensors for environmental monitoring. Strategy and examples.', *Pure Applied Chemistry,* Vol. 73, No. 12, p. 1969-1977.

Brett, M.A. and Brett, A.M.O. (1998), *Electroanalysis*, Oxford University Press Inc., New York.

Butler, J.A.V. (1924), 'Studies in heterogeneous equilibria. Part II. The kinetic interpretation of the Nernst theory of electromotive force', *Transactions of the Faraday Society,* Vol. 19, p. 729-733.

Campbell, J.K., Sun L. and Crooks, R.M. (1999), 'Electrochemistry using single carbon nanotubes', Vol. 121, p. 3779-3780.

Cardosi, M.F. and Turner, A.P.F. (1989), 'The realisation of electron transfer from biological molecules to electrodes', Oxford University Press, Oxford, p. 257-275.

Cass, A.E.G., Davis, G., Francis G. D., Hill, H.A.O., Aston, W.J., Higgins, I.J., Plotkin, E.V., Scott, L.D.L. and Turner, A.P.F. (1984), 'Ferrocene-mediated enzyme electrode for amperometric determination of glucose', *Analytical Chemistry,* Vol. 56, p. 667-671.

Castanón, M.J.L., Ordieres, A.J.M. and Blanco, P.T. (1997), 'Amperometric detection of ethanol with poly(*o*-phenylenediamine)- modified enzyme electrodes', *Biosensors and Bioelectronics,* Vol. 12, No. 6, p. 511-520.

Cattrall, R.W. (1997), *Chemical Sensors*, Oxford University Press, New York.

Centonze, D., Malitesta, C., Palmisano, F. and Zambonin, P.G. (1994), 'Permeation of solutes through an electropolymerised ultrathin poly-*o*-phenylenediamine film used as an enzyme-trapping membrane', *Electroanalysis,* Vol. 6, p. 423-429.

Chapman, D.L. (1913), 'A contribution to the theory of electrocapillarity', *Philosophical Magazine,* Vol. 25, p. 475-481.

Cheek, G., Wales, C.P. and Nowak, R.J. (1983), 'pH response of platinum and vitreous carbon electrodes modified by electropolymerised films', *Analytical Chemistry,* Vol. 55, p. 380-381.

Chemical Market Associates Inc. (2003), *World Chlor-Alkali Analysis*, 555 Pleasantville Road, New York, USA.

Cheung, H.M. and Gaddam, K. (2000), 'Ultrasound-assisted emulsion polymerization of methyl methacrylate and styrene', *Journal of Applied Polymer Science,* Vol. 76, p. 101-104.

Chiang, C.F., Tsai, C.T., Lin, S.T., Huo, C.P. and Lo, K.V. (2003), 'Disinfection of hospital water by continuous ozonation', *Journal of Environmental Science and Health,* Vol. A38, No. 12, p. 2895-2908.

Chiba, K., Ohsaka, T., Ohnuki, Y. and Oyama, N. (1987), 'Electropolymerisation preparation of a ladder polymer containing phenazine rings', *Journal of Electroanalytical Chemistry,* Vol. 219, p. 117-124.

Church, C.C. and Cartensen, E.L. (2001), '"Stable" inertial cavitation', *Ultrasound in Medicine and Biology,* Vol. 27, p. 1435-1437.

Clark, L.C.Jr. (inventor) (1970), *Membrane polarographic electrode system and method with electrochemical compensation*. U.S. Patent No.3, 539, 455.

Clark, L.C.Jr. (1956), 'Monitor and control of blood tissue oxygen tensions', *Transactions of the American Society for Artificial Internal Organs,* Vol. 2, p. 41-48.

Clark, L.C.Jr. and Lyons, C. (1962), 'Electrode systems for continuous monitoring in cardiovascular surgery', *Annals of the New York Academy of Sciences,* Vol. 102, p. 29-45.

Cooper, W.J., Sorber, C.A. and Meier, E.P. (1975), 'A rapid free available chlorine test with syringaldazine', *Journal of the American Water Works Association,* Vol. 67, p. 34-39.

Cottrell, F.G. (1902), 'Der reststrom bei galvanischer polarisation, betrachtet als ein diffusionsproblem', *Zeitschrift für Physikalische Chemie,* Vol. 61, p. 385-431.

Craik, S.A., Finch, G.R., Bolton, J.R. and Belosevic, M. (2000), 'Inactivation of *Giardia Muris* cysts using medium-pressure ultraviolet radiation in filtered drinking water', *Water Research,* Vol. 34, No. 18, p. 4325-4332.

Crawford, A.E. (1964), 'The measurement of cavitation', *Ultrasonics,* Vol. 2, No. 3, p. 120-123.

Crum, L.A. (1984), 'Rectified diffusion', *Ultrasonics,* Vol. 22, No. 5, p. 215-223.

Crum, L.A. (1994), 'Sonoluminescence', *Physics Today,* September publication, p. 22-29.

Cui, G., Yoo, J.H., Lee, J.S., Yoo, J., Uhm, J.H., Cha, S.G. and Nam, H. (2001), 'Effect of pre-treatment on the surface and electrochemical properties of screen-printed carbon paste electrodes', *The Analyst,* Vol. 126, p. 1399-1403.

Cunningham, W., Mathieson, K., McEwan, F.A., Blue, A., McGeachy, R., McLeod, J.A., Morris-Ellis, C., O'Shea, V., Smith, K.M., Litke, A. and Rahman, M. (2001), 'Fabrication of microelectrode arrays for neural measurements from retinal tissue', *Journal of Physics D: Applied Physics,* Vol. 34, p. 2804-2809.

Curie, J. and Curie, P. (1880), 'Cristallophysique: Développment, par pression, de l'électricité polaire dans les cristaux hémiedres a faces inclinées', *Comptes Rendus,* Vol. 91, p. 294-295.

Currie, L.A. (1968), 'Limits for qualitative detection and quantitative determination', *Analytical Chemistry,* Vol. 40, p. 586-593.

Currie, L.A. (1995), 'Nomenclature in evaluation of analytical methods including detection and quantification capabilities', *Pure Applied Chemistry,* Vol. 67, p. 1699-1723.

Curulli, A., Kelly, S., O'Sullivan, C., Guilbault, G.G. and Palleschi, G. (1998), 'A new interference-free lysine biosensor using a non-conducting polymer film', *Biosensors and Bioelectronics,* Vol. 13, p. 1245-1250.

D'Elia, L.F., Ortíz, L.R., Márquez, O.P., Márquez, J. and Martínez, Y. (2001), 'Electrochemical deposition of poly(*o*-phenylenediamine) films on type 304 stainless steel', *Journal of The Electrochemical Society,* Vol. 4, p. C297-C300.

Dai, H.P., Wu, Q.H., Sun, S.G. and Shiu, K.K. (1998), 'Electrochemical quartz crystal microbalance studies on the electropolymerisation processes of *ortho*-phenylenediamine in sulfuric acid solutions', *Journal of Electroanalytical Chemistry,* Vol. 456, p. 47-59.

Dayton, M.A., Brown, J.C., Stutts, K.J. and Wightmann, R.M. (1980), 'Faradaic electrochemistry at microvoltammetric electrodes', *Analytical Chemistry,* Vol. 52, p. 946-950.

Deakin, M.R., Stutts, K.J. and Wightman, R.M. (1985), 'The effect of pH on some outer-sphere electrode reactions at carbon electrodes', *Journal of Electroanalytical Chemistry,* Vol. 182, p. 113-122.

Dendy, P.P. (1988), 'Sonoluminescence and the ultrasound hazard debate', *Physics in Medical Biology,* Vol. 32, No. 11, p. 1233-1237.

Deng, H. and Van Berkel, G.J. (1999), 'Electrochemical polymerisation of aniline investigated using on-line electrochemistry/electrospray mass spectrometry', *Analytical Chemistry,* p. 4284-4293.

Devaraju, V., Lewin, P.A. and Bleeker, H. (2002), 'Determination of sensitivity versus frequency characteristics of miniature ultrasonic hydrophones below 1 MHz using planar scanning technique', *Journal of Ultrasound Medicine,* Vol. 21, p. 261-268.

Diekers, M., Hirsch, A., Luo, C. and Guldi, D.M. (2000), 'Synthesis, cyclic voltammetry, and photophysical properties of a bridged *o*-phenylenediamine-C_{60} dyad', *Organic Letters,* Vol. 2, No. 18, p. 2741-2744.

Dimaki, M. and Boggild, P. (2004), 'Dielectrophoresis of carbon nanotubes using microelectrodes: a numerical study', *Nanotechnology,* Vol. 15, p. 1095-1102.

Dock, E. and Ruzgas, T. (2003), 'Screen-printed carbon electrodes modified with cellobiose dehydrogenase: amplification factor for catechol vs. reversibility of ferricyanide', *Electroanalysis,* Vol. 15, No. 5-6, p. 492-498.

Doppler, C. (1843), 'Über das farbige Licht der Dopplesterne und einiger anderer Gestirne des Himmels', *Abhandlungen der königlichen böhmischen Gesellschaft der Wissenschaften,* Vol. 2, p. 465-482.

Doyle, P. (1994), *Marketing Management & Strategy*, Prentice-Hall International, New York, USA.

Dunn, D.J. (2001), *Fundamental Engineering Thermodynamics*, Longman, London, UK.

Egan, C., Shipley, D. and Howard, P. (1992), *Perspectives on Marketing Management*, John Wiley & Sons Limited, Chichester, Sussex, UK.

Eggins, B.R. (2002), *Chemical Sensors and Biosensors*, John Wiley & Sons Limited, Wiltshire, UK, p. 5-9.

Ekinci, E., Erdogdu, G. and Karagözler, A.E. (2001), 'Preparation, optimisation, and voltammetric characteristics of poly(*o*-phenylenediamine) film as a dopamine-selective polymeric membrane', *Journal of Applied Polymer Science,* Vol. 79, p. 327-332.

Emmerson, A.M. (2001), 'Emerging waterborne infections in health-care settings', *Emerging Infectious Disease,* Vol. 7, No. 2, p. 272-276.

Emr, S. and Yacynych, A. (1995), 'Use of polymer films in amperometric biosensors', *Electroanalysis,* Vol. 7, p. 913-923.

EPA-821-R-03-005 (February 2003), *U.S. Environmental Protection Agency: Technical Support Document for the Assessment of Detection and Quantitation Approaches*, Washington DC.

Epstein, S.S. (1974), 'Environmental determinants of human cancer', *Cancer Research,* Vol. 34, p. 2425-2435.

Erdey-Grúz, T. and Volmer, M. (1930), 'Zur theorie der wasserstoffüberspannung', *Zeitschrift für Physicalische Chemie,* Vol. 150A, p. 203-213.

Esty, D.C. and Chertow, M. (1997), *Thinking Ecologically: An Introduction*, Yale University Press, New Haven, Connecticut, USA.

Etter, P.C. (2003), *Underwater Acoustics Modelling and Simulation* (3rd edition), Spon Press, London, UK.

European Environment Agency (2002), *Europe's environment: the third assessment. Part 12: Environmental and human health,* accessed 20th June 2004, available at: http://reports.eea.eu.int/environmental_assessment_report_2003_10/en/kiev_chapt_12.pdf

Feeney, R. and Kounaves, S.P. (2000), 'Microfabricated ultramicroelectrode arrays: developments, advances, and applications in environmental analysis', *Electroanalysis,* Vol. 12, No. 9, p. 677-684.

Fick, A. (1855), 'Ueber diffusion', *Annalen der Physik, Leipzig,* Vol. 170, p. 59-86.

Fieser, L.F. (1930), 'An indirect method of studying the oxidation-reduction potentials of unstable systems, including those from the phenols and amines', *Journal of the American Chemical Society,* Vol. 52, No. 12, p. 5204-5241.

Fleischmann, M., Pons, S., Rolinson, D.R., and Schmidt, P.P. (1987), *Ultramicroelectrodes*, Datatech Systems, Morganton, USA.

Fletcher, S. and Horne, M.D. (1999), 'Random assemblies of microelectrodes (RAM™ electrodes) for electrochemical studies', *Electrochemistry Communications,* Vol. 1, p. 502-512.

Flynn, H.G. (1964), *Physics of Acoustic Cavitation on Liquids*, Academic Press Limited, New York, USA.

Fofonoff, T.A., Martel, S.M., Hatsopoulos, N.G., Donoghue, J.P. and Hunter, I.W. (2004), 'Microelectrode array fabrication by electrical discharge machining and chemical etching', *IEEE Transactions onn Biomedical Engineering,* Vol. 51, No. 6, p. 890-895.

Ford, D. and Saren, M. (2001), *Managing and Marketing Technology*, Thomson Business Press, London, UK.

Frass, A., Lehmann, G., Lomonosov, A. and Hess, P. (2001), 'Linear and nonlinear elastic surface waves: from seismic waves to materials science', *Analytical Sciences,* Vol. 17, p. S9-S12.

Frederick, J.R. (1965), *Ultrasonics Engineering*, John Wiley & Sons Limited, New York, USA.

Freedonia Group International (April 2002), *Chemical Sensors to 2006: Liquid, Gas and Biosensors*,

Frenzel, H. and Schultes, H. (1934), 'Lumineszenz im ultraschallbeschickten wasser', *Zeitschrift Für Physikalische Chemie,* Vol. B27, p. 421-424.

Fritsche, J. (1840), 'Ueber das anilin, ein neues zerselzungs-product des indigo', *Journal für Praktische Chemie,* Vol. 20, p. 453-459.

Gaitan, D.F., Crum, L.A., Church, C.C. and Roy, R.A. (1992), 'Sonoluminescence and bubble dynamics for a single, stable, cavitation bubble', *Journal of the Acoustical Society of America,* Vol. 91, No. 6, p. 3166-3183.

Galton, F. (1883), *Inquiries into Human Faculty and Development*, MacMillan, London.

Galán-Vidal, C.A., Muńoz, J., Domínguez, C. and Alegret, S. (1995), 'Chemical sensors, biosensors and thick-film technology', *Trends in Analytical Chemistry,* Vol. 14, No. 5, p. 225-231.

Garjonte, R. and Malinaukas, A. (1999), 'Amperometric glucose biosensor based on glucose oxidase immobilized in poly(*o*-phenylenediamine) layer', *Sensors and Actuators B,* Vol. 56, p. 85-92.

Ghiotto, A. and Penrose, J.D. (2000), 'Investigating the acoustic properties of the underwater implosions of light globes and evacuated spheres', *Austrailian Acoustical Society Conference,* Joondalup, Australia,

Gilmore, R.S. (1996), 'Review article: industrial ultrasonic imaging and microscopy', *Journal of Physics D: Applied Physics,* Vol. 29, p. 1389-1417.

Glaser, J.A., Foerst, D.L., McKee, G.D., Quave, S.A. and Budde, W.L. (1981), 'Trace analysis for wastewaters', *Environmental Science & Technology,* Vol. 15, p. 1426-1435.

Global Information Inc. (March 2004), Sensor products: amperometric electrochemical sensor demand in *Chemical Sensors: Liquid, Gas and Biosensors* (report)

Gobet, J., Rychen, P., Cardot, F. and Santoli, E. (2003), 'Microelectrode array sensor for water quality monitoring', *Water Science Technology,* Vol. 47, No. 2, p. 127-134.

Gokoglu, N., Yerlikaya, P. and Cengiz, E. (2003), 'Biogenic amines formation in sardine marinade during refrigerated storage', *Journal of Food Biochemistry,* Vol. 27, p. 361-447.

Gordon, G., Cooper, W.J., Rice, R.G. and Pacey, G.E. (1992a), 'Disinfectant Residual Measurement Methods', (2nd edition), Research Foundation, Colorado, UK, pp. 33-35.

Gordon, G., Cooper, W.J., Rice, R.G. and Pacey, G.E. (1992b), 'Disinfectant Residual Measurement Methods', (2nd edition), Research Foundation, Colorado, UK, pp. 62.

Gore, A. (1992), *Earth in the Balance*, Penguin, New York, USA.

Gottardi, W. (1999), 'Iodine and disinfection: theoretical study on mode of action, efficiency, stability, and analytical aspects in the aqueous system', *Archiv der Pharmazie - Pharmaceutical and Medicinal Chemistry,* Vol. 332, No. 5, p. 151-157.

Gouy, G. (1910), 'Sur la constitution de la charge électrique a la surface d'un électrolyte', *Comptes Rendus,* Vol. 149, p. 654-657.

Grahame, D.C. (1947), 'The electrical double layer and the theory of electrocapillarity', *Chemical Reviews,* Vol. 41, p. 441-501.

Granger, M.C. and Swain, G.M. (1999), 'The influence of surface interactions on the reversibility of ferri/ferrocyanide at boron-doped diamond thin-film electrodes', *Journal of the Electrochemical Society,* Vol. 146, p. 4551-4558.

Green, M.J. and Hilditch, P.I. (1991), 'Disposable single-use sensors', *Analytical Proceedings,* Vol. 28, p. 374-376.

Greenspan, M. and Tschiegg, C.E. (1967), 'Ultrasonic cavitation in ultra-pure water', *Journal of Research of The National Bureau of Standards, Section C,* Vol. 71, p. 229-234.

Grennan, K., Killard, A.J. and Smyth, M.R. (2001), 'Physical characterisations of a screen-printed electrode for use in an amperometric biosensor system', *Electroanalysis,* Vol. 13, No's. 8-9, p. 745-750.

Guilbault, G.G. (1976), *Analysis of Substrates*, Marcell Dekker Inc., New York.

Haas, C.N. (1999), *Water Quality and Treatment: a handbook of community water supplies (American Water Works Association)* (5th edition), McGraw-Hill, New York, USA.

Hall, T. and Hyde, R.A. (1992), *Water Treatment Processes and Practices*, WRc, Swindon, UK.

Hammer, M. (1996), *Beyond reengineering: how the process-centered organization is changing our work and our lives* (1st edition), Harper Collins Inc., New York, USA.

Hanna (2004), *Health & Safety Data Sheet for N,N-Diethyl-1,4-phenylenediammonium sulfate (DPD)*

Harp, D.L. (1995), *Current Technology of chlorine analysis for water and wastewater*, Hach Company, Loveland, Colorado, USA.

Hart, J.P. and Pemberton, R.M. (1997), *A Review of Screen-Printed Electrochemical Sensors*, Faculty of Applied Sciences, University of the West of England, Bristol, UK.

Hart, J.P.W.S.A. (1994), 'Screen-printed voltammetric and amperometric electrochemical sensors for decentralized testing', *Electroanalysis,* Vol. 6, p. 617-624.

Hashimoto, A., Kunikane, S. and Hirata, T. (2002), 'Prevalence of *Cryptosporidium* oocysts and *Giardia* cysts in the drinking water supply in Japan', *Water Research,* Vol. 36, p. 519-526.

Hatch, G. and Yang, V. (1983), 'Determining residual chlorine: effect of temperature on the titrametric starch-iodine end point', *Journal of the American Water Works Association,* Vol. 75, p. 154-156.

Heineman, W.R., Wieck, H.J. and Yacynych, A.M. (1980), 'Polymer film chemically modified electrode as a potentiometric sensor', *Analytical Chemistry,* Vol. 52, p. 345-346.

Hepher, M.J., Duckett, D. and Loening, A. (2000), 'High-speed video microscopy and computer enhanced imagery in the pursuit of bubble dynamics', *Ultrasonics Sonochemistry,* Vol. 7, p. 229-233.

Hernlem, B.J. and Tsai, L.S. (2000), 'Titration of chlorine: amperometric versus potentiometric', *Journal of the American Water Works Association,* Vol. 92, No. 12, p. 101-107.

Heyrovsky, J. (1922), 'Elektrolysa se rtutovou kapkovou kathodou', *Chemické Listy,* Vol. 16, p. 256-264.

Heyrovsky, J. (1948), 'Modern trends of polarographic analysis', *Analytica Chimica Acta,* Vol. 2, No. 2, p. 533-541.

Higson, S.P.J. (Filed 19th November 1996; publication date October 1996), '*Sensor*', International Patent PCT/GB96/0092.

Higson, S.P.J. (Filed September 2002; publication date April 2004), '*Heat-sealed protective film for electrochemical sensors*', International Patent WO 2004/029609.

Higson, S.P.J. and Vadgama, P. (1993), 'A study of electrical double layer effects in the pretreatment of two-electrode cells for enzyme electrodes', *Electroanalysis,* Vol. 5, p. 431-436.

Hodnett, M. and Zeqiri, B. (1997), 'A strategy for the development and standardisation of measurement methods for high power/cavitating ultrasonic fields: a review of high power field measurment techniques', *Ultrasonics Sonochemistry,* Vol. 4, p. 273-288.

Horst, C., Chen, Y.S., Kunz, U. and Hoffmann, U. (1996), 'Design, modeling and performance of a novel sonochemical reactor for heterogeneous reactions', *Chemical Engineering Science,* Vol. 51, No. 10, p. 1837-1846.

Howe, A.D., Forster, S., Morton, S., Marshall, R., Osborne, K.S. and Wright, P. (2002), 'Cryptosporidium oocysts in a water supply associated with cryptosporidiosis outbreak', *Emerging Infectious Diseases,* Vol. 8, No. 6, p. 619-624.

Hu, I.F., Karweik, D.H. and Kuwana, T. (1985), 'Activation and deactivation of glassy carbon electrodes', *Journal of Electroanalytical chemistry,* Vol. 188, p. 59-72.

Hua, I. and Thompson, J.E. (2000), 'Inactivation of *Escherichia Coli* by sonication at discrete ultrasonic frequencies', *Water Research,* Vol. 34, No. 15, p. 3888-3893.

Imisides, M.D., John, P., Riley, P.J. and Wallace, G.G. (1991), 'The use of electropolymerisation to produce new sensing surfaces: a review emphasizing electrodeposition of heteroaromatic compounds', *Electroanalysis,* Vol. 3, p. 879-889.

Imisides, M.D., John, R. and Wallace, G.G. (1996), 'Microsensors based on conducting polymers', *Chemtech,* Vol. 26, No. 5, p. 19-25.

Iqbal, S.S., Mayo, M.W., Bruno J.G., Bronk, B.V., Batt, C.A. and Chambers, J.P. (2000), 'A review of molecular recognition technologies for detection of biological threat agents', *Biosensors & Bioelectronics,* Vol. 15, p. 549-578.

Irvine, T. (1979), *Blevins, R.*, Krieger Publishers Company, Malabar, Florida, USA.

IUPAC (1997a), *Definition of a chemical sensor,* accessed February 18th 2004, available at: http://www.iupac.org/publications/analytical_compendium/Cha07sec4.pdf

IUPAC (1997b), *Limit of detection (in analysis),* accessed November 20th 2003, available at: http://www.iupac.org/goldbook/L03540.pdf

Janata, J. (2001), 'Centennial retrospective on chemical sensors', *Analytical Chemistry,* Vol. 73, No. 5, p. 150A-153A.

Janata, J. and Josowicz, M. (1998), 'Chemical sensors', *Analytical Chemistry,* Vol. 70, No. 12, p. 179R-208R.

Jang, D.H., Yoo, Y.S. and Oh, S.M. (1995), 'Electropolymerisation mechanism for poly(*o*-phenylenediamine) (PPD) and its electrocatalytic behaviour for O_2 reduction', *Bulletin of the Korean Chemical Society,* Vol. 16, No. 5, p. 392-396.

John, R. and Wallace, G.G. (1990), 'Dispensed mercury microelectrodes using non-conducting polymer coatings', *Analytica Chimica Acta,* Vol. 235, p. 451-455.

Junli, H., Li, W., Nanqi, R. and Fang, M. (1997), 'Disinfection effect of chlorine dioxide on bacteria in water', *Water Research,* Vol. 31, No. 3, p. 607-613.

Kalcher, K. (1990), 'Chemically modified carbon paste electrodes in voltammetric analysis', *Electroanalysis,* Vol. 2, p. 419-433.

Kano, N. (1984), 'Attractive quality and must-be quality', *Journal of the Japanese Society for Quality Control,* Vol. 1, No. 4, p. 39-48.

Kelly, S.C., O'Connell, P.J., O'Sullivan, C.K. and Guilbault, G.G. (2000), 'Development of an interferent free amperometric biosensor for determination of L-lysine in food', *Analytica Chimica Acta,* Vol. 412, p. 111-119.

Kim, C.H., Park, D.S. and Shim, Y.B. (2001), 'Adsorptive voltammetric determination of azobenzene in trace levels using the modified electrode with a sol-gel film containing mercury salt', *Analytical Sciences,* Vol. 17, p. i1057-i1060.

Kinoshita, K. (1988), *Carbon: The Electrochemical and Physicochemical Properties,* John Wiley & Sons Limited, New York, USA.

Knox, S. and Bickerton, D. (2003), 'The six conventions of corporate branding', *European Journal of Marketing,* Vol. 37, No. 7-8, p. 998-1016.

Konopka, S.J. and McDuffie, B. (1970), 'Diffusion coefficients of ferri- and ferrocyanide ions in aqueous media, using twin-electrode thin-layer electrochemistry', *Analytical Chemistry,* Vol. 42, No. 14, p. 1741-1746.

Kotler, P. (1999), *Marketing Management: Millenium Edition* (10th edition), Prentice Hall Incorporated, New Jersey, USA.

Koudelka-Hep, M. and van der Wal, P.D. (2000), 'Microelectrode sensors for biomedical and environmental applications', *Electrochimica Acta,* Vol. 45, No. 15, p. 2437-2441.

Krefting, D., Mettin, R. and Lauterborn, W. (2004), 'High-speed observation of acoustic cavitation erosion in multibubble systems', *Ultrasonics Sonochemistry,* Vol. 11, p. 119-123.

Kress-Rogers, E., Hugi, A., MacDougall, D.B., Joshi, P., Bee, S., Benson, I.B., Ridley, I., Reh, I.C., Kent, M., Berrie, P.G., Denbow, N., Roberts, I., Lyng J.G., Roedel, W., Gibson, D.M., Kilcast, D., Bilitewski, U., Warsinke, A., and Tothill, I. (2001), *Instrumentation and Sensors for the Food Industry*, Woodhead Publishing Limited, Abington Hall, Abington, Cambridge, UK.

Kruus, P. (1991), 'Sonochemical initiation of polymerisation', *Advances in Polymer Chemistry,* Vol. 2, p. 1-21.

Lauterborn, W., Kurz, T., Mettin, R. and Ohl, C.D. (1999), 'Experimental and theoretical bubble dynamics', *Advances in Chemical Physics,* Vol. 110, p. 295-380.

Lauterborn, W. and Ohl, C.D. (1997), 'Cavitation bubble dynamics', *Ultrasonics Sonochemistry,* Vol. 4, p. 65-75.

Lee, H.J., Beriet, C., Ferrigno, R. and Girault, H.H. (2001), 'Cyclic voltammetry at a regular microdisc electrode array', *Journal of Electroanalytical Chemistry,* Vol. 502, p. 138-145.

Leighton, T. (1994), *The Acoustic Bubble*, Academic Press Limited, London.

Leighton, T.G. (1995), 'Bubble population phenomena in acoustic cavitation', *Ultrasonics Sonochemistry,* Vol. 2, No. 2, p. S123-S136.

Leighton, T.G., Walton, A.J. and Pickworth, M.J.W. (1990), 'Primary Bjerknes forces', *European Journal of Physics,* Vol. 11, p. 47-50.

Lewis, D. (1992), 'Doubt cast on claims for 'dolphin-friendly' tuna', *New Scientist,* Vol. 134, No. 1820, p. 10-11.

Li, X.G., Huang, M.R. and Duan, W. (2002), 'Novel multifunctional polymers from aromatic diamines by oxidative polymerisations', *Chemical Reviews,* Vol. 102, p. 2925-3030.

Li, X.G., Huang, M.R. and Yang, Y. (2001), 'Synthesis and characterisation of *o*-phenylenediamine and xylidine copolmers', *Polymer,* Vol. 42, p. 4099-4107.

Lindley, J., Mason, T.J. and Lorimer, J.P. (1987), 'Sonochemically enhanced Ullmann reactions', *Ultrasonics,* Vol. 25, p. 45-48.

Loeb, G.E., Peck, R.A. and Martyniuk, J. (1995), 'Toward the ultimate metal electrode', *Journal of Neuroscience Methods,* Vol. 63, p. 175-183.

Logman, M.J., Budygin, E.A., Gainetdinov, R.R. and Wightman, R.M. (2000), 'Quantitation of in vivo measurements with carbon fibre microelectrodes', *Journal of Neuroscience methods,* Vol. 95, p. 95-102.

Lord Rayleigh (1885), 'On waves propagated along the plane surface of an elastic solid', *Proceedings of the London Mathematical Society,* Vol. 17, p. 4-11.

Lord Rayleigh (1917), 'On the pressure developed in a liquid during the collapse of a spherical cavity', *Philosophical Magazine,* Vol. 34, p. 94-98.

Lord, S.S. and Rogers, L.B. (1954), 'Polarographic studies with gold, graphite, and platinum electrodes', *Analytical Chemistry,* Vol. 26, p. 284-295.

Losito, L., Giglio, E.D., Cioffi, N. and Malitesta, C. (2001), 'Spectroscopic investigation on polymer films obtained by oxidation of *o*-phenylenediamine on platinum electrodes at different pHs', *Journal of Materials Science Chemistry,* Vol. 11, p. 1812-1817.

Losito, L., Palmisano, F. and Zambonin, P.G. (2003), '*o*-Phenylenediamine electropolymerisation by cyclic voltammetry combined with electrospray ionization-ion trap mass spectrometry', *Analytical Chemistry,* Vol. 75, p. 4988-4995.

Luche, J.L. (1987), 'Organometallic sonochemistry: successes, problems and by-products', *Ultrasonics,* Vol. 25, p. 40-44.

Luche, J.L., Einhorn, C., Einhorn, J., de Souza Barboza, J.C., Petrier, C., Dupuy, C., Delair, P., Allavena, C. and Tuschl, T. (1990), 'Ultrasonic waves as promoters of radical processes in chemistry: the case of organometallic reactions', *Ultrasonics,* Vol. 28, p. 316-321.

Madou, M.J. (1997), *Fundamentals of Microfabrication*, CRC Press, Boca Raton, Florida, USA.

Malinauskas, A., Bron, M. and Holze, R. (1998), 'Electrochemical and raman spectroscopic studies of electrosynthesised copolymers and bilayer structures of polyaniline and poly(*o*-phenylenediamine)', *Synthetic Metals,* Vol. 92, p. 127-137.

Malinovskaya, T.D., Aparnev, A.I., Egorov, Y.P. and Yukhin, Y.M. (2001), 'Carbon monoxide semiconductor sensors based on SnO_2-Bi_2O_3', *Russian Journal of Applied Chemistry,* Vol. 74, No. 11, p. 1864-1867.

Malitesta, C., Losito, L. and Zambonin, P.G. (1999), 'Molecularly imprinted electrosynthesised polymers: new materials for biomimetic sensors', *Analytical Chemistry,* Vol. 71, p. 1366-1370.

Malitesta, C., Palmisano, F., Torsi, L. and Zambonin, P.G. (1990), 'Glucose fast-response amperometric sensor based on glucose oxidase immobilized in an electropolymerised poly(*o*-phenylenediamine) film', *Analytical Chemistry,* Vol. 62, p. 2735-2740.

Marcus, R.A. (1965), 'On the theory of electron-transfer reactions. VI. Unified treatment for homogeneous and electrode reactions', *Journal of Chemical Physics,* Vol. 43, No. 2, p. 679-701.

Mark, H. (1945), 'Some applications of ultrasonics in high-polymer research', *Journal of the Acoustical Society of America,* Vol. 16, p. 183-187.

Marsh, J., Scantlebury, J.D. and Lyon, S.B. (2001), 'Poly(2-allyl)phenylene-oxide electropolymer film growth on steel', *Journal of Applied Polymer Science,* Vol. 79, p. 1563-1571.

Martinusz, K., Inzelt, G. and Horányi, G. (1995), 'Coupled electrochemical and radiometric study of anion migration in poly(*o*-phenylenediamine) films', *Journal of Electroanalytical Chemistry,* Vol. 395, p. 293-297.

Mason, T.J. (1999), *Sonochemistry*, Oxford University Press, Oxford, UK.

Mason, T.J. and Lorimer, J.P. (2002), *Applied Sonochemistry*, Wiley-VCH, Weinheim, Verlag, Germany.

Mason, T.J., Lorimer, J.P. and Moorhouse, J.P. (1989), 'Sonochemistry - using ultrasonic baths', *Education in Chemistry,* January publication, p. 13-15.

Matula, T.J., Cordry, S.M., Roy, R.A. and Crum, L.A. (1997), 'Bjerknes force and bubble levitation under single-bubble sonoluminescence conditions', *Journal of the Acoustical Society of America,* Vol. 102, No. 3, p. 1522-1527.

McCreery, R.L. (1991), *Carbon Electrodes: Structural Effects on Electron Transfer Kinetics*, Dekker, New York, US.

Mederos, A., Domínguez, S., Hernández-Molina, R., Sanchiz, J. and Brito, F. (1999), 'Coordinating ability of phenylenediamines', *Coordination Chemistry Reviews,* Vol. 193-195, p. 913-939.

Merck (1998), *Analytical Quality Assurance, Standard for free chlorine,* accessed Novemeber 4th 2000, available at: http://photometry.merck.de/servlet/PB/menu/1170360/1170360.html

Mettin, R., Luther, S., Ohl, C.D. and Lauterborn, W. (1999), 'Acoustic cavitation structures and simulations by a particle model', *Ultrasonics Sonochemistry,* Vol. 6, p. 25-29.

Minnaert, M. (1933), 'On musical air bubbles and sounds of running water', *Philosophical Magazine,* Vol. 16, p. 235-248.

Mintel (September 2003), *Self Diagnostics Report*, Mintel International Group Limited, 18-19 Long Lane, London, UK.

Mintel (June 2004), *Potable Water Industrial Report*, Mintel International Group Limited, 18-19 Long Lane, London, UK.

Misík, V. and Riesz, P. (2000), 'Free radical intermediates in sonodynamic therapy', *Annals of the New York Academy of Sciences,* Vol. 899, p. 335-348.

Moholkar, V., Sable, S.P. and Pandit, A.B. (2000), 'Mapping the cavitation intensity in an ultrasonic bath using the acoustic emission', *The American Institute of Chemical Engineers,* Vol. 46, No. 4, p. 684-694.

Morf, W.E. (1996), 'Theoretical treatment of the amperometric current response of multiple microelectrode arrays', *Analytica Chimica Acta,* Vol. 330, p. 139-149.

Morf, W.E. (1997), 'Theoretical treatment of the current vs. time response of microelectrode arrays to changes of potential, concentration, or flow', *Analytica Chimica Acta,* Vol. 341, p. 121-127.

Morf, W.E. and de Rooij, N.F. (1997), 'Performance of amperometric sensors based on multiple microelectrode arrays', *Sensors and Actuators B,* Vol. 44, p. 538-541.

Morris, R., Frant, D.J. and White, H.S. (1987), 'Electrochemistry at Pt band electrodes of width approaching molecular dimensions', *Journal of physical Chemistry,* Vol. 91, p. 3559-3564.

Mudambi, S.M., Doyle, P. and Wong, V. (1997), 'An exploration of branding in industrial markets', *Industrial Marketing Management,* Vol. 26, p. 433-446.

Murphy, L.J. (1998), 'Reduction of interference response at a hydrogen peroxide detecting electrode using electropolymerised films of substituted naphthalenes', *Analytical Chemistry,* Vol. 70, p. 2928-2935.

Muńoz, E. and Palmero, S. (2004), 'Speciation of arsenic by potentiometric stripping analysis using gold(III) solution as chemical reoxidant and a wall-jet flow cell', *Electroanalysis,* Vol. 16, No. 23, p. 1956-1963.

Myler, S. (2000), *The Exploitation of Thin-Polymer-Films and Microelectrode Arrays for the Development of Electrochemical Biosensors*, PhD Thesis, University of Manchester Institute of Science and Technology (UMIST), Manchester, UK.

Myler, S., Collyer, S.D., Davis, F., Gornall, D. and Higson, S.P.J. (*Article in press*), 'Sonochemically fabricated microelectrode arrays for biosensors - Part III. AC impedimetric study of aerobic and anaerobic response of alcohol oxidase within polyaniline', *Biosensors and Bioelectronics.*

Myler, S., Davis, F., Collyer, S.D. and Higson, S.P.J. (2004), 'Sonochemically fabricated microelectrode arrays for biosensors - part II. Modification with a polysiloxane coating', *Biosensors and Bioelectronics,* Vol. 20, p. 408-412.

Myler, S., Eaton, S. and Higson, S.P.J. (1997), 'Poly(*o*-phenylenediamine) ultra-thin polymer-film composite membranes for enzyme electrodes', *Analytica Chimica Acta,* Vol. 357, p. 55-61.

Neppiras, E.A. (1984), 'Acoustic cavitation: an introduction', *Ultrasonics,* Vol. 22, No. 1, p. 25-28.

Newman, J.D., Tigwell, L.J., Warner, P.J., and Turner, A.P.F. (May 2002), 'Biosensors - an inside view', *Seventh World Congress on Biosensors,* Kyoto, Japan, Elsevier, Amsterdam, p. 1-10.

Nguyen, T.Q., Liang, Q.Z. and Henning, K. (1997), 'Kinetics of ultrasonic and transient elongational flow degradation: a comparative study', *Polymer,* Vol. 38, No. 15, p. 3783-3793.

Niwa, O. and Tabei, H. (1994), 'Voltammetric measurements of reversible and quasi-reversible redox species using carbon film based interdigitated array microelectrodes', *Analytical Chemistry,* Vol. 66, No. 285-289,

Norton, J.D., White, H.S. and Feldberg, S.W. (1990), 'Effect of the electrical double layer on voltammetry at microelectrodes', *Journal of Physical Chemistry,* Vol. 94, p. 6772-6780.

Ogura, K., Kokura, M., Yano, J. and Shiigi, H. (1995), 'Spectroscopic and scanning tunnelling microscope characterisation of virgin and recast films of electrochemically prepared poly(*o*-phenylenediamine)', *Electrochimica Acta,* Vol. 40, No. 17, p. 2707-2714.

Ogura, K., Shiigi, H. and Nakayama, M. (1996), 'A new humidity sensor using the composite film derived from poly(*o*-phenylenediamine) and poly(vinyl alcohol)', *Journal of the Electrochemical Society,* Vol. 143, p. 2925-2929.

Ohnuki, Y., Matsuda, H., Ohsaka, T. and Oyama, N. (1983), 'Permselectivity of films prepared by electrochemical oxidation of phenol and amino-aromatic compounds', *Journal of Electroanalytical Chemistry and Interfacial Chemistry,* Vol. 158, p. 55-67.

Ooi, S.K. and Biggs, S. (2000), 'Ultrasonic initiation of polystyrene latex synthesis', *Ultrasonics Sonochemistry,* Vol. 7, p. 125-133.

Osaka, T. (1997), 'Review: Electrochemical formation and microstructure in thin films for high functional devices', *Electrochimica Acta,* Vol. 42, No. 20-22, p. 3015-3022.

Oyama, N., Chiba, K., Ohnuki, Y. and Ohsaka, T. (1985), 'Electropolymerized aniline derivative films possessing selective electron transfer mediation properties for the redox reaction of dissolved substrates', *The Chemical Society of Japan,* Vol. 6, p. 1172-1177.

Oyama, N., Ohsaka, T., Chiba, K. and Takahashi, K. (1988), 'Effects of supporting electrolyte and pH on charge transport within electropolymerized poly(*o*-phenylenediamine) films deposited on graphite electrodes', *Bulletin of the Chemical Society of Japan,* Vol. 61, p. 1095-1101.

Paeschke, M., Wollenberger, U., Lisec, T., Schnakenberg, U. and Hintshe, R. (1995), 'Highly selective electrochemical microsensors using submicrometer electrode arrays', *Sensors and Actuators (B),* Vol. 26-27, p. 394-397.

Palin, A.T. (1957), 'The determination of free and combined chlorine in water by the use of diethyl-*p*-phenylene diamine', *Journal of the American Water Works Association,* Vol. 49, p. 873-880.

Palin, A.T. (1974), 'Chemistry of Modern Water Chlorination', *Water Services,* Vol. 78, p. 7-12.

Payment, P., Siemiatycki, J., Richardson, L., Renaud, G., Franco, E. and Provost, M. (1997), 'A prospective epidemiological study of gastrointestinal health effects due to consumption of drinking water', *International Journal of Environmental Health Research,* Vol. 7, p. 5-31.

Penner, R.M., Heben, M.J., Longin, T.L. and Lewis, N.S. (1990), 'Fabrication and use of nanometer-sized electrodes in electrochemistry', *Science,* Vol. 250, p. 1118-1121.

Pharr, C.M. and Griffiths, P.R. (1997), 'Infrared spectroelectrochemical analysis of adsorbed hexacyanoferrate species formed during potential cycling in the ferrocyanide/ferricyanide redox couple', *Analytical Chemistry,* Vol. 69, p. 4673-4679.

Pierce, A.D. (1989), *Acoustics: an Introduction to its Physical Principles and Applications* (2nd edition), American Institute of Physics, Maryland, USA.

Pons, S. and Fleischmann, M. (1987), 'The behaviour of microelectrodes', *Analytical Chemistry,* Vol. 59, p. 1391A-1399A.

Pope, P.N. and Winter, A.T. (1985), 'An undergraduate experiment on acoustic impedance', *European Journal of Physics,* Vol. 6, p. 13-15.

Porter, M.E. (1980), *Competitive strategy: techniques for analyzing industries and competitors*, Free Press, New York, USA.

Porter, M.E. (1991), 'America's Green Strategy', *Scientific American,* Vol. 264, No. 4, p. 168-168.

Porter, M.E. and van der Linde, C. (1995a), 'Green and competitive: Ending the stalemate', *Harvard Business Review,* Vol. 73, No. 5, p. 120-134.

Porter, M.E. and van der Linde, C. (1995b), 'Towards a new conception of the environment-competitiveness relationship', *Journal of Economics Perspectives,* Vol. 9, No. 4, p. 97-118.

Prasad, B.M., Singh, D. and Misra, R.A. (1996), 'Synthesis and properties of poly(*o*-phenylenediamine)', *Journal of Polymer Materials,* Vol. 13, No. 2, p. 157-161.

Price, G., Hearn, M.P., Wallace, E.N.K. and Patel, A.M. (1996), 'Ultrasonically assisted synthesis and degradation of poly(dimethly siloxane)', *Polymer,* Vol. 37, No. 12, p. 2303-2308.

Price, G.J. (2003), 'Recent developments in sonochemical polymerisation', *Ultrasonics Sonochemistry,* Vol. 10, p. 277-283.

Pritchard, J., Law, K., Vakurov, A., Millner, P. and Higson, S.P.J. (2004), 'Sonochemically fabricated enzyme microelectrode arrays for the environmental monitoring of pesticides', *Biosensors and Bioelectronics,* Vol. 20, No. 4, p. 765-772

Prochazka, G.A. (1880), 'The boiling points of esters and ether esters of the oxi-acids', *Journal of the American Chemical Society,* Vol. 2, No. 4, p. 174-188.

Rawson, F.F. (1987), 'Ultrasonic technology in today's industry', *Physics Bulletin,* Vol. 38, p. 255-257.

Renaudin, V., Gondrexon, N., Boldo, P., Pétrier, C., Bernis, A. and Gonthier, Y. (1994), 'Method for determining the chemically active zones in a high-frequency ultrasonic reactor', *Ultrasonics Sonochemistry,* Vol. 1, No. 2, p. S81-S85.

Rice, M.E., Galus, Z. and Adams, R.N. (1983), 'Graphite paste electrodes', *Journal of Electroanalytical Chemistry,* Vol. 143, p. 89-102.

Rice, R.J. and McCreery, R.L. (1989), 'Quantitative relationship between electron transfer rate and surface microstructure of laser-modified graphite electrodes', *Analytical Chemistry,* Vol. 61, p. 1637-1641.

Richardson, S.D. (2003), 'Disinfection by-products and other emerging contaminants in drinking water', *Trends in Analytical Chemistry,* Vol. 22, No. 10, p. 666-684.

Ries, A. and Trout, J. (2001), *Positioning: The Battle for Your Mind*, McGraw-Hill Education, Maidenhead, UK.

Riesz, P., Berdahl, D. and Christman, C.L. (1985), 'Free radical generation by ultrasound in aqueous and non-aqueous solutions', *Environmental Health Perspectives,* Vol. 64, p. 233-252.

Rosemount Analytical (November 2001), *Chlorine Measurement by Amperometric Sensor*, report, accessed 4th July 2004, available at: http://www.emersonprocess.com/raihome/documents/Liq_AppData_43-6063_200111.pdf

Ross, B., Cammann, K., Mokwa, W. and Rospert, M. (1992), 'Ultramicroelectrode arrays as transducers for new amperometric oxygen sensors', *Sensors and Actuators B,* Vol. 7, p. 758-762.

Rubenstein, I. (1984), 'Voltammetric pH measurements with surface-modified electrodes and a voltammetric internal reference', *Analytical Chemistry,* Vol. 56, p. 1135-1137.

Russell, S. (1994), *Residual Chlorine: A Guide to Measurement in Water Applications*, WRc plc, Marlow, Buckingham, UK.

Ryan, M.R., Lowry, J.P. and O'Neill, R.D. (1997), 'Biosensor for neurotransmitter L-glutamic acid designed for efficient use of L-glutamate oxidase and effective rejection interference', *Analyst,* Vol. 122, p. 1419-1429.

Rúriková, D. and Kunáková, I. (1999), 'Determination of selenium in soils by cathodic stripping voltammetry after separation as gaseous selenium tetrabromide', *Chemical Papers,* Vol. 53, No. 4, p. 246-251.

Sarkar, P., Tothill I.E., Setford, S.J. and Turner, A.P.F. (1999), 'Screen-printed amperometric biosensors for the rapid measurement of L- and D-amino acids', *The Analyst,* Vol. 124, p. 865-870.

Sasso, S.V., Pierce, R.J., Walla, R. and Yacynych, A.M. (1990), 'Electropolymerised 1,2-diaminobenzene as a means to preventing interferences and fouling and to stabilize immobilized enzyme in electrochemical biosensors', *Analytical Chemistry,* Vol. 62, p. 1111-1117.

Schmitt, G., Schultz, J.W., Faßbender, F., Buß, G., Lüth, H. and Schöning, M.J. (1999), 'Passivation and corrosion of microelectrode arrays', *Electrochimica Acta,* Vol. 44, p. 3865-3883.

Schug, C., Schempp, S., Lamparter, P. and Steeb, S. (1999), 'Surface roughness of sputter-deposited gold films: a combined x-ray technique and AFM study', *Surface and Interface Analysis,* Vol. 27, p. 670-677.

Sehgal, C., Sutherland, R.G. and Verrall, R.E. (1980), 'Optical spectra of sonoluminescence of transient and stable cavitation in water saturated with various gases', *Journal of Physical Chemistry,* Vol. 84, No. 4, p. 388-395.

Shapira, D. and Saltmarsh, M.J. (2002), *Comments on possible of d-d fusion in sonoluminescence*Physics Division, Oak Ridge National Laboratory, Oak Ridge, Tennessee, USA.

Shlamovitz, G.Z., Iakobishvili, Z., Matz, I., Golovchiner, G., Lev, E., Siegal, R.J. and Birnbaum, Y. (2003), 'In vitro ultrasound augmented clot dissolution -what is the optimal timing of ultrasound application?', *Cardiovascular Drugs and Therapy,* Vol. 16, p. 521-526.

Shoup, D. and Szabo, A. (1984), 'Influence of insulation geometry on the current at microdisk electrodes', *Journal of Electroanalytical Chemistry,* Vol. 160, p. 27-31.

Shuqun, C., Xinda, Z., Zhaoyou, T., Yao, Y., Susu, B. and Dechu, Q. (2000), 'Effects of high-intensity focused ultrasound and anti-angiogenic agents on the ablation of experimental liver cancers', *Chinese Journal of Digestive Diseases,* Vol. 1, p. 35-38.

Silver, I.A. (1987), 'Microelectrodes in medicine', *Philosophical Transactions of the Royal Society of London,* Vol. B136, p. 161-167.

Sincero, A.P. and Sincero, G.A. (2003), *The Physical-Chemical Treatment of Water and Wastewater*, CRC Press, London, UK.

Sittampalam, G. and Wilson, G.S. (1983), 'Surface-modified electrochemical detector for liquid chromatography', *Analytical Chemistry,* Vol. 55, p. 1608-1610.

Smith-Bindman, R., Hosmer, W.D., Caponigro, M. and Cunningham, G. (2001), 'The variability in the interpretation of prenatal diagnostic ultrasound', *Ultrasound Obstetrics and Gynaecology,* Vol. 17, p. 326-332.

Snow, J. (1849), 'On the pathology and mode of the communication of cholera', *London Medical Gazette,* p. 745-752.

Southampton Electrochemistry Group (1985), *Instrumental Methods in Electrochemistry* (1st edition), Ellis Horwood, Chichester, UK.

Stafström, S., Brédas, J.L., Epstein, A.J., Woo, H.S., Tanner, D.B., Huang, W.S. and MacDiarmid, A.G. (1987), 'Polaron lattice in highly conducting polyaniline: theoretical and optical studies', *Physics Review Letters,* Vol. 59, No. 13, p. 1464-1467.

Stern, O. (1924), 'Zur theorie der elektrolytischen doppelschicht', *Zietschrift Elektrochemie,* Vol. 30, p. 508-516.

Stetter, J.R., Penrose W.R. and Yao, S. (2003), 'Sensors, chemical sensors, electrochemical sensors, and ECS', *Journal of the Electrochemical Society,* Vol. 150, No. 2, p. S11-S16.

Stoessel, S.J. (1993), 'The use of ultrasound to initiate ring-opening polymerisation', *Journal of Applied Polymer Chemistry,* Vol. 48, p. 505-507.

Štulík, K., Amatore, C., Holub, K., Mareček, V. and Kutner, W. (2000), 'Microelectrodes. Definitions, characterisation, and applications', *Pure Applied Chemistry,* Vol. 72, No. 8, p. 1483-1492.

Stumm, W. and Morgan, J.J. (1996), *Aquatics Chemistry* (3rd edition), John Wiley and Sons Limited, New York, USA.

Suslick, K.S. (1990), 'Sonochemistry', *Science,* Vol. 247, p. 1439-1445.

Suslick, K.S., Didenko, Y., Fang, M.M., Hyeon, T., Kolbeck, K.J., McNamara, W.B., Mdleleni, M.M. and Wong, M. (1999), 'Acoustic cavitation and its chemical consequences', *Philosophical Transactions of the Royal Society of London, Series A: Mathematical and Physical Sciences,* Vol. 357, p. 335-353.

Suslick, K.S., Hammerton, D.A. and Cline, R.E. (1986), 'The sonochemical hot spot', *Journal of the American Chemical Society,* Vol. 108, p. 5641-5642.

Svancara, I., Hvizdalová, M., Vytras, K. and Novotny, R. (1996), 'A microscopic study on carbon paste electrodes', *Electroanalysis,* Vol. 8, No. 1, p. 61-65.

Svancara, I. and Vytras, K. (2000), 'Physico-chemical processes in analytical electrochemistry with carbon paste electrodes. An overview', *Chemija,* Vol. 11, No. 1, p. 18-27.

Svancara, I., Vytras, K., Barek, J. and Zima, J. (2001), 'Carbon paste electrodes in modern electroanalysis', *Critical reviews in analytical chemistry,* Vol. 31, No. 4, p. 311-345.

Tafel, J. (1905), 'Über die polarisation bei kathodischer Wasserstoffentwicklung', *Zeitschrift für Physikalische Chemie,* Vol. 50, p. 641-712.

Taleyarkan, R.P., West, C.D., Cho, J.S., Lahey, R.T., Nigmatulin, R.I. and Block, R.C. (2002), 'Evidence for nuclear emission during acoustic cavitation', *Science,* Vol. 295, p. 1868-1873.

Tercier-Waeber, M.L., Buffle, J., Confalonieri, F., Riccardi, G., Sina, A., Graziottin, F., Fiaccabrino, G.C. and Koudelka-Hep, M. (1999), 'Submersible voltammetric probes for *in situ* real-time trace element measurements in surface water, groundwater and sediment-water interface', *Measurement Science Technology,* Vol. 10, p. 1202-1213.

Thornycroft, J. and Barnaby, S.W. (1895), 'Torpedo-boat destroyers', *Proceedings from the Institute of Civil Engineers,* Vol. 122, p. 51-69.

Townend, J. (2002), *Practical statistics for Environmental and Biological Scientists,* John Wiley & Sons Limited, Chichester, Sussex, UK.

Trojanowicz, M. (2002), 'Determination of pesticides using electrochemical enzymatic biosensors (review)', *Electroanalysis,* Vol. 14, No. 19-20, p. 1311-1328.

Tuziuti, T., Yasui, K. and Iida, Y. (2005), 'Spatial study on a multibubble system for sonochemistry by laser-light scattering', *Ultrasonics Sonochemistry,* Vol. 12, p. 73-77.

U.S. Census Bureau: *World Population Clock,*accessed 12th January 2004, available at: http://www.census.gov/main/www/popclock.html

Umezawa, Y., Umezawa, K., Buhlmann, P. and Hamada, N. (2002), 'Potentiometric selectivity coefficients of ion-selective electrodes, part 2: inorganic anions & part 3: organic ions', *Pure Applied Chemistry,* Vol. 74, p. 923-1099.

United Nations (2001), *International Rivers and Lakes Newsletter 35, Section XII: The global water crisis and the commodification of the world's water supply,* accessed 20th June 2004, available at: http://www.un.org/esa/sustdev/sdissues/water/rivers-lakes-news35.pdf

Updike, S.J. and Hicks, J.P. (1967), 'The enzyme electrode', *Nature,* Vol. 214, p. 986-988.

Vaezy, S., Martin, R., Mourad, P. and Crum, L. (1999), 'Hemostasis using high intensity focused ultrasound', *European Journal of Ultrasound,* Vol. 9, p. 79-87.

Van Dam, Y.K. and Apeldoorn, P.A. (1996), 'Sustainable Marketing', *Journal of Macromarketing,* Vol. 16, No. 2, p. 45-56.

Van der Hoff, B.M.E. and Glynn, P.A.R. (1974), 'The rate of degradation by ultrasonation of polystyrene in solution', *Journal of Macromolecular Science and Macromolecular Chemistry,* Vol. A8, p. 429-449.

Verrall, R.E. and Sehgal, C.M. (1987), 'Sonoluminescence', *Ultrasonics,* Vol. 25, p. 29-30.

Vlachy, V. (1999), 'Ionic effects beyond Poisson-Boltzmann theory', *Annual Review of*

Physical Chemistry, Vol. 50, p. 145-165.

Volkov, A., Tourillon, G., Lacaze, P.C. and Dubois, J.E. (1980), 'Electrochemical polymerisation of aromatic amines', *Journal of Electroanalytical Chemistry,* Vol. 115, p. 279-291.

Von Helmholtz (1853), 'Ueber einige gesetze der vertheilung elektrischer ströme in körperlichen leitern mit anwendung auf die thierisch-elektrischen versuche', *Annalen der Physik,* Vol. 89, p. 211-233.

Walker, I. (2002), *Chloramination - future best practice for the water industry?,* accessed 4th May 2004, available at: http://www.wrcplc.co.uk/downloads/news/chloramination_nov_02.pdf

Wallace, G.G., Spinks, G.M. and Kane-Maguire, L.A.P. (2002), 'Electrochemical Polymerisation', *Conductive Electroactive Polymers: Intelligent Materials Systems* (2nd edition), CRC Press, Boca Raton, Florida, USA, p. 122-127.

Walley, N. and Whitehead, B. (1994), 'It's not easy being green', *Harvard Business Review,* Vol. 72, No. 11-12, p. 45-52.

Wang, J. (1995), *Electrochemical Sensors For Environmental Monitoring: A Review of Recent Technology*, Solicitation No. LV-94-012, United States Environmental Protection Agency, Department of Chemistry and Biochemistry, New Mexico State University, Las Cruces, New Mexico, United States of America.

Wang, J. (2000), 'Analytical Electrochemistry', (2nd edition), Wiley-VCH, New York, USA, p. 140-170.

Wang, J., Luo, D. and Horiuchi, T. (1998), 'Anodic stripping with collection at interdigitated carbon film microelectrode arrays', *Electroanalysis,* Vol. 10, No. 2, p. 107-110.

Wang, J., Sadik, O.A. and Land, W.H. (2003), 'Targeting chemical and biological warfare agents at the molecular level', *Electroanalysis,* Vol. 15, No. 14, p. 1149-1159.

Westerhoff, P., Chao, P. and Mash, H. (2004), 'Reactivity of natural organic matter with aqueous chlorine and bromine', *Water Research,* Vol. 38, p. 1502-1513.

White, G.C. (1999), *Handbook of Chlorination and Alternative Disinfectants* (4th edition), John Wiley & Sons Limited, New York, USA.

Wightman, R.M. (1981), 'Microvoltammetric electrodes', *Analytical Chemistry,* Vol. 53, p. 1125A-1134A.

Wilde, E.W. (1991), 'Comparison of three methods for measuring residual chlorine', *Water Research,* Vol. 25, No. 10, p. 1303-1305.

William, D. and McCarthy, J.E. (1997), *Product Life Cycle: "Essentials of Marketing"* (7th edition), Richard D. Irwin Company, Chicago, USA.

Winokur, M., Moon, Y.B., Heeger, A.J., Barker, J., Bott, D.C. and Shirakawa, H. (1987), 'X-ray scattering from sodium-doped polyacetylene: incommensurate-commensurate and order-disorder transformations', *Physical Review Letters,* Vol. 58, p. 2329-2332.

Wood, L. (2000), 'Brands and brand equity: definition and management', *Management Decision,* Vol. 38, No. 9, p. 662-669.

World Health Organisation (2004), *Water sanitation and health: evaluation of the costs and benefits of water and sanitation improvements at the global level,* accessed 2nd June 2004, available at: http://www.who.int/water_sanitation_health/wsh0404summary/en/

Wu, C.C. and Chang, H.C. (2004), 'Estimating the thickness of hydrated ultrathin poly(*o*-phenylenediamine) film by atomic force microscopy', *Analytica Chimia Acta,* Vol. 505, p. 239-246.

Wu, L.L., Luo, J. and Lin, Z.H. (1996), 'Spectroelectrochemical studies of poly-*o*-phenylenediamine. Part 1. In situ resonance raman spectroscopy', *Journal of Electroanalytical Chemistry,* Vol. 417, p. 53-58.

www.matweb.com: *Materials property data,* accessed March 4th 2004, available at: www.matweb.com

Xu, C., Lemon, W. and Liu, C. (2002), 'Design and fabrication of a high-density metal microelectrode array for neural recording', *Sensors and Actuators A (Physical),* Vol. 96, p. 78-85.

Yacynych, A.M. and Mark, H.B. (1976), 'The spectroelectrochemical study of the oxidation of 1,2-diaminobenzene: alone and in the presence of Ni(II)', *Journal of the Electrochemical Society,* Vol. 123, p. 1346-1351.

Yanagida, H., Masubuchi, Y., Minagawa, K., Takimoto, J., Ogata, T. and Koyama, K. (2000), 'Dependence of sonochemical luminescence on various sound fields', *Ultrasonics,* Vol. 38, p. 671-675.

Yano, J. (1995), 'Electrochemical and structural studies on soluble and conducting polymer from *o*-phenylenediamine', *Journal of Polymer Science: Part A: Polymer Chemistry,* Vol. 33, p. 2435-2441.

Yano, J. and Higuchi, Y. (1990), 'Electrochromic properties of the polymer films derived from aniline derivatives and their dual-layer films', *Kobunshi Ronbunshu,* Vol. 47, No. 10, p. 817-824.

Yano, J., Kai, S. and Ogura, K. (1993), 'Poly(*o*-phenylenediamine)-Prussian blue composite film for a three-colour-expressible electrochromic display material', *Journal of Material Science Letters,* Vol. 12, p. 1791-1792.

Yano, J., Kitani, A., Vasquez, R.E. and Sasaki, K. (1985), 'Polymer film coated electrodes prepared by electrooxidation of aniline derivatives', *Nippon Kagaku Kaishi,* p. 1124-1130.

Yano, J., Shimoyama, A. and Ogura, K. (1992a), 'Poly(*o*-phenylenediamine)-film-coated elctrode having a permselective response to halogenide ions', *Journal of the Electrochemical Society,* Vol. 139, No. 5, p. L52-L53.

Yano, J., Shimoyama, A. and Ogura, K. (1992b), 'Poly(*o*-phenylenediamine)-film-coated electrode: incorporation of *o*-benzoquinone and permselectivity of I^- and Br^-', *Journal of the Chemical Society, Faraday transactions* , Vol. 88, No. 17, p. 2523-2527.

Yao, T., Satomura, M. and Nakahara, T. (1994), 'Amperometric flow-injection determination of glucose, urate and cholesterol in blood serum by using some immobilized enzyme reactors and a poly(1,2-diaminobenzene)-coated platinum electrode', *Analytica Chimica Acta,* Vol. 296, p. 271-276.

Yasui, K., Tuziuti, T. and Iida, Y. (2005), 'Dependence of the characteristics of bubbles on types of sonochemical reactors', *Ultrasonics Sonochemistry,* Vol. 12, p. 43-51.

Yau, T., Suzuki, S., Nishino, H. and Nakahara, T. (1995), 'On-line amperometric assay of glucose, L-glutamate, and acetylcholine using microdialysis probes and immobilized enzyme reactors', *Electroanalysis,* Vol. 7, p. 1114-1117.

Yinghuai, Z. (2004), 'Application of ultrasound technique in the synthesis of methanofullarene derivatives', *Journal of Physics and Chemistry of Solids,* Vol. 65, p. 349-353.

Zorn, M.E., Gibbons, R.D. and Sonzogni, W.C. (1999), 'Evaluation of approximate methods for calculating the limit of detection and limit of quantification', *Environmental Science & Technology,* Vol. 33, p. 2291-2295.

Zoski, C.G. (2002), 'Ultramicroelectrodes: design, fabrication, and characterisation', *Electroanalysis,* Vol. 14, No. 15-16, p. 1041-1051.

CHAPTER 11

Appendices

10.1 APPENDIX 1

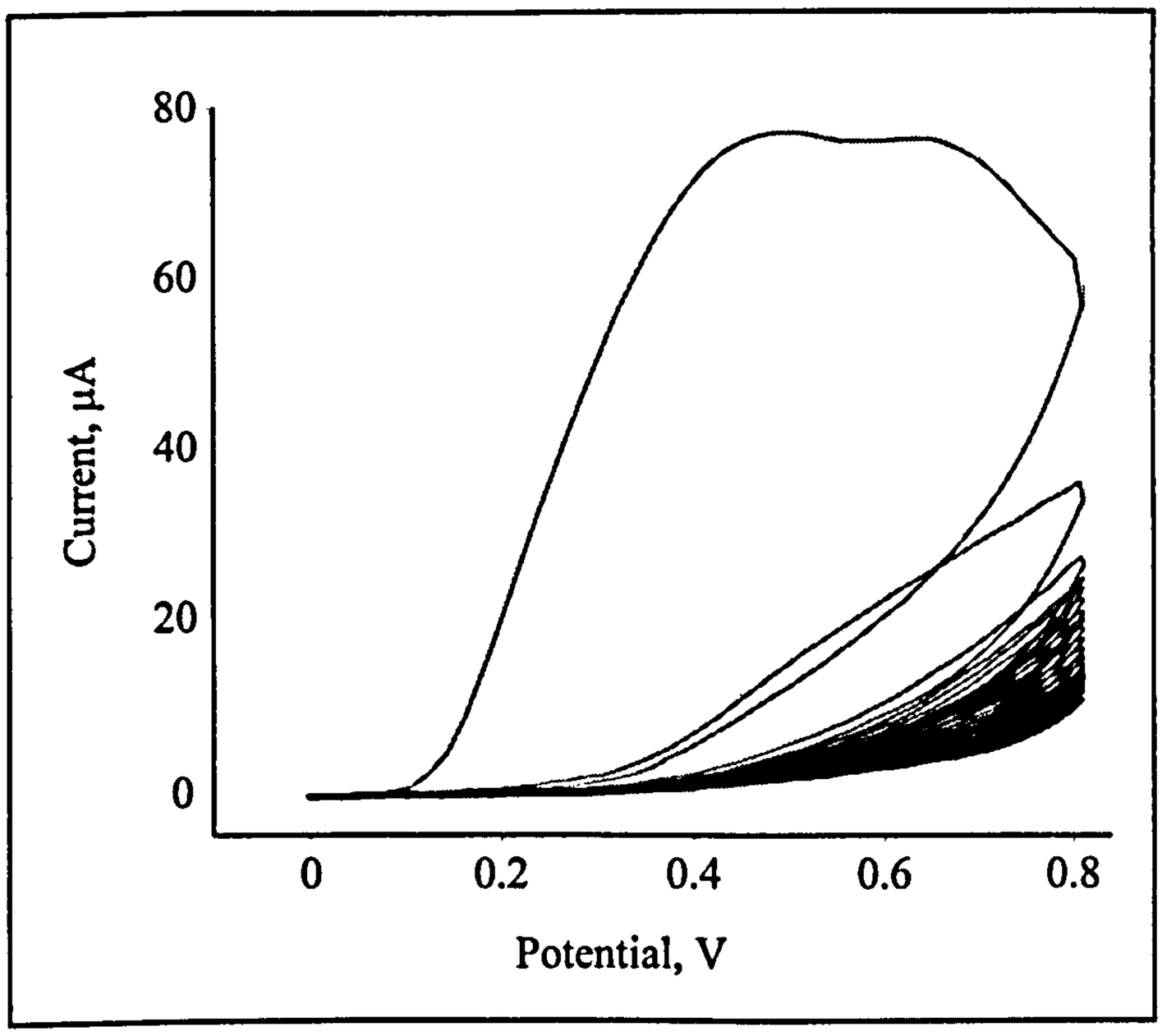

Figure 10.1: CV showing the electropolymerisation of P*o*PD with no resistor in series

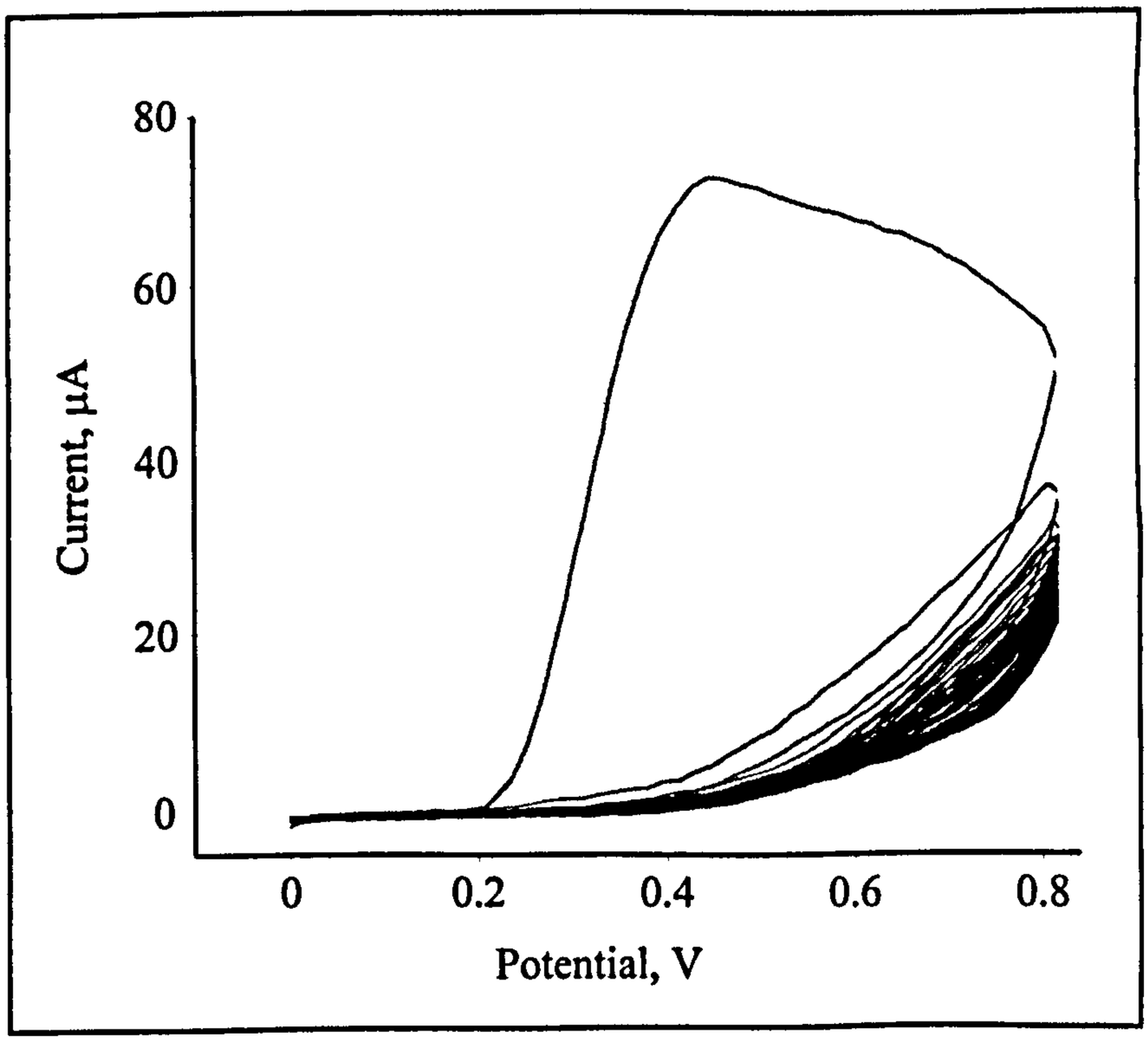

Figure 10.2: Effect of 1 KΩ resistor in series upon the electropolymerisation of P*o*PD

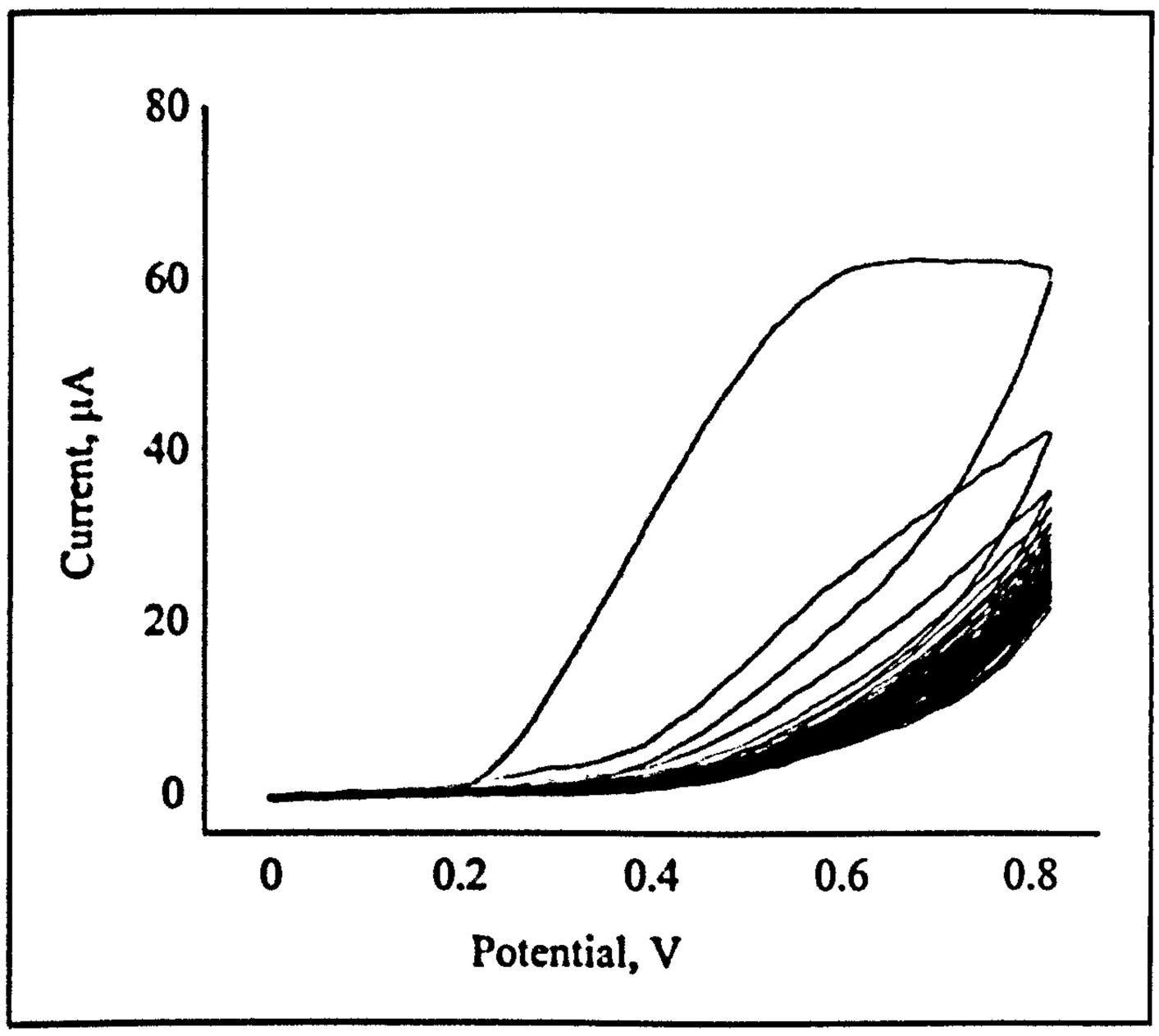

Figure 10.3: Effect of 2 KΩ resistor in series upon the electropolymerisation of PoPD

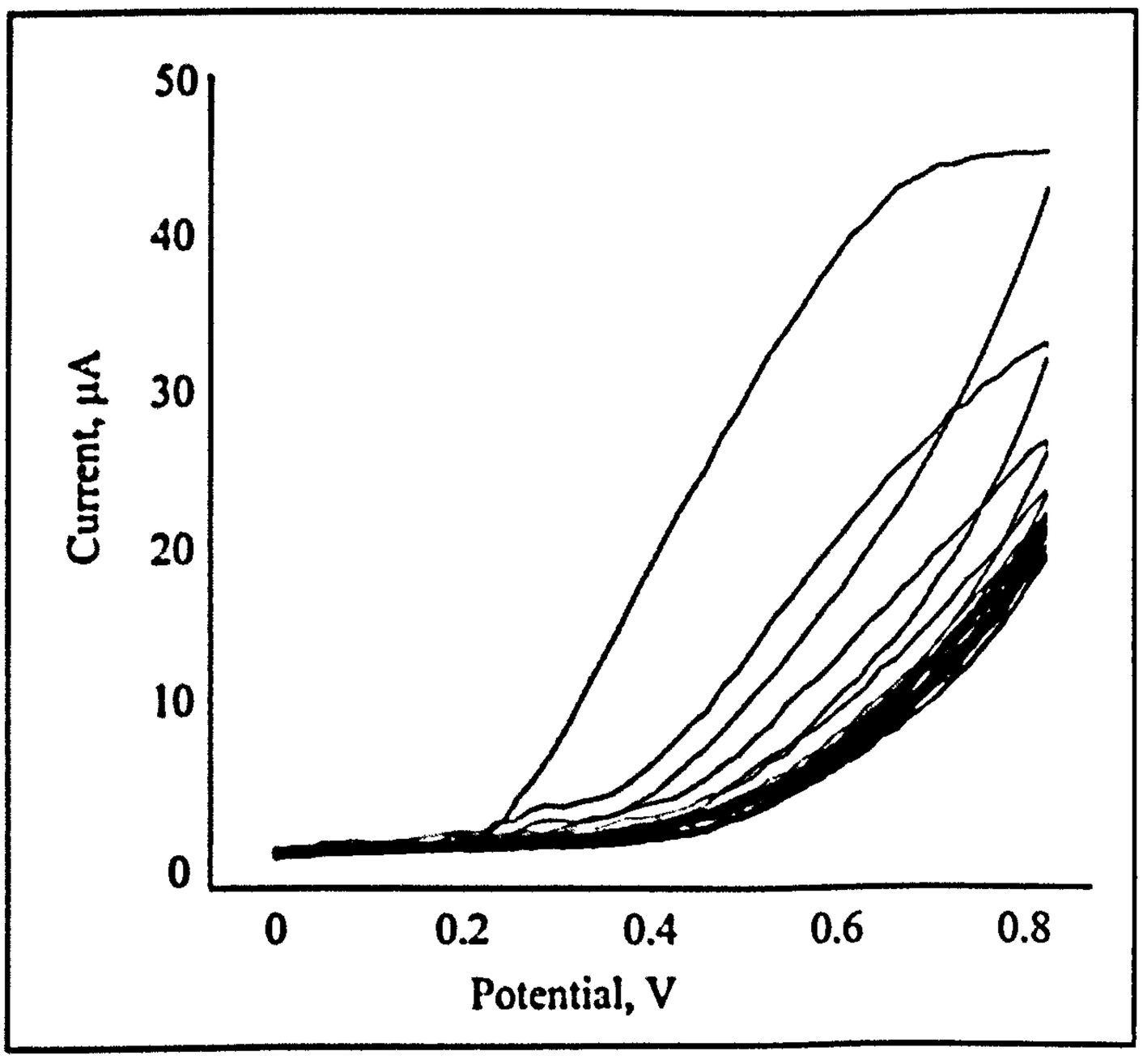

Figure 10.4: Effect of 3 KΩ resistor in series upon the electropolymerisation of PoPD

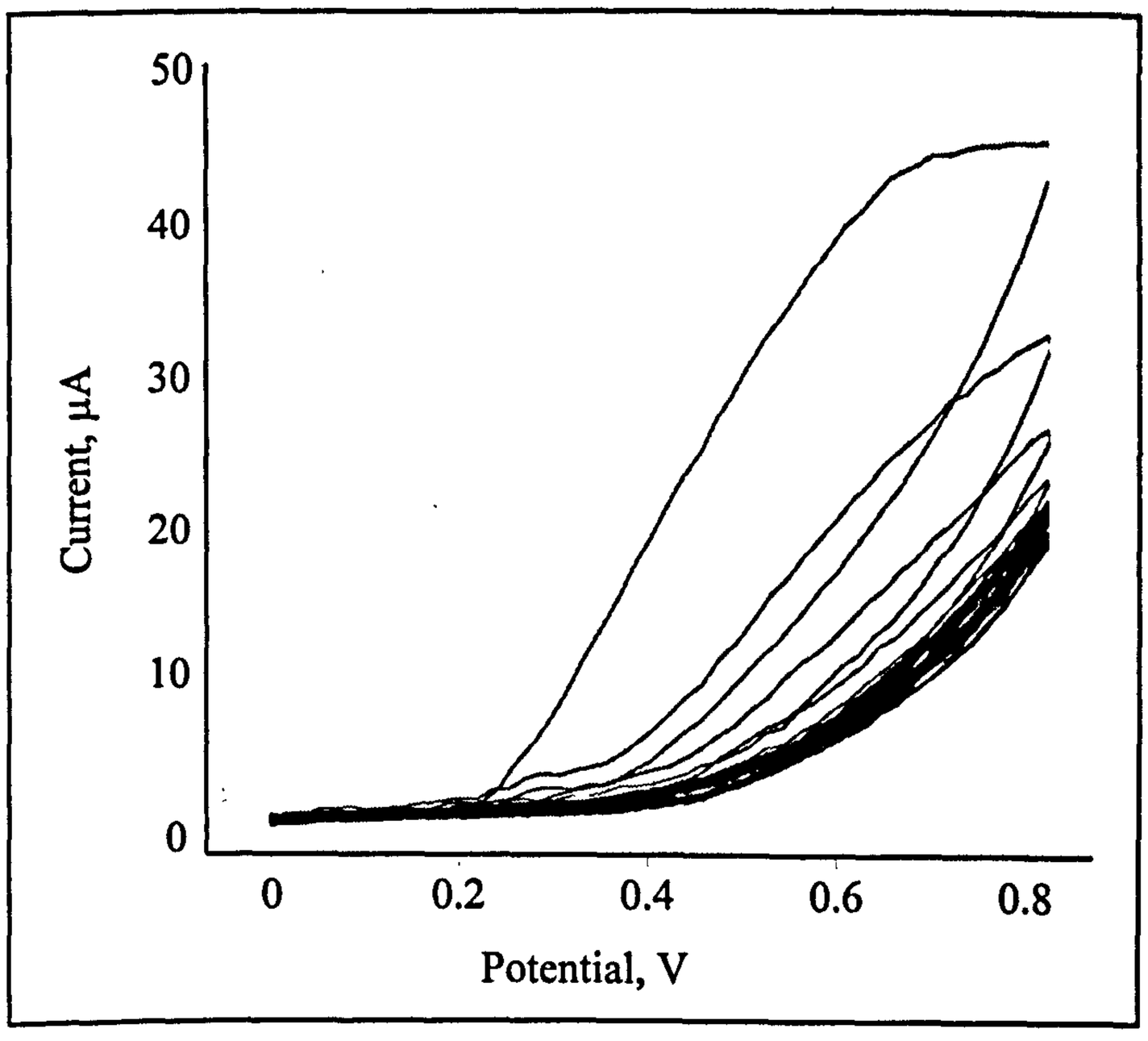

Figure 10.5: Effect of 5 KΩ resistor in series upon the electropolymerisation of PoPD

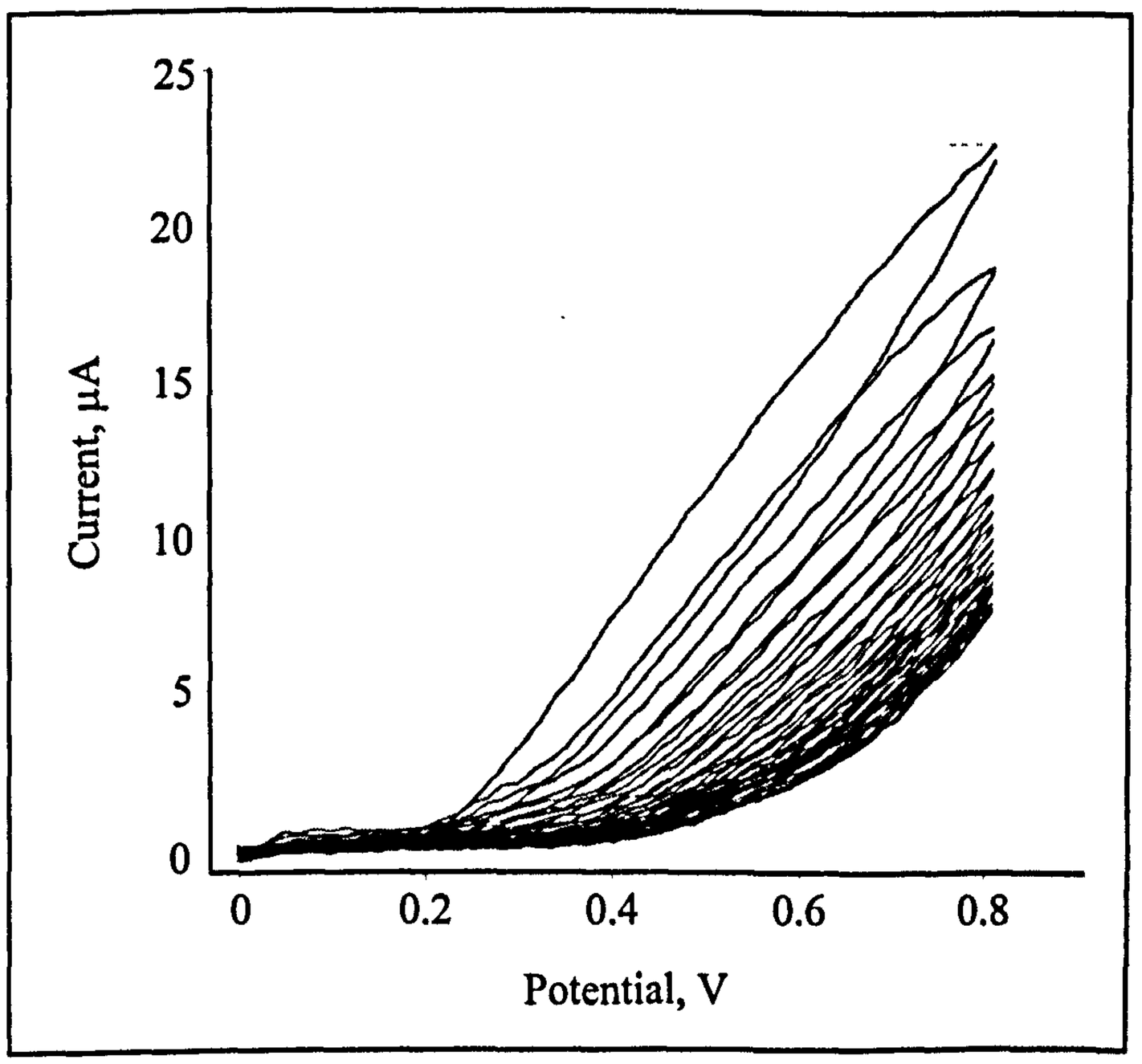

Figure 10.6: Effect of 10 KΩ resistor in series upon the electropolymerisation of PoPD

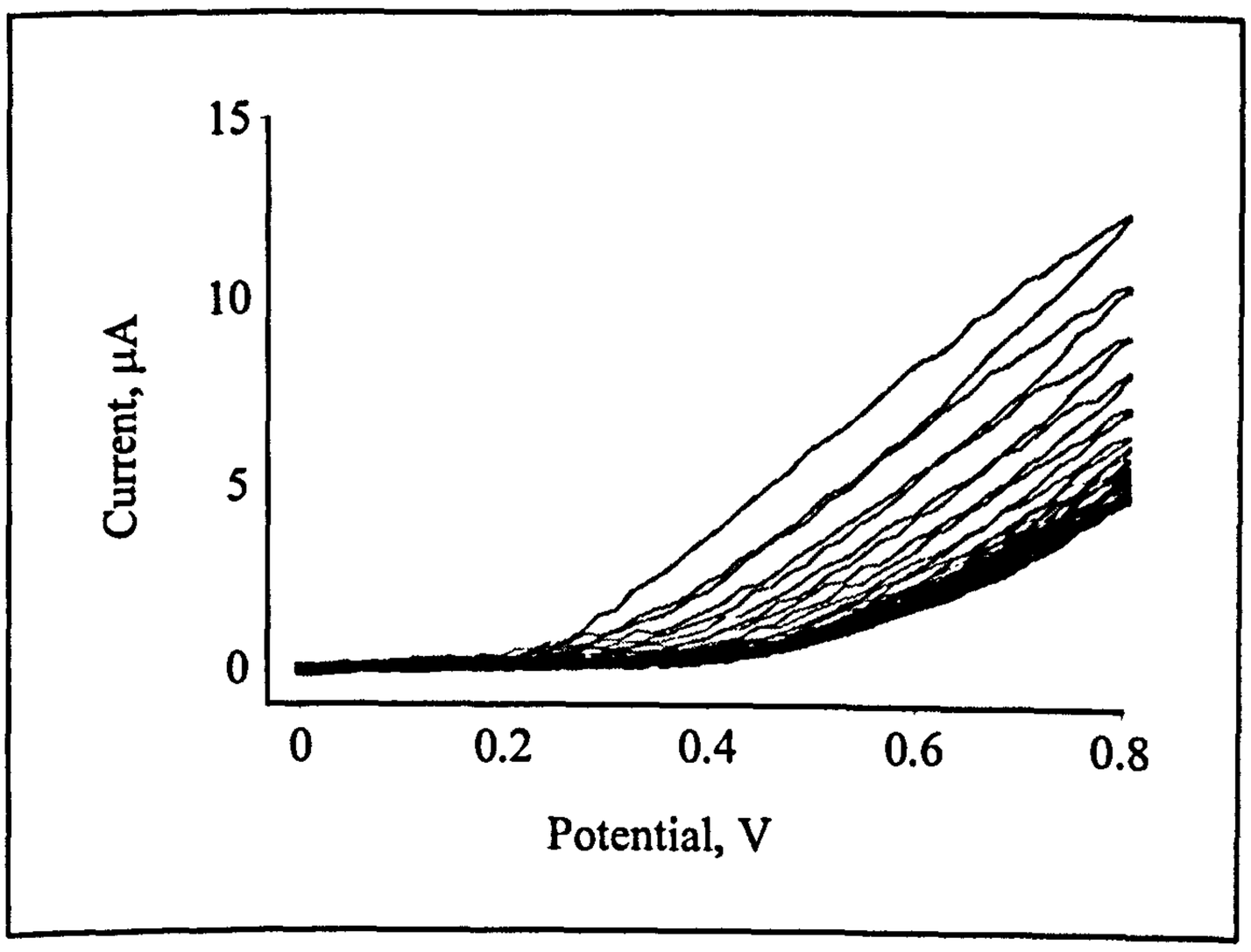

Figure 10.7: Effect of 10 KΩ resistor in series upon the electropolymerisation of PoPD

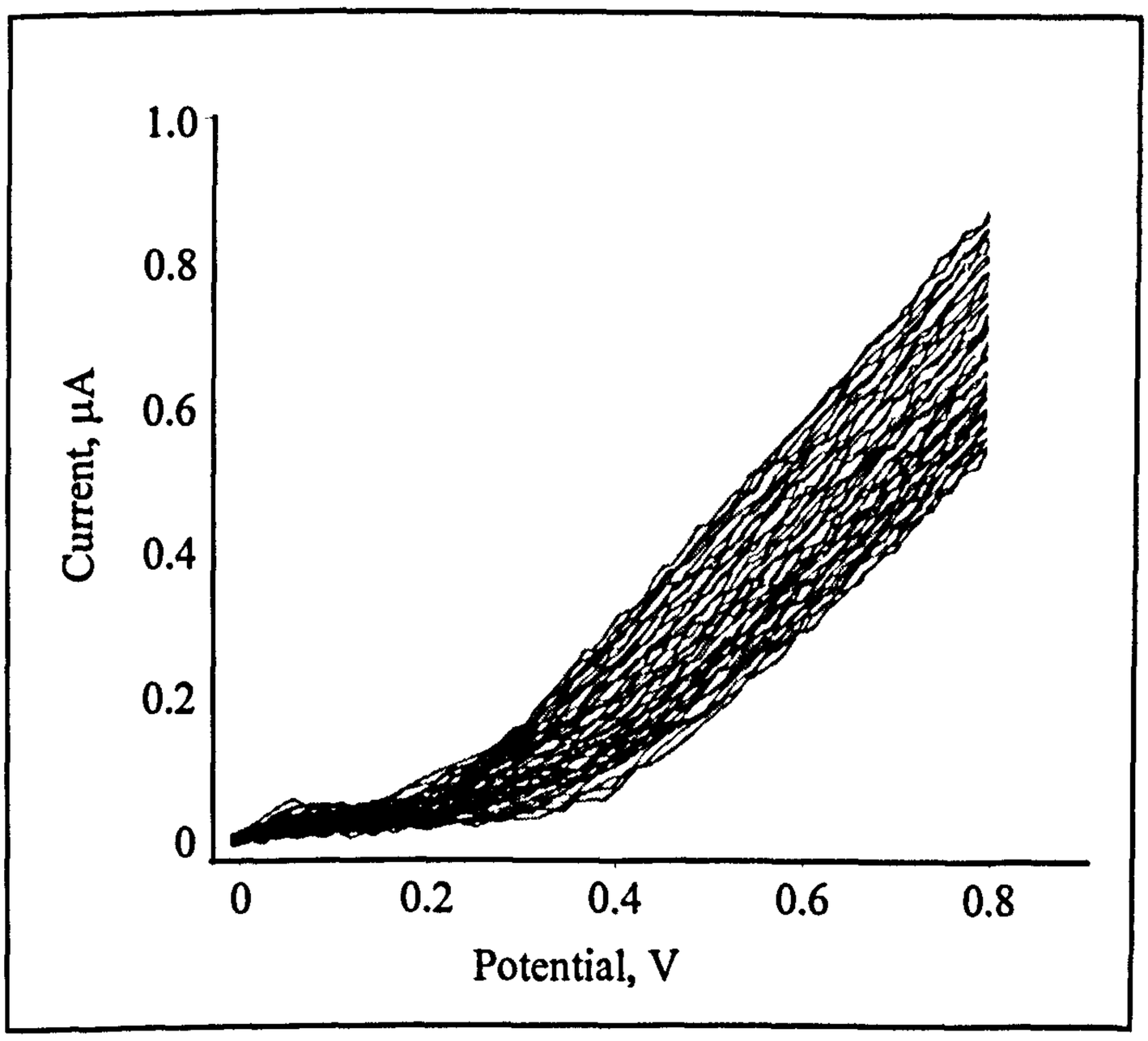

Figure 10.8: Effect of 100 KΩ resistor in series upon the electropolymerisation of PoPD

10.2 APPENDIX 2

Microarray Ltd Production potentiostat design specification

Issue 2

High level description

A 40 channel PC controlled potentiostat is required by the company to electro-polymerise bulk printed sheets of disposable sensor devices, in a new manufacturing process. It is intended for use primarily by a third party subcontract supplier, with relatively low skill level. Flexibility is important to allow tuning and development of the manufacturing process and for use in future applications.

The potentiostat software needs to be configured with a simple/automated front end with tight process controls and logging, for unskilled users, and an advanced and "unregulated" mode for development users.

Detailed requirements

40 identical channels

Control of an external ultrasonic bath via a means to be agreed, requiring an automated check to ensure that if the ultrasonic equipment is not functioning, the potentiostat will not start its production CV sweep

Capable of delivering up to 200mA per channel

Aqueous applications only

Polarisation potential range ± 1.5 volts

Integrated PC control

Data logging as follows:

- Basic data logging of up to 250 data sets in terms of 1st sweep and last sweep
- A random one in 10 channels to be logged in terms of full CV data
- Transportable as a data file that can be emailed
- A program suitable for the graphical display any of the 250 CVs
- A feature whereby a batch of 10 is halted if there is a problem with any of the channels, giving the operator the chance to either correct a problem with a particular channel(s) or continue with the unaffected channels
- Means of statistically analysing all 250 data sets for min/max voltages and currents, mean averages, statistical variation
- Able to generate a simple report of sweep success/failure (e.g. a typical report would read 250 CVs completed with zero errors or parameters outside limits)
- Time stamping for each CV

1/2

Microarray Ltd Production potentiostat design specification

Issue 2

- For problem solving or diagnosis measurement of the area under the CV characteristic is required
- For manufacturing process control and monitoring - the ability to plot trends throughout a batch of 250 routines, such as trend in max/min voltage/current

Simple user interface to allow minimal training requirement for production use with simple go/no go criteria fault detection

Password protected access to a more advanced user interface to allow skilled personnel to pull up detailed information, reports, and to monitor/adjust detailed process parameters

"Red and green light system" if first anodic sweep is below a certain threshold

Modes required:

- Cyclic voltammetry
- Potentiostatic
- Coulometry

Single housing/case for the complete system

Typical settings for polymerisation intended are 40 sweeps at 50 mV per second

2/2

D. W. Mills

Cranfield University, Silsoe